Martin Weckerle
Karlstraße 3
67433 Neustadt a.d. Weinstr.

Utilization of Correlation Matrices in Adaptive Array Processors for Time–Slotted CDMA Uplinks

deutscher Titel:

Nutzung von Korrelationsmatrizen in adaptiven Array-Prozessoren für zeitgeschlitzte CDMA-Aufwärtsstrecken

Vom Fachbereich Elektrotechnik und Informationstechnik
der Universität Kaiserslautern
zur Verleihung des akademischen Grades
Doktor der Ingenieurwissenschaften (Dr.–Ing.)
genehmigte Dissertation

von

Dipl.–Ing. Martin Weckerle

D 386

Tag der Einreichung:	4. Juli 2001
Tag der mündlichen Prüfung:	14. Mai 2002
Dekan des Fachbereichs:	Prof. Dr.–Ing. R. Urbansky
Vorsitzender der Prüfungskommission:	Prof. Dr.–Ing. habil. M. Pandit
1. Berichterstatter:	Prof. Dr.–Ing. habil. P.W. Baier
2. Berichterstatter:	o.Univ.–Prof. Dipl.–Ing. Dr. techn. E. Bonek

Die Deutsche Bibliothek – CIP-Einheitsaufnahme

Weckerle, Martin:
Utilization of correlation matrices in adaptive array processors for time–slotted CDMA uplinks /
Martin Weckerle. Universität Kaiserslautern. - Kaiserslautern : Univ., 2002
(Forschungsberichte Mobilkommunikation ; Bd. 11)
Zugl.: Kaiserslautern, Univ., Diss., 2002
ISBN 3-925178-83-X

Herausgeber: Prof. Dr.-Ing. habil. P.W. Baier
Lehrstuhl für hochfrequente Signalübertragung und -verarbeitung
Universität Kaiserslautern
Postfach 3049
67653 Kaiserslautern

Verfasser: Martin Weckerle

Verlag: Universität Kaiserslautern

Druck: ZBT - Abteilung Foto-Repro-Druck der Universität Kaiserslautern

D 386

ISSN 1438-6720
ISBN 3-925178-83-X

Vorwort

Die vorliegende Arbeit entstand in der Zeit von Juli 1997 bis Juni 2001 im Rahmen meiner Tätigkeit als wissenschaftlicher Mitarbeiter Prof. Dr.–Ing. habil. P.W. Baiers am Lehrstuhl für hochfrequente Signalübertragung und –verarbeitung der Universität Kaiserslautern. Ich möchte allen danken, die mich bei der Entstehung dieser Arbeit unterstützt haben.

Mein besonderer Dank gilt Herrn Prof. P.W. Baier für die Anregung und die Betreuung meiner Arbeit. Durch seine stete Diskussionsbereitschaft sowie durch zahlreiche Ratschläge und Hinweise hat er das Entstehen dieser Arbeit wesentlich gefördert.

Herrn Prof. Dipl.–Ing. Dr. techn. E. Bonek von der Technischen Universität Wien danke ich herzlich für die Übernahme des Koreferats. Durch den fachlichen Austausch im Rahmen des Forschungsprojekts COST 259 (European Cooperation in the Field of Scientific and Technical Research) der Europäischen Union entstanden wichtige Hinweise und zusätzliche Motivation, welche meiner Arbeit zugute kamen.

Weiterhin möchte ich Herrn Prof. Dr.–Ing. habil. M. Pandit für die Übernahme des Vorsitzes der Promotionskommission meinen Dank aussprechen.

Dem Unternehmensbereich ICM (Information Communication Mobile) der Siemens AG, München, insbesondere Herrn Dipl.–Ing. H. von der Neyen, gebührt ein weiterer Dank für die Förderung meiner Arbeit.

Beim Regionalen Hochschulrechenzentrum Kaiserslautern (RHRK) möchte ich mich für die Bereitstellung leistungsfähiger Rechnersysteme bedanken.

Meinen ehemaligen Kollegen am Lehrstuhl für hochfrequente Signalübertragung und –verarbeitung danke ich für die angenehme Arbeitsatmosphäre und für viele fruchtbare Diskussionen, die mir oftmals weitergeholfen haben. Ein besonderer Dank ergeht an die Herren Dr.–Ing. J.J. Blanz, Dr.–Ing. A. Papathanassiou und Dr.–Ing. R. Schmalenberger für die Unterstützung beim Einarbeiten in das TD–CDMA–Konzept mit adaptiven Antennen sowie an Herrn Dr.–Ing. T. Bing für seine stete Diskussionsbereitschaft.

Einen weiteren Dank möchte ich den Herren J.J. Catany Hernández, A. Dost, J. Gil Canals, J. Hennig, T. Pohlen und R. Reynes Carreras aussprechen, die im Rahmen ihrer Diplomarbeiten unter meiner Anleitung Beiträge zu dieser Dissertation geleistet haben.

Zahlreiche dankenswerte Anregungen und Hinweise für meine Arbeit resultierten auch aus Kontakten zu den Arbeitsgruppen Prof. Dr.techn. J.A. Nosseks, Prof. Dr.–Ing. J. Eberspächers und Prof. Dr.–Ing. J. Hagenauers, alle Technische Universität München, im Rahmen von Projekten, die durch die Deutsche Forschungsgemeinschaft (DFG) gefördert wurden.

Besonders herzlich bedanke ich mich bei meiner Familie, insbesondere bei meinen Eltern, die mir meine Ausbildung ermöglichten und mich stets unterstützt haben. Schließlich danke ich meiner Frau Daniela, die mir in dieser Zeit ein entscheidender Rückhalt war. Ihr möchte ich diese Arbeit widmen.

Neustadt, im Juli 2001 Martin Weckerle

Contents

1 Introduction

1.1 Adaptive array processing in the uplink of cellular mobile radio systems

1.1.1 General

A higher demand in wireless communications calls for higher systems capacities. The capacity of communications systems can be increased directly by enlarging the bandwidth of the existing communications channels or by allocating new frequencies to the service in question. However, since the electromagnetic spectrum is limited, thereby making it a valuable resource, and the electromagnetic environment is increasingly becoming congested with a proliferation of unintentional and intentional sources of interference, it may not be feasible in the future to increase system capacity by opening up new spectrum space for the wireless communications applications [LL96, Lee89, Bla98, Pap00, Bai96a]. Therefore, efficient use of the frequency resource is critical if communications engineers are to increase the capacity of communications systems [COS99, NTD+98, Cal88, Rap96, Bla98, NSC00, Pap00].

Considerations concerning efficient use of the available bandwidth play an important role in the worldwide standardization activities towards a global wideband mobile communications system, directed by the ITU (International Telecommunications Union) [ITU97]. The goal of these standardization activities, which are currently undergoing finalization, is a worldwide third-generation (3G) mobile radio air interface called IMT-2000 (International Mobile Telecommunications - 2000) [3GPP]. The existing second-generation (2G) systems will not meet the requirements for increased capacity in the near future [ASS98, NTD+98]. Advanced services requiring higher data rates, such as multimedia applications, wireless internet access, services offering flexibility as regards data rates and transmission qualities need the 3G systems design. Although 3G mobile radio systems will cope with the requirements of high data rates up to 2 Mbit/s, flexibility concerning the data rates and the transmission qualities, and efficient bandwidth utilization [BK95, ASS98, Pap00], they will not fulfill the requirement for capacity, if they exclusively use single antennas [Rap98, BBP97, BBS97, God97a, God97b, Pap00].

In recent years, adaptive antenna arrays have emerged as leading candidates for increasing the capacity of mobile radio networks by exploiting the directional inhomogeneity of the mobile radio channels [PaP97] and without increased bandwidth consumption. The received signal is obtained by means of an array of sensors located at different points in space in the field of interest. Each sensor of the array could be an omnidirectional antenna and is known as an element of the array. Adaptive array processing can be applied in the uplink, where the mobile station (MS) transmits and the base station (BS) of the cell concerned receives, and in the downlink, where the transmission situation is vice versa. In general, application of adaptive arrays can be considered for both the MS and the BS which leads to MIMO (multiple in, multiple out) [FoG98, Tel95, NSC00, PaP97] structures for the mobile radio channel. Fig. 1.1 shows a MIMO structure for the multiuser case, where several MSs transmit to one BS. MIMO structures have a high potential to increase the capacity. The optimum situation is to have uncorrelated radio channels for each link,

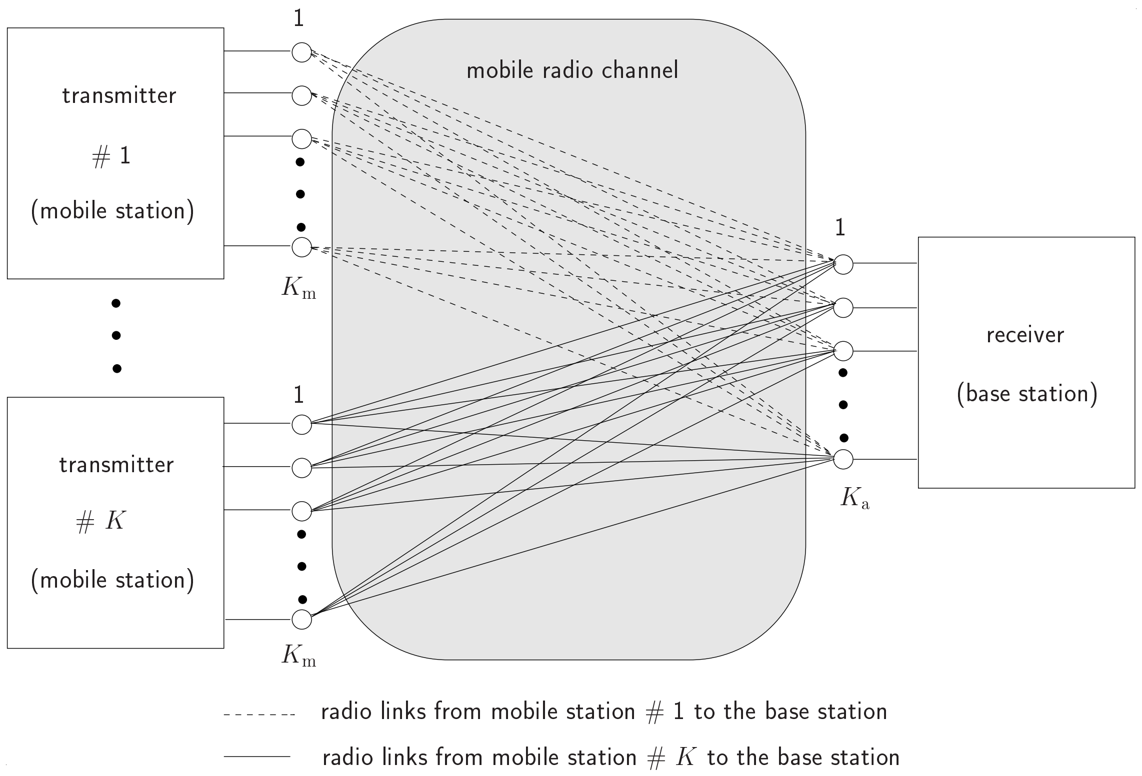

Fig. 1.1. Multiuser MIMO system in the uplink with K_m antenna elements at each MS and K_a antenna elements at the BS

as shown in Fig. 1.1. Hence, the capacity is increased by the number of existing radio links, i.e. by the product of the number of transmit and receive antennas as long as the number of receive antennas is greater than or equal to the number of transmit antennas [FoG98, TNSC99, Bac99]. For real applications and in real wave propagation environments the received signals at the different antenna elements are correlated, especially at the MSs, where the antennas are co-located close together due to size limitations. Therefore, the channels are not independent any more and special techniques have to be applied which ensure a certain independence. These techniques require new MSs, i.e. result in additional costs and the existing MSs cannot benefit from this MIMO structure. Furthermore, it is still difficult to have more than one or two antennas at the portable unit due to size limitations and cost of multiple chains of RF down conversion [NSC00]. At the

BS one does not have the problem of size limitations. Therefore, in the following one single antenna element at each MS and antenna arrays at the BSs in the uplink of a mobile radio system are considered, as shown in Fig. 1.2 and referred to as a SIMO (single in, multiple out) structure [PaP97]. The aim of array processing with SIMO

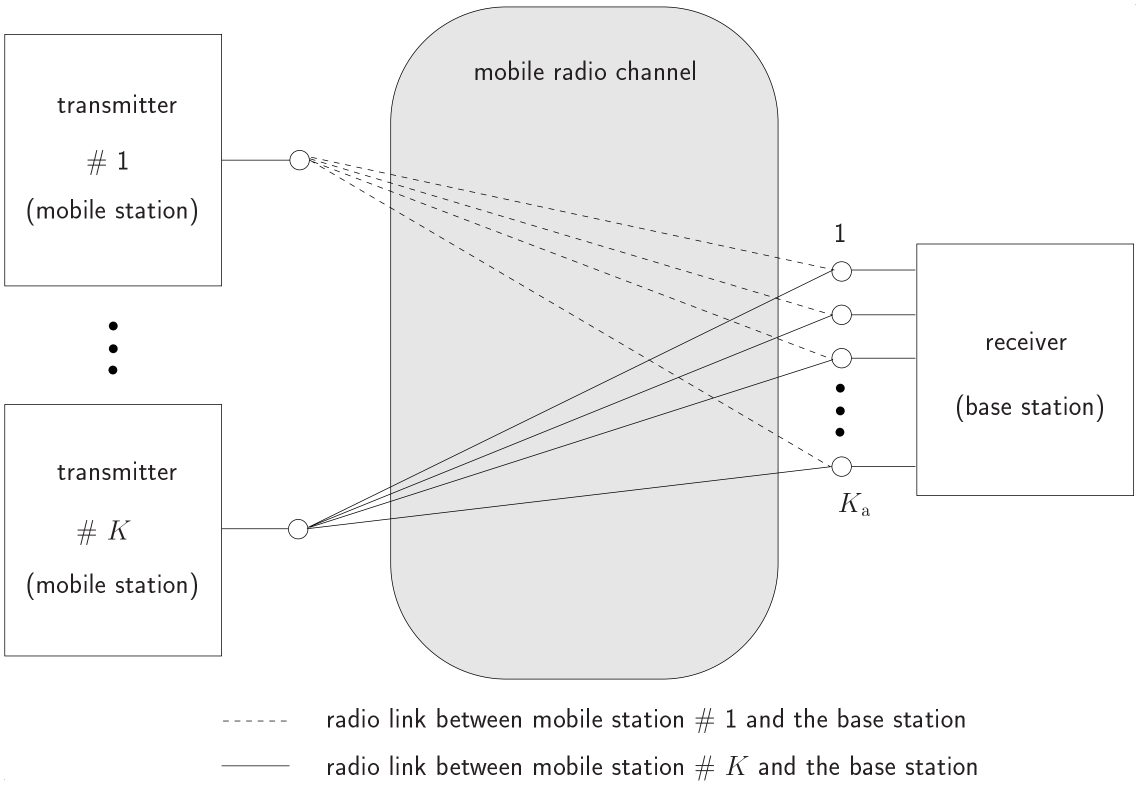

Fig. 1.2. Multiuser SIMO system in the uplink with one single antenna element at each MS and K_a antenna elements at the BS

structures in the uplink is to extract useful characteristics of the received signals, e.g. its direction of arrival (DOA) or correlation properties of the received signals [Hay85]. The increase in capacity by array processing without additional consumption of bandwidth can be realized by exploiting the above-mentioned signal characteristics in the processing of the signals received at the different antenna elements in such a way that as much power of the desired signals as possible is received while minimizing the received power of the undesired signals [God97a, MM80, LL96, Fuh97, Pap00]. Such a selective reception reduces interference and consequently allows frequencies to be reused more often in other cells. It also mitigates the effect of multipath fading, if selective reception is performed for each propagation path of each users signal [God97a, Gia99]. Signals from MSs which are more highly attenuated due to increased distances of the MSs to the BS are received with sufficient power, since as much power of the desired users as possible is received while the power of the undesired signals is minimized. Therefore, the BS coverage is increased and the number of cells and BSs sites required for the same coverage as a conventional system is reduced, which results in reduced costs of BS installation, operation and maintenance [God97a]. Instead of extending coverage, taking antenna arrays into account at the BS, it is also possible to reduce the transmission power of one MS by a certain amount without loss of data detection performance, even if the interference power originating from MSs other than the one under consideration is constant. Since, in general, this is true for each MS in the whole system, the transmission power of each MS can be reduced, resulting in system-wide interference reduction. This system-wide interference reduction eventually even results in a data detection performance improvement of the signals from all MSs in the whole system even though the transmission power of all MSs has been reduced.

The level of system performance improvement and increase of capacity depends on the multiple access scheme, equalization algorithms and channel estimation schemes of the target mobile radio system. Furthermore, it depends on the propagation conditions, i.e. spatial separation and location of the user signals and the interfering signals, the signal and interference power, their correlation properties and the scattering environment. It depends on the antenna configuration (whether the antenna array is one-dimensional or two-dimensional) and on the number K_{a} of antenna elements used in the array.

If array processing is applied in mobile radio communications, the following two different fundamental receiver structures incorporating antenna arrays have to be distinguished [Pap00]:

- The spatial and temporal signal processing is performed in two consecutive steps, see Fig. 1.3a [Tan94, KTBT99, FN94a, Far97, Fuh97, Pen99]. The signals received in the uplink at the different elements of the antenna array are processed only in the spatial domain. By utilizing proper element-specific weight factors at the different receive branches a kind of optimum combination of the received signals can be achieved in the uplink [MM80]. Mostly, the specific performance criterion considered for weighting and combining the signals received at the different antenna elements is to maximize the signal-to-noise ratio (SNR) or signal-to-interference ratio (SIR) [MM80]. The combined output signal can be feed into a conventional detector for temporal signal processing which is originally designed for a single antenna receiver. From this example it becomes obvious that one advantage of separate spatial and temporal signal processing is the fact that the spatial processing can be incorporated into an existing system without modifying the multiple access scheme, the modulation scheme and the subscriber handsets. This fact is an important issue relating to incorporation of adaptive antennas into the existing 2G radio systems [God97a, God97b, FN94a, Pap00, Pen99]. Temporal signal processing follows on independently from spatial signal processing. In multiuser systems for example this type of optimum combination of the signals in the spatial domain is undertaken for each user signal in order to separate the different users signals, which is the principle of the multiple access scheme Space Division Multiple Access (SDMA) [Tan94, FN97a, FN94a, Far97, Pen99, GR94]. Since these concepts treat spatial and temporal signal processing separately in two steps, they will always be less than optimum solutions.

- Spatial and temporal signal processing is performed jointly, as shown in Fig. 1.3b [Bla98, Pap00, WP99c, AMF99, Koh98, Bru00, BHSN00, FoG98, Tel95, NSC00]. In the uplink, all received signals at the antenna array are jointly processed in the spatial and temporal domain in a process called space-time signal processing [Pap00]. From a more general point of view there is no need to separate spatial and temporal signal processing. The array antenna is a part of the receiver. From the estimation principle point of view the fact that different signals are received at different antenna elements on the basis of the same unknown transmitted data symbols leads to the fact that the number of known parameters and therefore the *a priori* information concerning the received signal in the data estimation process increases by increasing the number K_a of antenna elements, whereas the number of unknown data symbols which is to be finally estimated remains the same. Therefore, the potential for improving the data estimation process increases by increasing the number K_a of antenna elements. Furthermore, the data estimation process can be improved by exploiting the option of joint optimization of the multi-antenna receiver in the space and time domains. The disadvantage of joint space-time signal processing is that it requires completely new base stations and receiver structures and it cannot be incorporated into existing uplink receivers.

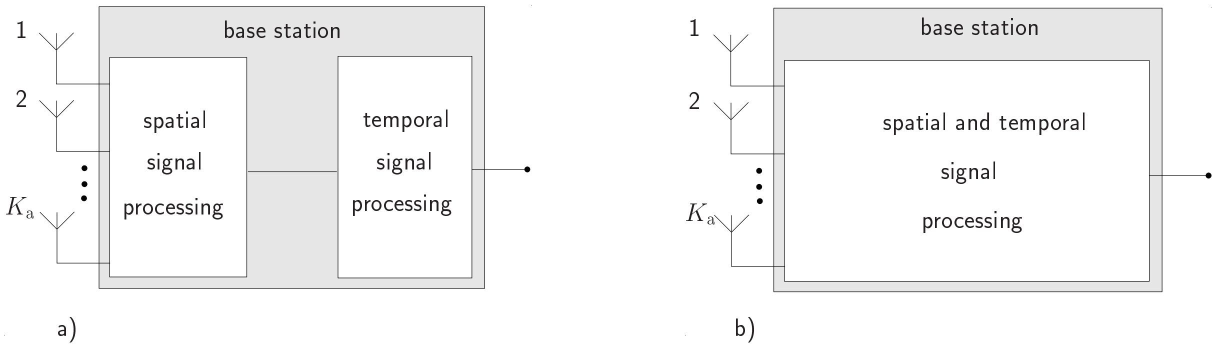

Fig. 1.3. Fundamental receiver structures
a) Separate spatial and temporal signal processing
b) Space-time signal processing

The source of energy responsible for illuminating the array may assume a variety of different forms. As seen from the location of the array, the radiation may be from diffused media and therefore distributed in nature, or it may be from isolated sources of finite angular extent. To exploit the full potential of antenna arrays, signal processing must be adapted according to the time varying propagation characteristics, which leads to adaptive array processing. Different algorithms can be applied to perform the adaptation of the signal processing according to a specified performance criterion. According to [Fuh97] two classes of algorithms for adaptive array processing basically exist:

- Temporal reference (TR) algorithms [Win93], which can be subdivided into algorithms that rely on knowledge of the time structure of the desired received signals, which can be obtained by using training sequences, and on blind algorithms that rely on the envelope properties of the signal to be received to realize the optimum performance according to the specified criterion. TR algorithms can be applied to single antenna receivers as well as to multi-antenna receivers with arbitrary distances between the antenna elements. The advantages of TR algorithms are [Fuh97]:
  - TR algorithms are independent of the antenna configuration,
  - they are independent of the propagation properties and
  - in systems using Time Division Duplex (TDD) information obtained in the uplink by using training sequences can be exploited in the downlink, e.g. for predistortion of the signals or Joint Transmission (JT) [BMW+00].

  Their disadvantages are:
  - Synchronization is required in order to find the position of the training sequence, except for the blind TR algorithms.
  - Since no DOAs are determined, this information cannot be exploited for downlink transmission.
- Spatial reference (SR) algorithms, which are based on algorithms for the estimation of the directions of arrival (DOAs) of wavefronts. Typical state of the art DOA estimation algorithms are MUSIC (Multiple Signal Classification) [Sch86], ESPRIT (Estimation of Signal Parameters via Rotational Invariance Techniques) [RK89, HN95] or SAGE (Space–Altering Generalized Expectation–Maximization) [FDHT96, THT98], which will be specified in Section 1.1.3. SR algorithms make use of the fact that the propagation delay between two neighboring antenna elements corresponds to a phase shift depending on the antenna distances and the DOA. If the array configuration is known, the DOAs can be determined. Based on the knowledge of the DOAs the received signals at the different antenna elements can be adaptively weighted and combined such a way that the array pattern is permanently optimized according to the specified performance criterion or that the prescribed objective function is satisfied. A presupposition for a useful application

of SR algorithms are narrowband signals. The farfield conditions should be fulfilled and antenna arrays with an antenna element spacing in the range of half of the carrier wavelength is recommended. The advantages of SR algorithms are:

– No training sequence is required. The separation of different signals corresponding to different users for example can be undertaken by short identifiers or by correlation of the different received signals [Fuh97].

– estimated DOAs can be considered for downlink transmission in order to focus as much power into the direction of the desired user as possible and no power into the direction of the undesired users which reduces the mean interference level in co-channel cells.

– different paths of each user signal can be resolved which leads to a reduced time dispersion.

The disadvantages of SR algorithms are:

– SR algorithms can only be applied for separate spatial and temporal signal processing.

– SR algorithms are limited to narrowband signals and to special antenna configurations.

– For usual mobile communication applications the number of incident signals exceeds the number of signals resolvable by the SR algorithm.

– The array configuration (array manifold) has to be known in detail. Due to seasonal variations in temperature or other environmental influences, the array has to be permanently carefully calibrated [Pen99, Fuh97].

– Mutual coupling of the antenna elements, which mean that the signal received by one antenna element does not only depend on the incident signals but on the signals on each of the other antenna elements [Pen99].

1.1.2 Consideration of signal correlation properties in the uplink

In Section 1.1.1 it has already been mentioned that the goal of array processing is to extract information concerning the characteristics of the signals of interest and the interfering signals in order to exploit this *a priori* information in an optimum manner. It is therefore necessary to know which *a priori* information is needed for optimum array processing and under what circumstances optimum array processing can be performed.

Optimum array processing techniques may be broadly classified as [MM80]:

- processing appropriate for ideal propagation conditions and
- processing appropriate for perturbed propagation conditions.

Ideal propagation conditions refer to the situation that exist when propagation takes place in an ideal non-random, non-dispersive medium where the desired signal is a plane wave and the receiving sensors are distortionless. In this case the optimum processor is said to be matched to a plane wave signal [MM80]. As has already been mentioned in Section 1.1.1, due to the DOA and the antenna spacing the received signals at the different antenna elements are certainly phase shifted with respect to each other. For operation under the above ideal conditions, the weighting of the input signals with respect to the phase shifts of the different signals received at the elements of the array succeeds in accomplishing the desired signal matching. Such ideal propagation conditions are never fulfilled in a mobile radio system. When perturbations in either the propagating medium or the receiving mechanism occur, the plane wave front signal assumption no longer holds, and the above-mentioned weighting of the input data will not produce the desired signal matching. Only under certain propagation conditions can DOA-based weighting perform in a satisfactory manner, although it is less than optimum. If the BS is located very high without having any scatterers in the near surroundings as, e.g. in large cells, the angular spreads of the different paths originating from one source might be quite small at the BS in the uplink. Taking the mean direction of incidence of the desired signals, great performance improvements can be achieved.

In contrast to the DOA-based weighting, if the desire is to match the array processor to a signal of arbitrary characteristics such as non-coherent wave front signals, signal matching can only be performed in a statistical manner [Cox72, Win84]. The considerable *a priori* information concerning the signal characteristics is the correlation properties of the signals received at the different antenna elements. If interfering signals are present as well, their correlation properties also have to be taken into account for optimum signal processing [MM80]. It is well known that when all elements in an array are uniformly weighted, i.e. the weight factors have the same absolute value, then the maximum SNR is obtained if the noise contributions from the various element channels have equal power and are spatially uncorrelated [App76]. When there is any directional interference, however, the noise from the various element channels will be spatially correlated. Consequently for linear spatial signal processing only the problem of selecting an optimum set of weights may be regarded as a problem of attempting to cancel out the correlated noise components [MM80]. Therefore, signal environment descriptions in terms of correlation matrices for both the desired and the undesired signals play a fundamental role in determining the optimum solution for the complex weights in the linear spatial signal processing unit.

Again, considering the sub-optimum DOA-based approach for spatial signal processing in the presence of interference with a small angular spread, broad nulls of the radiation pattern could be steered into the mean direction of incidence of the interfering signals. Since the number of steerable nulls in a radiation pattern is less than the number K_a of antenna elements, and since the number K_i of interfering signals can be expected to exceed the number K_a of antenna elements, only the strongest interferers can be suppressed with this technique.

Not only in spatial signal processing can the signal covariance matrices be considered, but also in joint space-time signal processing. As a consequence, because of signal processing in the spatial and temporal domains, not only the spatial covariance matrices but also the temporal covariance matrices can be utilized in space-time signal processing. Applying linear joint space-time signal processing for example, it may be regarded as basically an optimum filtering problem in the spatial and temporal domains to extract the desired signal. The best filter is the Wiener filter which minimizes the mean square error of the filter output with respect to the desired signal [Wha71]. The Wiener filter considers both the covariance matrices of the desired and the undesired signals.

Although signal covariance matrices are required for optimum linear array processing, there are two general problems in considering signal statistics in terms of correlation properties in signal processing of a mobile radio system:

- The correlation properties must be known at the receiver or at least the receiver structure must allow information about the correlation properties to be obtained.
- Due to the time variance of the propagation environment it is not possible to establish a covariance matrix based on the received signal, since establishing covariance matrices requires expected values to be determined. If spatial and temporal propagation conditions change very quickly as a result of fast movement of the MS, only estimates of the covariance matrices based on the signals received in short time periods can be determined.

1.1.3 Array processing concepts and state of the art

Previous Sections 1.1.1 and 1.1.2 have presented the general aspects concerning array processing in just the spatial domain or jointly in the spatial and temporal domains, a classification of adaptation algorithms and general aspects concerning optimum array processing taking account of signal correlation properties. In order to give an overview of the state of the art techniques involved in adaptive array processing, five different array processing concepts which have been originated and developed on the basis of different motivations such as performance measurements or application aspects will be presented below. These five different concepts are:

- beamforming,
- switched beams,
- space diversity,
- space-time coding and
- joint space-time detection.

This overview of different array processing concepts should help to classify the main topic of this thesis, which is joint space-time detection taking into account interference covariance matrices, in the field of array processing and to differentiate the concepts investigated in this thesis from other possible array processing concepts. Since this section only gives brief descriptions of the concepts presented, the reader is referred to the publications given in Table 1.1 and 1.2 for more detailed information concerning the above-mentioned array processing concepts and related topics. In many publications and research projects it has been demonstrated by computer simulation results or even by real time implementations that adaptive arrays help in a wide variety of ways to improve the performance of a communications system. Of course only some publications relevant to only a part of all the issues concerning the presented concepts are given in the Tables 1.1 and 1.2. Since, due to the high research interest, there is a tremendously large amount of published material concerning adaptive arrays, the quoted publications can only be seen as a small sample of all research activities.

According to the classification of array processing types in pure spatial signal processing and joint space-time signal processing and according to the applicable reference algorithm for adaptation given in Section 1.1.1, Fig. 1.4 shows how the five array processing concepts listed above can be classified in the field of array processing.

The beamforming approaches are the original adaptive array processing concepts. According to Fig. 1.4 beamforming concepts are considered for pure spatial signal processing and they are the only array processing concepts that rely on both TR and SR algorithms. The first approach to carrying out spatial signal processing of data sampled at an array of sensors was spatial filtering or beamforming, i.e. weighting and combining the signals at the different antenna elements which leads to a specific beam pattern and finally allows the beneficial selective reception of the desired signals and the suppression of the undesired signals. Among the early beamformers, there is the Bartlett beamformer, which is often called the conventional beamformer in literature, and which is an extension of classical Fourier-based spectral analysis [Bar48] for sensor array data. For an array of arbitrary geometry, this algorithm maximizes the power of the beamforming output for a given input signal for which direction of incidence is known. The Bartlett

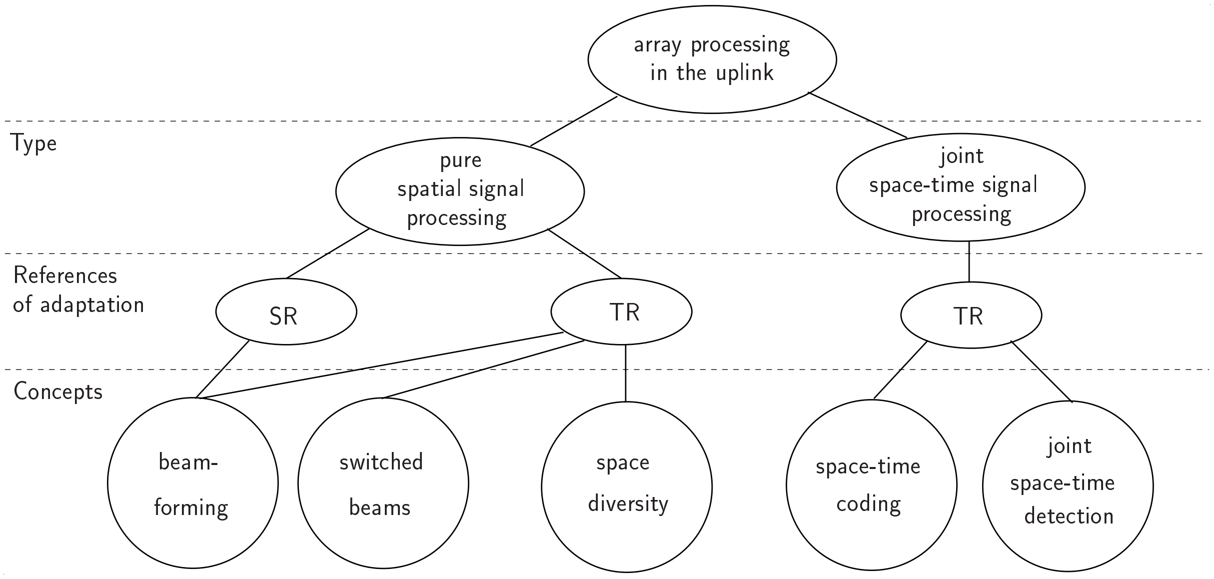

Fig. 1.4. Overview of different concepts for array processing in the uplink

beamformer was originally designed for analog signal processing. Since it does not consider any information relating to noise, the Capons beamformer attempts to minimize the power contributed by noise and any signals coming from directions other than the direction of incidence of the signal of interest while maintaining a fixed gain in the direction of incidence of the desired signal [Cap69]. In the early 1960s, when digital signal processing originates, the key capability of adaptive interference nulling was recognized and developed by Howells [How65]. Subsequently Applebaum established the control law associated with the Howells adaptive nulling scheme by analyzing an algorithm that maximized a generalized SNR [App66, App76, MM80]. Concurrently, the capability of self-training or self-optimizing control was applied to adaptive arrays by Widrow and others [WMGG67]. The self-optimizing control work established the least mean square error (LMS) algorithm that was based on the method of steepest descent. The Applebaum and Widrow algorithms are very similar, and both converge towards the optimum Wiener solution [MM80]. At the same time Adams [Ada66] developed an adaptive array processor based on maximizing the SNR at its output. A summary of these early research activities can be found in [SIT64, SIT76]. Other special beamformers, such as the null-steering beamformer, broadband beamformer or the optimum beamformer can be found in [And69, AnR69, MSC81, VoC92, MM80, Win84].

In general, for finding and adjusting the beamforming weights, TR and SR algorithms can be applied to adaptations, see Fig. 1.4. Adaptation is undertaken according to a specific performance criterion. The most popular performance measurements for finding

Table 1.1. Contributions on adaptive array processing (Part 1)

concept	reference	remarks
beamforming		introduction to adaptive antennas:
	[Ada66],[WMGG67]	- array configurations for broadband and narrowband signals
	[How65], [App66], [App76], [WMGG67], [SIT64], [SIT76]	- early research activities on adaptive antennas
	[God97a], [God97b], [PaP97]	- overview of adaptive array concepts and algorithms
	[BBA95]	- overview of adaptive antenna technology
		special beamformer:
	[Bar48],[Cap69]	- Bartlet beamformer, Capon's beamformer
	[And69] , [AnR69]	- Null-steering beamformer
	[MM80], [Win84]	- Optimum beamformer
	[MSC81] , [VoC92]	- Broadband beamforming
		TR algorithms:
	[Hay91],[Hsu82], [MM80],[Fuh97],	- relying on training signals
	[ShG94],[VTP97]	- blind TR algorithms
		SR algorithms:
	[Sch79],[Sch86], [Cap69],[Bur67],	- SE algorithms, e.g. MUSIC, ML, ME
	[RK89],[PK89], [Haa97a]	- PSBE algorithms, e.g. ESPRIT, Unitary ESPRIT
	[DLR77],[FDHT96]	- DPE algorithms, e.g. EM, SAGE
		SDMA: advantages and capacity considerations for TDMA systems:
	[Tan94],[FN94a], [FN97a],[Far97], [Pen99], [GR94]	- advantages
	[Har97], [GT95], [FN96b],[FN96a], [FN97b], [FKB97]	- capacity considerations
		CDMA systems:
	[GTM99], [SNXP93], [LRK99]	- DS/CDMA / W-CDMA
	[Pap00]	- TD-CDMA
	[DM80],[Pen99]	Calibration
	[KTBT99]	Real time implementations

Table 1.2. Contributions on adaptive array processing (Part 2)

concept	reference	remarks
switched beams	[God97a], [PaP97]	General description
	[BaS97], [LoP00]	Application examples
	[Lop96]	Investigations concerning capacity
space diversity	[Bre59],[SBS66]	Principles, classification
	[SJ67],[Lee82]	Combination methods MRC, EGC, SC for non-frequency selective channels
	[BaS91], [BaS92]	Combination and equalization for frequency selective channels
	[Bla98]	Diversity concepts for CDMA systems with multiuser detection
space-time coding	[FoG98] ,[Tel95], [RaC98]	Capacity considerations of multi-antenna systems
	[NSC00], [NTW], [TNSC99], [TSC98]	Overview of space-time coding
	[DAL00], [BaA00], [NSC00], [BHS00], [Bau99] [Fos96]	Special space-time encoder: - Spatial and delay diversity - Space-time block codes, - trellis coded modulation - Layered space-time architecture
joint space-time detection	[PCVM97], [LP96]	- Matched Desired IR Receiver - Maximum-Likelihood (ML) multiuser detector with linear arrays
	[Bla98], [Pap00] [WP99c],[AMF99]	TDD mode of UTRA: - Space-time multiuser detection - Considerations of intercell MAI covariance matrices
	[Koh98], [Bru00] [BHSN00] [HBD00] [DJFH97]	FDD mode of UTRA: - Joint space-time rake - space-time eigenrake - eigen beamforming - SAGE

the optimum weights are the mean square error (MSE) criterion, the SNR criterion, the maximum likelihood (ML) criterion and the minimum noise variance (MV) criterion which are presented and summarized in [MM80]. One of the most important TR algorithms relying on training sequences is the DMI (Direct Matrix Inversion) algorithm, which is the generalization of the Wiener filter in the spatial and temporal domain [Hay91]. Other representative algorithms of this class are the LS (Least Squares) [Hay91], the RLS (Recursive Least Squares) [Hay91], and the SQRLS (Square–Root RLS) [Hsu82] algorithms, which exhibit comparable performance in both settling time and output SNR performance [Fuh97]. The blind TR algorithms make use of the structure of the system matrix or the signal modulation structure, e.g. the constant modulus algorithm (CMA) [ShG94] makes use of the constant envelope property of the desired signals [Fuh97]. The classification of the most important blind TR algorithms is given in [VTP97].

The SR algorithms are based on DOA estimation. An extension of the following summary concerning DOA estimation algorithms can be found in [Pap00]. DOA estimation algorithms were originally developed for radar and sonar applications [Sch79, KT82, KT83, EJS81]. The possibility of using DOA estimation algorithms in mobile communications has been shown in [GR94, FHNP95, KS95, Pap00]. According to [KV96, FTH99, Pap00] the DOA estimation algorithms for mobile radio communications can be grouped into spectral estimation (SE) algorithms, parametric subspace–based estimation (PSBE) algorithms, and expectation–maximization (EM) algorithms. The SE algorithms, e.g., MUSIC [Sch79, Sch86], ML methods [Cap69, ZW88, SS90, WWR94], and the maximum entropy (ME) method of Burg [Bur67, Tho80], have been originally developed for frequency estimation. Examples of the PSBE algorithms are, e.g., ESPRIT [RK89] and Unitary ESPRIT, which offers increased estimation accuracy by inherently incorporating FBA (Forward–Backward Averaging), which practically doubles the number of available samples, and high-resolution capability by spatial smoothing techniques [Haa97a, PK89]. Representations of the DPE algorithms are, e.g. the expectation–maximization (EM) algorithm, which reduces the computational cost of joint ML by implementing as many separate maximization procedures, as the number of plane waves impinging at the antenna array [DLR77, FW88]. A second example of the DPE algorithms is the SAGE (Space–Altering Generalized Expectation–maximization) algorithm, which replaces the high–dimensional optimization procedure for computing the joint ML parameter estimation by several separate maximization processes performed sequentially [FDHT96, PFM94]. The SAGE algorithm has been successfully applied for joint parameter estimation and channel sounding in real-world mobile radio applications, see, e.g., [THT98, FTH99]. Among the disadvantages of SR algorithms which have already been presented in Section 1.1.1, the problem of the required array calibration has been mentioned. Investigations concerning this calibration problem can be found in [Pen99, DM80].

Recent publications show the applicability of beamforming to Time Division Multiple Access (TDMA) and Code Division Multiple Access (CDMA) mobile radio systems. A three–step strategy towards the introduction of adaptive antennas in TDMA systems is proposed in [Tan94]. The three steps are: Spatial filtering at the uplink only (SFU), spatial filtering for interference reduction (SFIR), and SDMA. The multiple access method SDMA and its advantages are also presented in detail in [FN94a, FN97a, Far97, Pen99] and [GR94]. Special topics in SDMA like dynamic channel allocation schemes, the spatial separation potential of adaptive antennas, and methods for maximizing the capacity in SDMA are presented in [Har97, GT95, FN96b, FN96a, FN97b]. It is noted that in [Tan94] a significant capacity increase is claimed for TDMA systems applying the SDMA principle compared to single antenna systems. This increase is in the order of $\sqrt{K_\mathrm{a} K}$, where K_a is the number of antenna elements used at the BS and K is the number of simultaneously active users within the same frequency band and time slot [Pap00]. Further, an overview of adaptive antenna technology is given in [BBA95]. Besides TDMA systems, examples of the applicability of beamforming concepts as well as the performance improvements in CDMA systems that they can achieve are shown in [GTM99, SNXP93, LRK99], if W-CDMA (Wideband CDMA) and DS/CDMA (Direct Sequence CDMA) is considered, and in [Pap00], if TD-CDMA (Time Division CDMA) is considered. Finally, the state of the art in beamforming techniques is not limited to theoretical work. Real time implementations already exist [KTBT99, KTT99].

The second array processing concept shown in Fig. 1.4 and in Table 1.2 is based on switched beams. A switched beam antenna has its narrow beams pre-defined, i.e. the beamforming does not form the basis of any adaptive process. The pre-defined beams are scanned in order to find and finally to select the beam that has the best SNR [PaP97, God97a]. This can be seen as a multi-sectorized site where resource management is undertaken at site level, while it is undertaken at sector level in the case of the usual multi-sectorized antenna [BaS97]. The performance of switched beam systems depends on a number of factors, including angular spread of the radio channel due to multipath propagation, relative angle of arrival of signals and interference, and the array topology. Performance gains in switched beam systems come from array gain, diversity gain, and reduced interference [PaP97]. The system losses arise from mismatch loss, beam-selection loss, and path diversity loss [PaP97]. In literature switched beam systems are not always seen as systems which perform adaptive processing, since no beam pattern is adaptively adjusted [PaP97]. Anyway, the adaptivity of this system lies in the switching which is performed on the basis of signal and interference power measurements. Therefore, the adaptation algorithm can be interpreted as a TR algorithm. Application examples and performance studies can be found in [BaS97, LoP00]. In [Lop96] it is claimed that a doubling of capacity is possible by using a 12-beam switched beam antenna system.

The third proposed array processing concept in the uplink is diversity reception. Diversity techniques can combat the fluctuations of the mobile radio channel by using a sophisticated combination of the independently fading channels which leads to a resulting transmission channel with increased mean SNR and a reduced standard deviation of the channel fading compared to each of the single transmission channels [Bre59, Bla98]. Therefore, diversity techniques belong to the array processing concepts. A classification of different diversity techniques can be found in [Bre59, SBS66, SJ67, Bla98], where the diversity techniques are subdivided in time, frequency, interferer and space diversity, where only the space diversity concepts belong to the array processing concepts. If the distance between adjacent antenna elements is larger than several wavelengths, the same shadowing effects cannot be expected to impair the received signals at the different antenna elements. Their might be major differences between the mean power of the received signals at the different antenna elements. By combining of these signals the slow fading can be mitigated. If the distance between the adjacent antenna elements is reduced, the received signals at the elements of the array might be affected by the same shadowing effects but the superposition of the different propagation paths is different, if the antenna elements are not located at exactly the same place. Fast fading can be mitigated by the combination of the signals received at the different antenna elements. The combining methods, which can be seen as the TR algorithms for adaptation are [Bre59, SBS66, SJ67]

- equal gain combining that adjusts the phases of the desired signals and combines them in-phase after equal weighting,
- maximum ratio combining, where the signals are weighted in proportion to the SNR and combined in-phase and
- selection combining, where the signal from one of the antennas is selected based upon the power of the desired signal, the total power, or the signal-to-interference ratio available at each antenna.

Since [Bre59, SBS66, SJ67] shows the combination methods for non-frequency selective channels, [BaS91, BaS92, Bla98] presents diversity combination and equalization for frequency selective channels. A summary of further references on diversity concepts can be found in [Bla98].

Fig. 1.4 shows that only TR algorithms can be applied to adaptation if joint space-time signal processing is performed. Knowledge of the temporal structure of the signals received at each antenna element, e.g. by applying training sequences, allows the weighting and combining to be performed in an optimum manner. Two different concepts are relevant in the field of space-time signal processing, namely space-time coding and joint space-time detection. Space-time coding can be seen as a combination of channel coding and diversity concepts [NSC00]. Space-time coding [NTW, BaA00] is a coding technique that is designed for use with multiple transmit antennas. It requires a MIMO channel structure, i.e. multiple antennas are utilized at the transmitter and at the receiver. In the case of space-time coding the information symbols feed to the individual transmit antenna elements are different, e.g. several symbols are dealt with at the same time, combined or delayed. The combination could be a baseband coding, where the information is spread over the antennas leading to essentially a number of quasi-independent channels [Bac99]. At the uplink receiver common equalization and channel decoding is performed. On the basis of channel estimations of the individual channel impulse responses (IRs) of each radio link between each transmit and each receive antenna in the uplink, the received information can be recovered by an optimum receiver. If the independence of the channels is also achieved for the interference due to transmit diversity, no correlations of the interference have to be considered at the receiver for optimum reception. Recently, several authors have pointed out the substantial capacities available in MIMO radio channels [FoG98, Tel95, RaC98]. Two main approaches have been proposed in order to achieve these capacities: the Layered Space-Time Architecture (BLAST) from Lucent Bell Labs [Fos96], and space-time codes from Tarokh and others at AT&T Laboratories [TSC98]. The simplest way to perform transmit diversity is spatial delay diversity, where the information is transmitted at the different antenna elements with different delays [DAL00]. Investigations relating to more sophisticated space-time coding, such as space-time block codes, space-time trellis codes, turbo trellis coded modulation or the concatenation of space-time block codes and turbo trellis coded modulation can be found in [NSC00, BHS00, Bau99]. Comprehensive information on the theoretical treatment of many of the transmit diversity schemes that have been studied before is presented by Narula et al. in [NTW]. Since multiple antennas are needed at the transmitter, space-time coding is not considered in this thesis.

The fifth array processing concept presented in this section is the joint space-time detection. Joint space-time detectors are data detectors which are extended for multi-antenna reception and exploit spatial and temporal signal properties jointly for the data detection process. In general joint space-time detectors make use of the knowledge of the channel parameters of all channel IRs of each user at each antenna element of the array and they can be applied to both multiuser and single user detection. Compared to space-time coding channel coding can be seen as an additional feature. If channel coding is considered in the transmitter, the uplink receiver performs space-time detection and channel coding in two steps. In contrast to space-time coding schemes, space-time detection in the uplink does not require multi-transmit antennas at the mobile terminal. It can be applied for both SIMO and MIMO channel structures. One of the first concepts in combining adaptive arrays with multiuser detectors for joint space-time detection is presented in [LP96], where the DOA information is incorporated in an ML multiuser detection process. The results presented are obtained under the assumption of non–frequency selective channels. In frequency selective channels the full potential of space-time detectors can be exploited, provided the channel IRs of each user at each antenna elements are known, which opens up the possibility of optimum spatial and temporal detection. In [PCVM97] a matched desired IR receiver (MDIR) is presented and in [Bla98] and [Pap00] linear joint space-time multiuser detection for the TD-CDMA uplink is performed by applying the zero-forcing (ZF) algorithm incorporating the jointly estimated channel IRs at each antenna element by a Steiner estimator [Ste95]. Although in [Bla98] the focus is on diversity techniques, the receiver structure under consideration can be represented as a joint space-time detector, since the channel IRs of each user and at each antenna element are considered for a joint temporal and spatial detection. The quality of the channel estimation is the performance limiting factor, because, if the channel IR is perfectly known at the receiver, the best linear unbiased data estimation can be performed with the ZF algorithm. Therefore, in [Pap00] the channel estimation is improved by incorporating *a priori* knowledge concerning the DOAs. In [DJFH97] a less than optimum ML approach is implemented by a combination of a non-linear multistage multiuser detector and the SAGE algorithm for channel parameter estimation for DS/CDMA systems. The sequential maximization of the likelihood function with respect to the transmitted symbols of all users and the channel parameters leads to a joint demodulation scheme which comprises the cancellation of ISI (inter symbol interference) and intracell MAI (multiple access interference) while simultaneously exploiting the available signal energy transmitted over frequency selective channels in a nearly optimum fashion.

The above-mentioned joint space-time detectors are designed for uncorrelated intercell MAI. However, if there is any directional intercell MAI, which particularly occurs if single transmit antennas are utilized, the received intercell MAI at the different antenna elements of the antenna array is correlated. According to Section 1.1.2, the correlation properties have to be taken into account for optimum detection. Although interference covariance matrices have been considered in a lot of investigations concerning beamforming, especially in the downlink [Ut99, Cz00, SB97a, SB97b], so far only slight attention has been paid to the consideration of signal and interference covariance matrices in space-time detection schemes. In [BHSN00, Bru00] a space-time eigenrake approach for single user detection in W-CDMA is proposed taking the covariance matrices of the desired signals and the intracell plus intercell MAI into account. In [AMF99] the intercell MAI covariance matrix is considered in a multiuser detection process applying a MMSE-BLE (minimum mean square error block linear equalizer) for TD–CDMA.

1.2 Time Division CDMA (TD–CDMA)

The customer base for 2G mobile radio systems is increasing much more quickly than expected, with around 400 million mobile subscribers worldwide in the year 2000 and nearly 1800 million in 2010 [Moh00]. Market expectations show an increasing demand for a wide range of services from voice at the low end through to high data rate services such as mobile multimedia. The explosive growth of internet usage is one of the major technical trends for future communications. Fixed internet penetration is growing in parallel to mobile radio access penetration. These developments are the major driver for 3G systems and result in a large potential market for mobile multimedia [Moh00].

In Europe work towards the 3G standard UMTS (Universal Mobile Telecommunications System) is led by ETSI (European Telecommunications Standards Institute) and a decision has already been reached concerning the standard of the multiple access air interface [NTD+98], which is one of the most important issues when developing a mobile radio system [Bai96c, Bai96b]. This air interface standard is termed UTRA (UMTS Terrestrial Radio Access) and defines different modes for the duplexing scheme TDD (Time Division Duplex) to be applied in the unpaired UMTS bands, and for the duplexing scheme FDD

(Frequency Division Duplex) to be applied in the paired UMTS bands [NTD+98]. In the TDD band the multiple access scheme TD–CDMA and in the FDD band the multiple access scheme W–CDMA will be applied.

The European UTRA concept has been recommended the ITU for the standardization of the worldwide 3G mobile air interface IMT-2000 [ETSI98]. The standardization activities are substantially supported by the third generation partnership project (3GPP) [3GPP]. 3GPP consists of members of standardization bodies in Europe (ETSI), US (T1), Japan (ARIB – Association of Radio Industry and Business), Korea (TTA – Telecommunications Technologies Association), and China (CWTS – China Wireless Telecommunication Standard). 3GPP merged the already well harmonized proposals by the regional standardization bodies including the European UTRA concept for a 3G standard which is still called UTRA and which is based on the evolved GSM core network. A second project, 3GPP2 [3GPP2], on the other hand, is working towards a 3G mobile radio standard, which is based on an IS95 evolution and was originally called cdma2000. Major international operators in the Operator Harmonization Group (OHG) have proposed a harmonized Global Third Generation (G3G) concept, which has been accepted by 3GPP and 3GPP2 [OHG99]. Finally, in November 1999 the ITU approved a comprehensive set of terrestrial radio interface specifications for IMT–2000. The G3G concept belongs to this set and, consequently, the UTRA specified by 3GPP with its TDD mode TD–CDMA is now part of the IMT–2000 family of terrestrial radio interfaces, see Fig. 1.5 [ITU00]. In Fig. 1.5 the five different members of this family are presented [ITU00]:

1. IMT–2000 CDMA Direct Spread (IMT–DS), based on UTRA FDD mode as specified by 3GPP.
2. IMT–2000 CDMA Multi-Carrier (IMT–MC), based on cdma2000 using FDD as specified by 3GPP2.
3. IMT–2000 TDMA Single-Carrier (IMT–SC), which is the IS–136 evolution UWC–136 (Universal Wireless Communications–136) [ITU00].
4. IMT–2000 CDMA TDD (IMT–TC), based on UTRA TDD mode as specified by 3GPP.
5. IMT–2000 FDMA/TDMA (IMT–FT), based on the DECT (Digital European Cordless Telephone) standard [ITU00].

In the TD–CDMA mobile radio air interface, which is considered in this thesis, the combination of the multiple access methods FDMA (Frequency Division Multiple Access) and TDMA (Time Division Multiple Access) known from GSM [MP92, PGH95] is supplemented by a CDMA component [Bai94, BK95, KBJ95, KB93, BKNS94b]. The TD–CDMA air interface concept has been verified by extensive computer simulations [BBNS94,

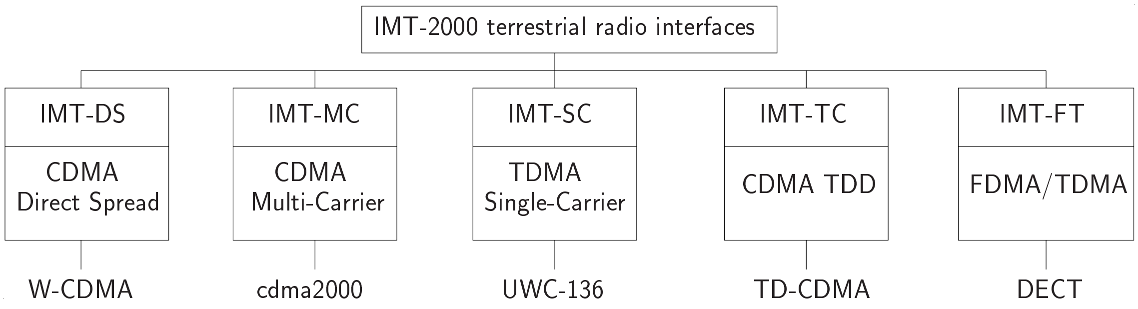

Fig. 1.5. IMT–2000 terrestrial radio interfaces [ITU00]

BKNS94b, BJN94, SB96, Kle96] and by field tests performed with a TD–CDMA hardware demonstrator [MSW97b, BEM+98a, BEM+98b].

Since TD–CDMA is a time–slotted CDMA mobile radio air interface, in the same frequency band and time slot, the latter also termed burst, K mobile users are active, each using a user-specific spreading code, which allows signal separation at the receiver [Naß95, Kle96]. The well–known frame structure of this TD–CDMA concept is illustrated in Fig. 1.6, where B, T_{fr}, N_{fr}, and T_{bu} denote the bandwidth of a frequency band, the duration of a TDMA frame, the number of bursts per TDMA frame, and the burst duration, respectively. As shown in Figs. 1.6 and 1.7, signal transmission in TD–CDMA takes place in bursts. Each burst of user k, $k = 1 \ldots K$, consists of

- two data sections (blocks),
- a user-specific midamble inserted between these data sections, which allows channel estimation at the receivers [SK93, Ste95], and
- a guard interval to prevent subsequently transmitted bursts from overlapping at the receiver [BKNS94b].

Each data block of a TDMA burst contains N symbols for each user k, $k = 1 \ldots K$, and each symbol is spread by a user-specific CDMA code, which is Q chips long, see Fig. 1.7. The midamble and the guard interval contain L_{m} and L_{g} chips, respectively, see Fig. 1.7. The adopted frame and burst structure of TD–CDMA is similar to that used in GSM. This is due to the fact that TD–CDMA has been historically developed as an evolution of GSM by introducing a supplementary CDMA component [BJK96, Bai96a, Bai96c]. Thus, TD–CDMA beneficially facilitates backward compatibility with GSM, which is the de facto world standard of 2G mobile radio systems [Bai94, BK95, Pap00].

Since TD–CDMA is an air interface for a cellular mobile radio system, reliability and transmission quality are determined by the MAI, i.e. TD-CDMA is interference limited [Cal88, Lee82, Lee89]. The influence of the MAI depends on, among other parameters, the data detection principle. In TD–CDMA the intracell MAI, i.e. the interference from other users assigned to the same BS, is eliminated by the joint detection (JD) algorithm [KB92b, Kle96] at the receivers. Therefore, in contrast to the situation in other CDMA mobile radio systems, e.g. W–CDMA, the intercell MAI, i.e. the interference from users of other cells, plays the most important role on the transmission quality and the reliability of the system. Moreover, in TD–CDMA channel estimation is performed jointly for all users assigned to the same BS and is based on the midamble training sequence inserted in each transmitted burst, see Figs. 1.6 and 1.7 [SK93, Ste95, Naß95, Bla98]. It is noted that joint data detection and joint channel estimation constitute the main characteristics of TD–CDMA receivers.

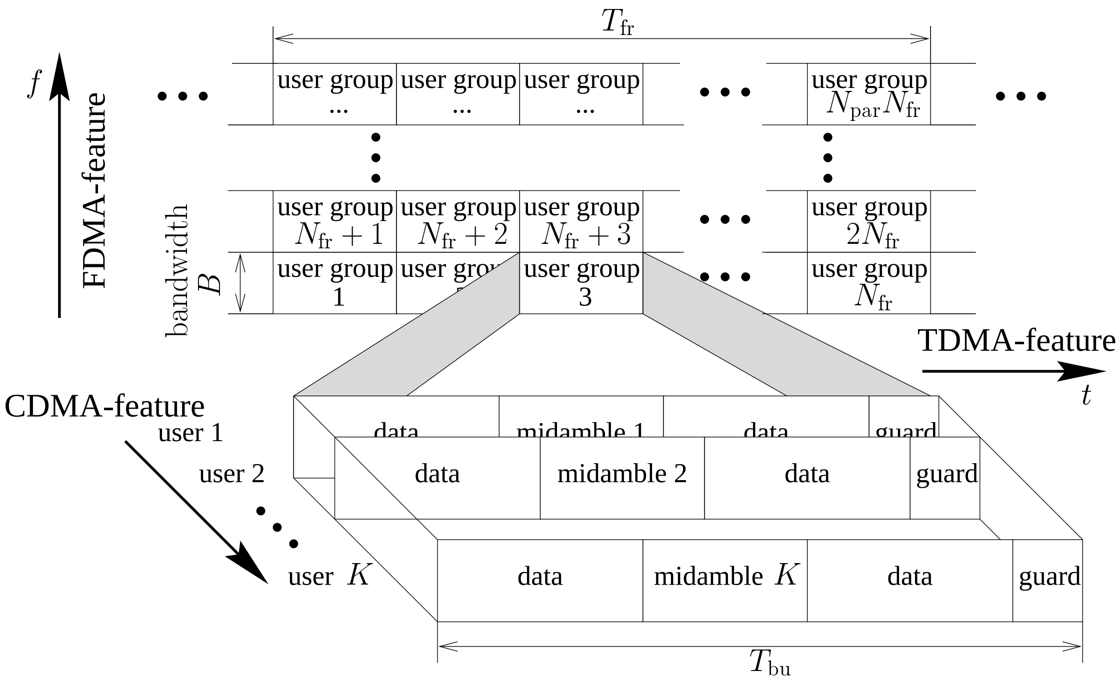

Fig. 1.6. Frame structure

As regards the UMTS requirements, TD–CDMA has some specific advantages. These advantages come from the TDMA component which is an essential feature of TD–CDMA. Thanks to this TDMA component, TD–CDMA is the obvious candidate to implement TDD and to be applied in the unpaired bands of the UMTS spectrum. As another advantage of the TDMA component, the number K of simultaneously active users is smaller than in CDMA concepts without TDMA, such as the UTRA mode W-CDMA

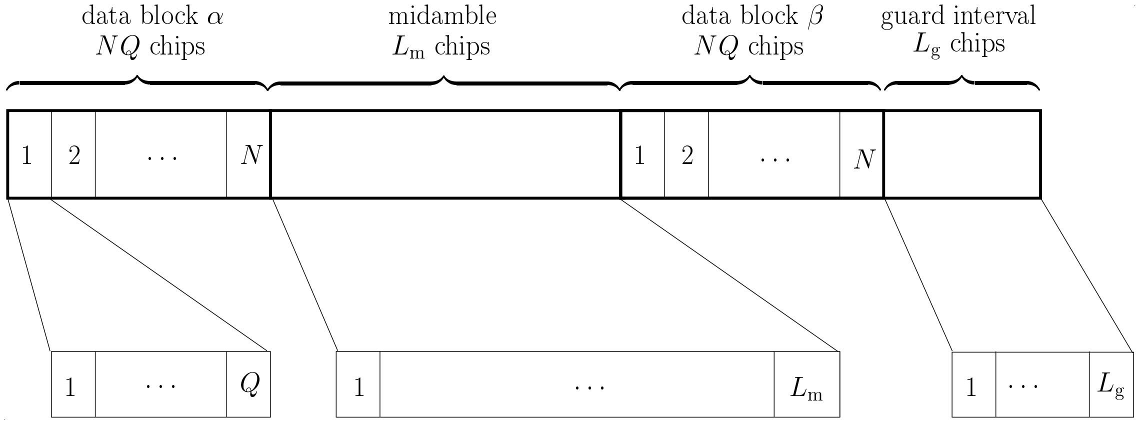

Fig. 1.7. Burst structure

[BaW98, BPW99, PBWS]. Besides the aforementioned interference reduction by joint detection, this smaller number K particularly facilitates the application of smart antennas which, for a given number of antenna elements, work more efficiently if the number of user signals to be handled by the smart antenna system is decreased. The TDMA component of TD–CDMA further allows reassignment to other time slots of mobile stations which are in critical interference conditions, a measure by which the requirement for soft handoff can be avoided [PWBB98, PW98]. Finally, because of its mobile operation in UTRA mode, TD–CDMA does not transmit continuously, it can, besides receiving signals from its own base station, listen to the base stations of the surrounding cells and, based on the signal strengths impinging from those cells, initiate a mobile-assisted handoff [BaW98].

As TD–CDMA is the obvious concept for use in the unpaired UMTS band, i.e. in the TDD mode, TD–CDMA paves the way for fully enjoying the benefits of TDD, namely [BaW98, Bin01]:

- Adaptive support of asymmetric data rates. The switching point can be adjusted within the frame in such a way that the desired optimum portioning of the total transmission capacity between uplink and downlink is achieved.
- Fast and precise open loop power control. Because the channel IRs are virtually equal in the TDD up- and downlink due to the reciprocity theorem, not only the attenuation variations caused by slow fading, but also those caused by fast fading are equal in both links.
- Channel adaptive predistortion. Thanks to the above-mentioned equality of the uplink and downlink channel IRs, the transmitted signals can be predistorted at the transmitters in such a way that they travel over the channels with reduced distortion and attenuation.

- Smart base station antennas for uplink and downlink. Direction of arrival estimates gained in the uplink receiver could be used to steer the antenna elements for downlink transmission with the view to optimum concentration of the radiated energy to the addressed mobile stations and to minimize interference to other mobiles.

- No duplex filter. This helps to reduce analog circuitry.

1.3 Goals of this thesis

Although a wide variety of state of the art techniques exist concerning adaptive array processing, there are still a lot of open questions, especially in the field of space-time receivers, where the spatial signal and temporal signal processing is performed commonly. Since in this case spatial and temporal signal processing are inseparable, it is only possible to investigate the performance of a whole receiver structure incorporating antenna array configurations. An analysis of performance enhancements by considering adaptive arrays and considering different system aspects such as different multiple access schemes and/or data detection and channel estimation algorithms for space-time signal processing separately is not possible. Therefore, a particular mobile radio concept has to be chosen as a basis for investigating space-time signal processing. The performance evaluation is only valid for the whole receiver structure. As has already been mentioned in Section 1.2, the target mobile radio system which forms the basis of the space-time processing investigations in this thesis is the TD–CDMA system. The combination of TD–CDMA with an antenna array has already been introduced in [BKNS94b, BJN94] and intensively studied in [Bla98] and [Pap00]. Performing space-time signal processing incorporating the estimation and consideration of the spatial and temporal correlation properties of the intercell MAI signals in data detection and estimation and consideration of the correlations of both the desired signals and the intercell MAI signals in the channel estimation is beyond the scope of [Bla98] and [Pap00]. Therefore, the design and investigation of a TD-CDMA receiver structure with the aforementioned capabilities is the main goal of this thesis. The performance of the introduced receiver structures are evaluated by simulation results. To measure the system performance the bit error rate (BER) for a given SIR is determined taking different channel models and different intercell MAI scenarios into account.

One possible solution to estimate and consider intercell MAI covariance matrices is to apply iterative receiver structures. Additionally such receiver structures can be combined with iterative multiuser detection. In [Ost01] an iterative multiuser detection scheme for a TD–CDMA system called multi-step joint detection (MSJD) is introduced considering single antenna receivers. A further goal of this thesis is the extention of MSJD by the use of antenna arrays and by the capability to estimate and consider the intercell MAI covariance matrix with the goal to evaluate the resulting system performance.

The list below gives a summary of goals of this thesis:

- To establish simple directional channel models for the signals of interest and for the undesired and interfering signals, respectively, as the basis for evaluation of the receiver structures to be proposed.
- Enhanced receiver design for the uplink of a TD-CDMA system with antenna arrays.
- Design and evaluation of different receiver concepts that incorporate the estimation of intercell MAI covariance matrices and channel IR correlation matrices.
- Investigation of the estimation quality of the intercell MAI covariance matrix.
- Design and investigation of joint space-time receiver structures that allow the intercell MAI covariance matrix to be exploited in order to improve data detection quality.
- Design and investigation of an iterative multi-user detection scheme that incorporates the estimation and consideration of the intercell MAI covariance matrix.
- Investigations concerning the signal reconstruction quality in the proposed iterative receiver structure.
- Investigations of joint space-time channel estimation concepts that incorporate estimation and consideration of the correlation matrix of the channel IRs.
- Performance analysis of the proposed concepts by computer simulation results.

1.4 Contents and important results

The following section briefly describes how the goals of this thesis presented in Section 1.3 are achieved. The structure and organization of this thesis is already given by the Table of Contents.

Chapter 2 defines and describes the different directional mobile radio channel models considered in the computer simulations of the receiver structures that will be described in the following sections. The development of directional channel models is not one of the main goals of this thesis. There are a lot of publications [COS89, COS99, ACTS98] and research activities relating to channel modelling. Recently worldwide discussions have particularly focused on directional channel models for the evaluation of systems with adaptive antennas [BBJ95, BKM96, COS01, FMB98, Höh90, KCW93b, MG96, MLKS98, SP98b]. Currently, there is no world wide standardized directional channel model although directional channel models are absolutely required for the evaluation of systems with adaptive antennas. This lack of an international standardized directional channel model means that everyone who investigates adaptive antennas by computer simulations has to choose one of the existing channel models or has to model the propagation characteristics himself. The performance of a system applying adaptive antennas will depend mainly on the chosen or established directional channel model. Therefore, a channel model should be as realistic as possible. On the other hand a simple channel models makes it easier to study certain effects and to study how the performance of a system with adaptive antennas is dependent on the wave propagation characteristics. Therefore, in Chapter 2 different simple directional channel models are introduced. A directional outdoor channel model is established by assigning channel IRs measured in a real environment to each active user. All propagation paths, i.e. measured channel taps, of one channel IR that is assigned to one single user are assumed to have the same DOA, which is called a single direction channel. Since TD–CDMA within UTRA is considered to operate in small cells, two directional indoor channel models are established and considered. In the first one the delay profile is taken from the ITU indoor/office models [ACTS98, ITU00a], where the channel taps can be assigned to different DOAs. The disadvantage of using the ITU channel model delay profile is that all paths of all simultaneously detected users have the same delay. This does not matter when simulating single user detection but it is too optimistic when simulating JD. To overcome this problem a simple ray–tracing model for a given rectangular room is presented. The advantage of the ray–tracing model presented is that, in the given room, two cells could be assumed which allows the channel IRs of the intercell MAI signals to be modelled in the same way as the channel IRs of desired signals.

For the evaluation of receiver structures and algorithms normally only link level simulations are performed, i.e. only one cell is looked at in the simulations without considering the intercell MAI. Since in a TD–CDMA system the only remaining interference is intercell MAI and since in this thesis spatial and temporal intercell MAI covariance matrices should be considered at the TD-CDMA receiver, it becomes obvious that intercell MAI models are required although only link level simulations are performed. Therefore, Chapter 3 presents a general approach for intercell MAI modelling based on the assumption of directionally continuous and directionally discrete intercell MAI signals. Other intercell MAI models with respect to the cluster size r as well as intercell MAI models with different spatial properties concerning the correlations of intercell MAI signals from different DOAs are also presented.

Chapter 4 introduces the antenna array configurations considered in this thesis. Four different arrangements of antenna elements are used to form the antenna arrays, namely one-dimensional linear arrangements as well as two-dimensional rectangular, cross and circular arrangements. The numbers K_{a} of antenna elements used for each array configuration are varied. A very simple propagation scenario with only one active user is considered to determine how the directional gain of an antenna array, with and without taking account of the intercell MAI covariance matrix, changes by changing the arrangements of the antenna elements. The assumed channel IRs consist of only one single tap with a single direction of incidence. The channel tap is known at the receiver. It is shown that in this case the space-time signal processing is equal to conventional beamforming with the aim of maximizing the SNR of the received signal. Depending on the array arrangement, the DOA of the users signal and whether or not the intercell MAI covariance matrix is considered in signal processing, different SNR gains with respect to one single omnidirectional antenna are investigated.

The time-discrete low pass representation of the channel IRs and the intercell MAI with respect to the burst structure of the TD–CDMA system under consideration, which is shown in Fig. 1.6, is introduced. Representation of the signals with vectors is finally required for the simulations and the mathematical description of the mobile radio system under consideration. To represent the signal correlations, the correlation matrix $\underline{\mathbf{R}}_{\tau,\mathrm{s}}$ of the channel IRs and the intercell MAI covariance matrices $\underline{\mathbf{R}}_{\mathrm{n}}$ and $\underline{\mathbf{R}}_{\mathrm{m}}$, respectively, of the intercell MAI, which are to be considered in data detection and in channel estimation are defined in Chapter 2 and 3, respectively.

The preferred detection scheme in TD–CDMA is joint detection (JD) [Kle96], where all the desired user signals which are simultaneously active in the same frequency band are detected jointly [Kle96, Wha71]. Therefore, the focus in Chapter 5 concerning data detection is on multiuser detection schemes that are extended to the use of antenna arrays and allow space-time signal processing to be performed. As regards linear multiuser detection schemes, they are easy to extend to antenna array processing. The linear detection problem in general can be seen as solving a set of linear equations. Extending this problem to antenna array processing only increases the number of equations but keeps the number of the unknown data symbols that are to be determined the same, which leads to an over-determined set of linear equations. Furthermore, consideration of correlation matrices of the desired signals and/or the interference is in the nature of optimum linear multiuser detection schemes which leads to space-time signal processing. Among the linear multiuser detection schemes the zero forcing block linear equalizer (ZF-BLE) and the minimum mean square error block linear equalizer (MMSE-BLE) are presented in Chapter 5. The conventional application of ZF-BLE for TD-CDMA is compared to the enhanced detection scheme, taking into account the intercell MAI covariance matrix $\underline{\mathbf{R}}_{\mathrm{n}}$. However, there is a concomitant noise enhancement with JD which leads to a SNR degradation. An empirically derived approximation of the SNR degradation by applying ZF-BLE is used to determine approximately the SNR degradation, depending on the number K of simultaneously active users and on the number K_{a} of antenna elements under consideration. Based on this cognition concerning SNR degradation, the non-linear multi-step joint detection (MSJD) algorithm is introduced. In MSJD the number K of simultaneously active user signals which are to be commonly detected is subdivided into a certain number of groups of user signals, each having a reduced SNR degradation when performing JD for each group than for performing JD for one large group of all user signals. Therefore, additional intracell MAI is caused by the presence of different signal groups which are not considered in each of the group-wise JD processes. The intracell MAI is mitigated by interference cancellation techniques. Fig. 1.8 shows the data detection principles considered in this thesis and the multiuser detection algorithms presented which take into consideration the intercell MAI covariance matrix $\underline{\mathbf{R}}_{\mathrm{n}}$ and the data covariance matrix $\underline{\mathbf{R}}_{\mathrm{d}}$. In the following the main focus is on the ZF algorithm without considering $\underline{\mathbf{R}}_{\mathrm{d}}$. There is no additional need to consider the spatial and temporal correlations of the channel IRs in data detection, since the estimated channel IRs include the information about the correlation properties of the desired signals and since the estimated channel IRs are considered in data detection by applying the ZF algorithm. The desired signals in data detection are the transmitted data symbols which do not have any spatial and temporal correlations. The spatial and temporal correlations are only based on the properties of the mobile radio channel and on the chosen antenna configuration but not on the transmitted symbols. Therefore the matrix $\underline{\mathbf{R}}_{\mathrm{d}}$ is not considered in data detection.

Chapter 6 presents different linear joint channel estimation (JCE) schemes for the TD–CDMA receiver. The ZF algorithm, which is considered for data detection, needs the knowledge of the channel IRs for temporal equalization of the received signals. The channel IRs are estimated using training sequences for channel estimation, which has already been mentioned in Section 1.1.3. With the knowledge of the channel IRs at each antenna element and by applying the ZF algorithm for data detection a spatial equalization of the received signals is implied. Conventional channel estimation in TD–CDMA is performed by the Steiner estimator [Ste95], which is originally designed for single antenna receivers and which performs a JCE based on the ZF algorithm with a reduced computational effort. Using a Steiner estimator at each antenna element is the easiest way to extend the channel estimation problem to antenna arrays. Three other channel estimation concepts are presented in Chapter 6, which additionally exploit the directional inhomogeneity of the mobile radio channel and the correlation properties of the channel IRs and the intercell MAI. The first one exploits the knowledge of the DOA of the impinging wave fronts in order to reduce the number of unknown channel taps in the estimation process, whereas the number of linear equations remains the same. Additionally, as a second channel estimation concept, the intercell MAI covariance matrix $\underline{\mathbf{R}}_{\mathrm{m}}$ can be considered. The third channel estimation concept is MMSE based and allows the correlation matrix $\underline{\mathbf{R}}_{\tau,\mathrm{s}}$ of the channel IRs and the intercell MAI covariance matrix $\underline{\mathbf{R}}_{\mathrm{m}}$ to be taken into consideration. Fig. 1.8 summarizes the considered JCE schemes. Chapter 6 is concluded by different possibilities for the evaluation of the channel estimation error.

A presupposition in Chapter 5 is that the matrices $\underline{\mathbf{R}}_{\mathrm{n}}$, $\underline{\mathbf{R}}_{\mathrm{m}}$ and $\underline{\mathbf{R}}_{\tau,\mathrm{s}}$ are known at the receiver. In the case of real implementations the required matrices must be estimated from the received signals. Two iterative concepts, including MSJD, and two non-iterative concepts for estimating the intercell MAI covariance matrices $\underline{\mathbf{R}}_{\mathrm{n}}$ and $\underline{\mathbf{R}}_{\mathrm{m}}$, respectively,

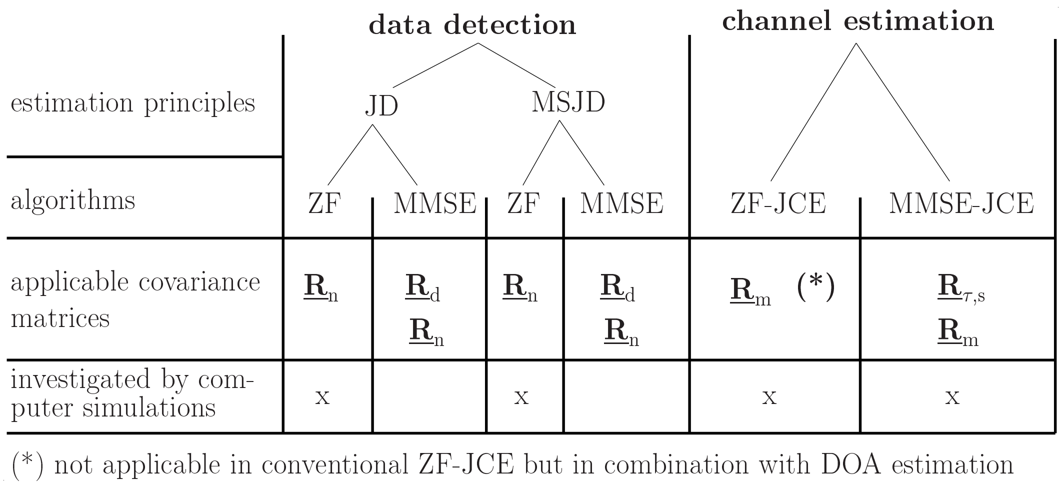

Fig. 1.8. Different data detection and channel estimation schemes and the corresponding covariance and correlation matrices

are introduced in Chapter 7. Since the iterative concept is based on signal reconstruction, estimations regarding the quality of the reconstructed signals based on the detected data symbols and depending on the bit error rate (BER) are also given. Furthermore, it is shown how the correlation matrix $\underline{\mathbf{R}}_{\tau,\mathrm{s}}$ of the channel IRs can be estimated from the previously estimated channel IRs at the different antenna elements.

Chapter 8 includes the performance analysis and verification of the different proposed TD-CDMA receiver concepts with adaptive arrays.

A summary of this thesis in English and German is presented in Chapter 9.

2 Directional models for mobile radio channels

2.1 Introduction

The radio channel has an obvious and direct influence on the performance of any wireless communication system [COS01]. Therefore, models of the mobile radio channel are required for mobile radio system design and optimization based on simulations [Moh95]. The modelling of mobile radio wave propagation requires a profound knowledge of the properties of the mobile radio channel. This knowledge can only be obtained by propagation measurements. World wide, numerous measurement campaigns have been performed in outdoor [KMT96, FRB97, Mar94, KaL91] and indoor [Zol93, Kat97, PaH89] environments in order to analyze the propagation properties of the mobile radio channel. Therefore, it is well known that in mobile radio communications a part of the electromagnetic energy radiated by the transmitter reaches the receiver by propagating through different paths [Par92, FL96, Pap00]. Even if the BS antenna is in an elevated location, it is not usually visible from the MS, because the MS is surrounded by buildings, trees, hills, etc. Therefore, the radio connection of a MS to a BS has to rely on physical effects like reflection, refraction, scattering and diffraction by the various objects in the propagation environment [Par92, BARY95]. Due to the multipath propagation the channel is time-dispersive or frequency-selective, if the delay spread of the channel IRs is equal to or larger than the inverse of the receiver filter bandwidth [Par92, Fuh97]. Another property of wireless channels is the presence of Doppler shift [Par92, ECSR98], which is caused by the motion of the receiver, the transmitter, and/or any other objects in the channel. Furthermore, the received signal power in mobile communications experiences fluctuations that can be divided into large-scale fading and small-scale fading. The large-scale fading is caused by shadowing effects in the propagation environment due to the morphology of the environment, and the small-scale fading is mainly caused by changing interference of signals from scatterers around the receiver while the receiver moves a few wavelengths [Par92, Fuh97]. The terms slow fading and fast fading are also sometimes used for the large-scale and the small-scale fading, respectively. Finally, directionally selective measurement results presented in the literature [Egg94, Egg95, FL96, KMT96, MG96, BKM96, FTH99, FMB98] demonstrate the directional inhomogeneity of the mobile radio channel dependent on the propagation environments.

Based on this knowledge concerning the propagation characteristics of the mobile radio channel, numerous channel models have been established which either are based on statistical properties of the wave propagation [MG96] or deterministical properties [Cic94, Zwi00], which are modelled by ray–tracing. Most existing channel models, like the famous COST 207 [COS89] (Cooperation in the Field of Scientific and Technical Research) models or the channel models standardized by the ITU [ACTS98, ITU00a], give only the power delay profile (PDP) [Bel63, Höh90, Höh92] and the Doppler spectrum [Pro89], but they do not include any information about the directional distribution of arriving waves. Systems with adaptive arrays allow the exploitation of these directional inhomogeneities of the mobile radio channel in order to improve the performance of the mobile radio system. Hence, for the evaluation of systems with adaptive arrays a channel model is required which, besides time variance and frequency selectivity, incorporates the directional inhomogeneity of the mobile radio channel. Recently, in many publications [ECSR98, Fuh97, Bla98, MLK98] various directional channel models have been proposed. A review of existing directional channel models for communication systems with antenna arrays is given in [ECSR98]. Furthermore, an overview of many European propagation measurements campaigns, undertaken by European research institutes and companies, who presented their results within the European COST 259 Action are summarized in [COS01]. Moreover, in [COS01] a consensus of many European companies and researchers for directional channel models for different propagation environments is introduced. However, as mentioned in Chapter 1 there still does not exist any international standardized directional channel model. This situation forces everybody who investigates systems with adaptive antennas to choose one of the existing models or to develop their own models.

In Section 2.2 a general description of spatial and directional channel IRs and a representation of channel correlation properties is given. An outdoor and two indoor directional channel models, which are considered in this thesis, are introduced in Sections 2.3, 2.4 and 2.5. The author has not chosen the directional channel model presented in [COS01], since most of the simulation results which are presented in Chapter 8 have been obtained before the channel model in [COS01] has emerged. With the outdoor channel model in Section 2.3 a new approach to channel modelling is presented, based on the fact that the measured channel IRs are used for system simulation. The model described in Section 2.3 is a single direction channel model in which non-directionally measured channel impulse responses will be interpreted as single direction channels. Using a channel model based on the stock of measurement data has the advantage that it is relatively quick and easy to access this stock during the simulation and that channel IRs do not have to be generated while the simulation program is running, resulting in saving in processing time. However, for this to be done, this stock of data must be obtained beforehand from comprehensive measurements, i.e. this type of modelling only makes sense if there is already measurement data available. The comprehensive measurement campaigns that have been performed to analyze the propagation characteristics of the mobile radio channel mean that a large number of measured channel IRs exist which are often no longer used for their original purpose, such as statistical evaluation of their amplitudes, powers, delays etc. Such stocks of channel IRs can then be included for channel modelling.

Assuming the existence of discrete DOAs on which the outdoor channel model is based, does not generally correspond to the real propagation conditions. Directional selective measurements of channel IR have shown [Egg95, FL96, KMT96] that the electromagnetic waves which are emitted by the transmitter do not generally all have the same discrete DOA at the receiver, but, depending on directional dispersion, arrive at the receiver at least spread over a specific angle range. Despite this it is often advantageous to simplify matters by assuming only individual discrete propagation directions between the MS and the BS, since in this case individual effects or dependencies between incidence direction and system performance may have to be explicitly investigated. Measurements have shown that in the outdoor area the azimuthal range of the incidence and departure directions at the MS is in general larger than at the BS [FL96], if the BS is elevated, i.e. is accommodated above the edge of the roof. Thus the simplified assumption of individual discrete propagation directions is an acceptable approximation of reality in particular in areas with elevated BS antennas and topology-related small angular dispersal between MS and BS.

The two indoor channel models considered in this thesis are not based on measured channel IRs, since the author does not have any indoor measurement results. Therefore, a synthetic directional channel model is introduced in Section 2.4, which considers multipath propagation for each user signal and which is an extension of the non-directional ITU indoor office (IO) B model [ACTS98, ITU00a]. Section 2.5 gives an alternative option for modelling channel IRs as well as interfering signals from adjacent cells in an indoor environment based on ray-tracing.

2.2 Spatial and directional channel IRs

In this section a SIMO (single input, multiple output) configuration with K_a antenna elements at the BS is described by spatial and directional channel IRs in the uplink and a representation of channel correlation properties is given. Such a description is required when modelling time slotted CDMA utilizing adaptive multi-element antennas at the BS.

Between each of the K_a BS antenna elements and the MS antennas of each of the K users there exists a radio channel. These radio channels can be characterized by $K_\mathrm{a} \cdot K$ channel IRs $\underline{h}_\mathrm{s}^{(k,k_\mathrm{a})}(\tau, t)$, $k = 1...K$, $k_\mathrm{a} = 1...K_\mathrm{a}$, where τ and t denote the delay and time, respectively [BBS97]. The $K_\mathrm{a} \cdot K$ channels depend on the propagation environment and on the antenna configuration [Bla98, Pap00].

In the description of the TD-CDMA system in Chapter 5 as well as in the description of the intercell MAI in Chapter 3 a time-discrete system model in the equivalent low pass domain is utilized. To illustrate linear signal processing, in the literature [Wha71, Kle96, Naß95, Bla98, Pap00] quite often a matrix-vector notation is used with vectors representing signals and matrices describing the signal processing. In the following, the dimensions of vectors and the dimensions of matrices are always given in chips, see also

Section 1.2 and Fig. 1.7. Therefore, the channel IRs $\underline{h}_{\mathrm{s}}^{(k,k_{\mathrm{a}})}(\tau,t)$, $k=1...K$, $k_{\mathrm{a}}=1...K_{\mathrm{a}}$, by sampling along the τ-axis, can be represented by $K_{\mathrm{a}}\cdot K$ complex vectors

$$\underline{\mathbf{h}}_{\mathrm{s}}^{(k,k_{\mathrm{a}})}=\left[\underline{h}_{\mathrm{s},1}^{(k,k_{\mathrm{a}})}\ldots\underline{h}_{\mathrm{s},W}^{(k,k_{\mathrm{a}})}\right]^{\mathrm{T}},\quad k=1...K,k_{\mathrm{a}}=1...K_{\mathrm{a}},\tag{2.1}$$

of dimension W [BBS97]. In the delay-discrete model the quantity W corresponds to the excess delay [BBS97]. With W being an integer and T_{c} being the duration of one single chip, and assuming that the maximum delay τ_{max} of all channel IRs considered in the simulations is less than $W\cdot T_{\mathrm{c}}$, a vector of dimension W is sufficient to describe the channel IR $\underline{h}_{\mathrm{s}}^{(k,k_{\mathrm{a}})}(\tau,t)$ of the user k at the antenna element k_{a}.

In (2.1) the dependency on time is not explicitly expressed, because a certain instant of time is considered in what follows. The $K_{\mathrm{a}}\cdot K$ channel IRs $\underline{\mathbf{h}}_{\mathrm{s}}^{(k,k_{\mathrm{a}})}$, $k=1...K$, $k_{\mathrm{a}}=1...K_{\mathrm{a}}$, of (2.1) are termed spatial channel IRs, because they are valid for the spatially separated BS antenna elements.

If the K_{a} antenna elements are far away from each other, the sets of paths constituting two different spatial channel IRs $\underline{\mathbf{h}}_{\mathrm{s}}^{(k,k_{\mathrm{a}})}$ and $\underline{\mathbf{h}}_{\mathrm{s}}^{(k,k_{\mathrm{a}}')}$, $k=1...K$, $k_{\mathrm{a}}\neq k_{\mathrm{a}}'$, are totally different from each other. This is not the case if the K_{a} BS antenna elements are more closely spaced so that the same set of waves is responsible for the properties of the K_{a} radio channels of user k. Such cases are considered in this thesis. Let us assume that in such cases K_{d} wave propagation paths with different DOAs are involved at the BS. For each of these K_{d} wave propagation paths a channel IR

$$\underline{\mathbf{h}}_{\mathrm{d}}^{(k,k_{\mathrm{d}})}=\left[\underline{h}_{\mathrm{d},1}^{(k,k_{\mathrm{d}})}\ldots\underline{h}_{\mathrm{d},W}^{(k,k_{\mathrm{d}})}\right]^{\mathrm{T}},\quad k_{\mathrm{d}}=1...K_{\mathrm{d}},k=1...K,\tag{2.2}$$

of user k can be introduced, which is valid for a reference point (RP) defined somewhere within the array of the K_{a} BS antenna elements [BPH99, Bla98]. The K_{d} channel IRs $\underline{\mathbf{h}}_{\mathrm{d}}^{(k,k_{\mathrm{d}})}$, $k_{\mathrm{d}}=1...K_{\mathrm{d}}$, of (2.2) of user k are termed directional channel IRs, because they hold for the K_{d} DOAs valid at the BS. With (2.2) we obtain the channel IR vectors

$$\underline{\mathbf{h}}_{\mathrm{RP}}^{(k)}=\sum_{k_{\mathrm{d}}=1}^{K_{\mathrm{d}}}\underline{\mathbf{h}}_{\mathrm{d}}^{(k,k_{\mathrm{d}})}\tag{2.3}$$

valid for the channel IR of user k in the case of an omnidirectional antenna at the RP. Now, with the K_{a} antenna element specific steering factors $\underline{a}_{k_{\mathrm{a}}}^{(k,k_{\mathrm{d}})}$, $k_{\mathrm{d}}=1...K_{\mathrm{d}}$, $k=1...K$, $k_{\mathrm{a}}=1...K_{\mathrm{a}}$, [MM80, RK89, BPH99] the spatial channel IRs $\underline{\mathbf{h}}_{\mathrm{s}}^{(k,k_{\mathrm{a}})}$, $k=1...K$, $k_{\mathrm{a}}=1...K_{\mathrm{a}}$, of (2.1) can be expressed by the $K\cdot K_{\mathrm{d}}$ directional channel IRs $\underline{\mathbf{h}}_{\mathrm{d}}^{(k,k_{\mathrm{d}})}$, $k_{\mathrm{d}}=1...K_{\mathrm{d}}$, $k=1...K$, of (2.2) as

$$\underline{\mathbf{h}}_{\mathrm{s}}^{(k,k_{\mathrm{a}})}=\sum_{k_{\mathrm{d}}=1}^{K_{\mathrm{d}}}\underline{\mathbf{h}}_{\mathrm{d}}^{(k,k_{\mathrm{d}})}\underline{a}_{k_{\mathrm{a}}}^{(k,k_{\mathrm{d}})},\quad k=1...K,k_{\mathrm{a}}=1...K_{\mathrm{a}}.\tag{2.4}$$

The steering factors $\underline{a}_{k_\mathrm{a}}^{(k,k_\mathrm{d})}$, $k_\mathrm{a} = 1...K_\mathrm{a}$, $k_\mathrm{d} = 1...K_\mathrm{d}$, $k = 1...K$, depend on the array geometry [BPH99, Bla98, Pap00], that is on the position of the array elements relative to RP, and on the radiation characteristics of the array elements. In the following only omnidirectional antenna elements are considered. Fig. 2.1 illustrates that the array element k_a has a distance $l^{(k_\mathrm{a})}$ to the RP and the angle spanned by the reference line (RL) and the line connecting the referred array element with the RP is termed $\alpha^{(k_\mathrm{a})}$. The K users

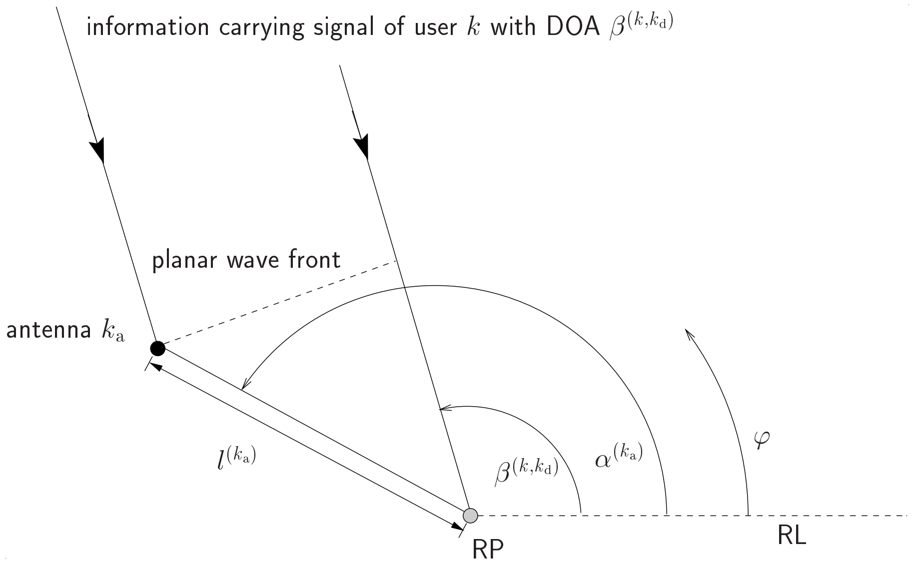

Fig. 2.1. Planar wave front of the information carrying signal of the user k impinging at the RP and the antenna element k_a with the DOA $\beta^{(k,k_\mathrm{d})}$ [BPH99]

are assumed to be in the far-field of the array. Consequently, the radiation of the user k impinging on the array via the wave propagation path k_d takes the form of a planar wave with the DOA $\beta^{(k,k_\mathrm{d})}$ [RK89], see Fig. 2.1. When antenna arrays [Haa97a, Bla98, Pap00] are used at the BS of a TD–CDMA mobile radio system, the narrowband assumption [MM80, RK89] is valid, i.e. the propagation time over the extent of the array is smaller than the inverse bandwidth of the signals. In this case the amplitudes and phases of the signals vary slowly with respect to the propagation time over the extent of the array. Hence, it is assumed that signals received at different antenna elements only differ in their arguments of their complex signal envelopes. Then, in the case of single direction channels, the propagation delay can be modelled by multiplying the signal complex envelope by a complex exponential [RK89, BPH99]. These complex exponentials are the phase factors $\mathrm{e}^{\mathrm{j}\psi(k,k_\mathrm{a},k_\mathrm{d})}$, where

$$\psi\left(k, k_\mathrm{a}, k_\mathrm{d}\right) = 2\pi \frac{l^{(k_\mathrm{a})}}{\lambda} \cos\left(\beta^{(k,k_\mathrm{d})} - \alpha^{(k_\mathrm{a})}\right), \quad k = 1...K, k_\mathrm{a} = 1...K_\mathrm{a}, k_\mathrm{d} = 1...K_\mathrm{d}, \qquad (2.5)$$

are the spatial frequencies with respect to the RP [RK89] and λ denotes the carrier wavelength. With (2.5) the steering factors $\underline{a}_{k_\mathrm{a}}^{(k,k_\mathrm{d})}$ of the antenna element k_a are given by

$$\underline{a}_{k_\mathrm{a}}^{(k,k_\mathrm{d})} = \mathrm{e}^{\mathrm{j}\psi(k,k_\mathrm{a},k_\mathrm{d})}, \quad k = 1...K, k_\mathrm{d} = 1...K_\mathrm{d}. \qquad (2.6)$$

The steering factors can be compiled to form the steering vectors

$$\underline{\mathbf{a}}^{(k,k_\mathrm{d})} = \left[\underline{a}_1^{(k,k_\mathrm{d})} ... \underline{a}_{K_\mathrm{a}}^{(k,k_\mathrm{d})}\right]^\mathrm{T}, \quad k = 1...K, k_\mathrm{d} = 1...K_\mathrm{d}, \tag{2.7}$$

of dimension K_a [MM80, RK89, Haa97a, BPH99].

Generally a finite number K_d of discrete directions is sufficient to describe the directional properties of mobile radio channels with satisfactory accuracy [BJL+02]. When defining these directions, two different approaches are possible: In the first approach a large number K_d of potential directions are *a priori* chosen with sufficiently narrow angular spacing, and the fact that only some of these directions are relevant has to be *a posteriori* taken into account by setting the directional channel IRs of the non-relevant directions to zero. In the second approach *a priori* only the relevant directions are considered, which means that these directions must be *a priori* known, a condition which cannot be easily fulfilled.

Within time intervals in the order of seconds the movements of the MSs are restricted to such small geographical domains that the shadowing conditions mentioned in Section 2.1 virtually do not change. Then, the momentary dynamics of the total fading are determined by small-scale fading only, which, in addition, can be considered to be stationary. Stationarity can be physically motivated by the results of channel measurements [BKM96] and means that the channel tap coefficients $\underline{h}_{\mathrm{s},w}^{(k,k_\mathrm{a})}$, see (2.1), and $\underline{h}_{\mathrm{d},w}^{(k,k_\mathrm{d})}$, see (2.2), are sample values of unbiased stationary complex processes. For this case correlation matrices of the spatial channel IR vectors $\underline{\mathbf{h}}_\mathrm{s}^{(k,k_\mathrm{a})}$ of (2.1) can be introduced [Wec00, JBM01] in order to describe the average channel properties by forming averages $\mathrm{E}\{\cdot\}$ over the real time t.

The correlation properties of the mobile radio channels can be studied with respect to delay, space and direction. The K_a spatial channel IR vectors $\underline{\mathbf{h}}_\mathrm{s}^{(k,k_\mathrm{a})}$, $k = 1...K$, $k_\mathrm{a} = 1...K_\mathrm{a}$, of (2.1) have the correlation matrices

$$\underline{\mathbf{R}}_{\tau,\mathrm{s}}^{(k,k',k_\mathrm{a},k_\mathrm{a}')} = \mathrm{E}\left\{\underline{\mathbf{h}}_\mathrm{s}^{(k,k_\mathrm{a})} \cdot \underline{\mathbf{h}}_\mathrm{s}^{(k',k_\mathrm{a}')*\mathrm{T}}\right\}, \quad k, k' = 1...K; k_\mathrm{a}, k_\mathrm{a}' = 1...K_\mathrm{a}, \tag{2.8}$$

where τ and s indicate that the elements of $\underline{\mathbf{R}}_{\tau,\mathrm{s}}{}^{(k,k',k_\mathrm{a},k_\mathrm{a}')}$ describe correlations with respect to both space and delay.

The vectors $\underline{\mathbf{h}}_\mathrm{s}^{(k,k_\mathrm{a})}$ of (2.1) of all users, $k = 1...K$, can be concatenated. This leads to the spatial antenna element specific channel IR vectors

$$\underline{\mathbf{h}}_\mathrm{s}^{(k_\mathrm{a})} = \left[\underline{\mathbf{h}}_\mathrm{s}^{(1,k_\mathrm{a})} .... \underline{\mathbf{h}}_\mathrm{s}^{(K,k_\mathrm{a})}\right]^\mathrm{T}, \quad k_\mathrm{a} = 1...K_\mathrm{a}, \tag{2.9}$$

of dimension KW. These vectors, with $\underline{\mathbf{R}}_{\tau,\mathrm{s}}^{(k,k',k_\mathrm{a},k_\mathrm{a}')}$ of (2.8), have the correlation matrices

$$\underline{\mathbf{R}}_{\tau}^{(k_\mathrm{a},k_\mathrm{a}')} = \mathrm{E}\left\{\underline{\mathbf{h}}_\mathrm{s}^{(k_\mathrm{a})} \cdot \underline{\mathbf{h}}_\mathrm{s}^{(k_\mathrm{a}')*\mathrm{T}}\right\} = \begin{pmatrix} \underline{\mathbf{R}}_{\tau,\mathrm{s}}^{(1,1,k_\mathrm{a},k_\mathrm{a}')} & \cdots & \underline{\mathbf{R}}_{\tau,\mathrm{s}}{}^{(1,K,k_\mathrm{a},k_\mathrm{a}')} \\ \vdots & \ddots & \vdots \\ \underline{\mathbf{R}}_{\tau,\mathrm{s}}{}^{(K,1,k_\mathrm{a},k_\mathrm{a}')} & \cdots & \underline{\mathbf{R}}_{\tau,\mathrm{s}}^{(K,K,k_\mathrm{a},k_\mathrm{a}')} \end{pmatrix}, \quad k_\mathrm{a}, k_\mathrm{a}' = 1...K_\mathrm{a}, \tag{2.10}$$

which describe for given antenna elements k_a and k_a', that is for a given spatial situation, the correlations with respect to the delay. Furthermore, the concatenation of the channel IRs $\underline{\mathbf{h}}_\mathrm{s}^{(k_\mathrm{a})}$, $k_\mathrm{a} = 1...K_\mathrm{a}$, of (2.9) yields the total spatial channel IR vector

$$\underline{\mathbf{h}}_\mathrm{s} = \left[\underline{\mathbf{h}}_\mathrm{s}^{(1)} .... \underline{\mathbf{h}}_\mathrm{s}^{(K_\mathrm{a})}\right]^\mathrm{T} \tag{2.11}$$

of dimension $K_\mathrm{a}KW$. This vector has the correlation matrix [Wec00]

$$\underline{\mathbf{R}}_{\tau,\mathrm{s}} = \mathrm{E}\left\{\underline{\mathbf{h}}_\mathrm{s} \cdot \underline{\mathbf{h}}_\mathrm{s}^{*\mathrm{T}}\right\} \tag{2.12}$$

of dimension $(K_\mathrm{a}KW) \times (K_\mathrm{a}KW)$. With $\underline{\mathbf{R}}_\tau^{(k_\mathrm{a},k_\mathrm{a}')}$ of (2.10) we can express $\underline{\mathbf{R}}_{\tau,\mathrm{s}}$ of (2.12) as

$$\underline{\mathbf{R}}_{\tau,\mathrm{s}} = \begin{pmatrix} \underline{\mathbf{R}}_\tau^{(1,1)} & \dots & \underline{\mathbf{R}}_\tau^{(1,K_\mathrm{a})} \\ \vdots & \ddots & \vdots \\ \underline{\mathbf{R}}_\tau^{(K_\mathrm{a},1)} & \dots & \underline{\mathbf{R}}_\tau^{(K_\mathrm{a},K_\mathrm{a})} \end{pmatrix}. \tag{2.13}$$

The structure of $\underline{\mathbf{R}}_{\tau,\mathrm{s}}$ of (2.13) is illustrated in Fig. 2.2 for the case K equal to two users and K_a equal to two antenna elements. The matrices $\underline{\mathbf{R}}_\tau^{(k_\mathrm{a},k_\mathrm{a})}$, $k_\mathrm{a} = 1...K_\mathrm{a}$, along the diagonal of $\underline{\mathbf{R}}_{\tau,\mathrm{s}}$ describe the correlations between the tap coefficients $\underline{h}_{\mathrm{s},w}^{(k_\mathrm{a})}$, $\underline{h}_{\mathrm{s},w'}^{(k_\mathrm{a})}$ of one and the same antenna element. The off-diagonal matrices $\underline{\mathbf{R}}_{\tau,\mathrm{s}}^{(k_\mathrm{a},k_\mathrm{a}')}$, $k_\mathrm{a}, k_\mathrm{a}' = 1...K_\mathrm{a}$, $k_\mathrm{a} \neq k_\mathrm{a}'$, describe correlations between tap coefficients of different antenna elements k_a, k_a' with respect to delay and space. In the simplest case correlations occur neither between different tap coefficients $\underline{h}_{\mathrm{s},w}^{(k_\mathrm{a})}$, $\underline{h}_{\mathrm{s},w'}^{(k_\mathrm{a})}$ of the same antenna element nor between tap coefficients $\underline{h}_{\mathrm{s},w}^{(k_\mathrm{a})}$, $\underline{h}_{\mathrm{s},w}^{(k_\mathrm{a}')}$, $k_\mathrm{a} \neq k_\mathrm{a}'$, of different antenna elements. Then, $\underline{\mathbf{R}}_{\tau,\mathrm{s}}$ of (2.13) is a purely diagonal matrix, and the scattering effects leading to $\underline{\mathbf{h}}_\mathrm{s}$ of (2.11) are uncorrelated with respect to delay and space.

Similar to (2.9) and (2.11)

$$\underline{\mathbf{h}}_\mathrm{d}^{(k)} = \left[\underline{\mathbf{h}}_\mathrm{d}^{(k,1)\mathrm{T}} \dots \underline{\mathbf{h}}_\mathrm{d}^{(k,K_\mathrm{d})\mathrm{T}}\right]^\mathrm{T} \tag{2.14}$$

expresses the directional channel IR of user k, where $\underline{\mathbf{h}}_\mathrm{d}^{(k,k_\mathrm{d})}$, $k_\mathrm{d} = 1...K_\mathrm{d}$, is defined in (2.2) and the total directional channel IR vector of all K users is written as

$$\underline{\mathbf{h}}_\mathrm{d} = \left[\underline{\mathbf{h}}_\mathrm{d}^{(1)\mathrm{T}} \dots \underline{\mathbf{h}}_\mathrm{d}^{(K)\mathrm{T}}\right]^\mathrm{T} \tag{2.15}$$

with the dimension $K_\mathrm{d}KW$. In the following the relationship between the total directional channel IR $\underline{\mathbf{h}}_\mathrm{d}$ of (2.15) and the total spatial channel IR $\underline{\mathbf{h}}_\mathrm{s}$ of (2.11) is shown. This relationship is of fundamental importance for an enhanced channel estimation scheme, which is described in [Pap00] and which will be briefly recapitulated in Chapter 6. With the steering vectors $\underline{\mathbf{a}}^{(k,k_\mathrm{d})}$, $k = 1...K$, $k_\mathrm{d} = 1...K_\mathrm{d}$, of (2.7) we can introduce the user specific steering matrices

$$\underline{\mathcal{A}}^{(k)} = \left[\underline{\mathbf{a}}^{(k,1)} \dots \underline{\mathbf{a}}^{(k,K_\mathrm{d})}\right], \quad k = 1...K. \tag{2.16}$$

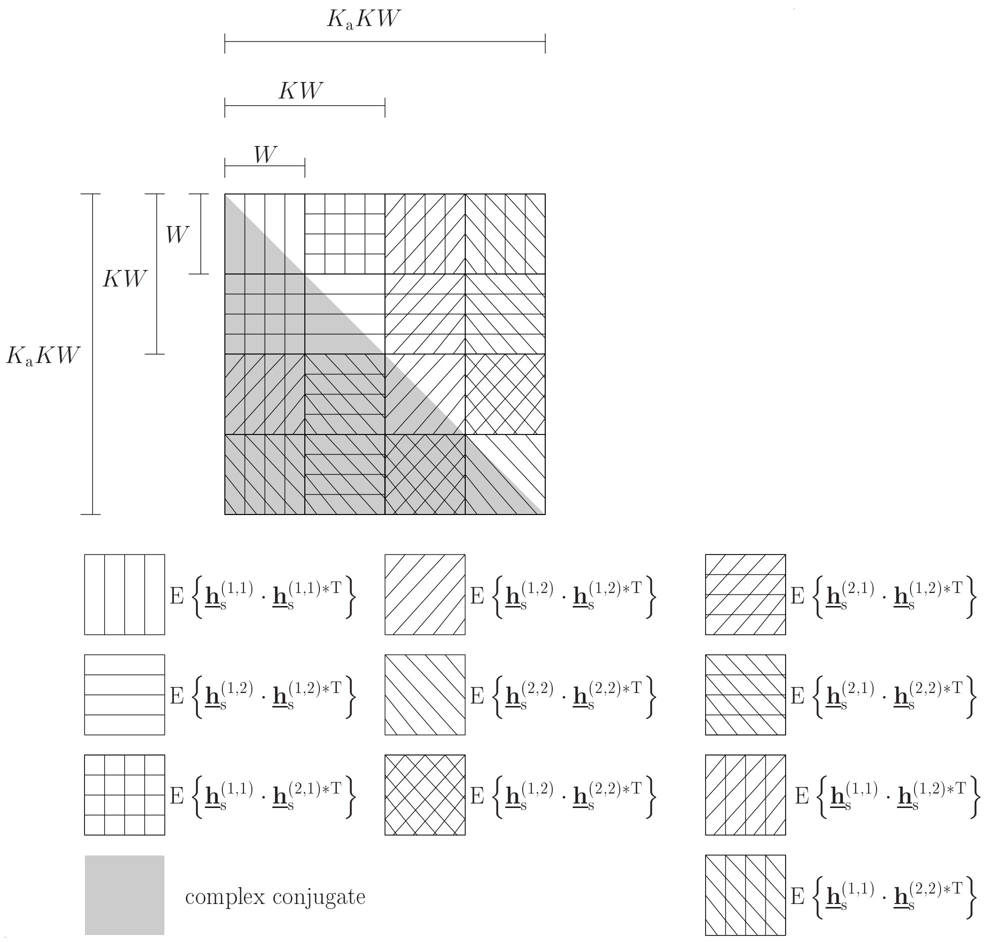

Fig. 2.2. Structure of the space/delay channel IR correlation matrix $\underline{\mathbf{R}}_{\tau,\mathrm{s}}$ of (2.13); $K = 2$; $K_\mathrm{a} = 2$

The rows of the K matrices $\underline{\mathcal{A}}^{(k)}$ of (2.16) can be represented by the vectors

$$\underline{\mathbf{a}}_\mathrm{d}^{(k,k_\mathrm{a})} = \left[\underline{a}_1^{(k,k_\mathrm{a})} \ldots \underline{a}_{K_\mathrm{d}}^{(k,k_\mathrm{a})}\right]^\mathrm{T}, \quad k = 1...K, k_\mathrm{a} = 1...K_\mathrm{a}, \tag{2.17}$$

which include the K_d spatial frequencies $\psi\left(k, k_\mathrm{a}, k_\mathrm{d}\right)$, $k_\mathrm{d} = 1...K_\mathrm{d}$, of (2.5), and which can be used to form the $W \times (K_\mathrm{d}W)$ matrices

$$\underline{\mathcal{A}}_\mathrm{d}^{(k,k_\mathrm{a})} = \underline{\mathbf{a}}_\mathrm{d}^{(k,k_\mathrm{a})\mathrm{T}} \otimes \mathbf{I}^{(W)}, \quad k = 1...K, k_\mathrm{a} = 1...K_\mathrm{a}, \tag{2.18}$$

where $\otimes$ denotes the Kronecker product [Gra81] and $\mathbf{I}^{(W)}$ is the $W \times W$ identity matrix. With the matrices $\underline{\mathcal{A}}_\mathrm{d}^{(k,k_\mathrm{a})}$, $k = 1...K$, $k_\mathrm{a} = 1...K_\mathrm{a}$, of (2.18) the $(KW) \times (K_\mathrm{d}KW)$ matrices

$$\underline{\mathcal{A}}_\mathrm{d}^{(k_\mathrm{a})} = \begin{bmatrix} \underline{\mathcal{A}}_\mathrm{d}^{(1,k_\mathrm{a})} & \ldots & 0 \\ 0 & \ddots & 0 \\ 0 & \ldots & \underline{\mathcal{A}}_\mathrm{d}^{(K,k_\mathrm{a})} \end{bmatrix}, \quad k_\mathrm{a} = 1...K_\mathrm{a}, \tag{2.19}$$

and finally the $(K_\mathrm{a}KW) \times (K_\mathrm{d}KW)$ matrix

$$\underline{\mathcal{A}}_\mathrm{d} = \left[\underline{\mathcal{A}}_\mathrm{d}^{(1)\mathrm{T}} \ldots \underline{\mathcal{A}}_\mathrm{d}^{(K_\mathrm{a})\mathrm{T}}\right]^\mathrm{T} \tag{2.20}$$

is given. The matrix $\underline{\mathcal{A}}_{\mathrm{d}}$ of (2.20) relates $\underline{\mathbf{h}}_{\mathrm{s}}$ of (2.11) and $\underline{\mathbf{h}}_{\mathrm{d}}$ of (2.15) [Pap00]:

$$\underline{\mathbf{h}}_{\mathrm{s}} = \underline{\mathcal{A}}_{\mathrm{d}}\ \underline{\mathbf{h}}_{\mathrm{d}}. \tag{2.21}$$

From (2.21) it becomes obvious that the directional information concerning the channel IRs, which is included in the matrix $\underline{\mathcal{A}}_{\mathrm{d}}$ of (2.20), can be separated from the temporal information included in the total directional channel IR vector $\underline{\mathbf{h}}_{\mathrm{d}}$ of (2.15).

For given directional channel IRs $\underline{\mathbf{h}}_{\mathrm{d}}^{(k,k_{\mathrm{d}})}$, $k_{\mathrm{d}} = 1...K_{\mathrm{d}}$, of (2.2) of user k, the spatial channel IRs $\underline{\mathbf{h}}_{\mathrm{s}}^{(k,k_{\mathrm{a}})}$, $k_{\mathrm{a}} = 1...K_{\mathrm{a}}$, of (2.1) of the user k are uniquely determined. The inverse is only true if the number K_{a} of antenna elements is at least as large as the number K_{d} of directions which have to be considered. In the case $K_{\mathrm{a}} < K_{\mathrm{d}}$ determining $\underline{\mathbf{h}}_{\mathrm{d}}^{(k,k_{\mathrm{d}})}$ for given $\underline{\mathbf{h}}_{\mathrm{s}}^{(k,k_{\mathrm{a}})}$ is not uniquely possible, that is an infinite number of solutions $\underline{\mathbf{h}}_{\mathrm{d}}^{(k,k_{\mathrm{d}})}$ result in the same $\underline{\mathbf{h}}_{\mathrm{s}}^{(k,k_{\mathrm{a}})}$ [BJL+02].

2.3 Directional outdoor channel model based on measurements

2.3.1 Measurement setup and measurement campaign

In this section, a channel model for uplink link level simulations is introduced, which, instead of synthetically generating the required channel IRs, uses measured IRs from propagation measurement campaigns. First, the measurement system and procedure is described, by which the complex IRs used in the simulations are obtained. The measurements were carried out using the Siemens Wideband Channel Sounder SIMOCS-2000, which was developed by Siemens in cooperation with the Research Group for RF Communications of the University of Kaiserslautern [FBKM93]. The SIMOCS-2000 consists of a mobile transmitter unit installed in a van and a stationary receiver unit. SIMOCS-2000 allows the determination of time variant-complex IRs by transmitting a digitally generated periodic spread spectrum test signal and by using optimum unbiased estimation in the receiver [FBKM93]. The main technical data of the SIMOCS-2000 are given in Table 2.1. The measurements were carried out in an urban macrocellular environment in Munich at a carrier frequency f_{c} of 1815 MHz using a bandwidth of 10 MHz. A vertically polarized antenna with an omnidirectional radiation pattern and a gain of 2.0 dBi was used as transmitter antenna, which was mounted on a van at a height of about 2 m above ground level. At the base station a vertically polarized antenna with a gain of 18 dBi, a half-power beam width of 65° and 7° in azimuth and elevation, respectively, was also used. It was located on the roof of a building, about 21 m above ground level. Surrounding buildings were about 20 m in height. For the measurement run, the van was driven along a route approximately orthogonal to the direction towards the base site. The run length

Table 2.1. Main technical data of the wideband channel sounder SIMOCS–2000 [EHWW98]

frequency range	700 MHz – 3 GHz
bandwidth	5 MHz, 10 MHz and 20 MHz
sequence period of the spread spectrum signal	12,8 μs, 25,6 μs, 51,2 μs and 102,4 μs
frequency stability	Rubidium–Standards in transmitter and receiver synchronized to GPS [Kap96]
dynamic range	$\geq$ 40 dB
measurement rate	selectable up to 1000 IRs per second
maximal measurable Doppler frequency	500 Hz
test signal	complex signal envelope of a periodic spread spectrum signal
signal processing	on–line calculation of complex IRs and monitoring

was about 300 m and the maximum vehicle speed was about 30 km/h. The center of the measurement run length was at a distance of 900 m to the BS site. The IRs were measured every 5.12 ms. Each measured channel IR consists of 256 samples. IRs with a maximum excess delay from multipath propagation of 25.6 μs can be measured, since the sampling rate is chosen to 0.1 μs. The sequence period time of the spread spectrum test signal must be larger than the maximal expected delay of 25.6 μs of the IRs in order to avoid an overlap in the temporal domain with the previously measured channel IRs. Therefore, the sequence period time is set to 51.2 μs.

Approximately 12000 IRs were recorded and stored in data files. The maximum delay spread of the IRs, which is defined in [Lor85], is 2.8 μs. Fig. 2.3 shows some examples of the magnitude $|\underline{h}\,(l,t)\,|$ of the measured channel IRs versus the measurement run length l and the delay τ.

2.3.2 Postprocessing of the measurement data

Because of the thermal noise at the receiver input the channel IRs measured in accordance with the procedures described in Section 2.3.1 are susceptible to noise. For this reason noise cancellation is performed before the channel IRs are used in the simulation. The basic principle of noise cancellation consists of determining a threshold N_t related to the amount of the sampling values, which allows the measured data to be separated into a useful signal and noise. All the magnitudes of a channel IR which are smaller than this threshold N_t are interpreted as noise and set to zero. Fig. 2.4 shows an example of a channel IR $\mid \underline{h}(\tau, t = \text{const.}) \mid$ at a fixed, but random instant of time $t = \text{const.}$ In

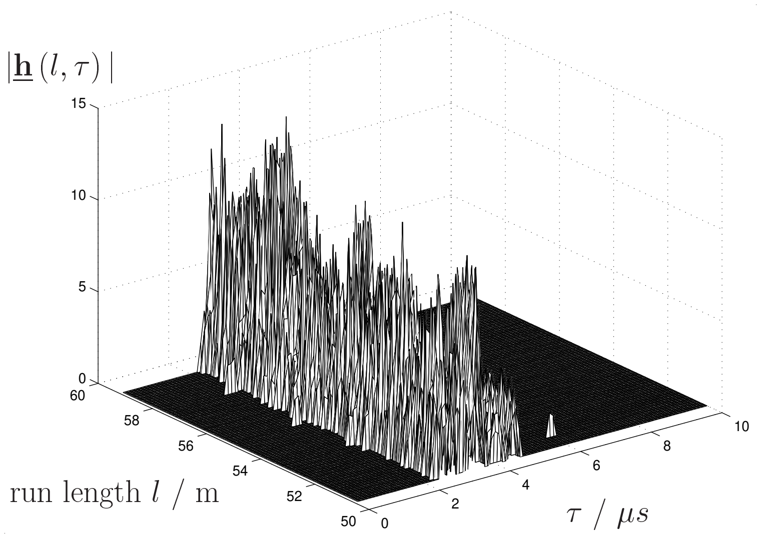

Fig. 2.3. Examples of measured channel IRs

Fig. 2.4 the delays τ_0 and τ_1 are shown, which delimit the proportion of the channel IR for which the magnitude $|\underline{h}(\tau, t)|$ exceeds the noise threshold N_t. To determine this noise threshold N_t, an estimate $\hat{\sigma}_\mathrm{t}^2$ of the noise power σ_t^2 is first determined. If the noise power σ_t^2 is known and if P_t is the probability of the noise magnitude exceeding the threshold N_t, N_t is given by [Feh94]

$$N_\mathrm{t} = \sqrt{-2 \cdot \sigma_\mathrm{t}^2 \cdot \ln(P_\mathrm{t})}. \tag{2.22}$$

In the following for noise cancellation of the channel IRs a probability P_t of 1% is considered. The noise power σ_t^2 is determined using an estimation process described in [Feh94] which is based on the well known process of Ordered Statistics quoted in other literature [Gov84, CoL66, Lew72, ShG81].

Since the measuring van covers a distance of several 100 m in an urban area, it can be assumed that because of shadowing effects the measured channel IRs will also be subject to slow, i.e. to large-scale fading. For the simulations of the TD–CDMA systems, for which the measured channel IRs are to be used, it is assumed that a slow power control will be used [Ste96, Sch99, Bla98] which will compensate for the large-scale fading. It can be assumed that because of the compensation for the large-scale fading, each subscriber signal will be received at an imaginary omnidirectional antenna in the RP with the same average power. Before performing the simulations the large-scale fading is thus eliminated from the measured channel IRs by a slow power control. This is based on the assumption that the powers $P(t)$ of the receive signals are composed multiplicatively of a rapidly fluctuating component $r(t)$ and a slowly fluctuating component $l(t)$ [Moh95, Lee85]:

$$P(t) = r(t) \cdot l(t), \tag{2.23}$$

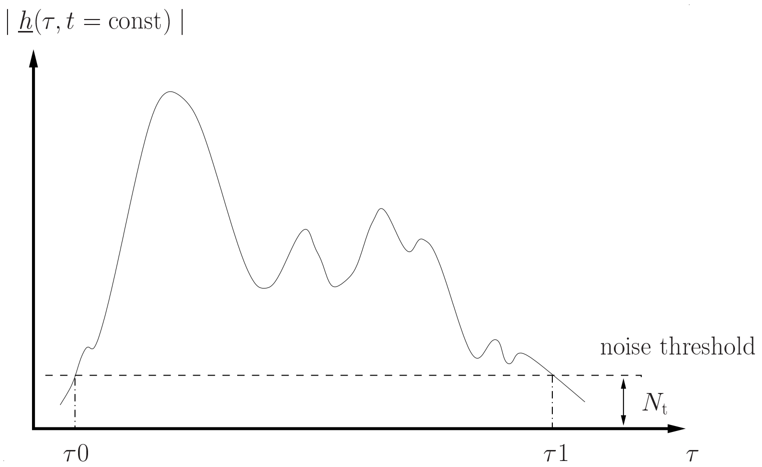

Fig. 2.4. Magnitude of a channel IR $| \underline{h}(\tau, t = \text{const.}) |$ with the noise threshold N_t. Definition of delays τ_0 and τ_1

where t is the continuous time. Here, at the measurement instant t_m the ratio of the receive power $P_r(t_m)$ to the transmit power $P_{tr}(t_m)$ within the measurement bandwidth B_m is [FKM94]

$$P(t_m) = \frac{P_r(t_m)}{P_{tr}(t_m)} = \frac{1}{4 \cdot B_m} \int_{\tau_0}^{\tau_1} | \underline{h}(\tau, t_m) |^2 \, d\tau. \tag{2.24}$$

A process to estimate the slow component $l(t)$ of $P(t)$, is to determine an average of $P(t_m)$ in each measurement instant t_m over a specific period 2Δ, over which it can be assumed that $l(t)$ does not change significantly. This assumption is approximately fulfilled, if the shadowing conditions in this period do not change significantly. As the result of the information given at each measurement instant t_m the local average value $\overline{P}(t_m)$ from $P(t_m)$ of (2.24) is obtained which is an estimate of the slow component $l(t)$. This described averaging technique is a sliding window average technique [Lee72]. Investigations for a suitable choice of length 2Δ of the sliding window, as for example in [Lee72], have shown that time intervals in which the measurement van covered a distance of 20 carrier wavelengths deliver good approximations of the shadowing components $l(t)$ so that the local mean value

$$\overline{P}(t_m) = \frac{1}{2\Delta} \int_{t_m - \Delta}^{t_m + \Delta} P(t') dt' \tag{2.25}$$

is produced. Fig. 2.5 shows the measured power curve $P(t_m)$ versus the measurement instants t_m and Fig. 2.6 shows the local mean value $\overline{P}(t_m)$ of (2.25), which was calculated by averaging over an interval of 20 carrier wavelengths.

With the equations (2.24) and (2.25) the rapidly varying component $r(t_m)$ of power $P(t_m)$

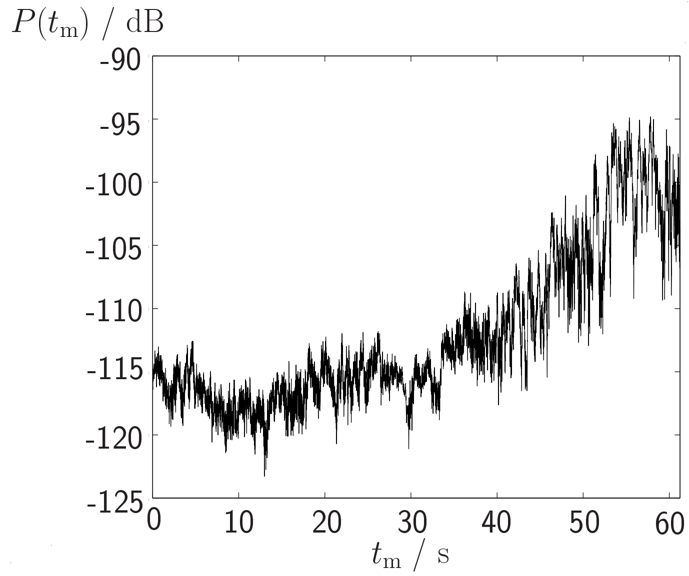

Fig. 2.5. Measured power $P(t_m)$ of (2.24) in dB of a measurement run

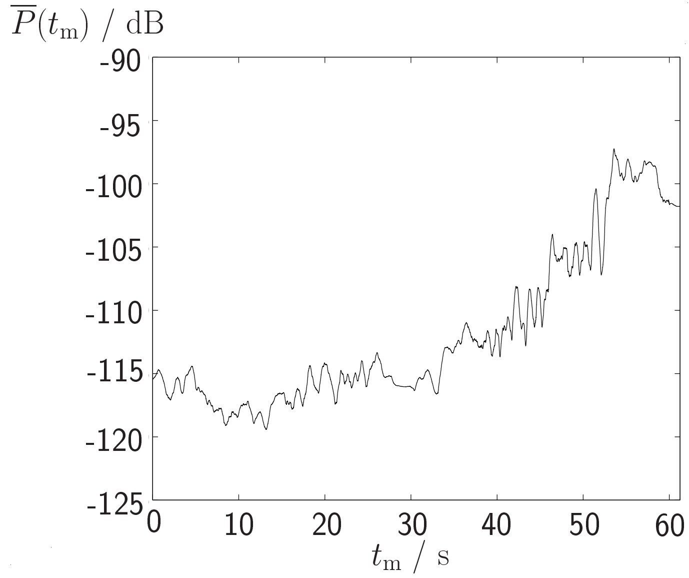

Fig. 2.6. Locally averaged value $\overline{P}(t_m)$ of (2.25) in dB for the case of using a sliding window with the length of 20 wavelengths

or the rapidly varying component $\underline{h}^{(r)}(\tau, t_m)$ of the IR $\underline{h}(\tau, t)$ can be calculated:

$$r(t_m) = \frac{P(t_m)}{\overline{P}(t_m)} \tag{2.26}$$

or

$$\underline{h}^{(r)}(\tau, t_m) = \frac{\underline{h}(\tau, t_m)}{\sqrt{4B_m\overline{P}(t_m)}}. \tag{2.27}$$

As a result of this process Fig. 2.7 shows the rapidly varying part $r(t_{\mathrm{m}})$ of power $P(t_{\mathrm{m}})$ according to Fig. 2.5. The graph in Fig. 2.7 shows that the slowly varying part $l(t)$ of power $P(t)$ is to a great deal eliminated.

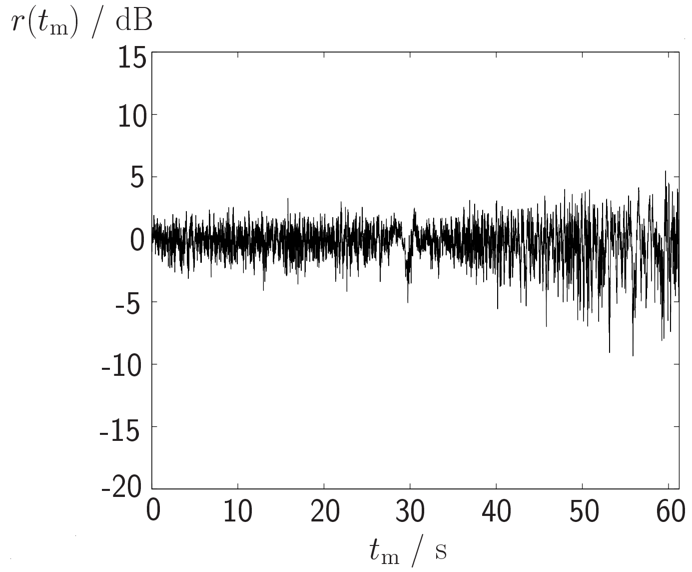

Fig. 2.7. Rapidly varying part $r(t_{\mathrm{m}})$ (small-scale fading) of the power levels $P(t_{\mathrm{m}})$ given in Fig. 2.5

Prior to the utilization of the measured channel IRs in the simulations of the considered TD–CDMA system, they have to be sampled at the chip rate $1/T_{\mathrm{c}}$. Notice that the chip rate $1/T_{\mathrm{c}}$ is a specific parameter of the considered TD–CDMA system, see Tab. 8.1, and it is not equal to the sampling rate of 0.1 μs of the measured channel IRs. Therefore, the measured channel IRs have to be band limited to the TD–CDMA system bandwidth and the sampling rate of the measured channel IRs has to be adapted to the chip rate $1/T_{\mathrm{c}}$ [ETSI98].

2.3.3 Channel model

Having eliminated the noise and the large–scale fading from the measured channel IRs as described in the previous section, we obtain a set of channel IRs which form the basis of the channel model to be described in the following. This channel model is considered for the simulations of the TD–CDMA system incorporating array processing. The measurements only allow information to be obtained about the time variance and the frequency selectivity of the channels. They do not allow information about the DOAs of the impinging wavefronts at the BS site, since the antenna used at the receiver has a half power beam width of 65°. Therefore, in order to obtain a directional model, it is assumed that each channel IR of the set of measured channel IRs represents a single direction channel, which means that it is assumed that each path of an IR is coming exactly from one discrete direction. Consequently, K_{d} is equal to 1. Each single direction channel is arbitrarily assigned to one user k and represents the directional channel IR $\underline{\mathbf{h}}_{\mathrm{d}}^{(k,1)}$ of (2.2) between user k and a RP at the BS site. Furthermore, it is assumed that the channel IR does not vary in time during the transmission of one burst, see Fig. 1.7. The K different users are assumed to be randomly distributed on a circle around the BS. The positions of the K users are kept fixed for the duration of four bursts. From the directional channel IRs $\underline{\mathbf{h}}_{\mathrm{d}}^{(k,1)}$ of (2.2) and knowing the steering factors $\underline{a}_{k_{\mathrm{a}}}^{(k,1)}$, $k_{\mathrm{a}} = 1...K_{\mathrm{a}}$, of (2.6) one can obtain the spatial channel IRs $\underline{\mathbf{h}}_{\mathrm{s}}^{(k,k_{\mathrm{a}})}$, $k_{\mathrm{a}} = 1...K_{\mathrm{a}}$, of (2.1) of user k according to (2.4).

2.4 ITU indoor channel model modified for systems with adaptive antennas

In this section the author presents a directional channel model for uplink link level simulations based on the tap-delay-line models standardized by ITU [ACTS98, ITU00a]. The ITU models are non–directional tap-delay-line channel models, which allow modelling of channel IRs $\underline{h}_{\mathrm{RP}}^{(k)}(\tau, t)$, $k = 1...K$, that are received by an omnidirectional antenna at the RP. Therefore, they cannot be used for simulations of systems with adaptive antennas. The power delay spectrum [Jak74] of a tap-delay-line channel model is not time continuous, but discrete. Moreover, a tap-delay-line model is characterized [ACTS98, ITU00a] by

- the number W_τ of channel taps,
- the delays τ_{w_τ}, $w_\tau = 2...W_\tau$, of the channel taps with respect to the first tap $w_\tau = 1$,
- the mean square absolute values $\mathrm{E}\left\{\mid \underline{h}_{w_\tau} \mid^2\right\}$ of the tap-coefficients $\underline{h}_{w_\tau}$, $w_\tau = 1...W_\tau$, with respect to the strongest tap and
- a given Doppler spectrum $S_{\mathrm{c}}(0, f_{\mathrm{d}})$ [Jak74].

The Doppler spectrum $S_{\mathrm{c}}(0, f_{\mathrm{d}})$ determines the mean power of the received waves which have the Doppler frequency f_{d} [Pro89]. In the ITU channel models the Doppler frequencies f_{d} are determined according to a given Doppler spectrum $S_{\mathrm{c}}(0, f_{\mathrm{d}})$ [ACTS98]. Hence, the statistical properties of the angular distribution of the power depending on the direction of departure (DOD) φ_{s}, see Fig. 2.8, at the MS, i.e. at the location of any moving user k, is *a priori* given [Jak74]. The ITU channel model, which in this thesis is modified in order to obtain a directional channel model, is the ITU indoor/office (IO) B model [ACTS98]. The parameters of this model are given in Table 2.2.

For modelling the channel IRs $\underline{h}_{\mathrm{RP}}^{(k)}(\tau, t)$ of user k at the RP, according to the non–directional ITU model, a large but fixed number E of waves with random zero phases ϑ_i, $i = 1...E$, are apportioned to the W_τ channel taps. The superposition of a certain number $E_{w_\tau} < E$ of waves belonging to the same channel tap w_τ leads to a certain power of this channel tap w_τ. With a fixed number E_{w_τ} of waves per tap and considering random zero phases ϑ_i, $i = 1...E_{w_\tau}$ each channel tap w_τ has a certain mean power, if several generated channel IRs are considered. The mean relative power of each channel tap w_τ with the relative delay τ_{w_τ} is given in Table 2.2. Hence, from the total number E of waves as many waves E_{w_τ} are assumed to have the same delay τ_{w_τ} and belong to the same channel tap w_τ, respectively, so that the mean relative power of each tap w_τ given in Table 2.2 is achieved. In Table 2.2 an example for the numbers E_{w_τ} of waves assigned to the taps w_τ is given for the case E equal to 300. The Doppler frequency f_{d} of each single wave is derived from a given Doppler spectrum $S_{\mathrm{c}}(0, f_{\mathrm{d}})$ [Höh90, ACTS98] in order to model the time variance of the channel IR $\underline{h}_{\mathrm{RP}}^{(k)}(\tau, t)$ of user k.

Table 2.2. ITU-Indoor-Office Parameter [ACTS98]

	Channel B Delay Spread = 100 ns		number of waves E_{w_τ} in the case of $E = 300$
Tap w_τ	Rel. Delay τ_{w_τ} / ns	Avg. Power / dB	
1	0	0	$E_1 = 173$
2	100	-3.6	$E_2 = 76$
3	200	-7.2	$E_3 = 34$
4	300	-10.8	$E_4 = 14$
5	500	-18	$E_5 = 2$
6	700	-25.2	$E_6 = 1$

Starting point of the directional modelling are the following assumptions and properties of the model:

- The number K_{d} of the directional channel IRs $\underline{\mathbf{h}}_{\mathrm{d}}^{(k,k_{\mathrm{d}})}$, $k_{\mathrm{d}} = 1...K_{\mathrm{d}}$, of (2.2) of user k is a parameter of the channel model, i.e. K_{d} can be arbitrarily chosen.
- K_{d} is equal for all K users.
- The K_{d} DOAs $\beta^{(k,k_{\mathrm{d}})}$, see Fig. 2.1, of the directional channel IRs $\underline{\mathbf{h}}_{\mathrm{d}}^{(k,k_{\mathrm{d}})}$, $k_{\mathrm{d}} = 1...K_{\mathrm{d}}$, of (2.2) of user k are uniformly distributed in the azimuth. The DOAs $\beta^{(k,k_{\mathrm{d}})}$ are kept fixed for the duration of four bursts. In the case of users being far away from

the BS and moving with low velocities $v^{(k)}$, $k = 1...K$, it can be expected that the changing of the DOAs $\beta^{(k,k_\mathrm{d})}$ during a time period of four bursts can be neglected. Therefore, it might not be unrealistic to keep the DOAs $\beta^{(k,k_\mathrm{d})}$ fixed.

- Each of the K_d directional channel IRs $\underline{\mathbf{h}}_\mathrm{d}^{(k,k_\mathrm{d})}$, $k_\mathrm{d} = 1...K_\mathrm{d}$, of (2.2) of user k has the same mean power at the RP.

The reason for the above approach of modelling directional channel IRs is that one can obtain performance results of the simulated mobile radio system dependent on the number K_d of DOAs. Always the same number K_d of DOAs $\beta^{(k,k_\mathrm{d})}$, $k_\mathrm{d} = 1...K_\mathrm{d}$, of the channel IR of user k would exist, if each tap would have been assigned to a different DOA because the number W_τ of assumed channel taps is fixed in the ITU models. Furthermore, none of the K_d DOAs is favoured, since they all have the same mean power.

Now, the basic considerations concerning the directional modelling mentioned before must be combined with the characteristics of the ITU IO B model. In the following description we refer to the channel IR of user k. The modelling of the remaining $K-1$ channel IRs is straightforward. Each of the E waves is uniquely assigned to one of the K_d DOAs. Always the same number $\frac{E}{K_\mathrm{d}}\rfloor$ of waves, where $\rfloor$ means that the quotient is rounded off to the next whole number, is assigned to each of the K_d DOAs. The assignment of the E waves to the W_τ taps and to the K_d DOAs $\beta^{(k,k_\mathrm{d})}$ is done as follows:

1. Each of the E waves is given a number $e = 1...E$.
2. All $\frac{E}{K_\mathrm{d}}\rfloor$ consecutive waves are assigned to the same DOA.
3. The waves with the numbers $e = (k_\mathrm{d}-1)\cdot\left(\frac{E}{K_\mathrm{d}}\rfloor\right) + 1...k_\mathrm{d}\cdot\left(\frac{E}{K_\mathrm{d}}\rfloor\right)$ are assigned to the DOA $\beta^{(k,k_\mathrm{d})}$.
4. According to the power delay profile of the ITU IO B model, see Table 2.2, the waves with the numbers $e = \left(\sum_{i=1}^{w_\tau-1} E_i\right) + 1...\sum_{i=1}^{w_\tau} E_i$ are assigned to the tap w_τ.

By the procedure described in the items one to four it may happen that certain waves are assigned to the same delay τ_{w_τ} although they have different DOAs $\beta^{(k,k_\mathrm{d})}$, $k_\mathrm{d} = 1...K_\mathrm{d}$. This is possible especially, if $K_\mathrm{d} > W_\tau$. Likewise it is possible that different waves are assigned to the same DOA $\beta^{(k,k_\mathrm{d})}$ but to different delays τ_{w_τ}, $w_\tau = 1...W_\tau$, which might happen in the case $K_\mathrm{d} < W_\tau$.

In opposite to the ITU channel model, where the Doppler frequency f_d of each single wave is derived based on the *a priori* given Doppler spectrum, in the channel model presented in this section the Doppler spectrum results from the Doppler frequencies. Knowing the

DOA $\beta^{(k,k_\mathrm{d})}$ and the delay τ_{w_τ} of each single wave and assuming single reflections for all waves between MS, i.e. any moving user k, and the RP at the BS site, the reflection point is located on an ellipse where the focuses are the locations of the RP and MS, see Fig. 2.8. Hence, the DOD $\varphi_\mathrm{s}^{(k,k_\mathrm{d})}$ of each wave at the MS can be determined by simple geometric calculation shown in [Bla98, Fuh97]. It is assumed that the MSs are moving on a circle around the BS, which, consequently, gives us the direction of movement φ_v of the MS k. With the given velocities $v^{(k)}$ of the MS k and considering the carrier wavelength λ, the

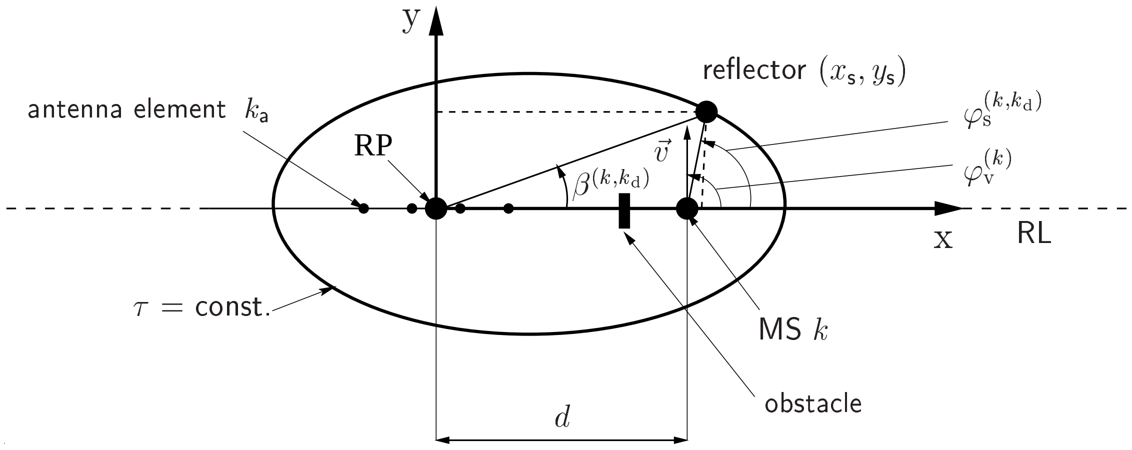

Fig. 2.8. Coordinate system for the determination of the coordinates of the reflection points

Doppler frequencies

$$f_\mathrm{d}^{(k,k_\mathrm{d})} = \frac{v^{(k)}}{\lambda} \cdot \cos(\varphi_\mathrm{s}^{(k,k_\mathrm{d})} - \varphi_\mathrm{v}^{(k)}), \quad k = 1...K, k_\mathrm{d} = 1...K_\mathrm{d}, \tag{2.28}$$

valid for all waves with the same DOA $\beta^{(k,k_\mathrm{d})}$ can be determined. To simplify the simulations, the velocity $v^{(k)}$ of the K MSs are assumed to be equal. Typical velocities $v^{(k)}$ for indoor propagation modelling are in the range of 1 to 3 km/h.

Knowing the DOA $\beta_{e,w_\tau}^{(k)}$ and the Doppler frequency $f_{\mathrm{d},e,w_\tau}^{(k)}$ of the waves $e = 1...E_{w_\tau}$ that belong to the channel tap w_τ with the delay τ_{w_τ}, the channel IR of user k received at an omnidirectional antenna at the RP is given by

$$\begin{aligned}&\underline{h}_\mathrm{RP}^{(k)}(\tau, t, \varphi) = \\ &\lim_{E\to\infty} \frac{1}{\sqrt{E}} \sum_{w_\tau=1}^{W_\tau} \sum_{e=1}^{E_{w_\tau}} \exp(\mathrm{j}\vartheta_{e,w_\tau}) \exp(\mathrm{j}2\pi f_{\mathrm{d},e,w_\tau}^{(k)} t) \delta(\tau - \tau_{w_\tau}) \delta(\varphi - \beta_{e,w_\tau}^{(k)}), \\ &k = 1...K,\end{aligned} \tag{2.29}$$

where ϑ_{e,w_τ} are random zero phases which are evenly distributed in the range $[0...2\pi[$, see [Bla98, Pap00]. From (2.29) one can obtain the channel IR of user k

$$\underline{h}_\mathrm{RP}^{(k)}(\tau, t) = \int_0^{2\pi} \underline{h}_\mathrm{RP}^{(k)}(\tau, t, \varphi) \,\mathrm{d}\varphi \tag{2.30}$$

as a function of delay τ and time t.

Fig. 2.9 shows the magnitude of the channel IR $\underline{h}_{\mathrm{RP}}^{(k)}(\tau, t)$ of (2.30) of user k. The velocity $v^{(k)}$ of user k is assumed to be 3 km/h and K_{d} equal to 8 DOAs are considered. Fig. 2.10 shows the magnitude $|\underline{h}_{\mathrm{RP}}^{(k)}(\tau, t_0, \varphi)|$ at a certain instant t_0 as a function of τ and the azimuth angle φ with $K_{\mathrm{d}} = 12$ DOAs.

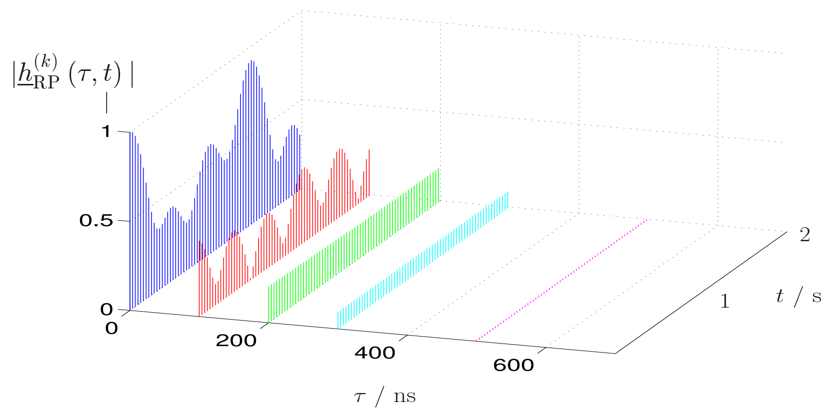

Fig. 2.9. Magnitude $|\underline{h}_{\mathrm{RP}}^{(k)}(\tau, t)|$ of (2.29); channel model ITU IO B; $v^{(k)} = 3$ km/h; $K_{\mathrm{d}} = 8$

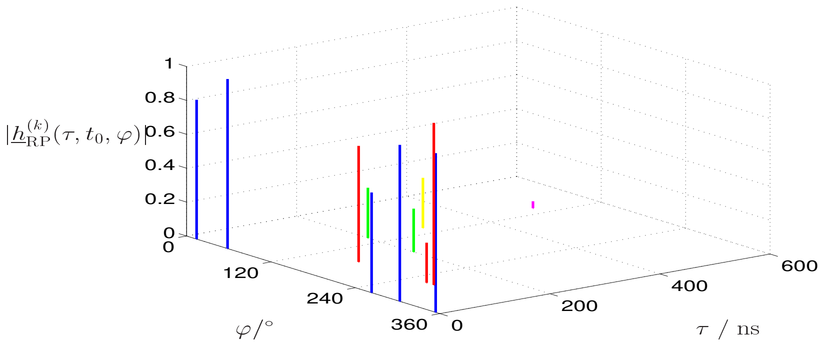

Fig. 2.10. Magnitude $|\underline{h}_{\mathrm{RP}}^{(k)}(\tau, t_0, \varphi)|$ of the channel IR of user k at the RP at the time t_0 as a function of τ and the azimuth angle φ; channel model ITU IO B; $v^{(k)} = 3$ km/h; $K_{\mathrm{d}} = 12$

2.5 Novel simple directional indoor channel model based on ray–tracing

In this section a simple 2-dimensional (2D) directional indoor channel model based on ray–tracing is introduced, which allows the modelling of the channel IRs valid for the desired signals of one cell and the modelling valid for the channel IRs of the signals of an adjacent cell in the same way. This channel model was developed by the author for the following reasons:

1. The standardized ITU channel models are tap-delay-line models with fixed delays for each tap [ETS98a]. Therefore, the delay profile is the same for each user. In a real propagation environment it is improbable that the channels of all users have the same delay profile, since in general the multipath propagation is different if the users are not located at the same place. For the simulations of systems with single user detection these channel models are sufficient, because each user signal is treated separately and the fact that the channels of all users have the same delay profile does not affect the simulations. When using joint detection, all channel IRs of all users of a cell have to be taken into account simultaneously in the simulations. Therefore, a more realistic modelling of the radio wave propagation, which is based on certain assumptions concerning the propagation environment and the propagation conditions, would be reasonable.

2. The UTRA proposed by ETSI and specified by 3GPP [3GPP] is part of the IMT-2000 family [ITU00]. The TDD mode TD–CDMA of UTRA is expected to support small cells and indoor areas. As an additional feature of the TD–CDMA receiver structure is the use of adaptive antennas. To evaluate the performance of systems with adaptive antennas in indoor environments, a directional indoor channel model is required. So far, there is no directional indoor channel model standardized by the ITU.

3. Especially for modelling the propagation for in-house scenarios with large rooms and many subscribers, it might be required to divide such a room into more than one cell. In this case, the channels valid for the desired user signals should be modelled in the same way as those valid for the interference.

The three issues mentioned above require the development of a new directional indoor channel model for the desired signals and the interference.

In the proposed model it is assumed that the service area is a rectangular room of length $x_{\max}$ equal to 50m and width $y_{\max}$ equal to 25m, see Fig. 2.11. The proposed channel model for desired signals and interference is a two dimensional model. The receivers and the transmitters utilize vertically polarized antennas which are placed at the same height. Only wave propagation in the horizontal plane is assumed and no reflections at the floor or the ceiling are considered. The room is divided into two equal cells as shown in Fig. 2.11. A BS is located in the centre of each cell. In the chosen coordinate system the BSs have the coordinates $(x_{\mathrm{BS}\mu}, y_{\mathrm{BS}\mu})$, $\mu = 1, 2$, see Fig. 2.12. In each cell K MSs are uniformly distributed. The $\mathrm{MS}_{\mu}^{(k)}$, $\mu = 1, 2$, $k = 1...K$, that belong to BS_{μ}, $\mu = 1, 2$ have the coordinates $(x_{\mathrm{BS}_{\mu}}^{(k)}, y_{\mathrm{BS}_{\mu}}^{(k)})$, $\mu = 1, 2$, $k = 1...K$. In the following, BS_1 is assumed to be the BS of the regarded cell, whereas BS_2 is the BS of the adjacent cell. The wall material of the room is assumed to be known. The attenuation of the walls is assumed to prevent transmission from inside to outside the room and vice versa. In general, the surface of real walls is rough which can lead to scattering of the waves impinging at the walls [Zol93]. Whether a wave is scattered or reflected at a wall depends on the wavelength λ, the reflection angle θ, which describes the deviation of the DOA of the waves from perpendicular impinging waves at the wall, and the roughness of the surface of the wall. The surface roughness is quantified by the mean difference h of local maximums and minimums of the surface height [Zol93]. Two reflected waves exist, one reflected at the maximum and the other one reflected at the minimum of the surface height, if a plane wave front impinges on the wall. The phase difference of two reflected waves must be smaller than $\pi/2$ in order to avoid scattering [Zol93]. This leads to the condition [Zol93]

$$h < \frac{\lambda}{8 \cdot \cos(\theta)}, \tag{2.31}$$

which must be fulfilled in order to have reflection of impinging waves and no scattering. In the following the roughness of the walls can be neglected for the considered wavelength λ, i.e. the walls are modelled as planes.

Only single reflections of the waves are assumed, see Fig. 2.11. Due to the assumed geometric properties of the environment and the limitation to single reflections, the propagation takes place over a limited number K_{d} of propagation paths. For each of the four walls the specular reflection conditions are fulfilled only at one point, which limits the number of reflected paths to four. Together with the direct path between MS and BS a maximum number of K_{d} equal to five propagation paths exists from $\mathrm{MS}_1^{(k)}$ to BS_1 and BS_2, see Fig. 2.11. Indoor propagation measurements [Gra94] justify the assumption of wave propagation over a limited number of main propagation paths and a larger number of less important paths, which are not considered in the described channel model.

With the coordinates $(x_{\mathrm{BS}_{\mu}}, y_{\mathrm{BS}_{\mu}})$, $\mu = 1, 2$, of the BS_{μ}, $\mu = 1, 2$, and $(x_{\mathrm{BS}_{\mu}}^{(k)}, y_{\mathrm{BS}_{\mu}}^{(k)})$, $\mu = 1, 2$, $k = 1...K$, of the $\mathrm{MS}_{\mu}^{(k)}$, $\mu = 1, 2$, $k = 1...K$, see Fig. 2.12, the DOA of the direct path

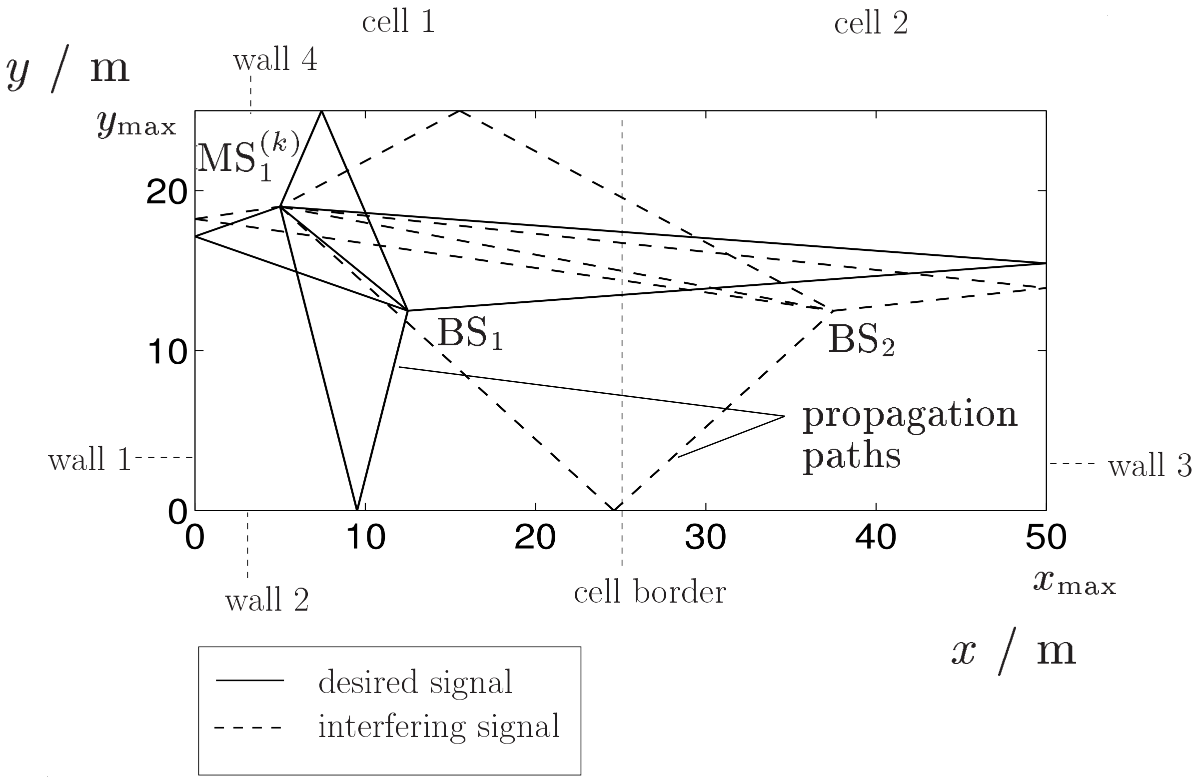

Fig. 2.11. Propagation environment for the directional indoor channel model

$k_{\mathrm{d}} = 1$ is

$$\beta_{\mathrm{BS}_\mu}^{(k,1)} = \arctan\left(\frac{|x_{\mathrm{BS}_\mu} - x_{\mathrm{BS}_\mu}^{(k)}|}{|y_{\mathrm{BS}_\mu} - y_{\mathrm{BS}_\mu}^{(k)}|}\right) \cdot \begin{cases} +\frac{\pi}{2} & \text{if} \quad x_{\mathrm{BS}_\mu} > x_{\mathrm{BS}_\mu}^{(k)}, y_{\mathrm{BS}_\mu} < y_{\mathrm{BS}_\mu}^{(k)} \\ \cdot(-1) + \frac{3\pi}{2} & \text{if} \quad x_{\mathrm{BS}_\mu} > x_{\mathrm{BS}_\mu}^{(k)}, y_{\mathrm{BS}_\mu} > y_{\mathrm{BS}_\mu}^{(k)} \\ +\frac{3\pi}{2} & \text{if} \quad x_{\mathrm{BS}_\mu} < x_{\mathrm{BS}_\mu}^{(k)}, y_{\mathrm{BS}_\mu} > y_{\mathrm{BS}_\mu}^{(k)} \\ \cdot(-1) + \frac{\pi}{2} & \text{if} \quad x_{\mathrm{BS}_\mu} < x_{\mathrm{BS}_\mu}^{(k)}, y_{\mathrm{BS}_\mu} < y_{\mathrm{BS}_\mu}^{(k)}, \end{cases}$$
$$k = 1...K, \mu = 1,2, \tag{2.32}$$

and the distance $d_{\mathrm{BS}_\mu}^{(k,1)}$ between $\mathrm{MS}_\mu^{(k)}$, $\mu = 1,2$, $k = 1...K$ and BS_μ, $\mu = 1,2$, is

$$d_{\mathrm{BS}_\mu}^{(k,1)} = \sqrt{\left(y_{\mathrm{BS}_\mu}^{(k)} - y_{\mathrm{BS}_\mu}\right)^2 + \left(x_{\mathrm{BS}_\mu} - x_{\mathrm{BS}_\mu}^{(k)}\right)^2}, \qquad k = 1...K, \mu = 1,2. \tag{2.33}$$

To determine the DOAs $\beta_{\mathrm{BS}_\mu}^{(k,k_{\mathrm{d}})}$, $k_{\mathrm{d}} = 2...5$, of the other four paths connecting $\mathrm{MS}_\mu^{(k)}$, $\mu = 1,2$, $k = 1...K$, and BS_μ, $\mu = 1,2$, the angles $\theta_{\mathrm{BS}_\mu}^{(k,k_{\mathrm{d}})}$, $k = 1...K$, $k_{\mathrm{d}} = 2...5$, $\mu = 1,2$, are required, see Fig. 2.12. Due to the geometric structure of the considered room, a unique solution for the angles $\theta_{\mathrm{BS}_\mu}^{(k,k_{\mathrm{d}})}$, $k = 1...K$, $k_{\mathrm{d}} = 2...5$, $\mu = 1,2$, exists. For all

Table 2.3. Angles $\theta_{\mathrm{BS}_\mu}^{(k,k_\mathrm{d})}$, $k=1...K$, $k_\mathrm{d}=2...5$, $\mu=1,2$ of the propagation paths originating in reflections at the four walls of the room dependent on the position of the MS

$\tan\left(\theta_{\mathrm{BS}_\mu}^{(k,k_\mathrm{d})}\right)=$	wall 1 $k_\mathrm{d}=2$	wall 2 $k_\mathrm{d}=3$	wall 3 $k_\mathrm{d}=4$	wall 4 $k_\mathrm{d}=5$
$x_{\mathrm{BS}_\mu}>x_{\mathrm{BS}_\mu}^{(k)}$, $y_{\mathrm{BS}_\mu}<y_{\mathrm{BS}_\mu}^{(k)}$	$\frac{y_{\mathrm{BS}_\mu}^{(k)}-y_{\mathrm{BS}_\mu}}{2x_{\mathrm{BS}_\mu}-x_{\mathrm{BS}_\mu}^{(k)}}$	$\frac{x_{\mathrm{BS}_\mu}-x_{\mathrm{BS}_\mu}^{(k)}}{2y_{\mathrm{BS}_\mu}^{(k)}-y_{\mathrm{BS}_\mu}}$	$\frac{y_{\mathrm{BS}_\mu}^{(k)}-y_{\mathrm{BS}_\mu}}{2\left(x_{\max}-x_{\mathrm{BS}_\mu}\right)-\left(x_{\max}-x_{\mathrm{BS}_\mu}^{(k)}\right)}$	$\frac{\left(\frac{x_{\max}}{2}-x_{\mathrm{BS}_\mu}^{(k)}\right)-\left(\frac{x_{\max}}{2}-x_{\mathrm{BS}_\mu}\right)}{2\left(\frac{x_{\max}}{2}-y_{\mathrm{BS}_\mu}\right)-\left(\frac{x_{\max}}{2}-y_{\mathrm{BS}_\mu}^{(k)}\right)}$
$x_{\mathrm{BS}_\mu}>x_{\mathrm{BS}_\mu}^{(k)}$, $y_{\mathrm{BS}_\mu}>y_{\mathrm{BS}_\mu}^{(k)}$	$\frac{y_{\mathrm{BS}_\mu}-y_{\mathrm{BS}_\mu}^{(k)}}{2x_{\mathrm{BS}_\mu}-x_{\mathrm{BS}_\mu}^{(k)}}$	$\frac{x_{\mathrm{BS}_\mu}-x_{\mathrm{BS}_\mu}^{(k)}}{2y_{\mathrm{BS}_\mu}-y_{\mathrm{BS}_\mu}^{(k)}}$	$\frac{y_{\mathrm{BS}_\mu}-y_{\mathrm{BS}_\mu}^{(k)}}{2\left(x_{\max}-x_{\mathrm{BS}_\mu}\right)-\left(x_{\max}-x_{\mathrm{BS}_\mu}^{(k)}\right)}$	$\frac{\left(\frac{x_{\max}}{2}-x_{\mathrm{BS}_\mu}^{(k)}\right)-\left(\frac{x_{\max}}{2}-x_{\mathrm{BS}_\mu}\right)}{2\left(\frac{x_{\max}}{2}-y_{\mathrm{BS}_\mu}^{(k)}\right)-\left(\frac{x_{\max}}{2}-y_{\mathrm{BS}_\mu}\right)}$
$x_{\mathrm{BS}_\mu}<x_{\mathrm{BS}_\mu}^{(k)}$, $y_{\mathrm{BS}_\mu}>y_{\mathrm{BS}_\mu}^{(k)}$	$\frac{y_{\mathrm{BS}_\mu}-y_{\mathrm{BS}_\mu}^{(k)}}{2x_{\mathrm{BS}_\mu}^{(k)}-x_{\mathrm{BS}_\mu}}$	$\frac{x_{\mathrm{BS}_\mu}^{(k)}-x_{\mathrm{BS}_\mu}}{2y_{\mathrm{BS}_\mu}-y_{\mathrm{BS}_\mu}^{(k)}}$	$\frac{y_{\mathrm{BS}_\mu}-y_{\mathrm{BS}_\mu}^{(k)}}{2\left(x_{\max}-x_{\mathrm{BS}_\mu}\right)-\left(x_{\max}-x_{\mathrm{BS}_\mu}^{(k)}\right)}$	$\frac{\left(\frac{x_{\max}}{2}-x_{\mathrm{BS}_\mu}\right)-\left(\frac{x_{\max}}{2}-x_{\mathrm{BS}_\mu}^{(k)}\right)}{2\left(\frac{x_{\max}}{2}-y_{\mathrm{BS}_\mu}^{(k)}\right)-\left(\frac{x_{\max}}{2}-y_{\mathrm{BS}_\mu}\right)}$
$x_{\mathrm{BS}_\mu}<x_{\mathrm{BS}_\mu}^{(k)}$, $y_{\mathrm{BS}_\mu}<y_{\mathrm{BS}_\mu}^{(k)}$	$\frac{y_{\mathrm{BS}_\mu}^{(k)}-y_{\mathrm{BS}_\mu}}{2x_{\mathrm{BS}_\mu}^{(k)}-x_{\mathrm{BS}_\mu}}$	$\frac{x_{\mathrm{BS}_\mu}^{(k)}-x_{\mathrm{BS}_\mu}}{2y_{\mathrm{BS}_\mu}^{(k)}-y_{\mathrm{BS}_\mu}}$	$\frac{y_{\mathrm{BS}_\mu}-y_{\mathrm{BS}_\mu}^{(k)}}{2\left(x_{\max}-x_{\mathrm{BS}_\mu}\right)-\left(x_{\max}-x_{\mathrm{BS}_\mu}^{(k)}\right)}$	$\frac{\left(\frac{x_{\max}}{2}-x_{\mathrm{BS}_\mu}\right)-\left(\frac{x_{\max}}{2}-x_{\mathrm{BS}_\mu}^{(k)}\right)}{2\left(\frac{x_{\max}}{2}-y_{\mathrm{BS}_\mu}\right)-\left(\frac{x_{\max}}{2}-y_{\mathrm{BS}_\mu}^{(k)}\right)}$

possible locations of the MSs the angles $\theta_{\mathrm{BS}_\mu}^{(k,k_\mathrm{d})}$, $k=1...K$, $k_\mathrm{d}=2...5$, $\mu=1,2$, are listed in Table 2.3.

With the angles $\theta_{\mathrm{BS}_\mu}^{(k,k_\mathrm{d})}$, $k=1...K$, $k_\mathrm{d}=2...5$, $\mu=1,2$, of Table 2.3 the DOAs

$$\beta_{\mathrm{BS}_\mu}^{(k,k_\mathrm{d})} = \theta_{\mathrm{BS}_\mu}^{(k,k_\mathrm{d})}\begin{cases}\cdot(-1)+\frac{k_\mathrm{d}\pi}{2}\bmod 2\pi & \text{if}\quad x_{\mathrm{BS}_\mu}>x_{\mathrm{BS}_\mu}^{(k)}, y_{\mathrm{BS}_\mu}<y_{\mathrm{BS}_\mu}^{(k)}\\ +\frac{k_\mathrm{d}\pi}{2}\bmod 2\pi & \text{if}\quad x_{\mathrm{BS}_\mu}>x_{\mathrm{BS}_\mu}^{(k)}, y_{\mathrm{BS}_\mu}>y_{\mathrm{BS}_\mu}^{(k)}\end{cases}, \quad k=1...K, k_\mathrm{d}=2...5, \mu=1,2, \tag{2.34}$$

of the reflected propagation paths can be determined.

The total propagation distances $d_{\mathrm{BS}_\mu}^{(k,k_\mathrm{d})}$, $k=1...K$, $k_\mathrm{d}=2...5$, $\mu=1,2$, of the reflected paths are the sum of the two partial distances $d_{\mathrm{BS}\mu,1}^{(k,k_\mathrm{d})}$ and $d_{\mathrm{BS}\mu,2}^{(k,k_\mathrm{d})}$, see Fig. 2.12. Therefore,

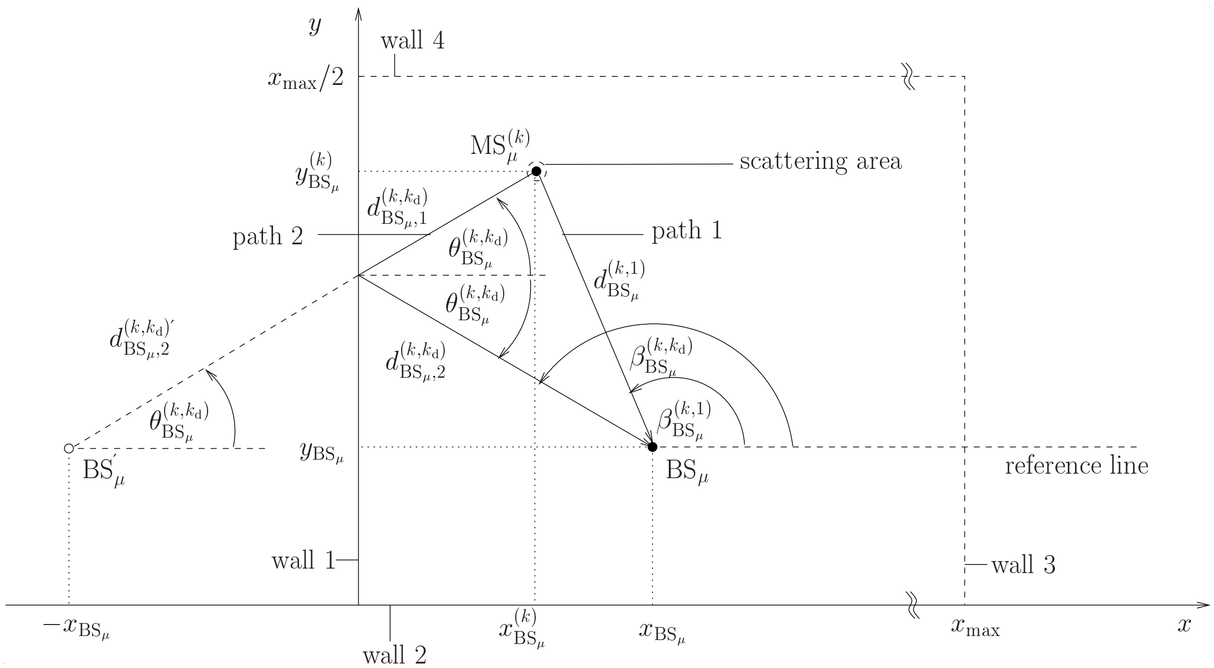

Fig. 2.12. Geometric properties of the propagation paths

the four reflected paths have the total lengths

$$d_{\mathrm{BS}_\mu}^{(k,2)} = \begin{cases} \sqrt{\left(y_{\mathrm{BS}_\mu} - y_{\mathrm{BS}_\mu}^{(k)}\right)^2 + \left(2x_{\mathrm{BS}_\mu} - x_{\mathrm{BS}_\mu}^{(k)}\right)^2}, & \text{if} \quad x_{\mathrm{BS}_\mu} > x_{\mathrm{BS}_\mu}^{(k)}, \\ \sqrt{\left(y_{\mathrm{BS}_\mu} - y_{\mathrm{BS}_\mu}^{(k)}\right)^2 + \left(x_{\mathrm{BS}_\mu} - 2x_{\mathrm{BS}_\mu}^{(k)}\right)^2}, & \text{if} \quad x_{\mathrm{BS}_\mu} < x_{\mathrm{BS}_\mu}^{(k)}, \end{cases} \tag{2.35}$$

$$d_{\mathrm{BS}_\mu}^{(k,3)} = \begin{cases} \sqrt{\left(2y_{\mathrm{BS}_\mu} - y_{\mathrm{BS}_\mu}^{(k)}\right)^2 + \left(x_{\mathrm{BS}_\mu} - x_{\mathrm{BS}_\mu}^{(k)}\right)^2}, & \text{if} \quad y_{\mathrm{BS}_\mu} > y_{\mathrm{BS}_\mu}^{(k)}, \\ \sqrt{\left(y_{\mathrm{BS}_\mu} - 2y_{\mathrm{BS}_\mu}^{(k)}\right)^2 + \left(x_{\mathrm{BS}_\mu} - x_{\mathrm{BS}_\mu}^{(k)}\right)^2}, & \text{if} \quad y_{\mathrm{BS}_\mu} < y_{\mathrm{BS}_\mu}^{(k)}, \end{cases} \tag{2.36}$$

$$d_{\mathrm{BS}_\mu}^{(k,4)} = \begin{cases} \sqrt{\left(y_{\mathrm{BS}_\mu} - y_{\mathrm{BS}_\mu}^{(k)}\right)^2 + \left(2\left(x_{\max} - x_{\mathrm{BS}_\mu}\right) - \left(x_{\max} - x_{\mathrm{BS}_\mu}^{(k)}\right)\right)^2}, & \text{if} \quad x_{\mathrm{BS}_\mu} < x_{\mathrm{BS}_\mu}^{(k)}, \\ \sqrt{\left(y_{\mathrm{BS}_\mu} - y_{\mathrm{BS}_\mu}^{(k)}\right)^2 + \left(\left(x_{\max} - x_{\mathrm{BS}_\mu}\right) - 2\left(x_{\max} - x_{\mathrm{BS}_\mu}^{(k)}\right)\right)^2}, & \text{if} \quad x_{\mathrm{BS}_\mu} > x_{\mathrm{BS}_\mu}^{(k)}, \end{cases} \tag{2.37}$$

$$d_{\mathrm{BS}_\mu}^{(k,5)} = \begin{cases} \sqrt{\left(\left(\frac{x_{\max}}{2} - y_{\mathrm{BS}_\mu}\right) - \left(\frac{x_{\max}}{2} - y_{\mathrm{BS}_\mu}^{(k)}\right)\right)^2 + \left(x_{\mathrm{BS}_\mu} - x_{\mathrm{BS}_\mu}^{(k)}\right)^2}, & \text{if} \quad x_{\mathrm{BS}_\mu} < x_{\mathrm{BS}_\mu}^{(k)}, \\ \sqrt{\left(\left(\frac{x_{\max}}{2} - y_{\mathrm{BS}_\mu}\right) - \left(\frac{x_{\max}}{2} - y_{\mathrm{BS}_\mu}^{(k)}\right)\right)^2 + \left(x_{\mathrm{BS}_\mu} - x_{\mathrm{BS}_\mu}^{(k)}\right)^2}, & \text{if} \quad x_{\mathrm{BS}_\mu} > x_{\mathrm{BS}_\mu}^{(k)}. \end{cases} \tag{2.38}$$

If the total path lengths $d_{\mathrm{BS}_\mu}^{(k,k_\mathrm{d})}$, $k = 1...K$, $k_\mathrm{d} = 1...5$, $\mu = 1, 2$, are known, the attenuation of the waves, which belong to each path can be determined. Depending on the angle $\theta_{\mathrm{BS}_\mu}^{(k,k_\mathrm{d})}$, $k_\mathrm{d} = 2...5$, $\mu = 1, 2$, and the complex permittivity number $\underline{\epsilon}_\mathrm{r}$ of the assumed wall material, the reflected waves belonging to the path k_{d} have an additional attenuation, which is given by the Fresnel reflection coefficient

$$\rho_{\perp}\left(\theta_{\mathrm{BS}_{\mu}}^{(k,k_{\mathrm{d}})}\right)=\frac{\cos\left(\theta_{\mathrm{BS}_{\mu}}^{(k,k_{\mathrm{d}})}\right)-\sqrt{\underline{\epsilon}_{\mathrm{r}}-\sin^{2}\left(\theta_{\mathrm{BS}_{\mu}}^{(k,k_{\mathrm{d}})}\right)}}{\cos\left(\theta_{\mathrm{BS}_{\mu}}^{(k,k_{\mathrm{d}})}\right)+\sqrt{\underline{\epsilon}_{\mathrm{r}}-\sin^{2}\left(\theta_{\mathrm{BS}_{\mu}}^{(k,k_{\mathrm{d}})}\right)}},\qquad k=1...K, k_{\mathrm{d}}=2...5, \mu=1,2, \tag{2.39}$$

for vertically polarized waves [Zol93]. Due to the assumption that all transmitter and receiver antennas are vertically polarized, it is sufficient to consider only the absolute value of the reflection coefficient of vertically polarized waves. Fig. 2.13 shows the reflection coefficient $\rho_{\perp}\left(\theta_{\mathrm{BS}_{\mu}}^{(k,k_{\mathrm{d}})}\right)$, $k=1...K$, $k_{\mathrm{d}}=2...5$, $\mu=1,2$, versus the angle $\theta_{\mathrm{BS}_{\mu}}^{(k,k_{\mathrm{d}})}$, $k=1...K$, $k_{\mathrm{d}}=2...5$, $\mu=1,2$, if walls made of concrete with $\underline{\epsilon}_{\mathrm{r}}$ equal $4.5+\mathrm{j}0.25$ are assumed [Zol93].

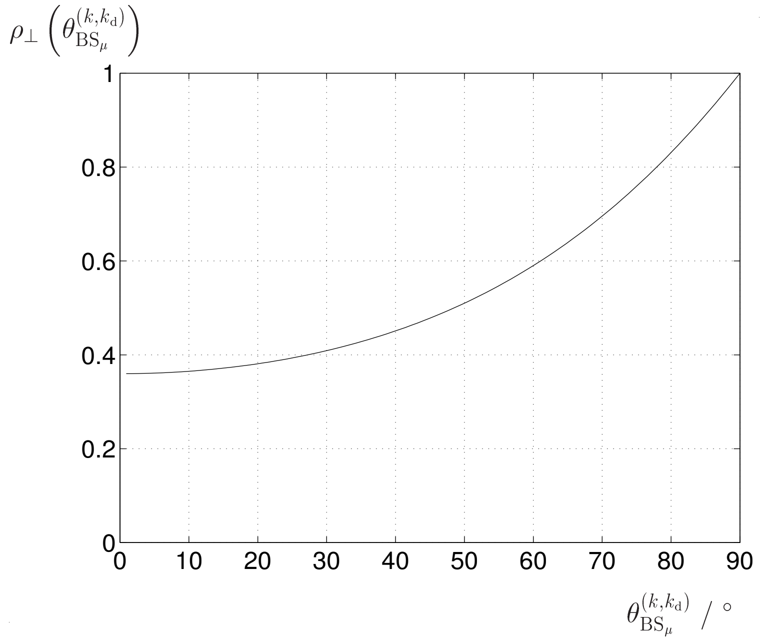

Fig. 2.13. Reflection coefficient $\rho_{\perp}\left(\theta_{\mathrm{BS}_{\mu}}^{(k,k_{\mathrm{d}})}\right)$ of vertical polarized waves versus the angle $\theta_{\mathrm{BS}_{\mu}}^{(k,k_{\mathrm{d}})}$, $k=1...K$, $k_{\mathrm{d}}=2...5$, $\mu=1,2$, $\underline{\epsilon}_{\mathrm{r}}=4.5+\mathrm{j}0.25$ [Zol93]

With c_0 the velocity of light and with the total distances $d_{\mathrm{BS}_{\mu}}^{(k,k_{\mathrm{d}})}$, $k=1...K$, $k_{\mathrm{d}}=1...5$, $\mu=1,2$, of (2.33), (2.35), (2.36), (2.37) and (2.38) the delay

$$\tau_{\mathrm{BS}_{\mu}}^{(k,k_{\mathrm{d}})}=\frac{d_{\mathrm{BS}_{\mu}}^{(k,k_{\mathrm{d}})}}{c_0},\qquad k=1...K, k_{\mathrm{d}}=1...5, \mu=1,2, \tag{2.40}$$

of each propagation path is given.

For developing a channel model consistent with the ITU channel models, besides the delays $\tau_{\mathrm{BS}_\mu}^{(k,k_\mathrm{d})}$, $k = 1...K$, $k_\mathrm{d} = 1...5$, $\mu = 1,2$, of (2.40) a power delay profile is required, which describes the mean relative power of a channel tap with a certain delay. Together with the total propagation distances $d_{\mathrm{BS}_\mu}^{(k,k_\mathrm{d})}$, $k = 1...K$, $k_\mathrm{d} = 1...5$, $\mu = 1,2$, of (2.33), (2.35), (2.36), (2.37) and (2.38) and the reflection coefficient $\rho_\perp\left(\theta_{\mathrm{BS}_\mu}^{(k,k_\mathrm{d})}\right)$, $k = 1...K$, $k_\mathrm{d} = 1...5$, $\mu = 1,2$, of (2.39) one obtains the power of the superimposed waves, which belong to the path k_d of the channel IR of user k in cell μ, with the delay $\tau_{\mathrm{BS}_\mu}^{(k,k_\mathrm{d})}$, $k = 1...K$, $k_\mathrm{d} = 1...5$, $\mu = 1,2$, of (2.40) with respect to the power of the superimposed waves, which belong to the direct path with $k_\mathrm{d} = 1$:

$$\rho_{\mathrm{T},\mu}^{(k,k_\mathrm{d})} = \begin{cases} 1, & \text{for} \quad k_\mathrm{d} = 1, \\ \left(\frac{d_{\mathrm{BS}_\mu}^{(k,1)}}{d_{\mathrm{BS}_\mu}^{(k,k_\mathrm{d})}}\right)^2 \cdot \rho_\perp\left(\theta_{\mathrm{BS}_\mu}^{(k,k_\mathrm{d})}\right), & \text{for} \quad k_\mathrm{d} = 2...5, \end{cases}$$
$$k = 1...K, \mu = 1,2. \tag{2.41}$$

It is further assumed that each MS is surrounded by a scattering area with a diameter negligibly small compared to the size of the room, see Fig. 2.12. The scatterers could be the mobile terminal on which the antenna is located, or even the body of a user which is close to the antenna. Each wave transmitted from each MS is scattered at one scattering point around the MS. The scattering points are assumed to be homogeneously distributed in the scattering area, see Fig. 2.14. Since the diameter of the scattering area is small compared to the size of the room and the walls, it can be assumed that the angles $\theta_{\mathrm{BS}_\mu}^{(k,k_\mathrm{d})}$, $k_\mathrm{d} = 1...K_\mathrm{d}$, $k = 1...K$, $\mu = 1,2$, for those waves scattered in the same direction are the same. These waves are assigned to one path. Since the power of superimposed waves of the path k_d is given by $\rho_{\mathrm{T},\mu}^{(k,k_\mathrm{d})}$, $k_\mathrm{d} = 1...K_\mathrm{d}$, $k = 1...K$, $\mu = 1,2$, of (2.41), the number of waves assigned to the path k_d of the user k of cell μ can be obtained by

$$E_{\mathrm{BS}_\mu}^{(k,k_\mathrm{d})} = \left(\frac{\rho_{\mathrm{T},\mu}^{(k,k_\mathrm{d})}}{\sum_{k_\mathrm{d}=1}^{5}\rho_{\mathrm{T},\mu}^{(k,k_\mathrm{d})}} \cdot E\right)\rfloor, \quad k = 1...K, k_\mathrm{d} = 1...5, \mu = 1,2. \tag{2.42}$$

The locations of the scatterers are kept fixed, while all K MSs are moving with velocity v into the direction given by the angle $\varphi_\mathrm{v}^{(k)}$. $\varphi_\mathrm{v}^{(k)}$ is uniformly distributed in the range $[0...2\pi[$, see Fig. 2.14. The movement of the MS takes place in such a small range that the position of the MS can be considered constant relative to the walls and the locations of the BS_μ, $\mu = 1,2$. With the velocity v and the wavelength λ we obtain the maximum Doppler frequency

$$f_{\mathrm{d,max}} = \frac{v}{\lambda}. \tag{2.43}$$

Based on the assumption of directionally uniform propagation of waves and homogeneously distributed scatters and with the maximum Doppler frequency $f_{\mathrm{d,max}}$ of (2.43),

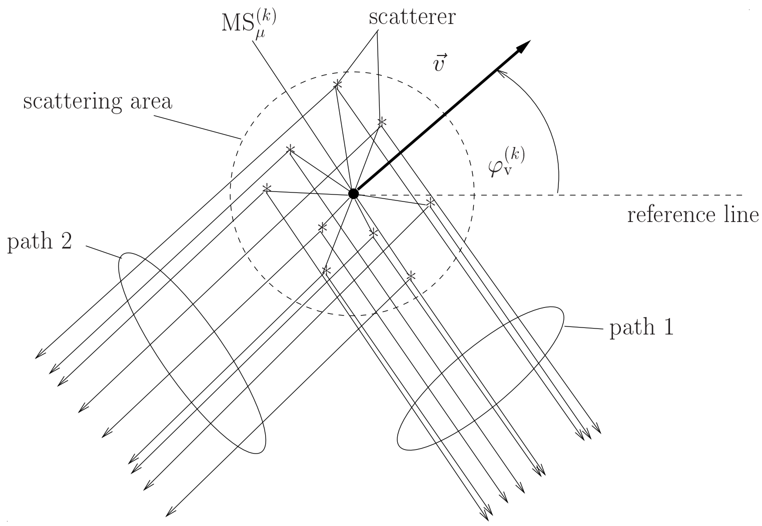

Fig. 2.14. Scattering area around the mobile station

the Doppler power spectrum is [COS89, Jak74]

$$S_{\mathrm{c}}\left(0, f_{\mathrm{d}}\right)=\begin{cases}\frac{1}{\sqrt{1-\left(f_{\mathrm{d}}/f_{\mathrm{d,max}}\right)^{2}}}, & \text{if} \quad \left|f_{\mathrm{d}}\right|<f_{\mathrm{d,max}},\\ 0, & \text{else.}\end{cases} \tag{2.44}$$

It is shown in [COS89] that under consideration of the Doppler power spectrum of (2.44) and the number of waves $E_{\mathrm{BS}_{\mu}}^{(k,k_{\mathrm{d}})}$ of (2.42) of the k_{d}-th path the Doppler frequencies $f_{\mathrm{d},\mu,i}^{(k,k_{\mathrm{d}})}$, $i=1...E_{\mathrm{BS}_{\mu}}^{(k,k_{\mathrm{d}})}$, $k=1...K$, $k_{\mathrm{d}}=1...5$, $\mu=1,2$, becomes

$$\begin{aligned} f_{\mathrm{d},\mu,i}^{(k,k_{\mathrm{d}})} &= -f_{\mathrm{d,max}}\cos\left(\pi u_{i}\right), \\ & u_{i}\in[0...1[, i=1...E_{\mathrm{BS}_{\mu}}^{(k,k_{\mathrm{d}})}, k=1...K, k_{\mathrm{d}}=1...5, \mu=1,2, \end{aligned} \tag{2.45}$$

where u_i is uniformly distributed in the range $[0...1[$.

$\vartheta_{\mathrm{BS}\mu,i}^{(k,k_{\mathrm{d}})}$, $i=1...E_{\mathrm{BS}_{\mu}}^{(k,k_{\mathrm{d}})}$, $k=1...K$, $k_{\mathrm{d}}=1...5$ $\mu=1,2$, is the zero phase of the i-th wave of the path k_{d} of the channel IR of user k in the cell μ and is assumed to be uniformly distributed in the range $[0...2\pi[$. Together with these phases, the Doppler frequencies $f_{\mathrm{d},\mu,i}^{(k,k_{\mathrm{d}})}$ of (2.45), the delays $\tau_{\mathrm{BS}_{\mu}}^{(k,k_{\mathrm{d}})}$, $k=1...K$, $k_{\mathrm{d}}=1...5$, $\mu=1,2$, of (2.40) and the DOAs $\beta_{\mathrm{BS}_{\mu}}^{(k,k_{\mathrm{d}})}$, $k=1...K$, $k_{\mathrm{d}}=1...5$, $\mu=1,2$, of (2.32) and (2.34), the directional channel IR of user k in the cell μ at a defined RP at the location of the BS_{μ} is

$$\begin{aligned} &\underline{h}_{\mathrm{RP,BS}_{\mu}}^{(k)}(\tau,t,\varphi)= \\ &\lim_{E\to\infty}\frac{1}{\sqrt{E}}\sum_{k_{\mathrm{d}}=1}^{K_{\mathrm{d}}}\sum_{i=1}^{E_{\mathrm{BS}_{\mu}}^{(k,k_{\mathrm{d}})}}\exp(\mathrm{j}\vartheta_{i,k_{\mathrm{d}}})\exp(\mathrm{j}2\pi f_{\mathrm{d},\mu,i}^{(k,k_{\mathrm{d}})}t)\delta(\tau-\tau_{\mathrm{BS}_{\mu}}^{(k,k_{\mathrm{d}})})\delta(\varphi-\beta_{\mathrm{BS}_{\mu}}^{(k,k_{\mathrm{d}})}), \\ &k=1...K, \mu=1,2. \end{aligned} \tag{2.46}$$

Fig. 2.15 shows the relative powers $\rho_{\mathrm{T},\mu}^{(k,k_\mathrm{d})}$, $k_\mathrm{d} = 1...K_\mathrm{d}$, with respect to the power of the first path $k_\mathrm{d} = 1$ of (2.41) and versus the delays $\tau_{\mathrm{BS}_\mu}^{(k,k_\mathrm{d})}$, $k_\mathrm{d} = 1...K_\mathrm{d}$, of (2.40) and Fig. 2.16 additionally shows $\rho_{\mathrm{T},\mu}^{(k,k_\mathrm{d})}$, $k_\mathrm{d} = 1...K_\mathrm{d}$, versus both the delays $\tau_{\mathrm{BS}_\mu}^{(k,k_\mathrm{d})}$, $k_\mathrm{d} = 1...K_\mathrm{d}$, and the DOAs $\beta^{(k,k_\mathrm{d})}$, $k_\mathrm{d} = 1...K_\mathrm{d}$, for the propagation scenario of Fig. 2.11.

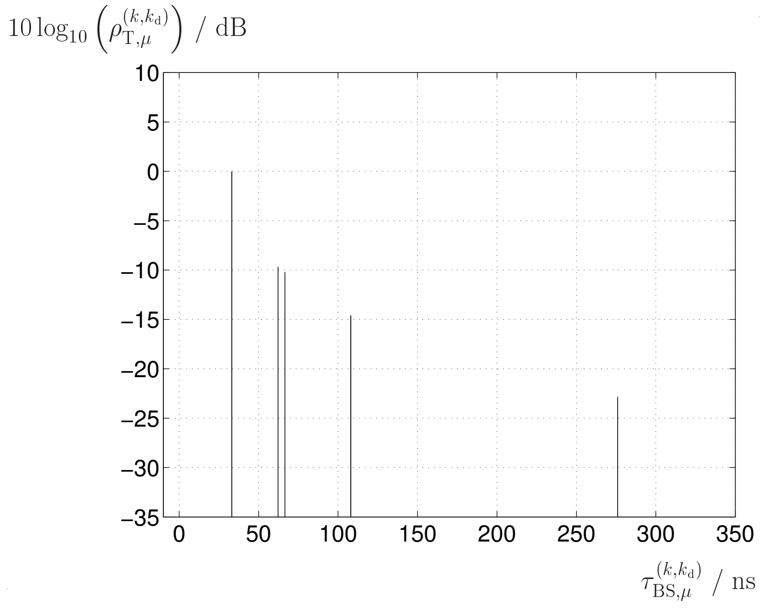

Fig. 2.15. Relative powers $\rho_{\mathrm{T},\mu}^{(k,k_\mathrm{d})}$, $K_\mathrm{d} = 1...K_\mathrm{d}$, of (2.41) with respect to $\rho_{\mathrm{T},\mu}^{(k,1)}$ versus the delays $\tau_{\mathrm{BS}_\mu}^{(k,k_\mathrm{d})}$, $k_\mathrm{d} = 1...K_\mathrm{d}$, of (2.40) valid for the channel IRs $\underline{h}_{\mathrm{RP,BS}\mu}^{(k)}(\tau, t_0, \varphi_0)$ of the propagation example given in Fig. 2.11

The implementation of the presented channel model in a time discrete system simulation tool can be done by limiting the channel bandwidth to the system bandwidth and sampling the bandlimited channel IRs with the sampling rate used in the simulation tool in order to obtain the corresponding channel IRs $\underline{h}_{\mathrm{RP,BS}_\mu}^{(k)}(\tau, t)$, $k = 1...K$, similar to (2.30) for a sampling time T_c equal to 0.461 μs, see Fig. 2.17. Furthermore, one can determine the vectors $\underline{\mathbf{h}}_\mathrm{s}^{(k,k_\mathrm{a})}$, $k = 1...K$, $k_\mathrm{a} = 1...K_\mathrm{a}$ of (2.1) by taking account of the K_a antenna element specific steering factors $\underline{a}_{k_\mathrm{a}}^{(k,k_\mathrm{d})}$, $k_\mathrm{d} = 1...K_\mathrm{d}$, $k = 1...K$, $k_\mathrm{a} = 1...K_\mathrm{a}$, of (2.6). According to (2.9) and (2.11) based on the vectors $\underline{\mathbf{h}}_\mathrm{s}^{(k,k_\mathrm{a})}$ the total channel IR vector $\underline{\mathbf{h}}_\mathrm{s}$ of (2.11) with the corresponding covariance matrix $\underline{\mathbf{R}}_{\tau,\mathrm{s}}$ of (2.13) is obtained for the proposed indoor channel model.

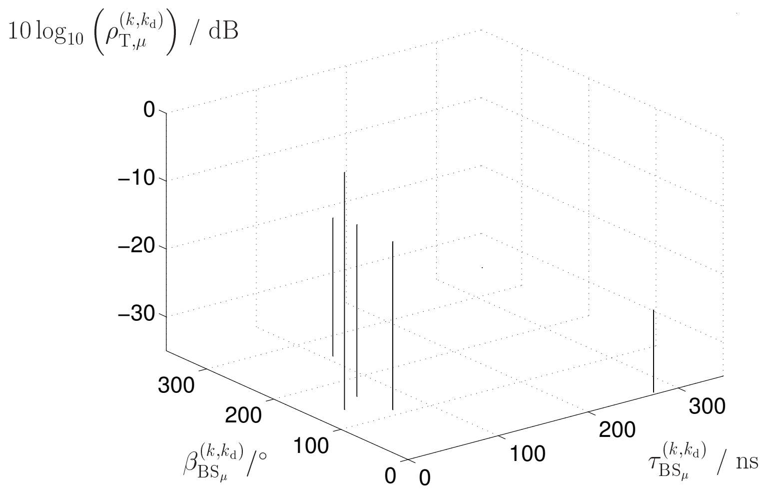

Fig. 2.16. Relative powers $\rho_{\mathrm{T},\mu}^{(k,k_\mathrm{d})}$, $k_\mathrm{d} = 1...K_\mathrm{d}$, of (2.41) with respect to $\rho_{\mathrm{T},\mu}^{(k,1)}$ versus the delays $\tau_{\mathrm{BS}_\mu}^{(k,k_\mathrm{d})}$, $k_\mathrm{d} = 1...K_\mathrm{d}$, of (2.40) and the DOAs $\beta^{(k,k_\mathrm{d})}$ valid for the channel IRs $\underline{h}_{\mathrm{RP,BS}\mu}^{(k)}(\tau, t_0, \varphi_0)$ of the propagation example given in Fig. 2.11

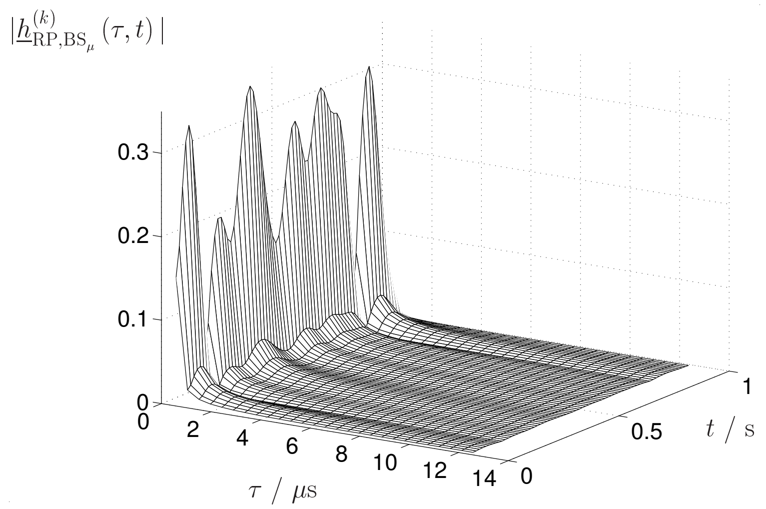

Fig. 2.17. Magnitude of $\underline{h}_{\mathrm{RP,BS}_\mu}^{(k)}(\tau, t)$; bandlimited and sampled with a sampling time T_c equal to 0.461 μs

3 Directional interference models

3.1 Introduction

The following Section 3.2 describes a method for modelling intercell MAI in cellular mobile radio systems with multi-antenna receivers. Intercell MAI is the co-channel interference which affects reception of desired signals at the regarded BS and which is caused by the users outside the cell under consideration, i.e. by users belonging to the other cells [BKNS94a, BKNS94b]. The intercell MAI modelling presented below is used in the link level simulations of the uplink under consideration of a multi-antenna TD–CDMA receiver. Besides intercell MAI, two other kinds of interference affect the transmission quality, namely intersymbol interference (ISI) and intracell MAI. ISI is caused by the superposition of signal components originating in temporally adjacent transmitted data symbols [Pro89, Kle96], and intracell MAI is caused by the user signals other than the desired signals that are simultaneously present in the same frequency band in the cell under consideration [Pro89, Kle96]. Both ISI and intracell MAI are eliminated by the linear joint detection (JD) scheme [Wha71, Ver86] proposed for TD-CDMA [BK95, Kle96, NTD$^+$98], which is also considered in this thesis. Therefore, ISI and intracell MAI are not considered in the following.

Proper modelling intercell MAI in a CDMA system requires generation of a channel model similar to the one for the desired signals also for the undesired signals, see Chapter 2, and transmission of random data symbols spread by arbitrary CDMA codes over the channels which have been generated by the created channel model. In order to reduce the computational effort for interference generation, it is assumed in state of the art interference modelling that intercell MAI can be represented by the equivalent low pass representation of a random Gaussian signal that has the same spectral form as the desired signals [Naß95, Bla98]. In the following this state of the art intercell MAI modelling is the basis for the modelling of the temporal correlations of intercell MAI. The state of the art modelling of the directional inhomogeneity of the intercell MAI is based on the assumption that each intercell MAI signal has a discrete DOA and that different intercell MAI signals are uncorrelated [Bla98]. In addition to the consideration of directionally discrete uncorrelated intercell MAI signals the intercell MAI model presented in Section 3.2 allows correlations between different intercell MAI signals to be considered and a directionally continuous modelling of intercell MAI.

After a description of the general intercell MAI model in Section 3.2, simplified versions of this model, which are finally used for the evaluation of the TD–CDMA system, are presented in Section 3.3.

3.2 General model

An antenna with the beam width $\mathrm{d}\varphi$, which is located at the RP receives from direction φ the intercell MAI signal

$$\underline{n}(\varphi, t) = \underline{n}_{\varphi}(\varphi, t)\,\mathrm{d}\varphi. \tag{3.1}$$

$\underline{n}_{\varphi}(\varphi, t)$ is termed azimuthal MAI density. The total intercell MAI signal which would be received by an omnidirectional antenna at the RP is

$$\underline{n}(t) = \int_0^{2\pi} \underline{n}_{\varphi}(\varphi, t)\,\mathrm{d}\varphi. \tag{3.2}$$

For each arbitrary angle φ_1 the signal $\underline{n}_{\varphi}(\varphi_1, t)\,\mathrm{d}\varphi_1$, which is received at the RP by an antenna with the beam width $\varphi_1 - \frac{\mathrm{d}\varphi}{2}...\varphi_1 + \frac{\mathrm{d}\varphi}{2}$, is assumed to be represented by a sample of a temporally stationary, ergodic, zero–mean Gaussian process which is linearly filtered by the GMSK chip impulse $C_0(t)$ [ETSI97] with the time–bandwidth product 0.3. The spectral form of intercell MAI results from the specified filter function and is equivalent to the spectral form of the desired signals in the mobile radio system under consideration. This means that the temporal correlation of each individual intercell MAI signal $\underline{n}_{\varphi}(\varphi, t)\,\mathrm{d}\varphi$ is known. If versions of the same interference signal with different delays come from a direction φ, then in general the spectral form of the total interference coming from this direction is not the same as the spectral form of the individual signals [Lük79], since specific relationships exist between these signals as regards delay and phase. It is assumed below that these relationships between delay and phase are constantly changing so that the spectral form of the total interference coming from direction φ is on average equal to the spectral form of the transmit signals. Modelling of the band-limited intercell MAI by filtering the sample functions of a stationary Gaussian process is state of the art and is described in detail in [Bla98] and for this reason is not presented in greater detail here.

The following assumes that the spectral form of the signals $\underline{n}_{\varphi}(\varphi, t)\,\mathrm{d}\varphi$, $\varphi \in [0...2\pi[$, is independent of azimuth angle φ. The intensity of signals $\underline{n}_{\varphi}(\varphi, t)\,\mathrm{d}\varphi$, $\varphi \in [0...2\pi[$ is described by the azimuthal intercell MAI density $\underline{n}_{\varphi}(\varphi, t)$, $\varphi \in [0...2\pi[$ and is given by the propagation conditions. With the model described below, azimuthal MAI density $\underline{n}_{\varphi}(\varphi, t)$, $\varphi \in [0...2\pi[$, serves as a basis for describing the assumed interference scenario. The selection of $\underline{n}_{\varphi}(\varphi, t)$, $\varphi \in [0...2\pi[$, determines a particular interference scenario. The temporal and directional auto correlation function of the azimuthal intercell MAI density $\underline{n}_{\varphi}(\varphi, t)$ at RP is

$$\underline{R}_{\varphi}(\varphi_1, \varphi_2, \Delta t) = \mathrm{E}\left\{\underline{n}_{\varphi}(\varphi_1, t) \cdot \underline{n}_{\varphi}^{*}(\varphi_2, t + \Delta t)\right\}, \quad \varphi_1, \varphi_2 \in [0...2\pi]. \tag{3.3}$$

Forming the expected value with operator $\mathrm{E}\{\cdot\}$ in (3.3), as also in the following equations, represents formation of an expected value over time t. Starting from (3.2) and (3.3), this produces a total average intercell MAI power to [Pap65]

$$\begin{aligned}\sigma^2 &= \mathrm{E}\left\{\left(\int_0^{2\pi} \underline{n}_\varphi(\varphi_1,t)\,\mathrm{d}\varphi_1\right)\cdot\left(\int_0^{2\pi} \underline{n}_\varphi^*(\varphi_2,t)\,\mathrm{d}\varphi_2\right)\right\}\\ &= \int_0^{2\pi}\int_0^{2\pi} \mathrm{E}\left\{\underline{n}_\varphi(\varphi_1,t)\cdot\underline{n}_\varphi^*(\varphi_2,t)\right\}\,\mathrm{d}\varphi_2\,\mathrm{d}\varphi_1\\ &= \int_0^{2\pi}\int_0^{2\pi} \underline{R}_\varphi(\varphi_1,\varphi_2,0)\,\mathrm{d}\varphi_2\,\mathrm{d}\varphi_1. \end{aligned} \tag{3.4}$$

at an omnidirectional antenna at the RP. An intercell MAI signal arriving at the RP at an angle φ received by an antenna at the RP with the beam width $\mathrm{d}\varphi$ therefore has an average amplitude of

$$\sigma(\varphi) = \sqrt{\underline{R}_\varphi(\varphi,\varphi,0)}\,\mathrm{d}\varphi. \tag{3.5}$$

From the general intercell MAI model considered in the following six different intercell MAI scenarios can be derived. The six intercell MAI scenarios differ with respect to correlation characteristics of the interference signals and with respect to the azimuthal power distribution of the incident intercell MAI at the RP:

- Signals $\underline{n}(\varphi_1,t)$ and $\underline{n}(\varphi_2,t)$, received from different angle ranges $\varphi_1-\frac{\mathrm{d}\varphi}{2}...\varphi_1+\frac{\mathrm{d}\varphi}{2}$ and $\varphi_2-\frac{\mathrm{d}\varphi}{2}...\varphi_2+\frac{\mathrm{d}\varphi}{2}$, $\varphi_1 \neq \varphi_2$, at an antenna with the beam width $\mathrm{d}\varphi$ are uncorrelated. For the spatial and temporal correlation function of the intercell MAI signal $\underline{n}(\varphi,t)$ of (3.1) the following applies:

$$\underline{R}_\mathrm{n}(\varphi_1,\varphi_2,\Delta t) = \mathrm{E}\left\{\underline{n}(\varphi_1,t)\cdot\underline{n}^*(\varphi_2,t+\Delta t)\right\}\begin{cases}\neq 0 & ,\text{if } \varphi_1=\varphi_2\\ =0 & ,\text{if } \varphi_1\neq\varphi_2.\end{cases} \tag{3.6}$$

- Signals $\underline{n}(\varphi_1,t)$ and $\underline{n}(\varphi_2,t)$, received from different angle ranges $\varphi_1-\frac{\mathrm{d}\varphi}{2}...\varphi_1+\frac{\mathrm{d}\varphi}{2}$ and $\varphi_2-\frac{\mathrm{d}\varphi}{2}...\varphi_2+\frac{\mathrm{d}\varphi}{2}$, $\varphi_1\neq\varphi_2$, at an antenna with the beam width $\mathrm{d}\varphi$ are correlated. The following applies to the spatial and temporal correlation function of the intercell MAI signal $\underline{n}(\varphi,t)$ of (3.1):

$$\underline{R}_\mathrm{n}(\varphi_1,\varphi_2,\Delta t) = \mathrm{E}\left\{\underline{n}(\varphi_1,t)\cdot\underline{n}^*(\varphi_2,t+\Delta t)\right\}\neq 0 \quad ,\text{for any } \varphi_1,\varphi_2. \tag{3.7}$$

In both cases the intercell MAI can comprise:

- directionally purely discrete intercell MAI signals,
- directionally purely continuous intercell MAI signals,
- a combination of both that is discrete and continuous intercell MAI signals.

Investigations concerning the assignment of the intercell MAI power to the existing interference sources in a cellular system [Ste96] showed that most of the interference power that impinges at a RP of a cell under consideration originates from only a small number of interference sources. The remaining intercell MAI power comes from a large number of intercell MAI signals, each contributing only a small part to the total intercell MAI power σ^2. Based on this investigation into the intercell MAI signals, it can be assumed that the combination of the directionally discrete and continuous intercell MAI is the most realistic intercell MAI scenario. In this combined scenario the power σ_c^2 of the directionally continuous component must be smaller than the power σ_d^2 of the directionally discrete component which is received at an omnidirectional antenna at the RP. It is assumed below that the directionally continuous component and the directionally discrete component are directionally uncorrelated. Consequently, the total intercell MAI power is given by

$$\sigma^2 = \sigma_\mathrm{c}^2 + \sigma_\mathrm{d}^2. \tag{3.8}$$

With the DOAs $\gamma_\mathrm{i}^{(k_\mathrm{i})}$, $k_\mathrm{i} = 1 \ldots K_\mathrm{i}$, of the directional intercell MAI signals the azimuthal MAI density $\underline{n}_\varphi(\varphi, t)$ can be described by utilizing the azimuthal MAI density of the continuous component $\underline{n}_\mathrm{c}(\varphi, t)$ and of the directional component $\underline{n}_\mathrm{d}(\varphi, t)$ according to

$$\underline{n}_\varphi(\varphi, t) = \underline{n}_\mathrm{c}(\varphi, t) + \sum_{k_\mathrm{i}=1}^{K_\mathrm{i}} \underline{n}_\mathrm{d}(\varphi, t) \cdot \delta\left(\varphi - \gamma_\mathrm{i}^{(k_\mathrm{i})}\right). \tag{3.9}$$

Fig. 3.1 shows an example of the combination of the directionally continuous component and the directionally discrete component with three discrete intercell MAI signals with the DOAs $\gamma_\mathrm{i}^{(k_\mathrm{i})}$, $k_\mathrm{i} = 1 \ldots 3$ at a certain time t_0.

The following assumes an antenna array with K_a antenna elements at the BS site. The distance $l^{(k_\mathrm{a})}$ of the array element k_a to an assumed RP and the angle $\alpha^{(k_\mathrm{a})}$ have already been introduced in Section 2.3.1, see Fig. 2.1. The far-field conditions and the narrowband assumption which are mentioned in Section 2.3.1 apply equally to the interfering signals and the desired signals. Note that similar to (2.6) the narrowband assumption implies that the effect of a time delay τ on the received waveforms is simply a phase shift [RK89], i.e.

$$\underline{n}_\varphi(\varphi, t + \tau) \approx \underline{n}_\varphi(\varphi, t) \cdot \mathrm{e}^{\mathrm{j}2\pi f_\mathrm{c}\tau}, \quad \varphi \in [0 \ldots 2\pi[, \tag{3.10}$$

if f_c is the carrier frequency. From Fig. 3.2 it becomes obvious that according to (2.5) the phase shifts are given by

$$\phi(\varphi, k_\mathrm{a}) = \frac{2\pi}{\lambda} \cdot l^{(k_\mathrm{a})} \cdot \cos\left(\varphi - \alpha^{(k_\mathrm{a})}\right), \quad k_\mathrm{a} = 1 \ldots K_\mathrm{a}, \varphi \in [0 \ldots 2\pi[, \tag{3.11}$$

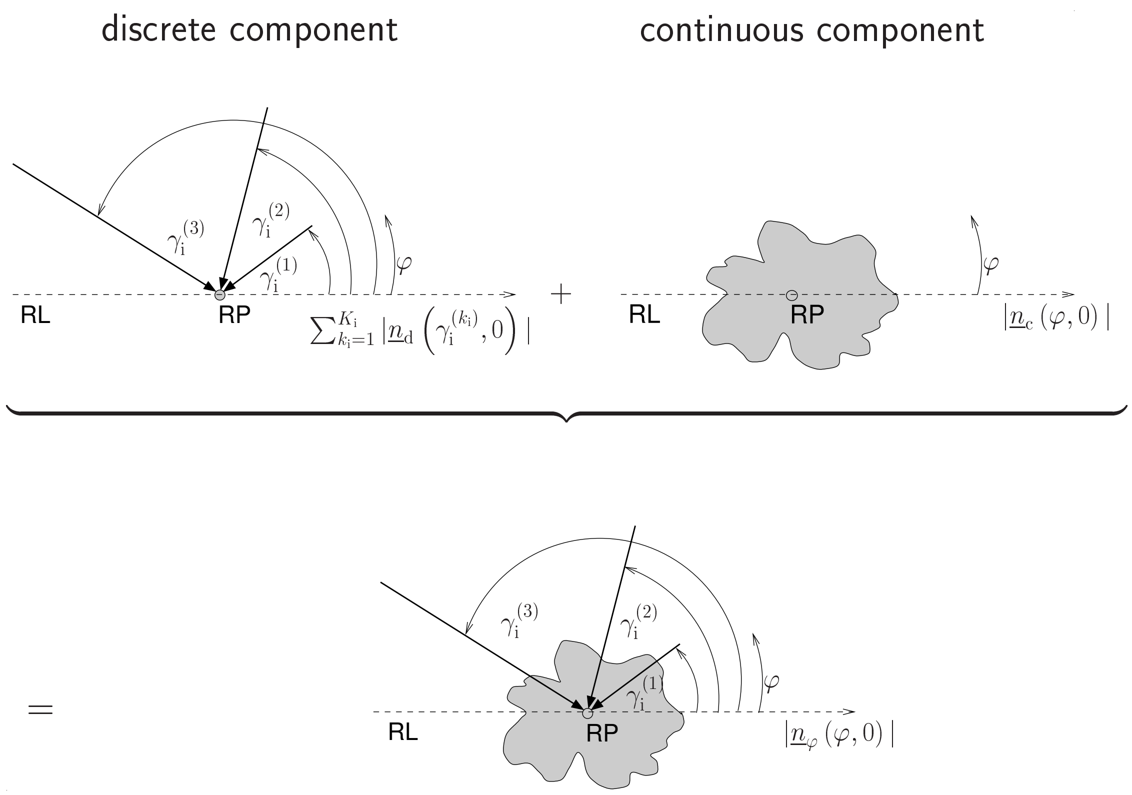

Fig. 3.1. General model with a discrete component which consists of $K_\mathrm{i} = 3$ intercell interferers and a continuous component

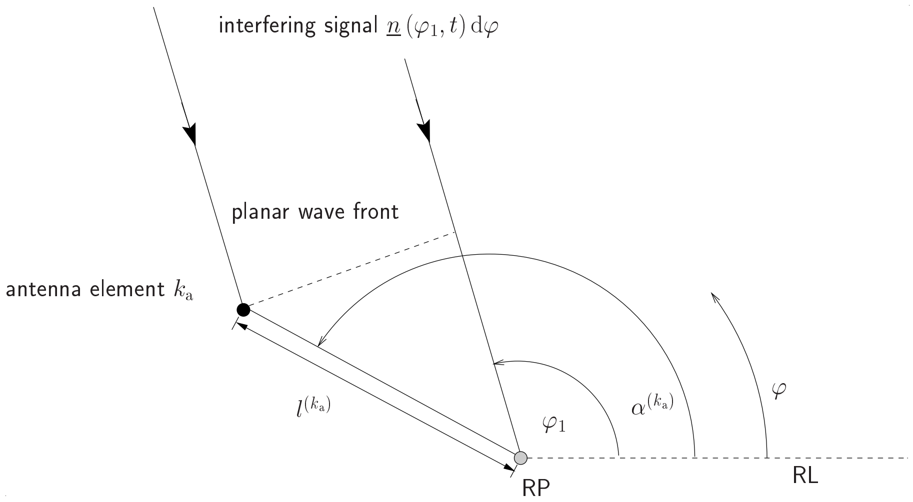

Fig. 3.2. Planar wave front of an intercell MAI signal impinging at the RP and the antenna element k_a [BPH99]

where λ is the carrier wavelength. Based on the density $\underline{n}_\varphi(\varphi, t)$ and considering the phase shifts $\phi(\varphi, k_\mathrm{a})$, $k_\mathrm{a} = 1...K_\mathrm{a}$, $\varphi \in [0...2\pi[$ of (3.11) we obtain the intercell MAI signal

$$\underline{n}^{(k_\mathrm{a})}(t) = \int_0^{2\pi} \underline{n}_\varphi(\varphi, t) \cdot \mathrm{e}^{\mathrm{j}\phi(\varphi, k_\mathrm{a})} \, \mathrm{d}\varphi, \tag{3.12}$$

which is received at the antenna element k_a having an omnidirectional beam pattern. From (3.3) and (3.12) we obtain the autocorrelation functions of the signals received at the antenna elements u and v

$$\underline{R}_\mathrm{n}^{(u,v)}(\Delta t) = \int_0^{2\pi} \int_0^{2\pi} \underline{R}_\varphi(\varphi_1, \varphi_2, \Delta t) \cdot \mathrm{e}^{\mathrm{j}(\phi(\varphi_1, u) - \phi(\varphi_2, v))} \, \mathrm{d}\varphi_2 \, \mathrm{d}\varphi_1, \quad u, v = 1...K_\mathrm{a}. \tag{3.13}$$

Now, only the time-discrete representation of the signals is considered with the objective of describing the correlation functions given by (3.6), (3.7) and (3.13) by covariance matrices. In opposite to the correlation matrix $\underline{\mathbf{R}}_{\tau,\mathrm{s}}$ of (2.12) these matrices are called covariance matrices, since the intercell MAI signals are assumed to be mean–free [Pap65]. The intercell MAI at the RP is temporally sampled by the chiprate $1/T_\mathrm{c}$ in order to obtain the samples

$$\underline{n}_{\mathrm{RP},s}(\varphi) = \underline{n}_\varphi(\varphi, (s-1) T_\mathrm{c}) \, \mathrm{d}\varphi, \quad s = 1...S, \tag{3.14}$$

which are dependent on the azimuth angle φ. With the samples $\underline{n}_{\mathrm{RP},s}(\varphi)$, $s = 1...S$, $\varphi \in [0...2\pi[$ of (3.14) each intercell MAI signal at the RP can be represented by the interference vectors

$$\underline{\mathbf{n}}_\mathrm{RP}(\varphi) = \left[\underline{n}_{\mathrm{RP},1}(\varphi) ... \underline{n}_{\mathrm{RP},S}(\varphi)\right]^\mathrm{T}, \ \ \varphi \in [0...2\pi[, \tag{3.15}$$

where each component of the vectors is a function of the azimuth angle φ and where S is the number of considered samples of the intercell MAI signal. According to the relation between $\underline{n}(\varphi, t)$ and $\underline{n}_\varphi(\varphi, t)$ given by (3.1) and considering (3.14) and (3.15) the azimuthal MAI density vector $\underline{\mathbf{n}}_\varphi(\varphi)$ can be defined by

$$\underline{\mathbf{n}}_\mathrm{RP}(\varphi) = \underline{\mathbf{n}}_\varphi(\varphi) \, \mathrm{d}\varphi. \tag{3.16}$$

With (3.5) the vectors of (3.15) can be normalized by

$$\underline{\tilde{\mathbf{n}}}_\mathrm{RP}(\varphi) = \frac{1}{\sqrt{\underline{R}_\varphi(\varphi, \varphi, 0) \, \mathrm{d}\varphi}} \underline{\mathbf{n}}_\mathrm{RP}(\varphi) \tag{3.17}$$

and we obtain

$$\underline{\tilde{\mathbf{n}}}_\mathrm{RP}(\varphi) = \frac{1}{\sqrt{\underline{R}_\varphi(\varphi, \varphi, 0)}} \underline{\mathbf{n}}_\varphi(\varphi) \tag{3.18}$$

by taking (3.16) into account. As already mentioned at the beginning of this section, independent of the azimuth angle φ all intercell MAI signals have the same spectral form.

Therefore, the normalized intercell MAI vectors $\underline{\tilde{\mathbf{n}}}_{\mathrm{RP}}(\varphi)$, $\varphi \in [0...2\pi[$, of (3.18) have the same normalized temporal covariance matrix

$$\begin{aligned}
\underline{\tilde{\mathbf{R}}}_{\mathrm{t}} &= \mathrm{E}\left\{\begin{pmatrix} \underline{\tilde{n}}_{\mathrm{RP},1}(\varphi) \\ \vdots \\ \underline{\tilde{n}}_{\mathrm{RP},S}(\varphi) \end{pmatrix} \cdot \left(\underline{\tilde{n}}^*_{\mathrm{RP},1}(\varphi) \ldots \underline{\tilde{n}}^*_{\mathrm{RP},S}(\varphi)\right)\right\} \\
&= \begin{bmatrix} \mathrm{E}\left\{\underline{\tilde{n}}_{\mathrm{RP},1}(\varphi)\cdot\underline{\tilde{n}}^*_{\mathrm{RP},1}(\varphi)\right\} & \ldots & \mathrm{E}\left\{\underline{\tilde{n}}_{\mathrm{RP},1}(\varphi)\cdot\underline{\tilde{n}}^*_{\mathrm{RP},S}(\varphi)\right\} \\ \vdots & \ddots & \vdots \\ \mathrm{E}\left\{\underline{\tilde{n}}_{\mathrm{RP},S}(\varphi)\cdot\underline{\tilde{n}}^*_{\mathrm{RP},1}(\varphi)\right\} & \ldots & \mathrm{E}\left\{\underline{\tilde{n}}_{\mathrm{RP},S}(\varphi)\cdot\underline{\tilde{n}}^*_{\mathrm{RP},S}(\varphi)\right\} \end{bmatrix}, \\
&\quad \varphi = [0...2\pi[, \qquad (3.19)
\end{aligned}$$

of the dimension $S \times S$. Consequently, the cross-correlations of two intercell MAI signals impinging from φ_1 and φ_2 can be represented by the normalized temporal $S\times S$ covariance matrix

$$\begin{aligned}
\underline{\tilde{\mathbf{R}}}_{\mathrm{RP}}(\varphi_1,\varphi_2) &= \mathrm{E}\left\{\begin{pmatrix} \underline{\tilde{n}}_{\mathrm{RP},1}(\varphi_1) \\ \vdots \\ \underline{\tilde{n}}_{\mathrm{RP},S}(\varphi_1) \end{pmatrix} \cdot \left(\underline{\tilde{n}}^*_{\mathrm{RP},1}(\varphi_2) \ldots \underline{\tilde{n}}^*_{\mathrm{RP},S}(\varphi_2)\right)\right\} \\
&= \begin{bmatrix} \mathrm{E}\left\{\underline{\tilde{n}}_{\mathrm{RP},1}(\varphi_1)\cdot\underline{\tilde{n}}^*_{\mathrm{RP},1}(\varphi_2)\right\} & \ldots & \mathrm{E}\left\{\underline{\tilde{n}}_{\mathrm{RP},1}(\varphi_1)\cdot\underline{\tilde{n}}^*_{\mathrm{RP},S}(\varphi_2)\right\} \\ \vdots & \ddots & \vdots \\ \mathrm{E}\left\{\underline{\tilde{n}}_{\mathrm{RP},S}(\varphi_1)\cdot\underline{\tilde{n}}^*_{\mathrm{RP},1}(\varphi_2)\right\} & \ldots & \mathrm{E}\left\{\underline{\tilde{n}}_{\mathrm{RP},S}(\varphi_1)\cdot\underline{\tilde{n}}^*_{\mathrm{RP},S}(\varphi_2)\right\} \end{bmatrix}, \\
&\quad \varphi_1,\varphi_2 = [0...2\pi[. \qquad (3.20)
\end{aligned}$$

The intercell MAI vector, which represents the MAI signal received at the antenna element k_{a}, is related according to (3.12) to the intercell MAI density vectors $\underline{\mathbf{n}}_{\varphi}(\varphi)$, $\varphi = [0...2\pi[$, of (3.16) via

$$\underline{\mathbf{n}}^{(k_{\mathrm{a}})} = \int_0^{2\pi} \underline{\mathbf{n}}_{\varphi}(\varphi)\cdot \mathrm{e}^{\mathrm{j}\phi(\varphi,k_{\mathrm{a}})}\,\mathrm{d}\varphi, \quad k_{\mathrm{a}} = 1...K_{\mathrm{a}}, \qquad (3.21)$$

[Bla98]. The covariance matrix of the intercell MAI vectors $\underline{\mathbf{n}}^{(u)}$ of the array element u and $\underline{\mathbf{n}}^{(v)}$ of the array element v is denoted by

$$\underline{\mathbf{R}}_{\mathrm{n}}^{(u,v)} = \mathrm{E}\{\underline{\mathbf{n}}^{(u)}\,\underline{\mathbf{n}}^{(v)*\mathrm{T}}\}, \quad u,v = 1...K_{\mathrm{a}}. \qquad (3.22)$$

Under consideration of (3.18), (3.20) and (3.21) the $S\times S$ matrices $\underline{\mathbf{R}}_{\mathrm{n}}^{(u,v)}$, $u,v = 1...K_{\mathrm{a}}$, of (3.22) can also be written as

$$\begin{aligned}
&\underline{\mathbf{R}}_{\mathrm{n}}^{(u,v)} \\
=\;& \mathrm{E}\left\{\left(\int_0^{2\pi} \underline{\mathbf{n}}_{\varphi}(\varphi_1)\cdot \mathrm{e}^{\mathrm{j}\phi(\varphi_1,u)}\,\mathrm{d}\varphi_1\right)\cdot\left(\int_0^{2\pi} \underline{\mathbf{n}}_{\varphi}^{*\mathrm{T}}(\varphi_2)\cdot \mathrm{e}^{-\mathrm{j}\phi(\varphi_2,v)}\,\mathrm{d}\varphi_2\right)\right\} \\
=\;& \int_0^{2\pi}\int_0^{2\pi} \mathrm{E}\left\{\underline{\mathbf{n}}_{\varphi}(\varphi_1)\cdot\underline{\mathbf{n}}_{\varphi}^{*\mathrm{T}}(\varphi_2)\right\}\cdot \mathrm{e}^{\mathrm{j}(\phi(\varphi_1,u)-\phi(\varphi_2,v))}\,\mathrm{d}\varphi_2\,\mathrm{d}\varphi_1 \\
=\;& \int_0^{2\pi}\int_0^{2\pi} \sqrt{\underline{R}_{\varphi}(\varphi_1,\varphi_1,0)\cdot\underline{R}_{\varphi}(\varphi_2,\varphi_2,0)}\cdot \mathrm{E}\left\{\underline{\tilde{\mathbf{n}}}_{\mathrm{RP}}(\varphi_1)\cdot\underline{\tilde{\mathbf{n}}}_{\mathrm{RP}}^{*\mathrm{T}}(\varphi_2)\right\} \\
&\cdot \mathrm{e}^{\mathrm{j}(\phi(\varphi_1,u)-\phi(\varphi_2,v))}\,\mathrm{d}\varphi_2\,\mathrm{d}\varphi_1 \\
=\;& \int_0^{2\pi}\int_0^{2\pi} \sqrt{\underline{R}_{\varphi}(\varphi_1,\varphi_1,0)\cdot\underline{R}_{\varphi}(\varphi_2,\varphi_2,0)}\cdot\underline{\tilde{\mathbf{R}}}_{\mathrm{RP}}(\varphi_1,\varphi_2)\cdot \mathrm{e}^{\mathrm{j}(\phi(\varphi_1,u)-\phi(\varphi_2,v))}\,\mathrm{d}\varphi_2\,\mathrm{d}\varphi_1, \\
& u,v = 1...K_{\mathrm{a}},
\end{aligned} \tag{3.23}$$

which represents (3.13) by using a matrix notation.

Finally, the general correlation functions of (3.6) and (3.7) can also be represented by a matrix. Therefore, the total intercell MAI vector

$$\underline{\mathbf{n}} = \left[\underline{\mathbf{n}}^{(1)\mathrm{T}}...\underline{\mathbf{n}}^{(K_{\mathrm{a}})\mathrm{T}}\right]^{\mathrm{T}}, \tag{3.24}$$

of dimension SK_{a} can be used, which is a concatenation of all K_{a} intercell MAI vectors $\underline{\mathbf{n}}^{(k_{\mathrm{a}})}$, $k_{\mathrm{a}} = 1...K_{\mathrm{a}}$, of (3.21), which are received at the K_{a} antenna elements. The corresponding total intercell MAI covariance matrix [Bla98]

$$\begin{aligned}
\underline{\mathbf{R}}_{\mathrm{n}} &= \mathrm{E}\left\{\underline{\mathbf{n}}\,\underline{\mathbf{n}}^{*\mathrm{T}}\right\} \\
&= \mathrm{E}\left\{\begin{pmatrix}\underline{\mathbf{n}}^{(1)} \\ \vdots \\ \underline{\mathbf{n}}^{(K_{\mathrm{a}})}\end{pmatrix}\cdot\left(\underline{\mathbf{n}}^{(1)*\mathrm{T}}...\underline{\mathbf{n}}^{(K_{\mathrm{a}})*\mathrm{T}}\right)\right\}
\end{aligned} \tag{3.25}$$

of the total intercell MAI vector $\underline{\mathbf{n}}$ of (3.24) with the dimension $(K_{\mathrm{a}}S)\times(K_{\mathrm{a}}S)$ can be expressed under consideration of the partial matrices $\underline{\mathbf{R}}_{\mathrm{n}}^{(u,v)}$, $u,v = 1...K_{\mathrm{a}}$, described by (3.23), as

$$\underline{\mathbf{R}}_{\mathrm{n}} = \begin{bmatrix} \underline{\mathbf{R}}_{\mathrm{n}}^{(1,1)} & \cdots & \underline{\mathbf{R}}_{\mathrm{n}}^{(1,K\mathrm{a})} \\ \vdots & \ddots & \vdots \\ \underline{\mathbf{R}}_{\mathrm{n}}^{(K_{\mathrm{a}},1)} & \cdots & \underline{\mathbf{R}}_{\mathrm{n}}^{(K\mathrm{a},K\mathrm{a})} \end{bmatrix}. \tag{3.26}$$

If we assume that the intercell MAI signals $\underline{\mathbf{n}}_{\mathrm{RP}}(\varphi)$, $\varphi = [0...2\pi[$, of (3.15) are uncorrelated, i.e.,

$$\underline{\tilde{\mathbf{R}}}_{\mathrm{RP}}(\varphi_1,\varphi_2) = \begin{cases} \underline{\tilde{\mathbf{R}}}_{\mathrm{t}} & ,\text{if } \varphi_1 = \varphi_2 \\ 0 & ,\text{if } \varphi_1 \neq \varphi_2 \end{cases}, \tag{3.27}$$

(3.23) takes the simple form

$$\underline{\mathbf{R}}_{\mathrm{n}}^{(u,v)} = \tilde{\underline{\mathbf{R}}}_{\mathrm{t}} \cdot \int_0^{2\pi} \underline{R}_{\varphi}\left(\varphi,\varphi,0\right) \cdot \mathrm{e}^{\mathrm{j}(\phi(\varphi,u)-\phi(\varphi,v))}\,\mathrm{d}\varphi, \quad u,v=1...K_{\mathrm{a}}. \tag{3.28}$$

With the scalars

$$\underline{r}^{(u,v)} = \underline{r}^{(v,u)*} = \int_0^{2\pi} \underline{R}_{\varphi}\left(\varphi,\varphi,0\right) \cdot \mathrm{e}^{\mathrm{j}(\phi(\varphi,u)-\phi(\varphi,v))}\,\mathrm{d}\varphi, \quad u,v=1...K_{\mathrm{a}}, \tag{3.29}$$

the partial covariance matrices $\underline{\mathbf{R}}_{\mathrm{n}}^{(u,v)}$, $u,v=1...K_{\mathrm{a}}$, of (3.23) of the total covariance matrix $\underline{\mathbf{R}}_{\mathrm{n}}$ of (3.25) can be written as

$$\underline{\mathbf{R}}_{\mathrm{n}}^{(u,v)} = \underline{r}^{(u,v)} \cdot \tilde{\underline{\mathbf{R}}}_{\mathrm{t}}, \quad u,v=1...K_{\mathrm{a}}. \tag{3.30}$$

As an example, a combination of a directional intercell MAI scenario with K_{i} discrete interferers having the powers $\left(\sigma^{(k_{\mathrm{i}})}\right)^2$, $k_{\mathrm{i}}=1...K_{\mathrm{i}}$, and the DOAs $\gamma_{\mathrm{i}}^{(k_{\mathrm{i}})}$, $k_{\mathrm{i}}=1...K_{\mathrm{i}}$, and a continuous intercell MAI scenario is considered. Assuming directionally uncorrelated intercell MAI and considering (3.3) and (3.9) we obtain

$$\underline{R}_{\varphi}\left(\varphi,\varphi,0\right) = \mathrm{E}\left\{\left|\underline{n}_{\mathrm{c}}\left(\varphi,t\right)\right|^2\right\} + \sum_{k_{\mathrm{i}}=1}^{K_{\mathrm{i}}} \mathrm{E}\left\{\left|\underline{n}_{\mathrm{d}}\left(\varphi,t\right)\right|^2\right\} \cdot \delta\left(\varphi-\gamma_{\mathrm{i}}^{(k_{\mathrm{i}})}\right), \quad \varphi\in[0...2\pi[. \tag{3.31}$$

With the azimuth power density

$$\rho_{\mathrm{c}}\left(\varphi\right) = \mathrm{E}\left\{\left|\underline{n}_{\mathrm{c}}\left(\varphi,t\right)\right|^2\right\}, \quad \varphi\in[0...2\pi[, \tag{3.32}$$

of the continuous component and with the interference powers

$$\left(\sigma^{(k_{\mathrm{i}})}\right)^2 = \int_0^{2\pi} \mathrm{E}\left\{\left|\underline{n}_{\mathrm{d}}\left(\gamma_{\mathrm{i}}^{(k_{\mathrm{i}})},t\right)\right|^2\right\} \cdot \delta\left(\varphi-\gamma_{\mathrm{i}}^{(k_{\mathrm{i}})}\right)\,\mathrm{d}\varphi, \quad k_{\mathrm{i}}=1...K_{\mathrm{i}}, \tag{3.33}$$

of the intercell MAI signals of the discrete component and considering (3.31), the scalars of (3.29) become

$$\begin{aligned}
\underline{r}^{(u,v)} &= \int_0^{2\pi} \left[\sum_{k_{\mathrm{i}}=1}^{K_{\mathrm{i}}} \mathrm{E}\left\{\left|\underline{n}_{\mathrm{d}}\left(\varphi,t\right)\right|^2\right\} \cdot \delta\left(\varphi-\gamma_{\mathrm{i}}^{(k_{\mathrm{i}})}\right) + \rho_{\mathrm{c}}\left(\varphi\right)\right] \cdot \mathrm{e}^{\mathrm{j}(\phi(\varphi,u)-\phi(\varphi,v))}\,\mathrm{d}\varphi \\
&= \underbrace{\sum_{k_{\mathrm{i}}=1}^{K_{\mathrm{i}}} \left(\sigma^{(k_{\mathrm{i}})}\right)^2 \cdot \mathrm{e}^{\mathrm{j}\left(\phi\left(\gamma_{\mathrm{i}}^{(k_{\mathrm{i}})},u\right)-\phi\left(\gamma_{\mathrm{i}}^{(k_{\mathrm{i}})},v\right)\right)}}_{\text{directional component}} \\
&\quad + \underbrace{\int_0^{2\pi} \rho_{\mathrm{c}}\left(\varphi\right) \cdot \mathrm{e}^{\mathrm{j}(\phi(\varphi,u)-\phi(\varphi,v))}\,\mathrm{d}\varphi,}_{\text{continuous component}} \quad u,v=1...K_{\mathrm{a}}.
\end{aligned} \tag{3.34}$$

Depending on which of the three interference scenarios - namely purely directional, purely continuous or a combination of both - is considered, the scalars $\underline{r}^{(u,v)}$, $u, v = 1...K_{\mathrm{a}}$, of (3.34) consist of a directional component and/or a continuous component. Due to (3.26) and (3.30), the total covariance matrix $\underline{\mathbf{R}}_{\mathrm{n}}$ of (3.25) can now be expressed as

$$\underline{\mathbf{R}}_{\mathrm{n}} = \begin{bmatrix} \underline{r}^{(1,1)} \cdot \tilde{\underline{\mathbf{R}}}_{\mathrm{t}} & \ldots & \underline{r}^{(1,K_{\mathrm{a}})} \cdot \tilde{\underline{\mathbf{R}}}_{\mathrm{t}} \\ \vdots & \ddots & \vdots \\ \underline{r}^{(1,K_{\mathrm{a}})*} \cdot \tilde{\underline{\mathbf{R}}}_{\mathrm{t}} & \ldots & \underline{r}^{(K_{\mathrm{a}},K_{\mathrm{a}})} \cdot \tilde{\underline{\mathbf{R}}}_{\mathrm{t}} \end{bmatrix}. \tag{3.35}$$

Since the scalars $\underline{r}^{(u,v)}$, $u, v = 1...K_{\mathrm{a}}$, of (3.29) represent the spatial correlations of the intercell MAI signals $\underline{\mathbf{n}}^{(k_{\mathrm{a}})}$, $k_{\mathrm{a}} = 1 \ldots K_{\mathrm{a}}$, received at the K_{a} antenna elements, a spatial covariance matrix

$$\underline{\mathbf{R}}_{\mathrm{s}} = \begin{bmatrix} \underline{r}^{(1,1)} & \ldots & \underline{r}^{(1,K_{\mathrm{a}})} \\ \vdots & \ddots & \vdots \\ \underline{r}^{(1,K_{\mathrm{a}})*} & \ldots & \underline{r}^{(K_{\mathrm{a}},K_{\mathrm{a}})} \end{bmatrix} \tag{3.36}$$

of the intercell MAI of dimension $K_{\mathrm{a}} \times K_{\mathrm{a}}$ can be established. The elements $\underline{r}^{(u,v)}$, $u, v = 1...K_{\mathrm{a}}$, of the matrix $\underline{\mathbf{R}}_{\mathrm{s}}$ of (3.36) include the phase factors $\phi(\varphi, k_{\mathrm{a}})$, $\varphi \in [0...2\pi[$, $k_{\mathrm{a}} = 1...K_{\mathrm{a}}$, given in (3.11). Therefore, the matrix $\underline{\mathbf{R}}_{\mathrm{s}}$ of (3.36) contains information concerning the directional properties of the intercell MAI. Utilizing the Kronecker product [Gra81], (3.35) takes the form [Bla98, WP99c, Pap00]

$$\underline{\mathbf{R}}_{\mathrm{n}} = \underline{\mathbf{R}}_{\mathrm{s}} \otimes \tilde{\underline{\mathbf{R}}}_{\mathrm{t}} \,. \tag{3.37}$$

From (3.35) and (3.37) it becomes obvious that the temporal correlations are the same at the K_{a} antenna elements, since the normalized temporal covariance matrix $\tilde{\underline{\mathbf{R}}}_{\mathrm{t}}$ is the same at each antenna element. In order to obtain the intercell MAI vectors

$$\underline{\mathbf{n}}^{(k_{\mathrm{a}})} = \left[\underline{n}_1^{(k_{\mathrm{a}})} ... \underline{n}_{\mathrm{S}}^{(k_{\mathrm{a}})}\right]^{\mathrm{T}}, \quad k_{\mathrm{a}} = 1...K_{\mathrm{a}}, \tag{3.38}$$

of (3.21), which are finally required for the simulations, first K_{a} vectors $\underline{\mathbf{n}}_{\mathrm{RP,k_a}}$, $k_{\mathrm{a}} = 1...K_{\mathrm{a}}$, of dimension S are taken from a zero-mean, stationary Gaussian process and are filtered with the GMSK chip impulse. After vectors $\underline{\mathbf{n}}_{\mathrm{RP,k_a}}$, $k_{\mathrm{a}} = 1...K_{\mathrm{a}}$ have been filtered, they are arranged in a $K_{\mathrm{a}} \times S$ matrix as follows:

$$\underline{\mathbf{N}}_{\mathrm{RP}} = \begin{bmatrix} \underline{\mathbf{n}}_{\mathrm{RP,1}}^{\mathrm{T}} \\ \vdots \\ \underline{\mathbf{n}}_{\mathrm{RP,K_a}}^{\mathrm{T}} \end{bmatrix}. \tag{3.39}$$

With the Cholesky decomposition

$$\underline{\mathbf{R}}_{\mathrm{s}} = \underline{\mathbf{L}}_{\mathrm{s}} \cdot \underline{\mathbf{L}}_{\mathrm{s}}^{*\mathrm{T}} \tag{3.40}$$

of the spatial covariance matrix $\underline{\mathbf{R}}_\mathrm{s}$ of (3.36), we obtain the $K_\mathrm{a} \times K_\mathrm{a}$ triangular matrix $\underline{\mathbf{L}}_\mathrm{s}$, which can be utilized to obtain the $K_\mathrm{a} \times S$ matrix

$$\underline{\mathbf{N}} = \underline{\mathbf{L}}_\mathrm{s} \cdot \underline{\mathbf{N}}_\mathrm{RP}^\mathrm{T}, \tag{3.41}$$

the rows of which contain the spatially and temporally correlated vectors $\underline{\mathbf{n}}^{(k_\mathrm{a})}$, $k_\mathrm{a} = 1...K_\mathrm{a}$, of (3.38). The concatenation according to (3.24) of the vectors $\underline{\mathbf{n}}^{(k_\mathrm{a})}$, $k_\mathrm{a} = 1...K_\mathrm{a}$, obtained via (3.41), forms the total intercell MAI vector $\underline{\mathbf{n}}$, which has the desired covariance matrix $\underline{\mathbf{R}}_\mathrm{n}$ of (3.26). From (3.19), (3.37), and (3.39) to (3.41) it becomes obvious that in the case of uncorrelated intercell MAI only the spatial covariance matrix $\underline{\mathbf{R}}_\mathrm{s}$ is required in order to characterize a certain intercell MAI scenario derived from this general model, since at least $\underline{\tilde{\mathbf{R}}}_\mathrm{t}$ from (3.19) is the same for all possible variations of the general model and, according to (3.19) also $\underline{\tilde{\mathbf{R}}}_\mathrm{t}$ is known.

So far, only directionally uncorrelated intercell MAI signals have been considered. In the following directional correlations of the intercell MAI signals are taken into account. Correlation of the intercell MAI can mean that a number of intercell MAI signals originate from the same source, i.e. are attributable to the same transmit signal of an interferer, and arrive at the RP by different paths with different DOAs. The multipath propagation means that different delayed versions of the same interference signal can arrive at the RP under different DOAs. The assumption was made at the start of the chapter that the relationship between the time delays of the different versions of an interference signal coming from a direction φ are constantly changing. The assumption made below is that specific time-delayed versions of an interference signal coming from different directions $\varphi_1 \neq \varphi_2$ have a fixed delay relationship to each other. Fig. 3.3 gives an impression of how the correlations can occur by having two times the same signal relatively delayed with respect to each other. The difference of the sum of the partial distances $d_1\,(m)$ and $d_2\,(m)$

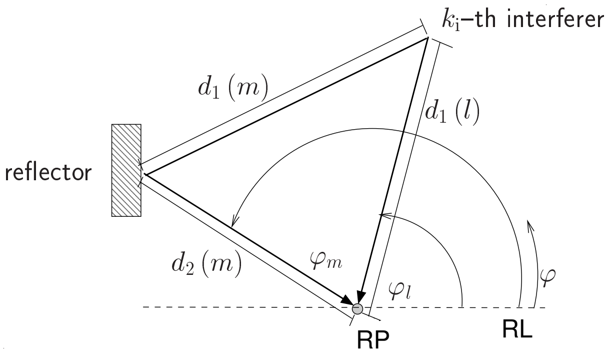

Fig. 3.3. Typical propagation scenario leading to correlations of the l–th and the m–th intercell MAI signal originating from the k_i–th interferer

of the m–th signal and the distance $d_1\,(l)$ of the l–th signal

$$\Delta d = (d_1\,(m) + d_2\,(m)) - d_1\,(l) \tag{3.42}$$

leads to a phase shift

$$\theta(l,m) = 2\pi \frac{\Delta d}{\lambda} \tag{3.43}$$

between the m–th and the l–th signal. For modeling the intercell MAI with correlated interference signals on the basis of overlaying of different time-delayed versions of the same interference signal, there are three distinct cases:

1. The relative delays of the different versions of the same interference signal are smaller than the half chiprate $T_\mathrm{c}/2$. As a result of discrete signal transmission the correlation function of the receive signals at the antenna element u and v $\underline{R}_\mathrm{n}^{(u,v)}(\Delta t)$ can be represented as shown in (3.13). If it is assumed that the receive signal m is correlated with the receive signal l at the RP, the receive signals m and l at the RP differ only in their power $\left(\sigma^{(l)}\right)^2$ and $\left(\sigma^{(m)}\right)^2$ according to (3.33) as well as through their DOAs φ_l and φ_m, see Fig. 3.3. The receive signal m is thus produced from the receive signal l for

$$\underline{\mathbf{n}}_\mathrm{RP}(\varphi_m) = \sqrt{\frac{\underline{R}_\varphi(\varphi_m,\varphi_m,0)}{\underline{R}_\varphi(\varphi_l,\varphi_l,0)}} \cdot \underline{\mathbf{n}}_\mathrm{RP}(\varphi_l), \quad \varphi_l,\varphi_m = [0...2\pi[. \tag{3.44}$$

Since signals $\underline{\mathbf{n}}_\mathrm{RP}(\varphi_l)$ and $\underline{\mathbf{n}}_\mathrm{RP}(\varphi_m)$ only differ in their power and not in their spectral form, the following is obtained taking account of (3.44) for covariance matrices according to (3.23)

$$\begin{aligned}\underline{\mathbf{R}}_\mathrm{n}^{(u,v)} &= \tilde{\underline{\mathbf{R}}}_\mathrm{t} \cdot \int_0^{2\pi}\int_0^{2\pi} \sqrt{\underline{R}_\varphi(\varphi_l,\varphi_l,0)\cdot \underline{R}_\varphi(\varphi_m,\varphi_m,0)} \cdot \mathrm{e}^{\mathrm{j}(\phi(\varphi_l,u)-\phi(\varphi_m,v))}\,\mathrm{d}\varphi_l\,\mathrm{d}\varphi_m,\\ & \quad u,v = 1...K_\mathrm{a}.\end{aligned} \tag{3.45}$$

According to (3.26) the total covariance matrix $\underline{\mathbf{R}}_\mathrm{n}$ with the partial matrices $\underline{\mathbf{R}}_\mathrm{n}^{(u,v)}$, $u,v = 1...K_\mathrm{a}$, of (3.45) can be obtained. From (3.45) it becomes obvious that the total covariance matrix $\underline{\mathbf{R}}_\mathrm{n}$ can be split up into a spatial covariance matrix $\underline{\mathbf{R}}_\mathrm{s}$ according to (3.36) - including the scalars

$$\begin{aligned}\underline{r}^{(u,v)} &= \int_0^{2\pi}\int_0^{2\pi} \sqrt{\underline{R}_\varphi(\varphi_l,\varphi_l,0)\cdot \underline{R}_\varphi(\varphi_m,\varphi_m,0)} \cdot \mathrm{e}^{\mathrm{j}(\phi(\varphi_l,u)-\phi(\varphi_m,v))}\,\mathrm{d}\varphi_l\,\mathrm{d}\varphi_m,\\ & \quad u,v = 1...K_\mathrm{a},\end{aligned} \tag{3.46}$$

– and a normalized temporal covariance matrix $\tilde{\underline{\mathbf{R}}}_\mathrm{t}$ of (3.19) by the Kronecker product according to (3.37). If $\underline{\mathbf{R}}_\mathrm{s}$ is known, the intercell MAI vectors $\underline{\mathbf{n}}^{(k_\mathrm{a})}$, $k_\mathrm{a} = 1...K_\mathrm{a}$, of (3.38) received at the K_a antenna elements according to the procedure described by the equations (3.39), (3.40) and (3.41) in Section 3.2 can be obtained.

2. The relative delays of the different versions of the same interference signal are greater than the duration of the GMSK chip pulse of $5T_\mathrm{c}$ [ETSI97]. The different versions of the same interference signal can be viewed as uncorrelated in this case. The intercell MAI is modelled in this case in a similar way to the modelling of uncorrelated intercell MAI described above.

3. The relative delays of the different versions of the same interference signal are greater than half the chiprate $T_c/2$ and less than the duration of the GMSK chip impulse of $5T_c$ [ETSI97], i.e. the relative delays of the different interference signals of a source must be taken into account as well in interference modelling. To simplify modelling only a small number K_i of interference sources will be assumed in this case. The interference signals of the K_i interference sources propagate over K_d paths to the RP. The intercell MAI signal k_d which comes from the source k_i can be described according to (3.15) with vector $\underline{\mathbf{n}}_{\mathrm{RP}}^{(k_i,k_d)}$ of dimension S. The interference signals $\underline{\mathbf{n}}_{\mathrm{RP}}^{(k_i,k_d)}$, $k_i = 1...K_i$, $k_d = 1...K_d$ have the DOAs $\gamma_i^{(k_i,k_d)}$, $k_i = 1...K_i$, $k_d = 1...K_d$, at the RP and in line with (3.33) powers $\left(\sigma^{(k_i,k_d)}\right)^2$, $k_i = 1...K_i$, $k_d = 1...K_d$. For modeling the temporal correlations of the sum signals which are produced, by overlaying the $\underline{\mathbf{n}}_{\mathrm{RP}}^{(k_i,k_d)}$, $k_i = 1...K_i$, $k_d = 1...K_d$, signals at the RP only the relative delays are relevant. This means that without restricting general applicability, interference signals $\underline{\mathbf{n}}_{\mathrm{RP}}^{(k_i,1)}$, $k_i = 1...K_i$ can be assigned the relative delay time

$$t^{(k_i,1)} = 0, \quad k_i = 1...K_i. \tag{3.47}$$

The remaining $K_d - 1$ interference signals of the source k_i are assigned according to their increasing relative delay time $t^{(k_i,k_d)} < t^{(k_i,k_d+1)}$, $k_d = 1...K_d - 1$ with ascending number k_d. This means that the version K_d of the interference signal originating from the source k_i is the version which is relatively delayed the longest. Only integer multiples of chip duration T_c are assumed as possible relative delay times, i.e.

$$\begin{aligned} t^{(k_i,k_d)} = q^{(k_i,k_d)} \cdot T_c, \quad q^{(k_i,k_d)} &= \left\{q^{(k_i,k_d)} \in \mathbb{N} \mid 0 \le q^{(k_i,k_d)} \le 5\right\}, \\ k_i &= 1...K_i, k_d = 1...K_d. \end{aligned} \tag{3.48}$$

For modelling the relative delays of the K_d versions of the intercell MAI signal originating from the source k_i, the starting point is a vectors $\underline{\mathbf{n}}_{\mathrm{v}}^{(k_i,K_d)}$ which contains $S + q^{(k_i,K_d)}$ samples of a Gaussian process filtered with the GMSK chip pulse. With carrier frequency f_c $K_d - 1$ further vectors are formed by

$$\begin{aligned} \underline{n}_{\mathrm{v},s}^{(k_i,k_d-1)} &= \frac{\sigma^{(k_i,k_d-1)}}{\sigma^{(k_i,k_d)}} \cdot \underline{n}_{\mathrm{v},s+q^{(k_i,k_d)}}^{(k_i,k_d)} \cdot \mathrm{e}^{\mathrm{j}2\pi f_c q^{(k_i,k_d)} T_c}, \\ & s = 1...S, k_i = 1...K_i, k_d = 2...K_d, \end{aligned} \tag{3.49}$$

in which case vectors $\underline{\mathbf{n}}_{\mathrm{v}}^{(k_i,k_d)}$, $k_i = 1...K_i$, $k_d = 1...K_d + 1$ have dimension $S + q^{(k_i,k_d)}$, $k_i = 1...K_i$, $k_d = 1...K_d$. Fig. 3.4 clarifies the relationship of the elements of the vectors $\underline{\mathbf{n}}_{\mathrm{v}}^{(k_i,k_d)}$, $k_i = 1...K_i$, $k_d = 1...K_d$ described by (3.49). The first S elements of vectors $\underline{\mathbf{n}}_{\mathrm{v}}^{(k_i,k_d)}$, $k_i = 1...K_i$, $k_d = 1...K_d$, in each case correspond to the elements

$$\underline{n}_{\mathrm{RP},s}^{(k_i,k_d)} = \underline{n}_{\mathrm{v},s}^{(k_i,k_d)} \quad s = 1...S, k_i = 1...K_i, k_d = 1...K_d, \tag{3.50}$$

which make up the vectors $\underline{\mathbf{n}}_{\mathrm{RP}}^{(k_i,k_d)}$, $k_i = 1...K_i$, $k_d = 1...K_d$. The signals required for interference simulation which are received at the K_a antenna elements of the

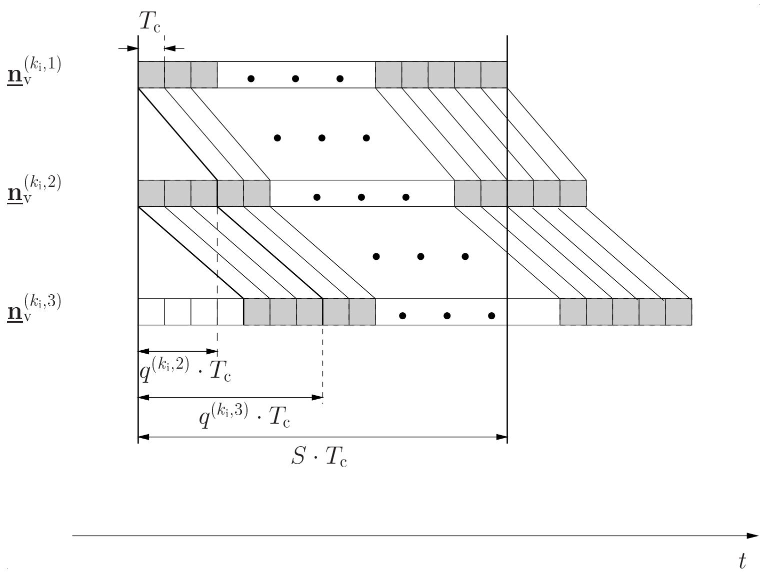

Fig. 3.4. Example of the relationship of the elements of the vectors $\underline{\mathbf{n}}_{\mathrm{v}}^{(k_{\mathrm{i}},k_{\mathrm{d}})}$, $k_{\mathrm{d}} = 1...3$, with the relative delays $q^{(k_{\mathrm{i}},k_{\mathrm{d}})} \cdot T_{\mathrm{c}}$ of $K_{\mathrm{d}} = 3$ vectors

antenna array, are produced in line with (3.21) and taking into consideration (3.50)

$$\underline{\mathbf{n}}^{(k_{\mathrm{a}})} = \sum_{k_{\mathrm{i}}=1}^{K_{\mathrm{i}}} \sum_{k_{\mathrm{d}}=1}^{K_{\mathrm{d}}} \underline{\mathbf{n}}_{\mathrm{RP}}^{(k_{\mathrm{i}},k_{\mathrm{d}})} \cdot \mathrm{e}^{\mathrm{j}\omega q^{(k_{\mathrm{i}},k_{\mathrm{d}})} T_{\mathrm{c}}} \cdot \mathrm{e}^{\mathrm{j}\phi\left(\gamma_{\mathrm{i}}^{(k_{\mathrm{i}},k_{\mathrm{d}})}, k_{\mathrm{a}}\right)}, \quad k_{\mathrm{a}} = 1...K_{\mathrm{a}}. \tag{3.51}$$

3.3 Special intercell MAI scenarios derived from the general model

3.3.1 Directionally uncorrelated interference scenarios

A great variety of intercell MAI scenarios and intercell MAI situations concerning the position of the interferes and the power of the individual interferers can be derived from the general intercell MAI model described in Section 3.2. Three special intercell MAI scenarios which are considered in the system simulations and which are based on the general intercell MAI model are described below. In the three scenarios exclusively temporarily uncorrelated intercell MAI signals $\underline{\mathbf{n}}_{\mathrm{RP}}(\varphi)$, $\varphi \in [0...2\pi[$, of (3.15) are assumed:

- Intercell MAI scenario 1: The intercell MAI consists only of the continuous component of the general intercell MAI model, which is described in Section 3.2. σ_{c}^2 is the total power of the continuous component of the intercell MAI and the azimuth power density at the RP

$$\rho_{\mathrm{c}}(\varphi) = \frac{\sigma_{\mathrm{c}}^2}{2\pi}, \quad \varphi \in [0...2\pi[, \tag{3.52}$$

which was introduced in (3.32) is constant see Fig. 3.5 a). Without loss of generality, we assume that the antenna element v is located at the RP. Hence, according to (3.11)

$$\phi(\varphi, v) = 0, \quad \varphi \in [0...2\pi[, \tag{3.53}$$

is obtained. Consequently, the scalars $\underline{r}^{(u,v)}$, $u, v = 1...K_{\mathrm{a}}$, of (3.29), which specify the spatial correlations between the intercell MAI signals $\underline{\mathbf{n}}^{(u)}$ and $\underline{\mathbf{n}}^{(v)}$ of (3.38), and, which finally form the spatial covariance matrix $\underline{\mathbf{R}}_{\mathrm{s}}$ of (3.36) of the continuous component, take the form [Bla98, BPH99, WPE98]

$$\begin{aligned} \underline{r}^{(u,v)} &= \int_0^{2\pi} \rho_{\mathrm{c}}(\varphi) \cdot \mathrm{e}^{\mathrm{j}2\pi \frac{l^{(u)}}{\lambda} \cos(\varphi)} \, \mathrm{d}\varphi \\ &= \frac{\sigma_{\mathrm{c}}^2}{2\pi} \int_0^{2\pi} \mathrm{e}^{\mathrm{j}2\pi \frac{l^{(u)}}{\lambda} \cos(\gamma_{\mathrm{i}})} \, \mathrm{d}\gamma_{\mathrm{i}} \\ &= \sigma_{\mathrm{c}}^2 \cdot \mathrm{J}_0 \left(2\pi \frac{l^{(u)}}{\lambda} \right), \end{aligned} \tag{3.54}$$

whereas $\mathrm{J}_0(\cdot)$ denotes the Bessel function of order zero. It has been assumed in (3.53) that the antenna element v is located at the RP. Now for the general case the distances $l^{(u)}$ in (3.54) must be replaced by the distances $l^{(u,v)}$ between the antenna elements u and v of the array. Therefore, the elements of the matrix $\underline{\mathbf{R}}_{\mathrm{s}}$ of (3.36) are given by

$$\underline{r}^{(u,v)} = \sigma_{\mathrm{c}}^2 \cdot \mathrm{J}_0 \left(2\pi \frac{l^{(u,v)}}{\lambda} \right). \tag{3.55}$$

The intercell MAI scenario 1 is illustrated in Fig. 3.5 a). By knowing the total spatial covariance matrix $\underline{\mathbf{R}}_{\mathrm{s}}$ from (3.36), we obtain the intercell MAI vectors $\underline{\mathbf{n}}^{(k_{\mathrm{a}})}$, $k_{\mathrm{a}} = 1...K_{\mathrm{a}}$, of (3.38) at the K_{a} antenna elements, which include the correlation properties of the intercell MAI scenario 1, according to the procedure described by the equations (3.39), (3.40) and (3.41) in Section 3.2.

- Intercell MAI scenario 2: The intercell MAI consists of both the discrete and the continuous component according to the general model presented in Section 3.2. the total power of the discrete component is σ_{d}^2 and it is assumed that the K_{i} directionally uncorrelated intercell MAI signals with its DOAs $\gamma_{\mathrm{i}}^{(k_{\mathrm{i}})}$, $k_{\mathrm{i}} = 1...K_{\mathrm{i}}$, have equal power

$$\left(\sigma^{(k_{\mathrm{i}})}\right)^2 = \frac{\sigma_{\mathrm{d}}^2}{K_{\mathrm{i}}}, \quad k_{\mathrm{i}} = 1...K_{\mathrm{i}}. \tag{3.56}$$

In the simulations the DOAs $\gamma_{\mathrm{i}}^{(k_{\mathrm{i}})}$, $k_{\mathrm{i}} = 1...K_{\mathrm{i}}$, are kept fixed or are assumed to be randomly distributed in the range $[0...2\pi[$. The continuous component of the intercell MAI scenario 2 is equal to the intercell MAI scenario 1, i.e. the azimuth power density of the continuous component $\rho_{\mathrm{c}}(\varphi)$, $\varphi \in [0...2\pi[$, is constant, see (3.52). Under consideration of (3.56) and (3.52) the scalars $\underline{r}^{(u,v)}$, $u, v = 1...K_{\mathrm{a}}$, of (3.34) can be determined by

$$\underline{r}^{(u,v)} = \underbrace{\frac{\sigma_{\mathrm{d}}^2}{K_{\mathrm{i}}} \sum_{k_{\mathrm{i}}=1}^{K_{\mathrm{i}}} \mathrm{e}^{\mathrm{j}\left(\phi\left(\gamma_{\mathrm{i}}^{(k_{\mathrm{i}})},u\right)-\phi\left(\gamma_{\mathrm{i}}^{(k_{\mathrm{i}})},v\right)\right)}}_{\text{discrete component}} + \underbrace{\sigma_{\mathrm{c}}^2 \cdot \mathrm{J}_0\left(2\pi\frac{l^{(u,v)}}{\lambda}\right)}_{\text{continuous component}}, \quad u, v = 1...K_{\mathrm{a}}. \tag{3.57}$$

With the scalars $\underline{r}^{(u,v)}$, $u, v = 1...K_{\mathrm{a}}$, of (3.57) the total spatial covariance matrix $\underline{\mathbf{R}}_{\mathrm{s}}$ of (3.36) is given which is required for the generation of the noise vectors $\underline{\mathbf{n}}^{(k_{\mathrm{a}})}$, $k_{\mathrm{a}} = 1...K_{\mathrm{a}}$, that correspond to the presented scenario 2. As it has been already described in Section 3.2, the vectors $\underline{\mathbf{n}}^{(k_{\mathrm{a}})}$, $k_{\mathrm{a}} = 1...K_{\mathrm{a}}$, can be obtained from the rows of the $K_{\mathrm{a}} \times S$ matrix $\underline{\mathbf{N}}$ of (3.41). Fig. 3.5 b) shows the intercell MAI scenario 2 with K_{i} equal to one intercell MAI signal of the discrete component.

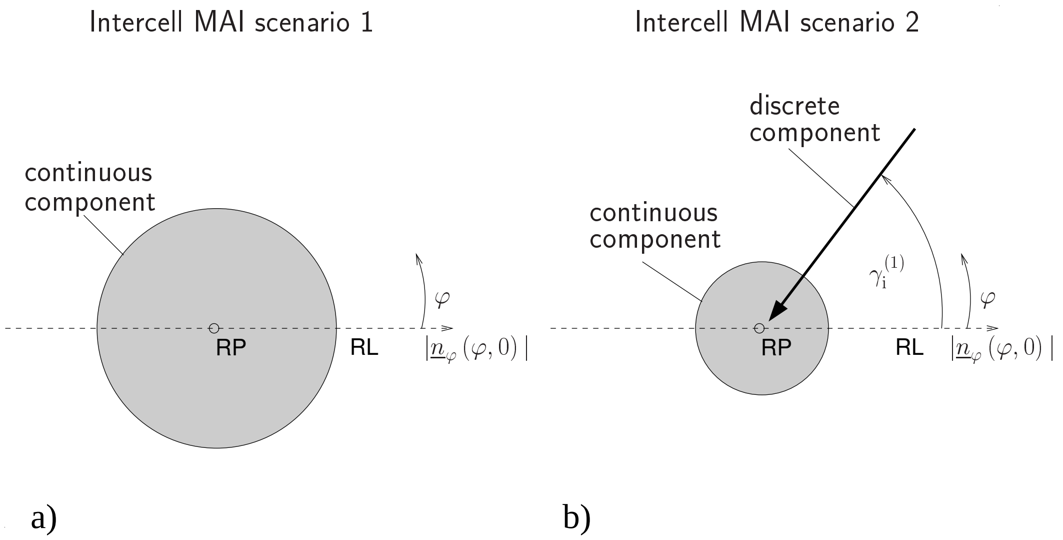

Fig. 3.5. a) Intercell MAI scenario 1; b) Intercell MAI scenario 2 with $K_{\mathrm{i}} = 1$

- Intercell MAI scenario 3: The intercell MAI consists only of the discrete component, where the intercell MAI power $\left(\sigma^{(k_{\mathrm{i}})}\right)^2$ of the k_{i}–th interferer is chosen according to the results of the investigations made by A. Steil [Ste96] concerning the interference power distribution on the intercell MAI sources in a cellular mobile radio system. In this investigation different cluster sizes r, which give the number of adjacent cells that utilize disjoint partial frequency bands of the total system bandwidth [Lee89, Hess93], are taken into account. In Section 3.2 it has already been mentioned that the general model is based on the assumption that only a few intercell MAI signals which originate from only a few interference sources mainly contribute to the total intercell MAI power σ^2 which is received at the RP. The remaining intercell

MAI originate from a large number of intercell MAI sources. With the computer program CEST [Ste96] it is possible to generate realizations of the intercell MAI with the total power σ^2, which is assumed to be received at one single omnidirectional antenna at the RP of a reference cell in a theoretically infinitely distended cell net. The intercell MAI power σ^2 generated by the program CEST has been analyzed by A. Steil with regard to the number of disturbing radio sources which contribute to the power σ^2, without respect to the DOAs [Ste97]. Now, the goal is to combine the results of A. Steil dependent on the cluster size r with regard the number K_i and the power $\left(\sigma^{(k_\mathrm{i})}\right)^2$, $k_\mathrm{i} = 1...K_\mathrm{i}$ of the intercell MAI signals with the general directional intercell MAI model of Section 3.2 in order to obtain a more realistic assignment of the intercell MAI power $\left(\sigma^{(k_\mathrm{i})}\right)^2$, $k_\mathrm{i} = 1...K_\mathrm{i}$, to the individual interferer than in the intercell MAI scenarios 1 and 2, where all interferers of one component have the same power and where no dependency on the cluster size r is considered. To obtain the desired values of $\left(\sigma^{(k_\mathrm{i})}\right)^2$, $k_\mathrm{i} = 1...K_\mathrm{i}$, with CEST, it has been presumed that the cellular mobile radio system under consideration is interference limited and that the results are obtained without the presence of intracell MAI. The results hold for any arbitrary but fixed cell of one reference cluster, which is representative for any cell of the assumed cell net [Ste96, Ste97]. The bar charts presented in the Figures 3.6 and 3.7 show the normalized values

$$\left(\tilde{\sigma}^{(k_\mathrm{i})}\right)^2 = \frac{\left(\sigma^{(k_\mathrm{i})}\right)^2}{\sigma^2}, \quad k_\mathrm{i} = 1 \ldots K_\mathrm{i}, \tag{3.58}$$

for a given standard deviation of intercell MAI power σ of 8 dB and under the assumption that an average number of $\bar{K}$ equal to four, six and eight users are active per cell. In Fig. 3.6 the cluster size r of one is chosen and in Fig. 3.7 a size r of three is chosen. In the Figs. 3.6 and 3.7 each bar consists of K_i equal to eight gray stripes which alternate in the intensity of their shade. The width of the stripe k_i of each bar is proportional to $\left(\tilde{\sigma}^{(k_\mathrm{i})}\right)^2$, $k_\mathrm{i} = 1 \ldots 8$. Known from the literature [Lee91, Par92, Ste92], the attenuation coefficient α, which is a measure for the decrease of received power, if the distance between transmitter and receiver is increased, is set to four. From the Figs. 3.6 and 3.7 it becomes obvious that the mean number of intercell MAI sources that contribute to σ^2 for a given percentage of, e.g. 60%, increases, if $\bar{K}$ is increased, and it decreases, if the cluster size r is increased. Regarding the bars in the Figs. 3.6 and 3.7 valid for the mean number $\bar{K}$ equal to four of active users per cell, one can see that dependent on the cluster size r, approximately four or two contributions to σ^2, respectively, already cause 60% of the total intercell MAI power σ^2. This result fits in with the statement given in Section 3.2 that the biggest part of the intercell MAI power originates only from a few intercell interference sources. Furthermore, the Figs. 3.6 and 3.7 show that the intercell interference diversity decreases if r is increased. To exploit the results given in the Figs. 3.6 and 3.7 in order to generate a directional intercell MAI scenario, it is assumed that the power $\left(\sigma^{(k_\mathrm{i})}\right)^2$ of the intercell MAI signal k_i

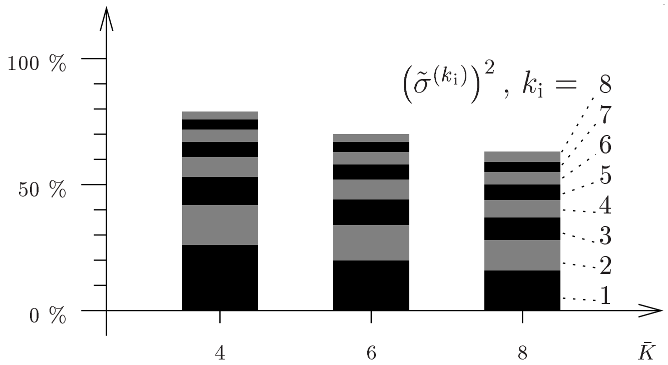

Fig. 3.6. Values of the k_i–th contribution $\left(\tilde{\sigma}^{(k_\mathrm{i})}\right)^2$ of (3.58) to the total intercell MAI power σ^2 at the RP; $r = 1$; $\alpha = 4$; $\sigma = 8\mathrm{dB}$; $C = \mathrm{const.}$ [Ste97]

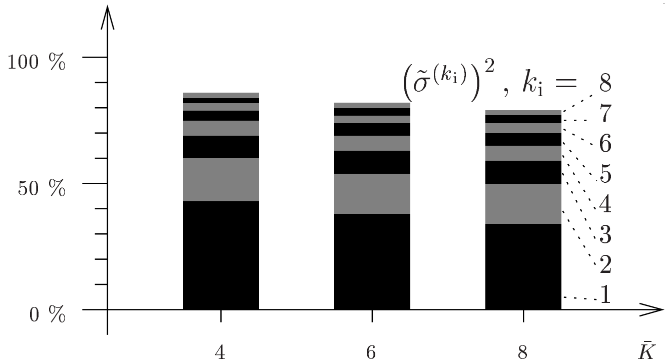

Fig. 3.7. Values of the k_i–th contribution $\left(\tilde{\sigma}^{(k_\mathrm{i})}\right)^2$ of (3.58) to the total intercell MAI power σ^2 at the RP; $r = 3$; $\alpha = 4$; $\sigma = 8\mathrm{dB}$; $C = \mathrm{const.}$ [Ste97]

impinges with the DOA $\gamma_\mathrm{i}^{(k_\mathrm{i})}$ at the RP. In the case of a cluster size r equal to one, it can be imagined that all K_i intercell interferers are arbitrarily located within the six adjacent cells with respect to the cell under consideration. If $\bar{K}$ equal to eight intercell interferers are active and if it is assumed that the relevant interferers are only located in the adjacent cells, the total number K_i of intercell interferers is equal to 48. The percentage parts $\left(\tilde{\sigma}^{(k_\mathrm{i})}\right)^2$, $k_\mathrm{i} = 1...8$, of the total intercell MAI power σ^2 of the eight strongest intercell interferers can be obtained from the Figs. 3.6 and 3.7. The remaining intercell MAI power is evenly distributed to the remaining 40 intercell MAI signals. All DOAs $\gamma_\mathrm{i}^{(k_\mathrm{i})}$, $k_\mathrm{i} = 1...K_\mathrm{i}$, are uniformly distributed in the azimuth. In the case of a cluster size r equal to three, the intercell interferers are not located in the adjacent cells. As becomes obvious from Fig. 3.8 in the case of r equal to three, there exist ranges of azimuth angles which are free of impinging intercell MAI, and there exist preferential directions of the intercell MAI, if only scattering nearby the mobile station is assumed. In this case the DOAs $\gamma_\mathrm{i}^{(k_\mathrm{i})}$, $k_\mathrm{i} = 1...K_\mathrm{i}$, are randomly distributed in the allowed azimuthal regions. With the DOAs $\gamma_\mathrm{i}^{(k_\mathrm{i})}$,

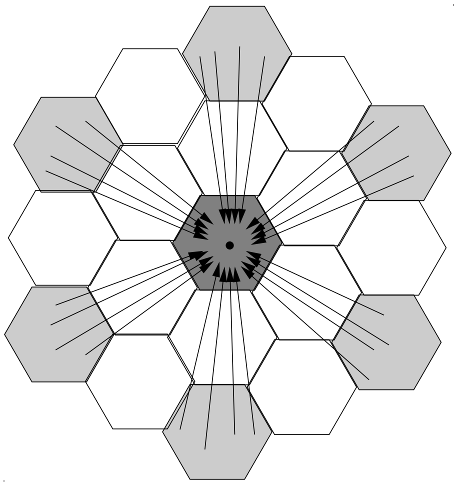

Fig. 3.8. Intercell MAI scenario with a cluster size r equal to three and $\bar{K} = 4$

$k_\mathrm{i} = 1...K_\mathrm{i}$, and the knowledge of the antenna geometry the phase factors $\phi(k_\mathrm{i}, k_\mathrm{a})$, $k_\mathrm{i} = 1...K_\mathrm{i}$, $k_\mathrm{a} = 1...K_\mathrm{a}$, from (3.11) are given. Furthermore, with the normalized values $\left(\tilde{\sigma}^{(k_\mathrm{i})}\right)^2$ of (3.58) and the total intercell MAI power the scalars

$$\underline{r}^{(u,v)} = \sigma^2 \sum_{k_\mathrm{i}=1}^{K_\mathrm{i}} \left(\tilde{\sigma}^{(k_\mathrm{i})}\right)^2 \cdot \mathrm{e}^{\mathrm{j}\left(\phi\left(\gamma_\mathrm{i}^{(k_\mathrm{i})}, u\right) - \phi\left(\gamma_\mathrm{i}^{(k_\mathrm{i})}, v\right)\right)}, \quad u, v = 1...K_\mathrm{a}, \tag{3.59}$$

which describes the components of the spatial covariance matrix $\underline{\mathbf{R}}_\mathrm{s}$ of (3.36) can be determined. Knowing $\underline{\mathbf{R}}_\mathrm{s}$ the intercell MAI vectors $\underline{\mathbf{n}}^{(k_\mathrm{a})}$, $k_\mathrm{a} = 1...K_\mathrm{a}$, at the K_a antenna elements valid for the scenario 3 can be obtained in the same way as it has been done for the scenarios 1 and 2.

3.3.2 Directionally correlated interference scenarios

In Section 3.3.1 it is assumed that each of the K_i intercell MAI signals that impinge at the RP has one single discrete DOA $\gamma_\mathrm{i}^{(k_\mathrm{i})}$, $k_\mathrm{i} = 1...K_\mathrm{i}$. In the case of multipath propagation this assumption must not be true. For instance, in Fig. 3.9 it is shown that the propagation of the signal of one single intercell interferer $K_\mathrm{i} = 1$ takes place via two paths with the different DOAs $\gamma_\mathrm{i}^{(1,1)}$ and $\gamma_\mathrm{i}^{(1,2)}$ at the RP. In Section 3.2 it has been shown that the sum of a signal propagating on two discrete paths has different correlation properties depending on Δd of (3.42), which gives the difference of the length of the two paths, and depending on their DOAs. Based on the general model presented in Section 3.2, the following scenario which includes directionally correlated intercell MAI signals is proposed for the consideration in the TD–CDMA system simulations. The scenario is characterized by the following properties:

- The temporal correlations of each single intercell MAI signal are given by $\underline{\tilde{\mathbf{R}}}_{\mathrm{t}}$ of (3.19).

- As it is shown in Fig. 3.9, the proposed intercell MAI scenario consists of a continuous and a discrete component, which in general are described in Section 3.2.

- All intercell MAI signals of the continuous component are uncorrelated and have equal power. The corresponding spatial covariance matrix $\underline{\mathbf{R}}_{\mathrm{s}}$ of (3.36) is equal to the spatial covariance matrix of the intercell MAI scenario 1 described in Section 3.3.1, with the components $\underline{r}^{(u,v)}$, $u, v = 1...K_{\mathrm{a}}$, of (3.55).

- Only K_{i} equal to one single intercell interferer is considered which contributes to the discrete component. The interference signal propagates via K_{d} equal to two paths with the different DOAs $\gamma_{\mathrm{i}}^{(1,1)}$ and $\gamma_{\mathrm{i}}^{(1,2)}$ and equal powers, i.e.

$$\left(\sigma^{(1,1)}\right)^2 = \left(\sigma^{(1,2)}\right)^2 = \frac{\sigma_{\mathrm{d}}^2}{2}. \tag{3.60}$$

  at the RP. In the description of the general model in Section 3.2 three possibilities concerning the relative delays of the K_{d} intercell MAI signals $\underline{\mathbf{n}}_{\mathrm{RP}}^{(k_{\mathrm{i}},k_{\mathrm{d}})}$, $k_{\mathrm{d}} = 1...K_{\mathrm{d}}$, from the intercell interferer k_{i} are described. The following two of these three possibilities in the case of K_{d} equal to two are considered in this special directionally correlated interference scenario:

  1. The signals $\underline{\mathbf{n}}_{\mathrm{RP}}^{(1,1)}$ and $\underline{\mathbf{n}}_{\mathrm{RP}}^{(1,2)}$ impinge at the RP with no relative delay, i.e. Δd of (3.42) is equal to zero. Hence, considering (3.60), (3.46) and (3.55) the scalars $\underline{r}^{(u,v)}$, $u, v = 1...K_{\mathrm{a}}$ of (3.46) take the form

$$\underline{r}^{(u,v)} = \frac{\sigma_{\mathrm{d}}^2}{2} \cdot \left(\mathrm{e}^{\mathrm{j}(\phi(1,u)-\phi(2,v))} + \mathrm{e}^{\mathrm{j}(\phi(2,u)-\phi(1,v))}\right) + \sigma_{\mathrm{c}}^2 \cdot \mathrm{J}_0\left(2\pi\frac{l^{(u,v)}}{\lambda}\right). \tag{3.61}$$

     If the scalars $\underline{r}^{(u,v)}$, $u, v = 1...K_{\mathrm{a}}$ of (3.61) are known, the spatial covariance matrix $\underline{\mathbf{R}}_{\mathrm{s}}$ of (3.36) is known and the intercell MAI signals received at the K_{a} antenna elements can be obtained in the same way as described in Section 3.3.1 for the directionally uncorrelated scenarios.

  2. The signals $\underline{\mathbf{n}}_{\mathrm{RP}}^{(1,1)}$ and $\underline{\mathbf{n}}_{\mathrm{RP}}^{(1,2)}$ impinge at the RP with a relative delay according to (3.49). In this case, the vectors $\underline{\mathbf{n}}^{(k_{\mathrm{a}})}$, $k_{\mathrm{a}} = 1...K_{\mathrm{a}}$, of the discrete component are obtained by (3.51).

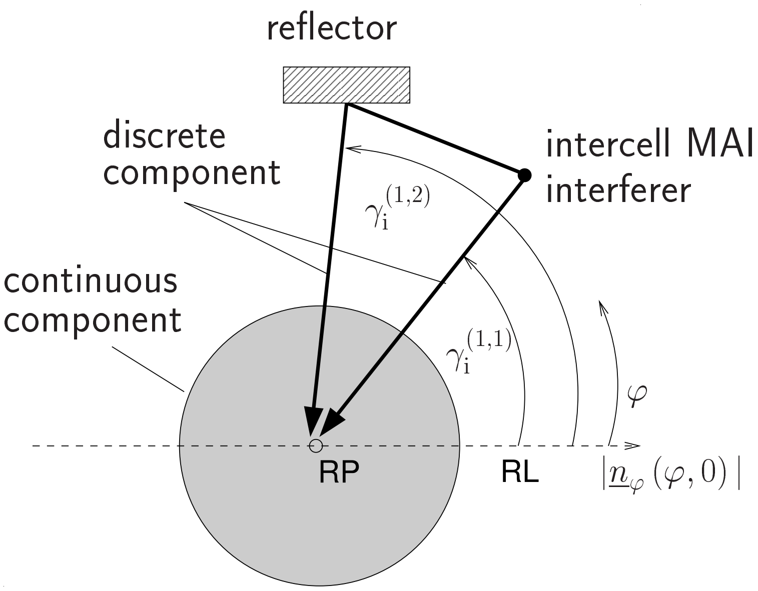

Fig. 3.9. Intercell MAI scenario with a continuous component and with $K_{\mathrm{i}} = 1$ interference source; $K_{\mathrm{d}} = 2$ paths with the DOAs $\gamma_{\mathrm{i}}^{(1,1)}$ and $\gamma_{\mathrm{i}}^{(1,2)}$ at the RP

4 Visualization of the potential of adaptive receiver antennas

4.1 Introduction

As already mentioned in Chapter 1, array antennas with omnidirectional antenna elements obtain specific directional characteristics through the appropriate processing of the receive or transmit signals of the individual elements [MM80]. The aim in the uplink is to carry out signal processing at the individual antenna elements in such a way that the resulting mean SIR γ at the output of the signal processing unit is greater than each of the mean SIRs $\gamma^{(k_\mathrm{a})}$, $k_\mathrm{a} = 1...K_\mathrm{a}$, at the individual receive antenna elements. When receiving via array antennas, the correlation characteristics of noise signals have an effect on the resulting mean SIR γ. To process the receive signals of the individual antenna elements, correlation characteristics of noise signals can be included in signal processing. This chapter is designed to establish how the mean SIR γ behaves compared to just a single omnidirectional receive antenna with and without taking account of the correlation characteristics of noise signals, respectively, i.e. with and without taking into consideration the spatial covariance matrix $\underline{\mathbf{R}}_\mathrm{s}$ of (3.36). The potential of different adaptive array antenna configurations to improve the mean SIR γ in the presence of spatially correlated interference is visualized by the directional array antenna gains. These directional array antenna gains are investigated for different array configurations dependent on the discrete DOA of a single desired user signal, where the DOA is perfectly known and considered in the signal processing. In addition the effect of choosing different intercell MAI scenarios on the directional dependent mean SIR γ at the output of the signal processing unit when considering and not considering the spatial covariance matrix $\underline{\mathbf{R}}_\mathrm{s}$ is investigated. The assumed interference scenarios are intercell MAI scenarios 1 and 2, presented in Section 3.3.1. The antenna array configurations considered in the following investigations are introduced in Section 4.2.

4.2 Array antenna configurations considered in this thesis

In this thesis four different antenna array configurations with K_a equal to 2,4,8 and 16 antenna elements are used, namely uniform linear arrays (ULA), uniform rectangular arrays (URA), cross arrays (CROSS), and ring arrays (RING), respectively. Fig. 4.1 shows the different configurations with K_a equal to 4 and 8 antenna elements, respectively. The antenna elements of the ULAs are spaced at half of the carrier wavelength λ. The URAs consists of ULAs, where the distances between the ULAs within the URAs are also $\lambda/2$.

The cross arrays consist of two perpendicular crossed ULAs. Dependent on the numbers K_a of antenna elements the ring arrays have a variable radius r_R, so that adjacent antenna elements have a distance of $\lambda/2$.

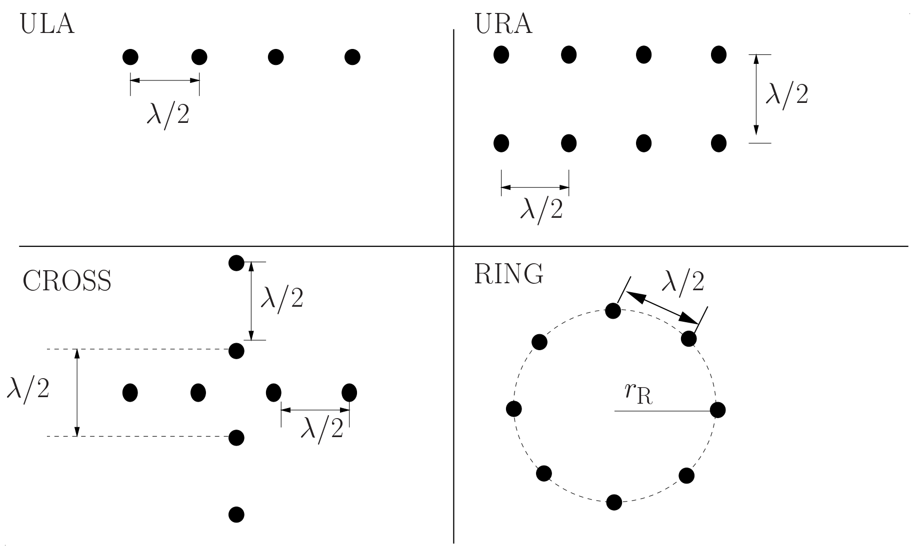

Fig. 4.1. Array antenna configurations ULA, URA, CROSS and RING

4.3 Directional array antenna gains under consideration of intercell MAI covariance matrices

In the following directional array antenna gains for the different array antenna configurations introduced in Section 4.2 with and without consideration of intercell MAI covariance matrices are determined and visualized. As mentioned in Section 4.1 a simple transmission model forms the basis for the investigations of the directional array antenna gains. This simple transmission scenario can be described as follows:

- Only one user, that is K is equal to one, is active.
- Only one symbol $\underline{s}$ with the square of the magnitude $|\underline{s}|^2$ equal to one is transmitted by the single user.
- Transmission takes place via an one-tap channel, i.e., no multipath propagation is considered and the dimension W of the directional channel IR vector $\underline{\mathbf{h}}_\mathrm{d}^{(1,1)}$ of (2.2) at the RP of the single user is equal to one.
- The square of the magnitude $|\underline{h}_\mathrm{d}^{(1,1)}|^2$ of (2.2) of the channel tap is equal to one.

- It is assumed that the signal of the single user impinges at the RP with the discrete DOA $\beta^{(1,1)}$, see Section 2.2.

Based on this description of the transmission model and according to (2.4), (2.5), (2.6), (2.9) and (2.11) the total spatial channel IR vector

$$\underline{\mathbf{h}}_{\mathrm{s}} = \left[\mathrm{e}^{\mathrm{j}\psi(1,1,1)} \ldots \mathrm{e}^{\mathrm{j}\psi(1,K_{\mathrm{a}},1)}\right]^{\mathrm{T}} \tag{4.1}$$

only consists of the K_{a} phase factors $\mathrm{e}^{\mathrm{j}\psi(1,k_{\mathrm{a}},1)}$, $k_{\mathrm{a}} = 1 \ldots K_{\mathrm{a}}$, of (2.6). Consequently, for the given transmission scenario the total spatial channel IR vector $\underline{\mathbf{h}}_{\mathrm{s}}$ of (4.1) is identical to the array steering vector $\underline{\mathbf{a}}^{(1,1)}$ of (2.7) with the dimension K_{a}. In order to simplify the equations, in the following $\underline{\mathbf{a}}$ denotes the array steering vector $\underline{\mathbf{a}}^{(1,1)}$ of (2.7), since only K equal to one user and K_{d} equal to one single DOA exists. Concerning the intercell MAI, the following assumptions are relevant:

- The considered intercell MAI can be represented by the intercell MAI scenarios 1 and 2, which were introduced in Section 3.3.1.
- Only one sample $\underline{n}_{\mathrm{RP}}$ of the intercell MAI signal with the total intercell MAI power

  $$\sigma^2 = \mathrm{E}\left\{|\underline{n}_{\mathrm{RP}}|^2\right\} \tag{4.2}$$

  is considered at the RP.

Hence, the total intercell MAI vector $\underline{\mathbf{n}}$ of (3.24) has only the dimension K_{a} and the total covariance matrix of the interference $\underline{\mathbf{R}}_{\mathrm{n}}$ of (3.25) is equal to the spatial covariance matrix $\underline{\mathbf{R}}_{\mathrm{s}}$ of (3.36), i.e.

$$\underline{\mathbf{R}}_{\mathrm{s}} = \mathrm{E}\left\{\underline{\mathbf{n}} \cdot \underline{\mathbf{n}}^{*\mathrm{T}}\right\}. \tag{4.3}$$

The received signals at the K_{a} antenna elements can be represented by the vector

$$\underline{\mathbf{e}} = \left[\underline{e}_1 \ldots \underline{e}_{K_{\mathrm{a}}}\right]^{\mathrm{T}} = \underline{\mathbf{a}} \cdot \underline{s} + \underline{\mathbf{n}} \tag{4.4}$$

of dimension K_{a}. The linear signal processing, i.e. in this case the combining of the received signals at the K_{a} antenna elements can be described by a weight vector

$$\underline{\mathbf{w}} = \left[\underline{w}_1 \ldots \underline{w}_{K_{\mathrm{a}}}\right]^{\mathrm{T}} \tag{4.5}$$

of dimension K_{a}, which leads to the array output signal

$$\underline{s}_{\mathrm{out}} = \underline{\mathbf{w}}^{\mathrm{T}} \cdot \underline{\mathbf{e}} = \underline{\mathbf{w}}^{\mathrm{T}} \cdot (\underline{\mathbf{a}} \cdot \underline{s} + \underline{\mathbf{n}}), \tag{4.6}$$

see Fig. 4.3. With (4.6) the mean SIR γ at the combiner output is given by

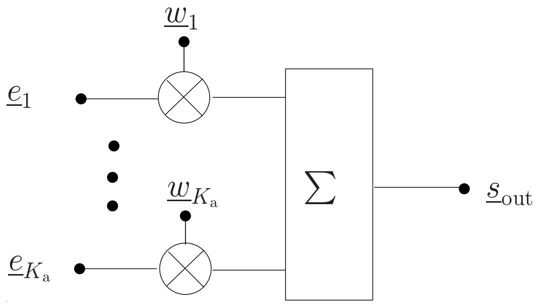

Fig. 4.2. Combining the weighted received signal $\underline{\mathbf{e}}$ according (4.6)

$$\gamma = \frac{\mathrm{E}\{|\ \underline{s}_\mathrm{out}\ |^2\}\ |_{\underline{\mathbf{n}}=0}}{\mathrm{E}\{|\ \underline{s}_\mathrm{out}\ |^2\}\ |_{\underline{s}=0}}. \tag{4.7}$$

With the weight vector $\underline{\mathbf{w}}$, the covariance matrix

$$\underline{\mathbf{R}}_\mathrm{x} = \mathrm{E}\left\{(\underline{\mathbf{a}} \cdot \underline{s}) \cdot (\underline{\mathbf{a}} \cdot \underline{s})^{*\mathrm{T}}\right\} = \underline{\mathbf{a}} \cdot \underline{\mathbf{a}}^{*\mathrm{T}} = K_\mathrm{a} \tag{4.8}$$

of the received signal $\underline{\mathbf{e}}\ |_{\underline{\mathbf{n}}=0}$ of (4.4) and with the spatial interference covariance matrix $\underline{\mathbf{R}}_\mathrm{s}$ of (4.3), the mean SIR γ of (4.7) can be written as [MM80]

$$\gamma = \frac{\underline{\mathbf{w}}^{*\mathrm{T}} \cdot \underline{\mathbf{R}}_\mathrm{x} \cdot \underline{\mathbf{w}}}{\underline{\mathbf{w}}^{*\mathrm{T}} \cdot \underline{\mathbf{R}}_\mathrm{s} \cdot \underline{\mathbf{w}}}. \tag{4.9}$$

It is well known [MM80] that γ of (4.9) is maximized by utilizing the vector

$$\underline{\mathbf{w}} = \frac{1}{\sigma^2} \cdot \underline{\mathbf{R}}_\mathrm{s}^{-1\mathrm{T}} \cdot \underline{\mathbf{a}}^*. \tag{4.10}$$

In the following it is assumed that the steering vector $\underline{\mathbf{a}}$ of (2.7) is perfectly known at the combiner, since the DOA $\beta^{(1,1)}$ of the user signal is assumed to be known. Furthermore, it is assumed that the matrix $\underline{\mathbf{R}}_\mathrm{s}$ is either perfectly known at the receiver or it is not known and, consequently, $\underline{\mathbf{R}}_\mathrm{s}$ must be replaced by a $K_\mathrm{a} \times K_\mathrm{a}$ identity matrix $\mathbf{I}^{(K_\mathrm{a})}$, which leads to the weight vector

$$\underline{\mathbf{w}} = \begin{cases} \frac{1}{\sigma^2} \cdot \underline{\mathbf{a}}^* & \text{, if } \underline{\mathbf{R}}_\mathrm{s} \text{ is not known,} \\ \frac{1}{\sigma^2} \cdot \underline{\mathbf{R}}_\mathrm{s}^{-1\mathrm{T}} \cdot \underline{\mathbf{a}}^* & \text{, else.} \end{cases} \tag{4.11}$$

With the weight vector $\underline{\mathbf{w}}$ of (4.11) and the covariance matrix $\underline{\mathbf{R}}_\mathrm{x}$ of (4.8) we obtain the mean SIR γ of (4.7) in the case of $K_\mathrm{a} > 1$ according to

$$\gamma_{K_\mathrm{a}>1} = \begin{cases} \frac{1}{\sigma^2} \cdot {K_\mathrm{a}}^2 \cdot \left(\underline{\mathbf{a}}^{*\mathrm{T}} \cdot \underline{\mathbf{R}}_\mathrm{s} \cdot \underline{\mathbf{a}}\right)^{-1} & \text{, if } \underline{\mathbf{R}}_\mathrm{s} \text{ is not considered in (4.11),} \\ \frac{1}{\sigma^2} \cdot \underline{\mathbf{a}}^{*\mathrm{T}} \cdot \underline{\mathbf{R}}_\mathrm{s}^{-1} \cdot \underline{\mathbf{a}} & \text{, if } \underline{\mathbf{R}}_\mathrm{s} \text{ is considered in (4.11).} \end{cases} \tag{4.12}$$

In the case of only a single receiver antenna, i.e. K_a equal to one, we obtain the mean SIR

$$\gamma_{\mathrm{K_a}=1} = \frac{\mathrm{E}\left\{|\underline{s}|^2\right\}}{\mathrm{E}\left\{|\underline{n}_\mathrm{RP}|^2\right\}} = \frac{1}{\sigma^2}, \tag{4.13}$$

if (4.2) is considered. With the mean SIRs $\gamma_{K_\mathrm{a}>1}$ of (4.12) and $\gamma_{K_\mathrm{a}=1}$ of (4.13) a SIR gain

$$g_\mathrm{a} = \frac{\gamma_{K_\mathrm{a}>1}}{\gamma_{K_\mathrm{a}=1}} \tag{4.14}$$

can be defined for the case that an antenna array with K_a omnidirectional antenna elements is utilized at the receiver instead of only a single omnidirectional antenna. Under the assumption of the above described simplified transmission model with only a single active user who transmits only a single symbol $\underline{s}$ via an one-tap channel and considering (4.12) and (4.13) the gain g_a of (4.14) takes the form

$$g_\mathrm{a} = \begin{cases} {K_\mathrm{a}}^2 \cdot \left(\underline{\mathbf{a}}^{*\mathrm{T}} \cdot \underline{\mathbf{R}}_\mathrm{s} \cdot \underline{\mathbf{a}}\right)^{-1} & \text{, if } \underline{\mathbf{R}}_\mathrm{s} \text{ is not considered in (4.11),} \\ \underline{\mathbf{a}}^{*\mathrm{T}} \cdot {\underline{\mathbf{R}}_\mathrm{s}}^{-1} \cdot \underline{\mathbf{a}} & \text{, if } \underline{\mathbf{R}}_\mathrm{s} \text{ is considered in (4.11).} \end{cases} \tag{4.15}$$

g_a of (4.15) is a function of the DOA $\beta^{(1,1)}$ and the mean azimuthal gain becomes

$$\overline{g}_\mathrm{a} = \frac{1}{2\pi} \int_0^{2\pi} g_\mathrm{a} \; \mathrm{d}\beta^{(1,1)}. \tag{4.16}$$

In the following the four different antenna configurations ULA, URA, CROSS and RING, which were introduced in Section 4.2, are considered at the receiver. For comparison the mean SIR $\gamma_{K_\mathrm{a}=1}$ of the signals received at a single antenna element is set to 0 dB.

Let us first assume that the spatial covariance matrix $\underline{\mathbf{R}}_\mathrm{s}$ of (3.36) of the intercell MAI is perfectly known at the receiver. For this case Figs. 4.3 a to d show the gain g_a of (4.15) for the different antenna configurations and for the spatial intercell MAI scenario 1 described in Section 3.3.1 versus the DOA $\beta^{(1,1)}$ of the desired signal. The steering vector $\underline{\mathbf{a}}$, which is equal to the total spatial channel IR vector $\underline{\mathbf{h}}_\mathrm{s}$ in (4.1), is changed depending on the DOA $\beta^{(1,1)}$ in order to obtain g_a of (4.15). The principal character of the curves in the Figs. 4.3 a to d depend on the considered antenna configurations. For instance, for K_a equal to 4 and $\beta^{(1,1)}$ equal to 0° the RING configuration has a maximum gain g_a of 7.5 dB, whereas the ULA has a minimum gain g_a of 3.6 dB. Further, the variance of the gain g_a with respect to $\beta^{(1,1)}$ is different for the different array configurations. This variance is lowest for the RING configuration. Therefore, if we consider the dependence of the BER of a receiver, the BER fluctuations when utilizing a RING configuration and changing the DOA $\beta^{(1,1)}$ over the whole azimuthal range are lower than when utilizing a ULA. For this reason the RING configuration should be preferred to the ULA where the users of the cell in question were to be evenly distributed over the azimuth. The Figs. 4.3

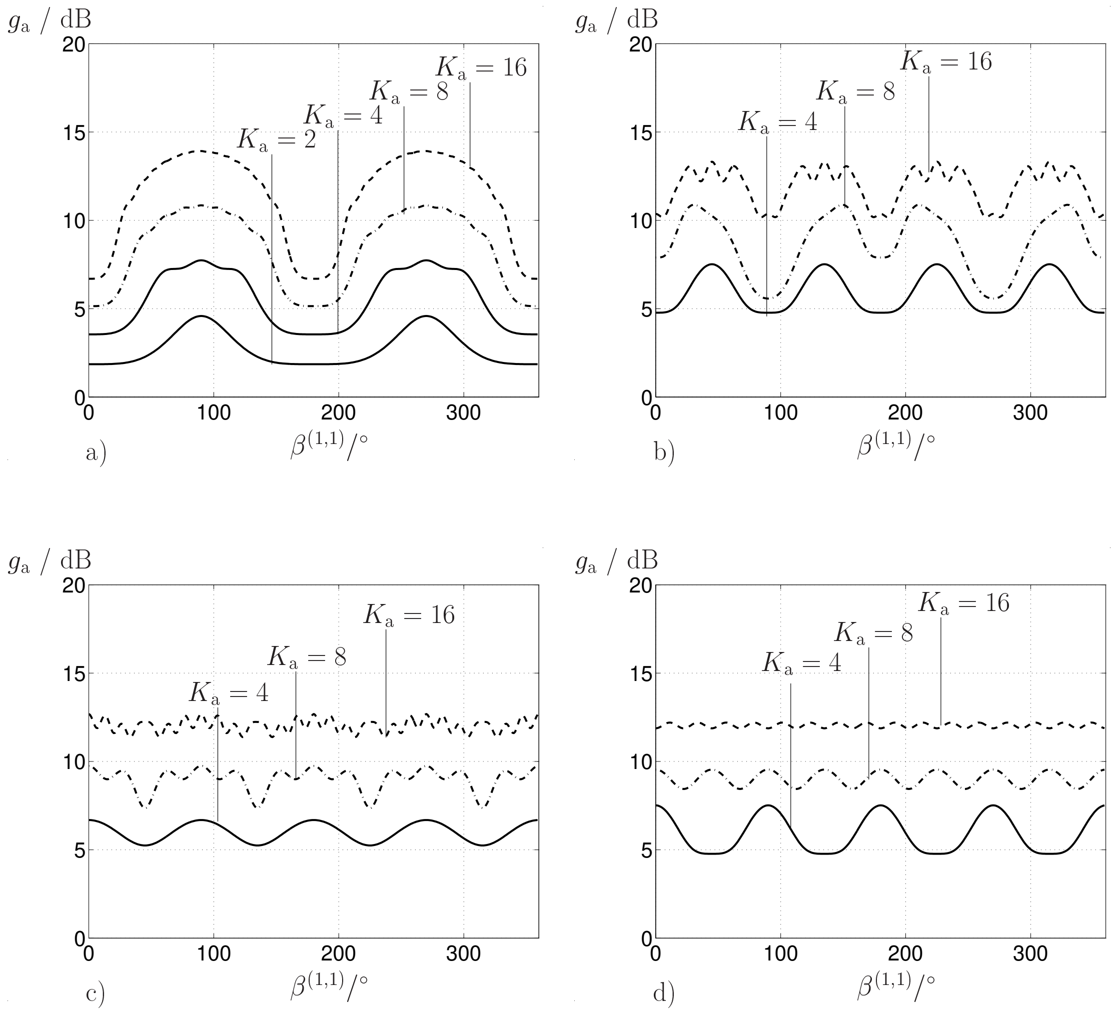

Fig. 4.3. g_a of (4.15) versus $\beta^{(1,1)}$; K_a equal to 4, 8 and 16 antenna elements; intercell MAI scenario 1; $\underline{\mathbf{R}}_s$ is perfectly known and considered in (4.15); a) ULA; b) URA; c) CROSS; d) RING

b and d also show that the RING and URA configurations with K_a equal to 4 are, up to a rotation of 45°, equivalent to each other.

Table 4.1 shows the mean gains $\overline{g}_a$ of (4.16) for the different array configurations. The desired signals received at the K_a antenna elements are constructively superimposed, whereas this is, in general, not the case for the undesired signals. Therefore, $\overline{g}_a$ of (4.16) is increased by 3 dB independently of the array configuration by doubling K_a. Even though the intercell MAI signals $\underline{\mathbf{n}}^{(k_a)}$, $k_a = 1...K_a$, received at the K_a antenna elements are spatially correlated, the consideration of the inverse $\underline{\mathbf{R}}_s^{-1}$ of the spatial covariance matrix in (4.15) causes a spatial decorrelation of the vectors $\underline{\mathbf{n}}^{(k_a)}$, $k_a = 1...K_a$, so that the received intercell MAI power is doubled by doubling K_a, whereas the power of the desired signals is increased by 4 by doubling K_a.

The Figs. 4.4 a to d show results corresponding to those of Figs. 4.3 a to d, if the spatial covariance matrix $\underline{\mathbf{R}}_{\mathrm{s}}$ of (3.36) is not considered in the signal processing of the receiver, i.e. $\underline{\mathbf{R}}_{\mathrm{s}}$ is not considered in (4.15). The mean gains $\overline{g}_{\mathrm{a}}$ of (4.16) for this case are listed in Table 4.2. A comparison of the values of Tables 4.1 and 4.2 shows that, except for the ULA, $\overline{g}_{\mathrm{a}}$ is increased by considering $\underline{\mathbf{R}}_{\mathrm{s}}$. Obviously, the spatial correlations of the intercell MAI have a degrading influence on the SIR. The differences of the gains g_{a}, which can be expected with and without consideration of $\underline{\mathbf{R}}_{\mathrm{s}}$ of (3.36), slightly increase with increasing number of antenna elements K_{a}, while the dependency of the gains on the DOA $\beta^{(1,1)}$ becomes less important.

Table 4.1. $\overline{g}_{\mathrm{a}}$ of (4.16) when utilizing different antenna array configurations with K_{a} equal to 4, 8 and 16 antenna elements; intercell MAI scenario 1; $\underline{\mathbf{R}}_{\mathrm{s}}$ is perfectly known and considered in (4.15)

	mean gain $\overline{g}_{\mathrm{a}}$				
antenna type	$K_{\mathrm{a}}=1$	$K_{\mathrm{a}}=2$	$K_{\mathrm{a}}=4$	$K_{\mathrm{a}}=8$	$K_{\mathrm{a}}=16$
ULA	0.0 dB	3.0 dB	6.0 dB	9.0 dB	12.0 dB
URA	–	–	6.0 dB	9.0 dB	12.0 dB
CROSS	–	–	6.0 dB	9.0 dB	12.0 dB
RING	–	–	6.0 dB	9.0 dB	12.0 dB

Table 4.2. $\overline{g}_{\mathrm{a}}$ of (4.16) when utilizing different antenna array configurations with K_{a} equal to 4, 8 and 16 antenna elements; intercell MAI scenario 1; $\underline{\mathbf{R}}_{\mathrm{s}}$ is not considered in (4.15)

	mean gain $\overline{g}_{\mathrm{a}}$				
antenna type	$K_{\mathrm{a}}=1$	$K_{\mathrm{a}}=2$	$K_{\mathrm{a}}=4$	$K_{\mathrm{a}}=8$	$K_{\mathrm{a}}=16$
ULA	0.0 dB	2.8 dB	5.8 dB	8.9 dB	11.9 dB
URA	–	–	4.9 dB	7.3 dB	9.1 dB
CROSS	–	–	5.6 dB	7.7 dB	10.2 dB
RING	–	–	4.9 dB	7.6 dB	10.4 dB

The results presented in the Figs. 4.3 and 4.4 show that the choice of the array configuration should depend on the expected propagation scenario, since the gains g_{a} of (4.15) have a different directional behavior. If it is expected that the user signal has a random DOA $\beta^{(1,1)}$ in the azimuth, then the RING configuration should be preferred. Otherwise, if it is only expected that user signals impinge at the RP from a certain small azimuthal range, the ULA configuration should be preferred. Considering the simple transmission model described in this section, the system performance is independent of the choice of the array configuration, if the spatial covariance matrix $\underline{\mathbf{R}}_{\mathrm{s}}$ is known at the receiver and

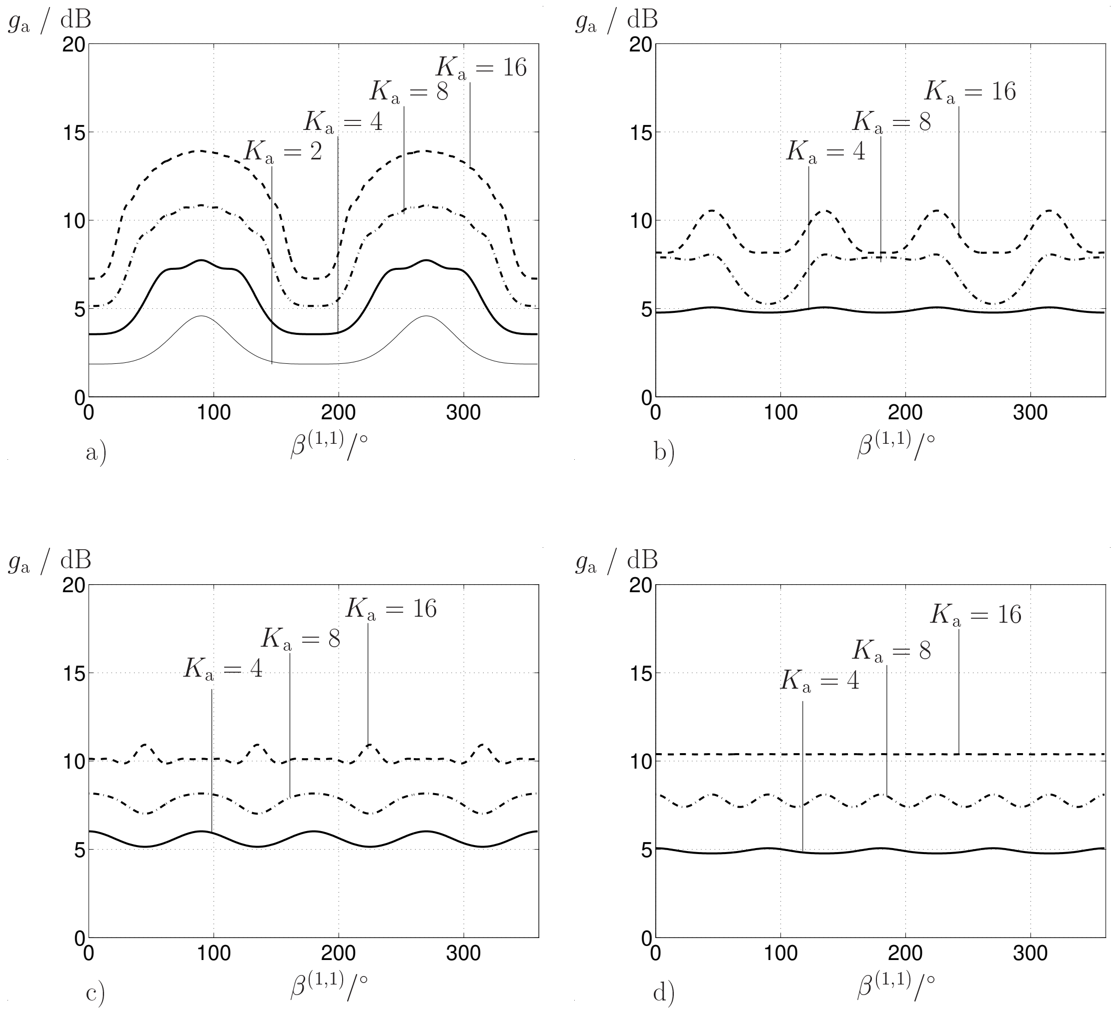

Fig. 4.4. g_a of (4.15) versus $\beta^{(1,1)}$; K_a equal to 4, 8 and 16 antenna elements; intercell MAI scenario 1; $\underline{\mathbf{R}}_s$ is not considered in (4.15); a) ULA; b) URA; c) CROSS; d) RING

used to form the weight vector $\underline{\mathbf{w}}$ according to (4.10). In the case of perfectly known matrix $\underline{\mathbf{R}}_s$ where all array configurations have the same mean gain $\overline{g}_a$, see Table 4.1, the use of the URA configuration can be recommended, since this configuration needs the smallest space.

According to the results of Table 4.2 the URA configuration is the worst choice, if the spatial covariance matrix $\underline{\mathbf{R}}_s$ is not considered. In this case the configurations like ULA and RING in which the antenna elements have a greater relative spacing are preferable. With increasing mutual distance of the antenna elements the spatial correlations of the signals received by the antenna elements decrease, and it becomes less important to consider the covariance matrix $\underline{\mathbf{R}}_s$. Consequently, no configuration can be uniquely favored. Therefore, in the TD–CDMA system simulations also different antenna configurations are considered to elaborate their differences in more detail. The correspondent simulation results are demonstrated in Chapter 8.

To demonstrate the dependence of the gains g_a of (4.15) on the interference scenario, the intercell MAI scenario 2 of Fig. 3.5 b with K_i equal to 1 strong interferer with a discrete DOA $\gamma_i^{(1)}$ and a continuous component is assumed, see Section 3.3.1. The intercell MAI signal of the strong interference source has the randomly selected DOA $\gamma_i^{(1)}$ equal to $100°$ and causes 80% of the total interference power σ^2, which would be received by an omnidirectional antenna in the RP. The remaining 20% of the total interference power σ^2 is caused by the continuous component. For the 4 antenna configurations ULA, URA, CROSS and RING K_a equal to 8 antenna elements are used. Figures 4.5 a to d show the gain g_a of (4.15) versus the discrete DOA $\beta^{(1,1)}$ of the desired signal.

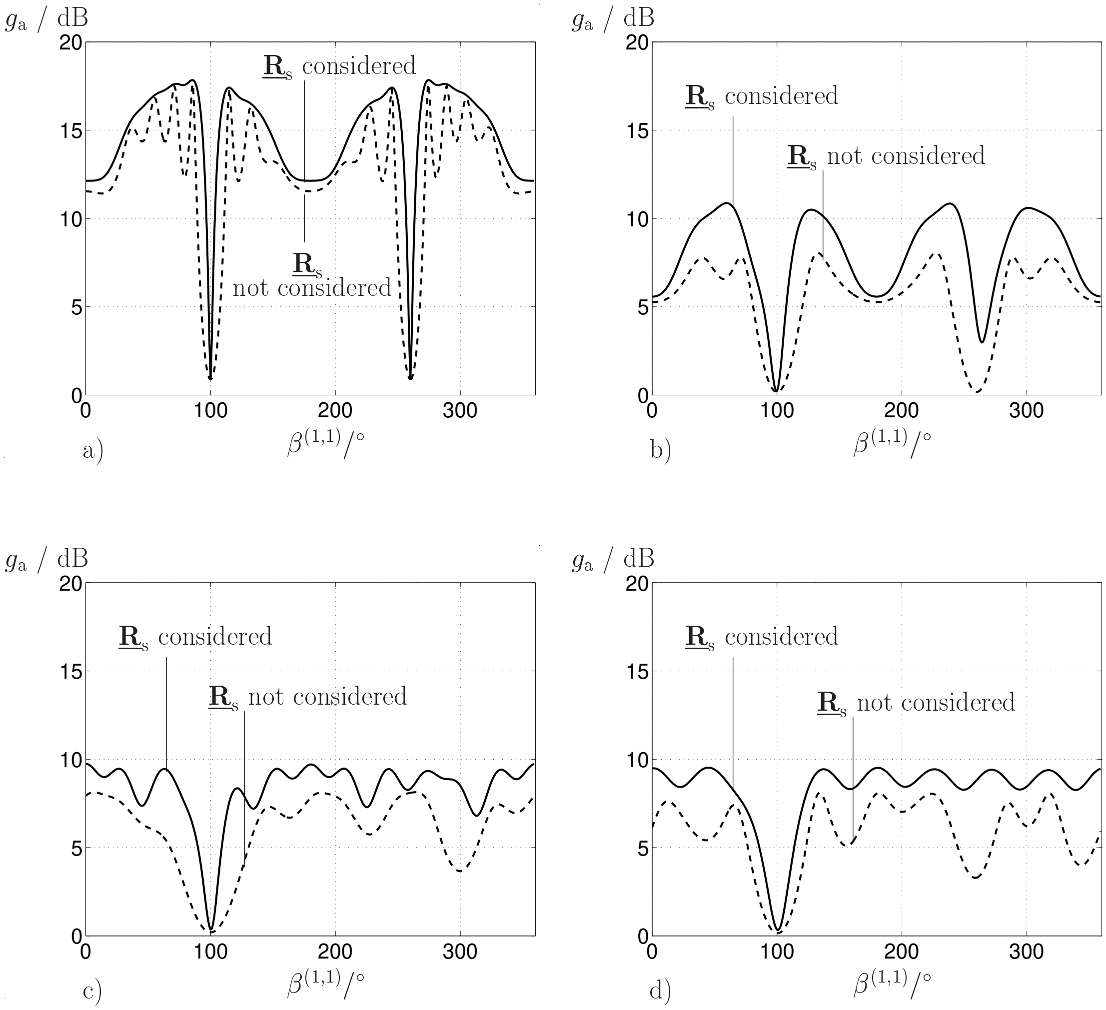

Fig. 4.5. g_a of (4.15) versus $\beta^{(1,1)}$ with and without consideration of $\underline{\mathbf{R}}_s$ in (4.15); $K_a = 8$; intercell MAI scenario 2; $\gamma_i^{(1)} = 100°$; 20% homogeneously distributed interference; a) ULA; b) URA; c) CROSS; d) RING

All curves in Figs. 4.5 a to d, have a minimum at $\beta^{(1,1)}$ is equal to $100°$. In cases of $\beta^{(1,1)}$ equal to $100°$ the signal processing by taking the weight vector $\underline{\mathbf{w}}$ of (4.5) into account

Table 4.3. $\overline{g}_{\mathrm{a}}$ of (4.16) for different array configurations with and without consideration of $\underline{\mathbf{R}}_{\mathrm{s}}$ in (4.15); $K_{\mathrm{a}} = 8$; intercell MAI scenario 2; $\gamma_{\mathrm{i}}^{(1)} = 100°$; 20% homogeneously distributed interference

	mean gain $\overline{g}_{\mathrm{a}}$	
antenna type	$\underline{\mathbf{R}}_{\mathrm{s}}$ not considered in (4.15)	$\underline{\mathbf{R}}_{\mathrm{s}}$ considered in (4.15)
ULA	13.5 dB	15.4 dB
URA	5.9 dB	8.5 dB
CROSS	6.4 dB	8.5 dB
RING	6.2 dB	8.5 dB

without considering $\underline{\mathbf{R}}_{\mathrm{s}}$ in (4.11) results in an antenna diagram which has aligned its main lobe in the direction of the desired user signal. Thus in the case of $\beta^{(1,1)}$ is equal to 100° this main lobe also points in the direction $\gamma_{\mathrm{i}}^{(1)}$ from which 80% of the total interference power comes. The directional interference signal is processed in the same way as the user signal, i.e. the antenna gain g_{a} is the same in direction $\beta^{(1,1)}$ equal to 100° for user and interference signal and the incident interference component from a discrete direction is not suppressed. For reasons of symmetry a second minimum occurs for the configurations ULA and URA at $\beta^{(1,1)}$ equal to 260°.

In scenarios in which the desired and undesired signals have the same directions, adaptive antennas cannot suppress the undesired signals without simultaneously suppressing the desired signals [MM80]. The comparatively high gains g_{a} in Fig. 4.5 a on using configuration ULA have to do with the favorable choice of direction $\gamma_{\mathrm{i}}^{(1)}$ equal to 100°. The width of the main lobe of configuration ULA for angles $\beta^{(1,1)}$ of around 90° to the RL is significantly smaller compared to two-dimensional antenna arrangements with small diameters [Ma74, MM80]. This means that directional interference components are better suppressed right from the outset than with antenna arrangements with a wider main lobe. Because of these sharply defined minima in cases of strongly directional interference, the mean gain $\overline{g}_{\mathrm{a}}$ of (4.16) is less than when taking account of the intercell MAI scenario 1. I.e. the correlation of the interference signals which are received at the K_{a} antenna elements, effects the mean SIR γ. Even when $\underline{\mathbf{R}}_{\mathrm{s}}$ is considered, the two-dimensional antenna configurations still all show the same mean gain $\overline{g}_{\mathrm{a}}$ of (4.16) in Table 4.3, although the mean gains $\overline{g}_{\mathrm{a}}$ of 8.5 dB are still 0.5 dB below the mean gains $\overline{g}_{\mathrm{a}}$ in Table 4.1.

However, it is generally evident from Figs. 4.5 a through d, that by taking account of the matrix $\underline{\mathbf{R}}_{\mathrm{s}}$ of (3.36) a larger gain g_{a} of (4.15) can be obtained.

5 Data detection

5.1 Introduction

This chapter deals with the data detection in the TD–CDMA uplink. The task of data detection algorithms is to determine an estimate of the transmitted data of all users K based on the received signal. In a TD-CDMA mobile radio system the data detection algorithms require *a priori* information about

- the CDMA codes,
- the spatial channel IRs $\underline{\mathbf{h}}_{\mathrm{s}}^{(k,k_{\mathrm{a}})}$, $k = 1...K$, $k_{\mathrm{a}} = 1...K_{\mathrm{a}}$ of (2.1),
- the data symbol alphabet $\mathbb{V}_{\mathrm{d}}$ of size M,
- in some cases information about the covariance matrices of the data symbols and
- in some cases information about the intercell MAI covariance matrix $\underline{\mathbf{R}}_{\mathrm{n}}$ of (3.25).

In general, in CDMA systems, where K users are simultaneously sharing the same frequency band, the data detection problem goes along with a signal separation problem. User signal separation in conjunction with data detection in a CDMA system can be performed by

- single user detection (SD) [Ver86, Pro89], or
- multiuser detection (MD) [Ver84, Ver86, Wha71, KB93].

SD is the conventional signal separation method, which has originally been designed for synchronous transmission with orthogonal CDMA codes over single tap channels, i.e. $W = 1$, see Chapter 2, with additive white Gaussian noise [Pro89]. Under these ideal transmission conditions, SD by applying filters matched to the user-specific CDMA codes is optimum [Pro89, KB92b]. In the case of multipath propagation this method is no longer optimum [KB92b]. The suboptimality of SD results from the fact that the user signal of interest is detected while all other user signals are treated as noise. In cellular mobile radio systems the interference caused by the simultaneously active users in one cell, and, which is termed intracell MAI, is not noise-like. Rather, the intracell MAI signals are signals of the own system with known user specific CDMA codes [Ver86, KB92b]. This knowledge can be exploited by MD algorithms in order to eliminate the intracell MAI. The MD schemes can be divided into [Kle96]

- interference cancellation (IC) schemes, which can be performed serially, i.e. successive, or in parallel, and
- joint detection (JD) schemes.

The basic idea of IC is [Pro89]

- to detect part of the transmitted data symbols,
- to reconstruct the contribution of these transmitted data symbols to the composite received signal,
- to subtract, i.e. cancel, this contribution from the composite received signal [Koh94] in order to achieve the desired signal separation and
- to detect once more the intracell MAI reduced signal.

In JD the data symbols of all users are detected jointly in one step, using all the *a priori* information about intracell MAI [KB93]. As already mentioned in Section 1.2, by applying JD the intracell MAI and the inter symbol interference (ISI) is eliminated. The data detection algorithms for TD-CDMA which enable JD have already been described and investigated in [Kle96]. These algorithms can be divided into three categories [Kle96, Pap00]:

- Maximum-likelihood (ML) algorithms, which are non-linear,
- linear algorithms, and
- iterative and decision feedback algorithms, respectively [Kle96].

From these different data detection algorithms two MD algorithms, namely a linear JD algorithm, see Section 5.3, and an iterative non-linear algorithm, see Section 5.4, which is a combination of linear JD and IC, are considered in this thesis. The optimum ML algorithms are not considered for TD–CDMA in the following due to their prohibitively high implementation complexity. Linear JD is performed by applying the zero-forcing block linear equalizer (ZF–BLE). The ZF–BLE is well known [Wha71, Ver98] and its applicability to TD–CDMA has already be shown in [Kle96]. The extension of the ZF–BLE to multi-antenna receivers has been shown in [Bla98]. Therefore, the ZF-BLE is only briefly described in Section 5.3.2. Typical of JD algorithms is a noise enhancement. An approximation of this noise enhancement when utilizing the ZF–BLE in a multi-antenna receiver is determined in Section 5.3.3. The iterative MD algorithm, which is described in

Section 5.4, is termed multi-step joint detection (MSJD) [Ost01, WBOW00]. For single antenna receivers a detailed description of the MSJD receiver can be found in [Ost01]. Therefore, only a brief description of MSJD with the extension to multi-element antennas [WWBJ00, Wec01] is given in Section 5.4.

The ZF–BLE and the MSJD algorithms, which are the two MD algorithms described in this chapter, form the basis of the novel extended receiver structures that incorporate the estimation and consideration of the intercell MAI covariance matrix $\underline{\mathbf{R}}_{\mathrm{n}}$ of (3.25). These extensions of the ZF–BLE, which is the state of the art data detector for TD–CDMA [Pap00], and of the MSJD are presented in Chapter 7.

Prior to the description of the detection algorithms, the time-discrete system model of the TD–CDMA air interface is given in Section 5.2. Throughout this chapter it is assumed that the channel IRs are perfectly known at the receiver. The problem of channel estimation in TD-CDMA is treated separately in Chapter 6. The relevant interference in the TD-CDMA system under consideration, which is represented by the vector $\underline{\mathbf{n}}$ of (3.24), is intercell MAI, see Chapter 3. Therefore, the thermal noise is neglected in the following.

5.2 System model

In this section the discrete time system model of a TD–CDMA air interface is described in the equivalent lowpass domain, when multi–element antenna configurations are used at the BS receiver [Bla98, Pap00]. The used matrix-vector-model of signal representation in TD–CDMA has already been introduced in [Kle96, Naß95]. Even the extension of this matrix-vector-model to the use of multi-element antennas at the BS has already been described in detail in [Bla98, Pap00]. Therefore, the system model is only briefly recapitulated in this Section. For more details the reader is referred to [Kle96, Naß95, Bla98, Pap00]. The multiple access scheme and the details of the burst and frame structures applied in TD–CDMA were already introduced in Chapter 1. It is assumed that TD–CDMA operates synchronously [Kle96, Naß95], and that burst synchronization is achieved by using particular access and synchronization bursts, as it is, e.g. also the case in GSM [ETSI88].

In the following only the first data blocks of the bursts will be considered, see Fig. 1.7. The consideration of the second data blocks would be straightforward. With K the number of users simultaneously active within a cell in the same frequency band, each burst of user k, $k = 1...K$, consists of

- two data sections

$$\underline{\mathbf{d}}^{(k)} = \left[\underline{d}_1^{(k)}...\underline{d}_N^{(k)}\right]^{\mathrm{T}} \tag{5.1}$$

of N M-ary complex data symbols $\underline{d}_n^{(k)}$ each with symbol duration T_s, which are elements of the complex set $\{\underline{v}_1 ... \underline{v}_M\}$ describing the symbol alphabet $\mathbb{V}_\mathrm{d}$, and

- a midamble $\underline{\mathbf{m}}^{(k)}$ of dimension L inserted between these data sections, which allows channel estimation at the receivers.

Prior to transmission each of the data symbols $\underline{d}_n^{(k)}$ of (5.1) is spectrally spread at the transmitter by a user specific CDMA code

$$\underline{\mathbf{c}}^{(k)} = \left[\underline{c}_1^{(k)} ... \underline{c}_Q^{(k)}\right]^\mathrm{T}, \quad k = 1...K, \tag{5.2}$$

of dimension Q. The $\tilde{M}$-ary complex elements $\underline{c}_q^{(k)}$, $q = 1...Q$, of (5.2), which are termed chips, are taken from the complex set $\{\underline{v}_{\mathrm{c},1} ... \underline{v}_{\mathrm{c},\tilde{M}}\}$. The chip duration T_c is equal to T_s/Q.

It is assumed that K_a antennas are utilized at the BS. Consequently, the mobile radio channel can be characterized by the $K_\mathrm{a} \cdot K$ spatial channel IR vectors $\underline{\mathbf{h}}_\mathrm{s}^{(k,k_\mathrm{a})}$, $k = 1...K$, $k_\mathrm{a} = 1...K_\mathrm{a}$ of (2.1) [PHFB97, BPH99]. The received signals which depend on the transmitted symbols can be represented by K_a vectors

$$\underline{\mathbf{e}}^{(k_\mathrm{a})} = \left[\underline{e}_1 ... \underline{e}_{NQ+W-1}\right]^\mathrm{T}, k_\mathrm{a} = 1...K_\mathrm{a}, \tag{5.3}$$

[PHFB97]. The vectors $\underline{\mathbf{e}}^{(k_\mathrm{a})}$, $k_\mathrm{a} = 1...K_\mathrm{a}$, of (5.3) contain, in addition to the desired signals, additive vectors

$$\underline{\mathbf{n}}^{(k_\mathrm{a})} = \left[\underline{n}_1^{(k_\mathrm{a})} ... \underline{n}_{NQ+W-1}^{(k_\mathrm{a})}\right]^\mathrm{T}, \quad k_\mathrm{a} = 1...K_\mathrm{a}, \tag{5.4}$$

which represent the received intercell MAI that affects the transmitted data blocks. The dimension S of the intercell MAI vector $\underline{\mathbf{n}}^{(k_\mathrm{a})}$ of (3.38) introduced in Section 3.2 now becomes $NQ+W-1$ due to the considered system parameters. The correlation properties of $\underline{\mathbf{n}}^{(k_\mathrm{a})}$ remain the same as described in Section 3.2. In Table 5.2 the vectors mentioned above and their dimensions are listed. These vectors are termed partial vectors, because they each pertain to only one user or one antenna.

The partial vectors can be serially concatenated to form total vectors [PHFB97], which, together with their dimensions, are also set out in Table 5.2.

The spatial IRs $\underline{\mathbf{h}}_\mathrm{s}^{(k,k_\mathrm{a})}$, $k = 1...K$, $k_\mathrm{a} = 1...K_\mathrm{a}$, of (2.1) and the CDMA codes $\underline{\mathbf{c}}^{(k)}$, see (5.2), determine the composite spatial channel IRs

$$\underline{\mathbf{b}}_\mathrm{s}^{(k,k_\mathrm{a})} = [\underline{b}_{\mathrm{s},1}^{(k,k_\mathrm{a})} \dots \underline{b}_{\mathrm{s},Q+W-1}^{(k,k_\mathrm{a})}]^\mathrm{T} = \underline{\mathbf{h}}_\mathrm{s}^{(k,k_\mathrm{a})} * \underline{\mathbf{c}}^{(k)}, \quad k = 1...K, k_\mathrm{a} = 1...K_\mathrm{a}. \tag{5.5}$$

The composite spatial channel IRs $\underline{\mathbf{b}}_\mathrm{s}^{(k,k_\mathrm{a})}$, $k = 1...K$, $k_\mathrm{a} = 1..K_\mathrm{a}$, of (5.5) are known at the receiver with an accuracy depending on the accuracy of the estimated spatial channel

Table 5.1. Partial and total vectors

	partial	dimension	total	dimension
data	$\underline{\mathbf{d}}^{(k)}$	N	$\underline{\mathbf{d}}$	KN
midamble	$\underline{\mathbf{m}}^{(k)}$	L		
spatial channel IRs	$\underline{\mathbf{h}}_{\mathrm{s}}^{(k,k_{\mathrm{a}})}$	W	$\underline{\mathbf{h}}$	$K_{\mathrm{a}}KW$
CDMA codes	$\underline{\mathbf{c}}^{(k)}$	Q	$\underline{\mathbf{c}}$	KQ
intercell MAI on data symbols	$\underline{\mathbf{n}}^{(k_{\mathrm{a}})}$	$NQ+W-1$	$\underline{\mathbf{n}}$	$K_{\mathrm{a}}\,(NQ+W-1)$
received signal based on transmitted symbols	$\underline{\mathbf{e}}^{(k_{\mathrm{a}})}$	$NQ+W-1$	$\underline{\mathbf{e}}$	$K_{\mathrm{a}}\,(NQ+W-1)$

IRs $\underline{\mathbf{h}}_{\mathrm{s}}^{(k,k_{\mathrm{a}})}$, $k=1...K$, $k_{\mathrm{a}}=1..K_{\mathrm{a}}$, of (2.1), since the vectors $\underline{\mathbf{c}}^{(k)}$, $k=1...K$, are known at the receiver. In the following it is assumed that the combined channel IRs $\underline{\mathbf{b}}_{\mathrm{s}}^{(k,k_{\mathrm{a}})}$, $k=1...K$, $k_{\mathrm{a}}=1..K_{\mathrm{a}}$, of (5.5) are perfectly known at the receiver. Setting out from $\underline{\mathbf{b}}_{\mathrm{s}}^{(k,k_{\mathrm{a}})}$, $k=1...K$, $k_{\mathrm{a}}=1..K_{\mathrm{a}}$, of (5.5) the system matrices $\underline{\mathbf{A}}^{(k,k_{\mathrm{a}})}$, $k=1...K$, $k_{\mathrm{a}}=1...K_{\mathrm{a}}$, with the elements [Pap00]

$$\underline{A}_{Q\cdot(n-1)+l,n}^{(k,k_{\mathrm{a}})} = \begin{cases} \underline{b}_l^{(k,k_{\mathrm{a}})} & \text{for} \quad n=1...N, \\ & \quad\quad\;\; l=1...Q+W-1, \\ 0 & \text{else}, \end{cases}$$
$$k=1...K, k_{\mathrm{a}}=1...K_{\mathrm{a}}, \tag{5.6}$$

can be established. The dimension of the system matrices $\underline{\mathbf{A}}^{(k,k_{\mathrm{a}})}$, $k=1...K$, $k_{\mathrm{a}}=1...K_{\mathrm{a}}$, is $(NQ+W-1)\times N$. From the system matrices $\underline{\mathbf{A}}^{(k,k_{\mathrm{a}})}$, $k=1...K$, $k_{\mathrm{a}}=1...K_{\mathrm{a}}$, with their elements given by (5.6), we obtain the user-specific system matrices [Bla98]

$$\underline{\mathbf{A}}^{(k)} = [\underline{\mathbf{A}}^{(k,1)\mathrm{T}} \dots \underline{\mathbf{A}}^{(k,K_{\mathrm{a}})\mathrm{T}}]^{\mathrm{T}}, \quad k=1...K, \tag{5.7}$$

of dimension $(K_{\mathrm{a}}(NQ+W-1))\times N$ and finally the total system matrix [Kle96, Naß95, Bla98, Pap00]

$$\underline{\mathbf{A}} = [\underline{\mathbf{A}}^{(1)} \dots \underline{\mathbf{A}}^{(K)}] \tag{5.8}$$

of dimension $(K_{\mathrm{a}}(NQ+W-1))\times(KN)$. From (5.1) we can form the total data vector

$$\underline{\mathbf{d}} = \left[\underline{\mathbf{d}}^{(1)\mathrm{T}} ... \underline{\mathbf{d}}^{(K)\mathrm{T}}\right]^{\mathrm{T}}. \tag{5.9}$$

Considering $\underline{\mathbf{n}}^{(k_{\mathrm{a}})}$, $k_{\mathrm{a}}=1...K_{\mathrm{a}}$, of (5.4) with the dimension $NQ+W-1$, we obtain the total intercell MAI vector $\underline{\mathbf{n}}$ according to (3.24) with dimension $K_{\mathrm{a}}(NQ+W-1)$. With $\underline{\mathbf{A}}$ of (5.8), with the total data vector $\underline{\mathbf{d}}$ of (5.9) and with the total intercell MAI vector $\underline{\mathbf{n}}$ of (3.24) with dimension $K_{\mathrm{a}}(NQ+W-1)$ we can express the total received signal, which depends on the transmitted data symbols, in the form of a total vector

$$\underline{\mathbf{e}} = \underline{\mathbf{A}}\,\underline{\mathbf{d}} + \underline{\mathbf{n}}. \tag{5.10}$$

With the matrices $\underline{\mathbf{A}}^{(k)}$ of (5.7) and the data vector $\underline{\mathbf{d}}^{(k)}$ of (5.1) the received signal

$$\underline{\mathbf{e}}_{\mathrm{d}}^{(k)} = \underline{\mathbf{A}}^{(k)} \, \underline{\mathbf{d}}^{(k)}, \quad k = 1...K, \tag{5.11}$$

which exclusively originates from transmitted signal of user k is obtained.

5.3 Linear multiuser detection

5.3.1 General

The prohibitively high implementation complexity of optimum non-linear MD algorithms like the maximum likelihood sequence estimation (MLSE) [For72, Ett76, Ver86] or the maximum likelihood symbol-to-symbol estimation (MLSSE) [HR90, Kle96], has led to the development of linear suboptimum estimators for TD–CDMA [Kle96]. In contrast to the optimum estimators, the linear estimators presented in [Kle96] are suboptimum in the sense that they deliver estimates of the total data vector $\underline{\mathbf{d}}$ without using the constraint that $\underline{\mathbf{d}}$ is taken from a finite data symbol alphabet $\mathbb{V}_{\mathrm{d}}$ during the estimation process [Kle96, Kay93]. However, they can be implemented with today's hardware and they achieve a performance which meets the specifications for the real-time operation of TD–CDMA [MSW97b, BEM+98a, BEM+98b].

The linear algorithms investigated in [Kle96] for the application in TD–CDMA are

- the decorrelating matched filter (DMF),
- the zero forcing block linear equalizer (ZF–BLE), and
- the minimum mean square error block linear equalizer (MMSE–BLE).

From the above mentioned linear algorithms which perform JD, the ZF–BLE is the state of the art algorithm for TD–CDMA with single antennas [MSW97b], see also Section 1.2. The ZF–BLE outperforms the DMF and the computational cost of the ZF–BLE is smaller than that of the MMSE–BLE [Kle96]. Furthermore, the MMSE–BLE requires the knowledge of the covariance matrix of the data vector $\underline{\mathbf{d}}$, see Table 5.2. The covariance matrix of the total data vector $\underline{\mathbf{d}}$ does not include any spatial correlations, since the data symbols themselves do not have any spatial dependency. However, the main focus in this thesis is on the exploitation of covariance matrices including spatial correlations. Therefore, the MMSE is not considered in this thesis for data detection and the ZF–BLE is exclusively considered.

5.3.2 ZF-BLE

As already mentioned in Section 5.1, the ZF-BLE is well known [Wha71, Ver98]. Therefore, only a brief description of the ZF-BLE follows in this section. For more detailed information concerning the ZF-BLE, especially in combination with CDMA, the reader is referred to [Ver98, Kle96, Naß95, Bla98].

In TD-CDMA the total received signal $\underline{\mathbf{e}}$ is determined by (5.10). The vector $\underline{\mathbf{e}}$ of (5.10) is known at the receiver. This is also approximately true for the system matrix $\underline{\mathbf{A}}$ of (5.8) with the accuracy of $\underline{\mathbf{A}}$ depending on the accuracy of the channel IR estimates $\hat{\underline{\mathbf{h}}}_{\mathrm{s}}$ [BPW99], see (2.11). As already mentioned in Section 5.1, throughout this chapter the channel IRs are assumed to be perfectly known at the receiver. Consequently, $\underline{\mathbf{A}}$ of (5.8) is also assumed to be perfectly known. The vectors $\underline{\mathbf{d}}$ and $\underline{\mathbf{n}}$ in (5.10) are unknown. However, the covariance matrix $\underline{\mathbf{R}}_{\mathrm{n}}$ of $\underline{\mathbf{n}}$, see (3.25), shall be assumed to be known. The task of data detection consists of determining $\underline{\mathbf{d}}$ of (5.9) from $\underline{\mathbf{e}}$ of (5.10). (5.10) can be considered as a linear system of equations for the KN unknown data symbols contained in $\underline{\mathbf{d}}$ [Pap00]. Then, by applying the ZF–BLE to perform JD, a linear estimate [Kle96, Naß95, Bla98]

$$\hat{\underline{\mathbf{d}}} = \left(\underline{\mathbf{A}}^{*\mathrm{T}} \underline{\mathbf{R}}_{\mathrm{n}}^{-1} \underline{\mathbf{A}}\right)^{-1} \underline{\mathbf{A}}^{*\mathrm{T}} \underline{\mathbf{R}}_{\mathrm{n}}^{-1} \underline{\mathbf{e}} \tag{5.12}$$

of $\underline{\mathbf{d}}$ can be obtained from (5.10). The ZF-BLE is based on the Gauß-Markov estimation [Kay93], which minimizes the quadratic form

$$\mathcal{Q}\left(\underline{\mathbf{d}}\right) = \left(\underline{\mathbf{e}} - \underline{\mathbf{A}}\,\underline{\mathbf{d}}\right)^{*\mathrm{T}}\ \underline{\mathbf{R}}_{\mathrm{n}}^{-1}\ \left(\underline{\mathbf{e}} - \underline{\mathbf{A}}\,\underline{\mathbf{d}}\right), \tag{5.13}$$

and which leads to an estimate of the data vector $\underline{\mathbf{d}}$ with minimum variance [Kay93]. By substituting $\underline{\mathbf{e}}$ of (5.10) in (5.12) we obtain

$$\hat{\underline{\mathbf{d}}} = \underline{\mathbf{d}} + \left(\underline{\mathbf{A}}^{*\mathrm{T}} \underline{\mathbf{R}}_{\mathrm{n}}^{-1} \underline{\mathbf{A}}\right)^{-1} \underline{\mathbf{A}}^{*\mathrm{T}} \underline{\mathbf{R}}_{\mathrm{n}}^{-1} \underline{\mathbf{n}}. \tag{5.14}$$

From (5.14) it is evident that $\hat{\underline{\mathbf{d}}}$ contains no ISI and MAI term, but only the desired symbols and a noise term with the covariance matrix $\left(\underline{\mathbf{A}}^{*\mathrm{T}} \underline{\mathbf{R}}_{\mathrm{n}}^{-1} \underline{\mathbf{A}}\right)^{-1}$ [Kle96]. Consequently, $\hat{\underline{\mathbf{d}}}$ of (5.12) and (5.14) is an unbiased estimate of $\underline{\mathbf{d}}$ [Wha71].

The main computational effort for solving (5.12) is the inversion of the matrix $\left(\underline{\mathbf{A}}^{*\mathrm{T}} \underline{\mathbf{R}}_{\mathrm{n}}^{-1} \underline{\mathbf{A}}\right)$. To reduce this effort the following approach is proposed in [Kle96, Bla98]: Setting out from the representation

$$\left(\underline{\mathbf{A}}^{*\mathrm{T}} \underline{\mathbf{R}}_{\mathrm{n}}^{-1} \underline{\mathbf{A}}\right)\ \hat{\underline{\mathbf{d}}} = \underline{\mathbf{A}}^{*\mathrm{T}} \underline{\mathbf{R}}_{\mathrm{n}}^{-1} \underline{\mathbf{e}} \tag{5.15}$$

of (5.12), first a Cholesky decomposition of the matrix $\left(\underline{\mathbf{A}}^{*\mathrm{T}} \underline{\mathbf{R}}_{\mathrm{n}}^{-1} \underline{\mathbf{A}}\right)$ is performed [Kle96, Naß95, Zur64] and then two trivial linear systems of equations are solved [Zur64].

For both the single antenna receiver and the receiver with antenna arrays the detector representation of (5.12) is valid, except for the dimensions of the vectors and matrices on the right hand side of (5.12). When considering K_a antenna elements at the BS receiver, the number of equations in the linear system of equations given in (5.12) is increased by the factor K_a, while the number of unknown symbols KN remains the same. From estimation theory it is known [Kay93] that in the case of an overdetermined linear system of equations the unknown components can be estimated more precisely than in a determined system. Furthermore, from (5.14) it becomes obvious that besides increasing the number K_a of antenna elements at the receiver an improvement of the data detection quality can only result from a reduction of the noise enhancement represented by the matrix $\left(\underline{\mathbf{A}}^{*\mathrm{T}}\underline{\mathbf{R}}_\mathrm{n}^{-1}\underline{\mathbf{A}}\right)^{-1}\underline{\mathbf{A}}^{*\mathrm{T}}\underline{\mathbf{R}}_\mathrm{n}^{-1}$ in (5.14). This noise enhancement, which is typical for JD processes [Ver98, Kle96], leads to an SNR degradation which is investigated in Section 5.3.2 especially when considering antenna arrays.

5.3.3 SNR degradation of the ZF-BLE

In this section an important property of JD processes concerning the relationship between the input and output SNR is discussed. This relationship can be quantitatively described by the SNR degradation [Kle96] which is valid in the presence of intracell MAI and ISI. An approximation of this SNR degradation is empirically determined.

According to (5.14) the JD process is transparent for the transmitted data [BPW99, Pap00]. The only effect of the JD process is a transformation of the input intercell MAI vector $\underline{\mathbf{n}}$ of (3.24) with the dimension $K_\mathrm{a}(NQ+W-1)$ into an output MAI vector $\left(\underline{\mathbf{A}}^{*\mathrm{T}}\underline{\mathbf{R}}_\mathrm{n}^{-1}\underline{\mathbf{A}}\right)^{-1}\underline{\mathbf{A}}^{*\mathrm{T}}\underline{\mathbf{R}}_\mathrm{n}^{-1}\underline{\mathbf{n}}$ according to (5.14). This transformation leads to a noise enhancement, which is typical for JD processes [Kle96], i.e. JD always goes along with a noise enhancement. Since JD enhances any kind of noise that affects the transmission of the desired signals, the author does not restrict the descriptions in this Section 5.3.3 to intercell MAI as in the previous sections. Therefore, instead of the SIR the SNR is considered in this section. To quantify these noise enhancements, in the following the ratio of the mean SNR γ_MF of the output signal of a filter matched to the composite spatial channel IRs $\underline{\mathbf{b}}_\mathrm{s}^{(k,k_\mathrm{a})}$, $k=1...K$, $k_\mathrm{a}=1...K_\mathrm{a}$ of (5.5) and the symbol SNR $\gamma_{\mathrm{ZF-BLE},i}$, $i=1...KN$, of the output signal of the ZF-BLE is determined. The ratio $\gamma_\mathrm{MF}/\gamma_{\mathrm{ZF-BLE},i}$, $i=1...KN$, is termed SNR degradation δ_i of the symbols $i=1...KN$ by applying ZF–BLE [Kle96].

In the literature [Ver86, MH94, Ver98, Lup89] the performance degradation of a multiuser detector due to intracell MAI is often quantified by the asymtotic efficiency introduced in [Ver84, Ver86]. If $e_k(\sigma_\mathrm{w})$ is actually the energy that the user k would require to achieve a certain BER $P_{\mathrm{b},k}(\sigma_\mathrm{w})$ without intracell MAI in an additive white Gaussian noise channel with power spectral density σ_w^2, and if w_k is actually the energy that the user k would require to achieve the same BER $P_{\mathrm{b},k}(\sigma_\mathrm{w})$ in the presence of intracell MAI, then the asymtotic efficiency of user k is defined as

$$\eta_k = \lim_{\sigma_{\mathrm{w}} \to 0} \frac{e_k(\sigma_{\mathrm{w}})}{w_k} \tag{5.16}$$

[Ver86, LV90]. In (5.16) neither intercell MAI nor ISI is considered. The asymtotic efficiency η_k of (5.16) is a limiting measure of how well a multiuser detector performs in the presence of intracell MAI relative to its performance in the absence of intracell MAI [MH94]. The worst case asymtotic efficiency for the data symbol n of user k over all possible energies of the other interfering and non-interfering data symbols [LV90] is the near-far resistance $\overline{\eta}_{k,n}$, which also has been introduced in [Ver86]. The near-far resistance $\overline{\eta}_{k,n}$ is a measure of the robustness of the detector with respect to variations in the received intracell MAI energies [MH94, Lup89]. It is a performance measure of the multiuser detector, which is independent of the symbol input SNR $\gamma_{\mathrm{in},i}$, $i = 1...KN$, of the detector and which is especially of interest in an environment where transmission energy changes in time. Let us establish the normalized $K \times K$ correlation matrix [Ver98]

$$\underline{\mathbf{R}}_{\mathrm{c}} = \frac{1}{Q} \cdot \begin{bmatrix} \underline{\mathbf{c}}^{(1)*\mathrm{T}} \\ \vdots \\ \underline{\mathbf{c}}^{(K)*\mathrm{T}} \end{bmatrix} \cdot \left[\underline{\mathbf{c}}^{(1)} \dots \underline{\mathbf{c}}^{(K)}\right] \tag{5.17}$$

of the CDMA codes $\underline{\mathbf{c}}^{(k)}$, $k = 1..K$, of (5.2), where Q is the dimension of the CDMA codes. In [Ver98] it is shown that with (5.17) and when assuming a single tap channel, i.e. $W = 1$, see Chapter 2, and transmitting only one single data symbol $N = 1$ per user, the near-far resistance $\overline{\eta}_{k,1}$ of the optimum multiuser detector takes the form

$$\overline{\eta}_{k,1} = \frac{1}{\left[\underline{\mathbf{R}}_{\mathrm{c}}^{-1}\right]_{k,k}}, \quad k = 1...K, \tag{5.18}$$

where $[\cdot]_{i,i}$ denotes the diagonal element i of the matrix in brackets.

In the following the connection between the near-far resistance $\overline{\eta}_{k,1}$ of (5.18) and the SNR degradation δ_k of user k when applying the ZF-BLE is shown. At first only a single element antenna is considered at the BS. Hence, instead of the $K \cdot K_{\mathrm{a}}$ composite spatial channel IRs $\underline{\mathbf{b}}_{\mathrm{s}}^{(k,k_{\mathrm{a}})}$, $k = 1...K$, $k_{\mathrm{a}} = 1...K_{\mathrm{a}}$, of (5.5) only the K composite channel IRs $\underline{\mathbf{b}}^{(k)}$, $k = 1...K$, of dimension $Q+W-1$ are relevant for the following description. It is assumed that the composite channel IRs $\underline{\mathbf{b}}^{(k)}$, $k = 1...K$, are perfectly known at the receiver and that each transmitted symbol $\underline{d}_i$, $i = 1...KN$, of all K users has the magnitude

$$\mid \underline{d}_i \mid = 1, \quad i = 1 \dots KN. \tag{5.19}$$

In the case of spatially and temporally uncorrelated intercell MAI and taking account of the mean output SNR γ_{MF} of the MF and the symbol output SNRs $\gamma_{\mathrm{ZF-BLE},i}$, $i = 1..KN$, of the ZF–BLE the SNR degradation takes the form

$$\delta_i = \frac{\gamma_{\mathrm{MF}}}{\gamma_{\mathrm{ZF-BLE},i}} = \mathrm{E}\{\mid \underline{\mathbf{b}}^{(k)} \mid^2\} \left[\left(\underline{\mathbf{A}}^{*\mathrm{T}}\underline{\mathbf{A}}\right)^{-1}\right]_{i,i}, \quad i = 1 \dots KN, \tag{5.20}$$

according to [Kle96, Pap00]. The term $\mathrm{E}\{|\ \underline{\mathbf{b}}^{(k)}\ |^2\}$ in (5.20) exclusively depends on the mean energy of the composite channel IRs. The system matrix $\underline{\mathbf{A}}$ consists of the composite channel IRs $\underline{\mathbf{b}}^{(k)}$, $k = 1...K$, see (5.6). Therefore, the normalized system matrix [Pap00]

$$\underline{\tilde{\mathbf{A}}} = \frac{1}{\sqrt{\mathrm{E}\{|\ \underline{\mathbf{b}}^{(k)}\ |^2\}}}\ \underline{\mathbf{A}} \tag{5.21}$$

is obtained. Then, the SNR degradation of (5.20) can be written as

$$\delta_i = \left[\left(\underline{\tilde{\mathbf{A}}}^{*\mathrm{T}}\underline{\tilde{\mathbf{A}}}\right)^{-1}\right]_{i,i}, \quad i = 1\ldots KN. \tag{5.22}$$

(5.22) shows that the SNR degradations δ_i, $i = 1...KN$, of the ZF–BLE exclusively depends on the elements of the normalized system matrix $\underline{\tilde{\mathbf{A}}}$ and not on the symbol input SNR $\gamma_{\mathrm{in},i}$, $i = 1...KN$, at the ZF–BLE. Furthermore, it can be seen from (5.22) that the analysis of the SNR degradation of the ZF–BLE can be interpreted as the analysis of the diagonal elements of an inverted matrix. The diagonal elements of an inverted matrix depend on the structure of the original matrix [Zur64]. Furthermore, assuming transmission via a single tap channel, i.e. $W = 1$, and transmitting only one single data symbol $N = 1$, the SNR degradations δ_k, $k = 1...K$, of (5.22) of the ZF-BLE are equal to the reciprocals of the near-far resistances $\overline{\eta}_{k,1}$, $k = 1...K$, of (5.18). This connection between the near-far resistances $\overline{\eta}_{k,1}$, $k = 1...K$, and the SNR degardations δ_k, $k = 1...K$, is not valid, when, e.g. the MMSE–BLE is applied. With $\sigma_{\mathrm{w}} \rightarrow 0$ the ZF–BLE converges to the performance of the MMSE–BLE [Ver98, Kle96]. Therefore, the asymtotic efficiency η_k of (5.16) is the same for ZF–BLE and MMSE–BLE, and, consequently, this is also true for the near-far resistances $\overline{\eta}_{k,1}$, $k = 1...K$, of (5.18) of both detectors. In opposite to the near-far resistances $\overline{\eta}_{k,1}$, $k = 1...K$, of (5.18) of ZF–BLE and MMSE–BLE, the SNR degradations of ZF–BLE and MMSE–BLE are different. Utilizing e.g. the MMSE–BLE, as shown in [Kle96] the SNR degardations $\delta_{\mathrm{MMSE},i}$, $i = 1...KN$, are not independent from the symbol input SNR $\gamma_{\mathrm{in},i}$, $i = 1...KN$, of the detector and, consequently, the SNR degardations $\delta_{\mathrm{MMSE},i}$, $i = 1...KN$, are different from the SNR degardations δ_i, $i = 1...KN$, valid for the ZF–BLE.

The aim of the following investigations is to find an approximation of the mean SNR degradation δ which is as simple as possible, assuming random CDMA codes. Over and above this, the effect of the ISI on the mean SNR degradation δ is investigated. The existing approximations of SNR degradation with use of random spreading codes, as for example in [BTB96] are based on geometric observation of vector spaces. As far as the author knows, the expectations of the near-far resistances $\mathrm{E}\{\overline{\eta}_{k,1}\}$ with random selection of the CDMA codes $\underline{\mathbf{c}}^{(k)}$, $k = 1...K$, of (5.2) were first determined in [Ver98] by extensive mathematical proof for

$$\mathrm{E}\{\overline{\eta}_{k,1}\} = 1 - \frac{K-1}{Q}, \quad k = 1...K. \tag{5.23}$$

In [Mue01] there are also corresponding observations as regards the expectation $\mathrm{E}\{\gamma_{\mathrm{out}}\}$ of the SNR γ_{out} at the output of a multiuser detector with use of random spreading codes.

All approximations and observations about mean SNR degradation δ or near-far resistance $\overline{\eta}_{k,1}$ previously referred to in the literature share the common feature that ISI was not included in the observations. In 1998 the author attempted to create a simple simulation concept which, on the basis of (5.22), empirically verifies the literature approximations of mean SNR degradation δ without taking account of ISI. In addition, in the simulation concept specified below the dependency of the mean SNR degradation δ on the number K of users and on the dimension $Q+W-1$ of the composite channel IRs $\underline{\mathbf{b}}^{(k)}$, $k=1...K$, is included in the investigations, in which case the influence of MAI and ISI are also taken into account.

To simplify matters the real and imaginary parts of the components of the effective channel IRs $\underline{\mathbf{b}}^{(k)}$, $k=1...K$, are obtained by sampling zero-mean white gaussian processes and not, as described in Section 5.2 by a convolution of the CDMA codes $\underline{\mathbf{c}}^{(k)}$, $k=1...K$, of (5.2) with the channel IRs $\underline{\mathbf{h}}_{\mathrm{RP}}^{(k)}$ of (2.3). For each user k a random composite channel IR $\underline{\mathbf{b}}^{(k)}$, $k=1...K$, of dimension $Q+W-1$ is selected, see Section 5.2. For the variance of the components $\underline{b}_l^{(k)}$, $k=1...K$, $l=1...Q+W-1$, of the vectors $\underline{\mathbf{b}}^{(k)}$, $k=1...K$, the following applies:

$$\mathrm{E}\{|\underline{b}_l^{(k)}|^2\}=1\,,k=1...K,l=1...Q+W-1. \tag{5.24}$$

The trivial case in which the dimension Q of the CDMA codes is equal to one is excluded from the following investigations, so that $Q>1$ holds. The following two cases are identified during the investigations:

- Exclusively intracell MAI and no ISI is considered. In this case it is sufficient to assume only one single transmit symbol per user and a transmission over a channel with only one single channel coefficient. If $W=1$ is the dimension of the channel IRs $\underline{\mathbf{h}}_{\mathrm{RP}}^{(k)}$, $k=1...K$, of (2.3) and $N=1$ is the number of transmit symbols, the matrix $\underline{\mathbf{A}}$ of (5.8) takes the form

$$\underline{\mathbf{A}}=[\underline{\mathbf{b}}^{(1)},\underline{\mathbf{b}}^{(2)},...,\underline{\mathbf{b}}^{(K)}] \tag{5.25}$$

  with the dimension $Q\times K$.

- Both ISI and also intracell MAI are taken into consideration. If consecutively transmitted data symbols are assigned the numbers $n=1...N$ and if $Q\geq W-1$, then a particular data symbol with the number n will only be influenced by the data symbol previously transmitted in time with the number $n-1$ and by the data symbol transmitted after it in time with the number $n+1$. In this case it is sufficient to assume in the simulations N equal to 3 transmitted data symbols per user. If

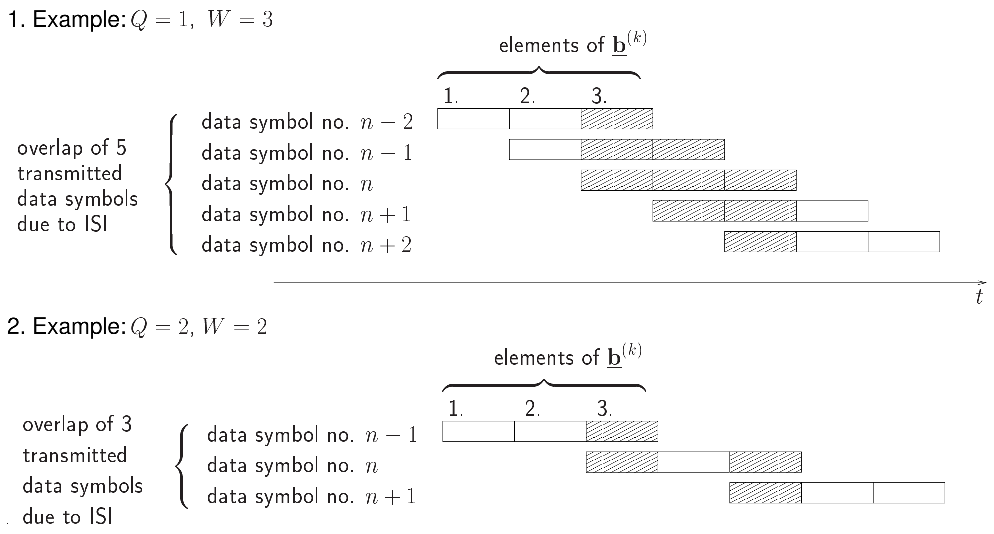

Fig. 5.1. Examples for different numbers N of data symbols which are required, depending on Q and W, to take full account of the ISI

$Q < W-1$, then more than 3 data symbols are involved in the ISI. Fig. 5.1 is valid for the example 1 ($Q=1$ and $W=3$) and example 2 ($Q=2$ and $W=2$) to illustrate the differing number N of required symbols to take full account of the ISI. In the case that $W>1$ the number N of considered data symbols is given by

$$N = \begin{cases} 3 & ,\text{if } Q \geq W-1, \\ 2\left(\frac{W-1}{Q}\rfloor - 1\right) & ,\text{if } Q < W-1. \end{cases}, \tag{5.26}$$

where $\rfloor$ means that the quotient $(W-1)/Q$ can be rounded off to a whole number. The system matrix $\underline{\mathbf{A}}$ of (5.21) then has the dimension $(NQ+W-1)\times(KN)$.

An experiment for determining the mean SNR degradation δ by approximation would be identified by the fact that a matrix $\underline{\tilde{\mathbf{A}}}$ of (5.21) taking into account ISI and intracell MAI will be formed and inverted in order to obtain the SNR degradations δ_i, $i=1...KN$, in accordance with (5.22). By averaging the SNR degradations δ_i, $i=1...KN$, and by averaging over a sufficiently large number of experiments δ_i, $i=1...KN$, a mean SNR degradation δ is determined. In Figs. 5.2 and 5.3 these mean SNR degradations are shown as a function of the dimension $Q+W-1$ of the composite channel IRs $\underline{\mathbf{b}}^{(k)}$, $k=1...K$, of the K users considered, where W is the dimension of the assumed channel IRs $\underline{\mathbf{h}}_{\mathrm{RP}}^{(k)}$, $k=1...K$. The curves in Fig. 5.2 show the mean SNR degradation δ depending on CDMA code dimension Q and the number of users K without taking account of ISI. In the case K equal to 1 no MAI occurs and the mean degradation δ is equal to 1 as expected, i.e the ZF-BLE algorithm does not cause any degradation. For K greater than 1 the mean SNR degradation δ assumes very large values, if Q is less than K. If we increase Q, the mean SNR degradation δ approaches 1 independently of K.

The curve for the mean SNR degradation δ depending on Q and K could be approximated by the author with the simulation concept presented by the function

$$\delta \approx \frac{Q+1}{Q-K+1}, \; K>1, \; Q>K. \tag{5.27}$$

For large numbers of users K (5.27) shows a good match with the approximations in [BTB96, Ver98, Mue01] as well as with the guide value of the expected values $\mathrm{E}\{\overline{\eta}_{k,1}\}$, $k = 1...K$, of the near-far resistances according to (5.23). The deviations between the reciprocals of δ of (5.27) and $\mathrm{E}\left\{\overline{\eta}_{k,1}\right\}$ of (5.23) are negligibly small for large numbers of users K. The dashed curves in Fig. 5.2 show the curve of function δ according to (5.27). These curves show the good quality of the approximation.

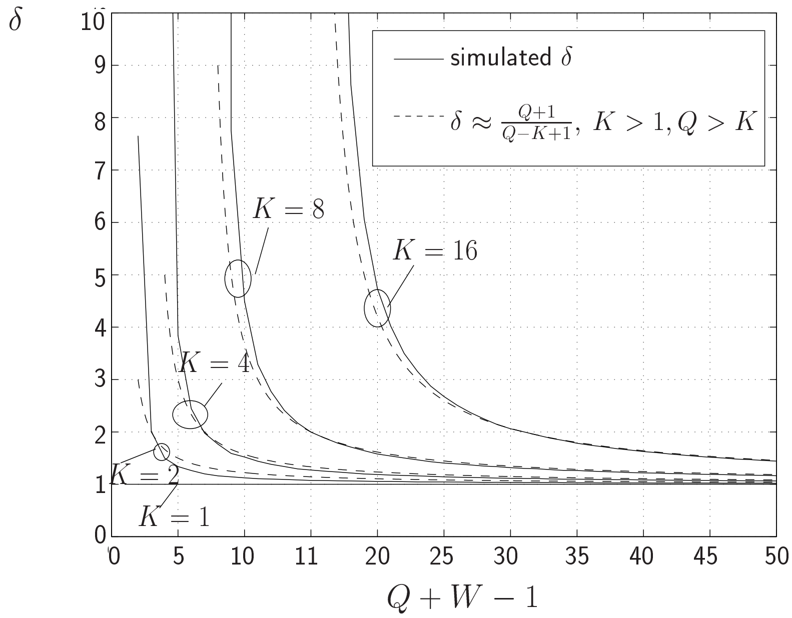

Fig. 5.2. Simulated and approximated mean SNR degradation δ for different numbers K of users versus $Q+W-1$ without consideration of ISI

The different curves in Fig. 5.3 are obtained by taking $K = 8$ users into account by variation in the dimension W of the channel IRs $\underline{\mathbf{h}}_{\mathrm{RP}}^{(k)}$, $k = 1...K$, of (2.3), in which case the dimension of the composite channel IRs $\underline{\mathbf{b}}^{(k)}$, $k = 1...K$, also changes, see (5.24). The striking feature of the curves shown in Fig. 5.3 is that the curves $W-1 = 1$ to $W-1 = 8$ are just copies, displaced along the $Q+W-1$ axis of the curves which apply for the case $W-1 = 0$, i.e. without ISI. Here the individual curves are displaced approximately by the amount $W-1$ from the curve $W-1 = 0$. If for example we assume the case of $Q = 15$ the amount of mean SNR degradation δ of (5.22) for $K = 8$ users is equal to 2 by approximation. If one now allows ISI, for example through the existence of channel IRs $\underline{\mathbf{h}}_{\mathrm{RP}}^{(k)}$ of (2.3) of dimension $W = 9$, the structure of the system matrix $\underline{\tilde{\mathbf{A}}}$ of (5.21) changes, since the dimensions of the composite channel IRs change and the arrangement of the composite channel IRs $\underline{\mathbf{b}}^{(k)}$, $k = 1...K$, in the system matrix $\underline{\mathbf{A}}$ changes, see (5.6). However, for the case $K = 8$, $Q = 15$ and $W - 1 = 8$, i.e. for $Q + W - 1 = 23$, despite the presence of ISI, the same SNR degradations figure $\delta = 2$ is still obtained as would be obtained without ISI. For the case $K = 8$ and $W - 1 = 1$ to $W - 1 = 8$ therefore ISI is negligible and the function δ according to (5.27) still applies.

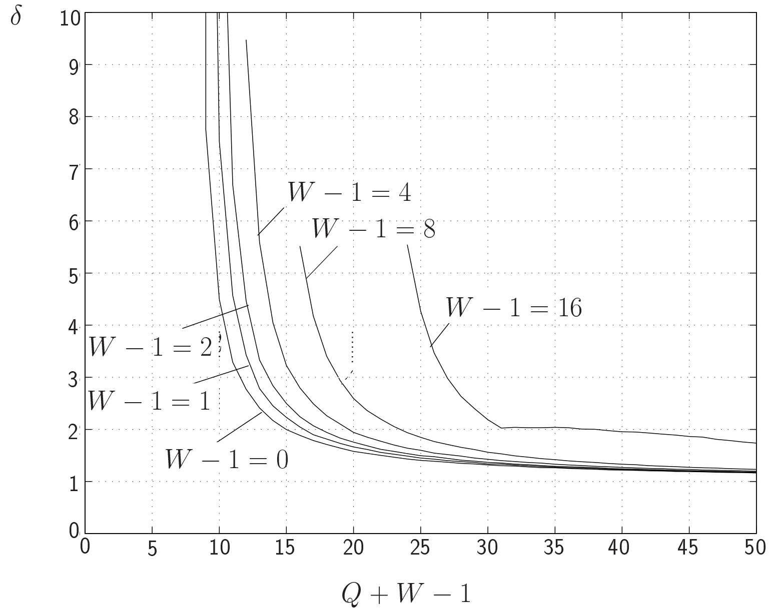

Fig. 5.3. Simulated mean SNR degradation δ versus $Q + W - 1$ under consideration of MAI and ISI; $K = 8$; $W > 1$

In Fig. 5.3 it is clear from curve $W - 1 = 16$ and in Fig. 5.4 from curves $W - 1 = 8$ and $W - 1 = 16$ that ISI is not basically negligible and that the approximation δ according (5.27) does not apply without restrictions. The results shown in the Figs. 5.3 and 5.4 allow the following statements to be made: If the composite channel IRs $\underline{\mathbf{b}}^{(k)}$, $k = 1...K$, at the receiver are perfectly known and if data vector $\underline{\mathbf{d}}$ in accordance with (5.12) is estimated, the effect of the ISI on the mean SNR degradation δ is basically negligible when

$$Q > K \geq W - 1. \tag{5.28}$$

The approximation of the SNR degradation δ ccording to (5.27) is applicable in the case (5.28). On the basis of the Figs. 5.3 and 5.4 is becomes clear that for the case

$$2K \leq W - 1 \leq Q \tag{5.29}$$

the ISI cannot be ignored and thus (5.27) cannot be usefully employed. If however

$$Q < W - 1, \tag{5.30}$$

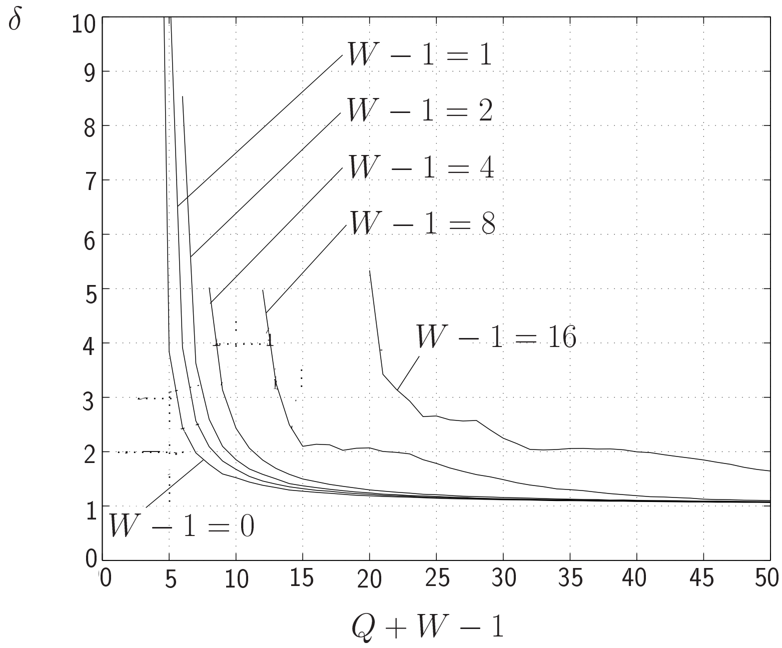

Fig. 5.4. Simulated mean SNR degradation δ versus $Q + W - 1$ under consideration of MAI and ISI; $K = 4$; $W > 1$

i.e. if the channel IRs are longer than the CDMA codes and if

$$2K \leq W - 1, \tag{5.31}$$

then N is greater than three, see (5.26). Despite the fact that the ISI extends in this case over a large number of symbols, δ is valid according to (5.27). If the system matrix $\underline{\mathbf{A}}$ of (5.8) is largely fully occupied, i.e. if it includes a few disappearing elements, the mean SNR degradation δ largely depends on the dimension $(NQ + W - 1) \times (KN)$ of the system matrix $\underline{\mathbf{A}}$. If N is now enlarged, then NQ and KN are the significant factors which determine the dimension of the matrix $\underline{\mathbf{A}}$. In this case the following applies:

$$\delta \approx \frac{NQ + W}{NQ + W - K} \approx \frac{Q + 1}{Q - K + 1}, \tag{5.32}$$

i.e. the approximation δ according to (5.27) can be used here.

With the knowledge of the mean SNR degradation δ we can determine the relation of the mean input SNR γ_{in} and the mean output SNR $\gamma_{\text{ZF-BLE}}$ of the ZF-BLE. With C the mean power of each desired information-carrying signal at each antenna and I the mean total noise and interference power, respectively, with respect to a single receiver antenna, the input SNR and SIR, respectively,

$$\gamma_{\text{in}} = \frac{C}{I} \tag{5.33}$$

is given. With (5.19) the output SNR

$$\gamma_{\mathrm{ZF-BLE}} = \frac{\mathrm{E}\{|\underline{d}_n^{(k)}|^2\}}{\mathrm{E}\{|\hat{\underline{d}}_n^{(k)} - \underline{d}_n^{(k)}|^2\}} = \frac{1}{\mathrm{E}\{|\hat{\underline{d}}_n^{(k)} - \underline{d}_n^{(k)}|^2\}} \tag{5.34}$$

at the output of the detector can be obtained. Taking into account the processing gain Q, we obtain from (5.27), (5.33) and (5.34) the approximation

$$\gamma_{\mathrm{ZF-BLE}} \approx \frac{(Q-K+1)\cdot Q}{Q+1}\cdot\gamma_{\mathrm{in}}. \tag{5.35}$$

It has been shown in this section that the approximated SNR degradation δ according to (5.27) obviously depends on the dimension of the Matrix $\tilde{\underline{\mathbf{A}}}$ of (5.21). To determine δ of (5.27) a system matrix $\underline{\mathbf{A}}$ with the dimension $Q\times K$ is sufficient, since the SNR degradation is the same for each transmitted data symbol. If the received signals at the K_{a} antenna elements were to be uncorrelated, (5.27) could be extended to

$$\delta \approx \frac{K_{\mathrm{a}}Q+1}{K_{\mathrm{a}}Q-K+1} \tag{5.36}$$

according to the changes in the dimensions of the system matrix $\underline{\mathbf{A}}$ when considering K_{a} antenna elements, see (5.6), (5.7) and (5.8). Fig. 5.5 shows the approximation δ of (5.36) for the cases K_{a} equal to 1,2,4 and 8 antennas.

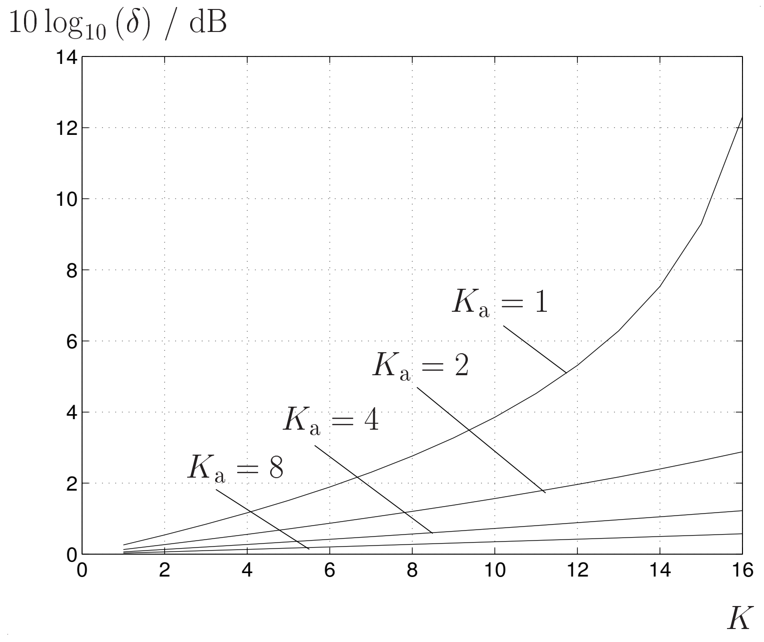

Fig. 5.5. Approximation (5.36) of the SNR degradation δ; $Q=16$; parameter: K_{a}

5.4 Multi-Step Joint Detection (MSJD) with adaptive arrays

5.4.1 General

The known linear JD algorithms [Ver98, Pro89, Kle96] utilized up to now for time-slotted CDMA can be improved by the introduction of iterative schemes [Poo00, Ree98, Moh98, MuH97] following the so-called turbo principle [Hag97] by which detector performances rather close to the performance of the ideal non-linear multiuser detector [Poo00] can be reached with reasonable computational effort. In the following a turbo scheme adapted to TD-CDMA is intoduced, which is termed Multi-Step Joint Detection (MSJD) by the author. MSJD is a combination of JD with an iterative interference elimination scheme. It is shown in [BJL+02] that MSJD can be interpreted as a complexity reduced version of the turbo multiuser detectors, which are known from literature [Poo00]. MSJD was developed at the Research Group for RF Communications of the University of Kaiserslautern [WBOW00], where the author has contributed to the development.

In Section 5.3.3 it is shown that intracell MAI besides intercell MAI is the dominant detrimental effect in CDMA systems. The main goal of MSJD is to reduce intracell MAI, and therefore, to enhance system performance of time-slotted CDMA for given levels of intercell MAI. However, similar to conventional JD, see (5.12), interference correlation matrices can be considered in data detection in order to mitigate intercell MAI. In the following we refer to the reduction of intracell MAI by MSJD. The possibility to consider intercell MAI correlations in MSJD is demonstrated in the mathematical description of MSJD which is given later on.

Due to the high SNR degradation δ especially in the single antenna case, see (5.36) and Fig. 5.5, the impact of intracell MAI is extremely high especially when the number K of simultaneously active users is equal to the dimension Q of the CDMA codes that is if the system is fully loaded. When applying the ZF algorithm, according to (5.36) the SNR degradation δ can be reduced by utilizing more than one antenna element. However, for otherwise fixed system parameters the transmission quality decreases with an increasing number K of user signals to be detected by conventional linear JD, see (5.36) and Fig. 5.5. At first sight there exists no obvious possibility to increase the transmission quality without reducing the number K of supportable users. However, a way out of this dilemma is revealed by the following insight: Considering intracell MAI reduction, the best we can do, if at least $K' < K$ of the data vectors $\underline{\mathbf{d}}^{(k)}$, $k = 1...K$ of (5.1) are perfectly known, is to reconstruct the received user signals $\underline{\mathbf{e}}_{\mathrm{d}}^{(k)}$, $k = 1...K'$, of (5.11) and subtract them from the received signal $\underline{\mathbf{e}}$ of (5.10) to get an intracell MAI reduced received signal. In general none of the K data vectors $\underline{\mathbf{d}}^{(k)}$, $k = 1...K$, are perfectly known. To reduce the data detection errors we apply FEC decoding, where the reduction of detection errors depends on the considered coding scheme and FEC code. In the following we use a convolutional code [ViO79] for FEC coding. Furthermore, we consider the FEC decoded bits for the signal reconstruction. Investigations concerning the signal reconstruction quality in the presence of incorrectly decoded bits are given in Section 7.2.3.

The concept of MSJD, independently of the number K_{a} of considered antenna elements, can be briefly summarized as follows:

1. By dividing the K users into two groups, the number of signals to be simultaneously separated by JD is divided by two compared to conventional JD, which leads to a smaller SNR degradation δ of (5.27) [Kle96].
2. When jointly detecting the signals of one user group, we now have to take into account intracell MAI, which is caused by the other group.
3. The subtraction of the reconstructed signals leads to remaining signals with a significantly reduced intracell MAI [KIH82b, KIH83].

For single antenna receivers a detailed description of MSJD is given in [Ost01]. In the following the mathematical description of the basic ideas of MSJD is briefly recapitulated considering system matrices $\underline{\mathbf{A}}^{(k)}$, $k = 1...K$, of (5.7) valid for systems with antenna arrays at the receiver. In [Ost01] it is shown that the division of the K users into two groups of the same size is optimum for MSJD. The first group $g = 1$ comprises the users $k = 1 \ldots K_{\mathrm{g}}$, whereas the second group $g = 2$ comprises the users $k = K_{\mathrm{g}} + 1 \ldots K$. If for instance the total number K of users is equal to 16 and $K_{\mathrm{g}} = 8$ holds, then the first group would contain the users $k = 1 \ldots 8$, and the second group would contain the users $k = 9 \ldots 16$. Now, with $\underline{\mathbf{d}}^{(k)}$ of (5.1), the data vectors

$$\underline{\mathbf{d}}_{\mathrm{G}}^{(1)} = \left[\underline{\mathbf{d}}^{(1)\mathrm{T}} \ldots \underline{\mathbf{d}}^{(K_{\mathrm{g}})\mathrm{T}}\right]^{\mathrm{T}} \tag{5.37}$$

and

$$\underline{\mathbf{d}}_{\mathrm{G}}^{(2)} = \left[\underline{\mathbf{d}}^{(K_{\mathrm{g}}+1)\mathrm{T}} \ldots \underline{\mathbf{d}}^{(K)\mathrm{T}}\right]^{\mathrm{T}} \tag{5.38}$$

of dimension $K_{\mathrm{g}}N$ and with the matrices $\underline{\mathbf{A}}^{(k)}$ of (5.7) the system matrices

$$\underline{\mathbf{A}}_{\mathrm{G}}^{(1)} = \left[\underline{\mathbf{A}}^{(1)} \ldots \underline{\mathbf{A}}^{(K_{\mathrm{g}})}\right] \tag{5.39}$$

and

$$\underline{\mathbf{A}}_{\mathrm{G}}^{(2)} = \left[\underline{\mathbf{A}}^{(K_{\mathrm{g}}+1)} \ldots \underline{\mathbf{A}}^{(K)}\right] \tag{5.40}$$

of dimension $(K_{\mathrm{a}}(NQ + W - 1)) \times (K_{\mathrm{g}}N)$ are introduced. Furthermore, the interference that affect the reception of the signals of group g are $\underline{\mathbf{n}}_{\mathrm{G}}^{(g)}$, $g = 1, 2$, and these vectors $\underline{\mathbf{n}}_{\mathrm{G}}^{(g)}$,

$g = 1, 2$, consist of the received signals of group $(3 - g)$ and the intercell MAI vector $\underline{\mathbf{n}}$ of (3.24), i.e.,

$$\underline{\mathbf{n}}_{\mathrm{G}}^{(1)} = \underline{\mathbf{A}}_{\mathrm{G}}^{(2)} \underline{\mathbf{d}}_{\mathrm{G}}^{(2)} + \underline{\mathbf{n}} \tag{5.41}$$

and

$$\underline{\mathbf{n}}_{\mathrm{G}}^{(2)} = \underline{\mathbf{A}}_{\mathrm{G}}^{(1)} \underline{\mathbf{d}}_{\mathrm{G}}^{(1)} + \underline{\mathbf{n}} \tag{5.42}$$

of dimension $K_{\mathrm{a}}(NQ + W - 1)$. With the noise vectors $\underline{\mathbf{n}}_{\mathrm{G}}^{(g)}$, $g = 1, 2$, and utilizing (5.37) and (5.38) to (5.39) and (5.40), the partial received signal originating in the users of group g can be written as

$$\underline{\mathbf{e}}_{\mathrm{G}}^{(g)} = \underline{\mathbf{A}}_{\mathrm{G}}^{(g)} \underline{\mathbf{d}}_{\mathrm{G}}^{(g)} + \underline{\mathbf{n}}_{\mathrm{G}}^{(g)}, \quad g = 1,\, 2, \tag{5.43}$$

of dimension $K_{\mathrm{a}}(NQ + W - 1)$. If the covariance matrices

$$\underline{\mathbf{R}}_{\mathrm{G}}^{(g)} = \mathrm{E}\left\{ \underline{\mathbf{n}}_{\mathrm{G}}^{(g)}\, \underline{\mathbf{n}}_{\mathrm{G}}^{(g)*\mathrm{T}} \right\}, \quad g = 1, 2, \tag{5.44}$$

of the noise vectors $\underline{\mathbf{n}}_{\mathrm{G}}^{(g)}$, $g = 1, 2$, of (5.41) and (5.42) are known at the receiver, we can apply the ZF-BLE algorithm, see Section 5.3.2, to obtain the estimates

$$\hat{\underline{\mathbf{d}}}_{\mathrm{G}}^{(g)} = \left(\underline{\mathbf{A}}_{\mathrm{G}}^{(g)*\mathrm{T}} \underline{\mathbf{R}}_{\mathrm{G}}^{(g)-1} \underline{\mathbf{A}}_{\mathrm{G}}^{(g)} \right)^{-1} \underline{\mathbf{A}}_{\mathrm{G}}^{(g)*\mathrm{T}} \underline{\mathbf{R}}_{\mathrm{G}}^{(g)-1} \underline{\mathbf{e}}, \quad g = 1, 2, \tag{5.45}$$

of the data vectors $\underline{\mathbf{d}}_{\mathrm{G}}^{(g)}$, $g = 1, 2$, of (5.37) and (5.38), respectively. The estimates $\hat{\underline{\mathbf{d}}}_{\mathrm{G}}^{(g)}$, $g = 1, 2$, obtained by (5.45) are not free from intracell MAI, because not all users $k = 1 \ldots K$, are included in the zero forcing equalization. Both the intracell and intercell MAI are included in the matrices $\underline{\mathbf{R}}_{\mathrm{G}}^{(g)}$, $g = 1, 2$, of (5.44). When considering antenna arrays at the receiver the matrices $\underline{\mathbf{R}}_{\mathrm{G}}^{(g)}$, $g = 1, 2$, of (5.44) include both spatial and temporal correlations of the intercell MAI and intracell MAI. In general, the matrices $\underline{\mathbf{R}}_{\mathrm{G}}^{(g)}$, $g = 1, 2$, of (5.44) are not known at the receiver. In this case they must be replaced by an identity matrix in (5.45), see [Ost01]. In Section 7.2.2 it is shown how at least the intercell MAI covariance matrix $\underline{\mathbf{R}}_{\mathrm{n}}$ of (3.25) can be estimated and considered in MSJD.

In the following, based on the estimates $\hat{\underline{\mathbf{d}}}_{\mathrm{G}}^{(g)}$, $g = 1, 2$, of (5.45) FEC decoding and interleaving are considered and 4PSK modulation is applied. Consequently, the data vectors $\underline{\mathbf{d}}^{(k)}$, $k = 1...K$, of (5.1) with dimension N result from K uncoded binary data vectors

$$\mathbf{u}^{(k)} = \left[u_1^{(k)} \ldots u_{M_{\mathrm{d}}}^{(k)} \right]^{\mathrm{T}}, \quad u_{m_{\mathrm{d}}}^{(k)} \in \{-1, +1\}, k = 1...K, m_{\mathrm{d}} = 1...M_{\mathrm{d}}, \tag{5.46}$$

of dimension M_{d} by convolutional encoding with rate R_{c} and constraint length K_{c}, interleaving and mapping on 4PSK data symbols. Then,

$$N = \frac{M_{\mathrm{d}} + K_{\mathrm{c}} - 1}{2R_{\mathrm{c}}} \tag{5.47}$$

holds. Now, with $\mathbf{u}^{(k)}$ of (5.46) the vectors

$$\mathbf{u}_{\mathrm{G}}^{(1)} = \left[\mathbf{u}^{(1)\mathrm{T}} \ldots \mathbf{u}^{(K_{\mathrm{g}})\mathrm{T}}\right]^{\mathrm{T}} \tag{5.48}$$

and

$$\mathbf{u}_{\mathrm{G}}^{(2)} = \left[\mathbf{u}^{(K_{\mathrm{g}}+1)\mathrm{T}} \ldots \mathbf{u}^{(K)\mathrm{T}}\right]^{\mathrm{T}}, \tag{5.49}$$

respectively, can be introduced. From the estimates $\hat{\underline{\mathbf{d}}}_{\mathrm{G}}^{(g)}$, $g = 1, 2$, of (5.45) estimates $\hat{\mathbf{u}}_{\mathrm{G}}^{(g)}$, $g = 1, 2$, of the uncoded data vectors $\mathbf{u}^{(k)}$ of (5.46) can be obtained by demapping, deinterleaving and decoding.

The impact of intracell MAI $\underline{\mathbf{A}}_{\mathrm{G}}^{(3-g)}\,\underline{\mathbf{d}}_{\mathrm{G}}^{(3-g)}$ when detecting the received signal $\underline{\mathbf{e}}_{\mathrm{G}}^{(g)}$, $g = 1, 2$, of (5.43) can be reduced by an at least approximate elimination of the signals not included in the JD process of each group [Var95]. An iterative process of groupwise JD and intracell MAI elimination is the basic idea of MSJD. The intracell MAI elimination in MSJD can be performed in parallel or serially. Therefore, in the following two Sections 5.4.2 and 5.4.3 parallel and serial MSJD are introduced including detailed descriptions of one iteration in the case of parallel and serial MSJD, respectively.

5.4.2 Parallel MSJD

Fig. 5.6 shows the receiver structure in case of parallel MSJD. In the following i is the step index of the actual iteration. The signal processing of each iteration i and group $g = 1$, 2 consists of five steps, which are indentified by the figures 1 to 5 in Fig. 5.6. These five steps can be described as follows:

1. Approximate elimination of the user signals $\underline{\mathbf{e}}_{\mathrm{d}}^{(k)}$, $k = 1 + K_{\mathrm{g}}(g-1)...K_{\mathrm{g}}(g-2) + K(g-1)$, of (5.11) of group $(3-g)$ by subtracting the reconstructed received signal $\hat{\underline{\mathbf{e}}}_{\mathrm{G}}^{(3-g)}(i-1)$ of the users of group $(3-g)$ from the received signal $\underline{\mathbf{e}}$ of (5.10):

$$\underline{\mathbf{e}}_{\mathrm{red}}^{(g)}(i) = \underline{\mathbf{e}} - \hat{\underline{\mathbf{e}}}_{\mathrm{G}}^{(3-g)}(i-1), \quad g = 1,\, 2\,. \tag{5.50}$$

   $\underline{\mathbf{e}}_{\mathrm{red}}^{(g)}(i)$ is a received signal of group g with reduced intracell MAI. For the first iteration $i = 1$ the signals $\hat{\underline{\mathbf{e}}}_{\mathrm{G}}^{(g)}(0)$, $g = 1$, 2, may be initialized by a vector equal to $\mathbf{0}$, because no reconstructions of the received signals from previous iterations are available.

2. Performing simultaneously groupwise multiuser detection with the ZF equalizer. Note that only for the first iteration $i = 1$, when $\hat{\underline{\mathbf{e}}}_{\mathrm{G}}^{(g)}$ is equal to the vector $\mathbf{0}$, the matrix $\underline{\mathbf{R}}_{\mathrm{G}}^{(g)}$ of (5.44) is the interference covariance matrix that has to be considered

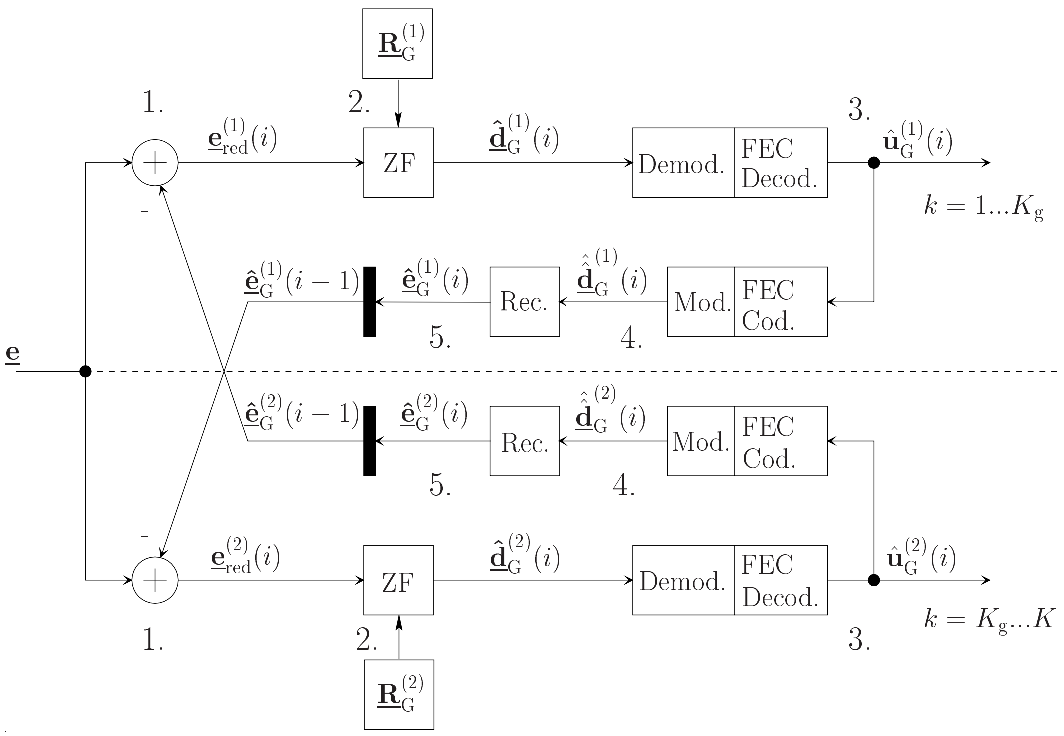

Fig. 5.6. Parallel MSJD; ZF: Zero Forcing; Rec.: Reconstruction [Ost01]

in the ZF process according to (5.45). In any other iteration $i > 1$ instead of $\underline{\mathbf{n}}_{\mathrm{G}}^{(g)}$, $g = 1, 2$, of (5.41) and (5.42) the noise that affects the reception of the signal $\underline{\mathbf{e}}_{\mathrm{red}}^{(g)}(i)$ consists of the total intercell MAI $\underline{\mathbf{n}}$ of (3.24) and the reconstruction errors $\underline{\mathbf{e}}_{\mathrm{G}}^{(3-g)} - \hat{\underline{\mathbf{e}}}_{\mathrm{G}}^{(3-g)}$, $g = 1, 2$. A more detailed analysis of the reconstruction errors is given in Chapter 7. Therefore, in the following a covariance matrix $\underline{\mathbf{R}}_{\mathrm{G}}^{(g)'}$ including the correlation properties of the intercell MAI $\underline{\mathbf{n}}$ of (3.24) and the correlations of the reconstruction errors $\underline{\mathbf{e}}_{\mathrm{G}}^{(3-g)} - \hat{\underline{\mathbf{e}}}_{\mathrm{G}}^{(3-g)}$, $g = 1, 2$ must be considered in the data detection process presumed that the matrix $\underline{\mathbf{R}}_{\mathrm{G}}^{(g)'}$ is known at the receiver. Consequently, according to (5.45) we obtain the estimates

$$\hat{\underline{\mathbf{d}}}_{\mathrm{G}}^{(g)}(i) = \left(\underline{\mathbf{A}}_{\mathrm{G}}^{(g)*\mathrm{T}} \underline{\mathbf{R}}_{\mathrm{G}}^{(g)'-1} \underline{\mathbf{A}}_{\mathrm{G}}^{(g)}\right)^{-1} \underline{\mathbf{A}}_{\mathrm{G}}^{(g)*\mathrm{T}} \underline{\mathbf{R}}_{\mathrm{G}}^{(g)'-1} \underline{\mathbf{e}}_{\mathrm{red}}^{(g)}(i), \quad g = 1, 2. \tag{5.51}$$

3. Calculating an estimate $\hat{\mathbf{u}}_{\mathrm{G}}^{(g)}(i)$ of the uncoded data vectors $\mathbf{u}_{\mathrm{G}}^{(g)}(i)$ of (5.48) and (5.49), respectively, by demapping, deinterleaving and FEC decoding of $\hat{\underline{\mathbf{d}}}_{\mathrm{G}}^{(g)}(i)$ of (5.51).

4. Generating improved estimates $\hat{\hat{\underline{\mathbf{d}}}}_{\mathrm{G}}^{(g)}(i)$ of the data vectors $\underline{\mathbf{d}}_{\mathrm{G}}^{(g)}(i)$ of (5.37) and (5.38), respectively, by re-encoding, re-interleaving and re-mapping of $\hat{\mathbf{u}}_{\mathrm{G}}^{(g)}(i)$.

5. Reconstructing the received signal $\underline{\mathbf{e}}_{\mathrm{G}}^{(g)}$ of (5.43) originating in the users of group g:

$$\hat{\underline{\mathbf{e}}}_{\mathrm{G}}^{(g)}(i) = \underline{\mathbf{A}}_{\mathrm{G}}^{(g)} \cdot \hat{\hat{\underline{\mathbf{d}}}}_{\mathrm{G}}^{(g)}(i), \quad g = 1,\ 2. \tag{5.52}$$

In the following iteration these hopefully improved reconstructions $\underline{\hat{\mathbf{e}}}_{\mathrm{G}}^{(g)}(i)$, $g = 1,\ 2$, of (5.52) will be used for the elimination in the first step, see (5.50).

The signal processing efforts required for linear multiuser detection of all users with the ZF-BLE on the one side and for MSJD on the other side are comparable, since the efforts for FEC decoding and signal reconstruction are neglectable compared to multiuser detection. In both cases the numbers of operations required for the matrix inversions in the ZF equalizers are dominant and are proportional to the third power of the number of jointly-detected user signals [PTVF92]. Consequently, a single ZF-BLE for a single group and iteration according to the concept of MSJD needs less operations than the ZF-BLE applied in linear multiuser detection. On the other hand two groups have to be processed in parallel in MSJD. In subsequent iterations the inverted matrices from the first iteration can be reused.

5.4.3 Serial MSJD

Section 5.4.2 describes how the two user groups are processed in parallel MSJD. In the following MSJD with serial interference elimination is presented. Fig. 5.7 shows the corresponding receiver structure similar to the one shown in Fig. 5.6. Whereas in parallel MSJD always two processes dealing with each signal group are performed simultaneously in one step, in serial MSJD these processes have to be performed sequentially. Hence, the number of steps needed for one iteration in serial MSJD is 10 instead of 5 in the case of parallel MSJD. The 10 steps of one iteration in serial MSJD are the following:

1. Approximate elimination of the user signals $\underline{\mathbf{e}}_{\mathrm{d}}^{(k)}$, $k = 1 + K_{\mathrm{g}} ... K$, of (5.11) of group $g = 2$ by subtracting the reconstructed received signal $\underline{\hat{\mathbf{e}}}_{\mathrm{G}}^{(2)}(i-1)$ of the users of group $g = 2$ according to (5.50) from the received signal $\underline{\mathbf{e}}$ of (5.10):
$$\underline{\mathbf{e}}_{\mathrm{red}}^{(1)}(i) = \underline{\mathbf{e}} - \underline{\hat{\mathbf{e}}}_{\mathrm{G}}^{(2)}(i-1). \tag{5.53}$$
$\underline{\mathbf{e}}_{\mathrm{red}}^{(1)}(i)$ is a received signal of group $g = 1$ with reduced intracell MAI. For the first iteration $i = 1$ the signals $\underline{\hat{\mathbf{e}}}_{\mathrm{G}}^{(2)}(0)$ may be initialized by a vector equal to $\mathbf{0}$, because no reconstructions of the received signals from previous iterations are available.

2. Performing JD of the signals of the group $g = 1$ with the ZF equalizer. Note that only for the first iteration $i = 1$, when $\underline{\hat{\mathbf{e}}}_{\mathrm{G}}^{(2)}$ is equal to the vector $\mathbf{0}$, the matrix $\underline{\mathbf{R}}_{\mathrm{G}}^{(g)}$ of (5.44) is the interference covariance matrix that has to be considered in the ZF process according to (5.45). Considering the covariance matrix $\underline{\mathbf{R}}_{\mathrm{G}}^{(1)'}$ according to the description given in step 2 in Section 5.4.2, we obtain the estimates
$$\underline{\hat{\mathbf{d}}}_{\mathrm{G}}^{(1)}(i) = \left(\underline{\mathbf{A}}_{\mathrm{G}}^{(1)*\mathrm{T}} \underline{\mathbf{R}}_{\mathrm{G}}^{(1)'-1} \underline{\mathbf{A}}_{\mathrm{G}}^{(1)}\right)^{-1} \underline{\mathbf{A}}_{\mathrm{G}}^{(1)*\mathrm{T}} \underline{\mathbf{R}}_{\mathrm{G}}^{(1)'-1} \underline{\mathbf{e}}_{\mathrm{red}}^{(1)}(i), \tag{5.54}$$
according to (5.51).

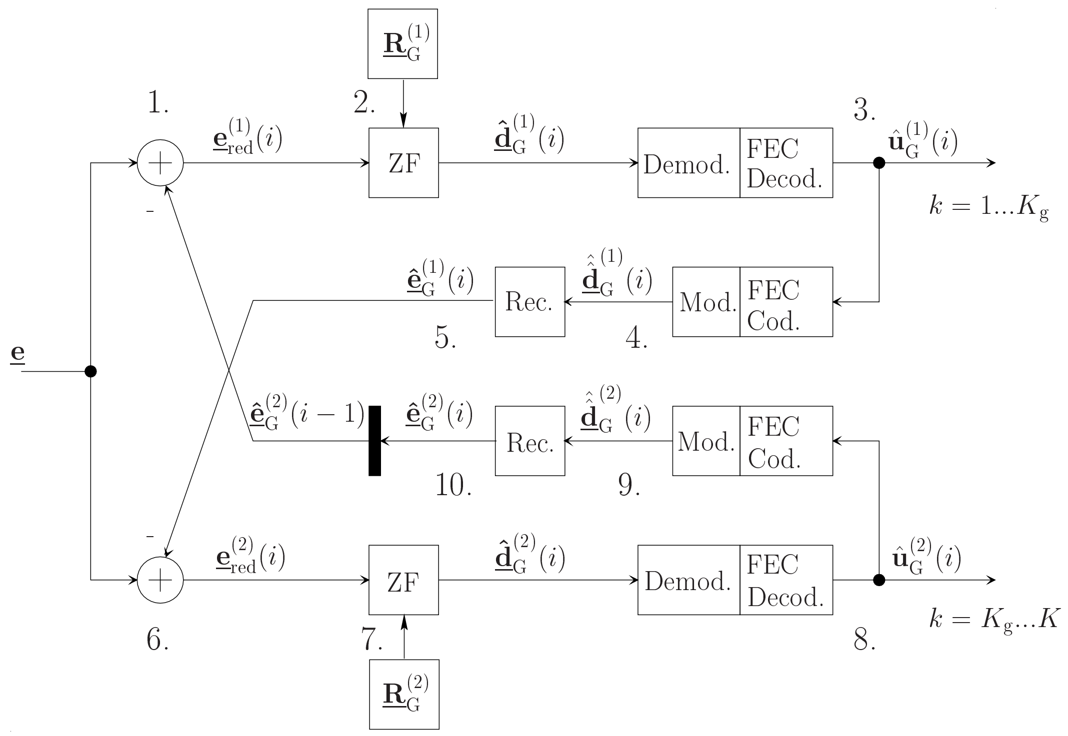

Fig. 5.7. Serial MSJD; ZF: Zero Forcing; Rec.: Reconstruction

3. Calculating an estimate $\hat{\mathbf{u}}_{\mathrm{G}}^{(1)}(i)$ of the uncoded data vectors $\mathbf{u}_{\mathrm{G}}^{(1)}(i)$ of (5.48), by demapping, deinterleaving and FEC decoding of $\hat{\underline{\mathbf{d}}}_{\mathrm{G}}^{(1)}(i)$ of (5.54).

4. Generating improved estimates $\hat{\hat{\underline{\mathbf{d}}}}_{\mathrm{G}}^{(1)}(i)$ of the data vectors $\underline{\mathbf{d}}_{\mathrm{G}}^{(1)}(i)$ of (5.37) by re-encoding, re-interleaving and re-mapping of $\hat{\mathbf{u}}_{\mathrm{G}}^{(1)}(i)$.

5. Reconstructing the received signal $\underline{\mathbf{e}}_{\mathrm{G}}^{(1)}$ of (5.43) originating in the users of group $g = 1$, see (5.52):

$$\hat{\underline{\mathbf{e}}}_{\mathrm{G}}^{(1)}(i) = \underline{\mathbf{A}}_{\mathrm{G}}^{(1)} \cdot \hat{\hat{\underline{\mathbf{d}}}}_{\mathrm{G}}^{(1)}(i). \tag{5.55}$$

6. Subtracting the reconstructed received signal $\hat{\underline{\mathbf{e}}}_{\mathrm{G}}^{(1)}(i)$ of (5.55) of the users of group $g = 1$ from the received signal $\underline{\mathbf{e}}$ of (5.10):

$$\underline{\mathbf{e}}_{\mathrm{red}}^{(2)}(i) = \underline{\mathbf{e}} - \hat{\underline{\mathbf{e}}}_{\mathrm{G}}^{(1)}(i). \tag{5.56}$$

7. Performing JD of the signals of the group $g = 2$ with the ZF equalizer. According to (5.51) and (5.54) we obtain the estimates

$$\hat{\underline{\mathbf{d}}}_{\mathrm{G}}^{(2)}(i) = \left(\underline{\mathbf{A}}_{\mathrm{G}}^{(2)^{*\mathrm{T}}} \underline{\mathbf{R}}_{\mathrm{G}}^{(2)'-1} \underline{\mathbf{A}}_{\mathrm{G}}^{(2)}\right)^{-1} \underline{\mathbf{A}}_{\mathrm{G}}^{(2)^{*\mathrm{T}}} \underline{\mathbf{R}}_{\mathrm{G}}^{(2)'-1} \underline{\mathbf{e}}_{\mathrm{red}}^{(2)}(i). \tag{5.57}$$

8. Calculating an estimate $\hat{\mathbf{u}}_{\mathrm{G}}^{(2)}(i)$ of the uncoded data vectors $\mathbf{u}_{\mathrm{G}}^{(2)}(i)$ of (5.49) by demapping, deinterleaving and FEC decoding of $\hat{\underline{\mathbf{d}}}_{\mathrm{G}}^{(2)}(i)$ of (5.57).

9. Generating improved estimates $\hat{\underline{\hat{\mathbf{d}}}}_{\mathrm{G}}^{(2)}(i)$ of the data vectors $\underline{\mathbf{d}}_{\mathrm{G}}^{(2)}(i)$ of (5.38) by re-encoding, re-interleaving and re-mapping of $\hat{\mathbf{u}}_{\mathrm{G}}^{(2)}(i)$.

10. Reconstructing the received signal $\underline{\mathbf{e}}_{\mathrm{G}}^{(2)}$ of (5.43) originating in the users of group $g = 2$:

$$\hat{\underline{\mathbf{e}}}_{\mathrm{G}}^{(2)}(i) = \underline{\mathbf{A}}_{\mathrm{G}}^{(2)} \cdot \hat{\underline{\hat{\mathbf{d}}}}_{\mathrm{G}}^{(2)}(i). \tag{5.58}$$

In the following iteration these hopefully improved reconstructions $\hat{\underline{\mathbf{e}}}_{\mathrm{G}}^{(2)}(i)$ of (5.58) will be used for the elimination in the first step, see (5.53).

Parallel MSJD offers the advantage over serial MSJD of lower signal processing time. However, the signal processing effort is the same. If, of the K user signals in the first group the K_{g} signals which show the lowest BER on detection are grouped together, these K_{g} user signals can be well reconstructed. With serial MSJD the total receive signal vector $\underline{\mathbf{e}}$ of (5.10) can then be cleaned up from the signals of the first group after the first detection step. Right after detection of the second user group a better BER performance of the signals of the second group is to be expected than if parallel MSJD is used. In general however it is not known before detection which signals have the lowest BER. Considerations in other possible strategies to assign users to user groups are presented in Section 5.4.4.

5.4.4 Strategies to assign users to user groups

For the description of parallel and serial MSJD in Sections 5.4.2 and 5.4.3 it was merely said that all K simultaneously active users are divided up into two user groups of equal size. A criterion in which each user k is assigned to one of the two groups was not taken into account in Sections 5.4.2 and 5.4.3. In the following three possible assignment criteria are presented of which the last two are compared by simulation results in Chapter 8. As well as an arbitrary assignment of the individual users to the two groups, the following assignment strategies are conceivable:

1. Assignment depending on the receive power of the user signals. This assignment principle is suitable for serial MSJD. In compliance with the normal procedure for serial intracell MAI elimination [KIHP90], the K_{g} user signals that were received with the highest power are assigned to the first group. All other users are assigned to the second group. With serial MSJD the advantage of this assignment criterion is that the user group with the strongest user signals will be detected first. Strong user signals can be well detected. In addition the intracell MAI in the first detection step is minimal for this assignment principle since only the weakest signals contribute

to intracell MAI. Because of the good detection result after the first detection step the user signals of the first group can be well reconstructed. The receive signal can thus be freed very well from the signals of the first group, which makes the second detection step easier. With parallel MSJD this assignment criteria plays no role.

2. All users who have the greatest physical distance from each other are assembled into a group. This assignment criterion only makes sense if array antennas are used on the receiver. If for example all users are arranged equidistantly on a circle around the BS, the assignment of the users to the two groups is as in Fig. 5.8 a. In [Pap00, PWBB98] it was shown that by using adaptive antennas on the BS the potential for separation of user signals is particularly great if the individual users are as far apart from each other as possible. By separating the user signals the MAI is reduced within the user group. If each detection process is considered for MSJD in itself and if the intracell MAI caused by the other group in each case is ignored, it is true that when array antennas and the assignment strategy described here are used, the BER performance of each individual JD step for MSJD will be improved in contrast to the case of arbitrary assignment of users to the two groups.

3. All users who are the closest to each other are collected into a group. This assignment criterion too only makes sense if array antennas are used on the receiver. Fig. 5.8 b shows the possible assignment of users to a group depending on their geographical position, if again an azimuthal equidistant user distribution on a circle around the BS is assumed. If the intercell MAI caused by the second group in each case is not taken into account, when the assignment strategy presented here is used the BER performance of each individual JD step is worse for MSJD than the assignment strategy presented under Point 2. Viewed overall, the following applies: The geographical proximity of the individual users of a group means that if adaptive antennas are used, no separation or hardly any separation of the individual user signals can be achieved, i.e the MAI of the user signals of a group is only reduced insignificantly. This means that joint detection of the user signals of a group is not improved to the extent that it is in the strategy mentioned in Point 2. For this the two groups are now geographically optimally spaced from each other. The MAI which is caused by the signals of the other group in each case is significantly reduced for the JD process of the signals of a group.

Using simulation results, an investigation is undertaken in Chapter 8 as to which of the last two strategies leads to a better BER behavior when using MSJD with array antennas. The assignment strategy mentioned in the first paragraph is not considered since in the simulations in Chapter 8 it is always assumed that all user signals are received at the BS with the same average power.

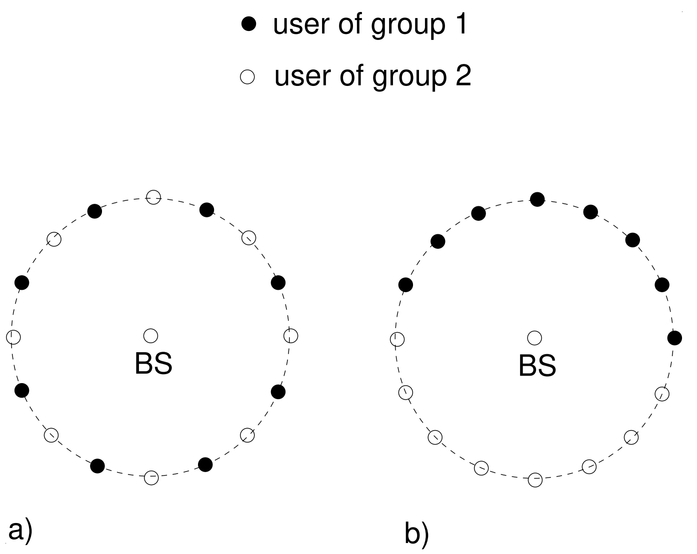

Fig. 5.8. Different strategies to assign users to user groups dependent on the user locations; a) Maximum distance strategy; b) Minimum distance strategy

6 Channel estimation

6.1 Introduction

The procedures used in the TD–CDMA system concept considered for data detection in accordance with the JD principle [Kle96, BKNS94b] are based on a coherent receiver [Pro89, Lük79] and require knowledge of the channel IRs of the K users at the K_a antenna elements contained in vector $\underline{\mathbf{h}}_\mathrm{s}$ of (2.11) with dimension $K_\mathrm{a}KW$, see Chapter 5. For systems with joint assessment of the data signals of the individual K users it is appropriate to jointly estimate the K spatial channel IRs $\underline{\mathbf{h}}_\mathrm{s}^{(k,k_\mathrm{a})}$, $k = 1...K$, $k_\mathrm{a} = 1...K_\mathrm{a}$, of (2.4) with dimension W of the K user signals at the K_a antenna elements. Mutual interference by simultaneous transmitting of midambles of the K users within the observed cell is therefore eliminated in a comparable way to the principle of JD.

The conventional joint channel estimation (JCE) for TD–CDMA in accordance with Steiner [Ste95], which was originally designed for single antenna receivers, only takes account of knowledge of the K transmitted midambles for obtaining the information about the channel IRs $\underline{\mathbf{h}}_\mathrm{RP}^{(k)}$, $k = 1...K$, of (2.3) of the K users. For receivers with K_a antenna elements a joint channel estimation of the spatial channel IRs $\underline{\mathbf{h}}_\mathrm{s}^{(k,k_\mathrm{a})}$, $k = 1...K$, $k_\mathrm{a} = 1...K_\mathrm{a}$, of (2.4) of the K users is performed for the signals received at each of the K_a antenna elements, so that overall all relevant $K \cdot K_\mathrm{a}$ channel IRs are estimated in the uplink. To make matters less complex here no information about directional inhomogeneities of the $K \cdot K_\mathrm{a}$ channel IRs to be estimated is taken into account. Taking account of the directional inhomogeneities of the intercell MAI is also, as will be shown in the following sections, not possible for the given system parameters [ETSI97] that are shown in Table 8.1 and for which the system simulation presented in Chapter 8 is relevant. Channel estimation in accordance with Steiner for a TD–CDMA system is summarized in Section 6.2.

To be able to take account of information about directional characteristics of both the $K \cdot K_\mathrm{a}$ channel IRs and of the intercell MAI with JCE, a channel estimation process was presented and investigated in [Pap00], which, with knowledge of the relevant K_d DOAs of the K user signals, allows a reduction of the number of unknown channel taps and consideration of the covariance matrix $\underline{\mathbf{R}}_\mathrm{n}$ of the intercell MAI. By reducing the number of unknowns in the equation system to be resolved for the channel estimation and by taking account of the matrix $\underline{\mathbf{R}}_\mathrm{n}$ of (3.25), the channel estimation is significantly improved [Pap00]. In [Pap00] the primary investigation concerns the achievable improvement of channel estimation as a result of the reduction of the number of unknowns in the equation system to be resolved. Here although the option of taking account of the matrix $\underline{\mathbf{R}}_\mathrm{n}$ in channel estimation is mentioned, it is not looked at in more detail. In Chapter 8 the possible performance improvements are determined by taking additional account of the estimated matrix $\underline{\mathbf{R}}_\mathrm{n}$ which is not considered in [Pap00]. The corresponding procedure for estimating the matrix $\underline{\mathbf{R}}_{\mathrm{n}}$ is described in Chapter 7. After the channel estimation principle fully described in [Pap00] has been addressed again in the following chapters of this thesis, this channel estimation procedure will be explained once more in brief in Section 6.3.

The channel estimation procedure presented in [Pap00] requires a DOA estimation. In numerous publications [HN95, RK89, PN97, PFB97a] the performance of the DOA estimation procedures such as MUSIC, ESPRIT or Unitary ESPRIT [RK89, HN95] has been demonstrated in outdoor scenarios. In indoor scenarios, it is not generally possible to assume discrete DOAs because of azimuthal wide dispersal of the signals impinging at the BS. DOA estimation procedures such as ESPRIT tend in this case to estimate the DOAs incorrectly, resulting in massive performance problems. Therefore, Section 6.4 describes a channel estimation process which takes account of the correlation matrix $\underline{\mathbf{R}}_{\tau,\mathrm{s}}$ of (2.13) of the channel IRs to be estimated and also the covariance matrix $\underline{\mathbf{R}}_{\mathrm{n}}$ of the intercell MAI. DOA estimation algorithms can be dispensed with completely here. The information about the directional inhomogeneities of the user signals is contained here in the matrix $\underline{\mathbf{R}}_{\tau,\mathrm{s}}$ and that of the intercell MAI signals in matrix $\underline{\mathbf{R}}_{\mathrm{n}}$.

Finally, in Section 6.5 two different channel estimation errors are introduced, to be used in Chapter 7 to assess the quality of the channel estimation with conventional ZF channel estimation and for the channel estimation described in Section 6.4.

6.2 Conventional channel estimation

The state of the art channel estimation technique in TD–CDMA was proposed by Steiner in [Ste95]. Steiner developed a technique for jointly estimating the channel IRs of each active user in the considered cell at a single antenna at the receiver. The estimation is performed by taking advantage of the midamble section inserted between the two data sections of the burst transmitted by each user k, $k = 1...K$, see Fig. 1.7. The novelty of the Steiner estimator consists in the design of the midamble training sequences known at the receiver. The midamble codes of all K users are derived from a single periodic basic code.

The received signal $\underline{\mathbf{e}}_{\mathrm{m}}$ at the BS, which is exclusively given by the midamble section and not by the data sections of the transmitted burst of each user, has dimension [SK93, Ste95]

$$L = L_{\mathrm{m}} - W + 1, \tag{6.1}$$

where L_{m} is the total length of the midamble in chips, see Fig. 1.7, and W is the dimension of each channel IR vector $\underline{\mathbf{h}}_{\mathrm{RP}}^{(k)}$, $k = 1 \ldots K$, see (2.3). By a cyclically shifted arrangement of the basic periodic code

$$\underline{\mathbf{m}}_{\mathrm{P}} = [\underline{m}_1 \ldots \underline{m}_L]^{\mathrm{T}} \tag{6.2}$$

of dimension L, from which the midamble of the user k is derived, the $L \times W$ Toeplitz matrix of the midamble training sequence for the user k [Ste95]

$$\underline{\mathbf{G}}^{(k)} = \begin{bmatrix} \underline{m}_W^{(k)} & \underline{m}_{W-1}^{(k)} & \cdots & \underline{m}_1^{(k)} \\ \underline{m}_{W+1}^{(k)} & \underline{m}_W^{(k)} & \cdots & \underline{m}_2^{(k)} \\ \vdots & \vdots & & \vdots \\ \underline{m}_{W-1}^{(k)} & \underline{m}_{W-2}^{(k)} & \cdots & \underline{m}_L^{(k)} \end{bmatrix} \tag{6.3}$$

is obtained. For JCE [Ste95] the matrix

$$\underline{\mathbf{G}} = \left[\underline{\mathbf{G}}^{(1)} \ldots \underline{\mathbf{G}}^{(K)}\right] \tag{6.4}$$

of all K user specific midamble training sequences is used. $\underline{\mathbf{G}}$ of (6.4) has the dimension $L \times (KW)$ and is known at the receiver. If the vector $\underline{\mathbf{h}}_{\mathrm{RP}}$ of dimension KW is obtained by the concatenation of the vectors $\underline{\mathbf{h}}_{\mathrm{RP}}^{(k)}$ of (2.3), and if we further admit an additive intercell MAI vector $\underline{\mathbf{n}}_{\mathrm{m}}$ of dimension L disturbing channel estimation, the received signal becomes [SK93, Ste95]

$$\underline{\mathbf{e}}_{\mathrm{m}} = \underline{\mathbf{G}}\, \underline{\mathbf{h}}_{\mathrm{RP}} + \underline{\mathbf{n}}_{\mathrm{m}}. \tag{6.5}$$

In the case of K_{a} antenna elements at the receiver, the total spatial channel IR vector $\underline{\mathbf{h}}_{\mathrm{s}}$ of (2.11) has the dimension $K_{\mathrm{a}}KW$, which includes the $K \cdot K_{\mathrm{a}}$ channel IRs received at the K_{a} antenna elements. Hence, the portion $\underline{\mathbf{e}}_{\mathrm{m}}$ of the total received signal from all antennas is given by

$$\underline{\mathbf{e}}_{\mathrm{m}} = \left(\mathbf{I}^{(K_{\mathrm{a}})} \otimes \underline{\mathbf{G}}\right) \underline{\mathbf{h}}_{\mathrm{s}} + \underline{\mathbf{n}}_{\mathrm{m}}, \tag{6.6}$$

where $\underline{\mathbf{n}}_{\mathrm{m}}$ now has the dimension $K_{\mathrm{a}}L$ and $\mathbf{I}^{(K_{\mathrm{a}})}$ is the $K_{\mathrm{a}} \times K_{\mathrm{a}}$ identity matrix. Consequently, $\underline{\mathbf{e}}_{\mathrm{m}}$ of (6.6) has the dimension $K_{\mathrm{a}}L$. In the following, to simplify the notation, the Kronecker product of $\mathbf{I}^{(K_{\mathrm{a}})}$ and $\underline{\mathbf{G}}$ will be represented by the matrix

$$\underline{\tilde{\mathbf{G}}} = \mathbf{I}^{(K_{\mathrm{a}})} \otimes \underline{\mathbf{G}} \tag{6.7}$$

with the dimension $(K_{\mathrm{a}}L) \times (K_{\mathrm{a}}KW)$. Taking account of the intercell MAI vector $\underline{\mathbf{n}}_{\mathrm{m}}$ that affects the channel estimation, the $(K_{\mathrm{a}}L) \times (K_{\mathrm{a}}L)$ covariance matrix of the intercell MAI

$$\underline{\mathbf{R}}_{\mathrm{m}} = \mathrm{E}\{\underline{\mathbf{n}}_{\mathrm{m}}\, \underline{\mathbf{n}}_{\mathrm{m}}^{*\mathrm{T}}\} \tag{6.8}$$

is specified according to (3.25). Here both the spatial and the temporal correlation characteristics of the intercell MAI represented by the vector $\underline{\mathbf{n}}_{\mathrm{m}}$ are equal to the intercell MAI that affects the data detection and is represented by the vector $\underline{\mathbf{n}}$ (3.24). The two interference signals $\underline{\mathbf{n}}$ and $\underline{\mathbf{n}}_{\mathrm{m}}$ originate from the same sources and are merely received with a slight time offset. Since the dimensioning of vectors $\underline{\mathbf{n}}_{\mathrm{m}}$ and $\underline{\mathbf{n}}$ are different, the dimensions of the associated covariance matrices $\underline{\mathbf{R}}_{\mathrm{m}}$ or $\underline{\mathbf{R}}_{\mathrm{n}}$ are also different. This is the reason for the different notations of the two covariance matrices of the intercell MAI.

If the ZF algorithm is now used for JCE, the estimated total spatial channel IR vector is obtained

$$\underline{\hat{\mathbf{h}}}_{\mathrm{s}} = \left(\underline{\tilde{\mathbf{G}}}^{*\mathrm{T}}\,\underline{\mathbf{R}}_{\mathrm{m}}^{-1}\,\underline{\tilde{\mathbf{G}}}\right)^{-1}\underline{\tilde{\mathbf{G}}}^{*\mathrm{T}}\,\underline{\mathbf{R}}_{\mathrm{m}}^{-1}\,\underline{\mathbf{e}}_{\mathrm{m}}. \tag{6.9}$$

In conventional TD–CDMA systems no information is obtained about covariance matrix $\underline{\mathbf{R}}_{\mathrm{m}}$. As a result, matrix $\underline{\mathbf{R}}_{\mathrm{m}}$ cannot be taken into consideration in (6.9). Starting from (6.9) the estimated spatial channel IR vector $\underline{\hat{\mathbf{h}}}_{\mathrm{s}}$, taking account of the channel estimation expanded to K_{a} receive antennas in accordance with Steiner is produced for

$$\underline{\hat{\mathbf{h}}}_{\mathrm{s}} = \left(\underline{\tilde{\mathbf{G}}}^{*\mathrm{T}}\,\underline{\tilde{\mathbf{G}}}\right)^{-1}\underline{\tilde{\mathbf{G}}}^{*\mathrm{T}}\,\underline{\mathbf{e}}_{\mathrm{m}}. \tag{6.10}$$

If all K user channel IRs $\underline{\mathbf{h}}^{(k)}$, $k = 1...K$, are estimated jointly, the midamble length can be chosen so that the matrix $\underline{\mathbf{G}}$ is square. For an additional corresponding choice of the midamble basic code [Ste95] the matrix $\underline{\mathbf{G}}$ of (6.4) can be inverted. This also applies for matrix $\underline{\tilde{\mathbf{G}}}$ of (6.7). Thus for (6.10) the following is obtained

$$\underline{\hat{\mathbf{h}}}_{\mathrm{s}} = \underline{\tilde{\mathbf{G}}}^{-1}\,\underline{\mathbf{e}}_{\mathrm{m}}. \tag{6.11}$$

The channel estimation process described by (6.11) is equivalent to K_{a} independent channel estimation processes at each of the K_{a} antenna elements at the receiver. The decisive benefit of the channel estimation process is its simplicity and the associated low level of complexity. The disadvantage is that despite using K_{a} receive antenna elements, no information about directional inhomogeneities, either of the spatial channel IRs $\underline{\mathbf{h}}_{\mathrm{s}}^{(k,k_{\mathrm{a}})}$, $k = 1...K$, $K_{\mathrm{a}} = 1...K_{\mathrm{a}}$, to be estimated, or of the intercell MAI $\underline{\mathbf{n}}_{\mathrm{m}}$ is taken into account.

6.3 Exploitation of the knowledge of the directions of arrival (DOA)

The following section shows a channel estimation process which, in contrast to the conventional channel estimation process shown in Section 6.2, allows utilization of directional inhomogeneities of both the user signals and the intercell MAI signals. As already mentioned in Section 6.1, a detailed description of this channel estimation process is to be found in [Pap00]. The investigations in [Pap00] are however restricted to taking account of the estimated DOAs of the user signals in channel estimation. Taking account of the estimated spatial correlation properties of the intercell MAI signals which this channel estimation process allows, is investigated in Chapter 8. For this reason this Section 6.3 only includes a brief description of the channel estimation process.

The basis of this channel estimation approach is a DOA estimation, which, e.g. can be realized by the ESPRIT or Unitary ESPRIT algorithm [RK89, HN95] or any other DOA estimation algorithm. In this section, a description of the ESPRIT algorithm is not given, since it is well known from literature [RK89, HN95, Haa97a]. Therefore, in the following the problem of DOA estimation is not considered, but it is assumed that the DOAs $\beta^{(k,k_\mathrm{d})}$, $k = 1...K$, $k_\mathrm{d} = 1...K_\mathrm{d}$, see Section 2.4, of each channel IR of the K users are perfectly known at the receiver. With the knowledge of the DOAs $\beta^{(k,k_\mathrm{d})}$, $k = 1...K$, $k_\mathrm{d} = 1...K_\mathrm{d}$, one can establish the $(K_\mathrm{a}KW) \times (K_\mathrm{d}KW)$ matrix $\underline{\boldsymbol{\mathcal{A}}}_\mathrm{d}$ of (2.21). The matrix $\underline{\boldsymbol{\mathcal{A}}}_\mathrm{d}$ of (2.21) gives the relation between the directional channel IR vector $\underline{\mathbf{h}}_\mathrm{d}$ of (2.15) and the total spatial channel IR vector $\underline{\mathbf{h}}_\mathrm{s}$ of length $K_\mathrm{a}KW$ given in (2.11). Then, the total received signal $\underline{\mathbf{e}}_\mathrm{m}$ from (6.6) becomes

$$\underline{\mathbf{e}}_\mathrm{m} = \left(\mathbf{I}^{(K_\mathrm{a})} \otimes \underline{\mathbf{G}}\right) \underline{\boldsymbol{\mathcal{A}}}_\mathrm{d}\underline{\mathbf{h}}_\mathrm{d} + \underline{\mathbf{n}}_\mathrm{m}. \tag{6.12}$$

If

$$K_\mathrm{d}KW < K_\mathrm{a}KW \tag{6.13}$$

is valid, the number of unknown directional channel impulse response components contained in $\underline{\mathbf{h}}_\mathrm{d}$ of (2.15) of dimension $K_\mathrm{d}KW$ is reduced compared to the number of unknown spatial channel IR components contained in $\underline{\mathbf{h}}_\mathrm{s}$ of (2.11) of dimension $K_\mathrm{a}KW$. Since the number of the unknown channel IR components in both (6.6) and (6.12) is the same, this reduction of the number of the unknown channel IR components leads to an improved quality of the channel estimate, see also [PHFB97, Pap00]. According to the maximum-likelihood principle we obtain from (6.12) the estimate

$$\hat{\underline{\mathbf{h}}}_\mathrm{d} = \left(\underline{\boldsymbol{\mathcal{A}}}_\mathrm{d}^{*\mathrm{T}} \left(\mathbf{I}^{(K_\mathrm{a})} \otimes \underline{\mathbf{G}}^{*\mathrm{T}}\right) \underline{\mathbf{R}}_\mathrm{m}^{-1} \left(\mathbf{I}^{(K_\mathrm{a})} \otimes \underline{\mathbf{G}}\right) \underline{\boldsymbol{\mathcal{A}}}_\mathrm{d}\right)^{-1} \underline{\boldsymbol{\mathcal{A}}}_\mathrm{d}^{*\mathrm{T}} \left(\mathbf{I}^{(K_\mathrm{a})} \otimes \underline{\mathbf{G}}^{*\mathrm{T}}\right) \underline{\mathbf{R}}_\mathrm{m}^{-1}\underline{\mathbf{e}}_\mathrm{m} \tag{6.14}$$

of the directional channel IR $\underline{\mathbf{h}}_\mathrm{d}$. With the matrix $\tilde{\underline{\mathbf{G}}}$ of (6.7) (6.14) can be written as

$$\hat{\underline{\mathbf{h}}}_\mathrm{d} = \left(\underline{\boldsymbol{\mathcal{A}}}_\mathrm{d}^{*\mathrm{T}}\ \tilde{\underline{\mathbf{G}}}\ \underline{\mathbf{R}}_\mathrm{m}^{-1}\ \tilde{\underline{\mathbf{G}}}\ \underline{\boldsymbol{\mathcal{A}}}_\mathrm{d}\right)^{-1}\ \underline{\boldsymbol{\mathcal{A}}}_\mathrm{d}^{*\mathrm{T}}\ \tilde{\underline{\mathbf{G}}}\ \underline{\mathbf{R}}_\mathrm{m}^{-1}\underline{\mathbf{e}}_\mathrm{m}. \tag{6.15}$$

(6.15) shows that the knowledge of the covariance matrix $\underline{\mathbf{R}}_\mathrm{m}$ of (6.8) is required for an maximum-likelihood channel estimation, which is the optimum estimation.

In this section only 1-dimensional (1D) information concerning the DOAs is considered, i.e. only information concerning the azimuth angle φ, which can be obtained from 1D DOA estimation techniques [RK89, Sch86]. In [Pap00] this enhanced channel estimation technique is further improved by utilizing the 2D Unitary ESPRIT algorithm [Haa97a] for 2D DOA estimation. The 2D DOA estimation algorithms allow the information of the DOAs of each component $\underline{h}_{\mathrm{RP},w}^{(k)}$, $w = 1...W$, of the spatial channel IR vectors $\underline{\mathbf{h}}_\mathrm{RP}^{(k)}$, $k = 1...K$, of (2.3) to be obtained. If each component $\underline{h}_{\mathrm{RP},w}^{(k)}$ of a channel IR vector can be assigned to one single DOA $\beta^{(k,w)}$, a matrix $\underline{\boldsymbol{\mathcal{A}}}_\mathrm{d}$ of (2.21) with the dimension $(K_\mathrm{a}KW) \times (KW)$, which includes all the spatial information, and a directional channel IR vector $\underline{\mathbf{h}}_\mathrm{d}$ of (2.15) with the dimension KW would be sufficient to describe the total spatial channel IR vector $\underline{\mathbf{h}}_\mathrm{s}$ according to (2.11). In this case, the number of unknown parameters in $\underline{\mathbf{h}}_{\mathrm{d}}$ of (2.15) is always reduced compared to the unknown parameters in $\underline{\mathbf{h}}_{\mathrm{s}}$ of (2.11), since

$$KW < K_{\mathrm{a}}KW \tag{6.16}$$

is always valid for K_{a} greater than one. This further enhanced channel estimation technique is not considered in this thesis. For more detailed information concerning this combined 2D DOA channel estimation concept, the reader is referred to [Pap00].

6.4 MMSE based channel estimation

The channel estimation process shown in Chapter 6.3 requires knowledge of the discrete K_{d} DOAs of the channel IR of K users. These must thus be determined before the actual channel estimation by using DOA estimation algorithms. In the following paragraphs a channel estimation process is presented that, instead of taking account of the discrete DOAs, allows account to be taken of the correlation characteristics of both the signals to be estimated, i.e. spatial channel IRs $\underline{\mathbf{h}}_{\mathrm{s}}^{(k,k_{\mathrm{a}})}$, $k = 1...K$, $k_{\mathrm{a}} = 1...K_{\mathrm{a}}$, of (2.1) and also the intercell MAI $\underline{\mathbf{n}}_{\mathrm{m}}$. For this, as already employed in Section 6.1 the principle of JCE of all channel IRs $\underline{\mathbf{h}}_{\mathrm{RP}}^{(k)}$, $k = 1...K$, of (2.3) of the K users is followed, through which intracell MAI is eliminated. A linear estimator which fulfills these requirements is the MMSE–BLE (Minimum Mean Square Error Block Linear Equalizer) [Wha71]. The MMSE–BLE in addition to the advantage of taking account of the correlation matrix $\underline{\mathbf{R}}_{\tau,\mathrm{s}}$ of the total spatial channel IR vector $\underline{\mathbf{h}}_{\mathrm{s}}$ to be estimated and the covariance matrix $\underline{\mathbf{R}}_{\mathrm{m}}$, see (6.8), of the total intercell MAI vector $\underline{\mathbf{n}}_{\mathrm{m}}$, also offers the benefit of a smaller SNR degradation δ compared to conventional channel estimation [Wha71, Kle96], whereby the MMSE is also of interest for single antenna receivers. Applied to channel estimation, the MMSE supplies as its answer the estimated total spatial channel IR vector

$$\hat{\underline{\mathbf{h}}}_{\mathrm{s,MMSE}} = \arg \min_{\underline{\mathbf{h}}_{\mathrm{s}}^{'} \in \mathbb{C}^{K_{\mathrm{a}}KW}} \mathrm{E}\{||\underline{\mathbf{h}}_{\mathrm{s}}^{'} - \underline{\mathbf{h}}_{\mathrm{s}}||^2\} \tag{6.17}$$

[Wha71] that has the smallest mean quadratic distance to the actual total spatial channel IR vector $\underline{\mathbf{h}}_{\mathrm{s}}$ of (2.11). When $\underline{\mathbf{h}}_{\mathrm{s}}$ and $\underline{\mathbf{n}}_{\mathrm{m}}$ are both Gaussian and independent, then, with channel estimation matrix $\tilde{\underline{\mathbf{G}}}$ of (6.7), the covariance matrix $\underline{\mathbf{R}}_{\mathrm{m}}$ of (6.8) and the matrix $\underline{\mathbf{R}}_{\tau,\mathrm{s}}$ of (2.13), which can be estimated with the process described in Chapter 7, the MMSE–BLE for channel estimation is given by [Wha71]

$$\hat{\underline{\mathbf{h}}}_{\mathrm{s,MMSE1}} = \left(\underline{\mathbf{R}}_{\tau,\mathrm{s}}{}^{-1} + \tilde{\underline{\mathbf{G}}}^{*\mathrm{T}}\, \underline{\mathbf{R}}_{\mathrm{m}}^{-1}\, \tilde{\underline{\mathbf{G}}}\right)^{-1} \tilde{\underline{\mathbf{G}}}^{*\mathrm{T}}\, \underline{\mathbf{R}}_{\mathrm{m}}^{-1}\, \underline{\mathbf{e}}_{\mathrm{m}} = \underline{\mathbf{M}}_{\mathrm{MMSE}}\, \underline{\mathbf{e}}_{\mathrm{m}}, \tag{6.18}$$

where

$$\underline{\mathbf{M}}_{\mathrm{MMSE}} = \left(\underline{\mathbf{R}}_{\tau,\mathrm{s}}{}^{-1} + \tilde{\underline{\mathbf{G}}}^{*\mathrm{T}}\, \underline{\mathbf{R}}_{\mathrm{m}}^{-1}\, \tilde{\underline{\mathbf{G}}}\right)^{-1} \tilde{\underline{\mathbf{G}}}^{*\mathrm{T}}\, \underline{\mathbf{R}}_{\mathrm{m}}^{-1}. \tag{6.19}$$

Since $\underline{\mathbf{h}}_{\mathrm{s}}$ is non-Gaussian the problem is to find the linear estimate

$$\hat{\underline{\mathbf{h}}}_{\mathrm{s}} = \underline{\mathbf{M}}_{\mathrm{MMSE}}\, \underline{\mathbf{e}}_{\mathrm{m}} + \underline{\mathbf{b}}_{\mathrm{MMSE}} \tag{6.20}$$

that minimizes the MSE [MM80]. In the following $\underline{\mathbf{b}}_{\mathrm{MMSE}}$ in (6.20) is neglected in order to reduce computational complexity. However, (6.18) still can be interpreted as a MMSE based scheme. Since the inverse matrices $\underline{\mathbf{R}}_{\tau,\mathrm{s}}{}^{-1}$ and $\underline{\mathbf{R}}_{\mathrm{m}}^{-1}$ are included in (6.19), this option of MMSE based channel estimation is referred to below as MMSE based channel estimation taking account of $\underline{\mathbf{R}}_{\tau,\mathrm{s}}{}^{-1}$ and $\underline{\mathbf{R}}_{\mathrm{m}}^{-1}$ or as MMSE–JCE I (MMSE-Joint Channel Estimation I). In the case of MMSE–JCE the set of equations

$$\left(\underline{\mathbf{R}}_{\tau,\mathrm{s}}{}^{-1} + \underline{\tilde{\mathbf{G}}}^{*\mathrm{T}}\, \underline{\mathbf{R}}_{\mathrm{m}}^{-1}\, \underline{\tilde{\mathbf{G}}}\right) \hat{\underline{\mathbf{h}}}_{\mathrm{s,MMSE}} = \underline{\tilde{\mathbf{G}}}^{*\mathrm{T}}\, \underline{\mathbf{R}}_{\mathrm{m}}^{-1}\, \underline{\mathbf{e}}_{\mathrm{m}} \tag{6.21}$$

of (6.18) can most easily be resolved by the Cholesky decomposition [Kle96, Naß95, Zur64] of the matrix $\left(\underline{\mathbf{R}}_{\tau,\mathrm{s}}{}^{-1} + \underline{\tilde{\mathbf{G}}}^{*\mathrm{T}}\, \underline{\mathbf{R}}_{\mathrm{m}}^{-1}\, \underline{\tilde{\mathbf{G}}}\right)$ and subsequent resolution of two trivial equation systems [Zur64]. The requirement for using (6.18) is that either the correlation matrix of the channel IRs $\underline{\mathbf{R}}_{\tau,\mathrm{s}}$ nor the matrix $\left(\underline{\mathbf{R}}_{\tau,\mathrm{s}}{}^{-1} + \underline{\tilde{\mathbf{G}}}^{*\mathrm{T}}\, \underline{\mathbf{R}}_{\mathrm{m}}^{-1}\, \underline{\tilde{\mathbf{G}}}\right)$ are singular. Even with a singular covariance matrix of intercell MAI $\underline{\mathbf{R}}_{\mathrm{m}}$ the matrix $\left(\underline{\tilde{\mathbf{G}}}^{*\mathrm{T}}\, \underline{\mathbf{R}}_{\mathrm{m}}^{-1}\, \underline{\tilde{\mathbf{G}}}\right)$ is not singular, so that the problem of the singularity of the matrix $\left(\underline{\mathbf{R}}_{\tau,\mathrm{s}}{}^{-1} + \underline{\tilde{\mathbf{G}}}^{*\mathrm{T}}\, \underline{\mathbf{R}}_{\mathrm{m}}^{-1}\, \underline{\tilde{\mathbf{G}}}\right)$ does not arise, provided $\underline{\mathbf{R}}_{\tau,\mathrm{s}}$ is not singular. Since on the diagonals of the matrix $\underline{\mathbf{R}}_{\tau,\mathrm{s}}$ the expectation values $\mathrm{E}\{|\underline{h}_{\mathrm{s},w}^{(k,k_{\mathrm{a}})}|\}$, $w = 1...W$, $k = 1...K$, $k_{\mathrm{a}} = 1...K_{\mathrm{a}}$, of the squares of the magnitudes $|\underline{h}_{\mathrm{s},w}^{(k,k_{\mathrm{a}})}|$, $w = 1...W$, $k = 1...K$, $k_{\mathrm{a}} = 1...K_{\mathrm{a}}$, of the channel IRs are to be found, these values can differ widely. The components $\underline{h}_{\mathrm{s},w}^{(k,k_{\mathrm{a}})}$, $w = 1...W$, $k = 1...K$, $k_{\mathrm{a}} = 1...K_{\mathrm{a}}$, of the channel IR vectors, which are to be assigned short delay times, which are e.g. valid for $w = 1$, have in general larger magnitudes than the components, which are e.g. valid for $w = W$. The latter can even be zero. In this case the matrix $\underline{\mathbf{R}}_{\tau,\mathrm{s}}$ is singular, since $\underline{\mathbf{R}}_{\tau,\mathrm{s}}$ then has zeros on its diagonal. The joint MMSE based channel estimation in accordance with (6.18) (MMSE–JCE I) cannot then be executed. These problems are rectified by transformations in accordance with the following equations, which contain the matrices $\underline{\mathbf{R}}_{\tau,\mathrm{s}}$, $\underline{\mathbf{R}}_{\mathrm{m}}$ and $\underline{\tilde{\mathbf{G}}}$ [Wha71]:

$$\begin{aligned}
& \underline{\tilde{\mathbf{G}}}^{*\mathrm{T}}\, \underline{\mathbf{R}}_{\mathrm{m}}^{-1} \left(\underline{\mathbf{R}}_{\mathrm{m}} + \underline{\tilde{\mathbf{G}}}\, \underline{\mathbf{R}}_{\tau,\mathrm{s}}\, \underline{\tilde{\mathbf{G}}}^{*\mathrm{T}}\right) \\
= \;& \underline{\tilde{\mathbf{G}}}^{*\mathrm{T}} + \underline{\tilde{\mathbf{G}}}^{*\mathrm{T}}\, \underline{\mathbf{R}}_{\mathrm{m}}^{-1}\, \underline{\tilde{\mathbf{G}}}\, \underline{\mathbf{R}}_{\tau,\mathrm{s}}\, \underline{\tilde{\mathbf{G}}}^{*\mathrm{T}} \\
= \;& \underline{\mathbf{R}}_{\tau,\mathrm{s}}{}^{-1}\, \underline{\mathbf{R}}_{\tau,\mathrm{s}}\, \underline{\tilde{\mathbf{G}}}^{*\mathrm{T}} + \underline{\mathbf{R}}_{\tau,\mathrm{s}}{}^{-1}\, \underline{\mathbf{R}}_{\tau,\mathrm{s}}\, \underline{\tilde{\mathbf{G}}}^{*\mathrm{T}}\, \underline{\mathbf{R}}_{\mathrm{m}}^{-1}\, \underline{\tilde{\mathbf{G}}}\, \underline{\mathbf{R}}_{\tau,\mathrm{s}}\, \underline{\tilde{\mathbf{G}}}^{*\mathrm{T}} \\
= \;& \left(\underline{\mathbf{R}}_{\tau,\mathrm{s}}{}^{-1} + \underline{\tilde{\mathbf{G}}}^{*\mathrm{T}}\, \underline{\mathbf{R}}_{\mathrm{m}}^{-1}\, \underline{\tilde{\mathbf{G}}}\right) \underline{\mathbf{R}}_{\tau,\mathrm{s}}\, \underline{\tilde{\mathbf{G}}}^{*\mathrm{T}}.
\end{aligned} \tag{6.22}$$

Where matrix $\left(\underline{\mathbf{R}}_{\mathrm{m}} + \underline{\tilde{\mathbf{G}}}\, \underline{\mathbf{R}}_{\tau,\mathrm{s}}\, \underline{\tilde{\mathbf{G}}}^{*\mathrm{T}}\right)$ in (6.22) is moved to the right hand side, giving

$$\underline{\tilde{\mathbf{G}}}^{*\mathrm{T}}\, \underline{\mathbf{R}}_{\mathrm{m}}^{-1} = \left(\underline{\mathbf{R}}_{\tau,\mathrm{s}}{}^{-1} + \underline{\tilde{\mathbf{G}}}^{*\mathrm{T}}\, \underline{\mathbf{R}}_{\mathrm{m}}^{-1}\, \underline{\tilde{\mathbf{G}}}\right) \underline{\mathbf{R}}_{\tau,\mathrm{s}}\, \underline{\tilde{\mathbf{G}}}^{*\mathrm{T}} \left(\underline{\mathbf{R}}_{\mathrm{m}} + \underline{\tilde{\mathbf{G}}}\, \underline{\mathbf{R}}_{\tau,\mathrm{s}}\, \underline{\tilde{\mathbf{G}}}^{*\mathrm{T}}\right)^{-1}. \tag{6.23}$$

Multiplying the matrix $\left(\underline{\mathbf{R}}_{\tau,\mathrm{s}}{}^{-1} + \underline{\tilde{\mathbf{G}}}^{*\mathrm{T}}\, \underline{\mathbf{R}}_{\mathrm{m}}^{-1}\, \underline{\tilde{\mathbf{G}}}\right)^{-1}$ from the left in the equation (6.23) produces the matrix $\underline{\mathbf{M}}_{\mathrm{MMSE}}$ of (6.19) jointly with (6.23) for

$$\begin{aligned}\underline{\mathbf{M}}_{\mathrm{MMSE}} &= \left(\underline{\mathbf{R}}_{\tau,\mathrm{s}}{}^{-1} + \underline{\tilde{\mathbf{G}}}^{*\mathrm{T}}\, \underline{\mathbf{R}}_{\mathrm{m}}^{-1}\, \underline{\tilde{\mathbf{G}}}\right)^{-1}\, \underline{\tilde{\mathbf{G}}}^{*\mathrm{T}}\, \underline{\mathbf{R}}_{\mathrm{m}}^{-1} \\ &= \underline{\mathbf{R}}_{\tau,\mathrm{s}}\, \underline{\tilde{\mathbf{G}}}^{*\mathrm{T}} \left(\underline{\mathbf{R}}_{\mathrm{m}} + \underline{\tilde{\mathbf{G}}}\, \underline{\mathbf{R}}_{\tau,\mathrm{s}}\, \underline{\tilde{\mathbf{G}}}^{*\mathrm{T}}\right)^{-1}. \end{aligned} \tag{6.24}$$

With $\underline{\mathbf{M}}_{\mathrm{MMSE}}$ according to (6.24) MMSE based channel estimation according to (6.18) can now be written as

$$\underline{\hat{\mathbf{h}}}_{\mathrm{s,MMSE2}} = \underline{\mathbf{R}}_{\tau,\mathrm{s}}\, \underline{\tilde{\mathbf{G}}}^{*\mathrm{T}} \left(\underline{\mathbf{R}}_{\mathrm{m}} + \underline{\tilde{\mathbf{G}}}\, \underline{\mathbf{R}}_{\tau,\mathrm{s}}\, \underline{\tilde{\mathbf{G}}}^{*\mathrm{T}}\right)^{-1} \underline{\mathbf{e}}_{\mathrm{m}}. \tag{6.25}$$

A minimal-effort resolution of the equation system, as is possible with (6.18) cannot be undertaken here. For this the possible singularity of the matrix $\underline{\mathbf{R}}_{\tau,\mathrm{s}}$ no longer prevents the estimation of the channel IRs with the MMSE-BLE. Below, in contrast to (6.18) this variant of the channel estimation is designated MMSE based channel estimation taking account of $\underline{\mathbf{R}}_{\tau,\mathrm{s}}$ and $\underline{\mathbf{R}}_{\mathrm{m}}$ or as MMSE–JCE II.

6.5 Channel estimation error

To assess the estimation quality of the spatial channel IRs $\underline{\hat{\mathbf{h}}}_{\mathrm{s}}^{(k,k_{\mathrm{a}})}$, $k = 1...K$, $k_{\mathrm{a}} = 1...K_{\mathrm{a}}$, which can be achieved with the channel estimation processes shown in Sections 6.3 and 6.4, two channel estimation errors are introduced below. Starting from the definition of the MMSE in accordance with (6.17), the most obvious assessment value of the quality of MMSE based channel estimation is the mean square error (MSE)

$$\epsilon_{\mathrm{h}}^2 = \frac{1}{K_{\mathrm{a}} \cdot K} \sum_{k_{\mathrm{a}}=1}^{K_{\mathrm{a}}} \sum_{k=1}^{K} \mathrm{E}\left\{ \sum_{w=1}^{W} \frac{|\underline{h}_{\mathrm{s},w}^{(k,k_{\mathrm{a}})} - \hat{\underline{h}}_{\mathrm{s},w}^{(k,k_{\mathrm{a}})}|^2}{|\underline{h}_{\mathrm{s},w}^{(k,k_{\mathrm{a}})}|^2} \right\}. \tag{6.26}$$

The diagrams in Chapter 8 show the Root Mean Square Error (RMSE)

$$\epsilon_{\mathrm{h}} = \sqrt{\epsilon_{\mathrm{h}}^2}. \tag{6.27}$$

After the MMSE determines an estimation result which has the smallest mean square estimation error, the MSE or RMSE applied to the estimation result of the MMSE channel estimation is always less that or equal to the MSE applied to the estimation result for conventional channel estimation. It therefore makes sense to adapt the measured value for assessing the quality of channel estimation more to the characteristics of the mobile radio channel. The different delay spread of mobile radio channel IRs as a result of different propagation characteristics in different countries means that the channel energy is more or less distributed over all components $\hat{\underline{h}}_{\mathrm{s},w}^{(k,k_{\mathrm{a}})}$, $w = 1...W$, $k = 1...K$, $k_{\mathrm{a}} = 1...K_{\mathrm{a}}$. In Indoor environments many of the W components of the spatial channel IRs $\hat{\underline{\mathbf{h}}}_{\mathrm{s}}^{(k,k_\mathrm{a})}$, $k = 1...K$, $k_\mathrm{a} = 1...K_\mathrm{a}$, can be approximately zero.

To obtain an accurate comparison between the quality of different channel estimation processes a quality measurement variable must be introduced that explicitly includes the energy of each individual components $\underline{h}_{\mathrm{s},w}^{(k,k_\mathrm{a})}$, $w = 1...W$, $k = 1...K$, $k_\mathrm{a} = 1...K_\mathrm{a}$ of the estimated channel IR vectors in quality assessment. The assessment of the quality of channel estimation should thus be independent of the channel energy. A measured value which fulfills the above requirements is shown in [Pap00] and below.

Since the sampled values of the channel IRs in the equivalent lowpass domain can be specified as complex values $\underline{h}_{\mathrm{s},w}^{(k,k_\mathrm{a})}$, $w = 1\dots W$, $k = 1\dots K$, $k_\mathrm{a} = 1\dots K_\mathrm{a}$, a separate consideration of the real parts $h_{\mathrm{r},w}^{(k,k_\mathrm{a})}$ and the imaginary parts $h_{\mathrm{i},w}^{(k,k_\mathrm{a})}$ is possible. $\Delta h_{\mathrm{r},w}^{(k,k_\mathrm{a})}$ is used below to indicate the differences between $h_{\mathrm{r},w}^{(k,k_\mathrm{a})}$ and the estimated values $\hat{h}_{\mathrm{r},w}^{(k,k_\mathrm{a})}$. Equally, the differences between the actual values $h_{\mathrm{i},w}^{(k,k_\mathrm{a})}$ and the estimated values $h_{\mathrm{i},w}^{(k,k_\mathrm{a})}$ are designated with $\Delta h_{\mathrm{i},w}^{(k,k_\mathrm{a})}$, so that

$$\Delta h_{\mathrm{r},w}^{(k,k_\mathrm{a})} = \hat{h}_{\mathrm{r},w}^{(k,k_\mathrm{a})} - h_{\mathrm{r},w}^{(k,k_\mathrm{a})}, \quad w = 1\dots W,\ k = 1\dots K,\ k_\mathrm{a} = 1\dots K_\mathrm{a}, \tag{6.28}$$

$$\Delta h_{\mathrm{i},w}^{(k,k_\mathrm{a})} = \hat{h}_{\mathrm{i},w}^{(k,k_\mathrm{a})} - h_{\mathrm{i},w}^{(k,k_\mathrm{a})}, \quad w = 1\dots W,\ k = 1\dots K,\ k_\mathrm{a} = 1\dots K_\mathrm{a}. \tag{6.29}$$

(6.28) and (6.29) allow a channel estimation error to be specified for the real part $\mathbf{h}_\mathrm{r}^{(k,k_\mathrm{a})}$ and the imaginary part $\mathbf{h}_\mathrm{i}^{(k,k_\mathrm{a})}$ of the spatial channel IRs $\hat{\underline{\mathbf{h}}}_{\mathrm{s}}^{(k,k_\mathrm{a})}$, $k = 1...K$, $k_\mathrm{a} = 1...K_\mathrm{a}$, as follows

$$\epsilon_{\mathrm{re}}^{(k,k_\mathrm{a})} = \mathrm{E}\left\{\frac{\sum\limits_{w=1}^{W} \mid \Delta h_{\mathrm{r},w}^{(k,k_\mathrm{a})} h_{\mathrm{r},w}^{(k,k_\mathrm{a})} \mid^2}{\sum\limits_{w=1}^{W}\left(h_{\mathrm{r},w}^{(k,k_\mathrm{a})}\right)^2}\right\},\ k = 1\dots K, k_\mathrm{a} = 1\dots K_\mathrm{a}, \tag{6.30}$$

$$\epsilon_{\mathrm{im}}^{(k,k_\mathrm{a})} = \mathrm{E}\left\{\frac{\sum\limits_{w=1}^{W} \mid \Delta h_{\mathrm{i},w}^{(k,k_\mathrm{a})} h_{\mathrm{i},w}^{(k,k_\mathrm{a})} \mid^2}{\sum\limits_{w=1}^{W}\left(h_{\mathrm{i},w}^{(k,k_\mathrm{a})}\right)^2}\right\},\ k = 1\dots K, k_\mathrm{a} = 1\dots K_\mathrm{a}. \tag{6.31}$$

Starting from (6.30) and (6.31) the mean channel estimation over all KK_a channel IRs

$$\epsilon_{\mathrm{re}} = \frac{1}{KK_\mathrm{a}}\sum_{k=1}^{K}\sum_{k_\mathrm{a}=1}^{K_\mathrm{a}} \epsilon_{\mathrm{re}}^{(k,k_\mathrm{a})} \tag{6.32}$$

$$\epsilon_{\mathrm{im}} = \frac{1}{KK_\mathrm{a}}\sum_{k=1}^{K}\sum_{k_\mathrm{a}=1}^{K_\mathrm{a}} \epsilon_{\mathrm{im}}^{(k,k_\mathrm{a})} \tag{6.33}$$

can be determined. In the following sections in Chapter 8 the values ϵ_h of (6.27), ϵ_re of (6.33) and ϵ_im of (6.33) are used to compare the quality of the MMSE based channel estimation with the quality of the conventional channel estimation.

7 Receiver concepts for estimating and exploiting correlation matrices

7.1 Introduction

In Section 5.3.2 it is shown that by applying the ZF algorithm for data detection knowledge of the intercell MAI covariance matrix $\underline{\mathbf{R}}_{\mathrm{n}}$ of (3.25) is required in order to get an optimum estimate $\hat{\underline{\mathbf{d}}}$ of (5.12) of the unknown total data vector $\underline{\mathbf{d}}$ of (5.9). Moreover, the intercell MAI covariance matrix $\underline{\mathbf{R}}_{\mathrm{m}}$ of (6.8) can also be considered in channel estimation, see Sections 6.2 and 6.3. For the MMSE based JCE presented in Section 6.4 both the correlation matrix $\underline{\mathbf{R}}_{\tau,\mathrm{s}}$ of (2.12) of the spatial channel IRs $\underline{\mathbf{h}}_{\mathrm{s}}$ of (2.11) and the intercell MAI covariance matrix $\underline{\mathbf{R}}_{\mathrm{m}}$ of (6.8) are even required. The state of the art receiver concepts for TD–CDMA consider neither the matrix $\underline{\mathbf{R}}_{\mathrm{n}}$ of (3.25) in data detection nor the matrices $\underline{\mathbf{R}}_{\mathrm{m}}$ of (6.8) and $\underline{\mathbf{R}}_{\tau,\mathrm{s}}$ of (2.12) in channel estimation [MSW97b]. The following sections present modified receiver concepts for TD–CDMA, incorporating the estimation and the utilization of these correlation and covariance matrices, respectively.

Prior to the description of the receiver concepts, three general remarks concerning the estimation of the intercell MAI covariance matrices $\underline{\mathbf{R}}_{\mathrm{n}}$, $\underline{\mathbf{R}}_{\mathrm{m}}$ and $\underline{\mathbf{R}}_{\mathrm{s}}$, respectively, and the relations between these matrices are presented below:

- It is assumed that the intercell MAI signals are directionally uncorrelated. In Chapter 3 it is shown that in this case the intercell MAI covariance matrix $\underline{\mathbf{R}}_{\mathrm{n}}$ of (3.25) can be represented by the Kronecker product of the spatial covariance matrix $\underline{\mathbf{R}}_{\mathrm{s}}$ of (3.36) and the temporal covariance matrix $\tilde{\underline{\mathbf{R}}}_{\mathrm{t}}$ of (3.19), see (3.37). The matrix $\tilde{\underline{\mathbf{R}}}_{\mathrm{t}}$ is *a priori* known at the receiver, since the spectral form of the interference given by the GMSK chip impulse filter [ETSI97] is known, see Section 3.2. Consequently, in scenarios with directionally uncorrelated intercell MAI it is sufficient to estimate only the spatial covariance matrix $\underline{\mathbf{R}}_{\mathrm{s}}$ of (3.36). With the *a priori* knowledge of $\underline{\mathbf{R}}_{\mathrm{s}}$ being a hermitian matrix, see Section 3.2, only the off-diagonal elements of the upper or lower triangular part of the matrix $\underline{\mathbf{R}}_{\mathrm{s}}$ must be estimated. Mainly we benefit in data detection from reduced computational effort, if estimating $\underline{\mathbf{R}}_{\mathrm{s}}$ only is sufficient. In data detection the inverted matrix $\underline{\mathbf{R}}_{\mathrm{n}}^{-1}$ is needed. In the case of directionally uncorrelated intercell MAI scenarios [Gra81]

$$\underline{\mathbf{R}}_{\mathrm{n}}^{-1} = \underline{\mathbf{R}}_{\mathrm{s}}^{-1} \otimes \tilde{\underline{\mathbf{R}}}_{\mathrm{t}}^{-1} \tag{7.1}$$

  holds. Therefore, prior to considering in data detection only $\underline{\mathbf{R}}_{\mathrm{s}}$ has to be inverted, since $\tilde{\underline{\mathbf{R}}}_{\mathrm{t}}^{-1}$ is always available, if the *a priori* known matrix $\tilde{\underline{\mathbf{R}}}_{\mathrm{t}}$ once has been inverted. Furthermore, independently of which of the two matrices $\underline{\mathbf{R}}_{\mathrm{n}}$ and $\underline{\mathbf{R}}_{\mathrm{m}}$ is needed in data detection and channel estimation, only the spatial covariance matrix $\underline{\mathbf{R}}_{\mathrm{s}}$ of (3.36) must be determined. The spatial covariance matrix $\underline{\mathbf{R}}_{\mathrm{s}}$ is the same in both cases, i.e. according to (3.37)

$$\underline{\mathbf{R}}_{\mathrm{m}} = \underline{\mathbf{R}}_{\mathrm{s}} \otimes \underline{\tilde{\mathbf{R}}}_{\mathrm{t,m}} \tag{7.2}$$

holds, where the matrix $\underline{\tilde{\mathbf{R}}}_{\mathrm{t,m}}$ of dimension $L \times L$ is equal to the the matrix $\underline{\tilde{\mathbf{R}}}_{\mathrm{t}}$ of (3.19) of dimension $(NQ + W - 1) \times (NQ + W - 1)$, except for their dimensions.

- If the preliminaries of directionally uncorrelated intercell MAI are not fulfilled at the BS site, then the temporal correlations of the intercell MAI signals received at the K_{a} antenna elements are not necessarily the same, see Section 3.2. In this case an estimation of the total covariance matrix $\underline{\mathbf{R}}_{\mathrm{n}}$ of (3.25) is required. The elements of the covariance matrix $\underline{\mathbf{R}}_{\mathrm{m}}$ of (6.8) can be obtained from the elements of the covariance matrix $\underline{\mathbf{R}}_{\mathrm{n}}$ of (3.25) according to

$$\begin{aligned} [\underline{\mathbf{R}}_{\mathrm{m}}]_{(u-1)L+i,(v-1)L+j} &= [\underline{\mathbf{R}}_{\mathrm{n}}]_{(u-1)(NQ+W-1)+i,(v-1)(NQ+W-1)+j}\,, \\ & i = 1...L, j = 1...L, u = 1...K_{\mathrm{a}}, v = 1...K_{\mathrm{a}}. \end{aligned} \tag{7.3}$$

Fig. 7.1 illustrates the relation between the elements of the matrices $\underline{\mathbf{R}}_{\mathrm{n}}$ of (3.25) and $\underline{\mathbf{R}}_{\mathrm{m}}$ of (6.8) given by (7.3), if $K_{\mathrm{a}} = 2$ antenna elements are utilized at the BS site. If,

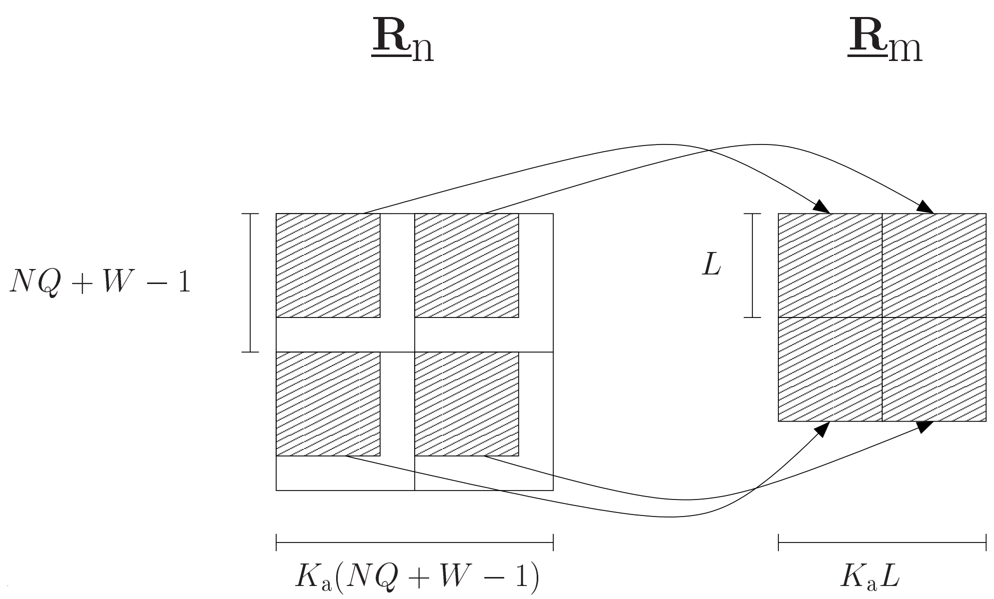

Fig. 7.1. Connection between the elements of the matrix $\underline{\mathbf{R}}_{\mathrm{n}}$ and the matrix $\underline{\mathbf{R}}_{\mathrm{m}}$ with $K_{\mathrm{a}} = 2$ antenna elements

in the reverse case, a receiver structure only allows the matrix $\underline{\mathbf{R}}_{\mathrm{m}}$ to be estimated, no connection can be made to the matrix $\underline{\mathbf{R}}_{\mathrm{n}}$. Therefore receiver concepts which only allow estimation of $\underline{\mathbf{R}}_{\mathrm{m}}$ should only be used in scenarios in which directional uncorrelated intercell MAI can be expected and thus must only estimate matrix $\underline{\mathbf{R}}_{\mathrm{s}}$.

- Regardless of the spatial correlation characteristics of the intercell MAI only the matrix $\underline{\mathbf{R}}_{\mathrm{s}}$ can ever be estimated. Basically the matrix $\underline{\tilde{\mathbf{R}}}_{\mathrm{t}}$ of (3.19) valid in the case of directional uncorrelated intercell MAI is used as the temporal covariance matrix. Estimating the spatial covariance matrix $\underline{\mathbf{R}}_{\mathrm{s}}$ is significantly less effort than estimating the intercell MAI covariance matrix $\underline{\mathbf{R}}_{\mathrm{n}}$, since matrix $\underline{\mathbf{R}}_{\mathrm{s}}$ contains fewer elements. Matrices $\underline{\mathbf{R}}_{\mathrm{n}}$ and $\underline{\mathbf{R}}_{\mathrm{m}}$ thus formed by (3.37) and (7.2) each lead to suboptimum solutions when considered in data detection or channel estimation if intercell MAI is directionally correlated. The corresponding performance results are shown in Chapter 8.

Three different concepts are presented below for the estimation of the intercell MAI covariance matrices $\underline{\mathbf{R}}_{\mathrm{n}}$, $\underline{\mathbf{R}}_{\mathrm{m}}$ and the spatial intercell MAI covariance matrix $\underline{\mathbf{R}}_{\mathrm{s}}$. The three concepts are described in detail in the Sections 7.2, 7.3 and 7.4:

- Based on the detected data vector $\hat{\underline{\mathbf{d}}}$ of (5.12) we reconstruct the received signal $\underline{\mathbf{e}}$ of (5.10), which depends exclusively on the transmitted data vector $\underline{\mathbf{d}}$ of (5.9) and subtract the reconstructed signal from the actual received signal $\underline{\mathbf{e}}$ in order to get an estimate of the intercell MAI vector $\underline{\mathbf{n}}$ of (3.24). From the estimate of the vector $\underline{\mathbf{n}}$ estimates of the spatial intercell MAI covariance matrix $\underline{\mathbf{R}}_{\mathrm{s}}$ of (3.36) and the intercell MAI covariance matrix $\underline{\mathbf{R}}_{\mathrm{n}}$ of (3.25) can be obtained.

- Based on the estimated total channel IR vector $\hat{\underline{\mathbf{h}}}_{\mathrm{s}}$ of (6.10) we reconstruct the received signal $\underline{\mathbf{e}}_{\mathrm{m}}$ of (6.6), which results exclusively on the transmitted midambles $\underline{\mathbf{m}}^{(k)}$, $k = 1...K$, see Section 5.2, and subtract the reconstructed signal from the actual received signal $\underline{\mathbf{e}}_{\mathrm{m}}$ in order to get an estimate of the intercell MAI vector $\underline{\mathbf{n}}_{\mathrm{m}}$, see (6.6). From the estimate of the vector $\underline{\mathbf{n}}_{\mathrm{m}}$ estimates of the spatial intercell MAI covariance matrix $\underline{\mathbf{R}}_{\mathrm{s}}$ of (3.36) and the intercell MAI covariance matrix $\underline{\mathbf{R}}_{\mathrm{m}}$ of (6.8) can be obtained.

- The estimated correlation matrix $\hat{\underline{\mathbf{R}}}_{\mathrm{e}}$ of the received signal $\underline{\mathbf{e}}$ of (5.10) and the correlation matrices $\hat{\underline{\mathbf{R}}}_{\mathrm{s}}^{(k)}$, $k = 1...K$, of the estimated spatial channel IRs $\hat{\underline{\mathbf{h}}}_{\mathrm{s}}^{(k,k_{\mathrm{a}})}$, $k = 1...K$, $k_{\mathrm{a}} = 1...K_{\mathrm{a}}$, of (2.1) are considered in order to obtain an estimate of the spatial covariance matrix $\underline{\mathbf{R}}_{\mathrm{s}}$ of (3.36). In contrast to the first two concepts, which allow the estimation of the total intercell MAI covariance matrix $\underline{\mathbf{R}}_{\mathrm{n}}$ of (3.25) or $\underline{\mathbf{R}}_{\mathrm{m}}$ of (6.8), this concept only allows the estimation of the spatial covariance matrix $\underline{\mathbf{R}}_{\mathrm{s}}$ of (3.36).

According to (3.25), e.g. the determination of the matrix $\underline{\mathbf{R}}_{\mathrm{n}}$ requires the determination of the expectation $\mathrm{E}\left\{\underline{\mathbf{n}}\,\underline{\mathbf{n}}^{*\mathrm{T}}\right\}$. Hence, in a real mobile radio system the following two problems arise:

- To determine the elements of the matrices $\underline{\mathbf{R}}_{\mathrm{n}}$, $\underline{\mathbf{R}}_{\mathrm{m}}$, $\underline{\mathbf{R}}_{\mathrm{s}}$ and $\underline{\mathbf{R}}_{\tau,\mathrm{s}}$ averaging can be only performed over a finite time period in order to obtain an estimate of the expectation.

- To be able to obtain and to exploit the correlations correctly, it is required that the directional and temporal correlations of the intercell MAI remain the same at least for the time period of the estimation of the covariance matrix.

These two problems lead right from the outset to estimation errors of matrices $\underline{\mathbf{R}}_{\mathrm{n}}$, $\underline{\mathbf{R}}_{\mathrm{m}}$, $\underline{\mathbf{R}}_{\mathrm{s}}$ and $\underline{\mathbf{R}}_{\tau,\mathrm{s}}$. For short time periods it can be assumed that the directional correlations of the intercell MAI remain the same, if the constellation of interfering sources does not change during these time periods and if the spatial correlations do not change very much with time due to the movement of the interfering sources. It is assumed below that this directional stationarity of the intercell MAI is valid for at least one burst so that for each received burst that is affected with the intercell MAI vector $\underline{\mathbf{n}}$ the corresponding covariance matrix $\underline{\mathbf{R}}_{\mathrm{n}}$ can be estimated. There are various approaches to the various procedures for estimating the matrices $\underline{\mathbf{R}}_{\mathrm{n}}$, $\underline{\mathbf{R}}_{\mathrm{m}}$, $\underline{\mathbf{R}}_{\mathrm{s}}$ and $\underline{\mathbf{R}}_{\tau,\mathrm{s}}$ as to how the problems mentioned above can be combatted. These approaches are each discussed in the sections in which the associated estimation procedure is also described.

For the estimation of the matrix $\underline{\mathbf{R}}_{\tau,\mathrm{s}}$ of (2.12) no signal reconstruction and no other correlation matrix besides $\underline{\mathbf{R}}_{\tau,\mathrm{s}}$ is involved in the estimation of process. A receiver structure that incorporates estimation of matrix $\underline{\mathbf{R}}_{\tau,\mathrm{s}}$ of (2.12) is shown in Section 7.5. The considerations concerning stationarity of the directional correlations and the consequences for the estimation of the intercell MAI covariance matrix $\underline{\mathbf{R}}_{\mathrm{n}}$ are also true for estimation of the correlation matrix $\underline{\mathbf{R}}_{\tau,\mathrm{s}}$ of (2.12) of the channel IRs.

7.2 Utilizing data signal reconstructions for estimating $\underline{\mathbf{R}}_{\mathrm{n}}$

7.2.1 ZF-BLE based structure

The receiver structure that incorporates estimation of $\underline{\mathbf{R}}_{\mathrm{n}}$ is shown in Fig. 7.2 [WPH99]. This receiver structure allows estimation of the total covariance matrix $\underline{\mathbf{R}}_{\mathrm{n}}$ as well as only estimation of the spatial covariance matrix $\underline{\mathbf{R}}_{\mathrm{s}}$ of the intercell MAI by an iterative approach. In the following i denotes the number of the considered iteration.

First, let us assume that the total spatial channel IRs $\underline{\mathbf{h}}_{\mathrm{s}}$ of (2.11) are perfectly known at the receiver. The system matrix $\underline{\mathbf{A}}$ of (5.8) is then also perfectly known. One iteration, including the estimation process of the covariance matrix $\underline{\mathbf{R}}_{\mathrm{n}}$ and the data detection applying the ZF–BLE, consists of the following steps, which also can be seen in Fig. 7.2:

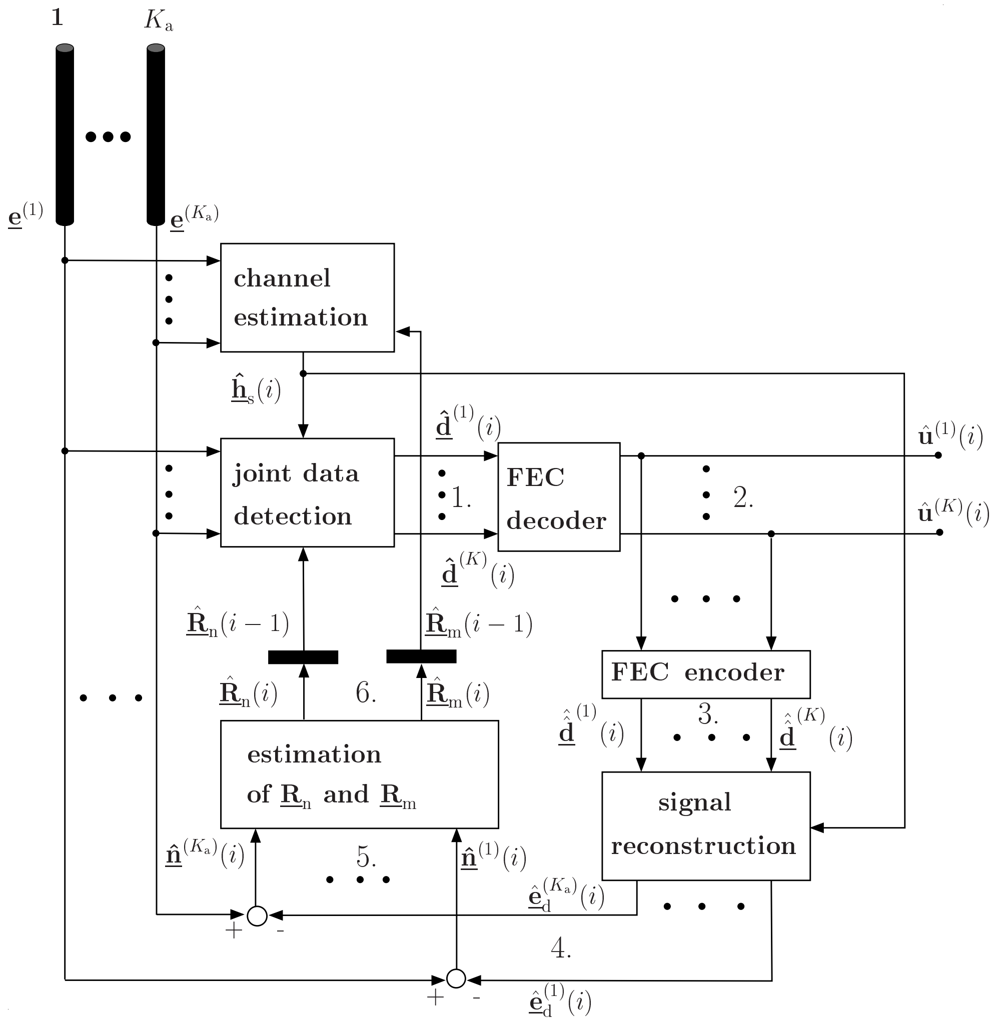

Fig. 7.2. Receiver structure incorporating the estimation of the covariance matrix $\underline{\mathbf{R}}_\mathrm{n}$ of the intercell MAI and considering forward error correction (FEC) coding [WPH99]

1. Joint data detection is performed by applying the ZF–BLE in order to obtain the estimated total data vector

$$\hat{\underline{\mathbf{d}}}(i) = \left(\underline{\mathbf{A}}^{*\mathrm{T}}\ \hat{\underline{\mathbf{R}}}_\mathrm{n}^{-1}(i-1)\ \underline{\mathbf{A}}\right)^{-1}\ \underline{\mathbf{A}}^{*\mathrm{T}}\ \hat{\underline{\mathbf{R}}}_\mathrm{n}^{-1}(i-1)\ \underline{\mathbf{e}} \tag{7.4}$$

   of iteration i according to (5.12). Notice that in the first iteration $i = 1$ the estimated covariance matrix $\hat{\underline{\mathbf{R}}}_\mathrm{n}(0)$ is equal to the identity matrix $\mathbf{I}^{(NQ+W-1)}$.

2. After having performed FEC decoding by using a convolutional decoder which uses $\hat{\underline{\mathbf{d}}}(i)$ of (7.4) as soft inputs the uncoded data vectors $\hat{\mathbf{u}}^{(k)}(i)$, $k = 1...K$, according to (5.46) are obtained.

3. The uncoded data vectors $\hat{\mathbf{u}}^{(k)}(i)$, $k = 1...K$, are FEC encoded again which leads to the vector $\hat{\hat{\underline{\mathbf{d}}}}(i)$.

4. With the system matrix $\underline{\mathbf{A}}$ of (5.8) and the vector $\hat{\hat{\underline{\mathbf{d}}}}(i)$ the signal reconstruction

$$\hat{\underline{\mathbf{e}}}_{\mathrm{d}}(i) = \underline{\mathbf{A}}\ \hat{\hat{\underline{\mathbf{d}}}}(i) \tag{7.5}$$

is obtained.

5. By subtracting the reconstructed signal $\hat{\underline{\mathbf{e}}}_{\mathrm{d}}(i)$ of (7.5) from the received signal $\underline{\mathbf{e}}$ of (5.10) an estimate

$$\hat{\underline{\mathbf{n}}}(i) = \underline{\mathbf{e}} - \hat{\underline{\mathbf{e}}}_{\mathrm{d}}(i) \tag{7.6}$$

of the total intercell MAI vector $\underline{\mathbf{n}}$ of (3.24) is obtained.

6. With the estimates $\hat{\underline{\mathbf{n}}}(i)$ of (7.6) we can obtain an estimation

$$\hat{\underline{\mathbf{R}}}_{\mathrm{n}}(i) = \hat{\underline{\mathbf{n}}}(i)\ \hat{\underline{\mathbf{n}}}^{*\mathrm{T}}(i) \tag{7.7}$$

of the intercell MAI covariance matrix $\underline{\mathbf{R}}_{\mathrm{n}}$ of (3.25). This estimate $\hat{\underline{\mathbf{R}}}_{\mathrm{n}}(i)$ will be considered in the data detection of the next iteration $i = 2$, see (7.4).

It is expected that the estimation quality, i.e. the accuracy of the estimate $\hat{\underline{\mathbf{R}}}_{\mathrm{n}}(i)$ of (7.7), is improved by increasing the number I_{t} of iterations as long as this iterative process converges. However, when estimating the covariance matrix $\underline{\mathbf{R}}_{\mathrm{n}}$ of (3.25) according to (7.7) only the instantaneously estimated samples of the total intercell MAI vector $\underline{\mathbf{n}}$ of (3.24) contribute to determination of $\hat{\underline{\mathbf{R}}}_{\mathrm{n}}(i)$, although the expectation $\mathrm{E}\left\{\hat{\underline{\mathbf{n}}}(i)\ \hat{\underline{\mathbf{n}}}^{*\mathrm{T}}(i)\right\}$ would be required. To more or less overcome this problem, a second possibility of improving the estimation of $\underline{\mathbf{R}}_{\mathrm{n}}$ and consequently data detection by the receiver structure of Fig. 7.2 is described below. So far, each transmitted burst has been treated separately, i.e. data detection is the same for each transmitted burst, independently of previously or subsequently transmitted bursts. Now, let us denote the received signal that depends on the transmitted burst of number n_{b} by the burst-specific vector $\underline{\mathbf{e}}_{n_{\mathrm{b}}}$ instead of $\underline{\mathbf{e}}$ of (5.10). Accordingly, the system matrix $\underline{\mathbf{A}}$ of (5.8) valid for burst number n_{b} is denoted by $\underline{\mathbf{A}}_{n_{\mathrm{b}}}$. Hence, according to (7.4) the detected data vector $\hat{\underline{\mathbf{d}}}_{n_{\mathrm{b}}}(i)$, which includes the detected data symbols $\hat{\underline{d}}_{n_{\mathrm{b}},i}$, $i = 1...KN$, which where transmitted in burst number n_{b}, is given by

$$\hat{\underline{\mathbf{d}}}_{n_{\mathrm{b}}}(i) = \left(\underline{\mathbf{A}}_{n_{\mathrm{b}}}^{*\mathrm{T}}\ \hat{\underline{\mathbf{R}}}_{\mathrm{n},n_{\mathrm{b}}}^{-1}(i-1)\ \underline{\mathbf{A}}_{n_{\mathrm{b}}}\right)^{-1}\ \underline{\mathbf{A}}_{n_{\mathrm{b}}}^{*\mathrm{T}}\ \hat{\underline{\mathbf{R}}}_{\mathrm{n},n_{\mathrm{b}}}^{-1}(i-1)\ \underline{\mathbf{e}}_{n_{\mathrm{b}}}. \tag{7.8}$$

Now, depending on the considered intercell MAI scenario, i.e. depending on the movement of the mobile terminals in the adjacent cells, we can consider one of the following three concepts to improve the estimate $\hat{\underline{\mathbf{R}}}_{\mathrm{n},n_{\mathrm{b}}}$:

- Covariance matrix $\underline{\mathbf{R}}_{\mathrm{n}}$ is estimated based on a fixed number N_{b} of received bursts. It is assumed that, based on the reception of burst number n_{b} and after I_{t} equal to one iteration, an estimate $\hat{\underline{\mathbf{R}}}_{\mathrm{n},n_\mathrm{b}}$ is obtained. Then, an improved estimate $\hat{\underline{\mathbf{R}}}_\mathrm{n}$ which can be considered in the detection of the last N_b received bursts is given by

$$\hat{\underline{\mathbf{R}}}_\mathrm{n} = \frac{1}{N_\mathrm{b}} \sum_{n_\mathrm{b}=1}^{N_\mathrm{b}} \hat{\underline{\mathbf{R}}}_{\mathrm{n},n_\mathrm{b}}. \tag{7.9}$$

- If it is known that the scenario does not change significantly with time due to movement of the interfering sources, then the covariance matrix $\hat{\underline{\mathbf{R}}}'_{\mathrm{n},n_\mathrm{b}-1}$ considered in the detection of the previously received burst number $n_\mathrm{b}-1$ can be considered together with the covariance matrix $\hat{\underline{\mathbf{R}}}_{\mathrm{n},n_\mathrm{b}}$ estimated in the actual burst number n_b to obtain the average

$$\hat{\underline{\mathbf{R}}}'_{\mathrm{n},n_\mathrm{b}} = \frac{1}{2}\left(\hat{\underline{\mathbf{R}}}_{\mathrm{n},n_\mathrm{b}} + \hat{\underline{\mathbf{R}}}'_{\mathrm{n},n_\mathrm{b}-1}\right). \tag{7.10}$$

- In item 1 and 2 it is always assumed that covariance matrix $\underline{\mathbf{R}}_\mathrm{n}$ is estimated by taking the detected data of the actual burst with the number n_b into account. The covariance matrix $\underline{\mathbf{R}}_{\mathrm{n},n_\mathrm{b}}$ estimated in this way is considered to improve the data detection of this actual burst number n_b. If the directional and temporal correlations of the intercell MAI do not vary, e.g. if the interfering sources are spatially fixed, then the covariance matrix estimated in burst $n_\mathrm{b}-1$ can be directly considered in the data detection without any iteration, i.e. for $i=1$ we obtain

$$\hat{\underline{\mathbf{d}}}_{n_\mathrm{b}}(1) = \left(\underline{\mathbf{A}}^{*\mathrm{T}}_{n_\mathrm{b}}\, \hat{\underline{\mathbf{R}}}^{-1}_{\mathrm{n},n_\mathrm{b}-1}\, \underline{\mathbf{A}}_{n_\mathrm{b}}\right)^{-1} \underline{\mathbf{A}}^{*\mathrm{T}}_{n_\mathrm{b}}\, \hat{\underline{\mathbf{R}}}^{-1}_{\mathrm{n},n_\mathrm{b}-1}\, \underline{\mathbf{e}}_{n_\mathrm{b}}. \tag{7.11}$$

  Although the interfering sources are assumed to be fixed, the system can be considered as adaptive, since it once, after an initial state, adapts itself to the given propagation environment.

In Section 7.1 it is mentioned that in the case of directionally uncorrelated intercell MAI it is sufficient to estimate the spatial covariance matrix $\underline{\mathbf{R}}_\mathrm{s}$ of (3.36), since the normalized temporal covariance matrix $\tilde{\underline{\mathbf{R}}}_\mathrm{t}$ of (3.19) is *a priori* known at the receiver. In the case of directionally uncorrelated intercell MAI the estimation procedure of the total intercell MAI vector $\underline{\mathbf{n}}$ of (3.24) described by (7.4), (7.5) and (7.6) remains the same. The partial vectors $\hat{\underline{\mathbf{n}}}^{(k_\mathrm{a})}(i)$, $k_\mathrm{a}=1...K_\mathrm{a}$, can be obtained from the estimated total intercell MAI vector $\hat{\underline{\mathbf{n}}}(i)$ of (7.6), since the vector $\underline{\mathbf{n}}$ is formed by the concatenation of the vectors $\underline{\mathbf{n}}^{(k_\mathrm{a})}$, $k_\mathrm{a}=1...K_\mathrm{a}$. Then, the estimates $\hat{\underline{\mathbf{n}}}^{(k_\mathrm{a})}(i)$, $k_\mathrm{a}=1...K_\mathrm{a}$, are arranged in a matrix

$$\hat{\underline{\mathbf{N}}}(i) = \begin{bmatrix} \hat{\underline{\mathbf{n}}}^{(1)\mathrm{T}}(i) \\ \vdots \\ \hat{\underline{\mathbf{n}}}^{(K_\mathrm{a})\mathrm{T}}(i) \end{bmatrix}, \tag{7.12}$$

according to (3.41). With (7.12) we can obtain the estimate

$$\hat{\underline{\mathbf{R}}}_{\mathrm{s}}(i) = \frac{1}{NQ+W-1} \, \hat{\underline{\mathbf{N}}}(i) \, \hat{\underline{\mathbf{N}}}^{*\mathrm{T}}(i) \tag{7.13}$$

of the spatial intercell MAI covariance matrix. The estimation of $\underline{\mathbf{R}}_{\mathrm{s}}$ according to (7.13) implies already an averaging over the $NQ+W-1$ samples of each signal $\hat{\underline{\mathbf{n}}}^{(k_{\mathrm{a}})}$, $k_{\mathrm{a}} = 1...K_{\mathrm{a}}$, in the time domain. Hence, the estimation quality of the matrix $\hat{\underline{\mathbf{R}}}_{\mathrm{s}}(i)$ of (7.13) in iteration i is expected to be better than the estimation quality of the total covariance matrix $\hat{\underline{\mathbf{R}}}_{\mathrm{n}}(i)$ of (7.7).

So far, we assumed that the total spatial channel IRs $\underline{\mathbf{h}}_{\mathrm{s}}$ of (2.11) are perfectly known at the receiver, i.e. $\underline{\mathbf{h}}_{\mathrm{s}}$ is known in the system matrix $\underline{\mathbf{A}}$ of (5.8) used for data detection and signal reconstruction. In the following channel estimation is also considered in the receiver structure of Fig. 7.2. The channel estimation can be performed either by applying the Steiner estimator, see Section 6.2, or by applying a channel estimation scheme, which allows consideration of the intercell MAI covariance matrix $\underline{\mathbf{R}}_{\mathrm{n}}$ or $\underline{\mathbf{R}}_{\mathrm{m}}$, see, e.g. Section 6.3. When applying the Steiner estimator for channel estimation only the system matrix $\underline{\mathbf{A}}$ in (7.4), (7.8) and (7.11) has to be replaced by the matrix $\hat{\underline{\mathbf{A}}}$ in which the estimated total spatial channel IR vector $\hat{\underline{\mathbf{h}}}_{\mathrm{s}}$ of (6.10) is considered. When the utilized channel estimation scheme allows the consideration of the covariance matrix $\underline{\mathbf{R}}_{\mathrm{m}}$ of (6.8), first $\underline{\mathbf{R}}_{\mathrm{n}}$ of (3.25) is estimated following one of the possibilities for the estimation of $\underline{\mathbf{R}}_{\mathrm{n}}$ described above. Then, $\underline{\mathbf{R}}_{\mathrm{m}}$ is obtained by extracting the relevant elements from the matrix $\underline{\mathbf{R}}_{\mathrm{n}}$ according to (7.3).

Advantages of the receiver concept presented in this section are:

- The signal reconstruction quality can be improved by considering FEC decoding and encoding.
- The knowledge of the symbol alphabet $\mathbb{V}_{\mathrm{d}}$, see 5.2, can be exploited, since signal reconstruction is based on quantized and not on continuous valued data symbols.
- All considered intercell MAI covariance matrices $\underline{\mathbf{R}}_{\mathrm{n}}$, $\underline{\mathbf{R}}_{\mathrm{m}}$, $\underline{\mathbf{R}}_{\mathrm{s}}$ can be estimated.

The disadvantages of this concept are:

- Data detection has to be performed at least once without considering covariance matrix $\underline{\mathbf{R}}_{\mathrm{n}}$ in order to obtain uncoded data vectors $\hat{\mathbf{u}}^{(k)}$, $k = 1...K$, which are required for the signal reconstruction that forms the basis for estimation of covariance matrix $\underline{\mathbf{R}}_{\mathrm{n}}$.

- Both the channel estimation errors and the detection errors affect the signal reconstruction being the basis of the estimation of $\underline{\mathbf{R}}_{\mathrm{n}}$.

In the following Section 7.2.2 the principles of estimating the matrix $\underline{\mathbf{R}}_{\mathrm{n}}$ are considered in MSJD. The effects of bit errors on the signal reconstruction quality are analyzed in Section 7.2.3.

7.2.2 MSJD based receiver structure

The principles of estimating and considering the intercell MAI covariance matrix $\underline{\mathbf{R}}_{\mathrm{n}}$ of (3.25) in MSJD are similar to those used for the estimation of $\underline{\mathbf{R}}_{\mathrm{n}}$ described in Section 7.2.1. Therefore, only brief descriptions of the parallel and serial MSJD concepts, see Section 5.4, which incorporate the estimation and utilization of the intercell MAI covariance matrix $\underline{\mathbf{R}}_{\mathrm{n}}$ are presented in the following.

Fig. 7.3 shows a parallel MSJD structure similar to Fig. 5.6 but extended to the estimation and consideration of $\underline{\mathbf{R}}_{\mathrm{n}}$. The estimation of the matices $\underline{\mathbf{R}}_{\mathrm{G}}^{(g)}$, $g = 1, 2$, of (5.44) is not considered. From Fig. 7.3 and taking account of the intracell MAI reduced signal $\underline{\hat{\mathbf{e}}}_{\mathrm{red}}^{(g)}(i)$ of (5.50) of iteration i, the reconstructed signals of $\underline{\hat{\mathbf{e}}}_{\mathrm{G}}^{(g)}(i)$ of (5.52) and the total received signal $\underline{\mathbf{e}}$ of (5.10) it can be seen that an estimate

$$
\begin{aligned}
\underline{\hat{\mathbf{n}}}(i) &= \underline{\mathbf{e}} - \underline{\hat{\mathbf{e}}}_{\mathrm{G}}^{(3-g)}(i) - \underline{\hat{\mathbf{e}}}_{\mathrm{G}}^{(g)}(i) \\
&= \sum_{g=1}^{2} \underline{\mathbf{A}}_{\mathrm{G}}^{(g)} \underline{\mathbf{d}}_{\mathrm{G}}^{(g)}(i) - \sum_{g=1}^{2} \underline{\mathbf{A}}_{\mathrm{G}}^{(g)} \hat{\hat{\underline{\mathbf{d}}}}_{\mathrm{G}}^{(g)}(i) + \underline{\mathbf{n}} \\
&= \underline{\hat{\mathbf{e}}}_{\mathrm{red}}^{(g)}(i) - \underline{\hat{\mathbf{e}}}_{\mathrm{G}}^{(g)}(i-1), \quad g = 1, 2,
\end{aligned}
\tag{7.14}
$$

of the total intercell MAI vector $\underline{\mathbf{n}}$ in the iteration i can be obtained.

Besides intercell MAI, the estimates $\underline{\hat{\mathbf{n}}}(i)$ of (7.14) include the reconstruction errors of both signal groups $g = 1, 2$. From the estimates $\underline{\hat{\mathbf{n}}}(i)$ of (7.14) the intercell MAI covariance matrix $\underline{\mathbf{R}}_{\mathrm{n}}$ can be estimated according to (7.7). Then, the estimate $\hat{\underline{\mathbf{R}}}_{\mathrm{n}}(i)$ of (7.7) can be considered in the detection. Based on the estimate $\underline{\hat{\mathbf{n}}}(i)$ also an estimate of the spatial covariance matrix $\underline{\mathbf{R}}_{\mathrm{s}}$ of (3.36) can be obtained. The comments given in Section 7.2.1 on the possibility of improving the estimation quality of both the spatial covariance matrix $\underline{\mathbf{R}}_{\mathrm{s}}$ of (3.36) and the total covariance matrix $\underline{\mathbf{R}}_{\mathrm{n}}$ of (3.25) by averaging techniques also hold, if MSJD is considered. The main difference concerning estimation of $\underline{\mathbf{R}}_{\mathrm{n}}$ in MSJD compared to the estimation procedure described in Section 7.2.1 is as follows: Each of the signal reconstructions $\underline{\hat{\mathbf{e}}}_{\mathrm{G}}^{(g)}(i)$, $g = 1, 2$, of (5.52) is based on data vectors $\hat{\underline{\mathbf{d}}}_{\mathrm{G}}^{(g)}(i)$, $g = 1, 2$, of (5.51) detected in the presence of intracell MAI, which is produced by the user group $(3 - g)$ with $g = 1, 2$. The uncoded detected data vectors $\hat{\mathbf{u}}^{(k)}(i)$ of (5.46) are expected to

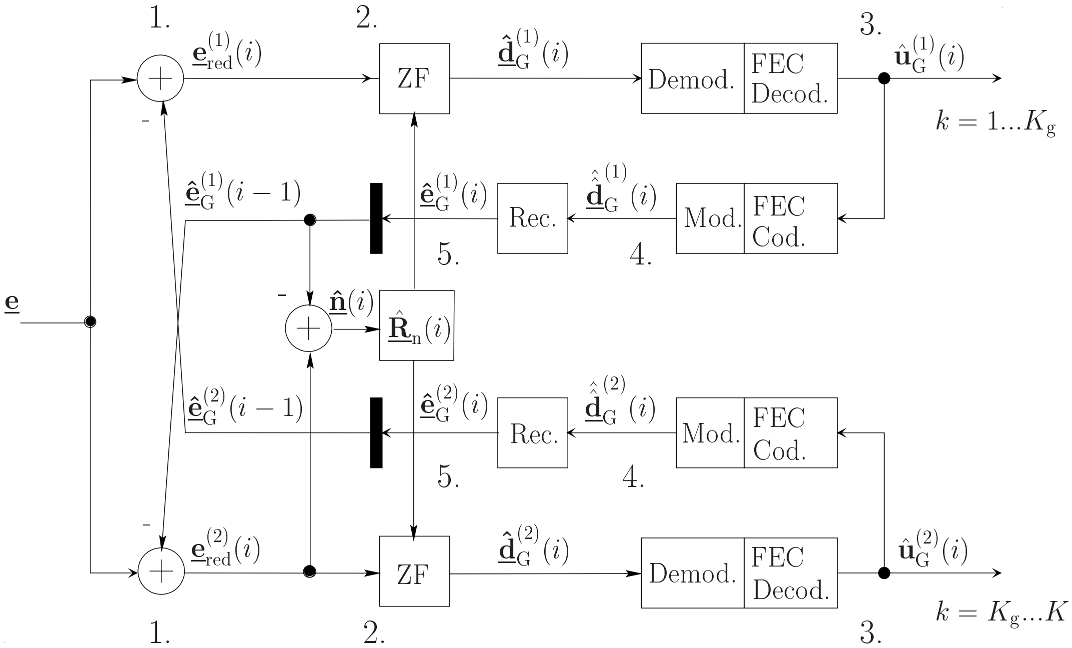

Fig. 7.3. Parallel MSJD receiver incorporating the estimation and consideration of the intercell MAI covariance matrix $\underline{\mathbf{R}}_{\mathrm{n}}$

include fewer bit errors, due to the absence of intracell MAI, than vectors $\hat{\underline{\mathbf{u}}}_{\mathrm{G}}^{(g)}(i)$, $g = 1, 2$, of (5.46). Consequently, the estimate $\hat{\underline{\mathbf{n}}}(i)$ of (7.6) in the iteration $i = 1$ is more precise than in (7.14). Therefore, it is recommended that an estimation of $\underline{\mathbf{R}}_{\mathrm{n}}$ or $\underline{\mathbf{R}}_{\mathrm{s}}$ should not be performed after the first detection step in MSJD, i.e. in the first iteration $i = 1$, but rather in subsequent iterations $i > 1$.

The possibility of estimating and considering $\underline{\mathbf{R}}_{\mathrm{n}}$ in serial MSJD is illustrated in Fig. 7.4. The main differences of parallel and serial MSJD were described in Section 5.4. Concerning estimation of matrix $\underline{\mathbf{R}}_{\mathrm{n}}$ in serial MSJD compared to parallel MSJD the difference is the following: In opposite to (7.14) the intracell MAI reduced signal $\hat{\underline{\mathbf{e}}}_{\mathrm{red}}^{(2)}(i)$ of (5.56) and the reconstructed signal $\hat{\underline{\mathbf{e}}}_{\mathrm{G}}^{(1)}(i)$ of (5.55) valid for the same iteration i are taken to obtain the estimate

$$\hat{\underline{\mathbf{n}}}(i) = \hat{\underline{\mathbf{e}}}_{\mathrm{red}}^{(2)}(i) - \hat{\underline{\mathbf{e}}}_{\mathrm{G}}^{(1)}(i) \tag{7.15}$$

of the intercell MAI. $\hat{\underline{\mathbf{n}}}(i)$ of (7.15) can be utilized to estimate $\underline{\mathbf{R}}_{\mathrm{n}}$ of (3.25) according to (7.7) or to estimate $\underline{\mathbf{R}}_{\mathrm{s}}$ according to (7.13). Then, these estimated matrices $\underline{\mathbf{R}}_{\mathrm{n}}$ or $\underline{\mathbf{R}}_{\mathrm{s}}$ can be utilized in the next iteration $i + 1$ in data detection.

In opposite to parallel MSJD the detection of the second user group $g = 2$ in serial MSJD is already done by considering an intracell MAI reduced signal $\hat{\underline{\mathbf{e}}}_{\mathrm{red}}^{(2)}(i)$, see (5.50), in the first iteration $i = 1$. Therefore, in serial MSJD it is expected that the estimation of the intercell MAI covariance matrix $\underline{\mathbf{R}}_{\mathrm{n}}$ of (3.25) is more accurate after the first data detection of both user groups $g = 1, 2$, i.e. after the first iteration $i = 1$, than in parallel MSJD.

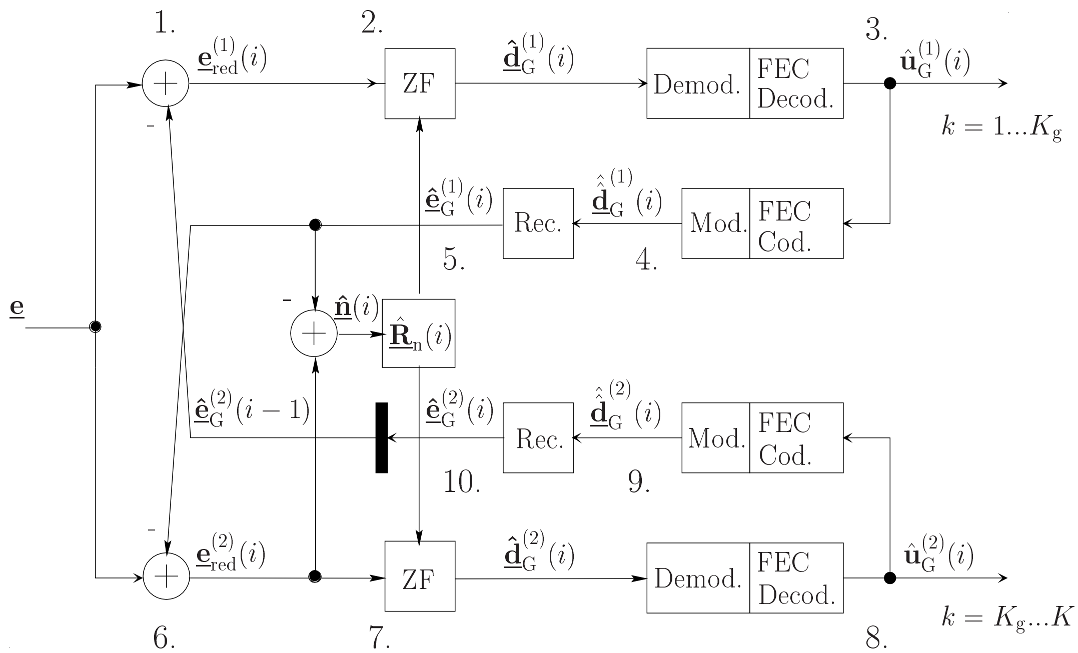

Fig. 7.4. Serial MSJD receiver incorporating the estimation and consideration of the intercell MAI matrix $\underline{\mathbf{R}}_{\mathrm{n}}$

In general, independently of using serial or parallel MSJD, the advantage of estimating and considering $\underline{\mathbf{R}}_{\mathrm{n}}$ in MSJD is that MSJD has an iterative structure which means that the additional effort of estimating $\underline{\mathbf{R}}_{\mathrm{n}}$ based on reconstructed signals is negligible compared to the approach shown in Section 7.2.1. The disadvantage when using MSJD is the expected lower estimation accuracy of the matrix $\underline{\mathbf{R}}_{\mathrm{n}}$, since the signal reconstructions, which form the basis of the estimation procedure of $\underline{\mathbf{R}}_{\mathrm{n}}$, are finally based on data detection results obtained in previous iterations, where the JD process is affected by intracell MAI.

The investigations of MSJD are performed without considering the errors of channel estimation. Therefore, there is no need to consider the estimated matrix $\hat{\underline{\mathbf{R}}}_{\mathrm{m}}$, see Section 7.1, in the channel estimation.

7.2.3 Signal reconstruction quality

With the receiver structures presented in Sections 7.2.1 and 7.2.2 a reconstruction of the received signal based on the detected and decoded data vectors $\hat{\mathbf{u}}^{(k)}$, $k = 1...K$, of (5.46) is performed for estimating the intercell MAI covariance matrix $\underline{\mathbf{R}}_{\mathrm{n}}$ of (3.25). The accuracy of the estimate $\hat{\underline{\mathbf{R}}}_{\mathrm{n}}$ is thus decisively determined by the quality of the signal reconstruction, see Section 7.2.1. This quality is effected both by estimation errors in data detection and also imperfection in channel estimation. The sections below investigate the effects of estimation errors in data detection on the quality of the signal reconstruction, incorporating FEC coding. The observations are made under the following assumptions:

- Only $K_{\mathrm{a}} = 1$ antenna element is assumed at the BS,

- the channel IRs $\underline{\mathbf{h}}_{\mathrm{RP}}^{(k)}$, $k = 1...K$, of (2.3) are perfectly known at the receiver and
- the intercell MAI vector $\underline{\mathbf{n}}$ of (3.24) is not taken into account.

The user-specific estimates $\hat{\underline{\mathbf{d}}}^{(k)}$, $k = 1...K$, of the data vectors $\underline{\mathbf{d}}^{(k)}$ of (5.1) are, as (5.9) shows contained in the data vectors $\hat{\underline{\mathbf{d}}}$ estimated in (5.12). If channel IRs $\underline{\mathbf{h}}_{\mathrm{RP}}^{(k)}$, $k = 1...K$, of (2.3) are perfectly known at the receiver, user-specific system matrices $\underline{\mathbf{A}}^{(k)}$, $k = 1...K$, of (5.7) and the data vectors $\hat{\underline{\mathbf{d}}}^{(k)}$, $k = 1...K$, can be used to determine the reconstructed receive signals

$$\hat{\underline{\mathbf{e}}}_{\mathrm{d}}^{(k)} = \underline{\mathbf{A}}^{(k)}\,\hat{\underline{\mathbf{d}}}^{(k)}, \quad k = 1...K, \tag{7.16}$$

of the K users. Starting from the actual receive signals $\underline{\mathbf{e}}_{\mathrm{d}}^{(k)}$, $k = 1...K$, of (5.11) without intercell MAI and the reconstructed signals $\hat{\underline{\mathbf{e}}}_{\mathrm{d}}^{(k)}$, $k = 1...K$, of (7.16) it is possible, instead of the quality of the signal reconstruction, to specify the reconstruction errors of the signal of user k for

$$\epsilon_{\mathrm{e}}^{(k)} = \frac{\mathrm{E}\{|\underline{\mathbf{e}}_{\mathrm{d}}^{(k)} - \hat{\underline{\mathbf{e}}}_{\mathrm{d}}^{(k)}|^2\}}{\mathrm{E}\{|\underline{\mathbf{e}}_{\mathrm{d}}^{(k)}|^2\}}, k = 1...K. \tag{7.17}$$

Fig. 7.5 shows the steps to be performed for signal reconstruction. If FEC coding is taken into account, the uncoded estimated data vectors $\hat{\mathbf{u}}^{(k)}$, $k = 1...K$, of (5.46) are again FEC coded during signal reconstruction. The code used is a 23, 35 non-systematic convolutional code (NSC-Code) [ViO79]. The encoder has a constrained length of K_{c}

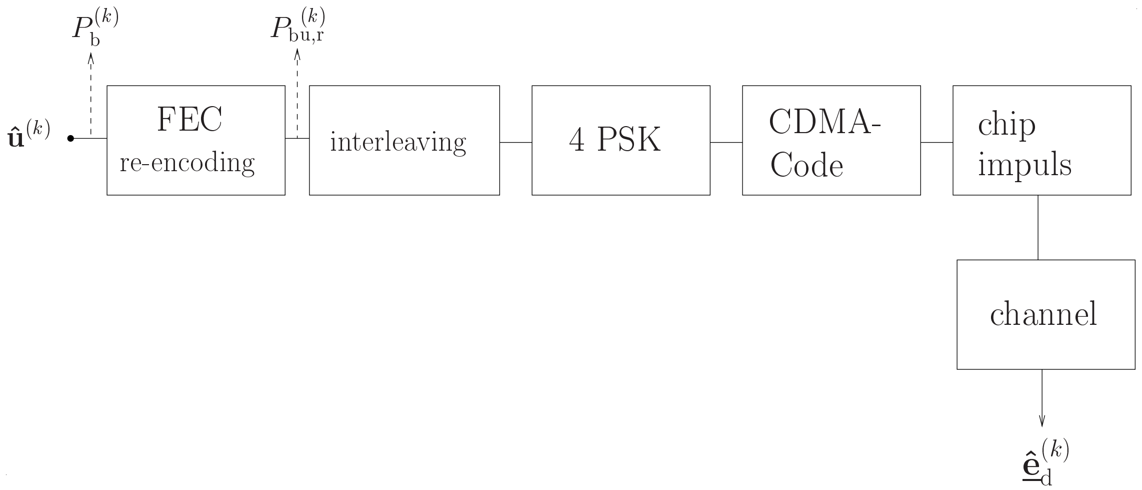

Fig. 7.5. Principle of signal reconstruction, starting from the uncoded, detected data $\hat{\mathbf{u}}^{(k)}$, $k = 1...K$, of (5.46)

equal to 5 and a code rate R_{c} equal to 0.5, see Fig. 7.6. In the following isolated bit errors are assumed, i.e. an errored bit at the input of the FEC encoder surrounded by correctly detected bits in succession assumes each of the five possible positions in the shift register of the encoder, see Fig. 7.6. With the number N_a of connections at the shift register and by the exclusive OR operations we obtain seven bit errors at the output of the encoder, if an isolated bit error is present at the input of the encoder. As Fig. 7.6 shows, of the 10 bits output in this case, the first two and the last two bits are incorrect and of the bit pairs output inbetween, one of each of the two bits is incorrect. With an

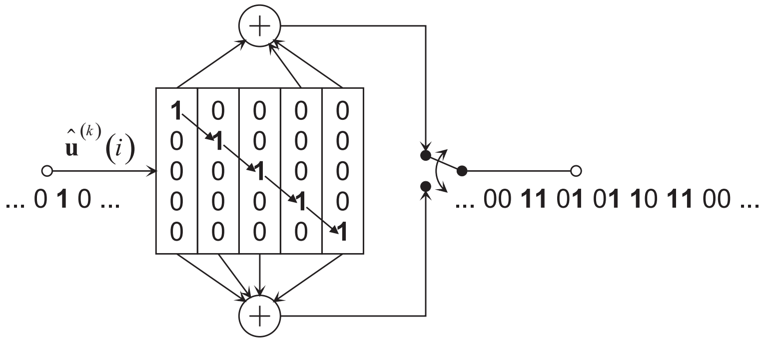

Fig. 7.6. Re-encoding in the case of a single bit error; $N_\mathrm{a} = 7$ connections at the shift register [WBOW00]

FEC encoder of rate R_c with N_a connections, isolated bit errors with a coded BER $P_\mathrm{b}^{(k)}$, $k = 1...K$, of the uncoded estimated data vectors $\hat{\mathbf{u}}^{(k)}$, $k = 1...K$, of (5.46) at the input of the encoder produce a BER amounting to

$$P_{\mathrm{bu,r}}^{(k)} = N_\mathrm{a} \cdot R_\mathrm{c} \cdot P_\mathrm{b}^{(k)}, \quad k = 1...K, \tag{7.18}$$

at the output of the encoder. With $N_\mathrm{a} = 7$ connections and a code rate $R_\mathrm{c} = 0.5$ the BER $P_{\mathrm{bu,r}}^{(k)}$, $k = 1...K$, at the output of the FEC encoder is greater than at the input of the encoder by a factor of 3.5.

After FEC coding the same interleaving structure must be used for signal reconstruction as in the transmitter of the observed system. The magnitude of the deviations of the actual received signal $\underline{\mathbf{e}}_\mathrm{d}^{(k)}$ of (5.11) from reconstructed signal $\hat{\underline{\mathbf{e}}}_\mathrm{d}^{(k)}$ of (7.16) depends on the selected modulation scheme. Multiplying the modulated signal by the CDMA code $\underline{\mathbf{c}}^{(k)}$ of (5.2) of user k as well as the convolution with the GMSK chip impulse [ETSI97] and the channel IR $\underline{\mathbf{h}}_\mathrm{RP}^{(k)}$ of (2.3) of user k have no role to play in the reconstruction error $\epsilon_\mathrm{e}^{(k)}$ of (7.17) provided the channel IR $\underline{\mathbf{h}}_\mathrm{RP}^{(k)}$ of user k is assumed to be perfectly known.

The assumption made below is that only isolated data errors occur in the uncoded estimated data vectors $\hat{\mathbf{u}}^{(k)}$, $k = 1...K$, of (5.46), i.e. that the gap between two subsequent bit errors is so large that for signal reconstruction the errors are not in the shift register of the FEC encoder at the same time. This thus excludes a mutual cancelation of two bit errors by the exclusive OR operations. As already explained above, each of these isolated errors at the input of the FEC encoder in signal reconstruction causes seven bit errors at the output of the FEC encoder or $K_{\mathrm{c}} = 5$ data symbol errors. In this case in two data symbols both bits are incorrect and in the remaining three data symbols one bit is incorrect in each case. According to (7.17) with 4 PSK modulation a deviation of 2 of reconstructed signal $\hat{\underline{\mathbf{e}}}_{\mathrm{d}}^{(k)}$ of (7.16) of user k from actual signal $\underline{\mathbf{e}}_{\mathrm{d}}^{(k)}$ of (5.11) is obtained when a data symbol error is present as a result of one incorrect bit in the data symbol. Furthermore, a deviation of 4 is obtained when both bits of a data symbol are incorrect. Taking account of the parameters from Chapter 8, for reconstruction error $\epsilon_{\mathrm{e}}^{(k)}$ of signal of user k the result is that, when N is the number of data symbols, M_{d} the number of uncoded bits, i.e. the dimensions of vectors $\hat{\mathbf{u}}^{(k)}$, $k = 1...K$, of (5.46), M the size of the data symbol alphabet and $P_{\mathrm{b}}^{(k)}$ the coded BER of the signal of user k,

$$\epsilon_{\mathrm{e}}^{(k)} = \frac{\frac{2}{5} \cdot 4 \cdot K_{\mathrm{c}} \cdot P_{\mathrm{b}}^{(k)} \cdot M_{\mathrm{d}} + \frac{3}{5} \cdot 2 \cdot K_{\mathrm{c}} \cdot P_{\mathrm{b}}^{(k)} \cdot M_{\mathrm{d}}}{N \cdot R_{\mathrm{c}} \cdot \log_2(M)} = 14 P_{\mathrm{b}}^{(k)}. \tag{7.19}$$

(7.19) shows a direct proportionality between the coded BER $P_{\mathrm{b}}^{(k)}$ and the reconstruction error $\epsilon_{\mathrm{e}}^{(k)}$ of the signal of user k.

There now follows an investigation into the effects of bundle errors on the reconstruction of the relevant user signals. For this only the reconstruction errors $\epsilon_{\mathrm{e}}^{(1)}$ of (7.17) and the coded BER $P_{\mathrm{b}}^{(1)}$ and the uncoded BER $P_{\mathrm{bu,r}}^{(1)}$ valid for signal reconstruction of the signal of an individual user $K = 1$ are considered. For the following considerations no system simulation is required since specific BERs $P_{\mathrm{b}}^{(1)}$ and bit error patterns are explicitly assumed, and the BER $P_{\mathrm{b}}^{(1)}$ is not obtained by transmission over a living channel. This means that the initial assumption is that the signals of the observed user are detected without errors. Before signal reconstruction, in a sequence of four bursts in each case X consecutive bit errors are inserted into the bits detected as error free and then signal reconstruction in accordance with Fig. 7.5 is undertaken.

In accordance with the underlaying parameters from Chapter 8 a burst contains two data blocks each with $N = 28$ data symbols. According to (5.47) and taking into consideration a code rate R_{c} of 0.5 a sequence of 192 uncoded bits is produced with the transmission of 4 bursts. The X bit errors thus represent an individual error bundle in a sequence of $192 - X$ error-free detected bits. Fig. 7.7 shows BERs $P_{\mathrm{b}}^{(1)}$ and $P_{\mathrm{bu,r}}^{(1)}$ and also the reconstruction error $\epsilon_{\mathrm{e}}^{(1)}$ of (7.17) of the signal of the observed user, depending on X. In addition the relationships $\epsilon_{\mathrm{e}}^{(1)}/P_{\mathrm{b}}^{(1)}$ and $P_{\mathrm{bu,r}}^{(1)}/P_{\mathrm{b}}^{(1)}$ are shown. For $X = 1$ the curve $\epsilon_{\mathrm{e}}^{(1)}/P_{\mathrm{b}}^{(1)}$ confirms the factor 14 by which the reconstruction error $\epsilon_{\mathrm{e}}^{(1)}$ of (7.17) with isolated single errors is greater than $P_{\mathrm{b}}^{(1)}$, see (7.19). Also confirmed is the factor 3.5, by which according to (7.18) $P_{\mathrm{bu,r}}^{(1)}$ is greater than $P_{\mathrm{b}}^{(1)}$ if it is assumed that only isolated errors occur. With X equals five consecutive incorrect bits the uncoded BER $P_{\mathrm{bu,r}}^{(1)}$ for reconstruction is equal to the coded BER $P_{\mathrm{b}}^{(1)}$. The reconstruction error $\epsilon_{\mathrm{e}}^{(1)}$ in this case is only greater by a factor of 4.2 than $P_{\mathrm{b}}^{(1)}$. Although the reconstruction error $\epsilon_{\mathrm{e}}^{(1)}$ relative to the coded BER $P_{\mathrm{b}}^{(1)}$

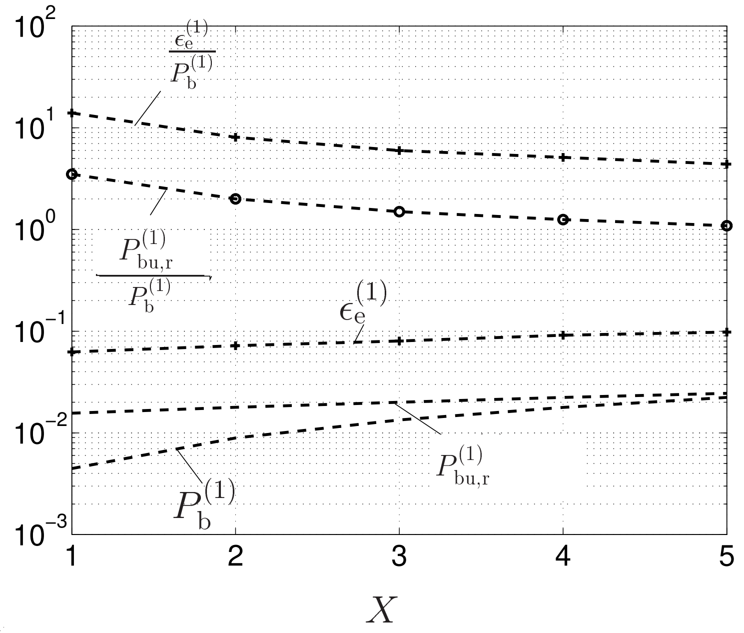

Fig. 7.7. BERs $P_{\mathrm{b}}^{(1)}$ and $P_{\mathrm{bu,r}}^{(1)}$ as well as reconstruction error $\epsilon_{\mathrm{e}}^{(1)}$ for individual bundle errors with X consecutive incorrect bits

is smaller when bundle errors occur and the bit error rate $P_{\mathrm{b}}^{(1)}$ rises, in absolute terms a lower reconstruction error $\epsilon_{\mathrm{e}}^{(1)}$ is obtained for a lower coded BER $P_{\mathrm{b}}^{(1)}$.

Instead of individual error bundles, the effects of signal reconstruction are investigated below when each Y-th bit in the uncoded detected data vectors $\hat{\mathbf{u}}^{(k)}$, $k = 1...K$, of (5.46) is incorrect. The results are shown in Fig. 7.8. If each Y equals 5^{th} bit is incorrect this ensures that at any point only a single incorrect bit is in the shift register of the encoder, there are again individual isolated errors. For $Y = 5$ the figure obtained for $\epsilon_{\mathrm{e}}^{(1)}/P_{\mathrm{b}}^{(1)}$ according to (7.19) is therefore again 14, see Fig. 7.8, and for $P_{\mathrm{bu,r}}^{(1)}/P_{\mathrm{b}}^{(1)}$ according to (7.18) the figure is 3.5. If we look at the unrealistic case in which each bit is incorrect, i.e. $Y = 1$, this result for $\epsilon_{\mathrm{e}}^{(1)}/P_{\mathrm{b}}^{(1)}$ is the figure 2, see Fig. 7.8. In this case the reconstruction error $\epsilon_{\mathrm{e}}^{(1)}$ in contrast to the factor 14 for isolated single errors, is only greater by a factor of 2 than the coded BER $P_{\mathrm{b}}^{(1)}$. The uncoded BER before signal reconstruction $P_{\mathrm{bu,r}}^{(1)}$ at the output of the encoder is in this case even smaller than $P_{\mathrm{b}}^{(1)}$, see Fig. 7.8.

With decreasing coded BERs $P_{\mathrm{b}}^{(1)}$ the difference between $P_{\mathrm{b}}^{(1)}$ and $P_{\mathrm{bu,r}}^{(1)}$ will increase, as Fig. 7.7 in particular shows. Taking account of FEC coding in signal reconstruction thus increases the uncoded BER $P_{\mathrm{bu,r}}^{(1)}$ underlying signal reconstruction. On the other hand FEC decoding has the effect that the coded BER $P_{\mathrm{b}}^{(k)}$ of uncoded data vectors $\hat{\mathbf{u}}^{(k)}$, $k = 1...K$, of (5.46) of each user k is smaller than the uncoded BER $P_{\mathrm{bu}}^{(k)}$ of the detected data $\hat{\underline{\mathbf{d}}}^{(k)}$, $k = 1...K$, of (5.1). In Chapter 8 an investigation is thus made using simulation results to see whether it is possible to dispense with FEC coding for signal reconstruction

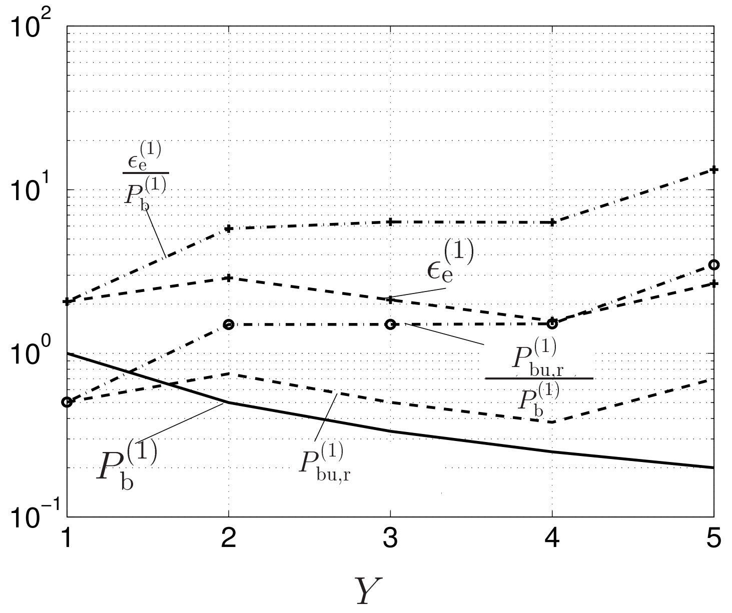

Fig. 7.8. BERs $P_{\mathrm{b}}^{(1)}$ and $P_{\mathrm{bu,r}}^{(1)}$ as well as reconstruction error $\epsilon_{\mathrm{e}}^{(1)}$ for bit sequences in which each Y-th bit is incorrect

or whether it is indispensable for signal reconstruction.

7.3 Exploiting channel IRs for estimating $\underline{\mathbf{R}}_{\mathrm{m}}$

Section 7.2 looks at two receiver concepts for estimating and considering the total intercell MAI covariance matrix $\underline{\mathbf{R}}_{\mathrm{n}}$ of (3.25) or the spatial intercell MAI covariance matrix $\underline{\mathbf{R}}_{\mathrm{s}}$ of (3.36). Both concepts rely on signal reconstruction based on exploiting detected data symbols. In the worst case, if the interferer constellations are changing permanently, then in the estimation concepts for $\underline{\mathbf{R}}_{\mathrm{n}}$ at least two data detection processes are required. One to obtain the data symbols, based on which the signal reconstruction is performed and the matrix $\underline{\mathbf{R}}_{\mathrm{n}}$ is estimated. Then, the estimated matrix $\hat{\underline{\mathbf{R}}}_{\mathrm{n}}$ of (7.7) can be considered soonest in a second data detection of the user signals.

In this section a concept for estimating the matrix $\underline{\mathbf{R}}_{\mathrm{m}}$ of (6.8) without the need for iterative detection structures is described. Such approaches were already mentioned in [AMF99]. The concept is based on reconstructing the portion of the received signal which depends exclusively on the transmitted midambles. The reconstructed signal is subtracted from the actual received signal $\underline{\mathbf{e}}_{\mathrm{m}}$ of (6.5). Fig. 7.9 shows the structure of the receiver concept described in this section.

First, a channel estimation is performed, see Fig. 7.9. In this channel estimation we can utilize

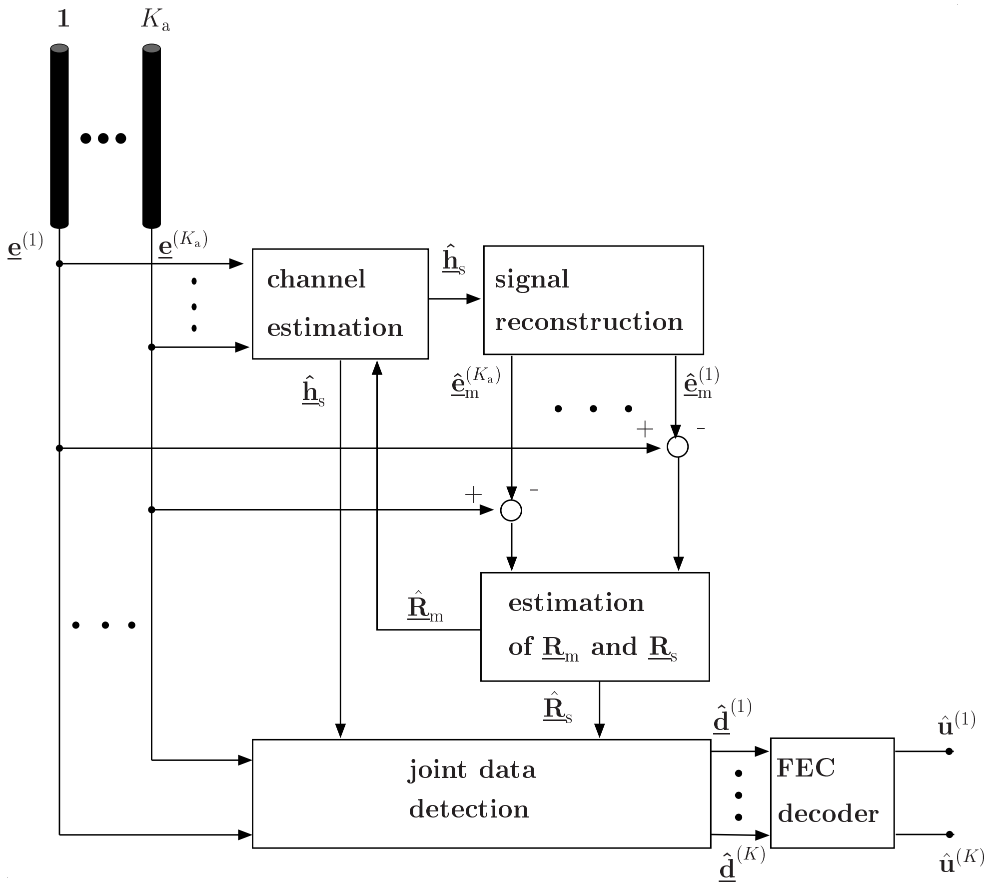

Fig. 7.9. Receiver concept incorporating the estimation of $\underline{\mathbf{R}}_m$ and $\underline{\mathbf{R}}_s$

- the Steiner estimator, see Section 6.2, or
- the DOA based channel estimation approach described in Section 6.3, if the DOAs $\beta^{(k,k_d)}$, $k = 1...K$, $k_d = 1...K_d$, of the user signals are known at the receiver, or
- the MMSE–JCE approach described in Section 6.4, if the correlation matrix $\underline{\mathbf{R}}_{\tau,s}$ of (2.12) of the spatial channel IR vector $\underline{\mathbf{h}}_s$ of (2.11) is available.

In any of these three channel estimation schemes according to (6.11), (6.15) and (6.25) first a channel estimation has to be performed, where $\underline{\mathbf{R}}_m$ is replaced by the identity matrix $\mathbf{I}^{(L)}$, since no knowledge of $\underline{\mathbf{R}}_m$ is available. With the matrix $\tilde{\underline{\mathbf{G}}}$ of (6.7) and with the estimated channel IR vectors $\hat{\underline{\mathbf{h}}}_s$, e.g. of (6.11) or (6.9), the reconstructions

$$\hat{\underline{\mathbf{e}}}_m = \tilde{\underline{\mathbf{G}}}\,\hat{\underline{\mathbf{h}}}_s \tag{7.20}$$

of the signal $\underline{\mathbf{e}}_m$ of (6.6) without intercell MAI can be determined. Similar to (7.6) an estimate

$$\hat{\underline{\mathbf{n}}}_m = \underline{\mathbf{e}}_m - \hat{\underline{\mathbf{e}}}_m \tag{7.21}$$

of the intercell MAI vector is obtained.

As already mentioned in Section 6.4 the vector $\underline{\mathbf{n}}_{\mathrm{m}}$ holds for the same correlation properties as $\underline{\mathbf{n}}$ of (3.24). Moreover, $\underline{\mathbf{n}}_{\mathrm{m}}$ and $\underline{\mathbf{n}}$ have the same spatial correlations. As already mentioned in Section 7.2.1 the vector $\underline{\mathbf{n}}$ of (3.24) is established by a concatenation of the partial vectors $\underline{\mathbf{n}}^{(k_{\mathrm{a}})}$, $k_{\mathrm{a}} = 1...K_{\mathrm{a}}$. Likewise, the intercell MAI vector $\hat{\underline{\mathbf{n}}}_{\mathrm{m}}$, $k_{\mathrm{a}} = 1...K_{\mathrm{a}}$, of (7.21) is a concatenation of the vectors $\hat{\underline{\mathbf{n}}}_{\mathrm{m}}^{(k_{\mathrm{a}})}$, $k_{\mathrm{a}} = 1...K_{\mathrm{a}}$, which represent the estimated intercell MAI received at the K_{a} antenna elements. Consequently, the vectors $\hat{\underline{\mathbf{n}}}_{\mathrm{m}}^{(k_{\mathrm{a}})}$, $k_{\mathrm{a}} = 1...K_{\mathrm{a}}$, can be extracted from $\hat{\underline{\mathbf{n}}}_{\mathrm{m}}$. With the estimates $\hat{\underline{\mathbf{n}}}_{\mathrm{m}}^{(k_{\mathrm{a}})}$, $k_{\mathrm{a}} = 1...K_{\mathrm{a}}$, the spatial covariance matrix $\underline{\mathbf{R}}_{\mathrm{s}}$ of (3.36) can be estimated similar to (7.13) by establishing a matrix

$$\hat{\underline{\mathbf{N}}}_{\mathrm{m}} = \begin{bmatrix} \hat{\underline{\mathbf{n}}}_{\mathrm{m}}^{(1)\mathrm{T}} \\ \vdots \\ \hat{\underline{\mathbf{n}}}_{\mathrm{m}}^{(K_{\mathrm{a}})\mathrm{T}} \end{bmatrix} \tag{7.22}$$

of dimension $K_{\mathrm{a}} \times L$ and by calculating

$$\hat{\underline{\mathbf{R}}}_{\mathrm{s}} = \frac{1}{L} \hat{\underline{\mathbf{N}}}_{\mathrm{m}} \, \hat{\underline{\mathbf{N}}}_{\mathrm{m}}^{*\mathrm{T}} . \tag{7.23}$$

According to (7.7) the estimate

$$\hat{\underline{\mathbf{R}}}_{\mathrm{m}} = \underline{\mathbf{n}}_{\mathrm{m}} \, \underline{\mathbf{n}}_{\mathrm{m}}^{*\mathrm{T}} \tag{7.24}$$

of the covariance matrix $\underline{\mathbf{R}}_{\mathrm{m}}$ based on the reception of the actual burst is obtained. The matrix $\hat{\underline{\mathbf{R}}}_{\mathrm{s}}$ of (7.23) can be directly considered in the data detection of the actual received burst with the number n_{b}, e.g. by applying the ZF–BLE according to (5.12). For the consideration of the matrix $\hat{\underline{\mathbf{R}}}_{\mathrm{m}}$ of (7.24) in the channel estimation by applying for instance (6.9), (6.15) or (6.25), there are two possibilities:

- For the actual received burst with the number n_{b} once more an channel estimation can be performed, now under consideration of $\hat{\underline{\mathbf{R}}}_{\mathrm{m}}$ of (7.24).
- The matrix $\hat{\underline{\mathbf{R}}}_{\mathrm{m}}$ of (7.24) can be considered in the channel estimation of the subsequent received burst with the number $n_{\mathrm{b}} + 1$.

The improvements of the estimation quality of the matrices $\hat{\underline{\mathbf{R}}}_{\mathrm{s}}$ of (7.23) and/or $\hat{\underline{\mathbf{R}}}_{\mathrm{m}}$ of (7.23) by taking more than a single burst into account in the estimation process, as it is described in Section 7.2.1 for the matrices $\hat{\underline{\mathbf{R}}}_{\mathrm{s}}(i)$ of (7.13) and $\hat{\underline{\mathbf{R}}}_{\mathrm{n}}(i)$ of (7.7), can also be considered here.

The advantage of the receiver concept described in this section is its simplicity, since no iterative data detection is required. The disadvantages are:

- No exploitation of the knowledge of the chip alphabet $\mathbb{V}_{\mathrm{m}}$ of the midambles,
- no consideration of FEC decoding for improving the quality of the reconstructed signal $\underline{\hat{\mathbf{e}}}_{\mathrm{m}}$ is possible, and,
- no estimation of the total intercell MAI covariance matrix $\underline{\mathbf{R}}_{\mathrm{n}}$ of (3.25) is possible.

With the TD–CDMA system parameters considered in this thesis, see Chapter 8, there is another important disadvantage. The matrix $\underline{\tilde{\mathbf{G}}}$ of (6.7) is a square and invertible matrix, if all spatial channel IRs $\underline{\mathbf{h}}_{\mathrm{s}}^{(k,k_{\mathrm{a}})}$, $k = 1...K$, $k_{\mathrm{a}} = 1...K_{\mathrm{a}}$, at all K_{a} antenna elements are jointly estimated. In this case, and considering (6.6) and (6.11), the estimate $\underline{\hat{\mathbf{n}}}_{\mathrm{m}}$ takes the form

$$\begin{aligned}
\underline{\hat{\mathbf{n}}}_{\mathrm{m}} &= \underline{\mathbf{e}}_{\mathrm{m}} - \underline{\hat{\mathbf{e}}}_{\mathrm{m}} \\
&= \underline{\tilde{\mathbf{G}}}\,\underline{\mathbf{h}}_{\mathrm{s}} + \underline{\mathbf{n}}_{\mathrm{m}} - \underline{\tilde{\mathbf{G}}}\,\underline{\hat{\mathbf{h}}}_{\mathrm{s}} \\
&= \underline{\tilde{\mathbf{G}}}\,\underline{\mathbf{h}}_{\mathrm{s}} + \underline{\mathbf{n}}_{\mathrm{m}} - \underline{\tilde{\mathbf{G}}}\,\underline{\tilde{\mathbf{G}}}^{-1}\,\underline{\mathbf{e}}_{\mathrm{m}} \\
&= \underline{\tilde{\mathbf{G}}}\,\underline{\mathbf{h}}_{\mathrm{s}} + \underline{\mathbf{n}}_{\mathrm{m}} - \underline{\tilde{\mathbf{G}}}\,\underline{\tilde{\mathbf{G}}}^{-1}\left(\underline{\tilde{\mathbf{G}}}\,\underline{\mathbf{h}}_{\mathrm{s}} + \underline{\mathbf{n}}\right) \\
&= \mathbf{0}.
\end{aligned} \tag{7.25}$$

From (7.25) it becomes obvious that an estimation of the intercell MAI $\underline{\mathbf{n}}_{\mathrm{m}}$ and, consequently, an estimation of the intercell MAI covariance matrix $\underline{\mathbf{R}}_{\mathrm{m}}$ is not possible with the considered system parameters. Hence, this receiver concept is not considered in this thesis.

7.4 Estimation of $\underline{\mathbf{R}}_{\mathrm{s}}$ based on spatial correlations of the received and reconstructed signals

After Sections 7.2 and 7.3 have presented receiver concepts which allow estimation of the intercell MAI covariance matrices $\underline{\mathbf{R}}_{\mathrm{n}}$ of (3.25) or $\underline{\mathbf{R}}_{\mathrm{m}}$ of (6.8) on the basis of signal reconstructions, the sections below describe a receiver concept based only on spatial correlations of the received signal $\underline{\mathbf{e}}$ of (5.10) and the spatial correlations of the user signals which allows estimation of the spatial intercell MAI covariance matrix $\underline{\mathbf{R}}_{\mathrm{s}}$ of (3.36). The matrix $\underline{\hat{\mathbf{R}}}_{\mathrm{s}}$ estimated in this way can then, like in the receiver structures already described in Sections 7.2 and 7.3 be taken into consideration in data detection and/or in channel estimation. The structure of the receiver concept presented in this section is shown in Fig. 7.10. A concept of this type has already be presented in [HMV00]. For this reason only the main basic features of the concept are repeated here.

At the receiver the received signal vector $\underline{\mathbf{e}}$ of (5.10) is first broken down into the K_{a} antenna-specific received signal vectors $\underline{\mathbf{e}}^{(k_{\mathrm{a}})}$, $k_{\mathrm{a}} = 1...K_{\mathrm{a}}$, see Table 5.2. The received

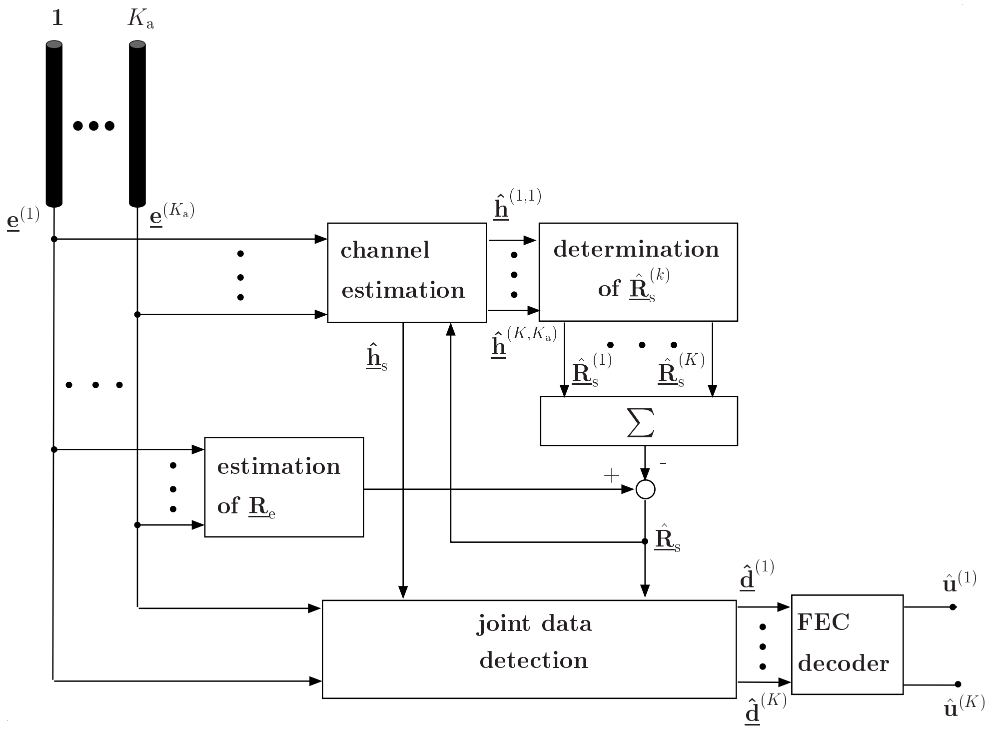

Fig. 7.10. Estimating and considering the spatial intercell MAI covariance matrix $\underline{\mathbf{R}}_{\mathrm{s}}$ starting from the estimated spatial correlation matrix $\hat{\underline{\mathbf{R}}}_{\mathrm{e}}$ of the received signal and the estimated spatial correlation matrices $\underline{\mathbf{R}}_{\mathrm{s}}^{(k)}$ of the $k = 1...K$ user signals

signal vectors $\underline{\mathbf{e}}^{(k_{\mathrm{a}})}$, $k_{\mathrm{a}} = 1...K_{\mathrm{a}}$, at the K_{a} antenna elements can then be arranged in the received signal matrix

$$\underline{\mathbf{E}} = \begin{bmatrix} \underline{\mathbf{e}}^{(1)\mathrm{T}} \\ \vdots \\ \underline{\mathbf{e}}^{(K_{\mathrm{a}})\mathrm{T}} \end{bmatrix} \tag{7.26}$$

of the dimension $K_{\mathrm{a}} \times (NQ + W - 1)$. (7.26) obtains an estimate

$$\hat{\underline{\mathbf{R}}}_{\mathrm{e}} = \frac{1}{NQ + W - 1} \underline{\mathbf{E}}\ \underline{\mathbf{E}}^{*\mathrm{T}} \tag{7.27}$$

with dimension $K_{\mathrm{a}} \times K_{\mathrm{a}}$ of the current spatial correlation matrix of the received signal. As already described in Section 7.2.1, the estimation quality of matrix $\hat{\underline{\mathbf{R}}}_{\mathrm{e}}$ of (7.27) can be improved by averages of further matrices $\hat{\underline{\mathbf{R}}}_{\mathrm{e}}$ estimated when receiving previous bursts, provided the user constellations and the spatial positions of the K users does not change or changes only marginally. The basic idea of estimating the spatial intercell MAI covariance matrix $\underline{\mathbf{R}}_{\mathrm{s}}$ of (3.36) with the receiver structure shown in Fig. 7.10 is that the spatial correlations of the received signal $\underline{\mathbf{e}}$ of (5.10) are precisely the total from the spatial correlations of the user signals and the spatial correlations of the intercell MAI, provided the user signals and the intercell MAI are uncorrelated. The required uncorrelatedness between the user signals and the intercell MAI is assumed below. In addition, the initial assumption is also made that the spatial correlation characteristics of the user signals will largely be determined by the spatial channel IRs $\underline{\mathbf{h}}_{\mathrm{s}}$ of (2.11). By using a conventional channel estimation in accordance with (6.11) the antenna specific channel IR $\underline{\mathbf{h}}_{\mathrm{s}}^{(k,k_{\mathrm{a}})}$, $k_{\mathrm{a}} = 1...K_{\mathrm{a}}$, of (2.1) of the K users can be estimated. If the estimated vectors $\hat{\underline{\mathbf{h}}}_{\mathrm{s}}^{(k,k_{\mathrm{a}})}$, $k_{\mathrm{a}} = 1...K_{\mathrm{a}}$, are arranged in the user-specific $K_{\mathrm{a}} \times W$ channel IR matrices

$$\hat{\underline{\mathbf{H}}}^{(k)} = \begin{bmatrix} \hat{\underline{\mathbf{h}}}_{\mathrm{s}}^{(k,1)\mathrm{T}} \\ \vdots \\ \hat{\underline{\mathbf{h}}}_{\mathrm{s}}^{(k,K_{\mathrm{a}})\mathrm{T}} \end{bmatrix}, \quad k = 1...K, \tag{7.28}$$

using (7.28), estimates

$$\hat{\underline{\mathbf{R}}}_{\mathrm{s}}^{(k)} = \frac{1}{W} \hat{\underline{\mathbf{H}}}\, \hat{\underline{\mathbf{H}}}^{*\mathrm{T}}, \quad k = 1...K, \tag{7.29}$$

of the user-specific spatial correlation matrices are obtained with dimensions $K_{\mathrm{a}} \times K_{\mathrm{a}}$. Just as already used for the estimate $\hat{\underline{\mathbf{R}}}_{\mathrm{e}}$ of (7.27) the estimated quality of the user-specific spatial correlation matrices $\hat{\underline{\mathbf{R}}}_{\mathrm{s}}^{(k)}$, $k = 1...K$, can be improved by averaging over a number of correlation matrices determined in different bursts if the above-mentioned conditions relating to user movement and constellations are fulfilled. With the estimates $\hat{\underline{\mathbf{R}}}_{\mathrm{e}}$ of (7.27) and $\hat{\underline{\mathbf{R}}}_{\mathrm{s}}^{(k)}$, $k = 1...K$, of (7.29) an estimate

$$\hat{\underline{\mathbf{R}}}_{\mathrm{s}} = \hat{\underline{\mathbf{R}}}_{\mathrm{e}} - \sum_{k=1}^{K} \hat{\underline{\mathbf{R}}}_{\mathrm{s}}^{(k)} \tag{7.30}$$

of the spatial intercell MAI covariance matrix $\underline{\mathbf{R}}_{\mathrm{s}}$ of (3.36) is obtained.

Compared with the receiver concept presented in Section 7.2.1, the procedure shown in this section for estimating the spatial intercell MAI covariance matrix $\underline{\mathbf{R}}_{\mathrm{s}}$ of (3.36) is much less effort. It is not possible to use the receiver structure presented here to estimate the total intercell MAI matrix $\underline{\mathbf{R}}_{\mathrm{n}}$ of (3.25). In Chapter 8 the BER performances of the receiver structures presented in this Section and in Section 7.2.1 will be compared by simulation results.

7.5 Receiver concept considering $\underline{\mathbf{R}}_{\mathrm{n}}$ and $\underline{\mathbf{R}}_{\tau,\mathrm{s}}$

The previous sections showed how data estimation could be improved by taking account of spatial and temporal correlation characteristics of the intercell MAI in the form of correlation and covariance matrices. One of the decisive benefits, in particular when making use of spatial covariance matrices is that the spatial covariance matrices include the information about the direction sensitivity of the intercell MAI, without the precondition of direction-discrete channel IRs and the use of DOA estimation algorithms being necessary. Since not only the intercell MAI $\underline{\mathbf{n}}$ of (3.24) but also desired signals of the users are generally not directionally discrete, see Chapter 2, it would seem sensible to have explicit utilization of the covariance matrices, not only of the intercell MAI, but also of the correlation matrices of the desired signals.

If the ZF–BLE is used for data estimation, when the covariance matrix $\underline{\mathbf{R}}_{\mathrm{n}}$ of (3.25) is already taken into account, a further improvement of data estimation can only be achieved by an improvement in the quality of the channel estimation. Accordingly the utilization of the correlation matrices of the desired signals has as its aim the improvement in channel estimation. In Section 6.4 MMSE based channel estimation has already been presented, which, in addition to taking account of the intercell MAI covariance matrix $\underline{\mathbf{R}}_{\mathrm{m}}$ of (6.8) also allows the consideration of the matrix $\underline{\mathbf{R}}_{\tau,\mathrm{s}}$ of (2.12) of the spatial channel IRs $\underline{\mathbf{h}}_{\mathrm{s}}$ of (2.11). As was shown in Chapter 2 the desired spatial correlations of the desired signals of the K users are included in matrix $\underline{\mathbf{R}}_{\tau,\mathrm{s}}$ of (2.12).

Therefore, in the following sections, the receiver concept presented in Section 7.2.1 which allows the intercell covariance matrix $\underline{\mathbf{R}}_{\mathrm{n}}$ to be estimated and taken into account in data detection, is expanded by the option of estimating and taking account of matrix $\underline{\mathbf{R}}_{\tau,\mathrm{s}}$ of (2.12) in the MMSE–JCE, see Section 6.4. Fig. 7.11 shows the receiver structure which belongs to the expanded concept. As well as matrix $\underline{\mathbf{R}}_{\tau,\mathrm{s}}$ of (2.12) it is also possible to take account of $\underline{\mathbf{R}}_{\mathrm{m}}$ of (6.8) for MMSE–JCE. An estimation of matrix $\hat{\underline{\mathbf{R}}}_{\mathrm{m}}$ can be obtained in accordance with (7.3) from estimated matrix $\hat{\underline{\mathbf{R}}}_{\mathrm{n}}$ of (7.7). Since estimation of matrices $\underline{\mathbf{R}}_{\mathrm{n}}$ and $\underline{\mathbf{R}}_{\mathrm{m}}$ using the receiver structure shown in Fig. 7.11 was described in detail in Section 7.2.1, the following paragraphs only deal with estimation of matrix $\underline{\mathbf{R}}_{\tau,\mathrm{s}}$ of (2.12).

Estimation of matrix $\underline{\mathbf{R}}_{\tau,\mathrm{s}}$ of (2.12) can be undertaken in a similar way to the description given in Section 7.2.1 for estimating matrix $\underline{\mathbf{R}}_{\mathrm{n}}$ of (3.25) as an iterative implementation. The necessary iterations can be conducted in parallel to the estimation of matrix $\underline{\mathbf{R}}_{\mathrm{n}}$. An iteration to estimate $\underline{\mathbf{R}}_{\tau,\mathrm{s}}$ can be described in the following steps:

- In iteration i as per (6.25) the estimated channel IR vector

  $$\hat{\underline{\mathbf{h}}}_{\mathrm{s,MMSE2}}(i) = \underline{\mathbf{R}}_{\tau,\mathrm{s}}(i-1)\ \tilde{\underline{\mathbf{G}}}^{*\mathrm{T}} \left(\underline{\mathbf{R}}_{\mathrm{m}}(i-1) + \tilde{\underline{\mathbf{G}}}\ \underline{\mathbf{R}}_{\tau,\mathrm{s}}(i-1)\ \tilde{\underline{\mathbf{G}}}^{*\mathrm{T}}\right)^{-1} \underline{\mathbf{e}}_{\mathrm{m}} \qquad (7.31)$$

  is obtained. In the first iteration, i.e. for $i=1$, matrix $\underline{\mathbf{R}}_{\tau,\mathrm{s}}(0) = \mathbf{I}^{(K_{\mathrm{a}}KW)}$ and matrix $\underline{\mathbf{R}}_{\mathrm{m}}(0) = 0$ are used. If you use $\underline{\mathbf{R}}_{\tau,\mathrm{s}}(0) = \mathbf{I}^{(K_{\mathrm{a}}KW)}$ and $\underline{\mathbf{R}}_{\mathrm{m}}(0) = 0$ in (7.31), channel estimation in accordance with (7.31) implements conventional channel estimation in accordance with (6.11).

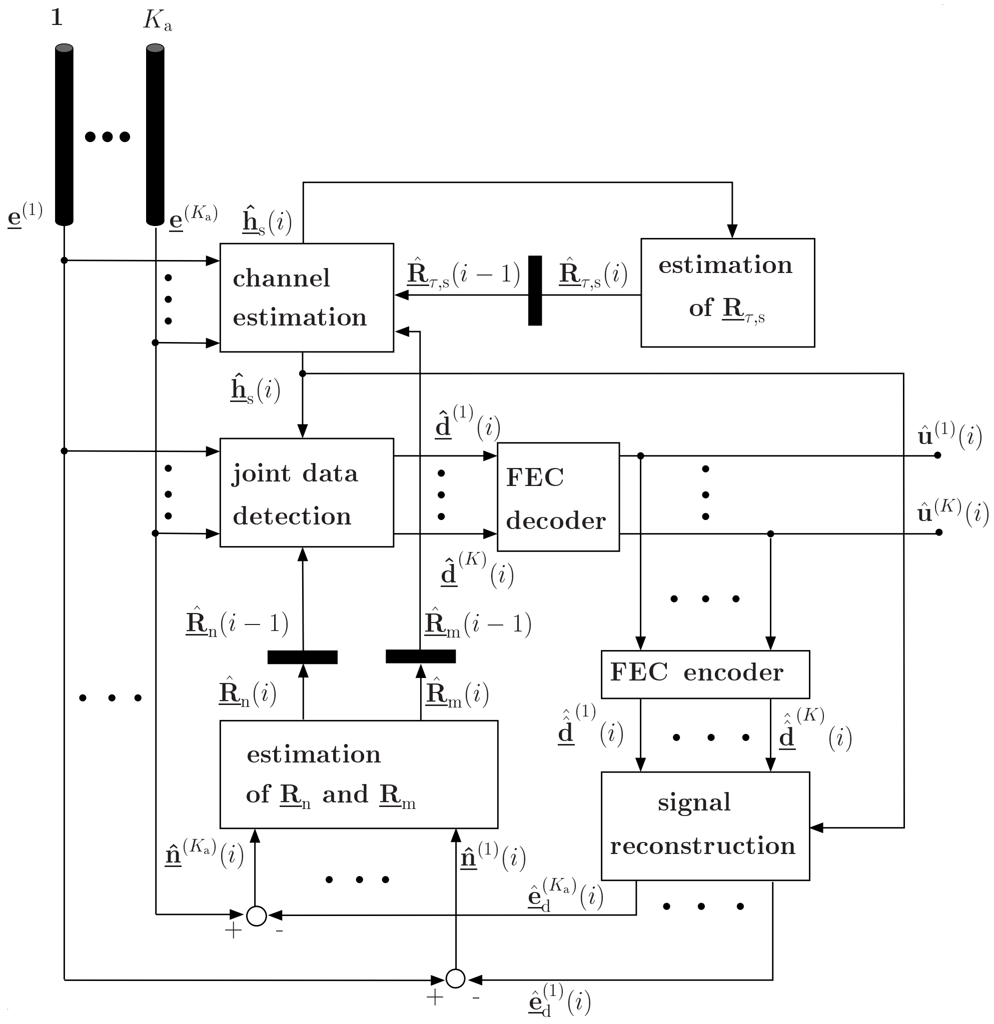

Fig. 7.11. Receiver structure which allows estimation and consideration of matrices $\underline{\mathbf{R}}_{\tau,s}$ in channel estimation and $\underline{\mathbf{R}}_m$ or $\underline{\mathbf{R}}_n$ in channel estimation and data detection, respectively

- Based on the estimated channel IR vector $\hat{\underline{\mathbf{h}}}_{s,MMSE2}(i)$ estimated in accordance with (7.31) the estimate

$$\hat{\underline{\mathbf{R}}}_{\tau,s}(i) = \hat{\underline{\mathbf{h}}}_{s,MMSE2}(i) \cdot \hat{\underline{\mathbf{h}}}^{*T}_{s,MMSE2}(i) \tag{7.32}$$

can be determined in iteration i. The estimate $\hat{\underline{\mathbf{R}}}_{\tau,s}(i)$ of (7.32) can then be considered again in the next step in channel estimation according to (7.31).

In general a channel estimation is undertaken in each burst and only one iteration $i = 1$ is taken into account for estimating $\underline{\mathbf{R}}_{\tau,s}$. For reasons of clarity the matrix estimated after the first iteration $\hat{\underline{\mathbf{R}}}_{\tau,s}(1)$ will be designated $\hat{\underline{\mathbf{R}}}_{\tau,s}$ in the following. Where the K users are moving slowly the changing of the DOAs of the user signals and thereby the changing of the spatial correlations of the channel IRs are only marginal. In this case channel IRs $\hat{\underline{\mathbf{h}}}_{\mathrm{s}}$ that were estimated in previous bursts can also be included in the determining of the estimate $\hat{\underline{\mathbf{R}}}_{\tau,\mathrm{s}}$, provided the composition of the user groups in the individual time slots does not change. As was already explained in Section 7.2.1 it is to be expected that estimation result $\hat{\underline{\mathbf{R}}}_{\tau,\mathrm{s}}$ will improve as the number of vectors $\hat{\underline{\mathbf{h}}}_{\mathrm{s}}$ from previous bursts used to determine matrix $\hat{\underline{\mathbf{R}}}_{\tau,\mathrm{s}}$ increases if users are not moving or moving only marginally. The options described in detail in Section 7.2.1 for improving the estimation quality of $\underline{\mathbf{R}}_{\mathrm{n}}$ of (3.25), such as for example averaging over several matrices $\hat{\underline{\mathbf{R}}}_{\mathrm{n}}$ determined in different bursts, can be applied in the same way to estimated matrix $\hat{\underline{\mathbf{R}}}_{\tau,\mathrm{s}}$.

8 Performance analysis of adaptive array processing for the TD-CDMA uplink

8.1 General

In this chapter, the performance of the receiver concepts presented in Chapter 7 is demonstrated by simulations in the uplink of a TD-CDMA mobile radio system. These receiver concepts utilize the data detection schemes shown in Chapter 5 and the channel estimation concepts of Chapter 6. In the simulations the channel models and intercell MAI models introduced in the Chapters 2 and 3 are considered. To measure and evaluate the performance of the different receiver concepts the achievable coded BER P_{b} under consideration of FEC coding and the uncoded BER P_{bu} without consideration of FEC coding, respectively, is determined. The coded BER P_{b} and uncoded BER P_{bu}, respectively, is one of the most important performance measures for digital receiver concepts [Pro89]. The average SIR, which is the relationship between the average power of a desired information carrying signal and the average total interference power σ^2, see Section 3.2, with respect to a single receiver antenna, is denoted by C/I. The average coded and uncoded BER P_{b} and P_{bu}, respectively, versus the average C/I is determined by a simulation model of data transmission, which includes the statistical and dynamic properties of the communications system to be investigated [Pap00]. When stochastic quantities are used in the simulation model, then the simulation model is termed Monte Carlo [BSS84, Edr94, Naß95, Bla98, Pap00]. The results produced by Monte Carlo simulations depend generally on the number of experiments conducted. As the number of experiments increase, the precision of the results increases [BSS84, JBS92]. There is certainly always a trade-off between simulation precision and simulation time. Relying on the analysis of [Naß95], if $10^{-\mu}$ denotes the coded BER P_{b} to be estimated by simulations, at least the transmission of $10^{\mu+3}$ bits must be simulated producing an estimate P_{b} which is, with a probability greater than 95%, within the confidence interval $[0.9{\cdot}10^{-\mu},\ 1.1\cdot10^{-\mu}]$ and therefore can be considered as reliable.

The simulation tool used is mainly based on the simulation program ADAMO (Antenna Diversity And MOre), which is described in detail in [Bla98]. In the simulations the antenna configurations described in Section 4.2 are utilized at the receivers with different numbers K_{a} of antenna elements. The simulations consider the cases of up to K equal to 8 users in the case of data detection by applying the ZF-BLE and up to K equal to 16 users in the case of data detection by applying MSJD.

8.2 Simulation concept

To determine the average coded and uncoded BER P_b and P_bu using Monte-Carlo simulation, data transmission within a reference cell embedded into a cell network is considered. Determination of the average BER P_b and P_bu is based on a large number of repeatedly conducted experiments. Each experiment comprises three stages:

1. In a first stage the channel model presented in Chapter 2 for modelling the propagation conditions is selected. For each of the K users in the reference cell considered, a directional channel IR $\underline{\mathbf{h}}_\mathrm{d}^{(k,k_\mathrm{d})}$, $k = 1...K$, $k_\mathrm{d} = 1...K_\mathrm{d}$, of (2.2) in accordance with the channel model selected, is generated. From the directional channel IRs $\underline{\mathbf{h}}_\mathrm{d}^{(k,k_\mathrm{d})}$, $k = 1...K$, $k_\mathrm{d} = 1...K_\mathrm{d}$, of (2.2), taking account of directions $\beta^{(k,k_\mathrm{d})}$, $k = 1...K$, $k_\mathrm{d} = 1...K_\mathrm{d}$, of the K users and of the antenna geometry, the K_a channel IRs $\underline{\mathbf{h}}_\mathrm{s}^{(k,k_\mathrm{a})}$, $k = 1...K$, $k_\mathrm{a} = 1...K_\mathrm{a}$, of (2.1) of the transmission channels between specific user k and the antenna element k_a at the BS of the reference cell are determined. The channel IRs $\underline{\mathbf{h}}_\mathrm{s}^{(k,k_\mathrm{a})}$, $k_\mathrm{a} = 1...K_\mathrm{a}$, of (2.1) of user k at the K_a antenna elements are not statistically independent of each other, but include the statistical linkages applicable for the underlying antenna configuration as a result of user-specific DOA, i.e. they are correlated in general. The K users are located either equidistant or random in the range $[0...2\pi[$ on a circle around the BS of the reference cell. One can thus assume that all K user signals are received at the RP with the same average power.

2. In a second stage the intercell MAI is generated in accordance with an interference model described in Section 3.3 and the intercell MAI covariance matrix $\underline{\mathbf{R}}_\mathrm{n}$ of (3.25) is determined. $\underline{\mathbf{R}}_\mathrm{n}$ is taken as known in the receiver for the investigations in Section 8.5.1 in order to determine the minimum average BER P_b or P_bu to be expected for a prespecified C/I for the receiver structure considered. The subsequent sections 8.5.2 to 8.7.3 additionally consider the estimated matrix $\hat{\underline{\mathbf{R}}}_\mathrm{s}$ of (7.13) in each case, regardless of whether the intercell MAI is directionally correlated or not. In the case of directionally correlated MAI this approach will not be optimum. It is obvious that a performance degradation is to be expected when not estimating the whole matrix $\underline{\mathbf{R}}_\mathrm{n}$. The corresponding simulation results can be found in Section 8.5.5. If the intercell MAI scenario 2 described in Section 3.3 is used, only $K_\mathrm{i} = 1$ single directional interferer is active, which causes 80% of the total interference power. The remaining 20% of the interference power is distributed directionally homogeneously in the azimuth.

3. In a third stage the transmission of the data symbols is simulated for a short period. The CDMA codes defined in [ETSI97] are used as user-specific CDMA codes $\underline{\mathbf{c}}^{(k)}$, $k = 1...K$, of (5.2). The user-specific BERs occurring during the short period required for the above-mentioned transmission of the data symbols are implementations of random variables P_b or P_bu.

As a result of an experiment the values of the current BER P_b or P_{bu} and of the current C/I are stored. After frequent repetition of the experiments the average BERs P_b and P_{bu} and the average C/I can be determined.

8.3 Simulation parameters

The parameters of the TD-CDMA system considered in this thesis are shown in Table 8.1. The parameters in Table 8.1 differ from those considered by 3GPP [3GPP] for TD-CDMA. The parameters correspond to the parameters defined by ESTI in 1997 [ETSI97]. To enable the comparability of the simulation results obtained in the period between 1997 and 2001 to be guaranteed, the TD-CDMA parameters defined by ESTI in 1997 are retained, i.e. the parameters were not permanently updated as part of standardization activities.

carrier frequency	f_c	1815 MHz
user bandwidth	B	1.6 MHz
number of users	K	8 / 16
burst duration	T_{bu}	577 μs
data symbols per data block	N	28
symbol duration	T_s	7.376 μs
chips per symbol	Q	16
chip duration	T_c	0.461 μs
midamble chips	L	296
modulation scheme		4PSK
chip impulse filter [ETSI97]		GMSK
convolutional encoder (FEC) 23,35 NSC-Code [ViO79] constraint length rate	 K_c R_c	 5 1/2
interleaving depth	I_d	4 bursts

Table 8.1. Parameters used in the simulations

8.4 BER performance dependent on different channel models and interference scenarios

8.4.1 Channel models

In this Chapter 8 simulation results which take account of the channel models presented in Chapter 2 are obtained. The selection of a channel model affects the BER performance of the receiver, i.e. the BER P_{b} determined for a given C/I depends decisively on the selected channel model. All results aimed at comparing the performance of different receiver structures, as described in Chapter 7, are obtained on the basis of the same channel model. This means that the comparability of results is always guaranteed. To get an impression of the influence of the choice of channel model, Fig. 8.1 shows a typical example of coded BER P_{b} of a TD-CDMA receiver with the parameters specified in Table 8.1 taking account of the following channel models with the parameters specified in each:

I : Channel model based on measurements, see Section 2.3,

- single direction channel, i.e. $K_{\mathrm{d}} = 1$,
- DOAs $\beta^{(k,1)}$, $k = 1...K$, are randomly changing in the range $[0...2\pi[$ every 4th bursts.

II : ITU IO B single direction channels, see Section 2.4,

- DOAs $\beta^{(k,1)}$, $k = 1...K$, are randomly changing in the range $[0...2\pi[$ every 4th bursts.

III : ITU IO B, multipath propagation, i.e. $K_{\mathrm{d}} = 4$, see Section 2.4,

- DOAs $\beta^{(k,k_{\mathrm{d}})}$, $k = 1...K$, $k_{\mathrm{d}} = 1...K_{\mathrm{d}}$, are randomly changing in the range $[0...2\pi[$ every 4th bursts.

IV : Indoor channel model, see Section 2.5,

- K users and K interferers are distributed randomly within the considered cell and the adjacent cell and
- positions of all users and interferers are kept fixed.

For all channel models the speed $v^{(k)}$=0 km/h, $k = 1...K$, is assumed for all K users. Furthermore, it is assumed that the channel IRs at the receiver are perfectly known. Except for the simulations considering channel model IV, the interference scenario underlying the simulations is the intercell MAI scenario 1 shown in Fig. 3.5 a, which is based on uncorrelated interference and azimuthal homogeneously distributed interference power σ^2. The assumed antenna arrangement is configuration URA, see Section 4.2, with $K_{\mathrm{a}} = 4$ antenna elements. In data detection according to (5.12) the covariance matrix $\underline{\mathbf{R}}_{\mathrm{s}}$ of (3.36) is not taken into account and is thus replaced by the identity matrix $\mathbf{I}^{(K_{\mathrm{a}})}$ of dimension $K_{\mathrm{a}} \times K_{\mathrm{a}}$.

The curves in Fig. 8.1 show that the channel model with the largest delay spread which is based on measured channel IRs, leads, as expected, to the worst BER results. Curves

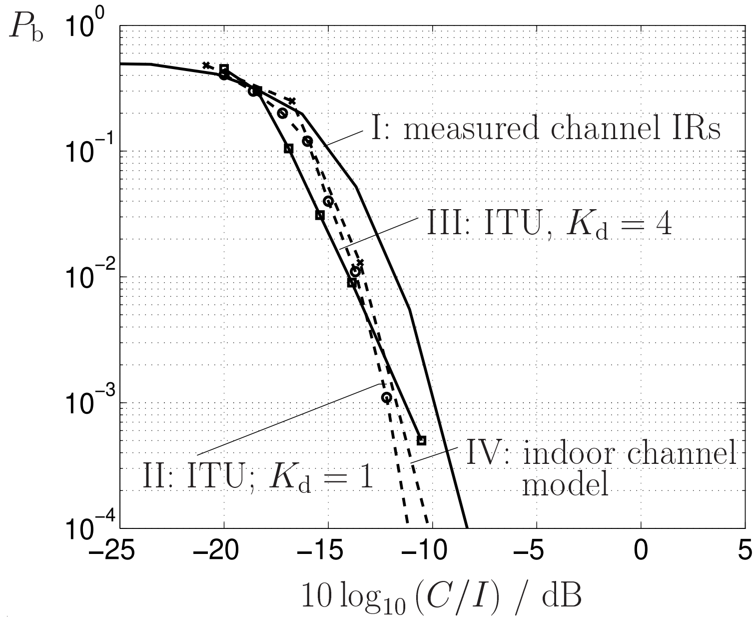

Fig. 8.1. Coded BER P_b performance for different channel models according to cases I-IV; $K_a = 4$; URA

II-IV, which are valid for the indoor channel models, show that the best BER performance is achieved in the case of single direction channels. In the case of single direction channels signal processing of the receiver signals at the K_a antenna elements means that the individual K user signals are best spatially separated from each other before detection. In the case of multipath propagation, the BER curves are flatter and the BER performance is generally worse.

8.4.2 Interference scenarios

Just as the choice of the channel model affects the BER behavior of the receiver, see Section 8.4.1, the choice of interference scenarios also affects the BER performance. Fig. 8.2 is a typical example of the coded BER P_b versus C/I for the following interference scenarios:

I : intercell MAI scenario 1 illustrated in Fig. 3.5 a,

II : intercell MAI scenario according to Fig. 3.8 considering a cluster size $r = 3$ and

III : intercell MAI scenario 2 illustrated in Fig. 3.5 b. The direction $\gamma_i^{(1)}$ of the strong interferer, which causes 80% of the total interference power σ^2, is changing randomly in the range $[0...2\pi[$ every 4^{th} bursts.

The underlying channel model is the model described in Section 2.3 based on measured channel IRs, i.e. the model designated in Section 8.4.1. As already described in the previous section, the antenna configuration URA with $K_\mathrm{a} = 4$ antenna elements is used for the simulations and in data detection in accordance with (5.12) the covariance matrix $\underline{\mathbf{R}}_\mathrm{s}$ of (3.36) is replaced by the identity matrix $\mathbf{I}^{(K_\mathrm{a})}$ of dimension $K_\mathrm{a} \times K_\mathrm{a}$.

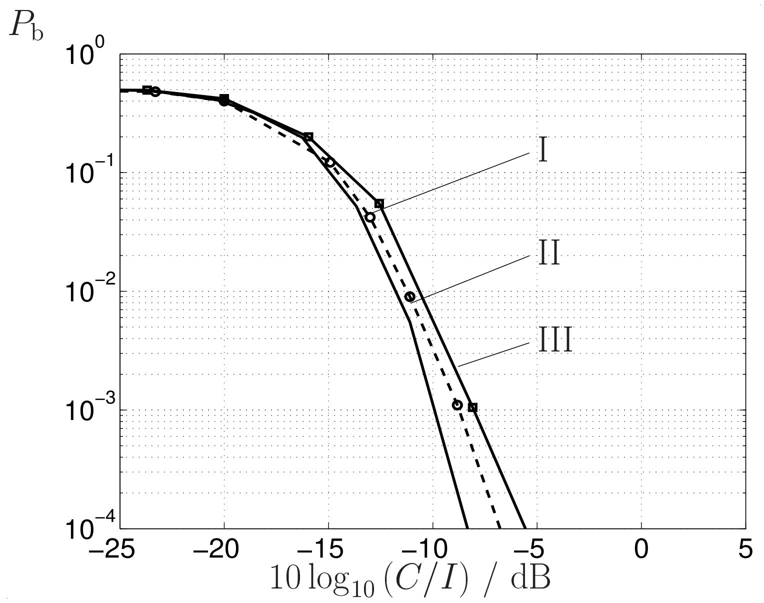

Fig. 8.2. Coded BER P_b performance considering different interference models according to cases I-III; $K_\mathrm{a} = 4$; URA

The curves in Fig. 8.2 show that the spatial correlations of the interference signals, which result from directionally discrete intercell MAI signals at the K_a receive antenna elements, lead to a BER performance degradation.

8.5 Simulation results applying ZF-BLE and considering known channel IRs

8.5.1 Perfect knowledge of the intercell interference covariance matrix $\underline{\mathbf{R}}_\mathrm{n}$

In this section, the performance improvements by using antenna arrays at the uplink receiver and by considering the spatial intercell MAI covariance matrix $\underline{\mathbf{R}}_\mathrm{s}$, see (3.36), in the JD process, see (5.12), are demonstrated. Two square array configurations (URA) with K_a equal to 4 and 16 antenna elements are used, see Fig. 4.1. The K users are assumed to be randomly distributed in the azimuth. The single direction channel model described in Section 2.3 based on measured channel IRs is considered. For each burst, the channel IRs of the K users are chosen randomly from the set of measured channel IRs. The channel IRs are kept fixed during the transmission of one burst. The DOAs $\beta^{(k,1)}$, $k = 1...K$, of the K users and, considering the intercell MAI scenario 2, the DOA $\gamma_{\mathrm{i}}^{(1)}$ of the single interfering signal are changing burst by burst during the simulations. The curves in Figs. 8.3 and 8.4 show the average coded and uncoded BER P_{b} and P_{bu}, respectively, versus the C/I for the below listed conditions concerning the spatial intercell MAI covariance matrix $\underline{\mathbf{R}}_{\mathrm{s}}$ of (3.36):

- Condition I: $\underline{\mathbf{R}}_{\mathrm{s}}$ is assumed to be perfectly known at the BS receiver and considered in the JD process according to (5.12).
- Condition II: $\underline{\mathbf{R}}_{\mathrm{s}}$ is not known at the BS receiver and is substituted by the identity matrix $\mathbf{I}^{(K_{\mathrm{a}})}$ in the JD process according to (5.12).

From Fig. 8.3 and 8.4 the benefits of considering the intercell MAI covariance matrix in the JD process become obvious. Taking into account the matrix $\underline{\mathbf{R}}_{\mathrm{s}}$ of (3.36), and – since $\tilde{\underline{\mathbf{R}}}_{\mathrm{t}}$ of (3.19) is *a priori* known – the total intercell MAI covariance matrix $\underline{\mathbf{R}}_{\mathrm{n}}$ of (3.25) offers a gain which varies between 1 dB and 5.5 dB at a coded BER $P_{\mathrm{b}} = 10^{-3}$, see Figs. 8.3 and 8.4, compared to the receiver which does not use this information. This variation of the achieved gain depends on the number K_{a} of antenna elements and on the considered interference scenario. Fig. 8.3 shows the BER curves with and without consideration of $\underline{\mathbf{R}}_{\mathrm{s}}$, assuming intercell MAI scenario 1. The performance improvement achieved by taking $\underline{\mathbf{R}}_{\mathrm{s}}$ into consideration increases as the number K_{a} of antenna elements increases, see Fig. 8.3. By assuming intercell MAI scenario 2, where most of the interference power impinges at the BS from a single discrete DOA $\gamma_{\mathrm{i}}^{(1)}$, the difference in BER performance with and without considering $\underline{\mathbf{R}}_{\mathrm{s}}$, see Fig. 8.4, compared to the intercell MAI scenario 1, see Fig. 8.3, obviously increases and it becomes more important to consider the matrix $\underline{\mathbf{R}}_{\mathrm{s}}$ in data detection.

In each of the results presented, consideration of the intercell MAI covariance matrix $\underline{\mathbf{R}}_{\mathrm{n}}$ in the JD process leads to an improved performance of TD-CDMA mobile radio systems with adaptive antennas.

Another important result, which can be seen from Figs. 8.3 and 8.4 is as follows: Depending on the chosen intercell MAI scenario, the ZF-BLE exhibits worse performance in the case of directional intercell MAI than it does in the case of omnidirectional MAI. The spatial correlations of the intercell MAI have an impact on the performance of the detector which can be mitigated by considering the intercell MAI covariance matrix $\underline{\mathbf{R}}_{\mathrm{s}}$ of (3.36) in data detection according to (5.12).

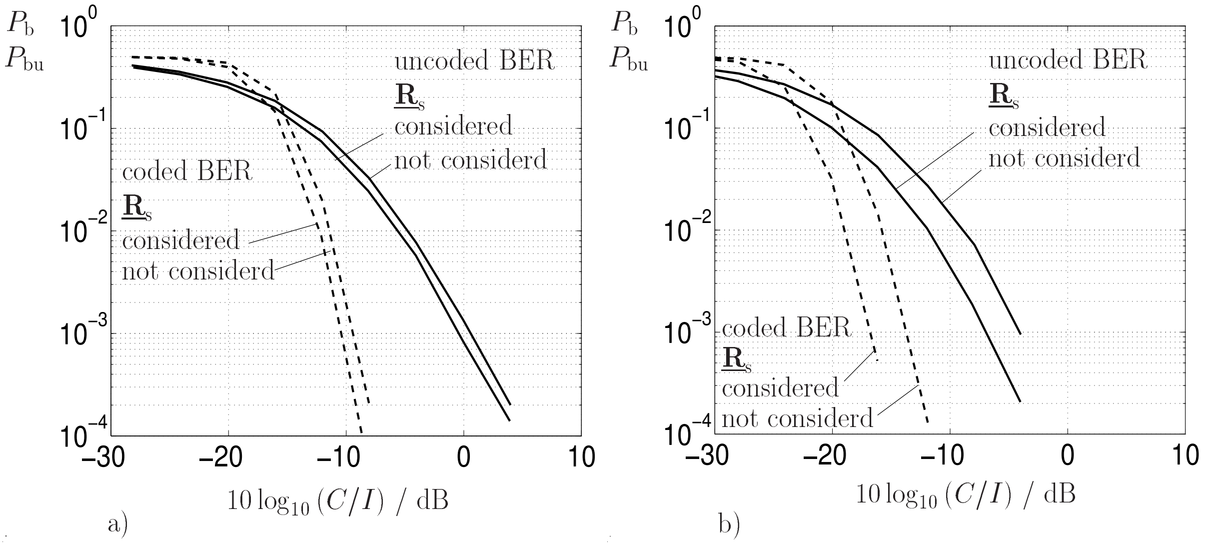

Fig. 8.3. Coded and uncoded BER P_b and P_{bu} versus C/I, when considering and not considering the intercell MAI covariance matrix $\underline{\mathbf{R}}_s$ in the JD process; intercell MAI scenario 1; URA with
a) $K_a = 4$ antenna elements and
b)$K_a = 16$ antenna elements [WP99c]

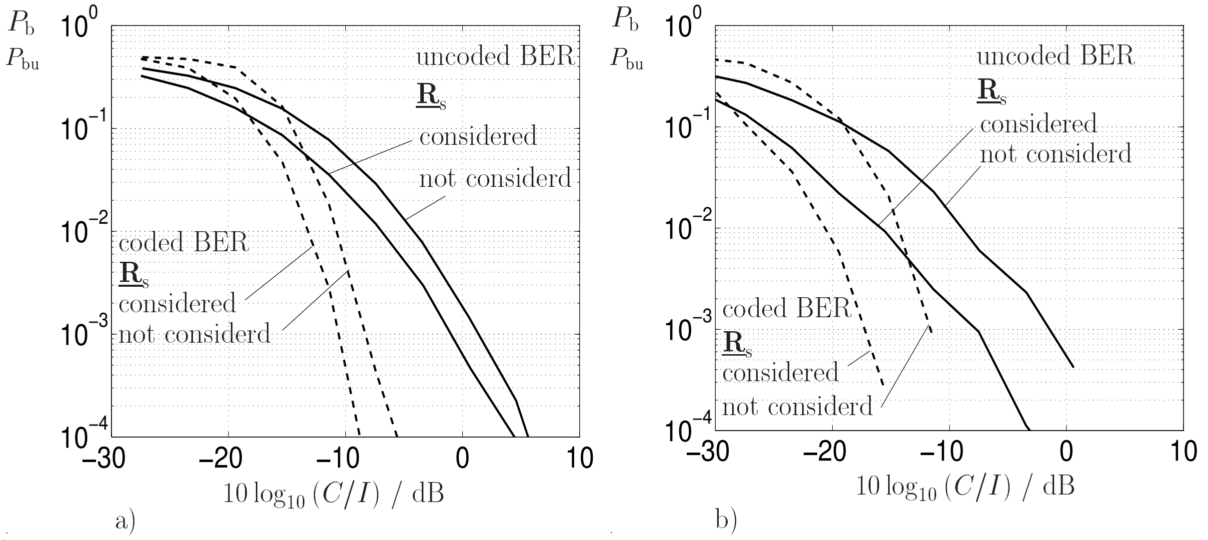

Fig. 8.4. Coded and uncoded BER P_b and P_{bu} versus C/I, when considering and not considering the intercell MAI covariance matrix $\underline{\mathbf{R}}_s$ in the JD process; intercell MAI scenario 2; URA with
a) $K_a = 4$ antenna elements and
b) $K_a = 16$ antenna elements [WP99c]

An example shows that by taking account of the spatial covariance matrix $\underline{\mathbf{R}}_s$ in data detection according to (5.12) strong directional interference can be completely suppressed to the same extent as with beam forming concepts. It is assumed that $K = 1$ user is active and that the DOA $\beta^{(1,1)}$ of the user signal amounts to 30°. The strong interferers have the DOA $\gamma_{\mathrm{i}}^{(1)} = 70°$. With receiver structures which have beam forming capabilities, beam forming can be described for each of the K user signals by K beam forming vectors $\underline{\mathbf{w}}^{(k)}$, $k = 1...K$, with K_{a} complex components [MM80], see also Section 4.3. If based on the channel IRs $\underline{\mathbf{h}}_{\mathrm{s}}^{(k,k_{\mathrm{a}})}$, $k = 1...K$, $k_{\mathrm{a}} = 1...K_{\mathrm{a}}$ of (2.1) a spatial correlation matrix $\underline{\mathbf{R}}_{\mathrm{s}}^{(k)}$, $k = 1...K$, according to (7.29) but valid for perfectly known channel IRs, is determined, the K beam forming vectors $\underline{\mathbf{w}}^{(k)}$, $k = 1...K$, are given by maximizing ratio

$$r\left(\underline{\mathbf{w}}^{(k)}\right) = \frac{\underline{\mathbf{w}}^{(k)*\mathrm{T}} \cdot \underline{\mathbf{R}}_{\mathrm{s}}^{(k)} \cdot \underline{\mathbf{w}}^{(k)}}{\underline{\mathbf{w}}^{(k)*\mathrm{T}} \cdot \underline{\mathbf{R}}_{\mathrm{s}} \cdot \underline{\mathbf{w}}^{(k)}} \tag{8.1}$$

[MM80]. Fig. 8.5 shows the beam forming diagrams for the scenario described above if antenna configuration URA with K_{a} equal to 4 antennas is used. The solid line shows the beam forming diagram when $\underline{\mathbf{R}}_{\mathrm{s}}$ in the receiver is assumed to be perfectly known. The

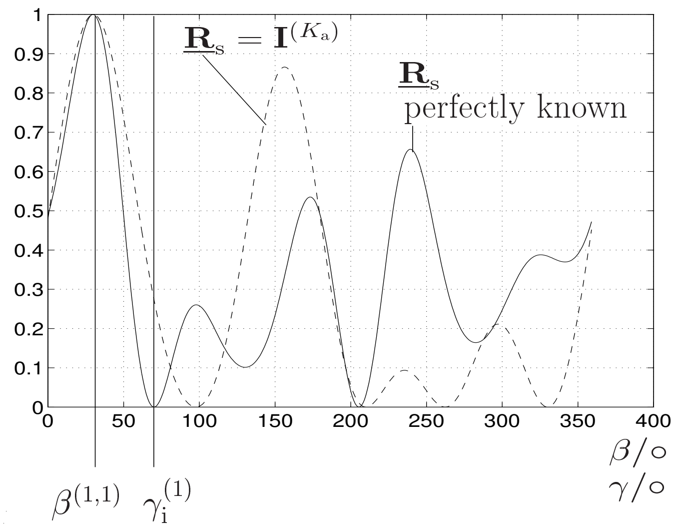

Fig. 8.5. Beam forming diagrams taking account and not taking account of $\underline{\mathbf{R}}_{\mathrm{s}}$; $K = 1$; $\beta^{(1,1)} = 30°$; $K_{\mathrm{i}} = 1$; $\gamma_{\mathrm{i}}^{(1)} = 70°$; antenna configuration URA; $K_{\mathrm{a}} = 4$; 99% purely directional intercell MAI

dashed beam forming diagram is produced if no information about matrix $\underline{\mathbf{R}}_{\mathrm{s}}$ is taken into consideration and $\underline{\mathbf{R}}_{\mathrm{s}}$ in (8.1) is replaced by the $K_{\mathrm{a}} \times K_{\mathrm{a}}$ identity matrix $\mathbf{I}^{(K_{\mathrm{a}})}$. With regard to comparison with spatial and temporal signal processing in accordance with (5.12), for which the inverse of matrix $\underline{\mathbf{R}}_{\mathrm{s}}$ is required, it is assumed that, instead of purely directional interference, 99% of the interference power impinges at the BS at an angle $\gamma_{\mathrm{i}}^{(1)} = 70°$ and 1% of the impinging interference power is homogeneously distributed in the azimuth, see Section 3.3.1. This ensures that matrix $\underline{\mathbf{R}}_{\mathrm{s}}$ will not be singular. Fig. 8.5 shows that the chosen arrangement of user signal DOA $\beta^{(1,1)}$ and DOA $\gamma_{\mathrm{i}}^{(1)}$ of the intercell MAI signal already suppresses 73% of the purely directional interference power without taking into account matrix $\underline{\mathbf{R}}_{\mathrm{s}}$, only 27% of the 99% of the total interference power arrives at the receiver. In comparison to omnidirectional receiving the C/I is increased by 5.57 dB in this case. This case, like the case below, ignores the fact that directionally homogeneous intercell MAI will be suppressed by the beam forming. In addition, by now taking account of matrix $\underline{\mathbf{R}}_{\mathrm{s}}$ in (8.1) the purely directional intercell MAI and thereby a total of 99% of the interference power can be suppressed. If one now assumes as an approximation that 99% of the entire interference power will be suppressed, this corresponds, when compared to omnidirectional receiving, to an increase in the C/I of 20 dB. If one compares the two cases, taking account of matrix $\underline{\mathbf{R}}_{\mathrm{s}}$ in (8.1), an increase in the C/I of 14.43 dB is to be expected compared to the case which does not take account of matrix $\underline{\mathbf{R}}_{\mathrm{s}}$ in (8.1), if the suppression of any directionally homogeneous intercell MAI component partly generated by the beam forming is ignored. The curves in Fig. 8.6 show the average uncoded BER P_{bu} which is produced with simulation of the behavior demonstrated in Section 7.2.1 with and without taking account of matrix $\underline{\mathbf{R}}_{\mathrm{s}}$ in data detection as a function of C/I, when the scenario described above and the same antenna configuration are taken into account. The

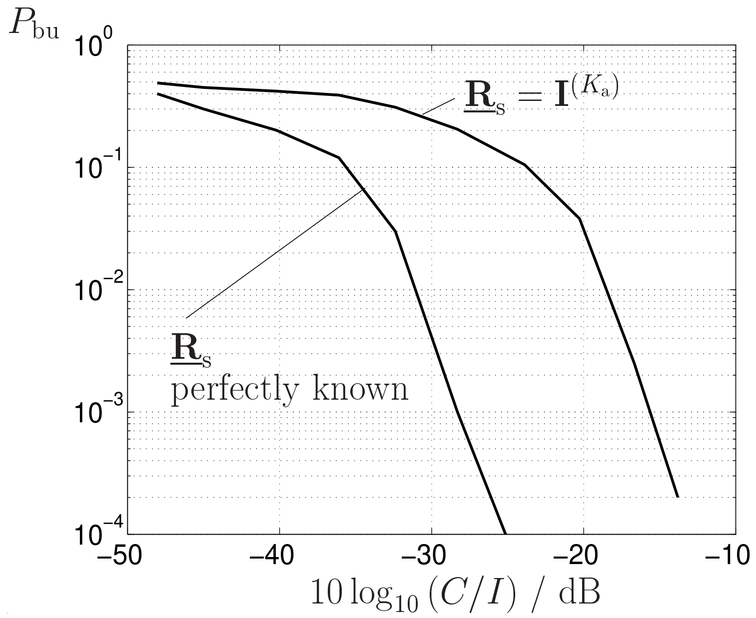

Fig. 8.6. Uncoded BER P_{bu} with and without taking account of matrix $\underline{\mathbf{R}}_{\mathrm{s}}$; $K = 1$; $\beta^{(1,1)} = 30°$; $K_{\mathrm{i}} = 1$; $\gamma_{\mathrm{i}}^{(1)} = 70°$; URA with $K_{\mathrm{a}} = 4$; 99% purely directional intercell MAI

same uncoded BER P_{bu} can be achieved by taking account of matrix $\underline{\mathbf{R}}_{\mathrm{s}}$ at a C/I which is 13 dB less than it would be without taking account of matrix $\underline{\mathbf{R}}_{\mathrm{s}}$. The deviation of the simulated result of 13 dB from the calculated 14.43 dB is attributable on the one hand to the factors ignored in the calculation as well as to possible simulation inaccuracies. The result tends to confirm however the suppression of the purely directional interference when matrix $\underline{\mathbf{R}}_{\mathrm{s}}$ is taken into consideration in (5.12).

8.5.2 Signal reconstruction quality

Section 8.5.1 showed that with perfect knowledge of matrix $\underline{\mathbf{R}}_{\mathrm{n}}$ of (3.25) or in the case of uncorrelated intercell MAI, with perfect knowledge of matrix $\underline{\mathbf{R}}_{\mathrm{s}}$ of (3.36) in data detection in accordance with (5.12) the uncoded and coded BER P_{bu} or P_{b} at a given C/I can be significantly reduced. This reduction is very much dependent on the selected intercell MAI scenario. Since matrix $\underline{\mathbf{R}}_{\mathrm{s}}$ is not generally known in the receiver, procedures for estimating the matrix $\underline{\mathbf{R}}_{\mathrm{s}}$ have already been described in Chapter 7. The estimation procedure described in Section 7.2.1 is based on the reconstruction of receive signal $\underline{\mathbf{e}}$ of (5.10) on the basis of the detected data vectors $\hat{\underline{\mathbf{d}}}$ of (5.12) or (7.4). Theoretical considerations about the quality of signal reconstruction, in particular considering or not considering the FEC coding, are also discussed in Section 7.2.2. In the following the goal of the investigations is to determine whether it is possible to dispense with FEC coding in signal reconstruction. Fig. 8.7 shows an extract of the receiver structure presented in Fig. 7.2, with the dashed line showing the possibility of reconstructing the signal without taking account of FEC coding. If for example with single isolated errors the uncoded BER $P_{\mathrm{bu,r}}$, see Fig. 8.7, is reduced by a factor of less than 3.5 by the FEC decoding in the receiver, see (7.18), and the coded BER P_{b} at the output of the receiver for signal reconstruction by FEC coding becomes a 3.5 times larger uncoded BER $P_{\mathrm{bu,r}}$, see (7.18), the considerations of the FEC encoding have a detrimental effect on the quality of the signal reconstruction. It would also be possible for the reduction of bit errors by FEC decoding to be increased again by FEC encoding. The effort that FEC decoding and coding require for signal reconstruction could then be saved.

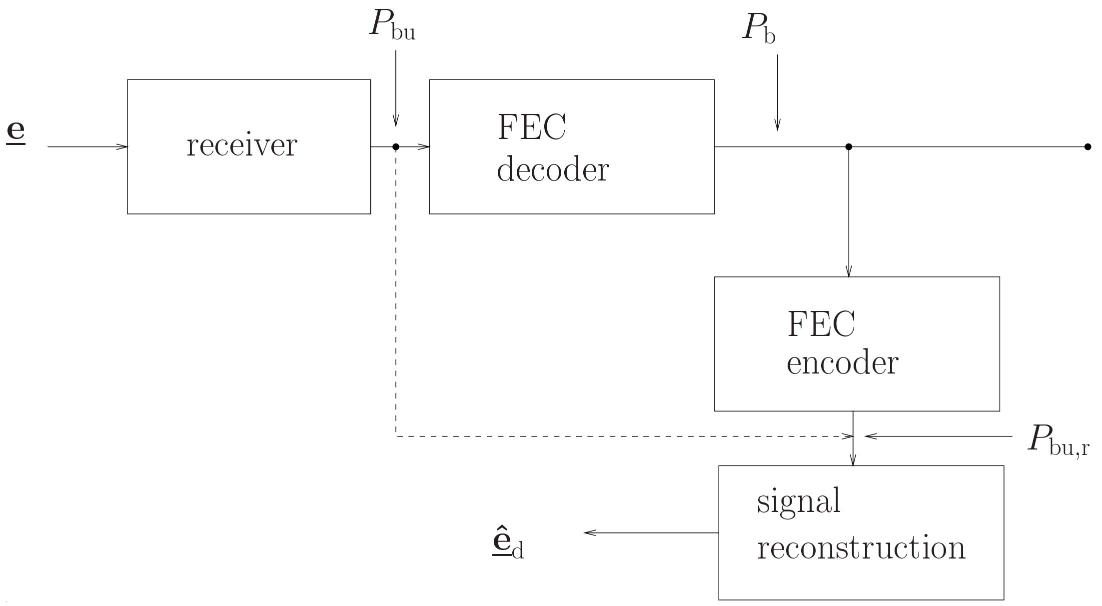

Fig. 8.7. Signal reconstruction without and with FEC coding

To determine the reconstruction error $\epsilon_{\mathrm{e}}^{(1)}$ while taking account of FEC coding and to determine the reconstruction error $\epsilon_{\mathrm{eu}}^{(1)}$ without considering FEC coding for signal reconstruction, simulations are conducted, starting from a receiver with $K_{\mathrm{a}} = 1$ antenna element and $K = 8$ users that are active simultaneously. For the signal of the first user $k = 1$ in each case, the curves in Fig. 8.8 show the uncoded BER $P_{\mathrm{bu}}^{(1)}$, the coded BER $P_{\mathrm{b}}^{(1)}$ and the reconstruction errors $\epsilon_{\mathrm{e}}^{(1)}$ and $\epsilon_{\mathrm{eu}}^{(1)}$ with and without considering FEC coding, as a function of the average C/I. If FEC coding is considered for signal reconstruction,

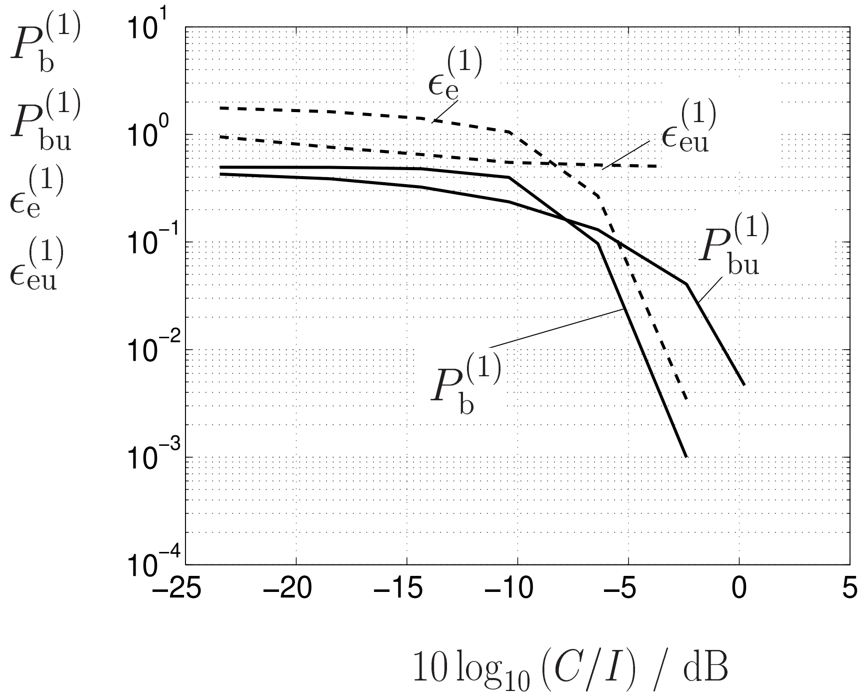

Fig. 8.8. Uncoded BER $P_{\mathrm{bu}}^{(1)}$ and coded BER $P_{\mathrm{b}}^{(1)}$; reconstruction error $\epsilon_{\mathrm{e}}^{(1)}$ with and reconstruction error $\epsilon_{\mathrm{eu}}^{(1)}$ without account taken of FEC coding versus average C/I; $K = 8$, $K_{\mathrm{a}} = 1$

reconstruction error $\epsilon_{\mathrm{e}}^{(1)}$ reduces significantly on reduction of the coded BER $P_{\mathrm{b}}^{(1)}$. For coded BER $P_{\mathrm{b}}^{(1)}$ below 0.2 it can be expected that individual errors will occur since then, with an appropriate interleaving scheme, there is the opportunity of only single isolated bit errors occurring at any one point in the shift register of the coder. According to the theoretical considerations, see (7.19), a factor 14 between coded BER $P_{\mathrm{b}}^{(1)}$ and reconstruction error $\epsilon_{\mathrm{e}}^{(1)}$ is to be expected. The curves in Fig. 8.8 however only show a factor of 3.5 between the coded BER $P_{\mathrm{b}}^{(1)}$ and the reconstruction error $\epsilon_{\mathrm{e}}^{(1)}$. Such a factor is obtained, as the curves in Fig. 7.7 show, if bundle errors occur. This means that despite of interleaving there are still bundle errors in the detected data.

Furthermore, the curves in Fig. 8.8 show that the reconstruction error $\epsilon_{\mathrm{eu}}^{(1)}$ for a small C/I is less than the reconstruction error $\epsilon_{\mathrm{e}}^{(1)}$, since $\epsilon_{\mathrm{eu}}^{(1)}$ is oriented to the lower uncoded BER

$P_{\mathrm{bu}}^{(1)}$ for small C/I values compared to $P_{\mathrm{b}}^{(1)}$. If the C/I value is increased, so improvement thus obtained in the reconstruction error $\epsilon_{\mathrm{eu}}^{(1)}$ is marginal although the uncoded BER $P_{\mathrm{bu}}^{(1)}$ reduces markedly. For the C/I values under consideration the reconstruction error $\epsilon_{\mathrm{eu}}^{(1)}$ is not less than 0.5. This leads one to assume that for signal reconstruction it is not possible to dispense with FEC coding to reduce the effort involved. In Section 8.5.3 simulation results show the effects of bad signal reconstruction on BER P_{b} and P_{bu} if FEC coding is dispensed with, if, based on the badly reconstructed signal, the covariance matrix $\underline{\mathbf{R}}_{\mathrm{n}}$ is estimated and is used in data detection in accordance with (5.12).

As well as signal reconstruction error $\epsilon_{\mathrm{e}}^{(1)}$, the errors of estimated intercell MAI $\hat{\underline{\mathbf{n}}}(1)$ according to (7.6) compared to actual intercell MAI $\underline{\mathbf{n}}$ of (3.24)

$$\sigma_{\mathrm{n}}^2 = \frac{\mathrm{E}\{|\underline{\mathbf{n}} - \hat{\underline{\mathbf{n}}}(1)|^2\}}{\mathrm{E}\{|\underline{\mathbf{n}}|^2\}} \tag{8.2}$$

and

$$\sigma_{\mathrm{A}}^2 = \frac{\mathrm{E}\{|\underline{\mathbf{n}} - \hat{\underline{\mathbf{n}}}(1)|^2\}}{\mathrm{E}\{|\underline{\mathbf{A}} \cdot \underline{\mathbf{d}}|^2\}} \tag{8.3}$$

are considered below. In (8.2) the deviation $\mathrm{E}\{|\underline{\mathbf{n}} - \hat{\underline{\mathbf{n}}}(1)|^2\}$ is related to the noise power $\mathrm{E}\{|\underline{\mathbf{n}}|^2\}$ and in (8.3) to the user signal power $\mathrm{E}\{|\underline{\mathbf{A}} \cdot \underline{\mathbf{d}}|^2\}$. The difference lies in the fact that when σ_{A}^2 is determined according to (8.3) for different C/I values, the denominator $\mathrm{E}\{|\underline{\mathbf{A}} \cdot \underline{\mathbf{d}}|^2\}$ is always the same since the different C/I values are set by varying the interference power. For σ_{n}^2 according to (8.2) denominator $\mathrm{E}\{|\underline{\mathbf{n}}|^2\}$ thus changes when the C/I is changed. To determine σ_{n}^2 and σ_{A}^2 it is further assumed below that the receiver has just one single antenna element, i.e. $K_{\mathrm{a}} = 1$. Let $K = 8$ users simultaneously active and arranged at random on a circle around the BS. The K users move at a speed $v^{(k)} = 3$ km/h, $k = 1...K$. For the simulation the ITU IO B channel model with single directions is used, see Section 2.4. For signal reconstruction FEC coding is taken into account. The curves in Fig. 8.9 show σ_{n}^2 according to (8.2) and σ_{A}^2 according to (8.3) for the estimated intercell MAI vector $\hat{\underline{\mathbf{n}}}(1)$ of (7.6) as a function of C/I. σ_{A}^2 of (8.3) becomes smaller when the C/I is increased, see Fig. 8.9. As the C/I becomes greater, the coded BER P_{b} becomes smaller. Since the channel IRs in the receiver are perfectly known, only coded BER P_{b} effects reconstruction error $\epsilon_{\mathrm{e}}^{(1)}$. The user signals of the $K = 8$ users can thus be well reconstructed with a large C/I and the quality of the estimate $\hat{\underline{\mathbf{n}}}(1)$ of (7.6) is correspondingly good. If the C/I is reduced, the coded BER P_{b} increases. The number of deviations of the individual components of the actual intercell MAI vector $\underline{\mathbf{n}}$ of (3.24) from the components of the estimate $\hat{\underline{\mathbf{n}}}(1)$ of (7.6) become larger and so does σ_{A}^2. σ_{A}^2 defined in accordance with (8.3) suggests however that the estimation of the intercell MAI for reduction of the C/I is less accurate. If the deviation $\mathrm{E}\{|\underline{\mathbf{n}} - \hat{\underline{\mathbf{n}}}(1)|^2\}$ in accordance with (8.2) is related to the intercell MAI power $\mathrm{E}\{|\underline{\mathbf{n}}|^2\}$, the estimated error thus defined becomes smaller with decreasing C/I. Although the coded BER P_{b} and thereby the number of different components in the vectors $\underline{\mathbf{n}}$ and $\hat{\underline{\mathbf{n}}}(1)$ increases as

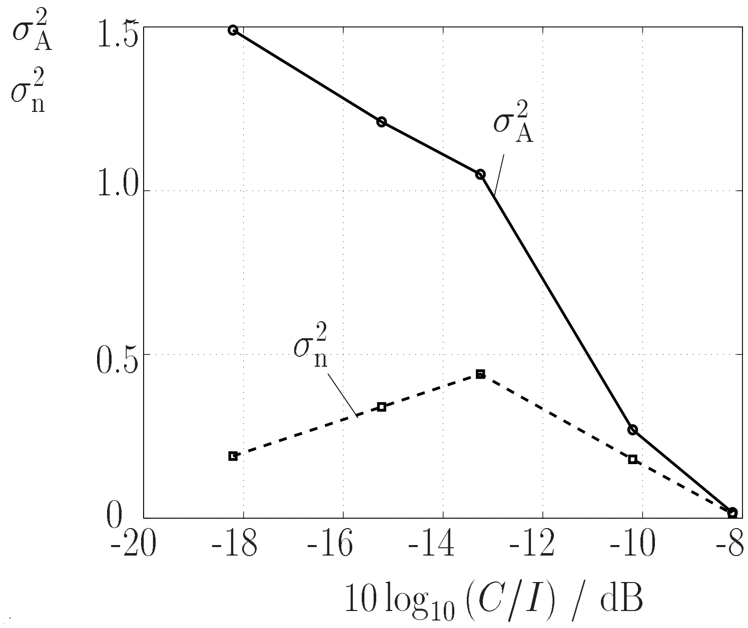

Fig. 8.9. σ_n^2 of (8.2) and σ_A^2 of (8.3) versus C/I; $K = 8$; $K_\mathrm{a} = 1$; ITU IO B; $K_\mathrm{d} = 1$; $v^{(k)} = 3$ km/h, $k = 1...K$

the C/I becomes smaller, each individual error is in the order of magnitude of the user signal power $\mathrm{E}\{|\underline{\mathbf{A}}\cdot\underline{\mathbf{d}}|^2\}$, which is comparably small compared to the intercell MAI power $\mathrm{E}\{|\underline{\mathbf{n}}|^2\}$. The σ_n^2 defined in accordance with (8.2) shows this type of behavior in Fig. 8.9. With a small C/I almost interference alone is received so that a good estimate of the interference can be made. With a very large C/I the number of different components in the vectors $\underline{\mathbf{n}}$ and $\underline{\hat{\mathbf{n}}}(1)$ is very small as a result of the low coded BER P_b so that σ_n^2 and also σ_A^2 is very small. The maximum value of σ_n^2 in Fig. 8.9 identifies the transition between the two effects described for large and small C/I values.

8.5.3 Consideration of the estimated intercell interference covariance matrix $\underline{\mathbf{R}}_\mathrm{n}$

In this section, first the accuracy of the estimation of the spatial covariance matrix $\underline{\mathbf{R}}_\mathrm{s}$, see (3.36), with the receiver structure proposed in Section 7.2.1 is determined. Then, in order to demonstrate the performance improvement by considering the estimated spatial covariance matrix $\underline{\hat{\mathbf{R}}}_\mathrm{s}$ in the JD process, the average coded and uncoded BER P_b and P_bu, respectively, are determined as a function of the average C/I.

The K users are assumed to be randomly distributed along the azimuth. In this section, intercell MAI scenario 2 with the fixed DOA $\gamma_\mathrm{i}^{(1)} = 90°$ is considered, see Section 3.3.1. According to (7.9) the estimate $\underline{\hat{\mathbf{R}}}_\mathrm{s}(1)$ is determined by taking $N_\mathrm{b} = 4$ bursts into account.

To quantify the accuracy of the estimate $\hat{\underline{\mathbf{R}}}_{\mathrm{s}}(1)$ of (7.5) an estimation error of the matrix $\underline{\mathbf{R}}_{\mathrm{s}}$ is defined by

$$\epsilon_{\mathrm{R_s}} = \mathrm{E}\left\{ \frac{1}{{K_{\mathrm{a}}}^2} \sum_{i=1}^{K_{\mathrm{a}}} \sum_{j=1}^{K_{\mathrm{a}}} \left| \underline{R}_{\mathrm{s}i,j} - \hat{\underline{R}}_{\mathrm{s}(1)i,j} \right| \right\}, \tag{8.4}$$

which is the expectation of the sum of all differences of the components of the matrices $\underline{\mathbf{R}}_{\mathrm{s}}$ and $\hat{\underline{\mathbf{R}}}_{\mathrm{s}}(1)$ devided by the number ${K_{\mathrm{a}}}^2$ of elements in the matrix $\underline{\mathbf{R}}_{\mathrm{s}}$. The curves in Fig. 8.10 show the estimation error $\epsilon_{\mathrm{R_s}}$ of the matrix $\underline{\mathbf{R}}_{\mathrm{s}}$ and the coded BER P_{b} without considering $\underline{\mathbf{R}}_{\mathrm{s}}$ in the JD process for a URA configuration with K_{a} equal to 4 antennas. In Fig. 8.10, the comparison of these two different types of curves demonstrates that the impact of a high coded BER P_{b} on the estimation of $\underline{\mathbf{R}}_{\mathrm{s}}$, described in Section 7.2.1, can be neglected. When assuming a high C/I, which causes a low coded BER P_{b}, see Fig. 8.10, the reconstruction $\hat{\underline{\mathbf{e}}}_{\mathrm{d}}(1)$, see (7.5), is equal to the interference-free received signal except for some deviations from the interference-free received signal due to bit errors in the detected signal that forms the basis of the signal reconstruction.

The fact that there only exit a few deviations of the reconstruction $\hat{\underline{\mathbf{e}}}_{\mathrm{d}}(1)$ of (7.5) from the interference-free received signal lead to a good estimation of the total vector $\hat{\underline{\mathbf{n}}}(1)$ from (7.6) and finally to a good estimation of $\underline{\mathbf{R}}_{\mathrm{s}}$. When decreasing the C/I, the number of bit errors increases and the estimation error $\epsilon_{\mathrm{R_s}}$ also slightly increases. By further increasing the intercell MAI power σ^2 the estimation error $\epsilon_{\mathrm{R_s}}$, see (8.4), decreases similar to σ_{n}^2 in Fig. 8.9. In the case of increasing σ^2 the number of bit errors also increases but each bit error causes only an estimation error in the size of the carrier power, which is small compared to the total intercell MAI power σ^2. The curve in Fig. 8.10 that shows the estimation error $\epsilon_{\mathrm{R_s}}$ versus C/I never reaches zero. The estimated spatial covariance matrix $\hat{\underline{\mathbf{R}}}_{\mathrm{s}}$ will never be equal to the real spatial covariance matrix $\underline{\mathbf{R}}_{\mathrm{s}}$ because of the finite number N_{b} of bursts considered in the estimation process described in Section 7.2.1.

To determine the dependence of $\epsilon_{\mathrm{R_s}}$ on the number N_{b}, see (7.9), of considered bursts in the estimation process, besides perfect channel estimation perfect data estimation is also assumed. The received signal can now be reconstructed perfectly interference-free. The curve in Fig. 8.11 shows $\epsilon_{\mathrm{R_s}}$ versus the number N_{b} of bursts considered in the estimation process. With an infinite number N_{b} of bursts the estimated matrix $\hat{\underline{\mathbf{R}}}_{\mathrm{s}}$ will be equal to the true matrix $\underline{\mathbf{R}}_{\mathrm{s}}$. To obtain the results shown in Fig. 8.11, the ULA configuration with $K_{\mathrm{a}} = 8$ antenna elements is used at the receiver. Only $K = 1$ user is active with a fixed DOA of $\beta^{(1,1)} = 135°$ and the strongest interferer has a fixed DOA of $\gamma_{\mathrm{i}}^{(1)} = 75°$.

In the following the performance improvements by considering the estimated matrix $\hat{\underline{\mathbf{R}}}_{\mathrm{s}}(1)$ determined by the estimation process described by (7.9) is shown. The curves in Fig. 8.12 show examples of the average coded BER P_{b} versus C/I for the conditions listed below concerning the spatial covariance matrix $\underline{\mathbf{R}}_{\mathrm{s}}$:

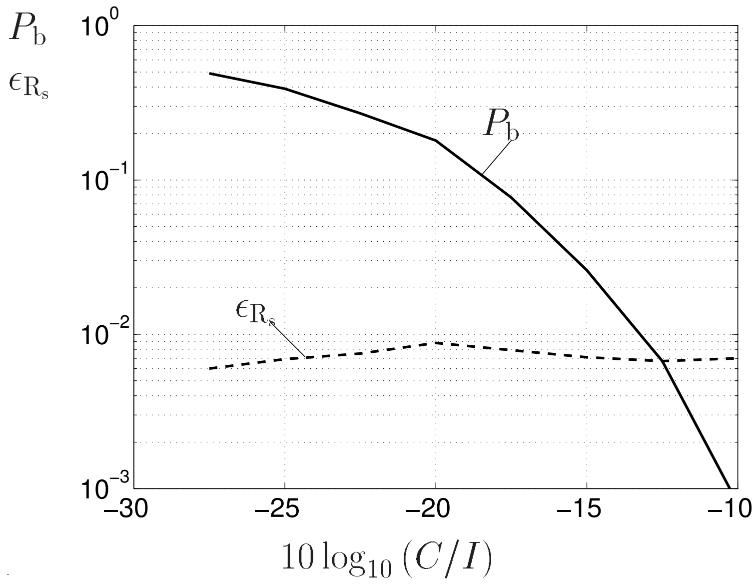

Fig. 8.10. P_b, when considering the intercell MAI covariance matrix $\underline{\mathbf{R}}_\mathrm{s}$ in the JD process, and $\epsilon_{\mathrm{R_s}}$ from (8.4) versus C/I; URA with $K_\mathrm{a} = 4$; $N_\mathrm{b} = 4$; intercell MAI scenario 2 with fixed DOA $\gamma_\mathrm{i}^{(1)} = 90°$ of the strongest interferer [WPH99]

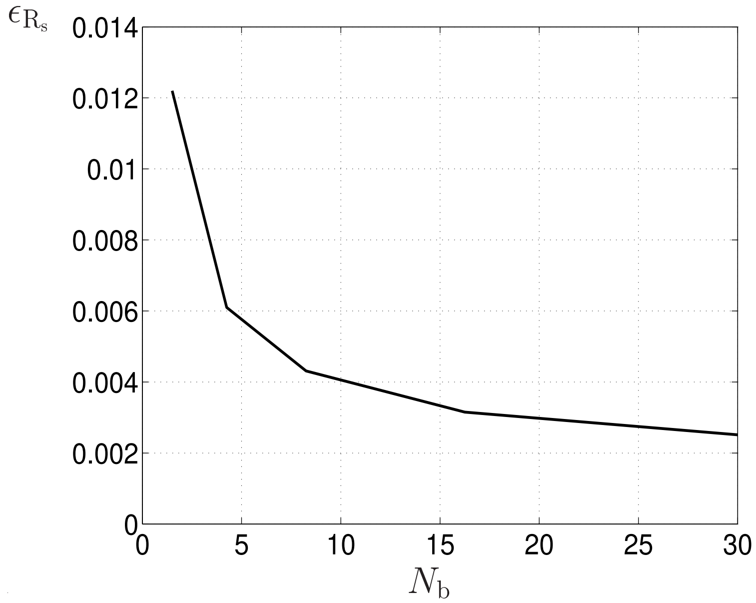

Fig. 8.11. $\epsilon_{\mathrm{R_s}}$ versus N_b; configuration ULA; $K_\mathrm{a} = 8$; $K = 1$; $\beta^{(1,1)} = 135°$; $\gamma_\mathrm{i}^{(1)} = 75°$

I : $\underline{\mathbf{R}}_\mathrm{s}$ is perfectly known at the BS receiver and considered in the JD process according to (5.12)

II : $\underline{\mathbf{R}}_\mathrm{s}$ is unknown at the BS receiver and is replaced by the identity matrix $\mathbf{I}^{(K_\mathrm{a})}$ in the JD process according to (5.12).

III : $\underline{\mathbf{R}}_{\mathrm{s}}$ is estimated according to (7.9) and considered after the first iteration $i = 1$ in the data detection according to (7.8).

IV : $\underline{\mathbf{R}}_{\mathrm{s}}$ is estimated according to (7.10) and is considered without any iteration in the data detection according to (7.11).

For determining the BER curves of Fig. 8.12, for each burst the channel IRs of the K users are chosen randomly from the set of measured channel IRs, see Section 2.3. Also the positions of the K users are randomly changing burst by burst during the simulation. The DOA $\gamma_{\mathrm{i}}^{(1)}$ of the strongest interferer is kept fixed at $\gamma_{\mathrm{i}}^{(1)} = 90°$. From Fig. 8.12 the benefits of considering the intercell MAI covariance matrix in the JD process become obvious. The

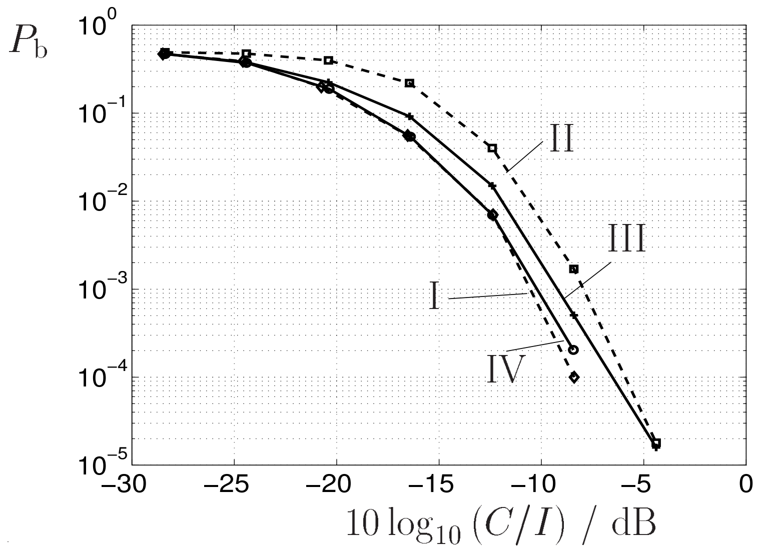

Fig. 8.12. Coded BER P_{b} versus C/I for an URA configuration under consideration of the cases I-IV; $K_{\mathrm{a}} = 4$; $N_{\mathrm{b}} = 4$; intercell MAI scenario 2 with fixed DOA $\gamma_{\mathrm{i}}^{(1)} = 90°$ of the strongest interferer

consideration of the spatial covariance matrix $\underline{\mathbf{R}}_{\mathrm{s}}$, and, since $\underline{\tilde{\mathbf{R}}}_{\mathrm{t}}$ is *a priori* known, of the total intercell MAI covariance matrix $\underline{\mathbf{R}}_{\mathrm{n}}$ offers a C/I gain which varies between 1 dB and 3 dB at a coded BER $P_{\mathrm{b}} = 10^{-3}$, see curves I, III, and IV of Fig. 8.12, compared to the performance of a receiver which does not use this information, see curve II. This variation of the achieved gain depends on the estimation quality of the spatial covariance matrix $\underline{\mathbf{R}}_{\mathrm{s}}$. As the curves I and IV of Fig. 8.12 show, the performance remains approximately the same, if $\underline{\mathbf{R}}_{\mathrm{s}}$ is estimated and permanently averaged according to (7.10), but already considered without any iteration in the data detection according to (7.11) with $i = 1$, compare the curves I and IV. If $\underline{\mathbf{R}}_{\mathrm{s}}$ is estimated and averaged according to (7.9) by taking into account the last N_{b} estimated matrices $\underline{\mathbf{R}}_{\mathrm{s}}$ but only considered after the first iteration

$i = 1$ in the data detection according to (7.8), see curve III of Fig. 8.12, a performance degradation of about 1dB at a coded BER $P_b = 10^{-3}$ is observed compared to curve IV.

Fig. 8.12 is valid for the intercell MAI scenario 2. The results shown in Fig. 8.13 illustrate that the achievable gains under consideration of matrix $\underline{\mathbf{R}}_s$ in JD are smaller in the case of omnidirectional intercell MAI, i.e. in the case of intercell MAI scenario 1, than in the case of directional intercell MAI. However, the curves in Fig. 8.13 demonstrate that even in the case of omnidirectional intercell MAI it is possible to estimate matrix $\underline{\mathbf{R}}_s$ and benefit from its consideration in JD. Only in the case of very high C/I, where the intercell MAI is low compared to the power of the desired signals, the estimation quality of the estimate $\hat{\underline{\mathbf{R}}}_s$ is not sufficiently accurate to have any beneficial influence when being considered in JD. In the case of a very high C/I only less interference is present compared to the desired signal power, which makes it difficult to estimate the interference exactly. Consequently, in this case the estimate $\hat{\underline{\mathbf{R}}}_s$ should not be considered in JD.

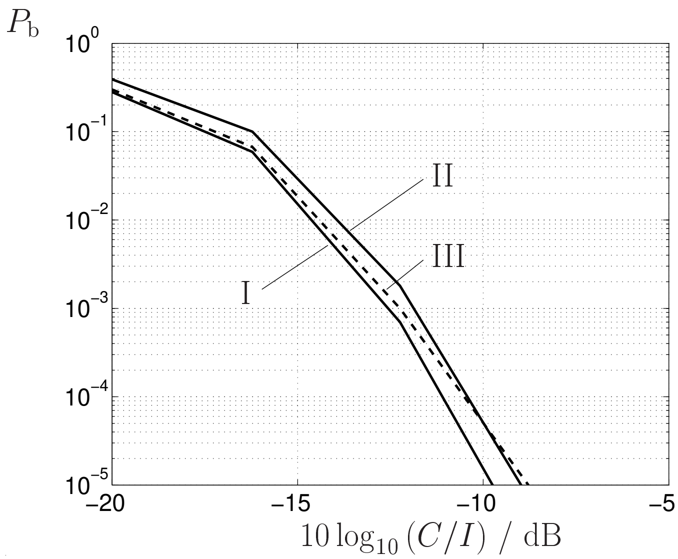

Fig. 8.13. Coded BER P_b versus C/I for an URA configuration under consideration of the cases I-III; $K_a = 4$; $N_b = 4$; intercell MAI scenario 1

In section 8.5.2 the reconstruction quality of the received signal has already been investigated. These investigations show that the signal reconstruction error $\epsilon_e^{(1)}$ without considering FEC coding is much greater than it would be if FEC coding is considered. Simulation will therefore be used below to check whether, despite dispensing with FEC coding in signal reconstruction, matrix $\underline{\mathbf{R}}_s$ can still be estimated just as well with perfectly known channel IRs, so that by taking account of $\hat{\underline{\mathbf{R}}}_s$ in data estimation according to (5.12) an improvement in system performance can be achieved.

The curves in Figs. 8.14 a and b show the uncoded BER P_{bu} and the coded BER P_b as a function of the C/I with and without taking account of the estimated matrix $\hat{\underline{\mathbf{R}}}_s(1)$ of

(7.13) for data detection in accordance with (7.4). The estimate $\hat{\underline{\mathbf{R}}}_{\mathrm{s}}$ is obtained without considering FEC coding in signal reconstruction. The selected antenna configuration is URA with $K_{\mathrm{a}} = 4$ antenna elements. The user signal and intercell MAI scenario is kept constant over $N_{\mathrm{b}} = 4$ bursts, and $N_{\mathrm{b}} = 4$ bursts will be used for estimation of $\hat{\underline{\mathbf{R}}}_{\mathrm{s}}$. For the user signal model the ITU IO B model with single direction channels is assumed which is described in Section 2.4. For the arrangement of the intercell MAI signals, intercell

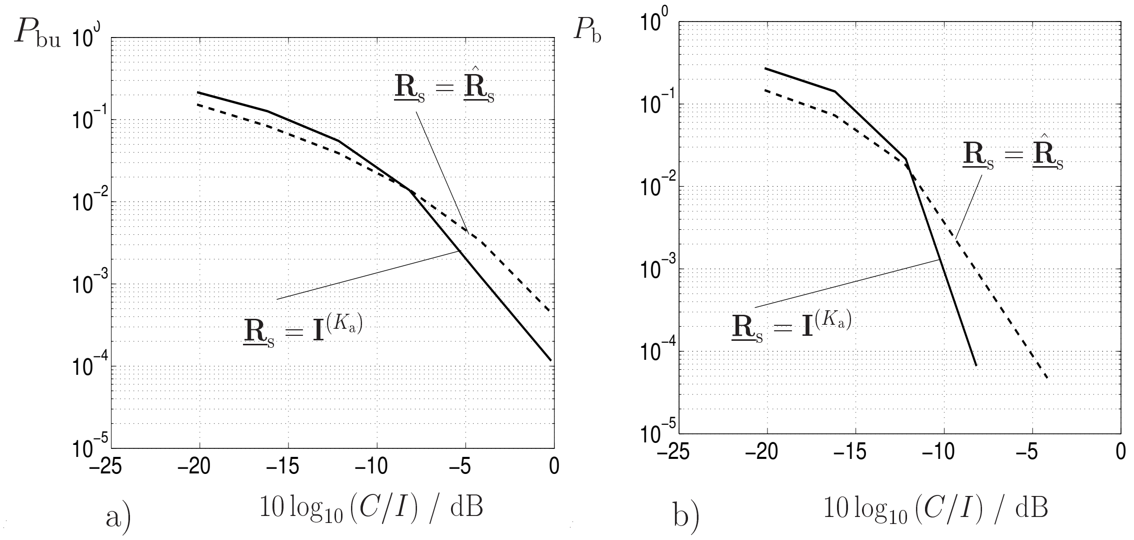

Fig. 8.14. BER with and without $\hat{\underline{\mathbf{R}}}_{\mathrm{s}}$, where $\hat{\underline{\mathbf{R}}}_{\mathrm{s}}$ is estimated without FEC in signal reconstruction; URA; $K_{\mathrm{a}} = 4$; $K = 2$; intercell MAI scenario 2; ITU IO B; $K_{\mathrm{d}} = 1$; $K_{\mathrm{i}} = 1$; 20% directionally homogenous interference
a) uncoded BER P_{bu}
b) coded BER P_{b}

MAI scenario 2 according to Section 3.3.1 with $K_{\mathrm{i}} = 1$ strong interferer is used as a basis, with the strong interferer causing 80% of the interference power. Direction $\gamma_{\mathrm{i}}^{(1)}$ of the strong interferer changes at random in the range $[0...2\pi[$ in all 4 bursts and is constant over 4 bursts. The curves in Figs. 8.14 a and b show that for a low C/I matrix $\hat{\underline{\mathbf{R}}}_{\mathrm{s}}$ is estimated well enough to effect a performance improvement when taken into account in data estimation. To achieve the coded and uncoded BER P_{b} or P_{bu} of 10^{-3} however, in the cases considered with $\hat{\underline{\mathbf{R}}}_{\mathrm{s}}$ taken into account in data estimation according to (5.12) a higher C/I is required than with replacing $\underline{\mathbf{R}}_{\mathrm{s}}$ by uniform matrix $\mathbf{I}^{(K_{\mathrm{a}})}$. The necessary quality of the estimate $\hat{\underline{\mathbf{R}}}_{\mathrm{s}}$ to enable $\hat{\underline{\mathbf{R}}}_{\mathrm{s}}$ to be used to good effect in data detection will obviously not be achieved without FEC coding for signal reconstruction.

8.5.4 Estimation of $\underline{\mathbf{R}}_{\mathrm{s}}$ based on spatial correlations of the received and reconstructed signals

In the previous section matrix $\underline{\mathbf{R}}_{\mathrm{s}}$ was estimated according to the procedure described in Section 7.2.1. By comparison, the receiver structure described in Section 7.4 will now be investigated. With this receiver structure, estimation of matrix $\underline{\mathbf{R}}_{\mathrm{s}}$ is based on previously determining the covariance matrices $\underline{\mathbf{R}}_{\mathrm{e}}$ of received signal and of the spatial correlation matrix of the channel IRs ${\underline{\mathbf{R}}_{\mathrm{s}}}^{(k)}$, $k = 1...K$, of the K user signals. The simulations make the following assumptions:

- $K = 8$ users are equidistantly spaced on a circle around the BS,
- the antenna configuration URA with $K_{\mathrm{a}} = 4$ antenna elements is used, channel model is the ITU IO B model with $K_{\mathrm{d}} = 1$, $v^{(k)} = 0$ km/h, $k = 1...K$, and
- Intercell MAI scenario 2 according to Section 3.3.1 with $K_{\mathrm{i}} = 1$, $\gamma_{\mathrm{i}}^{(1)} = 75°$ is assumed.

Figs. 8.15 a and b show the uncoded BER P_{bu} and coded BER P_{b} for the following cases:

I: $\underline{\mathbf{R}}_{\mathrm{s}}$ is perfectly known at the receiver.

II: $\underline{\mathbf{R}}_{\mathrm{s}}$ is estimated according to (7.7) with $i = 1$, averaged according to (7.10) to obtain $\hat{\underline{\mathbf{R}}}'_{\mathrm{s},n_{\mathrm{b}}}$, which is finally considered in data detection according to (7.11).

III: $\underline{\mathbf{R}}_{\mathrm{s}}$ is estimated according to (7.30), averaged according to (7.10) to obtain $\hat{\underline{\mathbf{R}}}'_{\mathrm{s},n_{\mathrm{b}}}$, which is finally considered in data detection according to (7.11).

IV: $\underline{\mathbf{R}}_{\mathrm{s}}$ is unknown at the receiver and is replaced by the identity matrix $\mathbf{I}^{(K_{\mathrm{a}})}$ in the JD process.

As is already the case for the curves in Fig. 8.12, the comparison of curves I and II in Figs. 8.15 a and b show an almost identical BER performance if the estimated matrix $\hat{\underline{\mathbf{R}}}_{\mathrm{s},n_{\mathrm{b}}}$ is averaged with estimation results from previously received bursts according to (7.10) and matrix $\hat{\underline{\mathbf{R}}}_{\mathrm{s},n_{\mathrm{b}}-1}$ determined in burst $n_{\mathrm{b}} - 1$ is considered for detection of the data of burst n_{b}. The shape of curve III in Fig. 8.15 a makes it clear that use of the receiver structure presented in Section 7.4 results in a worse BER performance than when the receiver used in Section 7.2.1 is used. Curves III and IV in Fig. 8.15 a even intersect at a C/I of -1 dB, i.e. with a larger C/I it would be better to use a conventional receiver than to use the receiver structure described in Section 7.4. If curves II and III of the coded BER P_{b} in Fig. 8.15 b are looked at, the difference of the BER performance is much smaller than

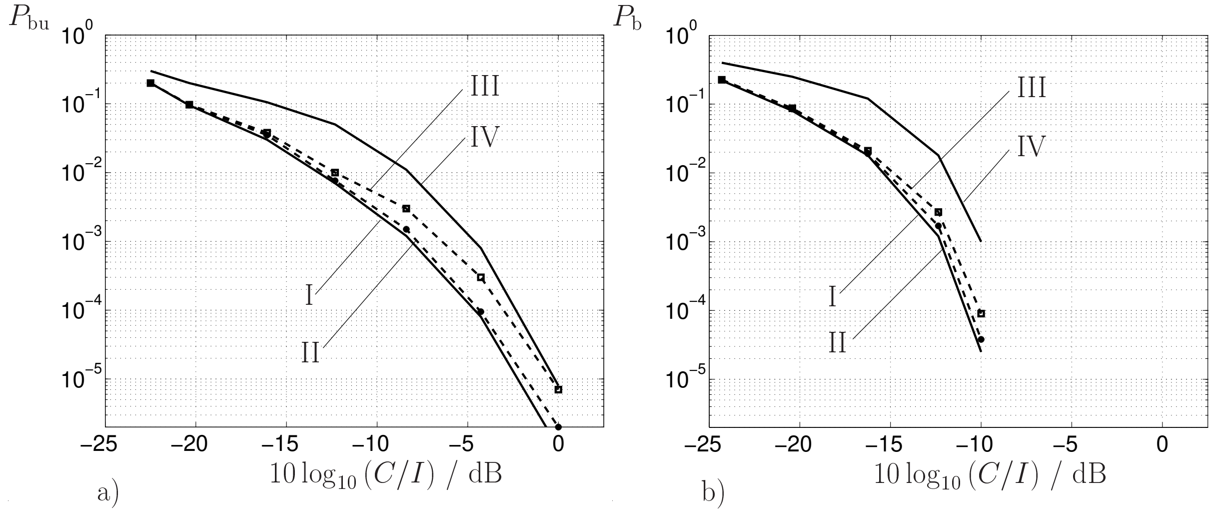

Fig. 8.15. BER versus C/I under consideration of the cases I-IV;
a) uncoded BER P_{bu} and
b) coded BER P_{b}

in the uncoded case. Estimation of matrix $\underline{\mathbf{R}}_{\mathrm{s}}$ obviously works particularly well with the two procedures if there is a relatively large amount of interference present, i.e. with a small C/I. With a large C/I the BER performance of the two procedures differs. If one looks at the receiver structure in accordance with Section 7.4, the estimation quality of $\hat{\underline{\mathbf{R}}}_{\mathrm{s}}$ is significantly affected by the estimation qualities of matrices $\hat{\underline{\mathbf{R}}}_{\mathrm{e}}$ of (7.27) and $\hat{\underline{\mathbf{R}}}_{\mathrm{s}}^{(k)}$, $k = 1...K$, of (7.29). These estimation qualities of $\hat{\underline{\mathbf{R}}}_{\mathrm{e}}$ and $\hat{\underline{\mathbf{R}}}_{\mathrm{s}}^{(k)}$, $k = 1...K$, can only be improved by taking account of several matrices $\hat{\underline{\mathbf{R}}}_{\mathrm{e}}$ and $\hat{\underline{\mathbf{R}}}_{\mathrm{s}}^{(k)}$, $k = 1...K$, and by averaging them since both the received signal and the channel IRs are perfectly known. Therefore, the C/I and the BER have no effect on the quality of estimations $\hat{\underline{\mathbf{R}}}_{\mathrm{e}}$ and $\hat{\underline{\mathbf{R}}}_{\mathrm{s}}^{(k)}$, $k = 1...K$. If the intercell MAI is small, the magnitudes of the components of the matrices $\hat{\underline{\mathbf{R}}}_{\mathrm{e}}$ and $\hat{\underline{\mathbf{R}}}_{\mathrm{s}}^{(k)}$, $k = 1...K$, are comparatively large values in comparison to the intercell MAI. Even if these large values are only subject to relatively small estimation errors, matrix $\underline{\mathbf{R}}_{\mathrm{s}}$ can no longer be recorded correctly according to (7.30).

If the receiver structure described in Section 7.2.1 is used, fewer bit errors occur with high C/I, which results in good signal reconstruction. In this case the intercell MAI can be determined exactly over most of the time of the burst under consideration. This thus leads to a good estimation $\hat{\underline{\mathbf{R}}}_{\mathrm{s}}$. This avoids additional sources of errors such as inclusion of estimations $\hat{\underline{\mathbf{R}}}_{\mathrm{e}}$ and $\hat{\underline{\mathbf{R}}}_{\mathrm{s}}^{(k)}$, $k = 1...K$, in the estimation of $\underline{\mathbf{R}}_{\mathrm{s}}$. If however we consider the coded BER P_{b} in Fig. 8.15 b, it is still evident that the procedure described in Section 7.4, allows an entirely acceptable improvement in the BER performance. However the investigations below will continue to be based on the procedure described in Section 7.2.1.

8.5.5 Directionally correlated intercell MAI

In the investigations performed in the previous sections it was assumed that the intercell MAI is directionally uncorrelated. With this proviso the effort of estimating the total covariance matrix $\underline{\mathbf{R}}_\mathrm{n}$ is reduced since the temporal covariance matrix $\tilde{\underline{\mathbf{R}}}_\mathrm{t}$ can be assumed to be known *a priori* and in addition is the same at any of the K_a receive antennas, see (3.37). In the outdoor area this type of simplification is acceptable as a first approximation. In this case the intercell MAI sources are frequently very far away from the disturbed BS. As measurements show [Mar97], the angular spread decreases as the distance between MS and BS increases. Intercell MAI signals from very distant MSs of the neighboring cell thereby arrive with a small angular spread at the disturbed BS. With multipath propagation of the intercell MAI signals, it can be assumed that the delay time difference of a signal on two different propagation paths is so large that the signals on the two paths can be assumed to be temporally uncorrelated when they arrive at the BS. In small cells or in the indoor area it must be assumed that the angular spread of the intercell MAI signals is larger than in the outdoor area [FL96, DZ94] and delay time differences of the same intercell MAI signal on different propagation paths can be so small that the intercell MAI signals can overlay each other constructively or destructively. The dependencies of the intercell MAI signals described above with different DOAs $\gamma_\mathrm{i}^{(k_\mathrm{i})}$, $k_\mathrm{i} = 1...K_\mathrm{i}$, cause significant changes in the temporal correlation of the intercell MAI signals at the K_a antenna elements. Hence, the *a priori* assumption of the temporal covariance matrix $\tilde{\underline{\mathbf{R}}}_\mathrm{t}$ for all K_a received intercell MAI signals at the K_a antenna elements is no longer valid, see Section 3.2. In this case, there are two options with regard to estimation of the total covariance matrix $\underline{\mathbf{R}}_\mathrm{n}$. Either the entire covariance matrix $\underline{\mathbf{R}}_\mathrm{n}$ is determined on the basis of the estimates $\hat{\underline{\mathbf{n}}}^{(k_\mathrm{a})}$, $k_\mathrm{a} = 1...K_\mathrm{a}$, which is possible using the procedure presented in Section 7.2.1, but represents considerable effort, or we dispense with exact knowledge of the total covariance matrix $\underline{\mathbf{R}}_\mathrm{n}$ and start from temporal uncorrelation of the intercell MAI signals, although the interference scenario does not correspond to it. In the latter case the effort of estimating matrix $\underline{\mathbf{R}}_\mathrm{n}$ is significantly reduced compared to the previously described estimation of the total matrix $\underline{\mathbf{R}}_\mathrm{n}$, since only the spatial covariance matrix $\underline{\mathbf{R}}_\mathrm{s}$ must be estimated. However performance degradation is to be expected here. This expected performance degradation is investigated below.

The investigations dispense with estimation and consideration of the spatial covariance matrix $\underline{\mathbf{R}}_\mathrm{s}$ and only investigates the effects on data detection when using the non correct temporal covariance matrix $\tilde{\underline{\mathbf{R}}}_\mathrm{t}$. These investigations are undertaken in accordance with the intercell MAI scenario 2 with $K_\mathrm{i} = 2$ intercell MAI signals with the DOAs $\gamma_\mathrm{i}^{(k_\mathrm{i})}$, $k_\mathrm{i} = 1, 2$ described in Section 3.3.2. The two interference signals might origin from the same source or from different sources. In the latter case we have $K_\mathrm{i} = 1$ interference source with transmitting an intercell MAI signal with $K_\mathrm{d} = 2$ DOAs. The two interferer signals are purely directional and each have the same power. Together these two interferer signals cause 80% of the total interference power. The remaining 20% of the interference

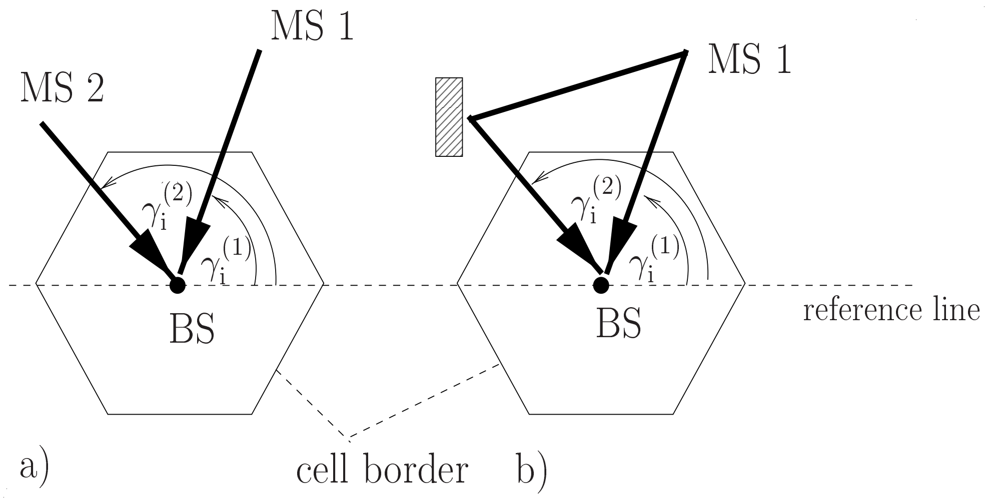

Fig. 8.16. Interference scenario
a) two independent interfering signals
b) two dependent interfering signals with the DOAs $\gamma_{\mathrm{i}}^{(1)}$ and $\gamma_{\mathrm{i}}^{(2)}$

power is directionally homogeneously distributed in the azimuth. In the data estimation in accordance with (5.12) the temporal covariance matrix $\underline{\tilde{\mathbf{R}}}_{\mathrm{t}}$ which is correct for the case of uncorrelated interference signals with various DOAs is assumed. Spatial covariance matrix $\underline{\mathbf{R}}_{\mathrm{s}}$ is replaced by uniform matrix $\mathbf{I}^{(K_{\mathrm{a}})}$ in data estimation in accordance with (5.12). As regards the interfering signals, a distinction is made between the following two cases shown in Fig. 8.16:

- The two interfering signals come from different sources and are independent.
- The two interfering signals come from the same source and are dependent.

For the two dependent interferer signals the fixed pairs of angles $(\gamma_{\mathrm{i}}^{(1)}, \gamma_{\mathrm{i}}^{(2)})$ equal to $(0°, 5°)$, $(0°, 15°)$, $(0°, 90°)$ and $(90°, 105°)$ are assumed. The user signals are modelled on the basis of the following assumptions:

- $K = 8$ users are distributed equidistantly on a circle around the BS,
- the channel model is the ITU IO B model with $K_{\mathrm{d}} = 1$, $v^{(k)} = 0$ km/h, $k = 1...K$, see Section 2.4.

If antenna configuration ULA is used, with $K_{\mathrm{a}} = 4$ antenna elements, it is assumed below that the intercell MAI signals are the same from the point of view of time at the location of the 4$^{\mathrm{th}}$ antenna element and only differ spatially in their DOAs $\gamma_{\mathrm{i}}^{(1)}$ and $\gamma_{\mathrm{i}}^{(2)}$. This

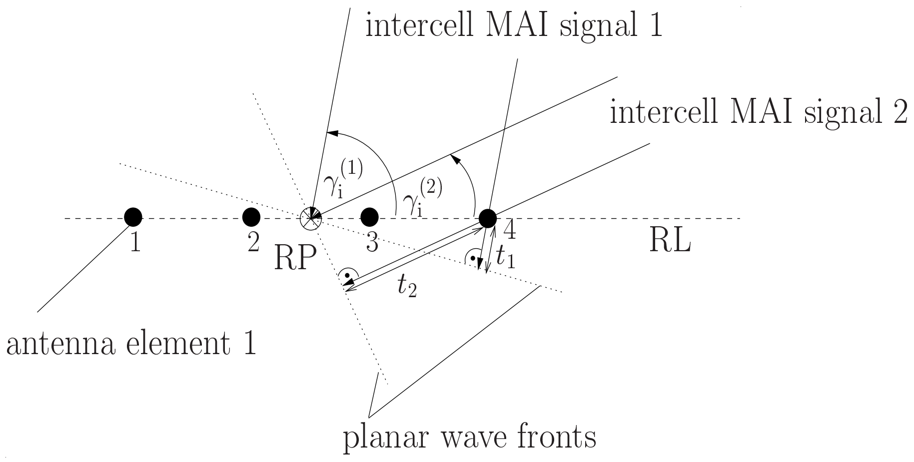

Fig. 8.17. Illustration of dependency of delays t_1 and t_2 and DOAs $\gamma_{\mathrm{i}}^{(1)}$ and $\gamma_{\mathrm{i}}^{(2)}$ in the case of constructive superposition at the 4^{th} antenna element

means that the two intercell MAI signals constructively overlap at the location of the 4^{th} antenna element. Consequently, the versions of the two interference signals 1 or 2 delayed by t_1 and t_2 overlap at the RP, see Fig. 8.17.

A special case for antenna configuration ULA is given if only for DOAs $\gamma_{\mathrm{i}}^{(1)}$ and $\gamma_{\mathrm{i}}^{(2)}$ of the interfering signals the pair of angles $\gamma_{\mathrm{i}}^{(1)}$ is equal to 90° and $\gamma_{\mathrm{i}}^{(2)}$ is equal to 0°. In accordance with Fig. 8.17 the delay of the first interfering signal typically t_1 is equal to zero and the delay of the second interfering signal t_2 is equal to $3/(4f_{\mathrm{c}})$, where f_{c} is the carrier frequency. This means that the same wave fronts arrive at antennas two and four, as shown in Fig. 8.18. At these points this leads to a constructive overlaying of the two interfering signals. Accordingly the interfering signals mutually extinguish each other at antennas one and three.

The curves in Figs. 8.19 to 8.21 show the coded and uncoded BERs P_{b} or P_{bu} as a function of the average C/I for the chosen pairs of angles for $K_{\mathrm{i}} = 2$ strong interferers when using antenna configuration ULA and RING. The following three cases are investigated here:

I : $K_{\mathrm{i}} = 2$ strong interferer signals with different DOAs are independent.

II : $K_{\mathrm{i}} = 2$ strong interferer signals with different DOAs are temporally the same when impinging at the RP.

III : $K_{\mathrm{i}} = 2$ strong interfering signals are temporally the same with different DOAs, but are shifted by t_1 and t_2 in time in the RP in accordance with in Fig. 8.17.

For the antenna configuration ULA with $K_{\mathrm{a}} = 4$ antenna elements, it can be seen from Figs. 8.19 a and b that with slight differences between DOAs $\gamma_{\mathrm{i}}^{(1)}$ and $\gamma_{\mathrm{i}}^{(2)}$ around 0°,

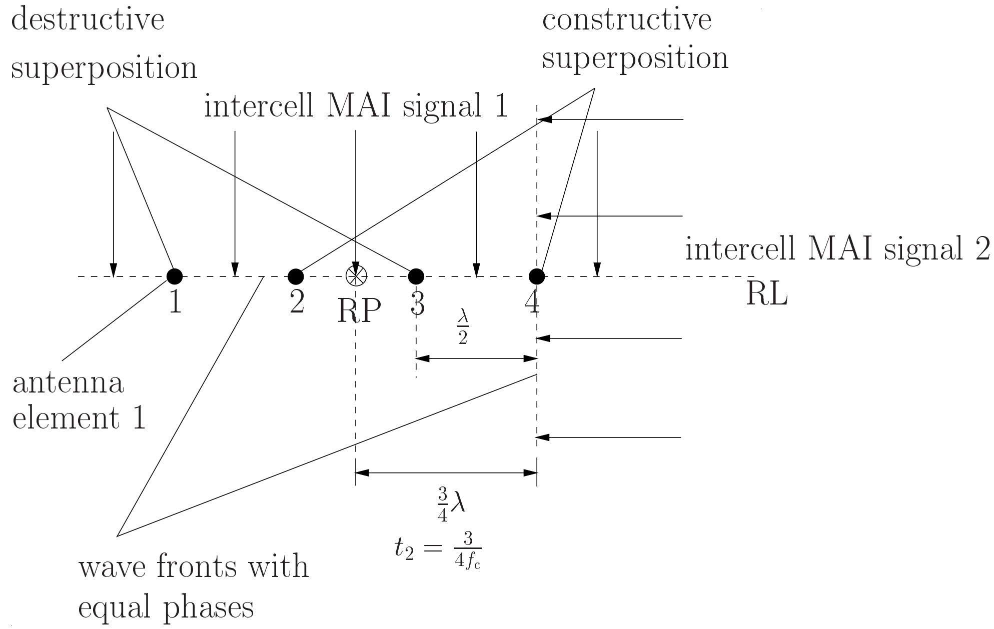

Fig. 8.18. Special case of antenna configuration ULA for $K_\mathrm{i} = 2$ identical interfering signals with different DOAs $\gamma_\mathrm{i}^{(1)} = 90°$ and $\gamma_\mathrm{i}^{(2)} = 0°$; delays $t_1 = 0$ and $t_2 = 3/(4f_0)$ as in Fig. 8.17

i.e. $\gamma_\mathrm{i}^{(1)}$, $\gamma_\mathrm{i}^{(2)} << 90°$, there are no difference of the BERs P_b and P_bu to be observed in the three cases considered. In opposite to the curves shown in Figs. 8.19 a and b a slight deterioration of the coded BER P_b for a given C/I is to be detected in Fig. 8.20 a for angles around 90°. For $\gamma_\mathrm{i}^{(1)} = 90°$ and $\gamma_\mathrm{i}^{(2)} = 105°$ there is a deterioration in C/I performance of 1.71 dB for a coded BER P_b equal to 10^{-3} when considering case III, i.e. when the two interfering signals are not only dependent but are also shifted in time by t_1 and t_2 according to Fig. 8.17. Even without the delay, i.e. when considering case II, C/I performance degradations of 0.57 dB are to be detected compared to the case I, if a coded BER P_b of 10^{-3} is to be achieved. The uncoded BER P_bu however does not show any deterioration of the coded BER P_b between the curves valid for cases I and II. Hence, the C/I deviations of 0.57 dB might be attributed to simulation inaccuracy. The special case shown for Fig. 8.20 b with $\gamma_\mathrm{i}^{(1)} = 90°$ and $\gamma_\mathrm{i}^{(2)} = 0°$ and the delays t_1 equal to zero and t_2 equal to $3/(4f_\mathrm{c})$, i.e. case III, reveals the greatest C/I performance degradation of 4.28 dB with a coded BER P_b of 10^{-3}.

The Figs. 8.21 a and b show the simulation results for antenna configuration RING with $K_\mathrm{a} = 8$ antenna elements. Case III with delays t_1 and t_2 according to Fig. 8.17 is not considered in Figs. 8.21 a and b. For a small difference in angle between the DOAs of the intercell MAI signals $\gamma_\mathrm{i}^{(1)}$ and $\gamma_\mathrm{i}^{(2)}$ of 5°, see Fig. 8.21 a, there are no effects on uncoded BER P_bu, if dependent interferers rather than independent ones are assumed. The deviations for the coded BER P_b can have arisen, as in Fig. 8.21 a,

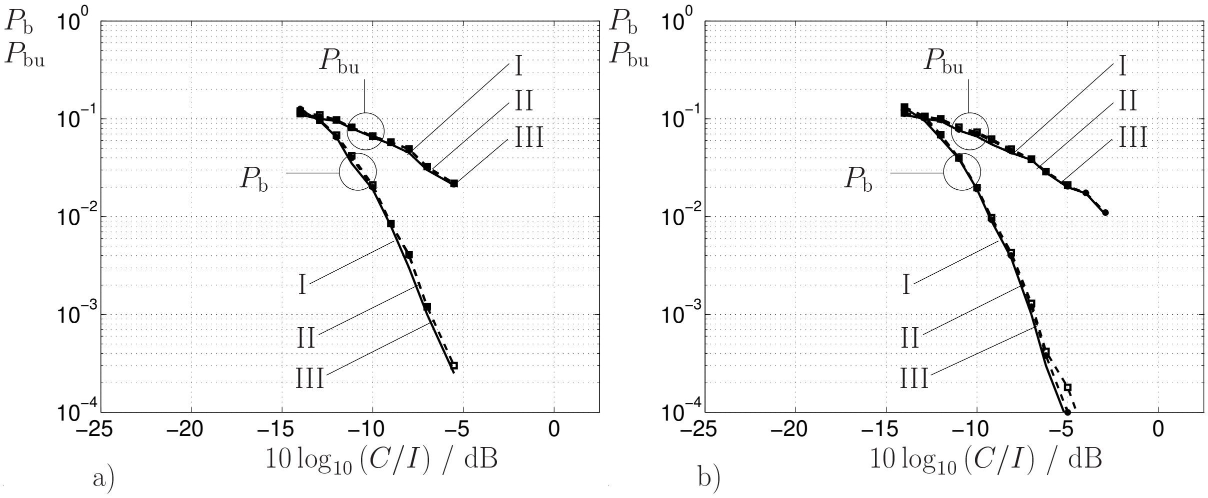

Fig. 8.19. Coded and uncoded BER P_b and $P_{bu}$with independent interfering signals and with dependent interfering signals with and without delays t_1 and t_2 according to Fig. 8.17; ULA; $K_a = 4$; directionally homogeneous interference component 20%;
a) $\gamma_i^{(1)} = 0°$, $\gamma_i^{(2)} = 5°$;
b) $\gamma_i^{(1)} = 0°$, $\gamma_i^{(2)} = 15°$

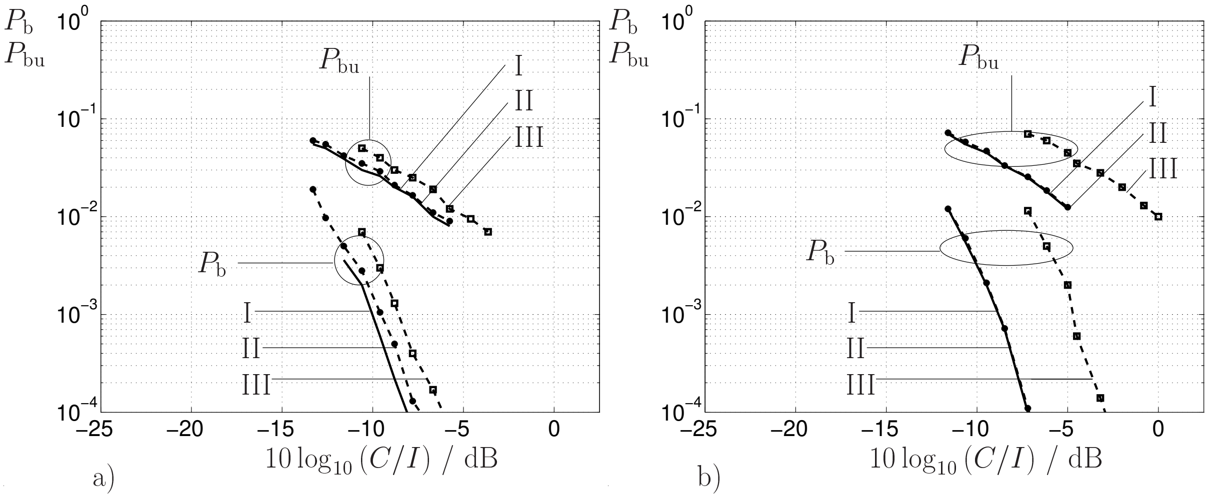

Fig. 8.20. Coded and uncoded BER P_b and P_{bu} for correlated and uncorrelated interfering signals with and without delays t_1 and t_2 according to Fig. 8.17; ULA; $K_a = 4$; directionally homogeneous interference component 20%;
a) $\gamma_i^{(1)} = 90°$, $\gamma_i^{(2)} = 105°$;
b) $\gamma_i^{(1)} = 0°$, $\gamma_i^{(2)} = 90°$

from simulation inaccuracies. Solely at 15° angle difference, see Fig. 8.21 b, can C/I performance degradations of 1.14 dB be detected for both uncoded BER P_{bu} as well as coded BER P_b of 10^{-3}.

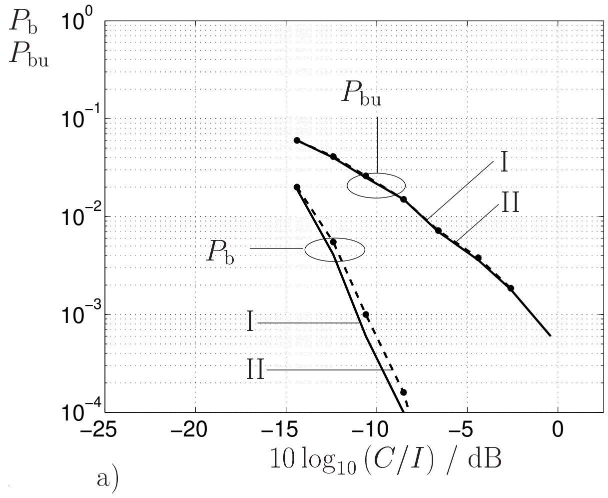

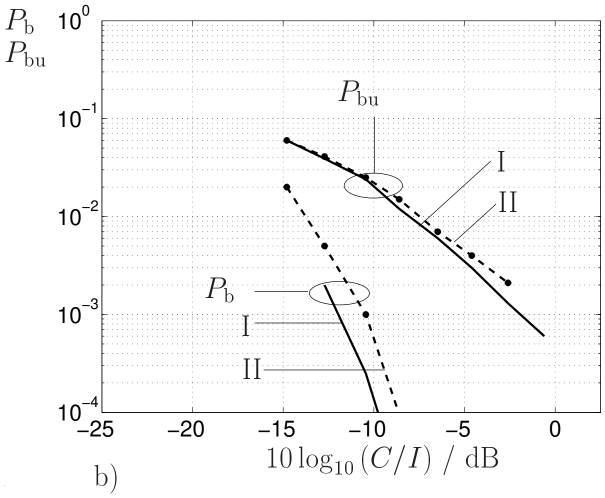

Fig. 8.21. Coded and uncoded BER P_b and P_{bu} for correlated and uncorrelated interfering signals; RING; $K_a = 8$; directionally homogeneous interference component 20%;
a) $\gamma_i^{(1)} = 0°$, $\gamma_i^{(2)} = 5°$;
b) $\gamma_i^{(1)} = 90°$, $\gamma_i^{(2)} = 105°$

All results in Figures 8.19 through 8.21 show that, though the same matrix $\tilde{\underline{\mathbf{R}}}_t$ is always considered, obvious performance degradations only occur in special unrealistic cases. In all other cases the performance degradations are negligibly small.

8.6 Simulation results applying MSJD and considering known channel IRs

8.6.1 Parallel MSJD

In this section the parallel MSJD receiver structure shown in Fig. 7.3 is considered. In contrast to the simulation conditions valid in previous sections, in the following Section $K = 16$ users instead of 8 are considered. The K users are equidistantly distributed on a circle around the BS and their positions are kept fixed during the simulations. The ITU IO B channel model with single direction channels described in Section 2.4 is used in the simulations. Moreover, the directionally uncorrelated intercell MAI scenarios 1 and 2 described in Section 3.3.1 are considered.

The combination of MSJD with adaptive antennas opens up the opportunity for including spatial criteria when forming the user groups $g = 1, 2$. In Section 5.4.4 there are already described three strategies for assigning users to the two user groups $g = 1, 2$.

The first assignment criterion described in Section 5.4.4 depends on the powers of the user signals. For parallel MSJD this assignment strategy does not have any significance, see Section 5.4.4, and is therefore not considered below. In addition all user signals are received with the same average power so that even with investigations of serial MSJD this strategy is not taken into account. This section only investigates the second strategy presented in Section 5.4.4 making the initial assumption that the users which have the greatest spatial distance from each other in each case are combined into the same group. With the assumed spatial distribution of users, that means that each second user signal will be assigned to group $g = 1$ and all others to group $g = 2$. This assignment strategy thus has the advantage that by using adaptive antennas, the individual user signals within a group can be better spatially separated [PWBB98, PW99] and thereby the detection of the individual signals of a group can be improved. The third assignment strategy described in Section 5.4.4 is considered in conjunction with the investigations for serial MSJD in Section 8.6.2.

The simulation results presented in Figs. 8.22 to 8.24, show the coded BER P_b as a function of the average C/I for use of conventional JD and parallel MSJD taking account of K_a equal to 2, 4 and 8 antenna elements. MSJD is initially executed in two iterations. Also shown is the coded BER P_b of group $g = 1$ after the first iteration $i = 1$ and the coded BER P_b of group $g = 1$ after the second iteration $i = 2$. In addition the achievable coded BERs P_b of group $g = 1$ are specified if, in the second iteration $i = 2$, the covariance matrix $\hat{\underline{\mathbf{R}}}_\mathrm{n}(1)$ of the intercell MAI estimated in accordance with Fig. 7.3 is taken into account. On the basis of the assumed intercell MAI scenarios 1 and 2, presented in Section 3.3.1, according to (3.37) the estimation of matrix $\underline{\mathbf{R}}_\mathrm{n}$ can be reduced to the estimation of the spatial covariance matrix $\underline{\mathbf{R}}_\mathrm{s}$. Therefore, as described in Section 7.2.1 only matrix $\underline{\mathbf{R}}_\mathrm{s}$ is estimated below and then the estimation result $\hat{\underline{\mathbf{R}}}_\mathrm{n}(1)$ of (3.37) is obtained, which is then taken into account in the relevant detection processes. To simplify matters, the covariance matrix $\hat{\underline{\mathbf{R}}}_\mathrm{n}(1)$ and $\hat{\underline{\mathbf{R}}}_\mathrm{s}(1)$ which is estimated in the first iteration $i = 1$, is designated $\hat{\underline{\mathbf{R}}}_\mathrm{n}$ and $\hat{\underline{\mathbf{R}}}_\mathrm{s}$.

Figs. 8.22 through 8.24 show simulation results assuming intercell MAI scenario 2 with $K_\mathrm{i} = 1$ strong intercell MAI signal. Direction $\gamma_\mathrm{i}^{(1)}$ of the strong intercell interferer, which makes up 80% of the total interference power, is equal to 255°. From the curves shown in Figs. 8.22 to 8.24 the following conclusions can be drawn:

- The coded BER P_b of the signals of group $g = 1$ is in most cases higher after the first iteration than the coded BER P_b that can be achieved when using conventional JD with the same C/I. The reason for this is the additional intracell interference that is caused by the signals of group $g = 2$ and has an effect on the detection of the signals of group $g = 1$ in the first iteration $i = 1$.

- With all results it is apparent that already in the second iteration $i = 2$ for the same C/I a lower coded BER P_b can be reached than with conventional JD.

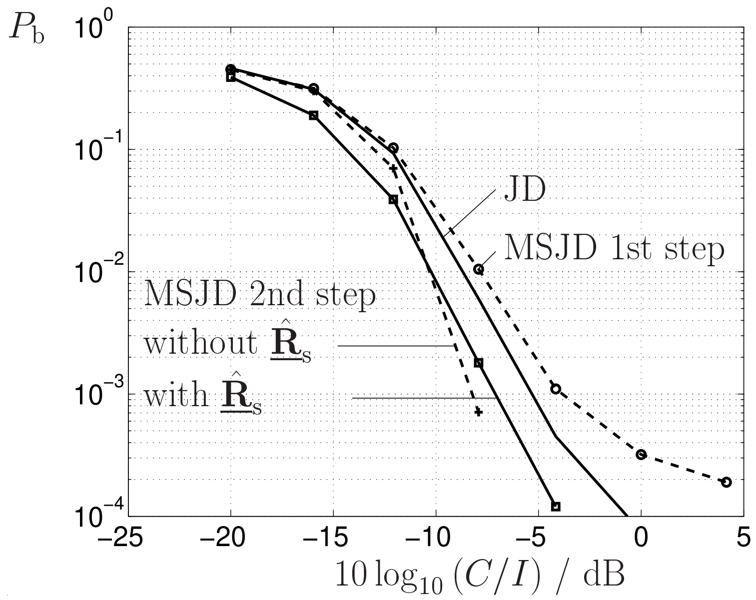

Fig. 8.22. Coded BER P_b with use of conventional JD, parallel MSJD in $i = 2$ iterations, and with consideration of $\hat{\underline{\mathbf{R}}}_s$ in MSJD; intercell MAI scenario 2; ULA; $K_a = 2$; $K = 16$

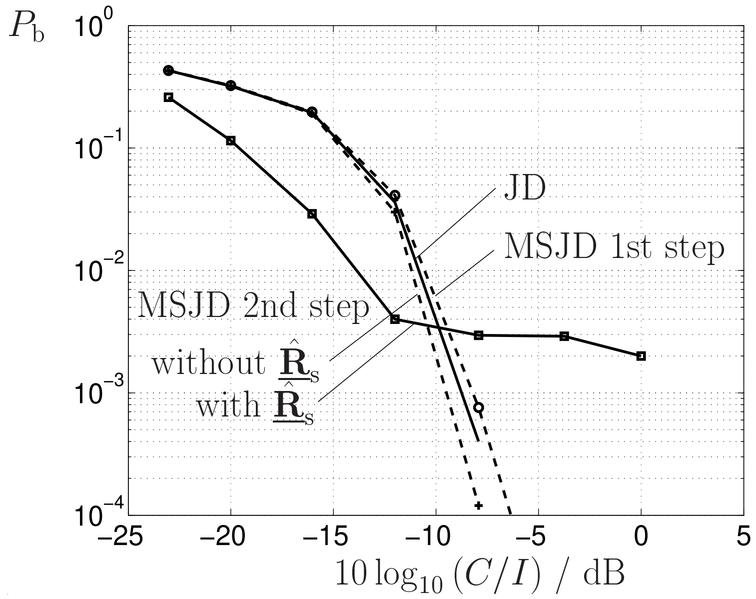

Fig. 8.23. Coded BER P_b with use of conventional JD, parallel MSJD in $i = 2$ iterations, and with consideration of $\hat{\underline{\mathbf{R}}}_s$ in MSJD; intercell MAI scenario 2; URA; $K_a = 4$; $K = 16$

- With an increase in the number of antenna elements K_a the reduction in the coded BER P_b that can be achieved using MSJD with a given C/I is less than with conventional JD. This result confirms the theoretical considerations given in Section

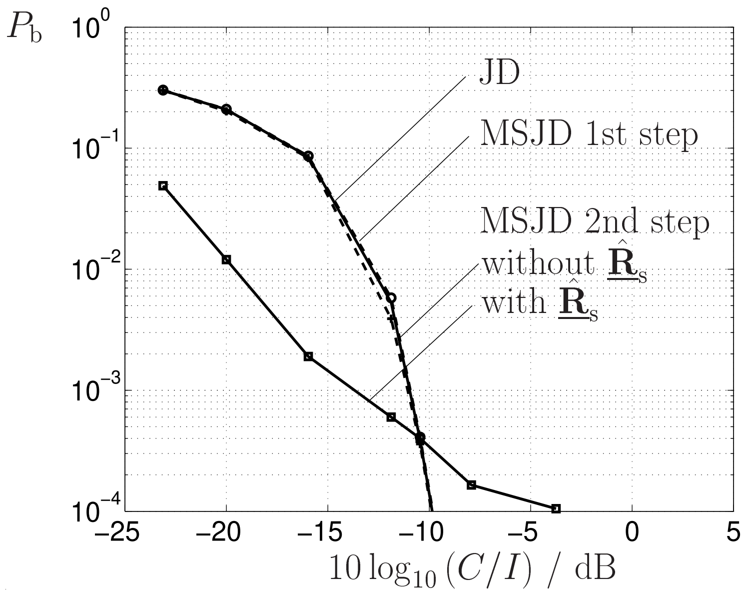

Fig. 8.24. Coded BER P_b with use of conventional JD, parallel MSJD in $i = 2$ iterations, and with consideration of $\hat{\underline{\mathbf{R}}}_s$ in MSJD; intercell MAI scenario 2; RING; $K_a = 8$; $K = 16$

5.3.3 with regard to reducing the SNR degradation on increasing the number of antenna elements K_a.

- An increase in the number of antenna elements K_a leads to a better spatial separability of the user signals within a group [PWBB98] and thereby to a reduction in intracell MAI for MSJD. This means that the coded BER P_b of the signals of group $g = 1$ after the first iteration $i = 1$ for e.g. $K_a = 4$ antenna elements is only insignificantly higher than the coded BER P_b for all $K = 16$ signals with conventional JD, see for example Fig. 8.23.

- When $K_a = 8$ antenna elements are used an improvement over conventional JD is only to be achieved by taking into consideration matrix $\hat{\underline{\mathbf{R}}}_s$. With MSJD no further significant improvement of the BER behavior can be obtained.

- If one takes into consideration the estimate $\hat{\underline{\mathbf{R}}}_s$ in the second iteration $i = 2$ with MSJD, the effects on system performance cannot be assessed in overall terms. For low C/I values the interference level is much higher than the level of the desired signal, and reconstruction errors due to detection errors in the first iteration $i = 1$ only have a negligible influence on the estimation of $\underline{\mathbf{n}}$ according to (7.6). Hence, $\underline{\mathbf{R}}_s$ can be estimated with an sufficient accuracy to improve the BER behavior when $\hat{\underline{\mathbf{R}}}_s$ is considered in the second iteration $i = 2$. The curves in Fig. 8.23 show that with $K_a = 4$ antenna elements the required C/I to achieve P_b equal to 10^{-2} is e.g. reduced by 2.6 dB. By increasing the C/I the estimation error of $\hat{\underline{\mathbf{R}}}_s$ increases.

The reconstruction errors of both groups $g = 1$ and $g = 2$ have an impact on the estimation quality of the matrix. Due to the additional intracell MAI in MSJD the signal reconstruction errors are higher than in conventional JD. Therefore, the quality of the estimate $\hat{\underline{\mathbf{R}}}_{\mathrm{s}}$ is worse. Consequently, the consideration of an inaccurate estimate $\hat{\underline{\mathbf{R}}}_{\mathrm{s}}$ in the second detection iteration $i = 2$ leads to a system performance inferior to that obtained in the case where $\hat{\underline{\mathbf{R}}}_{\mathrm{s}}$ is not considered.

The receiver structure presented in Fig. 7.3 shows that in parallel MSJD any number of iterations i is possible. For example the estimation $\hat{\underline{\mathbf{R}}}_{\mathrm{s}}(2)$ could also be taken into account in the third iteration $i = 3$. For $K_{\mathrm{a}} = 1$ antenna element the investigations in [Ost01] have shown that each MSJD step brings a further performance improvement. In [Ost01] it is also shown that the first step causes the greatest improvement in the receiver's BER behavior. However, as has already been explained in Section 5.3.3, when MSJD is combined with adaptive antennas with an increasing number K_{a} of antenna elements, the improvement in performance by using MSJD as opposed to JD is less, so that for example, with K_{a} equal to eight antenna elements, even in the first stage of MSJD only a slight improvement of the BER behavior can be achieved by MSJD. If the improvement in the BER behavior is already small in a first iteration and if all further steps now make even less of an improvement to the BER behavior, it can be assumed that for example a third iteration $i = 3$ will make hardly any difference in BER behavior compared to a second iteration $i = 2$. For this reason this section will not be investigating any MSJD receivers with $i > 2$ iteration.

It is assumed below that intercell MAI scenario 1 described in Section 3.3.1 is used for the simulations. The curves in Fig. 8.25 show a typical examples for the simulations results determined when using $K_{\mathrm{a}} = 2$ antenna elements. In Section 8.5.3 it has already been shown that with conventional JD, taking account of the perfectly known matrix $\underline{\mathbf{R}}_{\mathrm{s}}$ in data detection and assuming intercell MAI scenario 1 does not allow such great improvements as with the intercell MAI scenario 2. Errors in estimating matrix $\underline{\mathbf{R}}_{\mathrm{s}}$ can then lead that the performance improvement obtained by using $\hat{\underline{\mathbf{R}}}_{\mathrm{s}}$ is simply negated again, if the incorrect estimate $\hat{\underline{\mathbf{R}}}_{\mathrm{s}}$ is taken into account in data detection. As the simulation results in Fig. 8.25 show, this applies not only for the use of conventional JD, but in particular for MSJD.

The curves in Fig. 8.25 show especially for large values C/I that by considering the inaccurate estimate $\hat{\underline{\mathbf{R}}}_{\mathrm{s}}$ the system performance is inferior compared to the system performance achievable without consideration of $\hat{\underline{\mathbf{R}}}_{\mathrm{s}}$, if the interference is modelled according to the intercell MAI scenario 1.

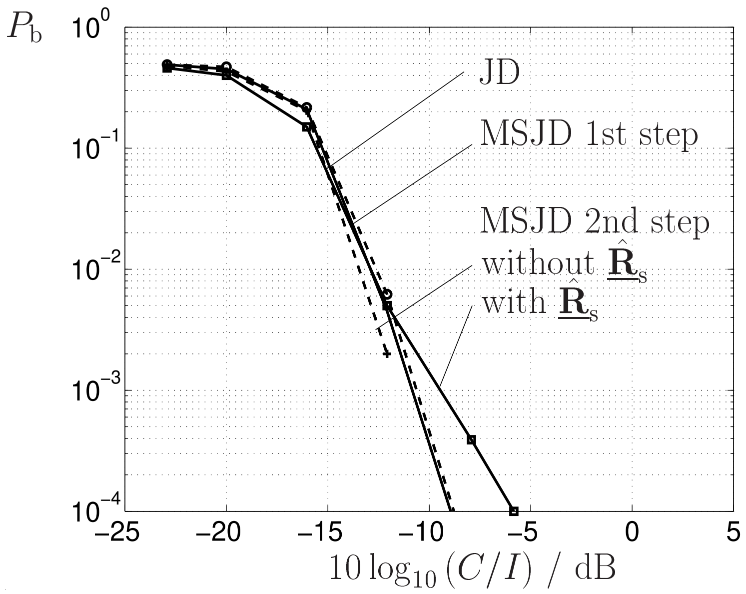

Fig. 8.25. Coded BER P_b with use of conventional JD, parallel MSJD in $i = 2$ iteration and with consideration of $\hat{\underline{\mathbf{R}}}_\mathrm{s}$ in MSJD; intercell MAI scenario 1; ULA; $K_\mathrm{a} = 2$; $K = 16$

8.6.2 Serial MSJD

Now that parallel MSJD has been considered in the previous section, this section will investigate serial MSJD. This involved comparing not only serial MSJD with parallel MSJD but also comparing two strategies for assigning signals to the two groups $g = 1, 2$ as described in Section 5.3.3. First of all, with other parameters being equal as in Section 8.6.1, and taking into consideration the same assignment strategy of the user signals in accordance with Fig. 5.8 a, the coded BER P_b versus C/I is looked at. The curves in Fig. 8.26 show the simulation results for $K_\mathrm{a} = 4$ antenna elements assuming intercell MAI scenario 2. This means that the results are comparable with those results presented in Fig. 8.23 in Section 8.6.1. Figs. 8.23 and 8.26 tend to show the same results. It is thus of no consequence for the detection quality whether parallel or serial MSJD is used. Below, with other parameters remaining the same, the criterion for assigning the user signals to the two user groups $g = 1, 2$ shown in Fig. 5.8 b are considered. Spatially adjacent users are combined into a group here. In contrast to the assignment strategy described in the previous Section 8.6.1 no spatial pre-separation of the individual user signals of a group is undertaken, but a separation of the two groups themselves.

The spatial separation of the user groups is obviously better for using MSJD than an improved spatial separation of each individual user signal, as the curves in Fig. 8.27 show. The suppression of the intracell MAI obtained by the spatial preliminary separation of

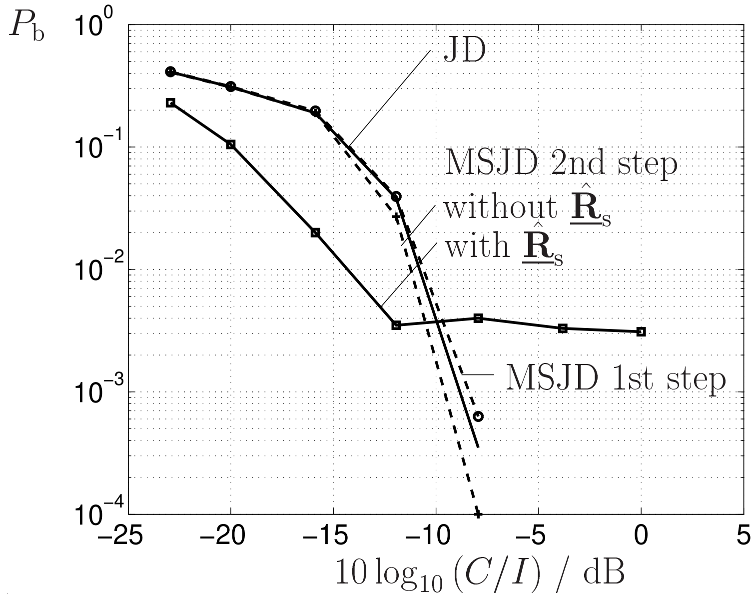

Fig. 8.26. Coded BER P_b with use of conventional JD, serial MSJD in $i = 2$ iterations and taking account of $\hat{\underline{\mathbf{R}}}_\mathrm{s}$ in MSJD; users spatially pre-separated; intercell MAI scenario 2; URA; $K_\mathrm{a} = 4$; $K = 16$

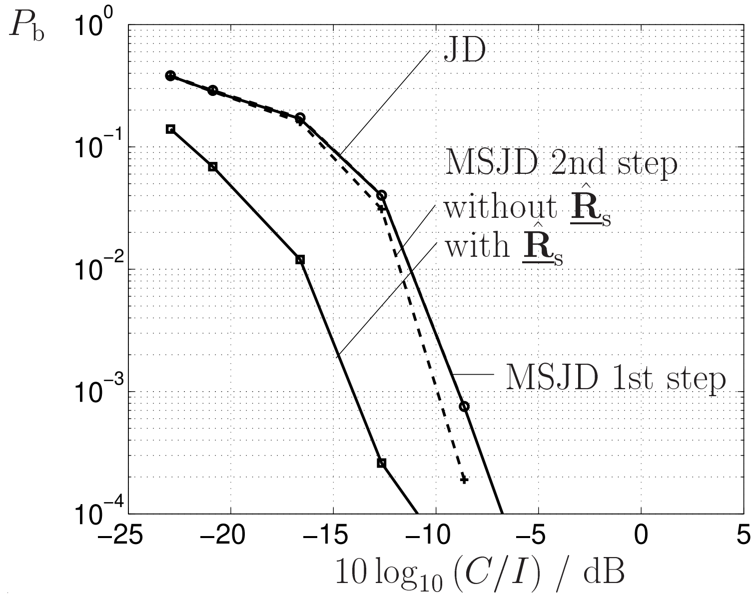

Fig. 8.27. Coded BER P_b with use of conventional JD, serial MSJD in $i = 2$ iteration and taking account of $\hat{\underline{\mathbf{R}}}_\mathrm{s}$ in MSJD; groups spatially pre-separated; intercell MAI scenario 2; URA; $K_\mathrm{a} = 4$; $K = 16$

the user groups results in a slightly improved BER behavior when MSJD is used that can be achieved by the spatial separation of the user signals within the individual groups. The massive intracell MAI that occurs for MSJD in a first iteration is reduced before detection of the first group $g = 1$, conditional on the use of an antenna array with the corresponding signal processing which causes a certain directional characteristic of the antenna array.

Selecting intercell MAI scenario 2 and the assumption that the DOA $\gamma_{\mathrm{i}}^{(1)} = 255°$ of the strong interferer is unchangeable, also makes the detection of the signals of group $g = 1$ especially easier as the curves in Fig. 8.27 show. The DOAs of the signals of group $g = 1$ do not lie in the range of $\gamma_{\mathrm{i}}^{(1)}$, see Fig. 5.8 b. The directional characteristic of the antenna obtained by the signal processing of the receive signals at the K_{a} antenna elements suppresses in this special case not only the intracell MAI, but also the intercell MAI. The good detection result that this achieves makes it easier to estimate the interference $\underline{\mathbf{n}}$ of (3.24), see Chapter 7 and thereby also facilitates estimation of the spatial intercell MAI covariance matrix $\underline{\mathbf{R}}_{\mathrm{s}}$. Taking account of the comparatively well estimated matrix $\underline{\mathbf{R}}_{\mathrm{s}}$ in the case considered in Fig. 8.27 leads, particularly with large C/I to a better BER behavior than is to be detected in the corresponding curves in Fig. 8.26.

8.7 Simulation results for the case of estimated channel IRs

8.7.1 Introduction

In the previous sections the channel IRs $\underline{\mathbf{h}}_{\mathrm{s}}^{(k,k_{\mathrm{a}})}$, $k = 1...K$, $k_{\mathrm{a}} = 1...K_{\mathrm{a}}$, of (2.1) at the receiver were assumed to be perfectly known.

In this section channel estimation is included in the investigations. Chapter 6 showed that even with channel estimation the intercell MAI covariance matrix $\underline{\mathbf{R}}_{\mathrm{n}}$ or $\underline{\mathbf{R}}_{\mathrm{m}}$ of (7.3) can be considered as beneficial. In Section 8.7.2 the channel estimation procedure presented in Section 6.3 is investigated using simulations. Here the necessary knowledge of the DOAs of the user signals is assumed to be known. Section 8.7.3 shows the simulation results of the MMSE based channel estimation procedure described in Section 6.4. MMSE–JCE allows account to be taken of both intercell MAI covariance matrix $\underline{\mathbf{R}}_{\mathrm{m}}$ and of the correlation matrix of the channel IRs $\underline{\mathbf{R}}_{\tau,\mathrm{s}}$ of (2.13).

8.7.2 Exploiting the knowledge of the DOAs

As has already been mentioned in Section 8.7.1, in the following simulation results are presented by considering the channel estimation scheme of Section 6.3 incorporating the exploitation of the knowledge of the DOAs of the desired user signals and the knowledge of the estimate $\hat{\underline{\mathbf{R}}}_{\mathrm{m}}$.

The following situation is assumed in the simulations:

- Antenna configuration: URA with $K_{\mathrm{a}} = 4$ antenna elements.
- Channel model: ITU IO B; single direction $K_{\mathrm{d}} = 1$; the DOAs $\beta^{(k,1)}$, $k = 1...K$, of each user signal is changing randomly within $[0...2\pi[$ every $N_{\mathrm{b}} = 4$ bursts; velocity of each user $v = 3$ km/h during the transmission of $N_{\mathrm{b}} = 4$ bursts.
- Number of users $K = 8$.
- Intercell MAI scenario 2, see Section 3.3.1; $K_{\mathrm{i}} = 1$; the main interference direction $\gamma_{\mathrm{i}}^{(1)}$ is changing randomly within $[0...2\pi[$ every $N_{\mathrm{b}} = 4$ bursts.
- The number N_{b} over which an averaging is performed to determine the estimate $\hat{\underline{\mathbf{R}}}_{\mathrm{s}}$ according to (7.9) is equal to 4.

Channel estimation is executed in accordance with (6.15). This assumes that matrix $\underline{\mathcal{A}}_{\mathrm{d}}$ of (2.20), which contains the DOA information, is perfectly known. Instead of matrix $\underline{\mathbf{R}}_{\mathrm{m}}$ only matrix $\underline{\mathbf{R}}_{\mathrm{s}}$ is estimated, since the interference scenario considered is a directionally uncorrelated scenario.

For the sake of comparison the following section also generates and discusses results assuming perfectly known channel IRs. Additionally the estimated matrix $\underline{\mathbf{R}}_{\mathrm{s}}$ is taken into consideration in data detection. The following seven cases are distinguished:

- The channel IRs are assumed to be perfectly known
  - I: The matrix $\underline{\mathbf{R}}_{\mathrm{s}}$ is considered in data detection
  - II: The estimated matrix $\hat{\underline{\mathbf{R}}}_{\mathrm{s}}$ is considered in data detection
  - III: The matrix $\underline{\mathbf{R}}_{\mathrm{s}}$ is replaced by $\underline{\mathbf{R}}_{\mathrm{s}} = \mathbf{I}^{(K_{\mathrm{a}})}$ in data detection
- The channel IRs are estimated
  - IV: The matrix $\underline{\mathbf{R}}_{\mathrm{s}}$ is considered in data detection and channel estimation
  - V: The estimated matrix $\hat{\underline{\mathbf{R}}}_{\mathrm{s}}$ is considered in data detection and channel estimation
  - VI: The estimated matrix $\hat{\underline{\mathbf{R}}}_{\mathrm{s}}$ is considered in data detection and $\underline{\mathbf{R}}_{\mathrm{s}}$ is replaced by $\underline{\mathbf{R}}_{\mathrm{s}} = \mathbf{I}^{(K_{\mathrm{a}})}$ in channel estimation
  - VII: The matrix $\underline{\mathbf{R}}_{\mathrm{s}}$ is replaced by $\underline{\mathbf{R}}_{\mathrm{s}} = \mathbf{I}^{(K_{\mathrm{a}})}$ in data detection and channel estimation

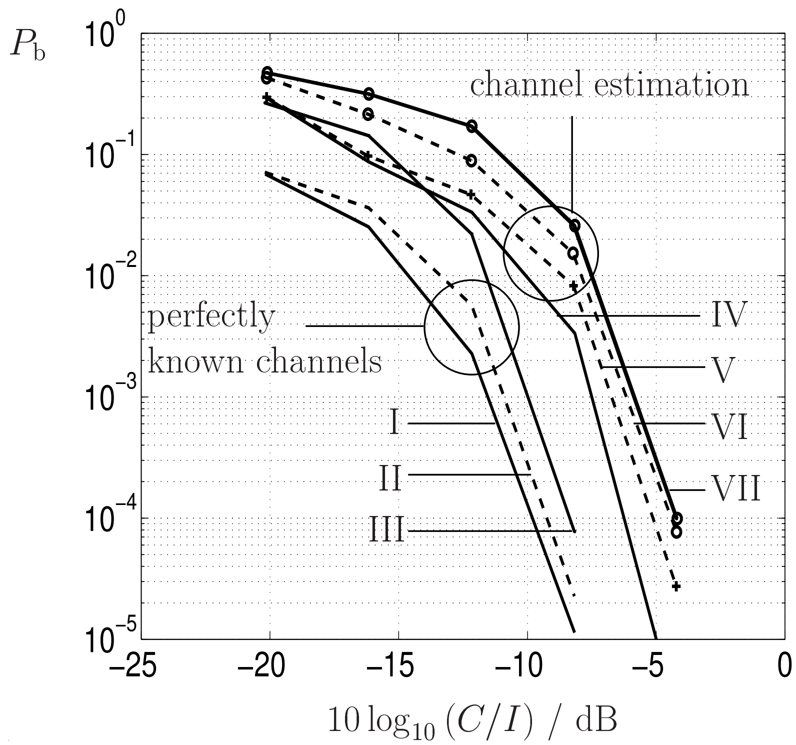

Fig. 8.28. Coded BER P_b for the cases I-VII; URA; $K_a = 4$; $K = 8$

The curves in Fig. 8.28 shows the simulation results. Curves I to III again show, as already demonstrated in Section 8.5.3, the BER performance in the case of perfectly known channel IRs. Cases IV through VII reflect the results taking into consideration channel estimation. The performance degradation is clearly evident when the channel IRs at the receiver are no longer perfectly known. Curve VII shows the worst performance. In this case solely the DOA information is utilized for channel estimation. If account is also taken of estimate $\hat{\underline{\mathbf{R}}}_s$ in channel estimation, a significant BER performance improvement with small C/I, but only a minimum BER performance improvement with higher C/I values can be achieved. Only additional consideration of the estimated matrix $\hat{\underline{\mathbf{R}}}_s$ in data detection leads to a considerable BER reduction with a given C/I. If matrix $\underline{\mathbf{R}}_s$ is perfectly known and if it is considered in both the channel estimation and data detection, the required C/I for a coded BER P_b of 10^{-3} can be reduced by 2 dB and, when using the estimate $\hat{\underline{\mathbf{R}}}_s$ by 1 dB.

8.7.3 MMSE based channel estimation

The following section contains simulation results which are generated under consideration of the MMSE based channel estimation presented in Section 6.4. This uses the same ITU IO B channel model as in the previous section.

If we want to determine the maximum performance improvement in channel estimation by MMSE, both matrices $\underline{\mathbf{R}}_{\tau,\mathrm{s}}$ of (2.13) and $\underline{\mathbf{R}}_{\mathrm{m}}$ of (6.8) must be perfectly known. Depending on the structure of the channel IRs, zeros can occur on the diagonals of the matrix $\underline{\mathbf{R}}_{\tau,\mathrm{s}}$, see (2.13). Matrix $\underline{\mathbf{R}}_{\tau,\mathrm{s}}$ is singular in this case. As explained in Section 6.4, this means that the use of the perfectly known matrix $\underline{\mathbf{R}}_{\tau,\mathrm{s}}$ cannot be considered in MMSE based channel estimation according to (6.18) (MMSE–JCE I). An assessment regarding the maximum improvement of channel estimation by using MMSE–BLE taking into consideration perfectly known matrix $\underline{\mathbf{R}}_{\tau,\mathrm{s}}$ versus the ZF–BLE is thus not possible with MMSE based channel estimation according to (6.18).

Section 6.4 showed that MMSE based channel estimation (6.18) can also be represented by (6.25). MMSE–JCE according to (6.25) (MMSE–JCE II) has the advantage that matrix $\underline{\mathbf{R}}_{\tau,\mathrm{s}}$ does not have to be directly inverted. The effects of this benefit on the quality of channel estimation are investigated below.

Fig. 8.29 shows the magnitudes $|\underline{\hat{R}}_{\tau,\mathrm{s},i,j}|$, $i,j = 1...K_{\mathrm{a}}KW$, of the components of an estimate $\underline{\hat{\mathbf{R}}}_{\tau,\mathrm{s}}$ for $K = 2$ users and $K_{\mathrm{a}} = 1$ antenna element at the receiver with a C/I of 0 dB. The zeros on the diagonals of estimate $\underline{\hat{\mathbf{R}}}_{\tau,\mathrm{s}}$ can be seen, which provide an indication of the singularity of the matrix $\underline{\hat{\mathbf{R}}}_{\tau,\mathrm{s}}$. By comparison, Fig. 8.30 shows matrix $\left(\underline{\hat{\mathbf{R}}}_{\mathrm{m}} + \underline{\tilde{\mathbf{G}}}\,\underline{\hat{\mathbf{R}}}_{\tau,\mathrm{s}}\,\underline{\tilde{\mathbf{G}}}^{*\mathrm{T}}\right)$ which is to be inverted when MMSE–BLE is used in accordance with (6.25), in which case estimated matrix $\underline{\hat{\mathbf{R}}}_{\tau,\mathrm{s}}$ is identical to the matrix depicted in Fig. 8.29. The fact that all diagonal elements are not equal to zero and the off-diagonal elements are smaller than the diagonal elements, leads to the conclusion that matrix $\left(\underline{\hat{\mathbf{R}}}_{\mathrm{m}} + \underline{\tilde{\mathbf{G}}}\,\underline{\hat{\mathbf{R}}}_{\tau,\mathrm{s}}\,\underline{\tilde{\mathbf{G}}}^{*\mathrm{T}}\right)$ is not singular and can thus be inverted.

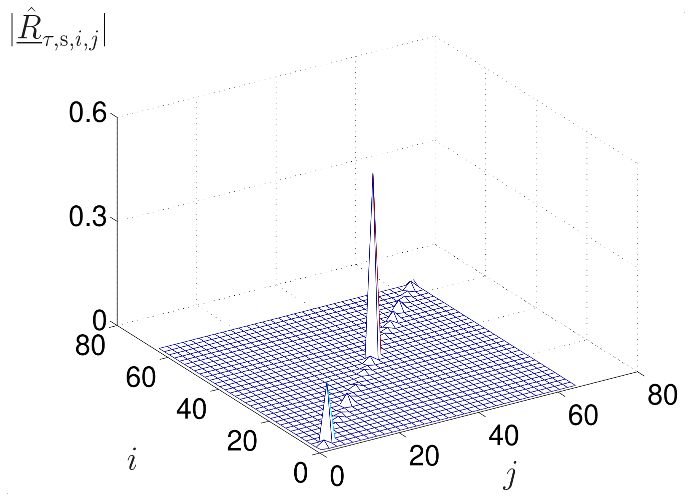

Fig. 8.29. Magnitudes $|\underline{\hat{R}}_{\tau,\mathrm{s},i,j}|$, $i,j = 1...K_{\mathrm{a}}KW$, of the components of an estimated matrix $\underline{\hat{\mathbf{R}}}_{\tau,\mathrm{s}}$; $K_{\mathrm{a}} = 1$; $K = 2$; $C/I = 0$ dB

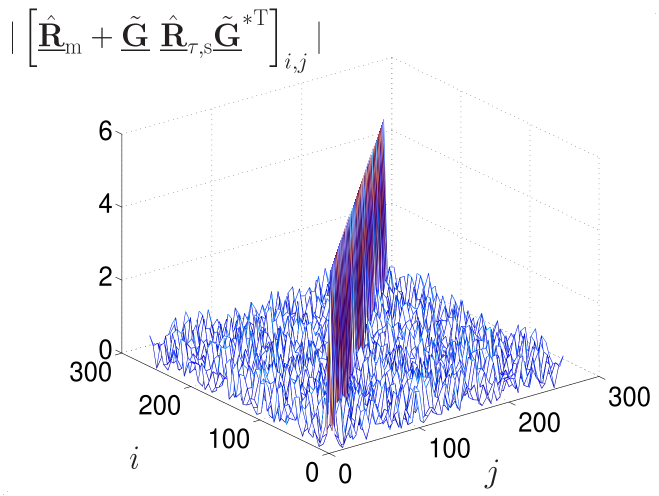

Fig. 8.30. Magnitudes $|\left[\underline{\hat{\mathbf{R}}}_{\mathrm{m}}+\underline{\tilde{\mathbf{G}}}\,\underline{\hat{\mathbf{R}}}_{\tau,\mathrm{s}}\,\underline{\tilde{\mathbf{G}}}^{*\mathrm{T}}\right]_{i,j}|$, $i,j=1...L-W+1$, of the components of a matrix $\underline{\hat{\mathbf{R}}}_{\mathrm{m}}+\underline{\tilde{\mathbf{G}}}\,\underline{\hat{\mathbf{R}}}_{\tau,\mathrm{s}}\,\underline{\tilde{\mathbf{G}}}^{*\mathrm{T}}$; $K_{\mathrm{a}}=1$; $K=2$; $C/I=0$ dB

The initial assumption is made that the total spatial channel IR vector $\underline{\mathbf{h}}_{\mathrm{s}}$ of (2.11) needed to form matrix $\underline{\hat{\mathbf{R}}}_{\tau,\mathrm{s}}$ in burst n_{b}, is perfectly known. With singular matrix $\underline{\hat{\mathbf{R}}}_{\tau,\mathrm{s}}$, generated according to (7.32) using the perfectly known total spatial channel IR vector $\underline{\mathbf{h}}_{\mathrm{s}}$, the investigation is to discover whether $\underline{\hat{\mathbf{R}}}_{\tau,\mathrm{s}}$ despite its singularity can be used, taking into consideration MMSE–JCE II according to (6.25) and which optimum channel estimation quality can be achieved with MMSE–JCE II. Fig. 8.31 shows the channel estimation matrix ϵ_{h} according to (6.27) for ZF channel estimation and MMSE–JCE II according to (6.25). In this case $K_{\mathrm{a}}=2$ antenna elements, $K=8$ users and intercell MAI scenario 1 described in Section 3.3.1 are taken into account. Spatial covariance matrix $\underline{\mathbf{R}}_{\mathrm{s}}$ of intercell MAI is replaced for MMSE–JCE II by the $K_{\mathrm{a}}\times K_{\mathrm{a}}$ identity matrix $\mathbf{I}^{(K_{\mathrm{a}})}$ and thereby not taken into account. As the curves in Fig. 8.31 show, taking into consideration the current nearly perfectly known matrix $\underline{\hat{\mathbf{R}}}_{\tau,\mathrm{s}}$, an almost perfect channel estimation can be achieved with MMSE–JCE II. Channel estimation error ϵ_{re} according to (6.33) in Fig. 8.32 shows the same tendency.

With its diagonal values, matrix $\underline{\mathbf{R}}_{\tau,\mathrm{s}}$ perfectly demonstrates the average of the sample values $\underline{h}_{\mathrm{s},w}^{(k,k_{\mathrm{a}})}$, $w=1...W$, $k=1...K$, $k_{\mathrm{a}}=1...K_{\mathrm{a}}$, of the channel IRs to be estimated. Utilizing *a priori* knowledge of the average energy of the sample values to be estimated with MMSE–JCE II leads, as the curves in Figs. 8.31 and 8.32 show, to a markedly better channel estimation result than by using ZF–JCE. Consideration of the almost perfectly known matrix $\underline{\hat{\mathbf{R}}}_{\tau,\mathrm{s}}$ already produces an almost optimum result, so that additionally considering matrix $\underline{\mathbf{R}}_{\mathrm{s}}$ in the MMSE–JCE can no longer bring any significant improvement in the channel estimation quality.

Below the estimate $\underline{\hat{\mathbf{R}}}_{\tau,\mathrm{s}}$ is obtained according to (7.32) considering the estimated total

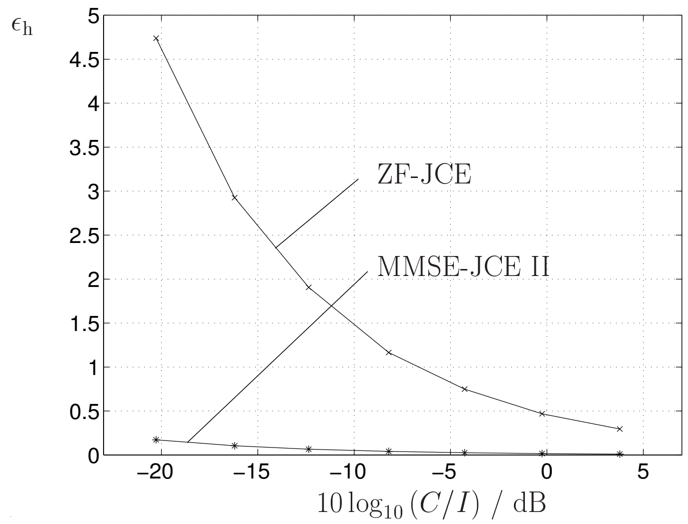

Fig. 8.31. RMSE ϵ_{h} with consideration of ZF–JCE and MMSE–JCE II with $\hat{\underline{\mathbf{R}}}_{\tau,\mathrm{s}}$ determined by taking account of perfectly known vector $\underline{\mathbf{h}}_{\mathrm{s}}$ and without consideration of the matrix $\hat{\underline{\mathbf{R}}}_{\mathrm{s}}$; intercell MAI scenario 1; ULA; $K_{\mathrm{a}} = 2$; $K = 8$

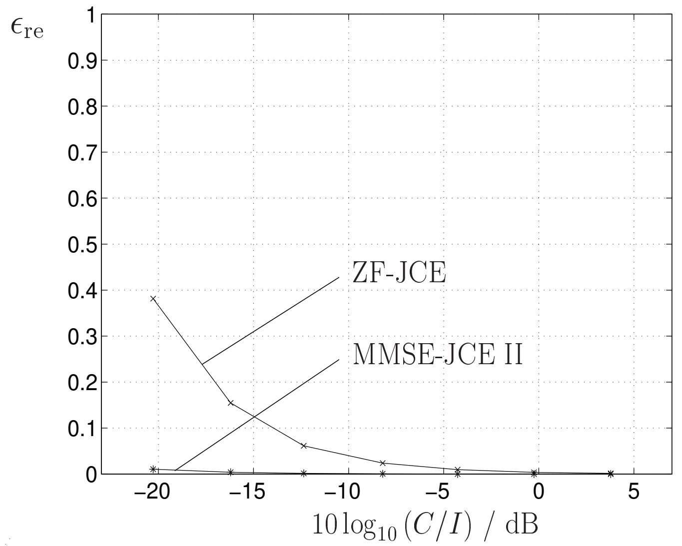

Fig. 8.32. Channel estimation error ϵ_{re} with consideration of ZF–JCE and MMSE–JCE II with $\hat{\underline{\mathbf{R}}}_{\tau,\mathrm{s}}$ determined by taking account of perfectly known vector $\underline{\mathbf{h}}_{\mathrm{s}}$ and without consideration of the matrix $\hat{\underline{\mathbf{R}}}_{\mathrm{s}}$; intercell MAI scenario 1; ULA; $K_{\mathrm{a}} = 2$; $K = 8$

spatial channel IR vector $\hat{\underline{\mathbf{h}}}_{\mathrm{s}}$, whereas $\hat{\underline{\mathbf{h}}}_{\mathrm{s}}$ is obtained by conventional channel estimation according to (6.11). Having determined $\hat{\underline{\mathbf{R}}}_{\tau,\mathrm{s}}$ that way, it is considered in MMSE based channel estimation according to (6.25) (MMSE–JCE II). The influence of the improvements to channel estimation on data detection is demonstrated by simulations. A URA configuration with $K_\mathrm{a} = 4$ antenna elements is used. A maximum number of $K = 8$ users are simultaneously active. The K users are equidistantly distributed on a circle around the BS, and their positions are kept fixed during the simulations. The once determined estimates $\hat{\underline{\mathbf{R}}}_{\mathcal{T},\mathrm{s}}$ and $\hat{\underline{\mathbf{R}}}_\mathrm{s}$ are continuously updated according to (7.10) by the estimation of $\underline{\mathbf{R}}_{\mathcal{T},\mathrm{s}}$ and $\underline{\mathbf{R}}_\mathrm{s}$ based on the currently received midamble section and data block, respectively. The curves in Fig. 8.33 show ϵ_h of (6.27) versus C/I for ZF–JCE and MMSE–JCE, respectively, with and without consideration of $\hat{\underline{\mathbf{R}}}_\mathrm{s}$. In all cases the channel estimation error ϵ_h is reduced by increasing C/I, and it is always lower when performing MMSE–JCE instead of ZF–JCE. For low values C/I, where much interference is present, consideration of the estimate $\hat{\underline{\mathbf{R}}}_\mathrm{s}$ in the MMSE–JCE further improves the channel estimation quality and reduces the channel estimation error ϵ_h. With increasing C/I, i.e. by reducing the interference, the consideration of the estimated spatial interference covariance matrix $\hat{\underline{\mathbf{R}}}_\mathrm{s}$ in the MMSE–JCE does not lead to any significant improvements of the channel estimation error ϵ_h compared to the case where the estimated spatial interference covariance matrix $\hat{\underline{\mathbf{R}}}_\mathrm{s}$ is not considered in MMSE–JCE.

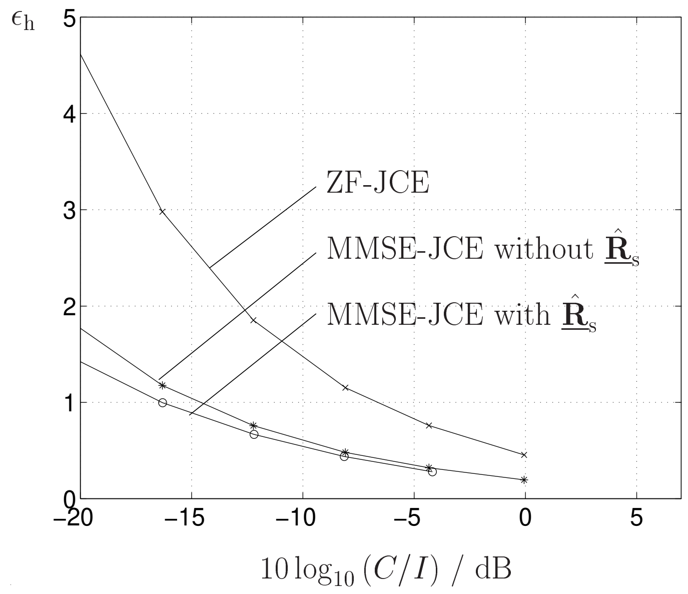

Fig. 8.33. Channel estimation error ϵ_h when using ZF–JCE and MMSE–JCE II with and without consideration of $\hat{\underline{\mathbf{R}}}_\mathrm{s}$ in JCE, respectively; $K = 8$; $K_\mathrm{a} = 4$; URA

In the following, the influence of the channel estimation quality improvements shown by the curves in Fig. 8.33 on the data detection is investigated. Therefore, the uncoded BERs P_bu for the following cases are shown in the Figs. 8.34 and 8.35:

- $\hat{\underline{\mathbf{R}}}_\mathrm{s}$ is not considered in data detection according to (5.12).

  I: ZF–JCE.

II: MMSE–JCE without consideration of $\underline{\hat{\mathbf{R}}}_{\mathrm{s}}$ in the channel estimation.

III: MMSE–JCE under consideration of $\underline{\hat{\mathbf{R}}}_{\mathrm{s}}$ in the channel estimation.

IV: The channel IRs are perfectly known at the receiver.

- $\underline{\hat{\mathbf{R}}}_{\mathrm{s}}$ is considered in the data detection according to (5.12).

V: MMSE–JCE under consideration of $\underline{\hat{\mathbf{R}}}_{\mathrm{s}}$ in the channel estimation.

VI: The channel IRs are perfectly known at the receiver.

With regard to BER, a channel estimate improvement at low values C/I has no effect since the high interference still has an impact on data detection, see (5.12). Fig. 8.33 shows that the great advantage of MMSE–JCE compared to ZF–JCE is based on the fact that, for achieving the same channel estimation quality, much lower values C/I are required when utilizing MMSE–JCE instead of ZF–JCE. The consequences for data detection become obvious from Fig. 8.34. The required C/I for an uncoded BER P_{bu} of 10^{-3} is reduced by 2.7 dB when applying MMSE–JCE instead of ZF–JCE, see the curves I and III in Fig. 8.34. Curves I and IV in Fig. 8.34 show that with perfect knowledge of the

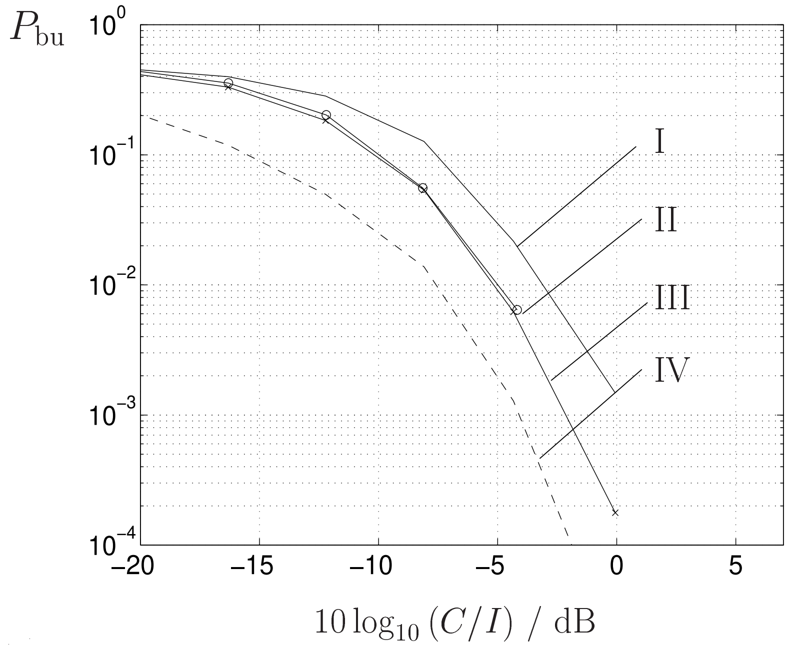

Fig. 8.34. Uncoded BER P_{bu} for the cases I-IV when applying ZF–JCE and MMSE–JCE II, respectively; $K = 8$; $K_{\mathrm{a}} = 4$; URA

channel IRs one can improve the system performance by 4.5 dB at an uncoded BER P_{bu} of 10^{-3}. Comparing curves II and III in Fig. 8.34, the channel estimation improvement at low C/I shown by ϵ_{h} in Fig. 8.33 which is obtained under consideration of $\underline{\hat{\mathbf{R}}}_{\mathrm{s}}$ in MMSE–JCE, shows hardly any beneficial influence on data detection. For high values

C/I BER curves II and III show no differences. As already mentioned, the estimate $\hat{\underline{\mathbf{R}}}_{\tau,\mathrm{s}}$ has on its diagonal the estimated values of the average energy of the components $\underline{h}_{\mathrm{s},w}^{(k,k_\mathrm{a})}$, $w = 1...W$, $k = 1...K$, $k_\mathrm{a} = 1...K_\mathrm{a}$ of the channel IRs vectors $\hat{\underline{\mathbf{h}}}_\mathrm{s}$. Consideration of the channel information regarding the average energy of the components $\underline{h}_{\mathrm{s},w}^{(k,k_\mathrm{a})}$, $w = 1...W$, $k = 1...K$, $k_\mathrm{a} = 1...K_\mathrm{a}$, in channel estimation suppresses a part of the interference. For example, for small components $\underline{h}_{\mathrm{s},w}^{(k,k_\mathrm{a})}$, $w = 1...W$, $k = 1...K$, $k_\mathrm{a} = 1...K_\mathrm{a}$, with strong interference, large estimated values $\hat{\underline{h}}_{\mathrm{s},w}^{(k,k_\mathrm{a})}$, $w = 1...W$, $k = 1...K$, $k_\mathrm{a} = 1...K_\mathrm{a}$ can be assumed with conventional channel estimation. If knowledge of the expected average energies of the components $\underline{h}_{\mathrm{s},w}^{(k,k_\mathrm{a})}$, $w = 1...W$, $k = 1...K$, $k_\mathrm{a} = 1...K_\mathrm{a}$, are also considered for MMSE–JCE and if components with strong interference $\hat{\underline{h}}_{\mathrm{s},w}^{(k,k_\mathrm{a})}$, $w = 1...W$, $k = 1...K$, $k_\mathrm{a} = 1...K_\mathrm{a}$, assume values which lie within the order of magnitude of the amounts of the actual components $\underline{h}_{\mathrm{s},w}^{(k,k_\mathrm{a})}$, $w = 1...W$, $k = 1...K$, $k_\mathrm{a} = 1...K_\mathrm{a}$, this coincidentally suppresses a part of the interference. Additional consideration of estimation $\hat{\underline{\mathbf{R}}}_\mathrm{s}$ then does not lead to any further significant improvement in channel estimation. This is shown particularly in Fig. 8.33 and in Fig. 8.34 for large C/I.

The curves in Fig. 8.35 shows the uncoded BERs P_bu valid for ZF–JCE and MMSE–JCE under consideration of $\hat{\underline{\mathbf{R}}}_\mathrm{s}$ in data detection according to (5.12). From the curves in Fig. 8.35 it becomes obvious that consideration of $\hat{\underline{\mathbf{R}}}_\mathrm{s}$ in data detection significantly improves the system performance. To reach an average uncoded BER P_bu of 10^{-3} a

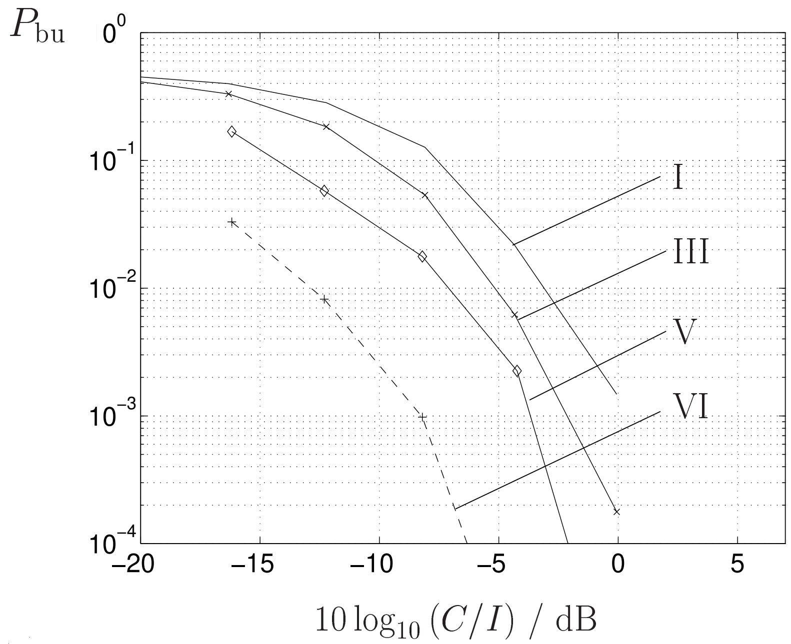

Fig. 8.35. Uncoded BER P_bu for the cases I, III, V and VI when applying ZF–JCE and MMSE–JCE II, respectively; $K = 8$; $K_\mathrm{a} = 4$; URA

specific C/I $\gamma_{\mathrm{ZF-JCE}}$ or $\gamma_{\mathrm{MMSE-JCE}}$ is necessary in each case when using ZF–JCE and

MMSE–JCE II without considering matrix $\underline{\hat{\mathbf{R}}}_{\mathrm{s}}$ or $\underline{\mathbf{R}}_{\mathrm{s}}$ in channel and data estimation.

In the same way a minimum C/I γ_{min} can be specified that with consideration of perfectly known channel IRs in data detection must be set to achieve P_{bu} equal to 10^{-3}. The differences

$$\Delta\gamma = \gamma_{\mathrm{ZF-JCE}} - \gamma_{\mathrm{MMSE-JCE}} \tag{8.5}$$

or

$$\Delta\gamma_{\mathrm{max}} = \gamma_{\mathrm{ZF-JCE}} - \gamma_{\mathrm{min}} \tag{8.6}$$

are shown in Fig. 8.36 depending on number of users K. In Fig. 8.36 this illustrates how the difference of the required C/I increases to achieve an uncoded BER P_{bu} of 10^{-3} with an increase in number of users K. As the number of users K increases, the rise in the SNR

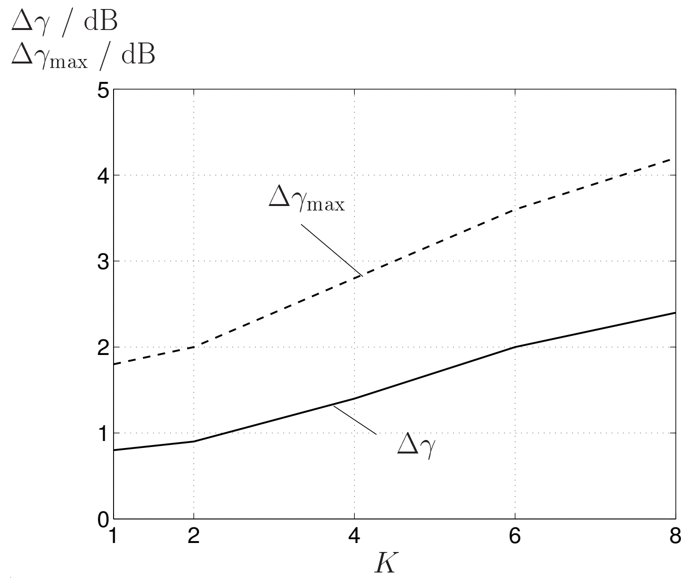

Fig. 8.36. Difference $\Delta\gamma$ according to (8.5) and $\Delta\gamma_{\mathrm{max}}$ according to (8.6) depending the number of users K; $K_{\mathrm{a}} = 4$; URA

degradation of channel estimation with MMSE is less than with channel estimation with the ZF algorithm and is therefore responsible for the increasing difference of the required C/I as the number of users K increases.

9 Summary

9.1 English

It is well known that the performance of mobile radio systems can be significantly enhanced by the application of adaptive antennas which consist of multi-element antenna arrays plus signal processing circuitry. In the thesis the utilization of such antennas as receive antennas in the uplink of mobile radio air interfaces of the type TD–CDMA is studied. Especially, the incorporation of covariance matrices of the received interference signals into the signal processing algorithms is investigated with a view to improve the system performance as compared to state of the art adaptive antenna technology. These covariance matrices implicitly contain information on the directions of incidence of the interference signals, and this information may be exploited to reduce the effective interference power when processing the signals received by the array elements. As a basis for the investigations, first directional models of the mobile radio channels and of the interference impinging at the receiver are developed, which can be implemented on the computer at low cost. These channel models cover both outdoor and indoor environments. They are partly based on measured channel impulse responses and, therefore, allow a description of the mobile radio channels which comes sufficiently close to reality. Concerning the interference models, two cases are considered. In the one case, the interference signals arriving from different directions are correlated, and in the other case these signals are uncorrelated. After a visualization of the potential of adaptive receive antennas, data detection and channel estimation schemes for the TD–CDMA uplink are presented, which rely on such antennas under the consideration of interference covariance matrices. Of special interest is the detection scheme MSJD (Multi Step Joint Detection), which is a novel iterative approach to multi-user detection. Concerning channel estimation, the incorporation of the knowledge of the interference covariance matrix and of the correlation matrix of the channel impulse responses is enabled by an MMSE (Minimum Mean Square Error) based channel estimator. The presented signal processing concepts using covariance matrices for channel estimation and data detection are merged in order to form entire receiver structures. Important tasks to be fulfilled in such receivers are the estimation of the interference covariance matrices and the reconstruction of the received desired signals. These reconstructions are required when applying MSJD in data detection. The considered receiver structures are implemented on the computer in order to enable system simulations. The obtained simulation results show that the developed schemes are very promising in cases, where the impinging interference is highly directional, whereas in cases with the interference directions being more homogeneously distributed over the azimuth the consideration of the interference covariance matrices is of only limited benefit. The thesis can serve as a basis for practical system implementations.

9.2 German

Das Verwenden adaptiver Antennen an den Basisstationen in der Aufwärtstrecke eines Mobilfunksystems eröffnet die Möglichkeit, die Richtungsinhomogenität des Mobilfunkkanals auszunutzen und eine signifkante Verbesserung der Performanz des Mobilfunksystems zu erreichen. Die adaptiven Antennen setzen sich dabei aus mehreren Antennenelementen zusammen, die eine Array-Antenne bilden, wobei die an jedem einzelnen Antennenelement empfangenen Signale einer gemeinsamen Signalverarbeitungseinheit zugeführt werden. Der richtungsselektive Einfall der von den einzelnen mobilen Teilnehmern kommenden Wellen an den Basisstationen des betrachteten zellularen Mobilfunksystems hat bestimmte räumliche und zeitliche Korrelationen der Empfangssignale an den einzelnen Antennenelementen zur Folge. In der vorliegenden Arbeit werden Möglichkeiten des Ausnutzens räumlicher und zeitlicher Korrelationseigenschaften sowohl der Nutz- als auch der Interferenzsignale in Form von Korrelations- bzw. Kovarianzmatrizen betrachtet, die im Rahmen einer gemeinsamen räumlichen und zeitlichen Signalverarbeitung Verbesserungen der Systemperformanz hervorrufen. Das Berücksichtigen dieser Korrelations- bzw. Kovarianzmatrizen impliziert ein Ausnutzen der Kenntnis der Einfallsrichtungen der Nutz- und der Interferenzsignale in der Signalverarbeitung, so daß die effektiv empfangene Interferenz reduziert und der Empfang der Nutzsignale begünstigt wird. Im allgemeinen sind insbesondere die räumlichen Korrelationseigenschaften der empfangenen Nutz- und Interferenzsignale a-priori bei der Signalverarbeitung nicht bekannt. Das Beschaffen dieser Information, d.h. das Schätzen der ensprechenden Korrelations- und Kovarianzmatrizen, ist somit auch ein zentrales Thema dieser Arbeit.

Die in der vorliegenden Arbeit betrachteten adaptiven Antennenkonzepte werden in der Aufwärtsstrecke eines Mobilfunksystems der dritten Generation untersucht, das auf dem Luftschnittstellenkonzept TD–CDMA (Time Division CDMA) basiert. TD–CDMA ist Bestandteil des von ETSI (European Telecommunications Standards Institute) gewählten Standards für das Luftschnittstellenkonzept von Mobilfunksystemen der dritten Generation in Europa, und TD–CDMA ist bei den Standardisierungsarbeiten von ITU (International Telecommunications Union) und 3GPP (3rd Generation Partnership Project) in den internationalen Standard der Luftschnittstellenkonzepte für Mobilfunksysteme der dritten Generation eingebracht worden.

Zur simulativen Bewertung der erzielbaren Performanzverbesserungen durch adaptive Antennen sind Modelle erforderlich, die neben der Zeitdispersion und Frequenzselektivität des Mobilfunkkanals auch die Richtungsinhomogenität des Mobilfunkkanals berücksichtigen, welche im wesentlichen von der Topologie des Ausbreitungsgebiets abhängigt. Solche Modelle sind gleichermaßen für Kanalimpulsantworten der Nutzsignale als auch für Interferenzsignale erforderlich. Unter Berücksichtigung des betrachteten zellularen TD-CDMA-Systems lassen sich Nutzsignale als Signale beschreiben, die von gleichzeitig im selben Frequenzband aktiven Teilnehmern einer Zelle ausgehen und an der Basisstation der betrachteten Zelle empfangen werden. Das gleichzeitige Senden der Nutzsignale der Teilnehmer einer Zelle führt zu Intrazellinterferenz an der Basisstation. Im Gegensatz dazu werden Interferenzsignale, die von Teilnehmern benachbarter Zellen stammen, als Interzellinterferenzsignale bezeichnet. Als Basis für die Systemuntersuchungen in der vorliegenden Arbeit werden einfache und leicht zu implementierende direktionale Kanalmodelle für die Nutzsignale entwickelt. In einer urbanen Umgebung gemessene Kanalimpulsantworten werden zur Kanalmodellierung herangezogen, wodurch eine ausreichende Nähe zur Realität gegeben ist. Nicht-richtungsselektiv gemessene Kanalimpulsantworten werden dabei diskreten Einfallsrichtungen am Empfänger zugeordnet. Für Simulationen in Innenraum-Bereichen wird ein direktionales Kanalmodell auf der Basis nicht-direktionaler ITU-Kanalmodelle erstellt. Dabei können unterschiedliche Kanalkoeffizienten einer nach dem ITU-Modell generierten Kanalimpulsantwort unterschiedlichen Einfallsrichtungen am Ort der Basisstation zugeordnet werden. Bei Verwenden der ITU-Modelle wird angenommen, daß alle Kanalimpulsantworten der Nutzsignale das gleiche Verzögerungs-Leistungsdichte-Spektrum besitzen. Für Untersuchungen von Mobilfunksystemen mit gemeinsamer Detektion der Teilnehmersignale, wie sie bei TD–CDMA vorzugsweise verwendet wird, kann diese Eigenschaft zu Ergebnissen führen, die zu optimistisch sind. Als Lösung dieses Problems wird ein einfaches Ray-Tracing-Modell zum Generieren von Kanalimpulsantworten vorgestellt, wobei ein rechteckiger Raum als Ausbreitungsgebiet angenommen wird. Dabei resultieren aufgrund der unterschiedlichen Positionen der Teilnehmer im Raum unterschiedliche Verzögerungs-Leitungsdichte-Spektren der Kanalimpulsantworten der einzelnen Teilnehmer. Durch die Modellierung von zwei Zellen in einem Raum können sowohl Nutz- als auch Interzellinterferenzsignale die gleichen Ausbreitungseigenschaften haben und gleichermaßen modelliert werden.

Bei Berücksichtigen von Interzellinterferenzsignalen, die aus benachbarten Zellen stammen, ist in zellularen Systemen die Anzahl der an einer Basisstation des betrachteten TD-CDMA-Systems zur empfangenen Interferenz beitragenden Interzellinterferezsignale im allgemeinen größer als die Anzahl der empfangenen Nutzsignale. Betrachtet man die Gesamtheit der sich an der Basisstation überlagernden Interzellinterferenzsignale, so muß demnach die Interferenzsignalmodellierung nicht zwingend in gleicher Weise wie die Kanalmodellierung erfolgen. Die Überlagerung einer Vielzahl von Interferenzsignalen erlaubt eine Modellierung der Interzellinterferenz als Musterfunktionen eines stationären mittelwertfreien Gauß-Prozesses, wobei die Interzellinterferenzsignale die gleiche spektrale Form wie die Nutzsignale aufweisen. Die zeitlichen Korrelationen eines einzelnen Interzellinterferenzsignals sind somit durch das Festlegen der spektralen Form gegeben. Räumliche Korrelationen der Interzellinterferenzsignale, d.h. Korrelationen von Interferenzsignalen, die an unterschiedlichen Antennenelementen empfangen werden, hängen von der Geometrie der Array-Antenne sowie von den Einfallsrichtungen der Interferenzsignale ab. In der vorliegenden Arbeit geht man bei der Interzellinterferenzmodellierung davon aus, daß Interzellinterferenzsignale, die aus unterschiedlichen Richtungen am Empfangsort eintreffen, entweder unkorreliert oder korreliert sind. Darüberhinaus werden unterschiedliche Interzellinterferenzszenarien betrachtet, die auf den Annahmen beruhen, daß die Interzellinterferenz aus einigen wenigen diskreten Richtungen, d.h. stark direktional, oder azimutal kontinuierlich an der Basisstation eintrifft. Im Rahmen dieser Betrachtungen wird mathematisch veranschaulicht, daß die räumlichen und zeitlichen Korrelationen der Interferenzsignale durch Kovarianzmatrizen dargestellt werden können.

In den simulativen Untersuchungen des TD-CDMA-Systems werden sowohl 1-dimensionale, d.h. lineare, als auch unterschiedliche 2-dimensionale, d.h. rechteckige, kreuzförmige und kreisförmige, Array-Antennenkonfigurationen betrachtet. Um einen Eindruck vom Verbesserungspotential der Systemperformanz durch den Einsatz adaptiver Antennen der oben genannten Konfigurationen zu vermitteln, wird für jede dieser Antennenkonfigurationen der richtungsabhängige Gewinn der Array-Antenne gegenüber einer einzelnen omnidirektionalen Antenne an der Basisstation unter Annahme eines einfachen Übertragungsmodells mit und ohne Berücksichtigen von Interferenzkovarianzmatrizen ermittelt und in Diagrammen veranschaulicht.

Ziel dieser Arbeit ist es, wie eingangs erwähnt wurde, die Signalverarbeitung, d.h. insbesondere die Datendetektion und die Kanalschätzung an den Basisstationen eines TD-CDMA-Systems mit adaptiven Antennen, durch Berücksichtigen von Korrelations- bzw. Kovarianzmatrizen zu verbessern. Das bevorzugte Detektionsverfahren in zeitgeschlitzten CDMA-Systemen ist die gemeinsame lineare Datendetektion der Teilnehmersignale (joint detection, JD), wobei alle Nutzsignale der gleichzeitig im selben Frequenzband aktiven Teilnehmer einer Zelle gemeinsam detektiert werden. Die gemeinsame Datendetektion wird unter Verwenden des ZF-Algorithmus (Zero Forcing) realisiert. Der ZF-Algorithmus eliminiert Intrazellinterferenz sowie Intersymbolinterferenz bei der Detektion. Im Gegenzug dazu wird die den Detektionsprozeß beeinträchtigende Interzellinterferenz erhöht, was im allgemeinen als Degradation des Signal-Stör-Verhältnisses bezeichnet wird. Naturgemäß erlaubt der ZF-Algorithmus das Berücksichtigen der Interzellinterferenzkovarianzmatrix. In konventionellen TD-CDMA-Systemen wird jedoch von dieser Möglichkeit bislang kein Gebrauch gemacht. Berücksichtigt man die Interzellinterferenzkovarianzmatrix im ZF-Algorithmus, so kann die effektiv empfangene Interferenz reduziert werden. Neben dem ZF-Algorithmus ist im Rahmen der Betrachtungen zur Datendetektion das Detektionsverfahren MSJD (Muti Step Joint Detection), das einen neuartigen Ansatz iterativer Mehrteilnehmerdetektion darstellt, von besonderem Interesse. Beim Verfahren MSJD werden die Detektionsergebnisse einer ersten bzw. vorhergehenden Stufe dazu benutzt, die Detektion einer Folgestufe zu verbessern. Hierbei wird die Zahl der gemeinsam in einer Zelle aktiven Teilnehmer in zwei Gruppen unterteilt, wobei alle Signale der Teilnehmer einer Gruppe gemeinsam detektiert werden. Die im Gegensatz zu konventionellem JD vergleichsweise geringere Anzahl an gemeinsam zu detektierenden Teilnehmersignalen pro Gruppe führt zu einer geringeren Degradation des Signal-Stör-Verhältnisses bei der Detektion. Gleichzeitig wird dabei die gemeinsame Detektion der Signale einer Gruppe durch Intrazellinterferenz beeinträchtigt, da nicht alle Teilnehmersignale der betrachteten Zelle in einem einzigen gemeinsamen Detektionsprozeß einbezogen werden und somit Intrazellinterferenz nicht vollständig eliminiert wird. Eine Reduktion dieser Intrazellinterferenz erreicht man dadurch, daß man mit den nach einem ersten Detektionsschritt vorliegenden Detektionsergebnissen die von einem Teil der Teilnehmer herrührenden Empfangssignale näherungsweise rekonstruiert und diese rekonstruierten Signale von dem ursprünglichen Empfangssignal abzieht. Man erhält ein modifiziertes Empfangssignal, das weniger Teilnehmersignale enthält. Hat man zwei Teilnehmergruppen und gehen die rekonstruierten Signale gerade auf die Signale einer Gruppe zurück, so erhält man nach Abzug der rekonstruierten Signale ein Empfangssignal, das im wesentlichen nur noch aus Signalen der anderen Gruppe besteht und somit erheblich weniger Intrazellinterferenz ausgesetzt ist als im vorangegangenen Detektionsschritt. Bei zusätzlichem Berücksichtigen adaptiver Antennen in MSJD kann die Intrazellinterferenz bereits im ersten Schritt reduziert werden, indem räumlich benachbarte Teilnehmer in einer Gruppe zusammengefaßt werden. Die Signale der Teilnehmer der beiden Gruppen erreichen die Basisstation im allgemeinen in diesem Fall aus unterschiedlichen Winkelbereichen, womit durch den Einsatz adaptiver Antennen die durch die Signale der einen Gruppe hervorgerufene Intrazellinterferenz bei der Detektion der Signale der jeweils anderen Gruppe reduziert werden kann. Ebenso wie der ZF-Algorithmus erlaubt auch MSJD das Berücksichtgen der Interzellinterferenzkovarianzmatrix in der Detektion der Teilnehmersignale der einzelnen Gruppen. Die simulative Untersuchung der erzielbaren Systemperformanz durch Berücksichtigen von Interferenzkovarianzmatrizen in MSJD ist ebenfalls Gegenstand dieser Arbeit.

Neben der Verbesserung von Datendetektionsalgorithmen unter Verwendung von Interferenzkovarianzmatrizen werden auch Kanalschätzverfahren untersucht, die ein Berücksichtigen dieser Matrizen erlauben. Der MMSE-Algorithmus (Minimum Mean Square Error) erlaubt neben dem Berücksichtigen der Interzellinterferenzkovarianzmatrix ebenso das Berücksichtigen der Korrelationsmatrix der zu schätzenden Kanalimpulsantworten. Die Korrelationsmatrix der Kanalimpulsantworten kann auf der Basis bereits zu früheren Zeitpunkten erhaltener Kanalschätzergebnisse gewonnen werden, wenn von einer hinreichend geringen Mobilität der Teilnehmer in dem betrachteten Mobilfunksystem ausgegangen werden kann. Die Korrelationsmatrizen der Kanalimpulsantworten beinhalten die Richtungsinformation der Nutzsignale. Da in der Datendetektion die Kanalinformation berücksichtigt wird, nutzt man implizit die Richtungsinformation der Nutzsignale auch bei der Datendetektion aus. Somit ist es nicht erforderlich, noch zusätzlich Korrelationsmatrizen der Nutzsignale in der Datendetektion zu berücksichtigen.

Die vorgestellten Signalverarbeitungskonzepte, die ein Berücksichtigen von Kovarianz- bzw. Korrelationsmatrizen sowohl in der Datendetektion als auch in der Kanalschätzung erlauben, werden in unterschiedlichen Empfängerstrukturen zusammengefaßt. Dabei unterscheiden sich die Empfängerstrukturen im wesentlichen durch die Art und Weise mit der sie die erforderliche Kenntnis der Korrelations- bzw. Kovarianzmatrizen erlangen. Von besonderem Interesse ist hierbei ein iteratives Verfahren, das auf der Basis rekonstruierter empfangener Nutzsignale ein Schätzen der Interzellinterferenzkovarianzmatrix ermöglicht. Entscheidend für die Schätzqualität der Kovarianzmatrix ist die Qualität der Signalrekonstruktion, die aus diesem Grund ebenfalls im Rahmen dieser Arbeit betrachtet wird.

Auf der Grundlage und unter Berücksichtigung der entwickelten Kanal- und Interferenzmodelle werden die Vorteile adaptiver Antennen in der vorliegenden Arbeit sowohl theoretisch als auch durch Simulationen der Aufwärtsstrecke des TD-CDMA-Systems dargestellt. Die erreichbare Bitfehlerrate bei gegebenen Signal-Stör-Verhältnis wird als Performanzmaß angenommen. Die Simulationsergebnisse zeigen exemplarisch, daß direktionale Interzellinterferenz, die zu räumlichen Korrelationen an den einzelnen Empfangsantennen eines Antennen-Arrays führt, einen degradierenden Einfluß auf die Bitfehlerrate des betrachteten TD-CDMA-Systems mit adaptiven Antennen hat. Das Berücksichtigen der Interzellinterferenzkovarianzmatrix mildert diesen degradierenden Effekt. Selbst eine Elimination stark direktionaler Interferenz kann durch das Berücksichtigen der genannten Kovarianzmatrix erreicht werden. Im Falle stark direktionaler Interzellinterferenz kann das erforderliche Signal-Stör-Verhältnis zum Erreichen einer Bitfehlerrate von 10^{-3} um 2.5 dB bzw. 5 dB reduziert werden, wenn vier bzw. 16 Antennenelemente am Empfänger berücksichtigt werden. Näherungsweise die Hälfte der Verbesserungen lassen sich erreichen, wenn die geschätzten Kovarianzmatrizen berücksichtigt werden. Im Falle direktional homogener Interzellinterferenz können nur geringe Performanzverbesserungen durch das Berücksichtigen von Kovarianzmatrizen erreicht werden. Bei diesen Szenarien ist es in Ausnahmefällen möglich, daß die Qualität der Schätzung der Kovarianzmatrizen nicht gut genug ist, so daß ihre Berücksichtigung zu einer schlechteren Performanz führt als das Nicht-Berücksichtigen.

Im allgemeinen stellt das Berücksichtigen der Kovarianzmatrizen in der TD-CDMA-Aufwärtsstrecke mit adaptiven Antennen eine Möglichkeit zum Verbessern der Bitfehlerrate in Mobilfunksystemen dar. Die vorliegende Arbeit kann somit als Basis für zukünftige Systemimplementierungen angesehen werden.

Appendix

A.1 Abbreviations

1D	1–Dimensional
2D	2–Dimensional
2G	2^{nd} Generation
3G	3^{rd} Generation
3GPP	3G Partnership Project
AWGN	Additive White Gaussian Noise
BER	Bit Error Rate
BLAST	Bell Labs LAyered Space–Time Architecture
BS	Base Station
CDMA	Code Division Multiple Access
CMA	Constant Modulus Algorithm
COST	European COoperation in the Field of Scientific and Technical Research
CROSS	CROSS shaped antenna array
DMI	Direct Matrix Inversion
DOA	Direction–Of–Arrival
DOD	Direction–Of–Departure
DPE	Deterministic Parametric Estimation
DS	Direct Sequence
EGC	Equal Gain Combining
EM	Expectation–Maximization
ESPRIT	Estimation of Signal Parameters via Rotational Invariance Techniques
ETSI	European Telecommunications Standards Institute
FDD	Frequency Division Duplex
FDMA	Frequency Division Multiple Access
FEC	Forward Error Correction
GMSK	Gaussian Minimum Shift Keying
GSM	Global System for Mobile Communications
IC	Interference Cancellation
IMT-2000	International Mobile Telecommunications 2000
IR	Impulse Response
ISI	InterSymbol Interference
ITU	International Telecommunications Union
JCE	Joint Channel Estimation
JD	Joint Detection
JT	Joint Transmission
LOS	Line Of Sight

LS	Least Square
MAI	Multiple Access Interference
MD	Multiuser Detection
MDL	Minimum Discription Length
ME	Maximum Entropy
MIMO	Multiple In, Multiple Out
ML	Maximum Likelihood
MLSE	Maximum Likelihood Sequence Estimation
MLSSE	Maximum Likelihood Symbol–by–Symbol Estimation
MMSE	Minimum Mean Square Error
MMSE-BLE	Minimum Mean Square Error Block Linear Equalizer
MRC	Maximal Ratio Combining
MS	Mobile Station
MSE	Mean Square Error
MSJD	Multi Step Joint Detection
MUSIC	MUltiple SIgnal Classification
MV	Minimum noise Variance
RF	Radio Frequency
RING	RING shaped antenna array
RL	Reference Line
RLS	Recursive Least Square
RMSE	Root Mean Square Error
RP	Reference Point
SAGE	Space–Altering Generalized Expectation–Maximization
SC	Selection Combining
SD	Single user Detection
SDMA	Space Division Multiple Access
SE	Spectral Estimation
SFIR	Spatial Filtering for Interference Reduction
SFU	Spatial Filtering at the Uplink
SIMO	Single In, Multiple Out
SIR	Signal–to–Interference Ratio
SNR	Signal–to–Noise Ratio
SQRLS	Square–Root RLS
SR	Spatial Reference
TD-CDMA	Time Division CDMA
TDD	Time Division Duplex
TDMA	Time Division Multiple Access
TR	Temporal Reference
UL	UpLink
ULA	Uinform Linear Array
UMTS	Universal Mobile Telecommunications System
URA	Uinform Rectangular Array

UTRA	UMTS Terrestrial Radio Access
W-CDMA	Wideband CDMA
ZF	Zero Forcing
ZF–BLE	Zero Forcing Block Linear Equalizer

A.2 Symbols

$\alpha^{(k_\mathrm{a})}$	angle spanned by RL and the line connecting RP with the antenna elements $k_\mathrm{a} = 1...K_\mathrm{a}$
$\underline{\mathbf{a}}^{(k,k_\mathrm{d})}$	steering vector for the k_d–th DOA of user k, $k_\mathrm{d} = 1\ldots K_\mathrm{d}$, $k = 1\ldots K$
$\underline{\mathbf{a}}_\mathrm{d}^{(k,k_\mathrm{a})}$	steering vector for the k_d DOAs of the IR of user k valid for the k_a–th antenna element, $k = 1...K$, $k_\mathrm{a} = 1...K_\mathrm{a}$
$\underline{a}_{k_\mathrm{d}}^{(k,k_\mathrm{a})}$	steering factor, k_d-th element of the steering vector $\underline{\mathbf{a}}_\mathrm{d}^{(k,k_\mathrm{a})}$, $k = 1...K$, $k_\mathrm{a} = 1...K_\mathrm{a}$
$\underline{a}_{k_\mathrm{a}}^{(k,k_\mathrm{d})}$	steering factor, k_a-th element of the steering vector $\underline{\mathbf{a}}^{(k,k_\mathrm{d})}$, $k = 1...K$, $k_\mathrm{d} = 1...K_\mathrm{d}$
$\underline{\mathbf{a}}$	steering vector in the case of $K = 1$ user and single direction channels, i.e. $K_\mathrm{d} = 1$
$\underline{\mathbf{A}}$	system matrix, which is determined by the CDMA codes $\underline{\mathbf{c}}^{(k)}$, $k = 1\ldots K$, and the total spatial channel IRs $\underline{\mathbf{h}}_\mathrm{s}^{(k)}$, $k = 1\ldots K$
$\hat{\underline{\mathbf{A}}}$	system matrix $\underline{\mathbf{A}}$ under consideration of the estimates $\hat{\underline{\mathbf{h}}}_\mathrm{s}^{(k)}$, $k = 1\ldots K$
$\underline{\mathbf{A}}^{(k)}$	k–th block of $\underline{\mathbf{A}}$, $k = 1...K$
$\underline{\mathbf{A}}^{(k,k_\mathrm{a})}$	(k, k_a)–th block of $\underline{\mathbf{A}}$, $k = 1...K$, $k_\mathrm{a} = 1...K_\mathrm{a}$
$\underline{\mathcal{A}}_\mathrm{d}$	steering matrix containing the matrices $\underline{\mathcal{A}}_\mathrm{d}^{(k_\mathrm{a})}$, $k_\mathrm{a} = 1...K_\mathrm{a}$
$\underline{\mathcal{A}}_\mathrm{d}^{(k_\mathrm{a})}$	steering matrices containing the matrices $\underline{\mathcal{A}}_\mathrm{d}^{(k,k_\mathrm{a})}$ of users $k = 1...K$, $k_\mathrm{a} = 1...K_\mathrm{a}$
$\underline{\mathcal{A}}_\mathrm{d}^{(k,k_\mathrm{a})}$	steering matrix containing the vectors $\underline{\mathbf{a}}_\mathrm{d}^{(k,k_\mathrm{a})}$, $k = 1...K$, $k_\mathrm{a} = 1...K_\mathrm{a}$
$\underline{\mathcal{A}}^{(k)}$	steering matrix of user k containing steering vectors $\underline{\mathbf{a}}^{(k,k_\mathrm{d})}$, $k_\mathrm{d} = 1...K_\mathrm{d}$
$\underline{\mathbf{A}}_\mathrm{G}^{(g)}$	system matrix $\underline{\mathbf{A}}$ valid for user group $g = 1, 2$, in MSJD
$\hat{\underline{\mathbf{A}}}_\mathrm{G}^{(g)}$	system matrix $\underline{\mathbf{A}}_\mathrm{G}^{(g)}$ valid for user group g in MSJD under consideration of the estimates $\hat{\underline{\mathbf{h}}}_\mathrm{s}^{(k)}$, $k = 1\ldots K$
$\beta^{(k,k_\mathrm{d})}$	azimuthal angle corresponding to the k_d–th DOA of user k, $k = 1...K$, $k_\mathrm{d} = 1\ldots K_\mathrm{d}$
$\beta_{e,w_\tau}^{(k)}$	azimuthal angle of the e–th wave, $e = 1...E_{w_\tau}$, belonging to the w_τ–th channel coefficient, $w_\tau = 1...W_\tau$, of user k, $k = 1...K$, $k_\mathrm{d} = 1\ldots K_\mathrm{d}$
$\beta_{\mathrm{BS}_\mu}^{(k,k_\mathrm{d})}$	azimuthal angle corresponding to the k_d–th DOA of user k impinging at BS μ, $\mu = 1, 2, = 1...K$, $k_\mathrm{d} = 1...K_\mathrm{d}$
$\underline{\mathbf{b}}^{(k)}$	composite channel IR of user k, $k = 1\ldots K$
$\underline{\mathbf{b}}_\mathrm{s}^{(k,k_\mathrm{a})}$	composite spatial channel IR of user k, $k = 1\ldots K$, at antenna k_a, $k_\mathrm{a} = 1\ldots K_\mathrm{a}$, valid for adaptive antennas
$\underline{b}_l^{(k)}$	composite channel coefficients of vector $\underline{\mathbf{b}}^{(k)}$

B	bandwidth of a partial frequency band
B_{m}	measurement bandwidth in the case of channel IR measurements
C	mean carrier received power of a desired signal
$\underline{\mathbf{c}}^{(k)}$	vector with the user specific CDMA code, $k = 1 \ldots K$
c_0	velocity of light
d	distance between BS and MS
$d_{\mathrm{BS}_\mu}^{(k,k_{\mathrm{d}})}$	path length of propagation path corresponding to the k_{d}–th DOA between BS μ and MS k, $\mu = 1, 2$, $k = 1...K$
$\underline{d}_n^{(k)}$	user specific data symbol, $n = 1 \ldots N$, $k = 1 \ldots K$
$\underline{\mathbf{d}}$	total data vector
$\underline{\mathbf{d}}^{(k)}$	user specific data vector, $k = 1 \ldots K$
$\hat{\underline{\mathbf{d}}}^{(k)}$	estimated user specific data vector, $k = 1 \ldots K$
$\hat{\underline{\mathbf{d}}}$	estimated total data vector
$\hat{\underline{\mathbf{d}}}(i)$	estimated total data vector valid for iteration i
$\hat{\underline{\mathbf{d}}}_{n_{\mathrm{b}}}(i)$	estimated total data vector of burst n_{b} valid for iteration i
$\underline{\mathbf{d}}_{\mathrm{G}}^{(g)}$	data vector of user group g in MSJD
$\hat{\underline{\mathbf{d}}}_{\mathrm{G}}^{(g)}$	estimated data vector of user group g in MSJD
$\underline{\mathbf{d}}_{\mathrm{G}}^{(g)}(i)$	data vector of user group g in MSJD valid for iteration i
$\hat{\underline{\mathbf{d}}}_{\mathrm{G}}^{(g)}(i)$	estimated data vector of user group g in MSJD valid for iteration i
$\hat{\hat{\underline{\mathbf{d}}}}_{\mathrm{G}}^{(g)}(i)$	estimated data vector of user group g in MSJD valid for iteration i after modulation and FEC encoding in signal reconstruction
Δd	difference of the length of two propagation paths
$\Delta\gamma$	difference of required SIR to achieve a BER P_{bu} equal to 10^{-3} applying ZF-JCE and MMSE-JCE
$\Delta\gamma_{\max}$	maximal difference of required SIR to achieve a BER P_{bu} equal to 10^{-3} applying conventional channel estimation and MMSE-JCE under consideration of $\underline{\mathbf{R}}_{\tau,\mathrm{s}}$
$\Delta h_{\mathrm{r},w}^{(k,k_{\mathrm{a}})}$	differences of the real parts of the estimated and the actual channel IRs of user k at antenna element k_{a}, $k = 1...K$, $k_{\mathrm{a}} = 1...K_{\mathrm{a}}$
$\Delta h_{\mathrm{i},w}^{(k,k_{\mathrm{a}})}$	differences of the imaginary parts of the estimated and the actual channel IRs of user k at antenna element k_{a}, $k = 1...K$, $k_{\mathrm{a}} = 1...K_{\mathrm{a}}$
δ_i	SNR degradation of TD–CDMA receivers, valid for each transmitted symbol $\underline{d}_i$, $i = 1 \ldots KN$
δ	mean SNR degradation of TD–CDMA receivers
$e_k(\sigma_{\mathrm{w}})$	energy that the user k requires to achieve the BER $P_{\mathrm{b},k}(\sigma_{\mathrm{w}})$ without intracell MAI in an AWGN channel
E	total numbers of waves contributing to a channel IR
E_{w_τ}	number of waves contributing to channel coefficient w_τ
$E_{\mathrm{BS}_\mu}^{(k,k_{\mathrm{d}})}$	number of waves assigned to the path k_{d} of the user k in cell μ, $k_{\mathrm{d}} = 1...K_{\mathrm{d}}$, $k = 1...K$, $\mu = 1, 2$
$\underline{\mathbf{e}}$	vector representing the received signal

$\underline{\mathbf{e}}^{(k_\mathrm{a})}$	vector representing the received signal at the antenna elements $k_\mathrm{a} = 1...K_\mathrm{a}$
$\underline{\mathbf{e}}_\mathrm{d}^{(k)}$	vector representing the received signal of user k without intercell MAI and noise
$\hat{\underline{\mathbf{e}}}_\mathrm{d}$	vector representing the reconstruction of the received signal based on $\hat{\underline{\mathbf{A}}}$ and $\hat{\underline{\mathbf{d}}}$
$\underline{\mathbf{e}}_\mathrm{G}^{(g)}$	vector representing the received signal of user group g in MSJD, $g = 1, 2$
$\hat{\underline{\mathbf{e}}}_\mathrm{G}^{(g)}(i)$	vector representing the estimated received signal of user group g valid for iteration i in MSJD, $g = 1, 2$
$\underline{\mathbf{e}}_\mathrm{red}^{(g)}(i)$	vector representing the intracell MAI reduced signal of user group g valid for iteration i in MSJD, $g = 1, 2$
$\hat{\underline{\mathbf{e}}}_\mathrm{red}^{(g)}(i)$	vector representing the estimated intracell MAI reduced signal of user group g valid for iteration i in MSJD, $g = 1, 2$
$\underline{\mathbf{e}}_\mathrm{m}$	vector representing the received total signal originating from the transmitted midambles and valid for channel estimation
$\hat{\underline{\mathbf{e}}}_\mathrm{m}$	vector representing the reconstruction of the $\underline{\mathbf{e}}_\mathrm{m}$ based on $\underline{\mathbf{h}}_\mathrm{s}$
$\underline{\mathbf{e}}_\mathrm{m}^{(k_\mathrm{a})}$	vector representing the signal originating from the transmitted midambles received at antenna element k_a, $k_\mathrm{a} = 1...K_\mathrm{a}$
$\underline{\mathbf{E}}$	matrix containing the vectors $\underline{\mathbf{e}}_\mathrm{m}^{(k_\mathrm{a})}$
$\epsilon_\mathrm{e}^{(k)}$	reconstruction error of the signal of user k; reconstruction based on coded data
$\epsilon_\mathrm{eu}^{(k)}$	reconstruction error of the signal of user k; reconstruction based on uncoded data
$\epsilon_{\underline{\mathbf{R}}_\mathrm{s}}$	estimation error of matrix $\underline{\mathbf{R}}_\mathrm{s}$
ϵ_h	RMSE of the estimated channel IRs
$\epsilon_\mathrm{re}^{(k,k_\mathrm{a})}$	estimation error of the real part of the estimated channel IRs $\hat{\underline{\mathbf{h}}}_\mathrm{s}^{(k,k_\mathrm{a})}$, $k = 1...K$, $k_\mathrm{a} = 1...K_\mathrm{a}$
$\epsilon_\mathrm{im}^{(k,k_\mathrm{a})}$	estimation error of the imaginary part of the estimated channel IRs $\hat{\underline{\mathbf{h}}}_\mathrm{s}^{(k,k_\mathrm{a})}$, $k = 1...K$, $k_\mathrm{a} = 1...K_\mathrm{a}$
ϵ_re	mean estimation error of the real part of the estimated channel IRs
ϵ_im	mean estimation error of the real part of the estimated channel IRs
η_k	asymptotic efficiency valid for user k, $k = 1...K$
$\overline{\eta}_{k,i}$	near-far resistance of a multiuser detector valid for symbol $\underline{d}_n^{(k)}$, $n = 1...N$, $k = 1...K$
$\overline{\eta}_k$	near-far resistance valid for user k, $k = 1...K$
f	frequency
f_c	Carrier frequency
f_d	Doppler frequency
$f_\mathrm{d,max}$	Maximum Doppler frequency
$f_\mathrm{d}^{(k,k_\mathrm{d})}$	Doppler frequency of k_d–th wave front of the channel IR of user k, $k = 1...K$, $k_\mathrm{d} = 1...K_\mathrm{d}$
γ	mean SIR per user and per antenna element

$\gamma_{K_\mathrm{a}=1}$	mean output SIR after signal processing in the case of $K_\mathrm{a}=1$ antenna element
$\gamma_{K_\mathrm{a}>1}$	mean output SIR after signal processing in the case of $K_\mathrm{a}>1$ antenna elements
$\gamma_\mathrm{i}^{(k_\mathrm{i})}$	azimuthal angle of the k_i–th intercell MAI signal, $k_\mathrm{i}=1\ldots K_\mathrm{i}$
$\gamma_\mathrm{i}^{(k_\mathrm{i},k_\mathrm{d})}$	azimuthal angle of the k_d–th intercell MAI signal from the k_i–th intercell MAI source, $k_\mathrm{i}=1\ldots K_\mathrm{i}$, $k_\mathrm{d}=1...K_\mathrm{d}$
$\gamma^{(k_\mathrm{a})}$	mean input SIR at the antenna element k_a, $k_\mathrm{a}=1...K_\mathrm{a}$
γ_MF	mean SIR of the output of a matched filter
$\gamma_\mathrm{ZF-BLE}$	mean SIR of the output of a ZF-BLE
$\gamma_\mathrm{MF,in}$	mean SIR of the input of a matched filter
$\gamma_\mathrm{ZF-BLE,in}$	mean SIR of the input of a ZF-BLE
$\gamma_\mathrm{ZF-JCE}$	required mean SIR to achieve a BER P_bu equal to 10^{-3} when using ZF-JCE
$\gamma_\mathrm{MMSE-JCE}$	required mean SIR to achieve a BER P_bu equal to 10^{-3} when using MMSE-JCE
γ_min	required SIR to achieve a BER P_bu equal to 10^{-3} in the case of perfectly known channel IRs
g_a	SIR gain when applying antenna arrays depending on the azimuth angle
$\overline{g}_\mathrm{a}$	mean SIR gain g_a
$\underline{\mathbf{G}}$	channel estimation matrix, exclusively determined by the user specific midambles
	matrix resulting from the Kronecker product of $\mathbf{I}^{(K_\mathrm{a})}$ and $\underline{\mathbf{G}}$
$\underline{\mathbf{G}}^{(k)}$	k–th block of $\underline{\mathbf{G}}$, $k=1\ldots K$
$\underline{\mathbf{h}}_\mathrm{d}^{(k,k_\mathrm{d})}$	directional channel IR corresponding to the k_d–th DOA of user k, $k=1...K$, $k_\mathrm{d}=1...K_\mathrm{d}$
$\underline{\mathbf{h}}_\mathrm{d}^{(k)}$	directional channel IR corresponding to the k_d–th DOA of user k, $k=1...K$
$\underline{\mathbf{h}}_\mathrm{d}$	vector containing all K_d directional channel impulse responses
$\underline{h}_\mathrm{RP}^{(k)}(\tau,t)$	channel IR of user k at the RP as a function of delay τ and time t, $k=1...K$
$\underline{h}_{\mathrm{RP,BS}_\mu}^{(k)}(\tau,t,\varphi)$	channel IR of user k at the RP of BS μ as a function of delay τ, time t and azimuth angle φ, $k=1...K$
$\underline{\mathbf{h}}_\mathrm{RP}^{(k)}$	vector representing $\underline{h}_\mathrm{RP}^{(k)}(\tau,t_0)$ at a specific instant t_0
$\underline{\mathbf{h}}_\mathrm{RP}$	vector containing all vectors $\underline{\mathbf{h}}_\mathrm{RP}^{(k)}$, $k=1...K$
$h_{\mathrm{r},w}^{(k,k_\mathrm{a})}$	real part of the element w of $\underline{\mathbf{h}}_\mathrm{s}^{(k,k_\mathrm{a})}$, $w=1...W$, $k=1...K$, $k_\mathrm{a}=1...K_\mathrm{a}$
$h_{\mathrm{i},w}^{(k,k_\mathrm{a})}$	imaginary part element w of $\underline{\mathbf{h}}_\mathrm{s}^{(k,k_\mathrm{a})}$, $w=1...W$, $k=1...K$, $k_\mathrm{a}=1...K_\mathrm{a}$
$\underline{h}_\mathrm{s}^{(k,k_\mathrm{a})}(\tau,t)$	channel IR of user k at antenna element k_a as a function of delay τ and time t, $k=1...K$, $k_\mathrm{a}=1...K_\mathrm{a}$
$\underline{\mathbf{h}}_\mathrm{s}^{(k,k_\mathrm{a})}$	vector representing $\underline{h}_\mathrm{s}^{(k,k_\mathrm{a})}(\tau,t_0)$ at a specific instant t_0
$\underline{h}_{\mathrm{s},w}^{(k,k_\mathrm{a})}$	element w of $\underline{\mathbf{h}}_\mathrm{s}^{(k,k_\mathrm{a})}$, $w=1...W$, $k=1...K$, $k_\mathrm{a}=1...K_\mathrm{a}$
$\underline{\mathbf{h}}_\mathrm{s}^{(k_\mathrm{a})}$	channel IR of all users valid for antenna element k_a, $k_\mathrm{a}=1...K_\mathrm{a}$

$\underline{\mathbf{h}}_{\mathrm{s}}$	total spatial channel IR vector containing all channel IRs $\underline{\mathbf{h}}_{\mathrm{s}}^{(k,k_{\mathrm{a}})}$, $k = 1\ldots K$, $k_{\mathrm{a}} = 1\ldots K_{\mathrm{a}}$
$\hat{\underline{\mathbf{h}}}_{\mathrm{s}}$	estimated total spatial channel IR vector
$\hat{\underline{\mathbf{h}}}_{\mathrm{s,MMSE1}}$	estimated total spatial channel IR vector by applying MMSE-JCE I
$\hat{\underline{\mathbf{h}}}_{\mathrm{s,MMSE2}}$	estimated total spatial channel IR vector by applying MMSE-JCE II
$\hat{\underline{\mathbf{H}}}$	matrix containing the vectors $\hat{\underline{\mathbf{h}}}_{\mathrm{s}}^{(k,k_{\mathrm{a}})}$, $k = 1...K$, $k_{\mathrm{a}} = 1...K_{\mathrm{a}}$
$\hat{\underline{\mathbf{H}}}^{(k)}$	k–th block of $\hat{\underline{\mathbf{H}}}$
i	iteration number in MSJD
I	mean received power per antenna element of interfering signals
$\mathbf{I}^{(K_{\mathrm{a}})}$	$K_{\mathrm{a}} \times K_{\mathrm{a}}$ identity matrix
I_{t}	number of iterations
j	imaginary unit
K	number of users active in a time slot
K_{a}	number of antenna elements at the BS
K_{c}	constrained length of a convolutional encoder
K_{d}	number of DOAs of user k, $k = 1\ldots K$, or of an intercell MAI source k_{i}, $k_{\mathrm{i}} = 1...K_{\mathrm{i}}$
K_{i}	number of intercell MAI signals or intercell MAI sources
K_{m}	number of antenna elements at the MS
λ	wavelength
$l(t)$	large–scale fading
$l^{(k_{\mathrm{a}})}$	distance of antenna element k_{a} from the RP of the array configuration, $k_{\mathrm{a}} = 1\ldots K_{\mathrm{a}}$
L	dimension of $\underline{\mathbf{e}}_{\mathrm{m}}$
L_{m}	length the midamble section of a burst
L_{g}	length the guard interval
$\underline{\mathbf{L}}_{\mathrm{s}}$	matrix resulting from the Cholesky decomposition of $\underline{\mathbf{R}}_{\mathrm{s}}$
M	size of the data symbol alphabet
M_{d}	dimension of the vectors $\mathbf{u}^{(k)}$, $k = 1...K$
$\underline{\mathbf{m}}^{(k)}$	vector representing the midamble of user k, $k = 1...K$
$\underline{\mathbf{m}}_{\mathrm{p}}$	basic code from which the midambles are derived
$\underline{\mathbf{M}}_{\mathrm{MMSE}}$	matrix describing the MMSE-BLE
$\mathrm{MS}_{\mu}^{(k)}$	MS of user k in cell μ, $k = 1...K$, $\mu = 1, 2$
N	number of symbols per data block and user
N_{b}	number of bursts
N_{fr}	number of time slots per TDMA frame
N_{t}	noise threshold of measured channel IRs
$\underline{n}(\varphi, t)$	intercell MAI as a function of the azimuth angle φ and the time t
$\underline{n}_{\varphi}(\varphi, t)$	azimuthal intercell MAI density
$\underline{n}(t)$	intercell MAI as a function of t
$\underline{n}_{\mathrm{c}}(\varphi, t)$	azimuthal intercell MAI density of the continuous component
$\underline{n}_{\mathrm{d}}(\varphi, t)$	azimuthal intercell MAI density of the discrete component

$\underline{n}^{(k_\mathrm{a})}(t)$	intercell MAI received at antenna element k_a, $k_\mathrm{a} = 1...K_\mathrm{a}$
$\underline{n}_{\mathrm{RP},s}(\varphi)$	sample s of the intercell MAI signal impinging from the azimuth angles φ at the RP
N_a	number of connections at the shift register of a convolutional encoder
$\underline{\mathbf{n}}_\mathrm{RP}(\varphi)$	vector containing the elements $\underline{n}_{\mathrm{RP},s}(\varphi)$
$\tilde{\underline{\mathbf{n}}}_\mathrm{RP}(\varphi)$	normalized vector $\underline{\mathbf{n}}_\mathrm{RP}(\varphi)$
$\underline{\mathbf{n}}_\varphi(\varphi)$	vector representing $\underline{n}_\varphi(\varphi, t)$
$\underline{\mathbf{n}}^{(k_\mathrm{a})}$	intercell MAI vector valid for antenna element k_a, $k_\mathrm{a} = 1 \ldots K_\mathrm{a}$, and for data detection
$\underline{\mathbf{n}}_\mathrm{m}^{(k_\mathrm{a})}$	intercell MAI vector valid for antenna element k_a, $k_\mathrm{a} = 1 \ldots K_\mathrm{a}$, and for channel estimation
$\underline{\mathbf{n}}$	intercell MAI vector valid for data detection
$\underline{\mathbf{n}}_\mathrm{m}$	intercell MAI vector valid for channel estimation
$\underline{\mathbf{n}}_\mathrm{RP}$	vector representing intercell MAI received at the RP and filtered with the GMSK chip impulse only
$\hat{\underline{\mathbf{n}}}$	estimate of the vector $\underline{\mathbf{n}}$
$\hat{\underline{\mathbf{n}}}(i)$	estimate of the vector $\underline{\mathbf{n}}$ valid for iteration i
$\hat{\underline{\mathbf{n}}}^{(k_\mathrm{a})}$	estimate of vector $\underline{\mathbf{n}}^{(k_\mathrm{a})}$
$\hat{\underline{\mathbf{n}}}_\mathrm{m}^{(k_\mathrm{a})}$	estimate of vector $\underline{\mathbf{n}}_\mathrm{m}^{(k_\mathrm{a})}$
$\hat{\underline{\mathbf{n}}}_\mathrm{m}$	estimate of vector $\underline{\mathbf{n}}_\mathrm{m}$
$\underline{\mathbf{n}}_\mathrm{G}^{(g)}$	intercell MAI vector valid for data detection of the user group g in MSJD
$\underline{\mathbf{n}}_\mathrm{G}^{(g)}(i)$	intercell MAI vector valid for data detection of the user group g in MSJD in iteration i
$\underline{\mathbf{N}}_\mathrm{RP}$	matrix consisting of K_a vectors $\underline{\mathbf{n}}_\mathrm{RP}$
$\underline{\mathbf{N}}$	matrix consisting of K_a intercell MAI vectors $\underline{\mathbf{n}}^{(k_\mathrm{a})}$, $k_\mathrm{a} = 1...K_\mathrm{a}$
$\hat{\underline{\mathbf{N}}}_\mathrm{m}$	matrix consisting of K_a estimated intercell MAI vectors $\hat{\underline{\mathbf{n}}}_\mathrm{m}^{(k_\mathrm{a})}$, $k_\mathrm{a} = 1...K_\mathrm{a}$
$\hat{\underline{\mathbf{N}}}(i)$	matrix consisting of K_a estimated intercell MAI vectors $\hat{\underline{\mathbf{n}}}^{(k_\mathrm{a})}$, $k_\mathrm{a} = 1...K_\mathrm{a}$ valid for iteration i
$\mathbf{0}$	zero vector
φ	azimuth angle
$\varphi_\mathrm{s}^{(k,k_\mathrm{d})}$	the DOD of k_d–th wave front of channel IR of user k
φ_v	direction of movement
$\phi(\varphi, k_\mathrm{a})$	phase shifts with respect to the RP of intercell MAI wave fronts impinging from angle φ at the antenna element k_a
P_b	average coded BER
P_bu	average uncoded BER
$P_\mathrm{bu,r}$	average uncoded BER in case of signal reconstruction
$P_\mathrm{b}^{(k)}$	average coded BER valid for user k, $k = 1...K$
$P_\mathrm{bu}^{(k)}$	average uncoded BER valid for user k, $k = 1...K$
$P_\mathrm{bu,r}^{(k)}$	average uncoded BER valid for user k in case of signal reconstruction
$P(t)$	power of the channel IRs as a function of time t

$P_{\mathrm{r}}(t_{\mathrm{m}})$	received power of the power of the channel IRs measured at instant t_{m}
$P_{\mathrm{tr}}(t_{\mathrm{m}})$	transmitted power at instant t_{m} for measuring the channel IRs
$\overline{P}(t_{\mathrm{m}})$	mean power of the channel IRs at the instant t_{m}
$P_{\mathrm{b},k}(\sigma_{\mathrm{w}})$	BER of user k without intracell MAI in AWGN channel with power spectral density σ_{w}^2
P_{t}	probability of noise exceeding the threshold N_{t}
$q^{(k_{\mathrm{i}},k_{\mathrm{d}})}$	integer describing the delay of wave front k_{d} of user k in terms of integer multiples of T_{c}, $k_{\mathrm{d}}=1...K_{\mathrm{d}}$, $k=1...K$
Q	dimension of $\underline{\mathbf{c}}^{(k)}$, $k=1\dots K$
r	cluster size
$r(t)$	small–scale fading of measured channel IRs
$\underline{r}^{(u,v)}$	elements of matrix $\underline{\mathbf{R}}_{\mathrm{s}}$
R_{c}	code rate
$\underline{\mathbf{R}}_{\mathrm{d}}$	covariance matrix of $\underline{\mathbf{d}}$
$\hat{\underline{\mathbf{R}}}_{\mathrm{e}}$	correlation matrix of the received signal described by vector $\underline{\mathbf{e}}$
$\underline{\mathbf{R}}_{\mathrm{G}}^{(g)}$	intercell and intracell MAI covariance matrix in MSJD valid for data detection of group g, $g=1,2$
$\underline{R}_{\varphi}(\varphi_1,\varphi_2,\Delta t)$	temporal and directional auto correlation function of the azimuthal intercell MAI density
$\underline{\mathbf{R}}_{\mathrm{m}}$	total intercell MAI covariance matrix valid for channel estimation
$\hat{\underline{\mathbf{R}}}_{\mathrm{m}}$	estimate of matrix $\underline{\mathbf{R}}_{\mathrm{m}}$
$\underline{R}_{\mathrm{n}}(\varphi_1,\varphi_2,\Delta t)$	temporal and directional auto correlation function of the intercell MAI
$\underline{\mathbf{R}}_{\mathrm{n}}$	total intercell MAI covariance matrix valid for data detection
$\underline{R}_{\mathrm{n}}^{(u,v)}(\Delta t)$	correlation function valid for interference received at the u–th and v–th antenna element
$\underline{\mathbf{R}}_{\mathrm{n}}^{(u,v)}$	covariance matrix of $\underline{\mathbf{n}}^{(u)}$ and $\underline{\mathbf{n}}^{(v)}$, $u,v=1\dots K_{\mathrm{a}}$
$\hat{\underline{\mathbf{R}}}_{\mathrm{n}}(i)$	estimate of $\underline{\mathbf{R}}_{\mathrm{n}}$ valid for iteration i
$\underline{\mathbf{R}}_{\mathrm{n},n_{\mathrm{b}}}$	matrix $\underline{\mathbf{R}}_{\mathrm{n}}$ valid for burst n_{b}
$\tilde{\underline{\mathbf{R}}}_{\mathrm{RP}}(\varphi_1,\varphi_2)$	covariance matrix of the normalized vectors $\tilde{\underline{\mathbf{n}}}_{\mathrm{RP}}(\varphi)$
$\underline{R}_{\mathrm{s},i,j}$	elements of matrix $\underline{\mathbf{R}}_{\mathrm{s}}$, $i,j=1...K_{\mathrm{a}}$
$\underline{\mathbf{R}}_{\mathrm{s}}$	spatial intercell MAI covariance matrix
$\hat{\underline{\mathbf{R}}}_{\mathrm{s}}(i)$	estimate of the spatial intercell MAI covariance matrix valid for iteration i
$\hat{\underline{\mathbf{R}}}_{\mathrm{s}}^{(k)}$	correlation matrix of the estimated channel IR of user k, $k=1...K$
$\hat{\underline{R}}_{\tau,\mathrm{s},i,j}$	estimated elements of matrix $\underline{\mathbf{R}}_{\tau,\mathrm{s}}$, $i,j=1...K_{\mathrm{a}}$
$\underline{\mathbf{R}}_{\tau,\mathrm{s}}^{(k,k',k_{\mathrm{a}},k_{\mathrm{a}}')}$	correlation matrix of the vectors $\underline{\mathbf{h}}_{\mathrm{s}}^{(k,k_{\mathrm{a}})}$, $k=1...K$, $k_{\mathrm{a}}=1...K_{\mathrm{a}}$
$\underline{\mathbf{R}}_{\tau}^{(k_{\mathrm{a}},k_{\mathrm{a}}')}$	correlation matrix of the vectors $\underline{\mathbf{h}}_{\mathrm{s}}^{(k_{\mathrm{a}})}$, $k_{\mathrm{a}}=1...K_{\mathrm{a}}$
$\underline{\mathbf{R}}_{\tau,\mathrm{s}}$	correlation matrix of the total spatial channel IR vector $\underline{\mathbf{h}}_{\mathrm{s}}$
$\tilde{\underline{\mathbf{R}}}_{\mathrm{t}}$	normalized temporal intercell MAI covariance matrix valid for data detection
$\tilde{\underline{\mathbf{R}}}_{\mathrm{t,m}}$	normalized temporal intercell MAI covariance matrix valid for channel estimation

$\underline{\mathbf{R}}_{\mathrm{x}}$	correlation matrix of the received signal $\underline{\mathbf{e}}$ if $\underline{\mathbf{n}} = 0$
$\underline{\rho}_{\mathrm{T},\mu}^{(k,k_{\mathrm{d}})}$	mean power of the superimposed waves of the channel IR of user k corresponding to the DOA k_{d}, $k_{\mathrm{d}} = 1...K_{\mathrm{d}}$, $k = 1...K$
$\rho_{\mathrm{c}}(\varphi)$	azimuthal intercell MAI power density of the continuous component
$\rho_{\perp}\left(\theta_{\mathrm{BS}_\mu}^{(k,k_{\mathrm{d}})}\right)$	Fresnel reflection coefficient in the case of reflection angle $\theta_{\mathrm{BS}_\mu}^{(k,k_{\mathrm{d}})}$
σ^2	intercell MAI power, which is assumed to be equal for all components of $\underline{\mathbf{n}}$
σ_{A}^2	power of the deviation of the real and the estimated intercell MAI signal with respect to the power of the noise-free received signal
σ_{c}^2	intercell MAI power of the continuous component
σ_{d}^2	intercell MAI power of the discrete component
σ_{n}^2	power of the deviation of the real and the estimated intercell MAI signal with respect to the power of the real intercell MAI
σ_{t}^2	noise power in the case of measured channel IRs
σ_{w}^2	power spectral density in the case of AWGN
$\left(\sigma^{(k_{\mathrm{i}})}\right)^2$	power of the k_{i}–th intercell MAI signal
$\left(\tilde{\sigma}^{(k_{\mathrm{i}})}\right)^2$	normalized power of the k_{i}–th intercell MAI signal
$\left(\sigma^{(k_{\mathrm{i}},k_{\mathrm{d}})}\right)^2$	power of the k_{d}–th intercell MAI signal originating from the k_{i}–th intercell MAI source
$\sigma(\varphi)$	average amplitude of $\underline{n}(\varphi, t)$
$\underline{s}$	single arbitrary transmit symbol
$\underline{s}_{\mathrm{out}}$	output symbol of an array processing unit
S	dimension of intercell MAI noise independent of the TD-CDMA system parameters
$S_{\mathrm{c}}(0, f_{\mathrm{d}})$	Doppler spectrum
$S_{\mathrm{c}}(\tau, f_{\mathrm{d}})$	scattering function
τ	delay parameter
τ_{w_τ}	delay of the channel coefficient w_τ
$\tau_{\mathrm{BS}_\mu}^{(k,k_{\mathrm{d}})}$	delay of the k_{d}–th DOA of the channel IR of user k in cell μ, $k_{\mathrm{d}} = 1...K_{\mathrm{d}}$, $k = 1...K$, $\mu = 1, 2$
t_{m}	measurement instant
$t^{(k_{\mathrm{i}},k_{\mathrm{d}})}$	relative time delay of k_{d} identical intercell MAI signals from source k_{i} with different DOAs impinging at the RP, $k_{\mathrm{i}} = 1...K_{\mathrm{i}}$, $k_{\mathrm{d}} = 1...K_{\mathrm{d}}$
T_{bu}	duration of a time slot
T_{c}	chip duration
T_{fr}	duration of a TDMA frame
T_{g}	duration of the guard interval
T_{s}	symbol duration
$\theta_{\mathrm{BS}_\mu}^{(k,k_{\mathrm{d}})}$	reflection angle corresponding to the k_{d}–th DOA valid the channel IR of user k in cell μ, $k_{\mathrm{d}} = 1...K_{\mathrm{d}}$, $k = 1...K$, $\mu = 1, 2$
$\mathbf{u}^{(k)}$	uncoded data vector of user k, $k = 1...K$

$\mathbf{u}_{\mathrm{G}}^{(g)}$	uncoded data vector of user k in MSJD valid for user group g, $k = 1...K$, $g = 1,2$
$\hat{\mathbf{u}}_{\mathrm{G}}^{(g)}(i)$	reconstructed uncoded data vector of user k in MSJD valid for user group g, $k = 1...K$, $g = 1,2$
v	user velocity
$v^{(k)}$	velocity of user k
$\vec{v}$	user velocity vector
$\mathbb{V}_{\mathrm{d}}$	data symbol alphabet
W	dimension of $\underline{\mathbf{h}}_{\mathrm{s}}^{(k,k_{\mathrm{a}})}$, $k = 1...K$, $k_{\mathrm{a}} = 1...K_{\mathrm{a}}$
$\underline{\mathbf{w}}$	weight vector
W_{τ}	number of channel coefficients in the case of ITU channels
$x_{\mathrm{BS}_{\mu}}$	x coordinate of the BS_{μ}
$y_{\mathrm{BS}_{\mu}}$	y coordinate of the BS_{μ}
$x_{\max}$	length of the room in case of indoor ray-tracing channel modelling
$y_{\max}$	broadness of the room in case of indoor ray-tracing channel modelling
$\vartheta_{e,w_{\tau}}$	random zero phases of wave e which is assigned to the channel coefficient w_{τ}
$\psi(k, k_{\mathrm{a}}, k_{\mathrm{d}})$	spatial frequencies valid for antenna k_{a}, corresponding to the k_{d}–th DOA of user k

References

[3GPP] 3GPP, "About the Third Generation Partnership Project (3GPP)", published in the Internet under the URL http://www.3gpp.org/ABOUT_3GPP/3gpp.htm, 1999.

[3GPP2] 3GPP, "Third Generation Partnership Project 2 (3GPP2) – Background", published in the Internet under the URL http://208.45.131.70/text/background.cfm, 1999.

[ACTS98] C. Anton, J.R. Fonollosa and M. Xavier, "System Simulation Specification", ACTS AC347/UPC/A31/PI/I/002/b1 SUNBEAM Specification, 1998.

[Ada66] R.T. Adams, "An adaptive antenna system for maximizing signal–to–noise ratio", Proc. WESCON Conference, Session 24, 1966, pp. 1–4.

[AMF99] C. Antón-Haro, X. Mestre and J.R. Fonollosa, "Array-based and joint detection methods for the TDD mode of UTRA", Proc. IEEE 10$^{\text{th}}$ International Symposium on Personal, Indoor and Mobile Radio Communications (PIMRC '99), Osaka, 1999, pp. 253–257.

[And63] T.W. Anderson, "Asymptotic theory for principal components analysis", Ann. Math. Statist., vol. 34, 1963, pp. 122–148.

[And69] V.C. Anderson, "DICANNE, a realizable adaptive process", Journal on Acoust. Soc. Amer., vol. 45, 1969, pp. 398–405.

[AnR69] V.C. Anderson and P. Rudnick, "Rejection of a coherent arrival at an array", Journal on Acoust. Soc. Amer., vol. 45, 1969, pp. 406–410.

[App66] S.P. Applebaum, "Adaptive arrays", Syracuse University Research Corporation, Rep. SPL TR66-1, 1966.

[App76] S.P. Applebaum, "Adaptive arrays", IEEE Transactions on Antennas and Propagation, vol. 24, 1976, pp. 585–598.

[AS84] E. Ashok and P.M. Schultheiss, "The effect of auxiliary source on the performance of the randomly perturbed array", Proc. IEEE International Conference on Acoustics, Speech, Signal Processing (ICASSP'95), vol. 40.1, San Diego, 1984.

[ASS98] F. Adachi, M. Sawahashi and H. Suda, "Wideband DS–CDMA for next–generation mobile communications systems", IEEE Communications Magazine, vol. 163, 1998, pp. 56–69.

[BaA00] G. Bauch and N. Al-Dhahir, "Reduced-complexity turbo equalization with multiple transmit and receive antennas over multipath fading channels", Proc. Conference on Information Sciences and Systems (CISS'00), Princeton, 2000, pp. WP3-13–WP3-18.

[Bac98] J. Bach Anderson, "Intelligent antennas in a scattering environment – An overview", Proc. IEEE Globecom'98, Sydney, 1998.

[Bac99] J. Bach Anderson, "Antenna arrays in mobile communications – Gain, diversity and channel capacity", Radio Science Bulletin, vol. 290, 1999, pp. 4–7.

[Bai94] P.W. Baier, "CDMA or TDMA? CDMA for GSM?", Proc. IEEE 5th International Symposium on Personal, Indoor and Mobile Radio Communications (PIMRC '94), The Hague, 1994, pp. 1280–1284.

[Bai96a] P.W. Baier, "Evaluating the multiple access options", Proc. IBC Conference Next Generation Mobile — Evolution or Revolution?, London, 1996.

[Bai96b] P.W. Baier, "A critical review of CDMA", Proc. IEEE 46th Vehicular Technology Conference (VTC '96), Atlanta, 1996, pp. 6–10.

[Bai96c] P.W. Baier, "CDMA, a challenging approach to multiple access", Proc. King's College Workshop on Wireless Multi-Media Communications, London, 1996, pp. 72–76.

[Bar48] M.S. Bartlett, "Smoothing periodograms from time series with continous spectra", Nature, vol. 161, 1948, pp. 686–687.

[BARY95] J. Bach Andersen, T.S. Rappaport and S. Yoshida, "Propagation measurements and models for wireless communications channels", IEEE Communications Magazine, vol. 33, 1995, pp. 42–49.

[BaS91] P. Balaban and J. Salz, "Dual diversity combining and equalization in digital cellular mobile radio", IEEE Transactions on Vehicular Technology, vol. VT-40, 1991, pp. 342–354.

[BaS92] P. Balaban and J. Salz, "Optimum diversity combining and equalization in digital data transmission with applications to digital cellular mobile radio", IEEE Transactions on Communications, vol. COM-40, 1992, pp. 885–907.

[BaS97] T. Bachelier and J.F. Sante, "Influence of mobility on capacity of DCS networks using switched-beam antennas", Proc. IEE Symposium on Intelligent antennas, Guildford, 1997.

[Bau99] G. Bauch, "Concatenation of space-time block codes and "turbo"-TCM", Proc. IEEE International Conference on Communications (ICC'99), Vancouver, 1999, pp. 1202–1206.

[BaW98] P.W. Baier and T. Weber, "CDMA for UMTS and IMT-2000", Proc. 1998 International Conference on Personal Mobile Radio and Spread Spectrum Communications (IPMSC98), Shanghai, 1998, pp. 1.6.1-1.6.20.

[BBA95] T. Bull, M. Barrett and R. Arnott, "Technology in smart antennas for universal advanced mobile infrastructure (TSUNAMI R2108) – Overview", Proc. RACE Mobile Telecommunications Summit, Cascais, 1995, pp. 88–97.

[BBJ95] J.J. Blanz, P.W. Baier and P. Jung, "A flexibly configurable statistical channel model for mobile radio systems with directional diversity", in [Wal95], 1995, pp. 93–100.

[BBNS94] P.W. Baier, J.J. Blanz, M.M. Naßhan and A. Steil, "Realistic simulations of a CDMA mobile radio system using joint detection and coherent receiver antenna diversity", Proc. IEE Colloquium on Spread Spectrum Techniques for Radio Communication Systems, London, 1994, pp. 1/1 – 1/5.

[BBP97] P.W. Baier, J.J. Blanz and A. Papathanassiou, "Joint detection CDMA and antenna diversity techniques", Proc. IEE Colloquium on CDMA Techniques and Applications for third Generation Mobile Systems, London, 1997, pp. 1/1 – 1/7.

[BBS97] P.W. Baier, J.J. Blanz and R.M. Schmalenberger, "Fundamentals of smart antennas for mobile radio applications", Proc. IEEE 8th International Symposium on Personal, Indoor and Mobile Radio Communications (PIMRC'97), Helsinki, 1997, in [GL97], pp. 345–376.

[Bel63] P.A. Bello, "Characterization of randomly time-variant linear channels", IEEE Transactions on Communication Systems, vol. CS-11, 1963, pp. 360–393.

[BEM$^+$98a] S. Bahrenburg, C. Euscher, J. Mayer, J. Schlee, and T. Weber, "Fading simulator measurements with a TD–CDMA hardware demonstrator", Proc. IEEE 5th International Conference on Telecommunications (ICT'98), vol. III, Chalkidiki, 1998, pp. 12–16.

[BEM$^+$98b] S. Bahrenburg, C. Euscher, J. Mayer, J. Schlee, and T. Weber, "Outdoor measurements with a TD (Time Division)–CDMA hardware demonstrator for UMTS", Proc. IEEE 4th International Symposium on Spread Spectrum Techniques & Applications (ISSSTA'96), Mainz, 1996, pp. 625–629.

[BHP$^+$97] J.J. Blanz, M. Haardt, A. Papathanassiou, I. Furió and P. Jung, "Combined direction of arrival and channel estimation for time-slotted CDMA", Proc. IEEE 4th International Conference on Telecommunications (ICT'97), Melbourne, 1997, pp. 395–400.

[BHSN00] C. Brunner, J.S. Hammerschmidt, A. Seeger, and J.A. Nossek, "Space-time eigenrake and downlink eigenbeamformer: Exploiting long-term and short-term channel properties in WCDMA", Proc. IEEE GLOBECOM, San Francisco, 2000.

[BHS00] G. Bauch, J. Hagenauer and N. Seshadri, "Turbo-TCM and transmit antenna diversity in multipath fading channels", Proc. International Symposium on Turbo Codes, Brest, 2000, pp. 189–192.

[Bin01] T. Bing, Zeitduplexbasierte Mobilkommunikation, untersucht am Beispiel eines TD-CDMA-Mobilfunksystems, Forschungsberichte Mobilkommunikation, vol. 8, University of Kaiserslautern, 2001. ISBN 3-925178-61-9.

[BJK96] P.W. Baier, P. Jung and A. Klein, "Taking the challenge of multiple access for third generation cellular mobile radio systems — a European view", IEEE Communications Magazine, vol. 34, 1996, pp. 82–89.

[BJL+02] P.W. Baier, C.A. Jötten, Y. Lu, I. Maniatis, M. Meurer, H. Tröger, T. Weber and M. Weckerle, "Recent progress in time slotted CDMA", to appear in 3rd Generation Mobile Communication Systems: Future Developements and Advanced Topics, edited by J.-G. Ma, Springer-Verlag, Berlin/Heidelberg/New York, 2002.

[BJN94] J.J. Blanz, P. Jung and M.M. Naßhan, "Realistic simulations of CDMA mobile radio systems using joint detection and coherent receiver antenna diversity", Proc. IEEE 3rd International Symposium on Spread Spectrum Techniques and Applications (ISSSTA '94), Oulu, 1994, pp. 193–197.

[BJSB96] J.J. Blanz, P. Jung, A.J. Steil and P.W. Baier, "Coherent receiver antenna diversity with directional antennas", Proc. IEEE 3rd International Conference on Telecommunications (ICT'96), Istanbul, 1996, pp. 410–417.

[BK91] A. Baier and W. Koch, "Potential of CDMA for 3rd generation mobile radio systems", Proc. Mobile Radio Conference, Nice, 1991.

[BK95] P.W. Baier and A. Klein, "Flexible hybrid multiple access schemes for 3rd generation mobile radio systems", E. Del Re, editor, Proc. Joint COST 227/231 Workshop on Mobile and Personal Communications, Florence, 1995, in [DR95], pp. 31–43.

[BKM96] J.J. Blanz, A. Klein and W. Mohr, "Measurement-based parameter adaptation of wideband spatial mobile radio channel models", Proc. IEEE 4th International Symposium on Spread Spectrum Techniques & Applications (ISSSTA'96), Mainz, 1996, pp. 91–97.

[BKNS94a] J.J. Blanz, A. Klein, M.M. Naßhan and A. Steil, "Capacity of a cellular CDMA mobile radio system applying joint detection", COST 231 Temporary Document TD (94) 2, Lisbon, 1994.

[BKNS94b] J.J. Blanz, A. Klein, M.M. Naßhan and A. Steil, "Performance of a cellular hybrid C/TDMA mobile radio system applying joint detection and coherent receiver antenna diversity", IEEE Journal on Selected Areas in Communications, vol. 12, 1994, pp. 568–579.

[BKNS94c] J.J. Blanz, A. Klein, M.M. Naßhan and A. Steil, "Cellular spectrum efficiency of a joint detection CDMA mobile radio system", Proc. International Zurich Seminar on Digital Communications, Zurich, 1994, in [Gün94], pp. 184–195.

[Bla98] J.J. Blanz, Empfangsantennendiversität in CDMA–Mobilfunksystemen mit gemeinsamer Detektion der Teilnehmersignale, Fortschrittberichte VDI, series 10, no. 535, VDI–Verlag, Düsseldorf, 1998.

[BM86] Y. Bresler and A. Markovski, "On the number of signals resolvable by a uniform linear array", IEEE Transactions on Acoustics, Speech, and Signal Processing, vol. 34, 1986, pp. 1361–1375.

[BMW+00] P.W. Baier, M. Meurer, T. Weber and H. Tröger, "Joint Transmission (JT), an alternative rationale for the downlink of Time Division CDMA using multi-element transmit antennas", Proc. IEEE 6th International Symposium on Spread Spectrum Techniques and Applications (ISSSTA 2000), invited paper, Parsippany, 2000, pp. 1-5.

[BN93] P.W. Baier and M.M. Naßhan, "Recent results concerning the benefit of joint detection in CDMA systems", Proc. IEE Colloquium on Spread Spectrum Techniques for Radio Communication Systems, London, 1993, pp. 5/1 – 5/4.

[BPH99] J.J. Blanz, A. Papathanassiou, M. Haardt, I. Furió and P.W. Baier, "Smart antennas for combined DOA and joint channel estimation in time–slotted CDMA mobile radio systems with joint detection", IEEE Transactions on Vehicular Technology, vol. 49, no. 2, 2000.

[BPW99] P.W. Baier, A. Papathanassiou and M. Weckerle, "Recent results on the benefits of adaptive antennas for TD–CDMA mobile radio systems", Proc. IEEE 6th International Conference on Telecommunications (ICT'99), Cheju, 1999, pp. 399–404.

[Bre59] D.G. Brennan, "Linear diversity combining techniques", Proc. of the IRE, vol. 47, 1959, pp. 1075–1102.

[Bru00] C. Brunner, "Efficient space-time processing schemes for WCDMA", Doctoral Dissertation, Munich University of Technology, 2000.

[BSPJ97] J.J. Blanz, R.M. Schmalenberger, A. Papathanassiou and P. Jung, "Smart antenna concepts for time-slotted CDMA", Proc. IEEE 47th Vehicular Technology Conference (VTC'97), Phoenix, 1997, pp. 11–15.

[BSS84] P. Balaban, K.S. Shanmugan and B.W. Stuck, "Computer–aided modeling, analysis, and design of communication systems: Introduction and issue overview", IEEE Journal on Selected Areas in Communications, vol. 2, 1984, pp. 1–8.

[BSWB00] T. Bing, E. Schulz, B. Wegmann and E. Bolinth, "Performance improvement of HIPERLAN/2 by adaptive receiver antennas", Proc. 5th International OFDM Workshop, Hamburg, 2000, pp. 2-1–2-4.

[BTB96] S.J. Baines, T.C. Tozer and A.G. Burr, "Performance limits for multi-user decorrelating detectors in DS-CDMA cellular radio systems", Proc. IEEE 4th International Symposium on Spread Spectrum Techniques & Applications (ISSSTA'96), Mainz, 1996, pp. 486-491.

[Bur67] J.P. Burg, "Maximum entropy spectral analysis", 37th Ann. Meeting, Society Exploration Geohysics, Oklahoma City, 1967.

[Cal88] G. Calhoun, Digital cellular radio, Artech House, Inc., Norwood, 1988.

[Cap69] J. Capon, "High–resolution frequency–wave number spectrum analysis", Proc. of the IEEE, vol. 57, 1969, pp. 1408–1418.

[Cic94] D.J. Cichon, Strahlenoptische Modellierung der Wellenausbreitung in urbanen Mikro- und Pikofunkzellen, Doctoral Dissertation, University of Karlsruhe, 1994. ISSN 0942-2935.

[CoL66] D.R. Cox and P.A.W. Lewis, The statistical analysis of series of events, Methuen, London, 1966.

[COS89] COST 207, Digital land mobile radio communications, Final Report COST Action 207, Office for Official Publications of the European Communities, Luxembourg, 1989.

[COS99] COST 231, Digital mobile radio towards future generation systems, Final Report COST Action 231, Office for Official Publications of the European Communities, Luxembourg, 1999.

[COS01] COST 259, Wireless flexible personalized communications, Final Report COST Action 259, edited by L.M. Correia, John Wiley & Sons Inc., 2001.

[Cox72] H. Cox, "Sensitivity considerations in adaptive beamforming", Proc. NATO Advanced Study Institute on Signal Processing, Loughborough, 1972, pp. 621–644.

[CYC92] P.R. Chang, W.H. Yang and K.K. Chan, "A neural network approach to MVDR beamforming problem", IEEE Transactions on Antennas and Propagation, vol. 40, 1992, pp. 313–322.

[Cz00] A. Czylwik, "Downlink beamforming for systems with Frequency Division Duplex (FDD)", COST 259 Temporary Document TD(00)034, Valencia, 2000.

[CZO87] H. Cox, R.M. Zeskind and M.M. Owen, "Robust adaptive beamforming", IEEE Transactions on Acoustics, Speech, and Signal Processing, vol. 35, 1987, pp. 1365–1376.

[CZO88] H. Cox, R.M. Zeskind and M.M. Owen, "Effects of amplitude and phase errors on linear predictive array processors", IEEE Transactions on Acoustics, Speech, and Signal Processing, vol. 36, 1988, pp. 10–19.

[DAL00] M.O. Damen, K. Abed-Meraim and T.J. Lim, "Transmit diversity as a combination od spatial and delay diversity", Proc. IEEE 6$^{\text{th}}$ International Symposium on Spread Spectrum Techniques & Applications (ISSSTA'00), Parsippany, 2000, pp. 137–140.

[DJFH97] D. Dahlhaus, A. Jarosch, B. Fleury and R. Heddergott, "Joint demodulation in DS/CDMA systems exploiting space and time diversity of the mobile radio channel", Proc. IEEE 8$^{\text{th}}$ International Symposium on Personal, Indoor and Mobile Radio Communications (PIMRC'97), Helsinki, 1997.

[DLDMV96] L. De Lathauwer, B. De Moor and J. Vandewalle, "Independent component analysis based on higher–order statistics only", Proc. IEEE SP Workshop on Statistical Signal Array Processing, Corfu, 1996, pp. 356–359.

[DLR77] A.P. Dempster, N.M. Laird and D.B. Rubin, "Maximum likelihood from incomplete data via the EM algorithm", Journal Royal Statist. Soc, Ser. B, vol. 39, 1977, pp. 477–489.

[DM80] C.N. Dorny and B.S. Meaghr, "Cohering of an experimental nonrigid array by self–survey", IEEE Transactions on Antennas and Propagation, vol. 28, 1980, pp. 902–904.

[DR95] E. Del Re, editor, Mobile and personal communications, Elsevier, Amsterdam, 1995.

[DZ94] U. Dersch and E. Zollinger, "Propagation mechanism in microcell and indoor environments", IEEE Transactions on Vehicular Technology, vol. 43, no. 4, 1994, pp. 1058-1066.

[ECSR98] R.B. Ertel, P. Cardieri, K.W. Sowerbi, T.S. Rappaport and J.R. Reed, "Overview of spatial channel models for antenna array communication systems", IEEE Personal Communications Magazine, vol. 5, no. 1, 1998, pp. 10–22.

[Edr94] M. Edrich, Einsatz computergestützter Methoden im nachrichtentechnischen Systementwurf, gezeigt an Beispielen aus der Spread–Spectrum–Technik, Fortschrittberichte VDI, series 10, no. 276, VDI–Verlag, Düsseldorf, 1994.

[Egg94] P.C.F. Eggers, "TSUNAMI: Spatial radio spreading as seen by directive antennas", COST 231 Temporary Document TD (94) 119, Darmstadt, 1994.

[Egg95] P.C.F. Eggers, "Angular dispersive mobile radio environments sensed by highly directive base station antennas", Proc. IEEE 6$^{\text{th}}$ International Symposium on Personal, Indoor and Mobile Radio Communications (PIMRC '95), Toronto, 1995, pp. 522–526.

[EHWW98] D. Emmer, E. Humburg, P. Weber and M. Weckerle, "Measurements of base station two-branch space and polarization diversity reception and comparison of the diversity gain based on the cdf of signal level and simulations of BER in a GSM system", Proc. IEEE 48$^{\text{th}}$ International Vehicular Technology Conference (VTC'98), Ottawa, 1998, pp. 5–10.

[EJS81] J.E. Evans, J.R. Johnson and D.F. Sun, "High resolution angular spectrum estimation techniques for terrain scattering analysis and angle of arrival estimation", Proc. ASSP Workshop on Spectral Estimation, Hamilton, 1981, pp. 134–139.

[ETO93] P.C.F. Eggers, J. Toftgard and A.M. Opera, "Antenna systems for base station diversity in urban small and micro cells", IEEE Journal on Selected Areas in Communications, vol. 11, 1993, pp. 1046–1056.

[ETSI88] ETSI/TC GSM Recommendations, Series 01–12, 1988.

[ETSI97] ETSI, "WB–TDMA/CDMA – System description and performance evaluation", ETSI SMG 2, TDoc 368/97, 1997.

[ETSI98] ETSI, "The ETSI UMTS Terrestrial Radio Access (UTRA) ITU–R RTT Candidate Submission", ETSI SMG 2, TDoc 260/98, 1998.

[ETS98a] ETSI, "Selection procedures for the choice of radio transmission technologies of the Universal Telecommunications System UMTS (UMTS 30.03)", ETSI TR 101 112, version 3.2.0, 1998.

[Ett76] W. van Etten, "Maximum likelihood receiver for multiple channel transmission systems", Transactions on Communications, vol. 24, 1976, pp. 276–283.

[Far97] C. Farsakh, Raummultiplex mit intelligenten Antennen in zellularen Mobilfunksystemen, Doctoral Dissertation, Munich University of Technology, 1997.

[FBB95] J. Fuhl, E. Bonek, P. Balducci, P. Nowak and H. Garn, "Internal antenna arrangements for personal communication systems", Proc. European Personal and Mobile Communications Conference (EPMCC'95), Bologna, 1995, pp. 62–67.

[FBKM93] T. Felhauer, P.W. Baier, W. König and W. Mohr, "Optimized wideband system for unbiased mobile radio channel sounding with periodic spread spectrum signals", IEICE Transactions on Communications, vol. E76–B, 1993, pp. 1016–1029.

[FDHT96] B.H. Fleury, D. Dahlhaus, R. Heddergott and M. Tschudin, "Wideband angle of arrival estimation using the SAGE algorithm", Proc. IEEE 4th International Symposium on Spread Spectrum Techniques & Applications (ISSSTA '96), Mainz, 1996, pp. 79–85.

[Feh94] T. Felhauer, Optimale erwartungstreue Algorithmen zur hochauflösenden Kanalschätzung mit Bandspreizsignalformen, Fortschrittberichte VDI, series 10, no. 278, VDI–Verlag, Düsseldorf, 1994.

[FHNP95] C. Farsakh, M. Haardt, J.A. Nossek and K. Pensel, "Adaptive antenna arrays in mobile radio systems", in [Wal95], pp. 101–108.

[FKB97] J. Fuhl, A. Kuchar and E. Bonek, "Capacity increase in cellular PCS by smart antennas", Proc. IEEE 47th Vehicular Technology Conference (VTC'97), Phoenix, 1997, pp. 1962–1966.

[FKM94] T. Felhauer, W. König and W. Mohr, "Wideband propagation measurements for characterizing the mobile radio channel and its parameters", Archiv für Elektronik und Übertragungstechnik (AEÜ), vol. 48, no. 6, 1994, pp. 321-331.

[FL96] B.H. Fleury and P.E. Leuthold, "Radiowave propagation in mobile communications: An overview of European research", IEEE Communications Magazine, vol. 34, 1996, pp. 70–81.

[FMB98] J. Fuhl, A.F. Molisch and E. Bonek, "Unified channel model for mobile radio systems with smart antennas", IEE Proc. - Radar, Sonar Navigation, vol. 145, no. 1, 1998, pp. 32–41.

[FN94a] C. Farsakh and J.A. Nossek, "Application of SDMA to mobile radio", Proc. IEEE 4th International Symposium on Personal, Indoor and Mobile Radio Communications (PIMRC'94), The Hague, 1994, pp. 736–739.

[FN96a] C. Farsakh and J.A. Nossek, "On the spatial separation potential of a uniform linear array", Proc. IEEE 46th Vehicular Technology Conference (VTC '96), Atlanta, 1996, pp. 1477–1480.

[FN96b] C. Farsakh and J.A. Nossek, "A real time downlink channel allocation scheme for an SDMA mobile radio system", Proc. IEEE 7th International Symposium on Personal, Indoor and Mobile Radio Communications (PIMRC'96), Taipei, 1996, pp. 1216–1220.

[FN97a] C. Farsakh and J.A. Nossek, "Adaptive antenna arrays in mobile radio systems", Proc. IEEE 47th Vehicular Technology Conference (VTC'97), Phoenix, 1997, pp. 2168–2172.

[FN97b] C. Farsakh and J.A. Nossek, "Maximizing the capacity of an SDMA mobile radio system", Proc. IEEE 4th International Conference on Telecommunications (ICT'97), Melbourne, 1997, pp. 813–818.

[FoG98] G.J. Foschini and M.J. Gans, "On limits of wireless communications in a fading environment when using multiple antennas", Wireless Communications Magazin, vol. 6, 1998, pp. 311–335.

[For72] G.D. Forney, "Maximum–likelihood sequence estimation of digital sequences in the presence of intersymbol interference", IEEE Transactions on Information Theory, vol. 18, 1972, pp. 363–378.

[Fos96] G.J. Foschini, "Layered space-time architecture for wireless communication in a fading environment when using multi-element antennas", Bell Labs Technical Journal, vol. 1, 1996, pp. 41-59.

[FRB97] J. Fuhl, J.P. Rossi and E. Bonek, "High resolution 3-D direction-of-arrival determination for urban mobile radio", IEEE Transactions on Antennas and Propagation, vol. 45, no. 4, 1997, pp. 672-681.

[FTH99] B.H. Fleury, M. Tschudin, R. Heddergott, D. Dahlhaus and K.I. Pedersen, "Channel parameter estimation in mobile radio environments using the SAGE algorithm", IEEE Journal on Selected Areas in Communications, vol. 17, 1999, pp. 434–450.

[Fuh97] J. Fuhl, Smart antennas for second and third generation mobile communications systems, Doctoral Dissertation, Technical University of Vienna, 1997.

[FW88] M. Feder and E. Weinstein, "Parameter estimation of superimposed signals using the EM algorithm", IEEE Transactions on Acoustics, Speech, and Signal Processing, vol. 36, 1988, pp. 477–489.

[Gab76] W.F. Gabriel, "Adaptive arrays – An introduction", Proc. IEEE, vol. 64, 1976, pp. 239–272.

[Gant91] F.R. Gantmacher, The theory of matrices, vol. 1, Chelsea Publishing Company, New York, 1991.

[Gia99] G.B. Giannakis, editor, "Highlights of signal processing for communications", IEEE Signal Processing Magazine, 1999, pp. 14–48.

[Gih91] K.S. Gihousen, et.al., "On the capacity of cellular CDMA systems", IEEE Transactions on Vehicular Technologies, vol. 40, no. 2, 1991, pp. 302–312.

[GL97] S.G. Glisic and P.A. Leppänen, editors, Wireless communications, Dordrecht, Kluwer, 1997.

[GM89] G.B. Giannakis and J.M. Mendel, "Identification of nonminimum phase systems using higher order statistics", IEEE Transactions on Acoustics, Speech, and Signal Processing, vol. 37, 1989, pp. 360–367.

[God97a] L.C. Godara, "Applications of antenna arrays to mobile communications, Part I: Performance improvement, feasibility, and system considerations", Proc. of the IEEE, vol. 85, 1997, pp. 1031–1060.

[God97b] L.C. Godara, "Applications of antenna arrays to mobile communications, Part II: Beam–forming and direction–of–arrival considerations", Proc. of the IEEE, vol. 85, 1997, pp. 1195–1245.

[Gol69] G.H. Golub, "Matrix decompositions and statistical calculations", in [MN69], 1969, pp. 365–397.

[Gov84] A.K. Govil, Definitions and formulae in statistics, Macmillan Press, London, 1984.

[GR94] M. Goldburg and R.H. Roy, "The impacts of SDMA on PCS system design", Proc. IEEE International Conference on Universal Personal Communications (ICUPC'94), San Diego, 1994, pp. 242–246.

[Gra81] A. Graham, Kronecker products and matrix calculus with applications, Ellis Horwood, Chichester, 1981.

[Gra94] F. Graf, Florian Digitale drahtlose Mikrofonsysteme mit Vielfachzugriff, Fortschrittberichte VDI, series 10, no. 284, VDI–Verlag, Düsseldorf, 1994.

[GT95] N. Gerlich and M. Tangemann, "Towards a channel allocation scheme for SDMA–based mobile communication systems", in [Wal95], pp. 109–116.

[GTB98] P.M. Grant, J.S. Thompson and B. Mulgrew, "Antenna arrays for cellular CDMA systems", Proc. IEEE 5th International Symposium on Spread Spectrum Techniques & Applications (ISSSTA'98), Sun City, 1998, pp. 404–410.

[Gün94] C.C. Günther, editor, Lecture Notes in Computer Science, vol. 783, Zurich, Springer–Verlag, 1994.

[GTM99] P.M. Grant, J.S. Thompson and B. Mulgrew, "Antenna arrays for cellular CDMA systems", published in CDMA techniques for third generation mobile systems, edited by F. Swarts et.al., Kluver Academic Publishers, Boston/Dordrecht/London, 1999.

[GVGZ92] S.A. Grandhi, R. Vijayan, D.J. Goodman, and J. Zander, "Centralized power control in cellular radio systems", IEEE Transactions on Vehicular Technology, vol. 42, 1992, pp. 466–468.

[GvL90] G.H. Golub and C.F. van Loan, editors, Matrix computations, The Johns Hopkin University Press, 1990.

[Haa97a] M. Haardt, Efficient one– two– and multidimensional array signal processing, Forschungsberichte, Shaker Verlag, Aachen, 1997.

[Haa97b] M. Haardt, "Structured least squares to improve the performance of ESPRIT–type algorithms", IEEE Transactions on Signal Processing, vol. 45, 1997, pp. 792–799.

[Hag97] J. Hagenauer, "The turbo principle: Tutorial introduction and state od the art", Proc. International Symposium on Turbo Codes and Related Topics, Brest, 1997, pp. 1-11.

[Har97] C. Hartmann, "Dynamic channel allocation in cellular communication systems with SDMA", Proc. 2nd European Personal Mobile Communications Conference (EPMCC'97), Bonn, 1997.

[Hat80] M. Hata, "Empirical formula for propagation loss in land mobile radio services", IEEE Transactions on Vehicular Technology, vol. 29, 1980, pp. 317–325.

[Hay85] S. Haykin, editor, Array signal processing , Prentice–Hall, Inc., Englewood Cliffs, New Jersey, 1985.

[Hay91] S. Haykin, Adaptive filter theory, Prentice–Hall, Inc., Englewood Cliffs, New Jersey, 2nd edition, 1991.

[HBD00] J.S. Hammerschmidt, C. Brunner and C. Drewes, "Eigenbeamforming - a novel concept in space and space-time processing", Proc. European Wireless 2000, Dresden, 2000.

[Hess93] G.C. Hess, Land–mobile radio system engineering, Artech House, Boston, 1993.

[HMV00] M. Haardt, C.F. Mecklenbräuker and M. Vollmer, "Adaptive antennas for third generation mobile radio systems", Proc. VDE World Microtechnologies Congress (MICRO.tec 2000), Hannover, 2000, pp. 201-206.

[HN95] M. Haardt and J.A. Nossek, "Unitary ESPRIT: How to obtain increased estimation accuracy with a reduced computational burden", IEEE Transactions on Signal Processing, vol. 43, 1995, pp. 1232–1242.

[Höh90] P. Höher, Kohärenter Empfang trelliscodierter PSK–Signale auf frequenzselektiven Mobilfunkkanälen — Entzerrung, Decodierung und Kanalparameterschätzung, Fortschrittberichte VDI, series 10, no. 147, VDI–Verlag, Düsseldorf, 1990.

[Höh92] P. Höher, “A statistical discrete–time model for the WSSUS multipath channel”, IEEE Transactions on Vehicular Technology, vol. 35, 1992, pp. 461–468.

[How65] P.W. Howells, “Intermediate Frequency Sidelobe Canceller”, U.S. Patent 3202990, 1965.

[HR90] J. Huber and A. Rüppel, “Zuverlässigkeitsschätzung für die Ausgangssymbole von Trellis–Decodern”, IEEE International Journal of Electronics and Communications, vol. 44, 1990, pp. 8–21.

[HS99] C. Hartmann and R. Steffen, “Dynamische Kanalvergabe in SDMA–Systemen mit unregelmäßigem Zell–Layout”, Proc. ITG Diskussionssitzung Systeme mit intelligenten Antennen, Stuttgart, 1999.

[Hsu82] F.M. Hsu, “Square root Kalman filtering for high–speed data received over fading dispersive HF channels”, IEEE Transactions on Information Theory, vol. 28, 1982, pp. 753–763.

[HV99] C. Hartmann and H.J. Vögel, “Teletraffic analysis of SDMA systems with inhomogeneous MS location, distribution and mobility“, Wireless Personal Communications, vol. 11/1, 1999, pp. 45–62.

[HZMN95] M. Haardt, M.D. Zoltowski, C.P. Mathews and J.A. Nossek, “2D unitary ESPRIT for efficient 2D parameter estimation”, Proc. IEEE International Conference on Acoustics, Speech, Signal Processing (ICASSP’95), Detroit, 1995, pp. 2096–2099.

[IK96] N. Ishi and R. Kohno, “Spatially and temporally joint transmitter–receiver using an adaptive array antenna”, IEICE Transactions on Communications, vol. E79–B, 1996, pp. 361–367.

[ITU97] Special Issue, “IMT–2000: Standards efforts of the ITU”, IEEE Personal Communications Magazine, 1997.

[ITU00] ITU, “IMT–2000: The global standard for third generation wireless communications”, published in the Internet under the URL http://www.itu.int/imt/what_is/imt/index.html, 2000.

[ITU00a] Rec. ITU-RM 1225, ”Guideline for evaluation of radio transmission technologies for IMT–2000”, 2000.

[Jak74] W. Jakes, Microwave mobile communications, John Wiley & Sons, New York, 1974.

[JBM01] C.A. Jötten, P.W. Baier and M. Meurer, “Transmit array processing for CDMA downlinks utilizing the duplexing scheme FDD”, Proc. 7$^{\text{th}}$ International Conference on Telecommunications (ICT 2001), Bucharest, 2001, pp. 419-424.

[JBS92] M.C. Jeruchim, P. Balaban and K.S. Shanmugan, Simulation of communication systems, Plenum Press, New York, 1992.

[KA97] D. Koulakiotis and A.H. Aghvami, "Evaluation of a DS/CDMA multi–user receiver employing a hybrid form of interference cancellation in Rayleigh fading channels", IEEE Communications Letters, vol. 2, 1997, pp. 61–63.

[KA98] D. Koulakiotis and A.H. Aghvami, "Hybrid interference cancellation, a multiuser detection scheme for W–DS/CDMA systems", Proc. IEEE 5^{th} International Conference on Telecommunications (ICT'98), Chalkidiki, 1998, pp. 318–322.

[KaL91] G. Kadel and R.W. Lorenz, "Breitbandige Ausbreitungsmessungen zur Charakterisierung des Funkkanals beim GSM System", Frequenz, vol. 45, no. 7-8, 1991, pp. 158-163.

[Kap96] E.D. Kaplan, Understanding GPS: Principles and applications, Artech House, Boston, 1996.

[Kat97] R. Kattenbach, Charakterisierung zeitvarianter Indoor–Funkkanäle anhand ihrer System- und Korrelationsfunktionen, Shaker Verlag, Aachen, 1997.

[Kay93] S.M. Kay, Fundamentals of statistical signal processing: Estimation theory, Prentice Hall, New Jersey, 1993.

[KB92a] A. Klein and P.W. Baier, "Optimum unbiased data estimation in mobile radio systems applying CDMA", COST 231 Temporary Document TD (92) 16, Vienna, 1992.

[KB92b] A. Klein and P.W. Baier, "Simultaneous cancellation of cross interference and ISI in CDMA mobile radio communications", Proc. IEEE 3^{rd} International Symposium on Personal, Indoor and Mobile Radio Communications (PIMRC '92), Boston, 1992, pp. 118–122.

[KB93] A. Klein and P.W. Baier, "Linear unbiased data estimation in mobile radio systems applying CDMA", IEEE Journal on Selected Areas in Communications, vol. 11, 1993, pp. 1058–1066.

[KBJ95] A. Klein, J.J. Blanz, P. Jung, M.M. Naßhan, A. Steil, B. Steiner and P. W. Baier, "Summarizing review of a JD–CDMA third generation mobile radio system concept developed within COST 231 – Part 2", COST 231 Temporary Document TD (95) 18, Berne, 1995.

[KCW93a] T. Kürner, D. Cichon and W. Wiesbeck, "Concepts and results for 3D digital terrain–based wave propagation models: An overview", IEEE Transactions on Communications, vol. 41, 1993, pp. 1002–1012.

[KCW93b] T. Kürner, D.J. Cichon and W. Wiesbeck, "Concepts and results for 3D digital terrain based wave propagation models — an overview", IEEE Journal on Selected Areas in Communications, vol. 11, 1993, pp. 1002–1012.

[KIH82a] R. Kohno, H. Imai and M. Hatori, "Cancellation techniques of co–channel interference in asynchronous spread spectrum multiple access systems", IECE Technical report, CS82–38, 1982, pp. 29–35.

[KIH82b] R. Kohno, H. Imai and M. Hatori, "Cancellation techniques of co–channel interference in asynchronous spread spectrum multiple access", IECE Technical Report, vol. CS82-38, 1982, pp. 29–35.

[KIH83] R. Kohno, H. Imai and M. Hatori, "Cancellation techniques of co–channel interference in asynchronous spread spectrum multiple access systems", Transactions of the IECE Japan, vol. J66–A, 1983, pp. 416–423.

[KIHP90] R. Kohno, H. Imai, M. Hatori and S. Pasupathy, "Combination of an adaptive array antenna and a canceller of interference for direct-sequence spread spectrum multiple access systems", IEEE Journal on Selected Areas in Communications, vol. 8, 1990, pp. 675-682.

[KKB93] A. Klein, K. Kaleh and P.W. Baier, "Zero forcing and minimum mean square error equalization for multi–user detection in code division multiple access", IEEE Transactions on Vehicular Technology, vol. 35, 1993, pp. 461–468.

[KKB94] A. Klein, G.K. Kaleh and P.W. Baier, "Equalizers for multi–user detection in code division multiple access mobile radio systems", Proc. IEEE 44$^{\text{th}}$ Vehicular Technology Conference (VTC '94), Stockholm, 1994, pp. 762–766.

[Kle96] A. Klein, Multi–user detection of CDMA–signals — algorithms and their application to cellular mobile radio, Fortschrittberichte VDI, series 10, no. 423, VDI–Verlag, Düsseldorf, 1996.

[Kle75] L. Kleinrock, Queueing systems, Volume I: Theory , John Wiley & Sons Inc., New York, 1975.

[KLF86] S.Y. Kung, C.K. Lo and R. Foka, "A Toeplitz approximation approach to coherent source direction finding", Proc. IEEE International Conference on Acoustics, Speech, Signal Processing (ICASSP'86), Tokyo, 1986, pp. 193–196.

[KM96] A. Klein and W. Mohr, "A statistical wideband mobile radio channel model including the directions-of-arrival", Proc. IEEE 4$^{\text{th}}$ International Symposium on Spread Spectrum Techniques & Applications (ISSSTA'96), Mainz, 1996, pp. 102–106.

[KMT96] A. Klein, W. Mohr, R. Thomas, P. Weber and B. Wirth, "Direction-of-arrival of partial waves in wideband mobile radio channels for intelligent antenna concepts", Proc. IEEE 46$^{\text{th}}$ Vehicular Technology Conference (VTC '96), Atlanta, 1996, pp. 849–853.

[Koh94] R. Kohno, "Spatial and temporal filtering for co–channel interference in CDMA", Proc. IEEE 3$^{\text{rd}}$ International Symposium on Spread Spectrum Techniques & Applications (ISSSTA'94), Oulu, 1994, pp. 51–60.

[Koh98] R. Kohno, "Spatial and temporal communication theory using adaptive antenna arrays", IEEE Personal Communications, vol. 5, no. 1, 1998, pp. 28–35.

[KP85] S.A. Kassam and H.V. Poor, "Robust techniques for signal processing: A survey", Proc. of the IEEE, vol. 73, 1985, pp. 433–481.

[KPK94] B.H. Khalaj, A. Paulraj, and T. Kailath, “2D RAKE receivers for CDMA cellular systems”, Proc. GLOBECOM’94, San Francisco, 1994, pp. 400–404.

[KS95] J. Kennedy and M.C. Sullivan, “Direction finding and smart antennas using software radio architectures”, IEEE Communications Magazine, vol. 33, 1995, pp. 62–68.

[KSS95] A. Klein, B. Steiner, and A. Steil, “Known and novel diversity approaches in a JD–CDMA system concept developed within COST 231”, Proc. IEEE 6th International Symposium on Personal, Indoor and Mobile Radio Communications (PIMRC ’95), Toronto, 1995, pp. 512–516.

[KT82] R. Kumaresan and D.W. Tufts, “Estimation of frequencies of multiple sinusoids: Making linear prediction perform like maximum likelihood”, Proc. IEEE, vol. 70, 1982, pp. 975–989.

[KT83] R. Kumaresan and D.W. Tufts, “Estimating the angles of arrival of multiple plane waves”, IEEE Transactions on Aerospace and Electronic Systems, vol. 19, 1983, pp. 134–139.

[KTBT99] A. Kuchar, M. Taferner, E. Bonek, M. Tangemann and C. Hoek, “A run-time optimized adaptive antenna array processor for GSM”, Proc. 3rd European Personal Mobile Communications Conference, Paris, 1999, pp. 307-312.

[KTT99] A. Kuchar, M. Taferner, M. Tangemann, C. Hoek, W. Rauscher, M. Strasser, G. Pospischil, and E. Bonek, “Real–time GSM smart antenna demonstrator”, Proc. ITG Diskussionssitzung Systeme mit intelligenten Antennen, Stuttgart, 1999.

[KV96] H. Krim and M. Viberg, “Two decades of array signal processing research”, IEEE Signal Processing Magazine, 1996, pp. 67–94.

[Lee82] W.C.Y. Lee, Mobile communications engineering, McGraw–Hill, New York, 1982.

[Lee85] W.C.Y. Lee, “Estimate of local average power of a mobile radio signal”, IEEE Transactions on Vehicular Technology, vol. 34, no. 1, pp. 22–27, 1985.

[Lee89] W.C.Y. Lee, Mobile cellular telecommunications systems, McGraw–Hill, New York, 1989.

[Lee91] W.C.Y. Lee, “Overview of cellular CDMA”, IEEE Transactions on Vehicular Technology, vol. VT–40, 1991, pp. 291–302.

[Lee72] W.C.Y. Lee, “Polarization diversity system for mobile radio. IEEE Transactions on Communications, vol. 20, 1972, pp. 912–923.

[Lew72] P.A.W. Lewis (editor), Stochastic point process. Statistical analysis, theory and applications, John Wiley & Sons Inc., New York, 1972.

[LH74] C.L. Lawson and R.J. Hanson, Solving least squares problems, Prentice–Hall, Inc., Englewood Cliffs, New Jersey, 1974.

[LK94] U. Liebenow and P. Kuhlmann, "Theoretical investigations and wideband measurements on wave propagation in hilly terrain", Proc. IEEE 44th Vehicular Technology Conference (VTC'94), Stockholm, 1994, pp. 1803–1806.

[LL96] J. Litva and T.K.-Y. Lo, Digital beamforming in wireless communications, Artech House Publishers, Boston, London, 1996.

[Loe92] K. Loew, "Comparison of urban propagation models with CW measurements", Proc. IEEE 42nd Vehicular Technology Conference (VTC '92), Denver, 1992, pp. 936–942.

[Lop96] A.R. Lopez, "Performance predictions for cellular switched-beam intelligent antenna systems", IEEE Communications Magazine, Oct. 1996, pp. 152–154.

[LoP00] A. Logothetis and H.V. Poor, "Fast switched-beam beamforming for optimal selection combining in frequency selective fading CDMA channels", Proc. IEEE 6th Internatioanl Symposium on Spread Spectrum Techniques & Applications (ISSSTA'00), Parsippany, 2000, pp. 20–24.

[Lor85] R.W. Lorenz, "Zeit- und Frequenzabhängigkeit der Übertragungsfunktion eines Funkkanals bei Mehrwegeausbreitung mit besonderer Berücksichtigung des Mobilfunkkanals," Der Fernmelde-Ingenieur, vol. 39, no. 4, 1985, pp. 1-45.

[LP96] W. Lee and R.L. Pickholtz, "Maximum likelihood multiuser detection with use of linear antenna arrays", published in the Internet under the URL http://www.seas.gwu.edu/faculty/pickholt/conference-papers.html, 1996.

[LRK99] M.P. Lötter, P. van Rooyen, and R. Kohno, "Spatial filtering and CDMA", published in CDMA techniques for third generation mobile systems, edited by F. Swarts et.al., Kluver Academic Publishers, Boston/Dordrecht/London, 1999.

[LT83] M.G. Larimore and J.R. Treichler, "Convergence behaviour of the constant modulus algorithm", Proc. IEEE International Conference on Acoustics, Speech, Signal Processing (ICASSP'83), 1983, pp. 13–16.

[Lük79] H.D. Lüke, Signalübertragung, Springer–Verlag, Berlin/Heidelberg/New York, 1979.

[Lup89] R. Lupas, "Near-far resistant linear multiuser detection", Doctoral Dissertation, Princeton University, Princeton, 1989.

[LV90] R. Lupas and S. Verdú, "Near-far resistance of multiuser detectors in asynchronous channels", IEEE Transactions on Communications, vol. 38, no. 4, 1990, pp. 496-508.

[LWK92] M. Lebherz, W. Wiesbeck and W. Krank, "A versatile wave propagation model for the VHF/UHF range considering three–dimensional terrain", IEEE Transactions on Communications, vol. 40, 1992, pp. 1121–1131.

[LZ97] H. Liu and M.D. Zoltowski, "Blind equalization in antenna array CDMA systems", IEEE Transactions on Signal Processing, vol. 45, 1997, pp. 161–172.

[Ma74] M.T. Ma, Theory and application of antenna arrays, John Wiley & Sons Inc., New York, 1974.

[Mar87] S.L. Marple, Jr., Digital Spectral Analysis with Applications, Prentice–Hall, Englewood Cliffs, New Jersey, 1987.

[Mar94] U. Martin, Ausbreitung in Mobilfunkkanälen: Beiträge zum Entwurf von Meßgeräten ud zur Echoschätzung, Doctoral Dissertation, University of Erlangen–Nürnberg, 1994.

[Mar97] U. Martin, "A directional radio channel model for densely build-up urban areas", Proc. 3rd ITG-Fachtagung "Mobile Kommunikation", 1997.

[May93] S. Mayrargue, "Spatial equalization of a radio–mobile channel without beamforming using the constant modulus algorithm (CMA)", Proc. IEEE International Conference on Acoustics, Speech, Signal Processing (ICASSP'93), vol. III, 1993, pp. 344–347.

[May99] J. Mayer, Signalisierungsprotokolle und Verkehrskapazität eines Mobilfunksystems der dritten Generation, Forschungsberichte Mobilkommunikation, vol. 2, University of Kaiserslautern, 1999. ISBN 3–925178–31–7.

[MDCM95] E. Moulines, P. Duhamel, J.F. Cardoso and S. Mayrargue, "Subspace methods for the blind identification of multichannel FIR filters", IEEE Transactions on Signal Processing, vol. 43, 1995, pp. 516–525.

[MG96] U. Martin and M. Grigat, "A statistical simulation model for the directional mobile radio channel and its configuration", Proc. IEEE 4th International Symposium on Spread Spectrum Techniques & Applications (ISSSTA'96), Mainz, 1996, pp. 86–90.

[MH94] U. Madhow and M.L. Honig, "MMSE interference suppression for direct-sequence spread-spectrum CDMA", IEEE Transactions on Communications, vol. 42, no. 12, 1994, pp. 3178-3188.

[MJ96] A. Mansour and C. Jutten, "A direct solution for blind separation of sources", IEEE Transactions on Signal Processing, vol. 44, 1996, pp. 746–748.

[MLK98] A.F. Molisch, J. Laurila and A. Kuchar, "Geometry–based stochastic model for mobile radio channels with directional components", COST 259 Temporary Document TD(98) 076, Duisburg, 1998.

[MLKS98] A.F. Molisch, J. Laurila, A. Kuchar and R. Schmalenberger, "Test scenarios for mobile radio systems with adaptive antennas", Proc. COST 252/259 Joint Workshop, Bradford, 1998, pp. 162–170.

[MM80] R.A. Monzingo and W.T. Miller, Introduction to adaptive arrays, Wiley & Sons, Inc. , New York, 1980.

[Moh95] W. Mohr, “Modelling of wideband mobile radio channels based on propagation measurements”, Proc. IEEE 6^{th} International Symposium on Personal, Indoor and Mobile Communications (PIMRC’95), Toronto, 1995, pp. 397–401.

[Moh98] M. Moher, “An iterative multiuser decoder for near-capacity communications”, IEEE Transactions on Communications, vol. 46, 1998, pp. 870-880.

[Moh00] W. Mohr, “European reserach projects towards third generation mobile radio systems and beyond”, Proc. IEEE 6^{th} International Symposium on Spread Spectrum Techniques & Applications (ISSSTA’00), keynote speech, Parsippany, 2000.

[MN69] R.C. Milton and J.A. Nelder, editors, Statistical calculations, Academic Press, New York, 1969.

[MP92] M. Mouly and M.B. Pautet, editors, The GSM–system for mobile communications, 1992.

[MSC81] J.T. Mayhan, A.J. Simmons, and W.C. Cummings, “Wideband adaptive nulling using tapped delay lines”, IEEE Transactions on Antennas and Propagation, vol. AP-29, 1981, pp. 923–936.

[MSW97a] J. Mayer, J. Schlee and T. Weber, “Protocol and signaling aspects of joint detection CDMA”, Proc. IEEE 8^{th} International Symposium on Personal, Indoor and Mobile Radio Communications (PIMRC ’97), Helsinki, 1997, pp. 867–871.

[MSW97b] J. Mayer, J. Schlee and T. Weber, “Realtime feasibility of joint detection CDMA”, Proc. 2^{nd} European Personal Mobile Communications Conference (EPMCC’97), Bonn, 1997, pp. 245–252.

[MSW98] J. Mayer, J. Schlee and T. Weber, “Handoff protocols in JD–CDMA”, Proc. IEEE 9^{th} International Symposium on Personal, Indoor and Mobile Radio Communications (PIMRC ’98), Boston, 1998, pp. 355–359.

[MuH97] R.R. Müller and J.B. Huber, ”Iterated soft decision interference cancellation for CDMA”, Proc. 9^{th} Tyrrhenian International Workshop on Digital Communications, Italy, 1997.

[Mue01] R.R. Müller, “Multiusers receivers for randomly spread signals: Fundamental limits with and without decision-feedback”, IEEE Transactions on Information Theory, vol. 47, no. 1, 2001, pp. 268-263.

[Naß95] M.M. Naßhan, Realitätsnahe Modellierung und Simulation nachrichtentechnischer Systeme, gezeigt am Beispiel eines CDMA–Mobilfunksystems, Fortschrittberichte VDI, series 10, no. 384, VDI–Verlag, Düsseldorf, 1995.

[Nit79] R. Nitzberg, “Effects of errors in adaptive weights”, IEEE Transactions on Aerospace and Electronic Systems, vol. 12, 1979, pp. 369–373.

[NPK94] A.F. Naguib, A. Paulraj and T. Kailath, “Capacity improvement with base–station antenna arrays in cellular CDMA”, IEEE Transactions on Vehicular Technology, vol. 43, 1994, pp. 691–698.

[NSC00] A.F. Naguib, N. Seshadri and A.R. Calderbank, "Space-time coding and signal processing for wireless communications", IEEE Signal Processing Magazine, 2000, pp. 76–92.

[NTD+98] E. Nikula, A. Toskala, E. Dahlman, L. Girard and A. Klein, "FRAMES multiple access for UMTS and IMT–2000", IEEE Personal Communications, April 1998, pp. 16–24.

[NTW] A. Narula, M. Trott and G. Wornell, " IEEE Transactions on Information Theory, to be published.

[OHG99] OHG, "Harmonized global 3G (G3G) technical framework for ITU IMT–2000 CDMA proposal", Operator Harmonization Group , submitted to ITU–R, Beijing, 1999.

[Ost01] J. Oster, Ein Beitrag zur Interzellinterferenzreduktion in zeitgeschlitzten CDMA-Systemen, Forschungsberichte Mobilkommunikation, vol. 9, University of Kaiserslautern, 2001. ISBN 3–925178–73–2.

[PaH89] K. Pahalvan and S.J. Howard, "Frequency domain measurements of indoor radio channels", Electronic Letters, vol. 25, no. 24, 1989, pp. 1645-1647.

[PaP97] A.J. Paulraj and C.B. Papadias, "Space-Time Processing for Wireless Communications", IEEE Signal Processing Magazine, vol. 14, no. 6, 1997, pp. 49-83.

[Pap65] A. Papoulis, Probability, random variables and stochastic processes, McGraw–Hill, Auckland, 1965.

[Pap00] A. Papathanassiou, Adaptive antennas for mobile radio systems using Time Division CDMA and joint detection, Forschungsberichte Mobilkommunikation, vol. 6, University of Kaiserslautern, 2000. ISBN 3–925178–48–1.

[Par92] J.D. Parsons, The mobile radio propagation channel, Pentech Press, London, 1992.

[PBHP98] A. Papathanassiou, J.J. Blanz, M. Haardt and P.W. Baier, "Spatial channel assignment considerations in a joint detection CDMA mobile radio system employing smart antennas", Proc. IEEE 5$^{\text{th}}$ International Conference on Telecommunications (ICT'98), vol. II, Chalkidiki, 1998, pp. 318–322.

[PBWS] A. Papathanassiou, J.J. Blanz, M. Weckerle and R. Schmalenberger, "Benefits of adaptive antennas in the uplink of TD-CDMA mobile radio systems", to appear in Third Generation Mobile Radio Systems, Springer–Verlag, Berlin/Heidelberg/new York.

[PCVM97] F.P. Pipon, P. Chevalier, P. Villa and J.-J. Monot, "Joint spatial and temporal equalization for channels with isi and cci: Theoretical and experimental results for a base station reception", Proc. IEEE Signal Processing Workshop on Signal Processing Advances in Wireless Communications, Paris, 1997, pp. 309–312.

[Pen99] K. Pensel, Signalverarbeitung für Mobilfunksysteme mit intelligenten Antennen, Doctoral Dissertation, Munich University of Technology, 1999.

[Per94] V. Perez, editor, Final propagation model, No. R2020/TDE/PS/DS/P/040/al, RACE UMTS Code Division Testbed (CODIT), Amsterdam, 1994.

[PFB97a] A. Papathanassiou, I. Furió, J.J. Blanz, M. Haardt and R. Schmalenberger, "Suboptimum combined direction of arrival and channel estimation for time–slotted CDMA with joint detection", COST 259 Temporary Document TD(97)025, Turin, 1997.

[PFB97b] A. Papathanassiou, I. Furió and J.J. Blanz, "Link level performance in the uplink of a joint detection CDMA mobile radio system employing multi–antenna array configurations", COST 259 Temporary Document TD(97)051, Lisbon, 1997.

[PFBP99] A. Papathanassiou, I. Furió, J.J. Blanz and P.W. Baier, "Smart antennas with two–dimensional array configurations for performance enhancement of a joint detection CDMA mobile radio system", Wireless Personal Communications, vol. 11/1, 1999, pp. 89–108.

[PFM94] K. Pedersen, B. Fleury and P. Mogensen, "High resolution of electromagnetic waves in time–varying radio channels", Proc. IEEE 8^{th} International Symposium on Personal, Indoor and Mobile Radio Communications (PIMRC'94), Helsinki, 1994.

[PGH95] J.E. Padgett, C.G. Günther and T. Hattori, "Overview of wireless personal communications", IEEE Communications Magazine, vol. 33, 1995, pp. 28–41.

[PH94] P. Patel and J. Holztmann, "Analysis of a successive interference cancellation scheme in a DS–CDMA system", IEEE Journal on Selected Areas in Communications, vol. 12, 1994, pp. 796–807.

[PHFB97] A. Papathanassiou, M. Haardt, I. Furió and J.J. Blanz, "Multi-user direction of arrival and channel estimation for time-slotted CDMA with joint detection", Proc. IEEE International Conference on Digital Signal Processing (DSP'97), Santorini, 1997, pp. 375–378.

[PHW99] A. Papathanassiou, C. Hartmann and T. Weber, "Uplink spectrum efficiency and capacity of TD–CDMA with adaptive antennas", COST 259 Temporary Document TD(99)113, Leidschendam, 1999.

[PK89] S.U. Pillai and B.H. Kwon, "Forward/Backward spatial smoothing techniques for coherent signal identification", IEEE Transactions on Acoustics, Speech, and Signal Processing, vol. 37, 1989, pp. 8–15.

[PN97] K. Pensel and J.A. Nossek, "DOA Estimation for SDMA Systems", COST 259 Temporary Document TD(97)024, Turin, 1997.

[PN98] K. Pensel and J.A. Nossek, "Uplink and downlink calibration of smart antennas", Proc. IEEE 5^{th} International Conference on Telecommunications (ICT'98), vol. II, Chalkidiki, 1998, pp. 323–327.

[POB99] A. Papathanassiou, J. Oster and P.W. Baier, "A novel simulation concept of reduced computational cost for TD–CDMA mobile radio systems with adaptive antennas", Proc. IEEE 50th Vehicular Technology Conference (VTC'99 Fall), Amsterdam, 1999, pp. 218–222.

[Poo00] H.V. Poor, "Turbo multiuser detection: An overview", Proc. IEEE 6th International Symposium on Spread Spectrum Techniques & Applications (ISSSTA 2000), Parsippany, 2000, pp. 583-587.

[Pro89] J.G. Proakis, Digital communications, McGraw–Hill, New York, 2nd edition, 1989.

[PSWB98] A. Papathanassiou, R. Schmalenberger, M. Weckerle and P.W. Baier, "User angular separation considerations on the uplink performance of a TD–CDMA mobile radio system", COST 259 Temporary Document TD(98)055, Bradford, 1998.

[PSWB99] A. Papathanassiou, R. Schmalenberger, M. Weckerle and P.W. Baier, "Advances in channel estimation techniques in TD–CDMA mobile radio systems with smart antennas", Proc. International Workshop on Mobile Communications (IWMC'99), Chania, 1999, pp. 11–20.

[PTVF92] W.H. Press, S.A. Teukolsky, W.T. Vetterling and B.P. Flannery, Numerical recipes in C, Cambridge University Press, New York, 1992.

[PW98] A. Papathanassiou and M. Weckerle, "A spatial channel assignment strategy for improving the performance of TD–CDMA mobile radio systems with smart antennas", Proc. ITG Diskussionssitzung Systeme mit intelligenten Antennen für UMTS und GSM, Karlsruhe, 1998.

[PW99] A. Papathanassiou and M. Weckerle, "Transmission quality enhancement by considering the spatial interference covariance matrix in a TD–CDMA mobile radio system with adaptive antennas", Proc. ITG Diskussionssitzung Systeme mit intelligenten Antennen, Stuttgart, 1999.

[PWBB98] A. Papathanassiou, M. Weckerle, J.J. Blanz and P.W. Baier, "Influence of user spatial separation on the uplink performance of a TD–CDMA mobile radio system with smart antennas", Proc. IEEE 5th International Symposium on Spread Spectrum Techniques & Applications (ISSSTA'98), Sun City, 1998, pp. 384–388.

[RaC98] G. Raleigh and J. Cioffi, "Spatio-temporal coding for wireless communication", IEEE Transactions on Communications, vol. 46, no. 3, 1998, pp. 357–366.

[Rap96] T.S. Rappaport, Wireless communications: Principles & Practice, Prentice-Hall, Inc., Upper Saddle River, New Jersey, 1996.

[Rap98] T.S. Rappaport, editor, Smart antennas: adaptive arrays, algorithms, and wireless position location, Published by the IEEE, 1998.

[Ree98] M.C. Reed *et al.*, "Iterative multiuser detection for CDMA with FEC: Near single user performance", IEEE Transactions on Communications, vol. 46, 1998, pp. 1693-1699.

[Ris78] J. Rissanen, "Modeling by shortest data description", Automatica, vol. 14, 1978, pp. 465–471.

[RK89] R.H. Roy and T. Kailath, "ESPRIT — estimation of signal parameters via rotational invariance techniques", IEEE Transactions on Signal Processing, vol. 37, 1989, pp. 984–995.

[RRPR97] Z. Rong, T.S. Rappaport, P. Petrus and J.H. Reed, "Simulation of multitarget adaptive algorithms for wireless CDMA systems", Proc. IEEE 47th Vehicular Technology Conference (VTC'97), Phoenix, 1997, pp. 1–5.

[RS87a] Y. Rockah and P.M. Schultheiss, "Array shape calibration using sources in unknown locations – part 1: Far field sources", IEEE Transactions on Acoustics, Speech, and Signal Processing, vol. 35, 1987, pp. 286–299.

[RS87b] Y. Rockah and P.M. Schultheiss, "Array shape calibration using sources in unknown locations – part 2: Near field sources and estimator implementation", IEEE Transactions on Acoustics, Speech, and Signal Processing, vol. 35, 1987, pp. 286–299.

[RTVW95] R. Rheinschmitt, M. Tangemann, J.O. Vallet and V. Weyl, "Network aspects of the introduction of adaptive arrays in mobile communication systems", Proc. RACE Mobile Telecommunications Summit, Cascais, 1995, pp. 367–371.

[RZ96] J. Ramos and M.D. Zoltowski, "Reduced complexity 2D RAKE receiver for CDMA", Proc. IEEE SP Workshop on Statistical Signal Array Processing, Corfu, 1996, pp. 502–505.

[RZ97] J. Ramos and M.D. Zoltowski, "Blind space–time processor for CDMA to maximize the SNIR", Proc. IEEE SP for Advanced Wireless Communications (SPAWC'97), Paris, 1997.

[SB96] A.J. Steil and J.J. Blanz, "Spectral efficiency of JD-CDMA mobile radio systems applying coherent receiver antenna diversity with directional antennas", Proc. IEEE 4th International Symposium on Spread Spectrum Techniques & Applications (ISSSTA '96), Mainz, 1996, pp. 313–319.

[SB97a] R. Schmalenberger and J.J. Blanz, "Multi antenna C/I balancing in the downlink of digital cellular mobile radio systems", Proc. IEEE 47th Vehicular Technology Conference (VTC'97), Phoenix, 1997, pp. 607–611.

[SB97b] R.M. Schmalenberger and J.J. Blanz, "A comparison of two different beamforming algorithms for multi antenna C/I balancing", Proc. European Personal Mobile Communications Conference (EPMCC'97), Bonn, 1997, pp. 483–490.

[SBS66] M. Schwartz, W.R. Bennett, and S. Stein, Communication systems and techniques, McGraw–Hill, New York, 1966.

[Sch78] G. Schwartz, "Estimating the dimension of a model", Ann. Math. Statist., vol. 6, 1978, pp. 461–464.

[Sch79] R.O. Schmidt, "Multiple emitter location and signal parameter estimation", Proc. RADC Spectrum Estimation Workshop, Griffiths AFB, New York, 1979, pp. 243–258.

[Sch86] R.O. Schmidt, "Multiple emitter location and signal parameter estimation", IEEE Transactions on Antennas and Propagation, vol. AP–34, 1986, pp. 276–280.

[Sch99] J. Schlee, Ein Hardware–Demonstrator zur Konzeptverifikation eines JD–CDMA–Mobilfunksystems Forschungsberichte Mobilkommunikation, vol. 1, University of Kaiserslautern, 1999. ISBN 3–925178–30–9.

[Sch01] R.M. Schmalenberger, Modell und Simulation der Abwärtsstrecke eines CDMA-Mobilfunksystems mit gemeinsamer Detektion der Teilnehmersignale und adaptiven Sendeantennen, Forschungsberichte Mobilkommunikation, vol. 7, University of Kaiserslautern, 2001. ISBN 3–925178–57–0.

[ShG81] S.S. Shapiro and A.J. Gross, Statistical modeling techniques, Dekker, New York, 1981.

[ShG94] J.J. Shynk, R.P. Gooch, "Performance analysis of the multistage CMA adaptive beamformer", 1994, pp. 316–320.

[Sie70] Telephone traffic theory, Tables and charts, Part I, Published by Siemens Aktiengesellschaft, Berlin–München, 1970.

[SIT64] "Special Issue on active and adaptive antennas", IEEE Transactions on Antennas and Propagation, vol. 12, 1964.

[SIT76] "Special Issue on adaptive antennas", IEEE Transactions on Antennas and Propagation, vol. 24, 1976.

[SJ67] S. Stein and J.J. Jones, Modern communication principles, McGraw-Hill, New York, 1967.

[SK93] B. Steiner and A. Klein, "Kanal– und Datenschätzung in synchronen CDMA–Mobilfunksystemen mit Interferenzeleminierung ", Kleinheubacher Berichte, vol. 36, 1993, pp. 253–268.

[SNXP93] B. Suard, A.F. Naguib, G. Xu and A. Paulraj, "Performance of CDMA mobile radio systems using antenna arrays", Proc. IEEE International Conference on Acoustics, Speech, and Signal Processing (ICASSP), Minneapolis, 1993, pp. 153–156.

[SOSL85] M.K. Simon, J.K. Omura, R.A. Scholtz and B.K. Levitt, Spread spectrum communications, vol. 1–3, Computer Science Press, Rockville, 1985.

[SP97] R. Schmalenberger and A. Papathanassiou, "Zwei kompatible Kanalmodelle für Simulationen auf System– und Linklevel", Proc. ITG Diskussionssitzung Modellszenarien für Systeme mit intelligenten Antennen, Kaiserslautern, 1997.

[SP98a] R. Schmalenberger and A. Papathanassiou, "Downlink spectrum efficiency of a JD-CDMA mobile radio system with array transmit antennas", COST 259 Temporary Document TD(98)094, Duisburg, 1998.

[SP98b] R. Schmalenberger and A. Papathanassiou, "Two compatible channel models for system and link level simulations of mobile radio systems", COST 259 Temporary Document TD(98)036, Bern, 1998.

[SS90] P. Stoica and K.C. Sharman, "Maximum likelihood methods for direction of arrival estimation", IEEE Transactions on Acoustics, Speech, and Signal Processing, vol. 38, 1990, pp. 1132–1143.

[Ste76] B.D. Steinberg, Principles of apperture and array system design, John Wiley & Sons Inc., New York, 1976.

[Ste92] R. Steele (editor), Mobile radio communications, Pentech Press, London, 1992.

[Ste95] B. Steiner, Ein Beitrag zur Mobilfunkkanalschätzung unter besonderer Berücksichtigung synchroner CDMA–Mobilfunksysteme mit Joint Detection, Fortschrittberichte VDI, series 10, no. 337, VDI–Verlag, Düsseldorf, 1995.

[Ste96] A. Steil, Spektrale Effizienz digitaler zellulare CDMA–Mobilfunksysteme mit gemeinsamer Detektion, Fortschrittberichte VDI, series 10, no. 437, VDI–Verlag, Düsseldorf, 1996.

[Ste97] A. Steil, "Statistics of the carrier–to–interference ratio in C/TDMA cellular mobile radio systems applying multi–user detection", Wireless Personal Communications, vol. 5, 1997, pp. 259–277.

[Ste98] M. Steinbauer, "A comprehensive transmission and channel model for directional radio channels", COST 259 Temporary Document TD(98)027, Bern, 1998.

[Tan94] M. Tangemann, "Introducing adaptive array antenna concepts in mobile communication systems", Proc. RACE Mobile Telecommunications Workshop, Amsterdam, 1994, pp. 2/714–727.

[TBM97] G. Tsoulos, M. Beach and J. McGeehan, "Wireless personal communications for the 21st century: European technological advances in adaptive antennas", IEEE Communications Magazine, vol. 35, 1997, pp. 102–109.

[Tel95] E. Teltar, "Capacity of multi-antenna Gaussian channels", AT&T Bell Labs Technical Memorandum, no. BL011217-950615-07TM, June 1995.

[TGM96] J.S. Thompson, P.M. Grant and B. Mulgrew, "Smart antenna arrays for CDMA systems", IEEE Communications Magazine, vol. 3, 1996, pp. 16–25.

[Tho80] T. Thorvaldsen, "Maximum entropy spectral analysis in antenna spatial filtering", IEEE Transactions on Antennas and Propagation, vol. 28, 1980, pp. 556–562.

[THT98] M. Tschudin, R. Heddergott and P. Truffer, "Validation of a high resolution measurement technique for estimating the parameters of impinging waves in indoor environments", Proc. IEEE 9$^{\text{th}}$ International Symposium on Personal, Indoor and Mobile Radio Communications (PIMRC'98), Boston, 1998, pp. 1411–1416.

[TNSC99] V. Tarokh, A.F. Naguib, N. Seshadri and A.R. Calderbank, "Space-time codes for high data rate wireless communication: Performance criteria in the presence of channel estimation errors, mobility, and multiple paths", and code construction", IEEE Transactions on Communications, vol. 47, 1999, pp. 199–207.

[TSA97] S. Tanaka, M. Sawahashi and F. Adachi, "Pilot symbol–assisted decision directed coherent adaptive array diversity for DS–CDMA mobile radio reverse link", IEICE Transactions on Fundamentals, vol. E80–A, 1997, pp. 2445–2454.

[TSC98] V. Tarokh, N. Seshadri and A.R. Calderbank, "Space-time codes for high data rate wireless communication: Performance criterion and code construction", IEEE Transactions on Information Theory, vol. 44, no. 2, 1998, pp. 744–765.

[TVP96] S. Talwar, M. Viberg and A. Paulraj, "Blind estimation of synchronous co–channel digital signals using an antenna array, Part I: Algorithms", IEEE Transactions on Signal Processing, vol. 44, 1996, pp. 1184–1197.

[TX97] M. Torlak and G. Xu, "Blind multiuser channel estimation in asynchronous CDMA systems", IEEE Transactions on Signal Processing, vol. 45, 1997, pp. 137–147.

[UHF90] WG 2 UHF Propagation, "Urban transmission loss models for mobile radio in the 900– and the 180–MHz bands", COST231 Temporary Document TD(90)119, Rev. 2, 1990.

[Ut99] W. Utschik, "Downlink beamforming for FDD mobile radio systems based on spatial covariances", COST259 Temporary Document TD(99)056, Vienna, 1999.

[Var95] M.K. Varanasi, "Group detection for synchronous Gaussian code-division multiple-access channels", IEEE Transactions on Information Theory, vol. 41, 1995, pp. 1083–1096.

[Vee97] A.J. van der Veen, "Analytical method for blind binary separation", IEEE Transactions on Signal Processing, vol. 45, 1997, pp. 178–182.

[Ver84] S. Verdú, Optimum multiuser signal detection, Doctoral Dissertation, University of Illinois at Urbana-Champaign, 1984.

[Ver86] S. Verdú, "Minimum probability of error for asynchronous Gaussian multiple–access channels", IEEE Transactions on Information Theory, vol. 32, 1986, pp. 85–96.

[Ver98] S. Verdú, Multiuser detection, Cambridge University Press, 1998.

[ViO79] A.J. Viterbi and J.K. Omura, Principles of digital communication and coding, McGraw-Hill, New York, 1979

[Vit95] A.J. Viterbi, Principles of spread spectrum communications, Addison–Wesley, 1995.

[VoC92] E.W. Vook and R.T. Compton, Jr., "Bandwidth performance of linear arrays with tapped delay line processing", IEEE Transactions on Aerosp. Electron. Syst., vol. 28, 1992, pp. 901–908.

[VOD92] A.J. van der Veen, P.B. Ober and E.F. Deprettere, "Azimuth and elevation computation in high resolution DOA estimation", IEEE Transactions on Signal Processing, vol. 40, 1992, pp. 1828–1832.

[VPP97] M.C. Vanderveen, C. Papadias and A. Paulraj, "Joint angle and delay estimation (JADE) for multipath signals arriving at an antenna array", IEEE Communications Letters, vol. 1, 1997, pp. 12–14.

[VTP97] A.J. van der Veen, S. Talwar and A. Paulraj, "A subspace approach to blind space–time signal processing for wireless communication systems", IEEE Transactions on Signal Processing, vol. 45, 1997, pp. 173–190.

[VVP97] A.J. van der Veen, M.C. Vanderveen and A. Paulraj, "Joint angle and delay estimation using shift–invariance techniques", IEEE Signal Processing Letters, vol. 4, 1997, pp. 142–145.

[Wal95] B. Walke, editor, ITG-Fachbericht, Mobile Kommunikation, vol. 135, VDE-Verlag, Berlin, 1995.

[WBOW00] T. Weber, P.W. Baier, J. Oster and M. Weckerle, "Performance enhancement of Time Division CDMA (TD-CDMA) by Multi-Step Joint Detection", Proc. 6$^{\text{th}}$ International Conference on Telecommunications (ICT 2000), Acapulco, 2000, pp. 1026-1032.

[Wec00] M. Weckerle, "MMSE based joint channel estimation for time division CDMA", Proc. IEEE 6$^{\text{th}}$ International Symposium on Spread Spectrum Techniques & Applications (ISSSTA 2000), Parsippany, 2000, pp. 525–529.

[Wec01] M. Weckerle, "Turbo methods for exploiting spatial and temporal covariance matrices in the TD-CDMA uplink with multi-element antennas", Proc. 4$^{\text{th}}$ European Personal Mobile Communications Conference (EPMCC'01), Vienna, 2001, no. 29.1.

[Wha71] A.D. Whalen, Detection of signals in noise, Academic Press, New York, 1971.

[Win93] J.H. Winters, "Signal Acquisition and Tracking with adaptive arrays in a digital mobile radio system IS-54 with flat fading", IEEE Transactions on Vehicular Technology, vol. 42, no. 4, 1993, pp. 377-384.

[Win84] J.H. Winters, "Optimum combining in digital mobile radio with cochannel interference", IEEE Journal on Selected Areas in Communications, vol. SAC-2, no. 4, 1984.

[WK85] M. Wax and T. Kailath, "Detection of signals by information theoretic criteria", IEEE Transactions on Acoustics, Speech, and Signal Processing, vol. 33, 1985, pp. 387–392.

[WMGG67] B. Widrow, P.E. Mantey, L.J. Griffiths and B.B. Goode, "Adaptive antenna systems", Proc. IEEE, vol. 55, 1967, pp. 2143–2159.

[WP99a] M. Weckerle and A. Papathanassiou, "Verfahren zum Schätzen der räumlichen Kovarianzmatrix der Störung in einem TD–CDMA–System mit adaptiven Antennen", Proc. ITG Diskussionssitzung Systeme mit intelligenten Antennen, Stuttgart, 1999.

[WP99b] M. Weckerle and A. Papathanassiou, "A novel multi–antenna TD–CDMA receiver concept incorporating the estimation and utilization of spatial interference covariance matrices", COST259 Temporary Document TD(99)059, Vienna, 1999.

[WP99c] M. Weckerle and A. Papathanassiou, "Performance analysis of multi-antenna TD-CDMA receivers with estimation and consideration of the interference covariance matrix", International Journal on Wireless Information Networks, vol. 6, no. 3, 1999, pp. 157–170.

[WPE98] M. Weckerle, A. Papathanassiou and D. Emmer, "The benefits of intelligent antenna arrays in TD–CDMA — A study based on measured channel impulse responses", Proc. IEEE 9$^{\text{th}}$ International Symposium on Personal, Indoor and Mobile Radio Communications (PIMRC '98), Boston, 1998, pp. 962–966.

[WPH99] M. Weckerle, A. Papathanassiou and M. Haardt, "Estimation and utilization of spatial interference covariance matrices in multi–antenna TD–CDMA systems", Proc. IEEE 10$^{\text{th}}$ International Symposium on Personal, Indoor and Mobile Radio Communications (PIMRC '99), Osaka, 1999, pp. 1198–1202.

[WPS99] M. Weckerle, A. Papathanassiou and R. Schmalenberger, "Consideration of the spatial interference covariance matrix in multi–antenna TD–CDMA systems", COST259 Temporary Document TD(99)018, Thessaloniki, 1999.

[WWBJ00] M. Weckerle, T. Weber, P.W. Baier and J. Oster, "Space-time signal processing utilizing multi-step joint detection for the uplink of time division CDMA", Proc. International Conference on Communication Technologies (ICCT 2000), Beijing, 2000, pp. 1330–1335.

[WWR94] Q. Wu, K.M. Wong and J.P. Reilly, "Maximum likelihood direction finding in unknown noise environments", IEEE Transactions on Signal Processing, vol. 42, 1994, pp. 980–983.

[XRK94] G. Xu, R.H. Roy and T. Kailath, "Detection of number of sources via exploitation of centro–symmetry property", IEEE Transactions on Signal Processing, vol. 42, 1994, pp. 102–112.

[YU93] W.S. Youn and C.K. Un, "A linearly constrained beamforming robust to array imperfections", IEEE Transactions on Signal Processing, vol. 41, 1993, pp. 1425–1428.

[Zan92a] J. Zander, "Performance of optimum transmitter power control in cellular radio systems", IEEE Transactions on Vehicular Technology, vol. 41, 1992, pp. 57–62.

[Zan92b] J. Zander, "Distributed cochannel interference control in cellular radio systems", IEEE Transactions on Vehicular Technology, vol. 41, 1992, pp. 305–311.

[ZB86] O. Zinke and H. Brunswig, Lehrbuch der Hochfrequenztechnik, vol. 1–2, Springer–Verlag, Berlin, 3rd edition, 1986.

[ZHM96] M.D. Zoltowski, M. Haardt and C.P. Mathews, "Closed–form 2–D angle estimation with rectangular arrays in element space or beamspace via unitary ESPRIT", IEEE Transactions on Signal Processing, vol. 44, 1996, pp. 316–328.

[Zol93] E. Zollinger, Eigenschaften von Funkübertragungsstrecken in Gebäuden, Doctoral Dissertation, Eidgenössische Technische Hochschule Zürich, 1993.

[ZS96] Z. Zvonar and M. Stojanovic, "Performance of antenna diversity multiuser receivers in CDMA channels with imperfect fading estimation", Wireless Personal Communications, vol. 3, 1996, pp. 91–110.

[Zur64] R. Zurmühl, Matrizen, Springer-Verlag, Berlin, 1964.

[ZW88] I. Ziskind and M. Wax, "Maximum likelihood localization of multiple sources by alternating projection", IEEE Transactions on Acoustics, Speech, and Signal Processing, vol. 36, 1988, pp. 1553–1560.

[Zwi00] T. Zwick, Die Modellierung von richtungsaufgelösten Mehrwegegebäudefunkkanälen durch markierte Poisson–Prozesse, Doctoral Dissertation, University of Karlsruhe, 2000.

Tabellarischer Lebenslauf

Name:	Martin Weckerle
Geburtsdatum:	6. Januar 1971
Geburtsort:	Neustadt a.d. Weinstraße
Familienstand:	verheiratet
Staatsangehörigkeit:	deutsch
Schulausbildung:	August 1977 – Juni 1981 Grundschule in Neustadt an der Weinstraße
	August 1981 – Mai 1990 Gymnasium in Neustadt an der Weinstraße
Schulabschluß:	Mai 1990 Allgemeine Hochschulreife
Grundwehrdienst:	Juli 1990 – Juni 1991
Studium:	Oktober 1991 – Juni 1997 Studium der Elektrotechnik an der Universität Kaiserslautern
Studienabschluß:	Diplom
Berufstätigkeit:	Juli 1997 – Mai 2001 wissenschaftlicher Mitarbeiter am Lehrstuhl für hochfrequente Signalübertragung und –verarbeitung der Universität Kaiserslautern
	seit Juni 2001 Mitarbeiter der Siemens AG in München